DYNAMIC ANALYSIS OF DIESEL ENGINE CRANKSHAFT SYSTEM USING FINITE ELEMENTS AND MULTIBODY SYSTEM SIMULATION PROGRAMS

by

Yasin Yılmaz

B.S., Mechanical Engineering, Middle East Technical University, 1996

M.S., Mechanical Engineering, Pamukkale University, 1999

Submitted to the Institute for Graduate Studies in
Science and Engineering in partial fulfillment of
the requirements for the degree of
Doctor of Philosophy

Graduate Program in Mechanical Engineering
Boğaziçi University

2008

DYNAMIC ANALYSIS OF DIESEL ENGINE CRANKSHAFT SYSTEM USING FINITE ELEMENTS AND MULTIBODY SYSTEM SIMULATION PROGRAMS

APPROVED BY:

Prof. Günay Anlaş
(Thesis Supervisor)

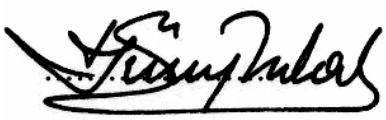

Prof. Ali Rana Atılgan

Assoc. Prof. İbrahim Emre Köse .....

Assoc. Prof. Stephen Ekwaro-Osire .....

Prof. Akın Tezel .....

DATE OF APPROVAL: 22.01.2008

ACKNOWLEDGEMENTS

I am particularly grateful to my thesis supervisor, Professor Günay Anlaş, for his technical support, leadership and professional guidance as well as his encouragement and mentoring during my study and research. I especially appreciate his patience and understanding.

I would like to express my gratitude to Professor Akın Tezel, Professor Ali Rana Atılgan, Associate Professor Stephen Ekwaro-Osire and Associate Professor İbrahim Emre Köse, who served as my committee members, for their valuable time used in reviewing and commenting on my dissertation.

My special thanks go to Mr. Umud E. Ozturk, Mr. Veysel Alkan, Mr. Alpay Oral, Mr. Ahmet H. Ertaş and all other fellow graduate students, who made my six year at Boğaziçi University an enjoyable one.

I also express my thanks to Ford Otosan, Engine and Powertrain Systems Department for providing support during this study.

Finally, I wish to thank my lovely wife Sema Yılmaz for her encouragement, support and understanding during the years of my dissertation work. Taking care of our son and managing a comfortable home are by no means easy. You have provided an extra motivation for me to move forward. I would also like to thank my son, Ahmet Berkay Yılmaz. You have been sharing all the joys and sorrows with me since you were born. Thank you all.

ABSTRACT

DYNAMIC ANALYSIS OF DIESEL ENGINE CRANKSHAFT SYSTEM USING FINITE ELEMENTS AND MULTIBODY SYSTEM SIMULATION PROGRAMS

In this thesis, dynamic analysis of in-line six cylinder diesel engine crankshaft system is carried out using analytical and numerical methods. The dynamic analysis of the crankshaft system consists of calculation of forces, displacements and stresses over a complete engine cycle (two revolutions of the crankshaft) under steady state (constant speed) conditions with a model of the whole cranktrain. Crankshaft system consists of crankshaft, engine block, pistons, piston pins, connecting rods, flywheel, torsional vibration damper, bearings and mounts that support the engine block. The loading on the system comes from the cylinder gas pressure and inertia of crankshaft system components.

In the analytical part of the study, first, the forces acting on the crankshaft system are determined. Then, main bearing loads are calculated using a statically determinate system approach for each crank throw. Finally, torsional vibration and stress analyses of the crankshaft system are performed. In the numerical analysis of the crankshaft system, Msc.Nastran and Msc.Adams programs are used. The dynamic stress distribution in the crankshaft is evaluated using a flexible crankshaft model that is obtained through finite elements and Component Mode Synthesis (CMS) technique. To study the effect of oil holes on crankshaft dynamic stresses, crankshaft models with and without oil holes are used. The effect of TV damper on crankshaft stresses is investigated. Bearings are modeled using hydrodynamic bearing models of ADAMS. Coupled axial, bending and torsional vibrations of the crankshaft system are considered. Effect of each part of the crankshaft system on crankshaft dynamic stress and vibration characteristics are investigated.

A separate chapter is devoted to effects of counterweight mass and position on main bearing load and crankshaft bending stresses. In the analysis, rigid, beam and 3D solid

(flexible) crankshaft models are used. Main bearing load results for rigid, beam and 3D solid models are compared and beam model is used in counterweight configuration analyses. Twelve-counterweight configurations with a zero degree counterweight angle and eight-counterweight configurations with thirty degree counterweight angle, each for 0%, 50% and 100% counterweight balancing rates, are considered. It is found that maximum main bearing load and web bending stress increase with increasing balancing rate, and average main bearing load increases with decreasing balancing rate. Both configurations show the same trend. For this specific engine, the load from gas pressure rather than inertia forces is the parameter with the most important influence on design of the crankshaft. Results of bearing loads and web bending stresses are tabulated.

ÖZET

DİZEL MOTORU KRANK MİLİ SİSTEMİNİN SONLU ELEMANLAR VE ÇOKLU-CİSİM SİSTEM SİMÜLASYON PROGRAMLARI KULLANILARAK DİNAMİK ANALİZİ

Bu tezde, analitik ve nümerik metodlar kullanılarak, altı silindirli sıra-tipi dizel motora ait krank mili sisteminin dinamik analizi gerçekleştirilmiştir. Krank mili sisteminin dinamik analizi, tüm sistem elemanları göz önünde bulundurularak sabit hızda bir motor çevrimi (iki krank mili dönüşü) boyunca krank mili üzerindeki kuvvet, yer değiştirme ve gerilimlerin hesaplanmasını içermektedir. Krank mili sistemi krank mili, motor bloğu, pistonlar, piston pimleri, biyel kolları, volan, burulma titreşim damperi, yataklar ve motor bloğunu taşıyan takozlardan oluşmaktadır. Sistem üzerindeki yükleme, silindir gaz basıncı ve krank mili sistem elemanlarının ataletlerinden gelmektedir.

Krank mili sisteminin analitik analizi kısmında, ilk önce krank mili sistemi üzerine etki eden kuvvetler belirlenmiştir. Sonrasında izostatik sistem yaklaşımı kullanılarak ana yatak yükleri hesaplanmıştır. Son olarak krank mili burulma titreşimi ve gerilme analizleri gerçekleştirilmiştir. Nümerik analiz kısmı için Msc.Nastran ve Msc.Adams programları kullanılmıştır. Krank mili üzerindeki dinamik stres dağılımını hesaplamak için, "Component Mode Synthesis" tekniği kullanılarak sonlu eleman analiziyle krank mili elastik cisim olarak modellenmiştir. Yağ deliklerinin krank mili dinamik gerilimleri üzerine etkisini belirlemek için, yağ delikli ve yağ deliksiz krank mili modelleri kullanılmıştır. Burulma titreşim damperinin krank mili stres dağılımına etkisi incelenmiştir. Ana yataklar ADAMS'ın hidrodinamik yatak modelleri kullanılarak modellenmiştir. Krank mili sisteminin eksenel, eğilme ve burulma titreşimleri hesaba katılmıştır. Krank mili sisteminin her bir elemanının krank mili dinamik stres ve titreşim karakteristikleri üzerine etkisi incelenmiştir.

Karşı-ağırlık kütle ve pozisyonunun ana yatak yükü ve krank mili eğilme gerilimi üzerine etkileri ayrı bir bölümde incelenmiştir. Analizlerde rijit, kiriş ve 3D katı krank mili modelleri kullanılmıştır. Bu modeller kullanılarak elde edilen ana yatak kuvvetleri karşılaştırılmış ve karşı-ağırlık konfigürasyonu analizlerinde kiriş krank mili modeli kullanılmıştır. % 0, % 50 and % 100 balans oranları için oniki ve sekiz karşı-ağırlık konfigürasyonları dikkate alınmıştır. Analizler sonucunda, artan balans oranıyla maksimum ana yatak kuvveti ve kol eğilme geriliminin arttığı, ve azalan balans oranıyla ortalama ana yatak kuvvetinin arttığı bulunmuştur. Her iki konfigürasyon aynı eğilimi göstermektedir. Bu motor için krank mili dizaynında atalet kuvvetlerinden daha çok gas basınç kuvveti önemli bir parametredir. Yatak kuvvetleri ve kol eğilme gerilimleri çizelgelenmiştir.

TABLE OF CONTENTS

ACKNOWLEDGEMENTS iii
ABSTRACT iv
ÖZET vi
LIST OF FIGURES xi
LIST OF TABLES xxvi
LIST OF SYMBOLS/ABBREVIATIONS xxxi
1. INTRODUCTION 1
1.1. Internal Combustion Engine Basics 4
1.1.1. Heat Engines 4
1.1.2. Engine Geometry 5
1.1.2.1. Piston Displacement 5
1.1.2.2. Piston Velocity 8
1.1.2.3. Piston Acceleration 9
1.1.2.4. Kinematics of Crank and Connecting Rod 9
1.1.2.5. Cylinder Volume 10
1.1.3. Thermodynamic Cycle of an Engine 11
1.2. Literature Review 12
1.3. Motivation and Objectives of the Study 22
1.4. Problem Statement 25
1.5. Thesis Outline 32
2. CRANKSHAFT TORSIONAL VIBRATION ANALYSIS 34
2.1. Introduction 34
2.2. Excitation Torque 36
2.2.1. Cylinder pressure torque 37
2.2.2. Reciprocating inertia torque 38
2.3. Dynamic Model of the Crankshaft System 40
2.4. Natural Frequencies 45
2.5. Torsional Vibration Analysis 49
2.5.1. Torsional Vibration Angle Amplitudes at Crankshaft Front End . . 51

2.5.2. Torsional Vibration Stress Amplitudes 64
2.5.3. Torsional Vibration Measurement 66
2.6. Torsional Vibration Sensitivity Analyses 69
2.6.1. Effect of TV Damper Specifications on Torsional Vibration 69
2.6.2. Effect of Cylinder Misfire on Forced Torsional Vibration 80
3. CLASSICAL FORCE AND STRESS ANALYSIS OF CRANKSHAFT SYSTEM 84
3.1. Introduction 84
3.2. Force Analysis of Crankshaft System 84
3.2.1. Pressure Forces 85
3.2.2. Inertia Forces 85
3.2.2.1. Inertia Force of the Connecting Rod 86
3.2.2.2. Inertia Forces of the Rotating Parts 88
3.2.2.3. Inertia Forces of the Reciprocating Parts 89
3.2.3. Force Resolution at the Crank Train and Main Bearing Forces . . . 90
3.3. Stress Analysis of Crankshaft System 96
3.3.1. Nominal Stresses due to Bending Moments and Radial Forces . . . 96
3.3.2. Actual Fillet Stresses due to Bending Moments and Radial Forces . 98
3.3.3. Combined Stresses for Bending and Torsion 99
3.3.4. Stress Concentration Factors 100
3.3.5. Results 101
4. DYNAMIC ANALYSIS OF CRANKSHAFT SYSTEM USING ADAMS . . . 107
4.1. Introduction 107
4.2. Modeling Crankshaft System Using ADAMS 108
4.2.1. Crankshaft Model Descriptions in ADAMS 108
4.2.2. Theory of Implementing Flexible Bodies in ADAMS 113
4.2.2.1. Component Mode Synthesis—The Craig-Bampton Method . 114
4.2.2.2. Mode Shape Orthonormalization 116
4.2.3. Bearing Types in ADAMS 118
4.2.4. Modeling Torsional Vibration Damper 120
4.2.5. Modeling Flywheel 123
4.2.6. Cranktrain Model 124
4.3.. Model Descriptions 126

4.4. Crankshaft Main Bearing Loads 133
4.5. Dynamic Stress Analyses 142
4.5.1. Beam Crankshaft Model 142
4.5.2. Flexible Crankshaft Model 144
4.5.3. Effect of TV Damper Stiffness and Damping on Crankshaft Stress . 157
4.6. Oil Film Thickness Analysis 161
5. COUNTERWEIGHT CONFIGURATION ANALYSIS 177
5.1. Introduction 177
5.2. Forces Acting on Crankshaft System and Balancing 180
5.3. Main Bearing Loads: Comparison of Crankshaft Models 183
5.4. Effect of counterweight configuration on main bearing load and crankshaft bending stress 188
5.4.1. Twelve counterweighs, $\gamma = 0°$, K=0%, K=50% and K=100% 188
5.4.2. Eight counterweights, $\gamma = 30°$, K=50% and K=100% 199
6. SUMMARY AND CONCLUSIONS 209
APPENDIX A: MATLAB CODE FOR TORSIONAL VIBRATION ANALYSIS . 215
APPENDIX B: STRESS RESULTS FOR BEAM CRANKSHAFT MODEL . . . 259
REFERENCES 272

LIST OF FIGURES

Figure 1.1. Piston-connecting rod assembly 6

Figure 1.2. Engine thermodynamic cycle events 12

Figure 1.3. Gas pressure values at different engine speeds for the 7.3 L engine . 26

Figure 1.4. Gas pressure values at different engine speeds for the 9.0 L engine . 26

Figure 1.5. Geometry of the 7.3L engine crankshaft system 27

Figure 1.6. Piston of the 7.3 L engine 28

Figure 1.7. Connecting rod of the 7.3 L engine 28

Figure 1.8. Crankshaft of the 7.3 L engine 29

Figure 1.9. Typical variation of radial and tangential force components acting on crankpin during one engine cycle 30

Figure 1.10. TV damper of the 7.3 L engine 30

Figure 1.11. Flywheel of the 7.3 L engine 31

Figure 1.12. Pulley of the 7.3 L engine 31

Figure 2.1. Lumped mass model of a crankshaft system 35

Figure 2.2. Total excitation torque variation with crank angle 40

Figure 2.3. Torsional vibration equivalent system of six cylinder engine without damper 42

Figure 2.4. Mode shapes corresponding to first two natural frequencies of 9 L engine crankshaft system 48

Figure 2.5. Crankshaft front end torsional vibration at 1200 rpm for 7.3 L engine 54

Figure 2.6. Crankshaft front end torsional vibration at 1480 rpm for 7.3 L engine 54

Figure 2.7. Crankshaft front end torsional vibration at 1600 rpm for 7.3 L engine 55

Figure 2.8. Crankshaft front end torsional vibration at 1700 rpm for 7.3 L engine 55

Figure 2.9. Crankshaft front end torsional vibration at 1850 rpm for 7.3 L engine 56

Figure 2.10. Crankshaft front end torsional vibration at 2220 rpm for 7.3 L engine 56

Figure 2.11. Crankshaft front end torsional vibration at 2400 rpm for 7.3 L engine 57

Figure 2.12. Torsional vibration angle amplitudes at crankshaft front end for 7.3 L engine w/o TV damper 57

Figure 2.13. Torsional vibration angle amplitudes at crankshaft front end for 7.3 L engine with TV damper 58

Figure 2.14. Crankshaft front end torsional vibration at 800 rpm for 9.0 L engine . 61

Figure 2.15. Crankshaft front end torsional vibration at 1000 rpm for 9.0 L engine 61

Figure 2.16. Crankshaft front end torsional vibration at 1200 rpm for 9.0 L engine 62

Figure 2.17. Crankshaft front end torsional vibration at 1350 rpm for 9.0 L engine 62

Figure 2.18. Crankshaft front end torsional vibration at 1675 rpm for 9.0 L engine 63

Figure 2.19. Crankshaft front end torsional vibration at 2000 rpm for 9.0 L engine 63

Figure 2.20. Crankshaft front end torsional vibration at 2200 rpm for 9.0 L engine 64

Figure 2.21. Torsional vibration stress amplitudes in crankshaft related to the crank pin diameter (7.3 L engine without damper) 65

Figure 2.22. Torsional vibration stress amplitudes in crankshaft related to the crank pin diameter (7.3 L engine with damper) 65

Figure 2.23. Total amplitude of crankshaft torsion vibration – Comparison of experimental and calculated data 67

Figure 2.24. Measured harmonic orders - 0.5th order to 3rd order 67

Figure 2.25. Measured harmonic orders - 3.5th order to 6th order 68

Figure 2.26. Measured harmonic orders - 6.5th order to 9th order 68

Figure 2.27. Measured harmonic orders - 9.5th order to 12th order 69

Figure 2.28. Effect of torsional stiffness change on natural frequencies 72

Figure 2.29. Effect of hub inertia change on natural frequencies 72

Figure 2.30. Effect of ring inertia change on natural frequencies 73

Figure 2.31. Effect of torsional stiffness change on front end torsional vibration at 2200 rpm engine speed 78

Figure 2.32. Effect of damping coefficient change on front end torsional vibration at 2200 rpm engine speed 78

Figure 2.33. Effect of hub inertia change on front end torsional vibration at 2200 rpm engine speed 79

Figure 2.34. Effect of ring inertia change on front end torsional vibration at 2200 rpm engine speed 79

Figure 2.35. Front end torsional vibration when cylinder # 1 misfires at 2000 rpm 81

Figure 2.36. Front end torsional vibration when cylinder # 2 misfires at 2000 rpm 81

Figure 2.37. Front end torsional vibration when cylinder # 3 misfires at 2000 rpm 82

Figure 2.38. Front end torsional vibration when cylinder # 4 misfires at 2000 rpm 82

Figure 2.39. Front end torsional vibration when cylinder # 5 misfires at 2000 rpm 83

Figure 2.40. Front end torsional vibration when cylinder # 6 misfires at 2000 rpm 83

Figure 3.1. Forces acting on crankshaft assembly 90

Figure 3.2. Forces acting on main bearings 91

Figure 3.3. Comparison of forces acting on main bearing #1 93

Figure 3.4. Comparison of forces acting on main bearing #2 93

Figure 3.5. Comparison of forces acting on main bearing #3 94

Figure 3.6. Comparison of forces acting on main bearing #4 94

Figure 3.7. Comparison of forces acting on main bearing #5 95

Figure 3.8. Comparison of forces acting on main bearing #6 95

Figure 3.9. Comparison of forces acting on main bearing #7 96

Figure 3.10. Crankthrow and cross section A-A for crankshaft stress analysis . . 97

Figure 4.1. Crankshaft design scheme 108

Figure 4.2. Geometry of web parts 109

Figure 4.3. Rigid crankshaft model 110

Figure 4.4. Torsional-flexible crankshaft model 111

Figure 4.5. Beam crankshaft model 111

Figure 4.6. Flexible crankshaft model 112

Figure 4.7. Two constraint modes for the left end of a beam that has attachment points at the two ends 114

Figure 4.8. Two fixed-boundary normal modes for a beam that has attachment points at the two ends 115

Figure 4.9. Process of modeling 3D Hydrodynamic Bearing in ADAMS/Engine . 120

Figure 4.10. Linear TV Damper with implemented force element 121

Figure 4.11. Extended Poynting-Thomson model of force component implemented in rubber TV damper 122

Figure 4.12. Cross-section of viscous TV damper 122

Figure 4.13. Schematic representation of a single-mass flywheel 123

Figure 4.14. Geometry of a dual-mass flywheel 124

Figure 4.15. Schematic representation of a cranktrain model 125

Figure 4.16. Cranktrain dynamic analysis procedure 125

Figure 4.17. Location of main bearings, pins and webs 126

Figure 4.18. Crankshaft finite element model 129

Figure 4.19. Flexible crankshaft model for the crankshaft with oil holes 130

Figure 4.20. Cranktrain model for beam crankshaft 132

Figure 4.21. Cranktrain model for flexible crankshaft 132

Figure 4.22. Gas pressure curves at different engine speeds for 7.3 L engine . . . 133

Figure 4.23. Forces acting on main bearing #1, beam crankshaft model 135

Figure 4.24. Forces acting on main bearing #1, flexible crankshaft model 135

Figure 4.25. Forces acting on main bearing #1, (AVL/Excite) 135

Figure 4.26. Forces acting on main bearing #2, beam crankshaft model 136

Figure 4.27. Forces acting on main bearing #2, flexible crankshaft model 136

Figure 4.28. Forces acting on main bearing #2, (AVL/Excite) 136

Figure 4.29. Forces acting on main bearing #3, beam crankshaft model 137

Figure 4.30. Forces acting on main bearing #3, flexible crankshaft model 137

Figure 4.31. Forces acting on main bearing #3, (AVL/Excite) 137

Figure 4.32. Forces acting on main bearing #4, beam crankshaft model 138

Figure 4.33. Forces acting on main bearing #4, flexible crankshaft model 138

Figure 4.34. Forces acting on main bearing #4, (AVL/Excite) 138

Figure 4.35. Forces acting on main bearing #5, beam crankshaft model 139

Figure 4.36. Forces acting on main bearing #5, flexible crankshaft model 139

Figure 4.37. Forces acting on main bearing #5, (AVL/Excite) 139

Figure 4.38. Forces acting on main bearing #6, beam crankshaft model 140

Figure 4.39. Forces acting on main bearing #6, flexible crankshaft model 140

Figure 4.40. Forces acting on main bearing #6, (AVL/Excite) 140

Figure 4.41. Forces acting on main bearing #7, beam crankshaft model 141

Figure 4.42. Forces acting on main bearing #7, flexible crankshaft model 141

Figure 4.43. Forces acting on main bearing #7, (AVL/Excite) 141

Figure 4.44. Locations of main pin, crank pin and webs for beam crankshaft model 142

Figure 4.45. Time history of Von Mises stress at Web #12, fillet to main journal (no oil holes, without TV damper) 144

Figure 4.46. Time history of maximum and minimum principle stresses at Web #12, fillet to main journal (no oil holes, without TV damper) 145

Figure 4.47. Time history of Von Mises stress at Web #12, fillet to crank pin (no oil holes, without TV damper) 145

Figure 4.48. Time history of maximum and minimum principle stresses at Web #12, fillet to crank pin (no oil holes, without TV damper) 146

Figure 4.49. Stress state at Web #12, fillet to main journal (no oil holes, without TV damper) 146

Figure 4.50. Stress state at Web #12, fillet to crank pin (no oil holes, without TV damper) 147

Figure 4.51. Time history of Von Mises stress at Web #12, fillet to main journal (no oil holes, with TV damper) 147

Figure 4.52. Time history of maximum and minimum principle stresses at Web #12, fillet to main journal (no oil holes, with TV damper) 148

Figure 4.53. Time history of Von Mises stress at Web #12, fillet to crank pin (no oil holes, with TV damper) 148

Figure 4.54. Time history of maximum and minimum principle stresses at Web #12, fillet to crank pin (no oil holes, with TV damper) 149

Figure 4.55. Stress state at Web #12, fillet to main journal 7 (no oil holes, with TV damper) 149

Figure 4.56. Stress state at Web #12, fillet to crank pin (no oil holes, with TV damper) 150

Figure 4.57. Time history of Von Mises stress at Web #12, fillet to main journal (with oil holes, without TV damper) 150

Figure 4.58. Time history of maximum and minimum principle stresses at Web #12, fillet to main journal (with oil holes, without TV damper) . . . 151

Figure 4.59. Time history of Von Mises stress at Web #12, fillet to crank pin (with oil holes, without TV damper) 151

Figure 4.60. Time history of maximum and minimum principle stresses at Web #12, fillet to crank pin (with oil holes, without TV damper) 152

Figure 4.61. Stress state at Web #12, fillet to main journal (with oil holes, without TV damper) 152

Figure 4.62. Stress state at Web #12, fillet to crank pin (with oil holes, without TV damper) 153

Figure 4.63. Time history of Von Mises stress at Web #12, fillet to main journal (with oil holes, with TV damper) 153

Figure 4.64. Time history of maximum and minimum principle stresses at Web #12, fillet to main journal (with oil holes, with TV damper) 154

Figure 4.65. Time history of Von Mises stress at Web #12, fillet to crank pin (with oil holes, with TV damper) 154

Figure 4.66. Time history of maximum and minimum principle stresses at Web #12, fillet to crank pin (with oil holes, with TV damper) 155

Figure 4.67. Stress state at Web #12, fillet to main journal (with oil holes, with TV damper) 155

Figure 4.68. Stress state at Web #12, fillet to crank pin (with oil holes, with TV damper) 156

Figure 4.69. Time history of Von Mises stress at Web #12 for different torsional stiffness values of the damper (Node 273404), fillet to main journal 7 157

Figure 4.70. Time history of Von Mises stress at Web #12 for different torsional stiffness values of the damper (Node 273514), fillet to main journal 7 158

Figure 4.71. Time history of Von Mises stress at Web #12 for different torsional stiffness values of the damper (Node 277307), fillet to crank pin . . 158

Figure 4.72. Time history of Von Mises stress at Web #12 for different damping values of the damper (Node 273404), fillet to main journal 7 159

Figure 4.73. Time history of Von Mises stress at Web #12 for different damping values of the damper (Node 273514), fillet to main journal 7 160

Figure 4.74. Time history of Von Mises stress at Web #12 for different damping values of the damper (Node 277307), fillet to crankpin 160

Figure 4.75. Minimum oil film thickness for main bearing #1 using 2D Hydro-dynamic model 163

Figure 4.76. Minimum oil film thickness for main bearing #2 using 2D Hydro-dynamic model 163

Figure 4.77. Minimum oil film thickness for main bearing #3 using 2D Hydro-dynamic model 164

Figure 4.78. Minimum oil film thickness for main bearing #4 using 2D Hydrodynamic model 164

Figure 4.79. Minimum oil film thickness for main bearing #5 using 2D Hydrodynamic model 165

Figure 4.80. Minimum oil film thickness for main bearing #6 using 2D Hydrodynamic model 165

Figure 4.81. Minimum oil film thickness for main bearing #7 using 2D Hydrodynamic model 166

Figure 4.82. Orbital curve for main bearing #1 using 2D Hydrodynamic model . 166

Figure 4.83. Orbital curve for main bearing #2 using 2D Hydrodynamic model . 167

Figure 4.84. Orbital curve for main bearing #3 using 2D Hydrodynamic model . 167

Figure 4.85. Orbital curve for main bearing #4 using 2D Hydrodynamic model . 168

Figure 4.86. Orbital curve for main bearing #5 using 2D Hydrodynamic model . 168

Figure 4.87. Orbital curve for main bearing #6 using 2D Hydrodynamic model . 169

Figure 4.88. Orbital curve for main bearing #7 using 2D Hydrodynamic model . 169

Figure 4.89. Minimum oil film thickness for main bearing #1 using 3D Hydrodynamic model 170

Figure 4.90. Minimum oil film thickness for main bearing #2 using 3D Hydrodynamic model 170

Figure 4.91. Minimum oil film thickness for main bearing #3 using 3D Hydro-

dynamic model 171

Figure 4.92. Minimum oil film thickness for main bearing #4 using 3D Hydrodynamic model 171

Figure 4.93. Minimum oil film thickness for main bearing #5 using 3D Hydrodynamic model 172

Figure 4.94. Minimum oil film thickness for main bearing #6 using 3D Hydrodynamic model 172

Figure 4.95. Minimum oil film thickness for main bearing #7 using 3D Hydrodynamic model 173

Figure 4.96. Orbital curve for main bearing #1 using 3D Hydrodynamic model . 173

Figure 4.97. Orbital curve for main bearing #2 using 3D Hydrodynamic model . 174

Figure 4.98. Orbital curve for main bearing #3 using 3D Hydrodynamic model . 174

Figure 4.99. Orbital curve for main bearing #4 using 3D Hydrodynamic model . 175

Figure 4.100. Orbital curve for main bearing #5 using 3D Hydrodynamic model . 175

Figure 4.101. Orbital curve for main bearing #6 using 3D Hydrodynamic model . 176

Figure 4.102. Orbital curve for main bearing #7 using 3D Hydrodynamic model . 176

Figure 5.1. 3D solid model of the 9.0 L engine crankshaft 178

Figure 5.2. Eight counterweight arrangement of the 9.0 L engine crankshaft . . 178

Figure 5.3. Model of the crankshaft system 180

Figure 5.4. First and second order vector stars 182

Figure 5.5. Gas pressure values at different engine speeds for the 9.0 L engine . 183

Figure 5.6. Forces acting on main bearing #1 for rigid, beam and 3D solid crankshaft models at 1000 rpm engine speed 184

Figure 5.7. Forces acting on main bearing #2 for rigid, beam and 3D solid crankshaft models at 1000 rpm engine speed 185

Figure 5.8. Forces acting on main bearing #3 for rigid, beam and 3D solid crankshaft models at 1000 rpm engine speed 185

Figure 5.9. Forces acting on main bearing #4 for rigid, beam and 3D solid crankshaft models at 1000 rpm engine speed 186

Figure 5.10. Forces acting on main bearing #5 for rigid, beam and 3D solid crankshaft models at 1000 rpm engine speed 186

Figure 5.11. Forces acting on main bearing #6 for rigid, beam and 3D solid crankshaft models at 1000 rpm engine speed 187

Figure 5.12. Forces acting on main bearing #7 for rigid, beam and 3D solid crankshaft models at 1000 rpm engine speed 187

Figure 5.13. Maximum bearing forces at bearing #1 for twelve-counterweight configurations 189

Figure 5.14. Average bearing forces at bearing #1 for twelve-counterweight configurations 189

Figure 5.15. Maximum bearing forces at bearing #2 for twelve-counterweight configurations 190

Figure 5.16. Average bearing forces at bearing #2 for twelve-counterweight configurations 190

Figure 5.17. Maximum bearing forces at bearing #3 for twelve-counterweight configurations 191

Figure 5.18. Average bearing forces at bearing #3 for twelve-counterweight configurations 191

Figure 5.19. Maximum bearing forces at bearing #4 for twelve-counterweight configurations 192

Figure 5.20. Average bearing forces at bearing #4 for twelve-counterweight configurations 192

Figure 5.21. Maximum bearing forces at bearing #5 for twelve-counterweight configurations 193

Figure 5.22. Average bearing forces at bearing #5 for twelve-counterweight configurations 193

Figure 5.23. Maximum bearing forces at bearing #6 for twelve-counterweight configurations 194

Figure 5.24. Average bearing forces at bearing #6 for twelve-counterweight configurations 194

Figure 5.25. Maximum bearing forces at bearing #7 for twelve-counterweight configurations 195

Figure 5.26. Average bearing forces at bearing #7 for twelve-counterweight configurations 195

Figure 5.27. Maximum bearing forces at bearing #1 for eight-counterweight configurations 199

Figure 5.28. Average bearing forces at bearing #1 for eight-counterweight configurations 200

Figure 5.29. Maximum bearing forces at bearing #2 for eight-counterweight configurations 200

Figure 5.30. Average bearing forces at bearing #2 for eight-counterweight configurations 201

Figure 5.31. Maximum bearing forces at bearing #3 for eight-counterweight configurations 201

Figure 5.32. Average bearing forces at bearing #3 for eight-counterweight configurations 202

Figure 5.33. Maximum bearing forces at bearing #4 for eight-counterweight configurations 202

Figure 5.34. Average bearing forces at bearing #4 for eight-counterweight configurations 203

Figure 5.35. Maximum bearing forces at bearing #5 for eight-counterweight configurations 203

Figure 5.36. Average bearing forces at bearing #5 for eight-counterweight configurations 204

Figure 5.37. Maximum bearing forces at bearing #6 for eight-counterweight configurations 204

Figure 5.38. Average bearing forces at bearing #6 for eight-counterweight configurations 205

Figure 5.39. Maximum bearing forces at bearing #7 for eight-counterweight configurations 205

Figure 5.40. Average bearing forces at bearing #7 for eight-counterweight configurations 206

LIST OF TABLES

Table 1.1. Engine data for 7.3 L and 9.0 L engines 25

Table 2.1. Inertia torque harmonic coefficients for the first six harmonics . . . 39

Table 2.2. Inertia, stiffness and damping values for the crankshaft system of 7.3L engine 42

Table 2.3. Inertia, stiffness and damping values for the crankshaft system of 9.0L engine 43

Table 2.4. Crank train parameters for the 7.3 L and 9.0 L engine crankshaft systems 43

Table 2.5. Natural frequencies of the 7.3 L and 9.0 L engine crankshaft systems . 47

Table 2.6. Crankshaft front end torsional vibration amplitudes for 7.3 L engine w/o TV damper 52

Table 2.7. Crankshaft front end torsional vibration amplitudes for 7.3 L engine with TV damper 53

Table 2.8. Crankshaft front end torsional vibration amplitudes for 9.0 L engine w/o TV damper 59

Table 2.9. Crankshaft front end torsional vibration amplitudes for 9.0 L engine with TV damper 60

Table 2.10. Natural frequencies of the 9.0 L engine crankshaft system 70

Table 2.11. Effect of TV damper torsional stiffness change on natural frequencies of the 9.0L engine crankshaft system 70

Table 2.12. Effect of TV damper hub inertia change on natural frequencies of the 9.0 L engine crankshaft system 71

Table 2.13. Effect of TV damper ring inertia change on natural frequencies of the 9.0 L engine crankshaft system 71

Table 2.14. Crankshaft front end torsional vibration amplitudes at 2200 rpm for first 16 orders with various torsional stiffness values of the TV damper 74

Table 2.15. Crankshaft front end torsional vibration amplitudes at 2200 rpm for first 16 orders with various damping coefficients of the TV damper . . 75

Table 2.16. Crankshaft front end torsional vibration amplitudes at 2200 rpm for first 16 orders with various hub inertia values of the TV damper . . . 76

Table 2.17. Crankshaft front end torsional vibration amplitudes at 2200 rpm for first 16 orders with various ring inertia values of the TV damper . . . 77

Table 3.1. Crankshaft dimensions and stress concentration factors 101

Table 3.2. Torsional Vibration Stress Amplitudes referred to the crank pin diameter 102

Table 3.3. Torsional Vibration Stress Amplitudes referred to the main pin diameter 102

Table 3.4. Actual fillet stresses due to bending moments and radial forces . . . 103

Table 3.5. Combined stresses at the crank pin fillet of the webs 104

Table 3.6. Combined stresses at the main pin fillet of the webs 105

Table 4.1. 7.3 L engine crankshaft counterweight positions and masses 127

Table 4.2. 7.3 L engine crankshaft web geometry 128

Table 4.3. Modal frequencies of the 7.3 L engine crankshaft 131

Table 4.4. Maximum stresses for beam crankshaft model 143

Table 4.5. Maximum Von Mises stress change at main pin and crank pin fillets of Web #12 with respect to stiffness of the TV damper 159

Table 4.6. Maximum Von Mises stress change at main pin and crank pin fillets of Web 12 with respect to damping coefficient of the TV damper . . . 161

Table 4.7. Dynamic viscosity change of SAE 10W-40 oil with respect to temperature 162

Table 4.8. Input data for oil film thickness calculation 162

Table 5.1. CAD mass properties of the crank throws 179

Table 5.2. Balancing system data 179

Table 5.3. Maximum bending stresses for no counterweight configuration, K=0% 196

Table 5.4. Maximum bending stresses for twelve-counterweight configuration with K=50% 197

Table 5.5. Maximum bending stresses for twelve-counterweight configuration with K=100% 198

Table 5.6. Maximum bending stress for eight counterweights, $\gamma = 30°$, K=50% counterweight configuration 207

Table 5.7. Maximum bending stress for eight counterweights, $\gamma = 30°$, K=100% counterweight configuration 208

LIST OF SYMBOLS / ABBREVIATIONS

A	Area of the projected web cross section
C_d^*	Complex viscous damping coefficient
D	Bore diameter
F	Bearing force component acting in the crank throw direction
F_i	Inertia force
F_T	Tangential force acting on the crankpin
F_p	Gas pressure force
J_h	Damper housing inertia
J_i , i = 1, 2,…,6	Cylinder inertias
J_p	Pulley inertia
J_r	Damper ring inertia
k	Harmonic order
K	Balancing rate
$\mathbf{K}$	Stiffness matrix
$\hat{\mathbf{K}}$	Generalized stiffness matrix
l	Effective connecting rod length
L	Stroke
$\mathbf{M}$	Mass matrix
$\hat{\mathbf{M}}$	Generalized mass matrix
$m_{cr\text{-}r}$	Connecting rod rotating mass
m_{cr_tr}	Connecting rod translating mass
m_p	Piston mass
M_B	Bending moment in the center of the crank web due to the bearing force component
$\mathbf{N}$	Transformation matrix
P_{cc}	Pressures inside the crank case
P_{cyl}	Pressures inside the cylinder
$\mathbf{q}$	Vector of modal coordinates

r	Crank radius
r_R	Distance from the crankshaft center of rotation to the center of gravity of the rotating mass
s	Piston displacement
$\dot{s}$	Piston velocity
$\ddot{s}$	Piston acceleration
T_p	Cylinder pressure torque
T_r	Reciprocating inertia torque
$\mathbf{u}$	Displacement vector
U_{CW}	Static unbalance of counterweight
U_{Crank_throw}	Static unbalance of crank throw
V	Combustion chamber volume
V_c	Clearance volume
V_d	Displacement volume
W_i	Indicated work
$\mathbf{X}$	Amplitude matrix
Z	Sectional modulus
α	Stress concentration factor for the crankpin fillet
β_B	Stress concentration factor for the main journal fillet for bending loading
β_Q	Stress concentration factor for the main journal fillet for compressive loading
$\mathbf{\Phi}$	Shape function matrix
$\mathbf{\Phi}^*$	Matrix of orthogonalized Craig-Bampton modes
γ	Offset angle of counterweight mass
θ	Angular position of the crankshaft
σ_a	Stress amplitude
σ_c	Maximum stress in crankpin fillet
σ_C	Combined stress
σ_j	Maximum stress in main journal fillet

σ_m	Mean stress
σ_T	Fillet stress amplitude due to torsion
σ_{BN}	Nominal bending stress related to the normal crank web cross- section
σ_{QN}	Nominal tensile or compressive stress in the normal crank web cross section due to radial forces in the crank web
ω	Crankshaft angular velocity

ADAMS	Automatic dynamic analysis of mechanical systems
CAE	Computer aided engineering
CI	Compression ignition
DOF	Degree of freedom
EVC	Exhaust valve closing
EVO	Exhaust valve opening
FEM	Finite element method
IVC	Intake valve closing
IVO	Inlet valve opening
MSS	Multibody system simulation
NVH	Noise, vibration and harshness
PFP	Peak firing pressure
SI	Spark ignition
TDC	Top dead center
TV	Torsional vibration

1. INTRODUCTION

New internal combustion engines must satisfy requirements such as increased engine power, decreased engine size and improved fuel economy, simultaneously. Moreover, reducing engine vibrations and making more reliable and durable models have become important aspects for the automotive industry. To overcome these challenges, a designer needs improved tools to predict dynamic response, durability and vibration characteristics of engine components if competitive designs are to be realized.

The dynamics of the crankshaft and the reciprocating engine components play an increasing role in the assessment of engine performance and structural design. Extensive static and dynamic analyses have been performed on vital engine components such as crankshafts to improve their durability, and noise, vibration and harshness (NVH) performance. In engine design, the performance of each component is strongly dependent on the performance of other components. This is particularly true for the crankshaft system of internal combustion engines.

The crankshaft system consists of the crankshaft, piston, connecting rod, crankshaft front and rear gears, flywheel, crankshaft pulley, torsional vibration damper, fan adapter, bolts and main bearings. The loading on the system comes from the cylinder pressure and inertia of rotating and reciprocating parts of the crankshaft assembly, the piston-connecting rod inertia and the inertia of other crankshaft accessories. The cylinder force acting on the piston head is transmitted to the crankpin through the piston-connecting rod assembly. The inertia of the piston-connecting rod provides a load on the crankpin as well. The radial component of the crankpin load causes crankshaft to bend and transmitted to the engine block at main bearing locations. The tangential component of the transmitted force, on the other hand, is utilized in the rotation of the crankshaft. With every power stroke the transmitted force is initially increased in magnitude and is subsequently reduced at the end of the stroke. This action results in twist-untwist action of the crankshaft, causing torsional vibrations to occur.

Engine crankshafts are subjected to significant vibrations (axial, torsional and bending) within their normal operating range. These vibrations affect dynamic stress distribution in crankshafts and bearing caps. An accurate prediction of dynamic stress levels is important for durability, low weight and high fatigue life. The crankshaft dynamic response is also needed for optimizing crankshaft accessories such as damper, pulley and flywheel. Thus an accurate prediction for the dynamic characteristics of crankshaft system using analytical, numerical and experimental methods is essential for modern engines.

Dynamic analysis of internal combustion engine crankshaft system consists of calculation of forces, stresses and dynamic response of the crankshaft over a complete engine cycle (two revolutions of the crankshaft) under steady state conditions with a model of the whole cranktrain which is supported by a cylinder block structure at the main bearing locations. For correct determination of forces, stresses and dynamic response of the crankshaft, influence of the flywheel and torsional vibration damper as well as the nonlinear behavior of the oil film in the bearings should be considered.

Crankshafts have remained as one of the most difficult structural geometries to be analyzed for dynamic response, load deformation behavior and dynamic stress distribution. In the past, they were designed using simplified models, empirical formulae and in-house experience. With the increasing power of modern computers, analyses based on computer aided engineering (CAE), finite element method (FEM) and multibody system simulation (MSS) have come into use for the analysis of crankshaft dynamics which otherwise cannot be accurately studied with existing analytical methods.

An increasing amount of CAE is needed in the development processes of modern engines. The calculations have to be quick on one hand and must deliver reliable results on the other hand. Since prototypes are not available early in the design process, especially in the “pre-prototype phase”, usage of virtual prototypes is required and it represents a very important part in the development process. During this period, results from calculations and the engineering experience of designers are the basis for design decisions. For more innovative designs where less engineering expertise is available, the importance of calculations increases dramatically in the concept phase. With increasing power of modern computers and growing experience of engineers, it is possible today to create accurate

results without model adaptation. If CAE can partially replace expensive testing investigations, a large potential of cost reduction and efficiency will be used in development process.

In the case of the dynamics of a cranktrain, it is necessary to describe the structural dynamic behavior of included parts and interaction between them. An additional problem is that the cranktrain components are coupled by oil films, which have to be described by non-linear hydrodynamic differential equations. FEM and MSS are both commonly used in engine analysis. However, neither FEM nor MSS, when used alone, is well suited for understanding the details of the dynamics of a cranktrain.

FEM can be used to address NVH problems. It can also be used to solve for stresses and strains to assess durability. These simulations often use a very high number of degrees of freedom (DOF) to match the structural behavior and the stress-strain distribution, including local effects. Therefore, it is common to use fixed boundary conditions and to neglect the interaction between parts; consequently, a linear formulation of the dynamic equations is used which allows transformation into the frequency domain to save simulation time. However, the coupling between the different engine parts is often nonlinear and large dynamic effects are important to describe the behavior of the whole engine.

The interaction of parts in a dynamic system may be investigated using MSS. This kind of simulation has been used very effectively in investigations of vehicle dynamics, where the dynamic structural stiffness of the parts is much higher than the stiffness of the elements connecting them. Every part of the system has 6 DOFs and may be coupled to other parts by specific constraints. The total number of DOFs in the system is small compared to typical FEM models, so it is possible to include non-linear effects and to analyze in the time domain for simulations of short duration.

Consequently, neither FEM nor MSS alone is well suited for detailed dynamic analysis where large motions and non-linear effects are important. In standard MSS models, rigid parts are coupled by joints, constraining DOFs, or by linear or nonlinear springs and dampers. To introduce flexibility into the MSS solution, dynamic stiffness of

each FE part is reduced to transfer functions between attachment points. A time domain solution that includes flexibility of engine components is then possible in MSS program with a reduced number of DOFs. The transfer behavior of the oil films that couple the engine parts may be described in MSS through the use of numerical solutions of hydrodynamic differential equations.

In the following sections, first a brief introduction is given on internal combustion engines. Second, studies in literature on dynamic analysis of internal combustion engines are examined. Third, motivation and objectives of the study are introduced. Finally, problem statement and thesis outline are given.

1.1. Internal Combustion Engine Basics

Basic concepts on reciprocating internal combustion engines that will be used in subsequent chapters are introduced in this section. The introduction is limited to four-stroke cycle engines.

1.1.1. Heat Engines

A heat engine converts thermal energy to mechanical work, by letting a working fluid go through a thermodynamic cycle. This involves heat transfer and volume change of the working fluid. The simplest type of heat engine accepts heat from a high-temperature reservoir, outputs mechanical work, and expels waste heat to a low-temperature reservoir. Mainly there are two types of heat engines: “internal combustion” and “external combustion” engines.

In external combustion engines, fuel is burned in the air and used to create a heated working fluid (such as boiling water or hot air). This heated vapor is then used to drive a piston or turbine to create power. Steam and Stirling engines are examples of external combustion engines.

In internal combustion (IC) engines, a combustible mixture of fuel and air is taken into the engine, burned and the expanding hot gases are used directly to produce power by

either pushing a piston or by causing a turbine to spin. The combustion process itself is responsible from power production. A reciprocating internal combustion engine utilizes a cylinder-piston-crank arrangement to produce power. There are two types of reciprocating internal combustion engines: Spark-Ignition (Otto-cycle) and Compression-Ignition (Diesel-cycle) engines.

Spark-ignition engines require a spark plug to operate. In these engines, combustion is initiated by passing an electric discharge between the electrodes of a spark plug through the combustible gas mixture. This causes the fuel to ignite and burn. In a diesel engine, high air temperatures and pressures prior to combustion are due to the compression of air alone rather than an air-fuel mixture. Compression of air alone eliminates the possibility of autiognition during compression and makes high compression ratios possible. However, because of the high pressures and temperatures, Diesel engines must be designed to be structurally stronger. Therefore, they tend to be heavier than SI engines with the same brake power. The energy release process in the Diesel engine is controlled by the rate of injection of fuel. After a brief ignition lag, the first fuel injected into the combustion chamber autoignites and the resulting high gas temperature sustains the combustion of the remainder of the fuel stream as it enters the combustion chamber.

1.1.2. Engine Geometry

The basic geometry of a reciprocating internal combustion engine is shown in Figure 1.1. The figure includes cylinder, piston, crankshaft, and connecting rod. Most geometric and kinematic properties of the engine can be derived from this simple schematics.

1.1.2.1. Piston Displacement. The vertical position of the piston is completely determined by the crank angle θ. This section derives an expression for the vertical piston position as a function of crank angle. Let θ define the angular position of the crank with respect to Top Dead Center (TDC). Designating the piston position with respect to TDC by s as shown in Figure 1.1, piston displacement, s, can be expressed as

$$s = (r + l) - (r\cos\theta + l\cos\beta). \tag{1.1}$$

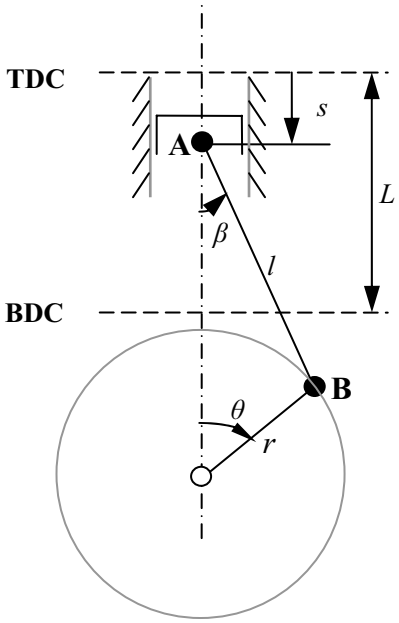

Figure 1.1. Piston-connecting rod assembly

Define,

$$\lambda = \frac{r}{l} \tag{1.2}$$

then equation (1.1) takes the following form:

$$s = r\left[\left(1+\frac{1}{\lambda}\right)-\left(\cos\theta+\frac{1}{\lambda}\cos\beta\right)\right]. \tag{1.3}$$

From Figure 1.1, it can be seen that,

$$\sin\beta = \lambda\sin\theta \tag{1.4}$$

Using

$$\cos\beta = \sqrt{1-\sin^2\beta} \tag{1.5}$$

together with equation (1.4) one gets

$$\cos\beta = \sqrt{1-\lambda^2\sin^2\theta}. \tag{1.6}$$

Substituting equation (1.6) in (1.3), the position of the piston in terms of the crank angle θ, and dimensions of the crank and the connecting rod is obtained as follows:

$$s = r\left[1+\frac{1}{\lambda}-\cos\theta-\frac{1}{\lambda}\sqrt{1-\lambda^2\sin^2\theta}\right]. \tag{1.7}$$

Using the binomial theorem, the radical in equation (1.7) can be expanded into the following series:

$$\sqrt{1-\lambda^2\sin^2\theta} = 1-\frac{\lambda^2}{2}\sin^2\theta-\frac{\lambda^4}{8}\sin^4\theta-\frac{\lambda^6}{16}\sin^6\theta+\ldots \tag{1.8}$$

The powers of $\sin\theta$ may be replaced by their equivalent multiple angles as shown below:

$$\sin^2\theta = \frac{1}{2}-\frac{1}{2}\cos 2\theta, \tag{1.9a}$$

$$\sin^4\theta = \frac{3}{8}-\frac{1}{2}\cos 2\theta+\frac{1}{8}\cos 4\theta, \tag{1.9b}$$

$$\sin^6\theta = \frac{5}{16}-\frac{15}{32}\cos 2\theta+\frac{3}{16}\cos 4\theta-\frac{1}{32}\cos 6\theta. \tag{1.9c}$$

Substituting equations (1.9 a-c) in equation (1.8), and then substituting the resulting equation in equation (1.7), the piston displacement can be expressed as:

$$s = r\left(A_0+A_1\cos\theta+\frac{A_2}{4}\cos 2\theta+\frac{A_4}{16}\cos 4\theta+\frac{A_6}{36}\cos 6\theta+\ldots\right) \tag{1.10}$$

where

$$A_0 = 1 + \frac{1}{4}\lambda + \frac{3}{64}\lambda^3 + \frac{5}{256}\lambda^5 + \ldots,$$

$$A_1 = -1,$$

$$A_2 = -\left(\lambda + \frac{1}{4}\lambda^3 + \frac{15}{128}\lambda^5 + \ldots\right),$$

$$A_4 = \frac{1}{4}\lambda^3 + \frac{3}{16}\lambda^5 + \ldots,$$

$$A_6 = -\left(\frac{9}{128}\lambda^5 + \ldots\right).$$

Usually λ takes values between 0.2 and 0.33, therefore only the first and second order harmonic components have significant contribution to piston displacement. Neglecting all other higher order components, an error of less than 1% occurs and equation (1.10) reduces to the following form:

$$s = r\left(1 + \frac{\lambda}{4} - \cos\theta - \frac{\lambda}{4}\cos 2\theta\right). \tag{1.11}$$

1.1.2.2. Piston Velocity. If the crank is assumed to rotate at a constant angular velocity ω which is the case for most applications, the piston velocity can be written as

$$\dot{s} = \frac{ds}{dt} = \frac{ds}{d\theta}\frac{d\theta}{dt} = -r\,\omega\left(A_1 \sin\theta + \frac{A_2}{2}\sin 2\theta + \frac{A_4}{4}\sin 4\theta + \frac{A_6}{6}\sin 6\theta + ..\right). \tag{1.12}$$

Using the reduced equation (1.11) for *s*, the piston velocity takes the following form:

$$\dot{s} = r\,\omega\left(\sin\theta + \frac{\lambda}{2}\sin 2\theta\right). \tag{1.13}$$

1.1.2.3. Piston Acceleration. The piston acceleration can be expressed as (ω is taken to be constant)

$$\ddot{s} = \frac{d\dot{s}}{dt} = \frac{d\dot{s}}{d\theta}\frac{d\theta}{dt} = \omega\frac{d\dot{s}}{d\theta} = -r\,\omega^2\left(A_1\cos\theta + A_2\cos 2\theta + A_4\cos 4\theta + A_6\cos 6\theta + \ldots\right). \quad (1.14)$$

Reasons for expressing the piston acceleration in series form are: First, it greatly facilitates the addition of forces with varying phase relations such as in multi cylinder engines and second, this form is helpful in solving vibration problems. Using the simplified formula, the acceleration of the piston can be approximated as

$$\ddot{s} = r\,\omega^2\left(\cos\theta + \lambda\cos 2\theta\right). \quad (1.15)$$

1.1.2.4. Kinematics of Crank and Connecting Rod. If $\omega = \text{constant}$, the crank acceleration has only a normal component which is directed along the crank radius toward the axis of rotation. Its value varies linearly from zero at the center of rotation to a maximum value of $r\,\omega^2$ at the axis of the crankpin.

The connecting rod has a planar motion. Its position may be determined for each crank angle considering the position of axis of articulation between piston and connecting rod, which is given by piston displacement and the angle β made by the connecting rod axis with the cylinder axis. According to equation (1.4), this angle is

$$\beta = \sin^{-1}\left(\lambda\cdot\sin\theta\right) \quad (1.16)$$

The instantaneous angular speed of the connecting-rod may be determined by differentiating equation (1.16) with respect to time:

$$\omega_{cr} = \frac{d\beta}{dt} = \frac{d\beta}{d\theta}\cdot\frac{d\theta}{dt} = \omega\cdot\frac{d\beta}{d\theta} \quad (1.17)$$

$d\beta/d\theta$ can be obtained by differentiating equation (1.4) and using equation (1.6) as shown below:

$$\cos\beta.d\beta = \lambda\cos\theta.d\theta \tag{1.18}$$

$$\frac{d\beta}{d\theta} = \frac{\lambda\cos\theta}{\cos\beta} = \frac{\lambda\cos\theta}{\sqrt{1-\lambda^2\sin^2\theta}} \tag{1.19}$$

Substituting equation (1.19) into (1.17), the following expression for the instantaneous angular velocity of the connecting rod can be obtained:

$$\omega_{cr} = \lambda\cdot\omega\cdot\frac{\cos\theta}{\sqrt{1-\lambda^2\sin^2\theta}}. \tag{1.20}$$

The angular acceleration of the connecting-rod can be obtained from equation (1.20) as follows:

$$\alpha_{cr} = \frac{d\omega_{cr}}{dt} = \frac{d\omega_{cr}}{d\theta}\frac{d\theta}{dt} = \omega\frac{d\omega_{cr}}{d\theta} = -\lambda\omega^2(1-\lambda^2)\frac{\sin\theta}{(1-\lambda^2\sin^2\theta)^{3/2}}. \tag{1.21}$$

1.1.2.5. Cylinder Volume. At TDC, the volume of the combustion chamber is the clearance volume, V_c. For any other crank position, the combustion chamber volume is the sum of the clearance volume and the volume with bore diameter D and height s. The total combustion chamber volume can be expressed as a function of the crank angle as

$$V(\theta) = V_c + \frac{\pi D^2}{4}\cdot s(\theta). \tag{1.22}$$

The difference between the maximum and minimum combustion chamber volume is called the displacement volume, V_d, and is given by

$$V_d = V(\pi) - V(0) = \left(V_c + \frac{\pi D^2}{4} \cdot s(\pi) \right) - \left(V_c + \frac{\pi D^2}{4} \cdot s(0) \right)$$
$$= \left(V_c + \frac{\pi D^2}{4} \cdot 2r \right) - V_c = \frac{\pi D^2}{4} \cdot 2r = \frac{\pi D^2}{4} \cdot L \tag{1.23}$$

where L is the stroke.

1.1.3. Thermodynamic Cycle of an Engine

The thermodynamic cycle of a four-stroke cycle engine spans two full revolutions of the crankshaft, and consists of four distinct strokes: intake, compression, expansion, and exhaust. The flow of gases is controlled by intake and exhaust valves, which are actuated by the cams on the camshaft. The camshaft rotational speed is half of the engine speed, and thus allows for the two-revolution (720 crank-angle degrees) thermodynamic cycle.

During the air intake phase, new air flows into the cylinder through the inlet valve sucked by the movement of the piston and compressed by turbo charging system. The pressure in the cylinder is approximately equal to turbo pressure. During compression, both valves are closed and the piston is moving upward by compressing the air trapped inside the cylinder. Approximately at the top piston position, diesel fuel is injected and combustion starts as a result of high temperature and pressure. The piston then moves downwards and the phase is called expansion because the cylinder volume expands. At the bottom piston position, the outlet valve opens and the burned gases exit the cylinder during the exhaust phase. The sequence of events in a four stroke engine is plotted in a cylinder pressure-crank angle diagram given in Figure 1.2.

The mechanical work transferred from cylinder gases to piston during the course of one thermodynamic cycle is called the indicated work, and is given by

$$W_i = \int_{\theta=0}^{4\pi} p(\theta) \cdot dV(\theta) \tag{1.25}$$

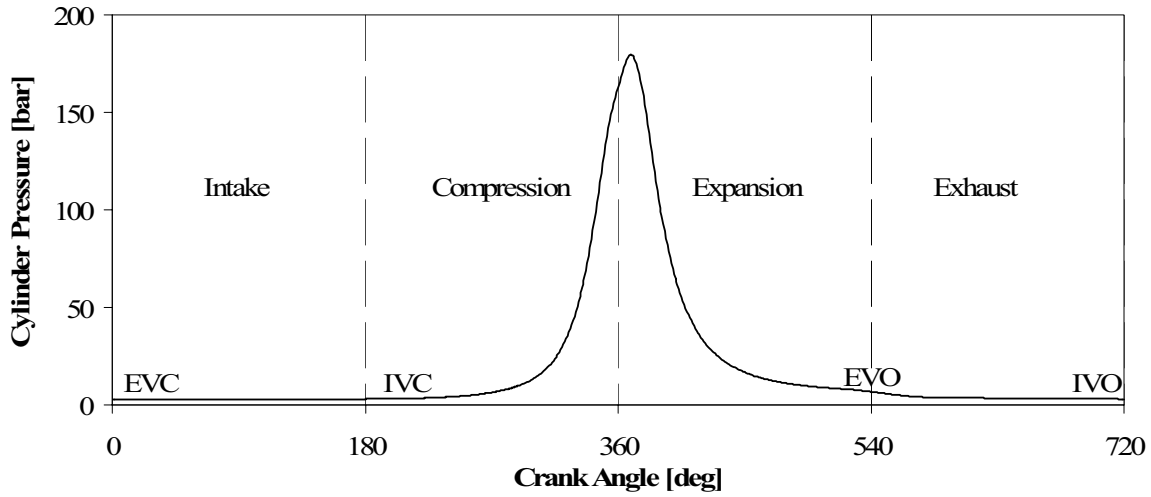

Figure 1.2. Engine thermodynamic cycle events (EVC : Exhaust valve closing, IVC : Intake valve closing, EVO : Exhaust valve opening, IVO : Inlet valve opening)

1.2. Literature Review

No literature review can be totally comprehensive when considering a field as large as internal combustion engine modeling. Books such as Heywood and Ferguson give some information what is available [1, 2]. In the development process of internal combustion engines two kinds of simulation techniques have been successfully used in recent years:

- Thermodynamic and fluid dynamic simulations give information about combustion and gas exchange of the engine and help mostly to optimize the thermodynamic processes due to fuel consumption and emissions.
- Mechanical simulations serve to understand the influence of the engine parameters on durability of engine components and NVH.

For the mechanical simulations, which is the task of this study, different numerical techniques are used depending on the specific purpose. The most important tools used in this manner are the analytical solution of simple equations often implemented as small programs, linear and nonlinear FEM analysis including postprocessors for the evaluation of specific technical equations (e.g. vibrations and durability), and dynamic MSS in time

domain for the evaluation of the dynamic interaction between several parts [3]. Now, a literature review will be given on dynamic analysis of crankshaft system of internal combustion engines.

To simplify the analysis of the three-dimensional vibrations of automobile engine crankshafts under firing conditions, in a two part study, Okamura et al. [4] have idealized the crankshaft by a set of jointed structures consisting of simple round rods and simple beam blocks of rectangular cross-section. The front pulley, timing gear, and the flywheel were idealized by a set of masses and moments of inertia. The main journal bearings were idealized by a set of linear springs and dash-pots. They derived the dynamic stiffness matrix for each member of the crankshaft system from the transfer matrix and then, constructing the dynamic stiffness matrix for the total crankshaft system, calculated the natural frequencies and mode shapes. In the first part of the study they shown the background of the modeling and computation procedures and applied them to free vibrations in several different automobile engine crankshafts. In the second part of the study Morita and Okamura [5] have applied the modeling and analysis procedures described in the first part to forced vibrations of a four-cylinder in-line engine crankshaft system under firing conditions and compared the obtained results with experimental ones.

Rajendran and Narasimhan [6] examined the effect of inertia variation on the free vibration characteristics of crankshafts under combined torsional and bending vibrations. In their study, they investigated single-cylinder engine crankshaft geometry. The parametric excitations due to inertia variation and the consequent instability have been neglected in the analysis. They have computed the free vibration characteristics under pseudostatic condition of the crankshaft and justified the approach for small engines, where only higher order critical speeds lie in the operating speed range.

Boysal and Rahnejat [7] dealt with torsional vibration analysis of a multi-body single cylinder internal combustion engine model. Their model incorporates the simultaneous solution of large displacement dynamics of engine components, infinitesimal vibrations of support bearings, and the trapped air-fuel cylinder transient pressures. They obtained time histories of the dynamic response of inertial members such as the piston, the flywheel and

the connecting rod. They also obtained the torsional vibrations of the crankshaft and whirl of journal bearings.

Brusa et al. [8] studied the torsional vibration of crankshafts with account taken to the variation of the geometry of the system with the crank angle. They have dealt with both the free behavior and the response to external excitations. They obtained a mathematical model which has the form of a set of linear differential equations with periodic coefficients.

Kang et al. [9] investigated the coupled modes, including coupled torsional-flexural vibration and coupled longitudinal-flexural vibration for non-rotating crankshafts which are free-free suspended. Using beam and solid elements, they determined the natural frequencies and mode shapes of two crankshafts from a four-cylinder in-line engine and a six-cylinder V-shaped engine by the FEM and compared with experimental data from modal testing. They used ANSYS software for FEM analysis and found that the solid element is more appropriate than the beam element in the modal analysis of crankshafts.

Nehme et al. [10] developed a distributed mass model to predict the rigid and flexible motions of the piston assembly/connecting rod/crankshaft mechanism of a single cylinder engine. The model takes into consideration the torsional vibration and out-of-plane transverse deformation of the crankshaft along with the out-of-plane transverse deformation of the connecting rod. They treated the crank journals, crankpins, and crank arms as simple beam elements and the flywheel, crank gear, and counterweights as rigid bodies.

Chalhoub et al. [11] investigated the effects of structural deformations of the crankshaft/connecting rod/piston mechanism on the estimation of the instantaneous engine friction torque. They considered a model, accounting for the rigid and flexible motions of the crank-slider mechanism and including engine component friction formulations. In their study, to estimate the engine friction torque, the torsional vibrations and the rigid body angular velocity of the crankshafts have been used along with the engine load torque and the cylinder gas pressure in the (P-ω) method.

Nehme et al. [12] investigated the effects of filtering the actual angular displacement, velocity and acceleration of the crankshaft on the computation of the instantaneous engine friction torque. They prepared a crank-slider mechanism to generate the rigid and flexible motions of the crankshaft/connecting-rod/piston mechanism and to determine the instantaneous engine friction torque. Again, the (P-ω) method have been used to estimate the instantaneous engine friction torque based on the actual and the filtered angular displacement, velocity and acceleration of the crankshaft.

Mourelatos [13] performed a structural analysis using dynamic substructuring with Ritz vectors for predicting the dynamic response of an engine crankshaft, based on the finite element method. He performed a two-level dynamic substructuring using a load-dependent Ritz vectors and coupled the rotating crankshaft with the non-rotating, compliant engine block. They compared the results with the equivalent superelement analysis in MSC/NASTRAN using the free and forced vibrations of a slender cylindrical beam and free vibrations of a four cylinder engine crankshafts. He also compared the results obtained for the dynamic response of engine crankshafts with the analytical predictions and experimental results for the torsional vibrations of an in line five cylinder engine and the bending vibrations of the crankshaft-flywheel assembly of a V6 engine.

Mourelatos [14] proposed a system model for analyzing the dynamic behavior of an internal combustion engine crankshaft. The analyzed model couples the crankshaft structural dynamics, the main bearing hydrodynamic lubrication and the engine block stiffness using a system approach. He used a two-level dynamic substructuring technique to predict the crankshaft dynamic response based on the finite-element method and compared the obtained results with the experimental ones.

Hoffman and Dowling [15] dealt with fully coupled rigid internal combustion engine dynamics and vibration in a two part study. In the first part, they presented a seven-degree of freedom model for low frequency engine vibrations that utilizes fully coupled rigid body dynamics for the pistons, connecting rods, crankshaft, flywheel and engine block. Then in the second part [16], they presented time and frequency domain comparisons of this model to experimental measurements made on an inline six-cylinder heavy duty Diesel engine running at full load at peak torque (1200 rpm) and rated (2100 rpm) speeds.

Ma and Perkins [17] developed the equations of motion for the major components in an internal combustion engine using a recursive formulation. These components include the rigid engine block, pistons, connecting rods, flexible crankshaft, balance shafts, main bearings and engine mounts. They employed relative coordinates that automatically satisfy all constraints and therefore lead to the minimum set of ordinary differential equations of motion. They demonstrated the procedure on a V-6 engine under free and firing conditions and compared the predicted engine responses with results from an ADAMS model. They obtained the results using different bearing models, including linear, nonlinear, and hydrodynamic bearing models.

Metallidis and Natsiavas [18] presented dynamic models of single- and multi-cylinder reciprocating machines which may involve torsional flexibility in the crankshaft, taking into account the dependence of the engine moment of inertia on the crankshaft rotation. They presented numerical results for linear and nonlinear engine models by applying appropriate methodologies, leading to direct determination of steady-state response of the system.

Zweiri et al. [19] presented a dynamic model for a single cylinder diesel engine that can simulate engine performance under both transient and steady state operating conditions. The model is based on an analysis of all the major forces internal to the engine and dynamometer. The model has been implemented in MATLAB/SIMULINK.

Zweiri et al. [20] developed an engine friction model in order to determine the instantaneous friction components at any crank angle during the overall engine response. The main friction components are the piston assembly, the bearing, the valve train and the auxiliaries.

Zweiri et al. [21] presented a combined non-linear dynamic, instantaneous friction model in the crank angle domain for a single cylinder diesel engine. The model is used to predict the in-cycle variation of engine states for transient and steady state operating conditions.

Pasricha and Carnegie [22] investigated the effects of variable inertia on the damped torsional vibrations of a single cylinder diesel engine. Equation of motion of the crankshaft is linearized for small displacements to predict important characteristics of the motion. For numerical analysis modified Euler's equations has been used. The waveform responses are studied at different speeds of engine rotation.

Drew et al. [23] investigated the torsional excitation of variable inertia effects in a single-cylinder reciprocating engine using a combination of experimental measurements and system modeling. A torsional exciter was used to measure the variation of the second torsional natural frequency of the stationary test system as a function of crank angle, which is equivalent to measuring the inertia variation of the system for that mode.

Geveci et al. [24] investigated the harmonic components of the crankshaft rotational speed signal of a six-cylinder diesel engine from a cylinder health diagnostics point of view. Effect of cylinder imbalance on the individual harmonic components of the engine speed signal is analyzed. A crank angle domain numerical model of the crankshaft dynamics for a six cylinder

Burla et al. [25] developed a parametric model for three dimensional finite element analysis of crankshaft torsional vibrations using parametric modeling. They used ANSYS to obtain finite element model of the crankshaft and modeled main journal bearings as linear springs and dashpots. The piston and reciprocating masses are lumped at the ends of the crank pins. They assumed that the gas force and inertia force for a given cylinder are equally supported by the adjacent crank journals.

Parakash et al. [26] used a combination of classical methods and finite element method to calculate the dynamic response and life estimate of the crankshaft. ANSYS software was used for finite element modeling of the crankshaft using 3-dimensional solid elements. They found out the displacements and stresses at all locations of the crankshaft using mode superposition method.

Raub et al. [27] applied a combined finite element method, multibody system simulation and hydrodynamic bearing simulation technique to solve for engine crankshaft

and cylinder block dynamics. They implemented the cylinder block and crankshaft in the MSS program, ADAMS/Engine, as flexible structures and obtained the displacements and deformations of the crank train parts and the main bearing reaction forces.

Ortjohann et al. [28] presented a method for 3-D durability analysis of crankshafts with coupled dynamic simulation including modal reduction. They used FE software NASTRAN to model the crankshaft and to take into account the stiffness of it. With modal reduction the complete deformation order information of the FEA simulation are reduced to the necessary information for the dynamic multibody system simulation software, ADAMS/Engine.

Kodama et al. [29] carried out experiments to determine the dynamic characteristics of high viscosity silicone oil damper and optimum clearance between the casing and the inertia ring. They measured the torsional angular, axial and lateral vibration displacements at the damper inertia ring and the casing varying the clearance dimensions of the peripheral, lateral gap filled with viscous fluid and kinematic viscosity of the silicone oil.

Henry et al. [30] introduced a procedure to assess crankshaft durability. First step of the procedure includes mesh generation, calculation of internal and external loads and torsional dynamic response due to rotation. The second step is the finite element method calculation which includes the preparation of input files for each loading condition. In the third step, boundary condition file is generated. In the final step, fatigue safety factor is determined using Dang Van fatigue criterion.

Kreuter and Pischinger [31] presented status of rules and methods for assessment of stresses in crankshafts of internal combustion engines. They analyzed the loads acting upon the crankshaft and compared the various classical calculation procedures used for durability analysis of crankshafts.

Borges et al. [32] studied stress distribution in a light automotive crankshaft crank using a geometrically restricted finite element model. They used ANSYS software for FEM analysis and a three dimensional model made of photoelastic material with the same boundary conditions to verify the results. This study was based on static load analysis and

investigated loading at a specific crank angle. The numerical results obtained showed that the overall stress distribution over the crank is uniform and the only region with high stress concentration was the crank-pin fillet.

Montazersadgh and Fatemi [33] carried out dynamic load and stress analysis of a single cylinder four stroke engine crankshaft and obtained the variation of stress magnitude at critical locations. They calculated the load acting on the crankshaft analytically and compared the results with the ones obtained by ADAMS simulation. They obtained the FE model in ABAQUS and applied the calculated loads and boundary conditions to this model. They found the critical engine speed and critical region on the crankshaft and investigated the stress variation over the engine cycle. They verified the results from FE analysis by strain gages attached to several locations on the crankshaft.

Wu and Yang [34] presented a computer programming technique of using extended transfer matrix method to the analysis of torsion-and-flexure coupled vibration of damped shafting system subjected to external excitations. The work has applications to marine propulsion systems.

Koser and Pasin [35] studied the torsional vibrations of the drive shaft of the mechanisms having variable inertia characteristics by modeling the shaft as a continuous element with distributed mass and investigated the forced response of the drive shaft. They used a system composed of an electric motor and a single mechanism.

Heath and McNamara [36] used a combination of finite element and classical analysis techniques for crankshaft stress analysis. They described the hierarchy of methods used for crankshaft stress analysis with case studies. At the highest level, they introduced a method for including load sharing effects of the flexible crankshaft within a flexible block interconnected by nonlinear oil films. This method includes the FE modeling of the complete crankshaft and consideration of its stress field throughout an engine cycle.

Priebsch et al. [37] introduced a method, which takes into account coupled torsional, bending and axial vibrations, for the design analyses of the stress and vibration of crankshafts. They considered hydrodynamic oil film and stiffness of the bearing structure

to model the main bearings. The calculation of forced vibrations is carried out using the gas and mass forces acting upon the rotating crankshaft.

Fessler and Sood [38] used models of single throws of crankshafts to find the stress distributions in some diesel engine crankshafts. They loaded the crankshafts by free and restrained torsion, radial and tangential forces and bending moments, and by axial tension. They obtained stress distributions in the fillets by frozen stress photoelasticity. They also measured some peak stresses with strain gauges and expressed the results as multiples of convenient nominal stresses.

Bickley et al. [39, 40] investigated the stresses and deformations in overlapped diesel engine crankshafts using single-throw, epoxy resin models loaded in pure torsion or bending. They considered the bending loads due to radial or tangential components of the connecting rod force and those due to pure radial bending or radial bending due to journal displacement. They measured the deformations and stresses in the crankpin and journal fillets after the photoelastic frozen-stress cycle. They obtained the greatest principle stress at each angular position around the journal and crankpin fillets. They expressed the results as stress concentration factors based on nominal stresses in a bar of same diameter as the crankpin.

Fessler et al. [41] investigated the effect of regrinding bearing surfaces on stresses in overlapped crankshafts. They carried out strain-gauged model tests and finite element calculations for simply supported, single-crank throws out for four shapes: the standard design, reduced crankpin only, reduced journal only and both bearing surface diameters reduced by 5 percent. They applied radial loading of the crankpin, pure radial bending and pure torsion separately. They normalized the stresses with respect to the nominal bending stress in the neck between crankpin and journal fillets. They found that resulting stress concentration factors were reduced by regrinding.

In a three part study, Warrior et al. [42-44] studied the design of overlapped crankshafts. In the first part [42], they determined the surface stress distributions of crankpin fillets under radial bending and pure torsion using FE program, ABAQUS. They used two dimensional (plane stain) and three dimensional elements to mesh the crankshaft.

They compared the stress concentration factors with symmetrically notched and shouldered bars in pure bending. In the second part [43], they investigated the effects of crank web shape on the peak stresses in crankpin and main journal fillets using the boundary element software, BEASY. They found that under radial bending and torsion, increasing the web thickness or increasing the overlap reduces the peak fillet stresses and stiffens the crankshaft. They presented empirical equations for the maximum stresses for bending, torsion and twist. In the third part [44], they analyzed the effects of different holes in the crankpin and journal fillet stress distributions using boundary element technique. They found that significant reductions in journal fillet peak stresses can be achieved under radial bending, but crankpin fillet maxima are slightly increased. Under torsion, there is a change in fillet stress distribution, but little variation in stress concentration factors. Under both load cases, the stiffness of the crankshaft is slightly reduced.

Filipi and Assanis [45] developed a nonlinear, transient, single-cylinder diesel engine simulation for predictions of instantaneous engine speed and torque. They determined the instantaneous crankshaft speed from the solution of the engine external load dynamics equation, where the engine torque is tracked on a crank-angle basis. They showed that selecting the proper value of the engine moment of inertia is important in order to control the amplitude of angular velocity fluctuations and ensure stable engine operation. They also showed that the variation in the inertial forces on the reciprocating components with speed has an important effect on the instantaneous torque profile and consequently on angular velocity fluctuations.

Taraza et al. [46] determined the gas-pressure torque of a multicylinder engine from measurements of the crankshaft's speed variation under steady state operation. They obtained the harmonic components of the crankshaft's speed by a Discrete Fourier Transform. They correlated the harmonic components of the speed variation to corresponding components of the engine torque sing a lumped mass model of the shafting and calculated the indicated mean effective pressure.

Taraza et al. [47] presented a friction model of a diesel engine that accounts for the individual contributions of the main components of the mechanical losses and the influence of specific design and operating parameters on the mechanical losses. The main

components considered in the model are the piston-ring assembly, the valve train, the bearings and auxiliaries.

Stanley and Taraza [48] obtained maximum and average main bearing loads of four and six cylinder symmetric in-line engines using rigid crankshaft model and estimated ideal counterweight mass that will result in acceptable maximum bearing load. They developed relationships for rapid determination of main bearing loads using geometric parameters and operating conditions of the engine.

Lu et al. [49] studied the free and forced bending vibrations of four-cylinder and six cylinder direct-injection diesel engine crankshaft systems using distributed continuous models. They obtained the general frequency equation and mode shapes for the bending vibration of the crankshaft under operating conditions using the transfer matrix method. They compared the bending vibration amplitudes at crankshaft front free end with experimental ones.

Aminudin et al. [50] analyzed the dynamic behavior of an in-line four-cylinder engine crankshaft under firing conditions assuming that pin and web parts of the crankshaft have a uniform cross-section in order to simplify the modal analysis. They used root mean square values to calculate the energy at each bearing journal.

1.3. Motivation and Objectives of the Study

In an internal combustion engine, the crankshaft is connected to other engine components such as flywheel, damper and pulley, and therefore the system must be considered together as a whole. In the literature survey given above, there is a lack of study on such experimental and numerical analyses. Either the researchers analyzed effect of each component of the crankshaft system individually or made some simplifying assumptions for their effects on the crankshaft dynamics that lead to some error in the results when compared to experimental ones. Some others used simplified analytical techniques which again cannot completely describe the crankshaft dynamics.

For example, in some studies, the inertial effects of the flywheel and other parts in the system are not included. Some studies considered only the effect of torsional vibration of the crankshaft. In many cases, the most effective vibrations are the ones linked to modes which are essentially torsional. However it must be remembered that the assumption of uncoupling can be a rough approximation. Axial, torsional and lateral vibrations, which induce vibration stresses, occur simultaneously in crankshafts of multi cylinder engines. The crankshaft of a multi-cylinder engine has a phase difference between the adjacent crank throw planes, and axial, torsional and lateral vibrations are all coupled. Another problem in the dynamic analysis of engine crankshafts is the implementation of boundary conditions and in some studies effect of hydrodynamic oil film pressure in the bearings is neglected.

Classical crankshaft analyses make some approximations and use a number of tabulated empirical formulas that limit their precision. The connecting rod is usually represented by a lumped mass system because it is stiffer than the crankshaft. The lower end of the connecting rod is attached to the crankpin. Whereas the inertial forces associated with the reciprocating upper end of the connecting rod along with the piston mass, are lumped with the equivalent gas force. Crankshaft is assumed to be a rigid structure and analyses are based on each single crank throw. No bending vibration effect is considered and this can lead to considerable errors for crankshaft systems with heavy flywheels. Bearings are considered as only constraining parts and hydrodynamic oil film pressure in the bearings are not considered. Therefore an extensive study is still needed to compensate for the inadequacy of the dynamic analysis of the crankshaft system.

The improvements in the level of computing power and capabilities resulted in great advances in many technological fields. With the help of current computers and codes, large scale mechanical models can be analyzed in more effective and reliable ways. One research area which benefited considerably from these advances is the area of engine dynamics and vibrations. Among others FEM and MSS programs are powerful tools and are capable of providing a systematic procedure for direct dynamic stress and vibration analysis of crankshafts which otherwise cannot be accurately studied with existing analytical methods.

Finite element analyses are generally based on quasistatic computations which means, for each time step a large number of data is needed concerning the corresponding load and boundary conditions. This is not practical, if number of degrees of freedom of the analyzed structure is too large. Moreover, in quasistatic simulations, no vibration effects are considered that can lead to considerable errors if the analyzed system is a complex one like a cranktrain and vibration effects have major role on the system. With MSS programs, it's possible to describe dynamic interactions between system components and to include the nonlinear effects. Flexibility of the cranktrain components can also be included into the analyses using finite elements. As a result, using finite elements and multibody dynamics packages simultaneously, dynamic modeling of the flexible component can be done. ADAMS/Engine is such an environment where interaction of crankshaft system components with each other can easily be defined and crankshaft flexibility can be included into the analyses using a separate FE program. Using a finite element program large number of degree of freedoms of a flexible structure may be considerably reduced and used in the dynamic analysis.

In this study, dynamic analysis of the crankshaft system of an inline 6-cylinder diesel engine is carried out using finite element and multibody dynamics considering the flexibility of the crankshaft and effect of crankshaft system components. Coupled axial, bending and torsional vibrations of the crankshaft system are taken into account. Effect of each part of the crankshaft system on the crankshaft dynamic stress and vibration characteristics are determined. For the numerical analysis of the crankshaft system, Msc.Nastran and Msc.Adams (Automatic Dynamic Analysis of Mechanical Systems) software programs are used.

With this study, a general procedure is obtained for the dynamic stress and vibration analyses of crankshaft system of internal combustion engines, and for the determination of effects of different crankshaft system components on dynamic stress and vibration characteristics of the crankshaft. The deficiencies associated with classical crankshaft analyses are eliminated.

1.4. Problem Statement

In this study all analyses are carried out for two types of in-line six cylinder heavy duty diesel engines: 7.3 L and 9.0 L. The data for these engines are given in Table 1.1. Cylinder pressure curves for 7.3 L and 9.0 L engines at different engine speeds under full load are given in Figures 1.3 and 1.4. The simulations are carried out at these engine speeds.

The crankshaft system of these engines consists of various parts such as crankshaft, piston, connecting rod, flywheel, torsional vibration (TV) damper, crankshaft front and rear gears and pulley. A schematic representation of the 7.3 L diesel engine crankshaft system is given in Figure 1.5.

Table 1.1. Engine data for 7.3 L and 9.0 L engines

	Unit	**7.3 L Engine**	**9.0 L Engine**
Combustion System	-	Diesel	Diesel
Configuration	-	6 cylinder	6 cylinder
Cylinder Arrangement	-	in-line	in-line
Bore Diameter	mm	112	115
Stroke	mm	124	144
Axial Cylinder Distance	mm	134	134
Peak Firing Pressure	MPa	18	19
Rated Power at speed	kW/rpm	221/2400	295/2200
Max. Torque at speed	Nm/rpm	1100/1200	1600/1200-1700
Crankshaft Type	-	Forged with 8 integral counterweights	Forged with 8 integral counterweights
Main Journal Diameter	mm	88	95
Pin Diameter	mm	77	81
Firing Order	-	1-5-3-6-2-4	1-5-3-6-2-4

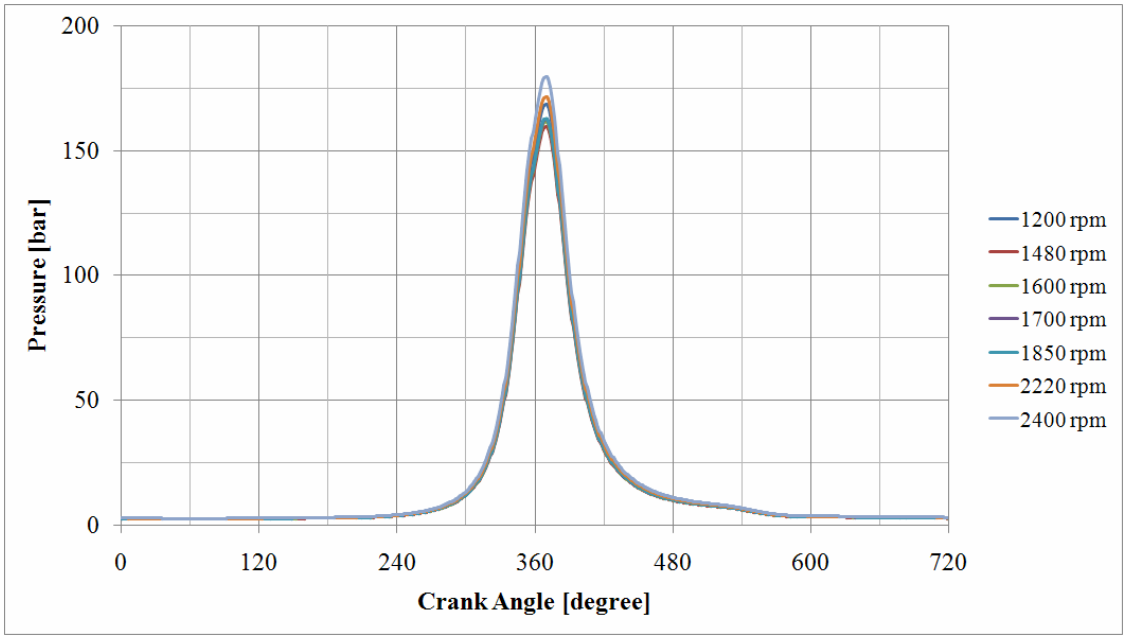

Figure 1.3. Gas pressure values at different engine speeds for the 7.3 L engine

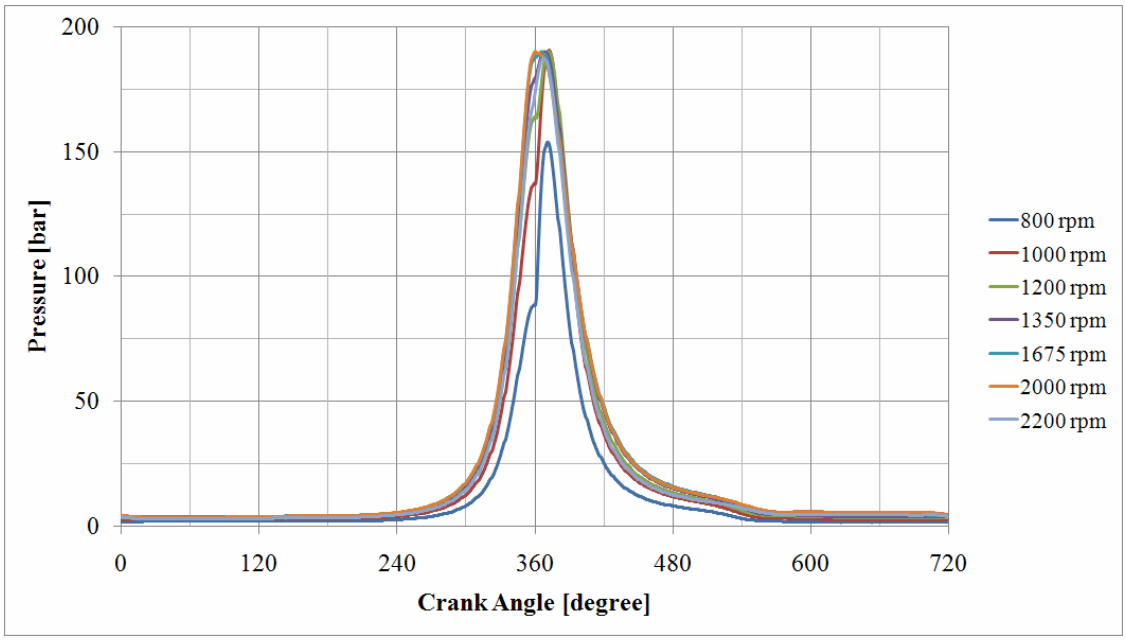

Figure 1.4. Gas pressure values at different engine speeds for the 9.0 L engine

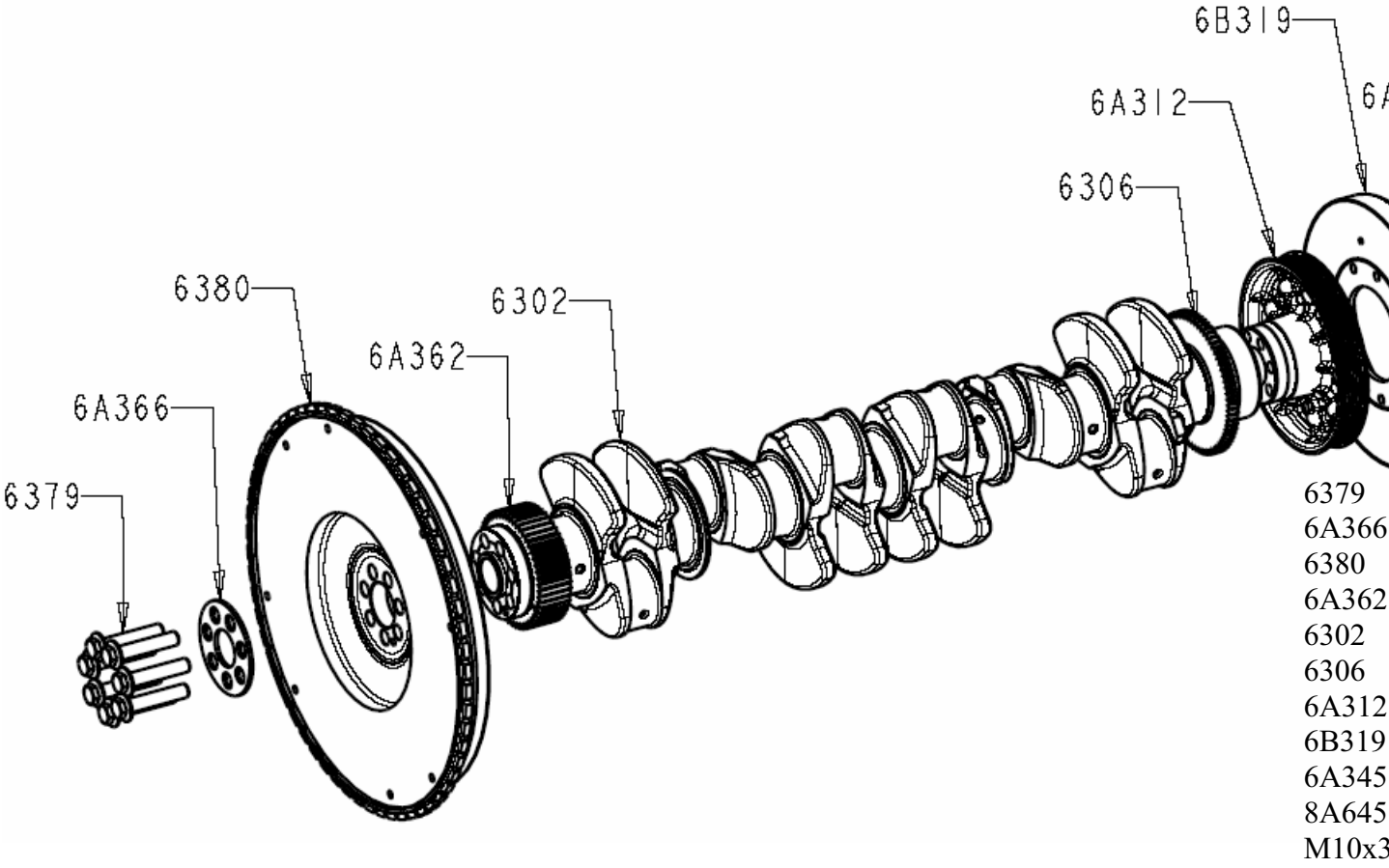

Figure 1.5. Geometry of the 7.3L engine crankshaft system [51]

The forces on the system are generated by pressure inside the cylinder and inertia of rotating and reciprocating components. The piston-connecting rod and crankshaft mechanism transform the linear motion of the piston to rotational motion of the crankshaft. Cylinder pressure force and inertial forces of the piston and connecting rod are transmitted to crank pin by this mechanism. Detailed geometries of the piston, connecting rod and crankshaft of the 7.3 L engine are shown in Figures 1.6-1.8, respectively.

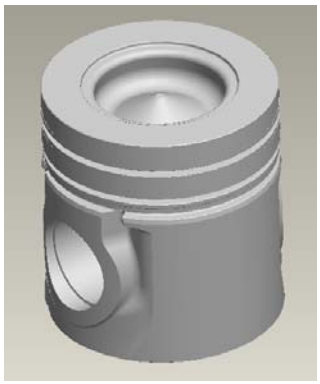

Figure 1.6. Piston of the 7.3 L engine [51]

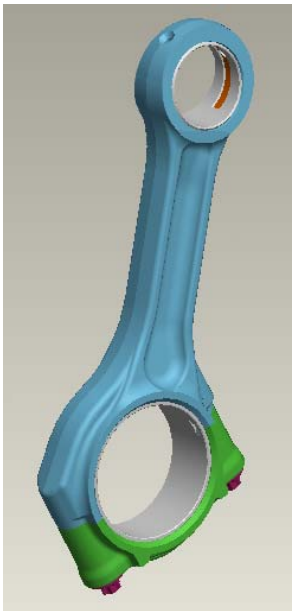

Figure 1.7. Connecting rod of the 7.3 L engine [51]

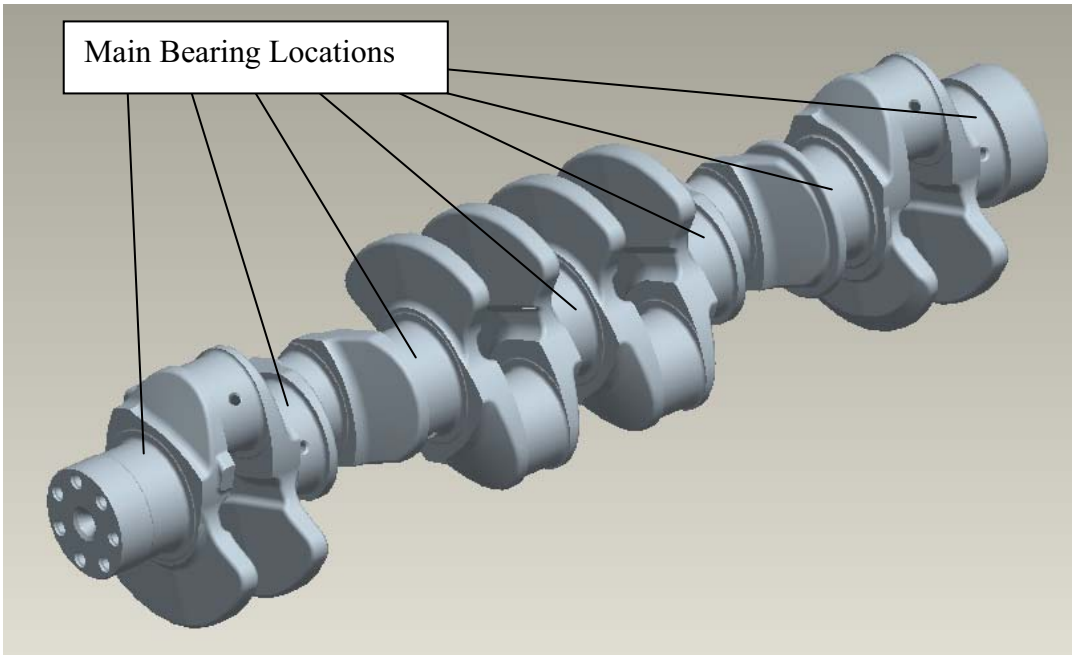

Figure 1.8. Crankshaft of the 7.3 L engine [51]

The crankshaft is supported by the cylinder block at main bearing locations. The radial component of the transmitted force tries to bend the crankshaft, whereas the tangential force component rotates the crankshaft. These forces are not constant during engine cycle. Typical variation of these forces in an engine cycle for a single cylinder is shown in Figure 1.9. The variation of these forces causes the bending and torsional vibrations of the crankshaft. Depending on the variation of tangential force component at the crankpin, the torque from the cylinder oscillates. So, a torsional vibration (TV) damper is connected to front end of the crankshaft to dampen the speed fluctuations and to reduce torsional vibration amplitudes and torsional stresses of the crankshaft. The geometry of the TV damper of 7.3 L engine is shown in Figure 1.10. A flywheel is connected to the other end of the crankshaft. The flywheel has a high moment of inertia in order to smooth the torque which is transmitted to the drive line. So, the flywheel is used for smoother operation of the engine. The flywheel of the 7.3 L engine is shown in Figure 1.11.

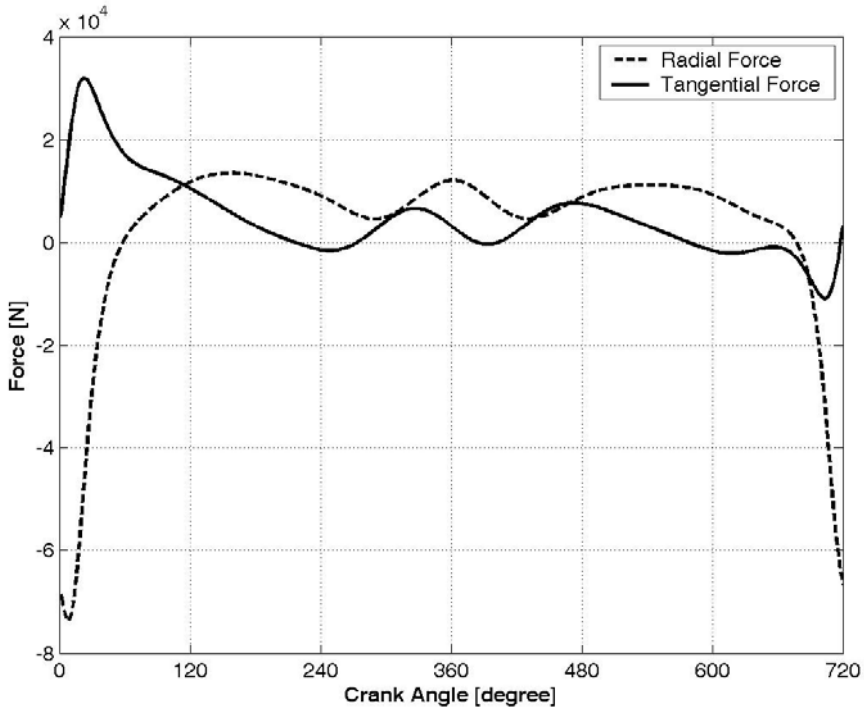

Figure 1.9. Typical variation of radial and tangential force components acting on crankpin during one engine cycle

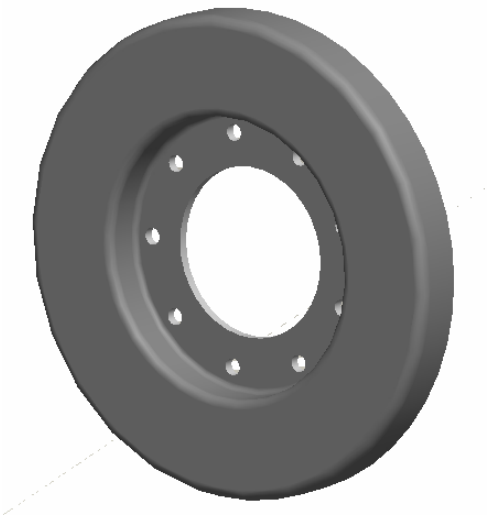

Figure 1.10. TV damper of the 7.3 L engine [51]

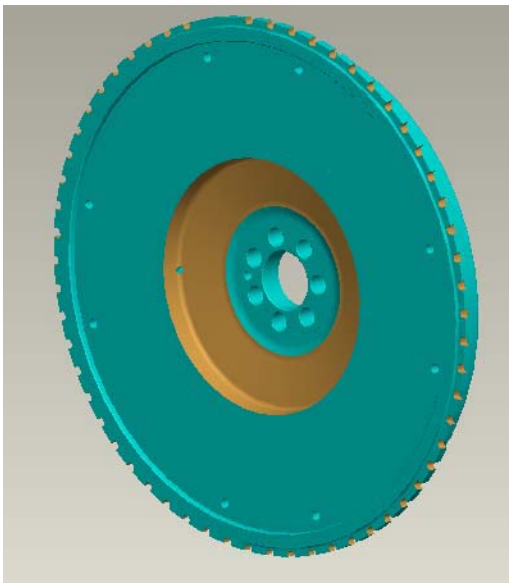

Figure 1.11. Flywheel of the 7.3 L engine [51]

Pulley and gears are used to transmit motion to accessories like water pump, fuel pump, air compressor, power steering pump, alternator and camshaft. Detailed geometry of the pulley of the 7.3 L engine is given in Figure 1.12.

Figure 1.12. Pulley of the 7.3 L engine [51]

1.5. Thesis Outline

This thesis consists of six main chapters. The first chapter is the introduction and it consists of basic concepts related to reciprocating internal combustion engines, a summary of previous research work relevant to the work presented in this thesis, background and motivation behind this work. It presents the problem statement and main objectives of this study at the end of the chapter.

The second chapter presents free and forced torsional vibration analysis of the crankshaft system. First the excitation torque on the system is determined. Then the dynamic model of the crankshaft system is constructed using lumped masses that are positioned at the crankshaft front and rear end as well as at the centers of the cylinders. Natural frequencies, vibration amplitudes at the crankshaft front end, and torsional stresses at each section of the crankshaft are calculated for two different equivalent systems, with and without a TV damper. Torsional vibration amplitude results are compared to experimental ones. Finally, effect of stiffness, damping coefficient, ring inertia and hub inertia change of the TV damper on natural frequencies and torsional vibration amplitudes at the crankshaft front end are investigated, and effect of cylinder misfire on forced torsional vibration of the crankshaft system is discussed.

The third chapter introduces traditional methods that are used for crankshaft force and stress analysis. Main bearing forces are calculated using a rigid crankshaft model and statically determinate system and considering gas pressure and inertial forces. Nominal stresses due to bending moments and radial forces are calculated. Using stress concentration factors and nominal stresses obtained for bending and torsion, local stresses in the fillet regions are determined. Combined stresses are determined according to the energy of distortion theory.

The fourth chapter presents an advanced method for dynamic analysis of crankshaft system using MSC.NASTRAN and ADAMS. In this chapter, details of modeling crankshaft system in ADAMS environment are introduced first. Then, dynamic analysis of the crankshaft system, which represents the calculation of forces, displacements and

stresses on the crankshaft over a complete engine cycle (two revolutions of the crankshaft) under steady state conditions, is performed taking coupled axial, torsional and bending vibrations into consideration. Effects of crankshaft system components on the stress and vibration characteristics of the crankshaft are also investigated.

The fifth chapter is devoted to counterweight configuration analysis. Effect of counterweight mass and position on main bearing loads and crankshaft bending stresses are investigated for different counterweight configurations. A comparison of different crankshaft models (e.g. rigid, beam and flexible) is also done in this chapter from main bearing load point of view.

The sixth chapter summarizes the findings from the work done in this research and presents the general recommendations for future work developments that can be incorporated.

2. CRANSHAFT TORSIONAL VIBRATION ANALYSIS

2.1. Introduction

Torsional vibration is generated in crankshafts of internal combustion engines as a result of the following factors:

- Motion of piston and connecting rod masses generate alternating torques often referred to as “inertia” torques,
- Following the explosion of the charge, a torque pulse is applied to the crankshaft throw. The resulting periodic excitation causes the engine angular velocity to fluctuate in both rigid body and flexible modes,
- Engines with several cylinders have flexible crankshafts due to their long length.

If torsional vibration is not controlled, it can result in crankshaft failure or failure of any accessories that are driven by the crankshaft, typically at the front end of the engine because the inertia of the flywheel reduces the fluctuation at the rear end of the engine. This potentially damaging vibration, especially in diesel engines, can be controlled by a torsional vibration damper that is located at the front end of the crankshaft.

The purpose of standard engine torsional vibration analysis is to use knowledge of the system forcing function, system boundary conditions, and system dynamics to predict the dynamic torsional response of the engine and powertrain. For evaluation of the torsional vibration behavior of a crankshaft system, lumped mass model is generally used, and torsional vibration angle amplitudes and torsional stresses are calculated at each node of the system. In particular, the calculation of torsional vibration amplitudes at front or rear ends is important because they can be compared to experimental results thus gives a tool for validating the lumped mass system model.

The basic forcing function for an engine is the torque applied at each crankshaft pin. The applied torque is a combination of torque resulting from the cylinder pressure applied to the top of the piston (gas pressure torque) and the torque required to accelerate the

reciprocating mass of the piston and connecting rod (inertia torque). The applied torque for each cylinder varies as a function of crankshaft angle over an engine cycle. For a four stroke engine, one engine cycle corresponds to two complete revolutions of the crankshaft. Therefore, fundamental frequency of the excitation and response is one half engine speed or ½ order. The applied torque at each cylinder contains significant energy for the first 24 harmonics of the fundamental engine cycle speed (½ to 12^{th} engine orders). The order content of the applied torque can be found by using a Fourier series expansion of the applied torque for exactly one engine cycle. The derivation of the order domain excitation torque is presented in Section 2.2.

A lumped mass model is used in classical torsional vibration analysis to represent the torsional dynamics of the crankshaft and powertrain over the frequency range of interest. A schematic view of a typical lumped mass model is shown in Figure 2.1. The dynamic model of the cranktrain consists of lumped masses corresponding to each cylinder throw and other parts of the system (flywheel, pulleys, couplings, etc.) connected by ideal springs. On each mass and between successive masses, friction torques act and they are represented as dampers. These are absolute damping acting on masses at cylinder locations due to friction between piston and liner, and relative damping between each mass because of the presence of oil film in main bearings of the crankshaft.

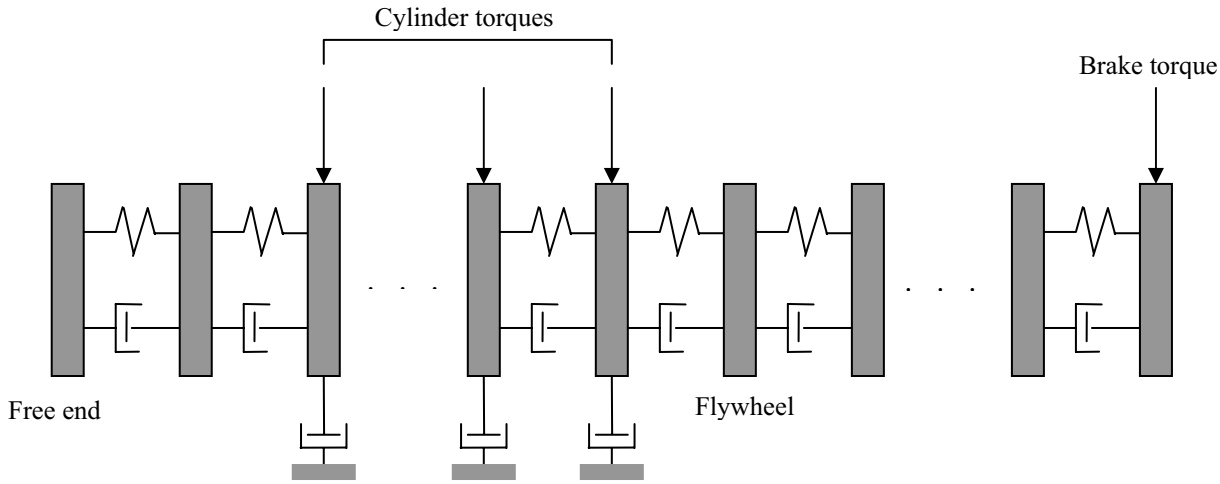

Figure 2.1. Lumped mass model of a crankshaft system

2.2. Excitation Torque

The excitation torque on the crankshaft consists of cylinder pressure torque, piston and connecting rod reciprocating inertia torque, brake torque, and torques from connecting gears and pulley. Gears and pulley are used to drive the valve train, the oil pump, the fuel pump and other accessories. The excitation torques from accessories are usually neglected as they are much smaller compared to the cylinder pressure torque and the reciprocating inertia torque. The brake torque fluctuation could be large if a relatively stiff coupling is used to connect the crankshaft to the external loading. When a softer clutch is used, the brake torque fluctuation is usually small and the torque can be assumed to be constant. So the applied load only has energy for the zero frequency and is zero for all other frequencies.

The torque applied at the crankshaft pin is not readily available. This torque is calculated using a known or assumed cylinder pressure curve and geometry of piston-connecting rod mechanism (see Figure 1.1). This model is used to relate a known cylinder pressure curve and known slider crank parameters to the applied torque at the crankshaft pin.

The equation for the applied excitation torque at the crankshaft throw is derived using the following assumptions:

- The connecting rod is rigid,
- The connecting rod consists of two concentrated masses: one at the piston side and the other at the crank side. So the mass at the piston side reciprocates with the piston and the other mass rotates with the crankshaft.
- The crankshaft rotates at constant angular velocity, ω.

The tangential force F_T acting on the crankpin due to gas pressure and reciprocating mass is:

$$F_T = \left(F_p + F_r\right) \cdot \frac{\sin\left(\theta + \beta\right)}{\cos\beta} \tag{2.1}$$

where F_p is the gas pressure force and F_r is the inertia force due to the acceleration of the piston and the reciprocating portion of the connecting rod. That is:

$$F_p = \frac{\pi \cdot D^2}{4} \cdot \left[P_{cyl}\left(\theta\right) - P_{cc}\left(\theta\right)\right] = \frac{\pi \cdot D^2}{4} \cdot P\left(\theta\right) \tag{2.2}$$

$$F_r = -\left(m_p + m_{cr\_tr}\right) \cdot \ddot{s} = -m_{rec} \cdot \ddot{s} \tag{2.3}$$

where $P_{cyl}\left(\theta\right)$ and $P_{cc}\left(\theta\right)$ are the pressures inside the cylinder and crank case, respectively. D is the bore diameter of the cylinder. m_p and m_{cr_tr} are piston mass and reciprocating portion of the connecting rod mass, respectively.

By convention F_T is considered positive when it turns the crank in the same direction as ω. This force produces the torque which acts on the crank.

$$T = r \cdot F_T \tag{2.4}$$

So the excitation torque can be analyzed in two parts: cylinder pressure torque and reciprocating inertia torque.

2.2.1. Cylinder Pressure Torque

Contribution of the gas pressure force to the engine torque is

$$T_p\left(\theta\right) = r \cdot \frac{\pi \cdot D^2}{4} \cdot P\left(\theta\right) \cdot \frac{\sin\left(\theta + \beta\right)}{\cos\beta} = r \cdot \frac{\pi \cdot D^2}{4} \cdot P\left(\theta\right) \cdot \left(\sin\theta + \frac{r \cdot \sin\theta \cdot \cos\theta}{\sqrt{l^2 - r^2 \cdot \sin^2\theta}}\right). \tag{2.5}$$

Because T_p is a periodic function of θ with a period of 4π, it can be expressed by the following Fourier series:

$$T_p(\theta) = A_{p_0} + \sum_{k=0.5,1.0,1.5,\ldots} \left[A_{p_k} \cdot \cos\left(k \cdot \theta\right) + B_{p_k} \cdot \sin\left(k \cdot \theta\right) \right] \tag{2.6}$$

where

$$A_{p_0} = \frac{1}{4\pi} \int_0^{4\pi} T_p\left(\theta\right) \cdot d\theta$$

$$A_{p_k} = \frac{1}{2\pi} \int_0^{4\pi} T_p\left(\theta\right) \cdot \cos\left(k \cdot \theta\right) \cdot d\theta$$

$$B_{p_k} = \frac{1}{2\pi} \int_0^{4\pi} T_p\left(\theta\right) \cdot \sin\left(k \cdot \theta\right) \cdot d\theta$$

Usually the gas pressure torque is represented quite accurately by considering harmonics up to k = 12. Due to half orders, 24 distinct harmonic orders must be considered for four stroke engines [46].

2.2.2. Reciprocating Inertia Torque

Torque from reciprocating inertia force is

$$T_r\left(\theta\right) = -r \cdot m_{rec} \cdot \ddot{s} \cdot \left(\sin\theta + \frac{r \cdot \sin\theta \cdot \cos\theta}{\sqrt{l^2 - r^2 \cdot \sin^2\theta}} \right). \tag{2.7}$$

In equation (2.7), $\ddot{s}$ is the piston acceleration, and it is given in equation (1.14). Substituting equation (1.14) in (2.7) and using trigonometric relations, T_r can be expressed in series form as

$$T_r\left(\theta\right) = m_{rec} \cdot \left(r \cdot \omega\right)^2 \cdot \sum_{k=1,2,3,\ldots} B_{r_k} \cdot \sin\left(k \cdot \theta\right) \tag{2.8}$$

Coefficients B_{r_k} are rapidly decreasing to very small values with increasing harmonic order so only the first six harmonic coefficients have some significance. Values for the coefficients of the first six harmonic components are given in Table 2.1.

The total excitation torque on the crankshaft can be obtained by adding the reciprocating inertia torque and the gas pressure torque from equations (2.6) and (2.8):

$$T(\theta) = T_p(\theta) + T_r(\theta) = A_0 + \sum_{k=0.5,1.0,1.5,\ldots} \left[A_k \cdot \cos(k \cdot \theta) + B_k \cdot \sin(k \cdot \theta) \right]. \qquad (2.9)$$

As an example, variation of the total excitation torque with 720^o crank rotation is shown in Figure 2.2 for 9.0 L diesel engine at 2200 rpm.

Table 2.1. Inertia torque harmonic coefficients for the first six harmonics

Harmonic order, k	Trigonometric function	Harmonic coefficient
1	$\sin\theta$	$\frac{1}{4}\cdot\left(\frac{r}{l}\right)+\frac{1}{16}\cdot\left(\frac{r}{l}\right)^3+\frac{15}{512}\cdot\left(\frac{r}{l}\right)^5$
2	$\sin 2\theta$	$-\frac{1}{2}-\frac{1}{32}\cdot\left(\frac{r}{l}\right)^4-\frac{1}{32}\cdot\left(\frac{r}{l}\right)^6$
3	$\sin 3\theta$	$-\frac{3}{4}\cdot\left(\frac{r}{l}\right)-\frac{9}{32}\cdot\left(\frac{r}{l}\right)^3-\frac{81}{512}\cdot\left(\frac{r}{l}\right)^5$
4	$\sin 4\theta$	$-\frac{1}{4}\cdot\left(\frac{r}{l}\right)^2-\frac{1}{8}\cdot\left(\frac{r}{l}\right)^4-\frac{1}{16}\cdot\left(\frac{r}{l}\right)^6$
5	$\sin 5\theta$	$\frac{5}{32}\cdot\left(\frac{r}{l}\right)^3+\frac{75}{512}\cdot\left(\frac{r}{l}\right)^5$
6	$\sin 6\theta$	$\frac{3}{32}\cdot\left(\frac{r}{l}\right)^4+\frac{3}{32}\cdot\left(\frac{r}{l}\right)^6$

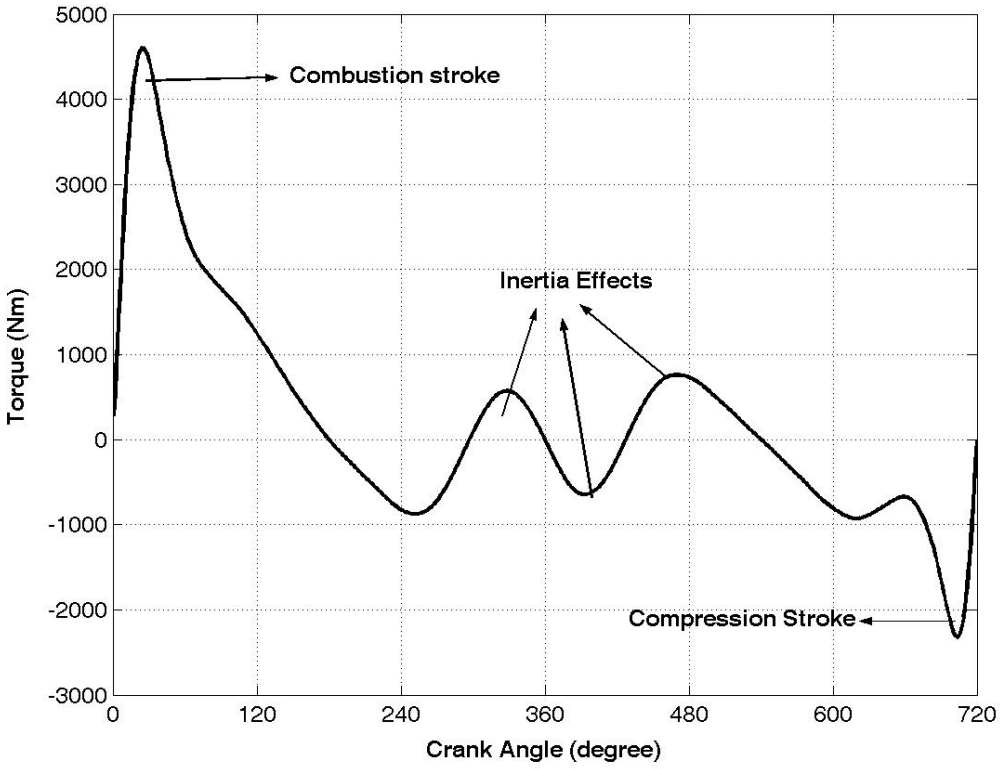

Figure 2.2. Total excitation torque variation with crank angle, $T(\theta) = T_p(\theta) + T_r(\theta)$

2.3. Dynamic Model of the Crankshaft System

The lumped mass model is used to simulate torsional vibration of 7.3 L and 9.0 L six cylinder diesel engines crankshaft systems. The schematic representation of a typical six cylinder engine crankshaft system is shown in Figure 2.3. In this model, a number of concentrated masses are positioned at the crankshaft front and rear ends as well as at the centers of the cylinders. The inertia, stiffness and damping values for the crankshaft systems of 7.3L and 9.0L engines are given in Tables 2.2 and 2.3. The polar moment of inertia of an individual cylinder is calculated as total of the inertias of one main journal, two adjacent crank webs, one crank pin and equivalent inertias of the piston and connecting rod. Each cylinder inertia is denoted as J_i where i denotes the number of cylinder (i = 1, 2, 3,…,6). All crankshaft inertias are calculated using three dimensional

drawings in ProEngineer. The crankshaft front end inertia includes the pulley inertia, J_p and the damper housing inertia, J_h. Inertia of the damper ring is denoted as J_r. The crankshaft rear end inertia is based on data of clutch given by the supplier and on 3-dimensional CAD data of the flywheel and denoted as J_{fw}. These masses are connected to each other by massless shafts of torsional stiffnesses, $K_1, K_2, ..., K_7$. The stiffness of the equivalent shaft sections are calculated using finite elements. Bearing and piston-ring frictions are assumed to be locally linear, viscous and acting on individual cylinder inertias. They are denoted as C_1, C_2, C_3, C_4, C_5 and C_6. In addition to these damping values, an absolute damping, C_p, is applied on the crankshaft front end for the belt drive system. Reciprocating and rotating masses of the connecting rods as well as other cranktrain parameters for these engines are given in Table 2.4.

A standard viscous damper with an outer diameter of 310 mm and a width of 32 mm is used for 7.3L engine with the following main specifications:

Total weight	: 11.80 kg (Hub mass=4.94 kg, Ring mass=6.86 kg)
Inertia of the ring	: 0.127 kgm^2
Inertia of the housing	: 0.056 kgm^2
Viscosity of the silicon oil	: 0.50 m^2/s at 80 ^{o}C
Torsional stiffness	: 125000 Nm/rad
Relative damping coefficient	: 95 Nms/rad

In 9.0 L engine, the same TV damper is used but with fan blades for increased heat radiation. The silicon oil viscosity and related to this parameter torsional stiffness and damping coefficients for this TV damper are also different.

Viscosity of the silicon oil	: 0.15 m^2/s at 80 ^{o}C
Torsional stiffness	: 69500 Nm/rad
Relative damping	: 73.67 Nms/rad

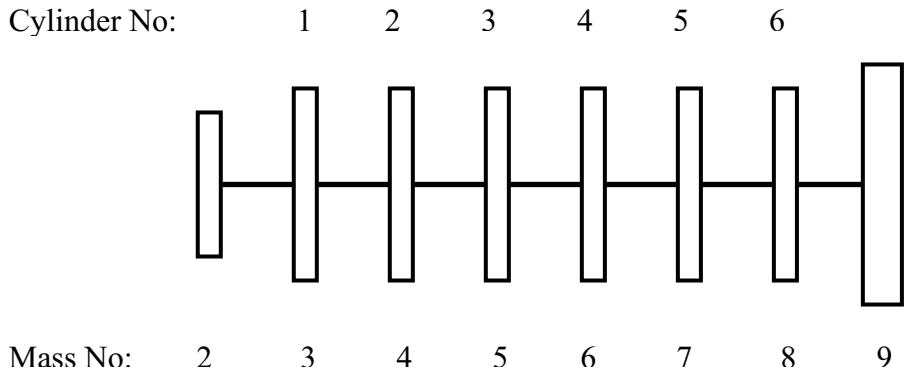

Figure 2.3. Torsional vibration equivalent system of six cylinder engine without damper

Table 2.2. Inertia, stiffness and damping values for the crankshaft system of 7.3L engine

Mass No	Designation	Moment of inertia (kgm^2)	Stiffness (10^6 Nm/rad)	Absolute Damping (Nms/rad)
2	Crankshaft front end (w/o damper)	0.0350	1.54	2.8
3	Cylinder No. 1	0.0545	1.78	5.7
4	Cylinder No. 2	0.0335	1.78	5.7
5	Cylinder No. 3	0.0545	1.78	5.7
6	Cylinder No. 4	0.0545	1.78	5.7
7	Cylinder No. 5	0.0335	1.78	5.7
8	Cylinder No. 6	0.0545	2.38	5.7
9	Flywheel and clutch	2.1200		

Table 2.3. Inertia, stiffness and damping values for the crankshaft system of 9.0L engine

Mass No	Designation	Moment of inertia (kgm^2)	Stiffness (10^6 Nm/rad)	Absolute Damping (Nms/rad)
2	Crankshaft front end (w/o damper)	0.0350	3.26	4.10
3	Cylinder No. 1	0.0627	2.27	8.19
4	Cylinder No. 2	0.0429	2.27	8.19
5	Cylinder No. 3	0.0627	2.27	8.19
6	Cylinder No. 4	0.0627	2.27	8.19
7	Cylinder No. 5	0.0429	2.27	8.19
8	Cylinder No. 6	0.0627	3.50	8.19
9	Flywheel and clutch	2.8000		

Table 2.4. Crank train parameters for the 7.3 L and 9.0 L engine crankshaft systems

	Unit	7.3 L engine	9.0 L engine
Crank radius	mm	62	72
Connecting rod length	mm	222	239
Cylinder spacing	mm	134	134
Mass of complete piston	kg	2.79	3.42
Connecting rod reciprocating mass	kg	0.77	0.92
Reciprocating mass (total per cylinder)	kg	3.55	4.32
Connecting rod rotating mass	kg	1.89	2.01

For the silicon oil filling the space between the damper housing and ring, the following complex viscous damping coefficient representation is used [52], [53]:

$$C_d^{\ *} = C_d - j\frac{K_d}{\omega} \tag{2.10}$$

Input torques to the system are cylinder pressure torques, piston and connecting rod reciprocating inertia torques, and load torque. The excitation torques from accessories are usually neglected as they are small compared to cylinder pressure torque and reciprocating inertia torque. These torques are represented as $T_{p1}, T_{p2}, ..., T_{p6}, T_{r1}, T_{r2}, ..., T_{r6}$ and T_L respectively. The equations of motion for the rigid disks are given with the following equations:

$$\left.\begin{aligned}
&J_r \cdot \ddot{\theta}_r + C_d^{\ *} \cdot \left(\dot{\theta}_r - \dot{\theta}_p\right) = 0 \\
&\left(J_h + J_p\right) \cdot \ddot{\theta}_p + C_d^{\ *} \cdot \left(\dot{\theta}_p - \dot{\theta}_r\right) + C_p \cdot \dot{\theta}_p + K_1 \cdot \left(\theta_p - \theta_1\right) = 0 \\
&J_1 \cdot \ddot{\theta}_1 + C_1 \cdot \dot{\theta}_1 + K_1 \cdot \left(\theta_1 - \theta_p\right) + K_2 \cdot \left(\theta_1 - \theta_2\right) = T_{p1} + T_{r1} \\
&J_2 \cdot \ddot{\theta}_2 + C_2 \cdot \dot{\theta}_2 + K_2 \cdot \left(\theta_2 - \theta_1\right) + K_3 \cdot \left(\theta_2 - \theta_3\right) = T_{p2} + T_{r2} \\
&J_3 \cdot \ddot{\theta}_3 + C_3 \cdot \dot{\theta}_3 + K_3 \cdot \left(\theta_3 - \theta_2\right) + K_4 \cdot \left(\theta_3 - \theta_4\right) = T_{p3} + T_{r3} \\
&J_4 \cdot \ddot{\theta}_4 + C_4 \cdot \dot{\theta}_4 + K_4 \cdot \left(\theta_4 - \theta_3\right) + K_5 \cdot \left(\theta_4 - \theta_5\right) = T_{p4} + T_{r4} \\
&J_5 \cdot \ddot{\theta}_5 + C_5 \cdot \dot{\theta}_5 + K_5 \cdot \left(\theta_5 - \theta_4\right) + K_5 \cdot \left(\theta_5 - \theta_6\right) = T_{p5} + T_{r5} \\
&J_6 \cdot \ddot{\theta}_6 + C_6 \cdot \dot{\theta}_6 + K_6 \cdot \left(\theta_6 - \theta_5\right) + K_7 \cdot \left(\theta_6 - \theta_{fw}\right) = T_{p6} + T_{r6} \\
&J_{fw} \cdot \ddot{\theta}_{fw} + K_7 \cdot \left(\theta_{fw} - \theta_6\right) = T_L
\end{aligned}\right\} \tag{2.11}$$

where $\theta_r, \theta_p, \theta_1, ..., \theta_6, \theta_{fw}$ are the angular displacements of the TV damper ring, pulley, each cylinder and flywheel masses, respectively.

2.4. Natural Frequencies

Natural frequencies of the torsional vibration system are determined by solving the following differential equations:

$$\left.\begin{aligned}
&J_r \cdot \ddot{\theta}_r + K_d \cdot \left(\theta_r - \theta_p\right) = 0 \\
&\left(J_h + J_p\right) \cdot \ddot{\theta}_p + K_d \cdot \left(\theta_p - \theta_r\right) + K_1 \cdot \left(\theta_p - \theta_1\right) = 0 \\
&J_1 \cdot \ddot{\theta}_1 + K_1 \cdot \left(\theta_1 - \theta_p\right) + K_2 \cdot \left(\theta_1 - \theta_2\right) = 0 \\
&J_2 \cdot \ddot{\theta}_2 + K_2 \cdot \left(\theta_2 - \theta_1\right) + K_3 \cdot \left(\theta_2 - \theta_3\right) = 0 \\
&J_3 \cdot \ddot{\theta}_3 + K_3 \cdot \left(\theta_3 - \theta_2\right) + K_4 \cdot \left(\theta_3 - \theta_4\right) = 0 \\
&J_4 \cdot \ddot{\theta}_4 + K_4 \cdot \left(\theta_4 - \theta_3\right) + K_5 \cdot \left(\theta_4 - \theta_5\right) = 0 \\
&J_5 \cdot \ddot{\theta}_5 + K_5 \cdot \left(\theta_5 - \theta_4\right) + K_5 \cdot \left(\theta_5 - \theta_6\right) = 0 \\
&J_6 \cdot \ddot{\theta}_6 + K_6 \cdot \left(\theta_6 - \theta_5\right) + K_7 \cdot \left(\theta_6 - \theta_{fw}\right) = 0 \\
&J_{fw} \cdot \ddot{\theta}_{fw} + K_7 \cdot \left(\theta_{fw} - \theta_6\right) = 0
\end{aligned}\right\} \qquad (2.12)$$

Substituting the following equation for θ_i into equation (2.12)

$$\theta_i = \Theta_i \cdot \cos\left(\omega t\right) \qquad i = 1, 2, ..., 9 \qquad (2.13)$$

the system of differential equations is transformed into the following system of algebraic equations:

$$\left.\begin{aligned}
&-J_r\cdot\omega^2\cdot\Theta_r+K_d\cdot\left(\Theta_r-\Theta_p\right)=0\\
&-\left(J_h+J_p\right)\cdot\omega^2\cdot\Theta_p+K_d\cdot\left(\Theta_p-\Theta_r\right)+K_1\cdot\left(\Theta_p-\Theta_1\right)=0\\
&-J_1\cdot\omega^2\cdot\Theta_1+K_1\cdot\left(\Theta_1-\Theta_p\right)+K_2\cdot\left(\Theta_1-\Theta_2\right)=0\\
&-J_2\cdot\omega^2\cdot\Theta_2+K_2\cdot\left(\Theta_2-\Theta_1\right)+K_3\cdot\left(\Theta_2-\Theta_3\right)=0\\
&-J_3\cdot\omega^2\cdot\Theta_3+K_3\cdot\left(\Theta_3-\Theta_2\right)+K_4\cdot\left(\Theta_3-\Theta_4\right)=0\\
&-J_4\cdot\omega^2\cdot\Theta_4+K_4\cdot\left(\Theta_4-\Theta_3\right)+K_5\cdot\left(\Theta_4-\Theta_5\right)=0\\
&-J_5\cdot\omega^2\cdot\Theta_5+K_5\cdot\left(\Theta_5-\Theta_4\right)+K_5\cdot\left(\Theta_5-\Theta_6\right)=0\\
&-J_6\cdot\omega^2\cdot\Theta_6+K_6\cdot\left(\Theta_6-\Theta_5\right)+K_7\cdot\left(\Theta_6-\Theta_{fw}\right)=0\\
&-J_{fw}\cdot\omega^2\cdot\Theta_{fw}+K_7\cdot\left(\Theta_{fw}-\Theta_6\right)=0
\end{aligned}\right\} \tag{2.14}$$

Equation (2.14) can be written in matrix form as shown below:

$$-\omega^2\cdot\mathbf{M}\cdot\mathbf{X}+\mathbf{K}\cdot\mathbf{X}=\mathbf{0} \tag{2.15}$$

where **M** is the mass matrix, **K** is the stiffness matrix and **X** is the amplitude matrix. They are given as:

$$\mathbf{M}=\begin{bmatrix}
J_r & 0 & 0 & 0 & 0 & 0 & 0 & 0 & 0\\
0 & J_h+J_p & 0 & 0 & 0 & 0 & 0 & 0 & 0\\
0 & 0 & J_1 & 0 & 0 & 0 & 0 & 0 & 0\\
0 & 0 & 0 & J_2 & 0 & 0 & 0 & 0 & 0\\
0 & 0 & 0 & 0 & J_3 & 0 & 0 & 0 & 0\\
0 & 0 & 0 & 0 & 0 & J_4 & 0 & 0 & 0\\
0 & 0 & 0 & 0 & 0 & 0 & J_5 & 0 & 0\\
0 & 0 & 0 & 0 & 0 & 0 & 0 & J_6 & 0\\
0 & 0 & 0 & 0 & 0 & 0 & 0 & 0 & J_{fw}
\end{bmatrix},$$

$$\mathbf{K} = \begin{bmatrix} K_d & -K_d & 0 & 0 & 0 & 0 & 0 & 0 & 0 \\ -K_d & K_d + K_1 & -K_1 & 0 & 0 & 0 & 0 & 0 & 0 \\ 0 & -K_1 & K_1 + K_2 & -K_2 & 0 & 0 & 0 & 0 & 0 \\ 0 & 0 & -K_2 & K_2 + K_3 & -K_3 & 0 & 0 & 0 & 0 \\ 0 & 0 & 0 & -K_3 & K_3 + K_4 & -K_4 & 0 & 0 & 0 \\ 0 & 0 & 0 & 0 & -K_4 & K_4 + K_5 & -K_5 & 0 & 0 \\ 0 & 0 & 0 & 0 & 0 & -K_5 & K_5 + K_6 & -K_6 & 0 \\ 0 & 0 & 0 & 0 & 0 & 0 & -K_6 & K_6 + K_7 & -K_7 \\ 0 & 0 & 0 & 0 & 0 & 0 & 0 & -K_7 & K_7 \end{bmatrix},$$

$$\mathbf{X}^{\mathrm{T}} = \begin{bmatrix} \Theta_r & \Theta_p & \Theta_1 & \Theta_2 & \Theta_3 & \Theta_4 & \Theta_5 & \Theta_6 & \Theta_{fw} \end{bmatrix}.$$

From these matrices the natural frequencies ω and eigenvectors **X** (mode shapes) can be found solving the generalized eigenvalue problem

$$\mathbf{M}^{-1} \cdot \mathbf{K} \cdot \mathbf{X} = \omega^2 \cdot \mathbf{X} \tag{2.16}$$

For 7.3 L and 9.0 L engine crankshaft systems with and without TV damper, the computed natural frequencies for first two modes are given in Table 2.5. As an example corresponding mode shapes of 9.0 L engine cranktrain with damper case are shown in Figure 2.4.

Table 2.5. Natural frequencies of the 7.3 L and 9.0 L engine crankshaft systems

	ω_1 (rad/sec)	ω_2 (rad/sec)
7.3 L engine crankshaft system w/o damper	1453	4014
7.3 L engine crankshaft system with damper	793	1577
9.0 L engine crankshaft system w/o damper	1549	4356
9.0 L engine crankshaft system with damper	684	1495

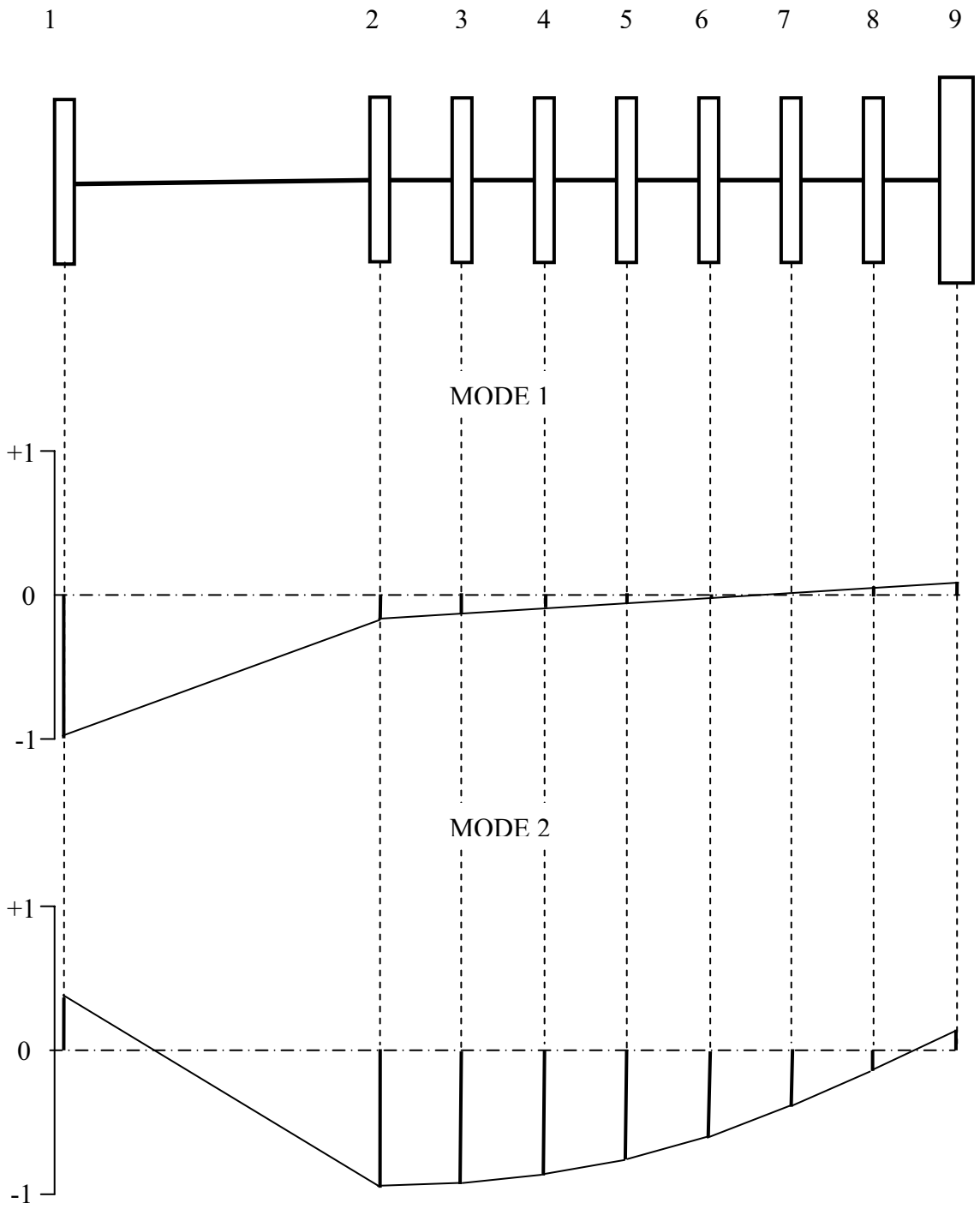

Figure 2.4. Mode shapes corresponding to first two natural frequencies of 9 L engine crankshaft system

2.5. Torsional Vibration Analysis

The evaluation of the torsional vibration behavior in view of engine related criteria is based on vibration amplitudes at each node of the system as well as on torsional vibration stresses in the higher stressed sections of the crankshaft. In particular, the calculation of torsional vibration amplitudes at the crankshaft front or rear ends are important since these values can be compared to experimental analysis results thus gives a tool for validating the modeled lumped mass system.

An essential step in performing torsional vibration analysis of the crankshaft system is the choice of appropriate boundary conditions. The standard boundary condition for a crank train torsional analysis is zero applied torque at the free ends of the system. The left end of the system is the free end of the crankshaft nose (TV damper side). The right end of the system is the point of applied load. If the applied load is assumed constant, the applied load only has energy for the zero frequency component and the applied load (and hence the right boundary torque condition) is zero for all frequencies other than the zero frequency. In cases where the applied load is not constant, the applied boundary condition for applied at the right end of the system (flywheel side) is no longer zero. In this case, the right boundary condition is treated as an additional unknown quantity in the analysis and the system equations are altered accordingly. Such an analysis is carried out in ADAMS which is given in Chapter 5.

Having established the excitation torque, system model and boundary conditions, the dynamic response of the cranktrain system can be calculated. The computations of the forced torsional vibration characteristics of crankshaft system are carried out by various authors, [54], [55], [56]. Analysis techniques are split into two basic categories: order domain and time domain.

Order domain techniques include Holzer analysis, impedance modeling and transfer matrices. In all of these methods, the system is analyzed in order domain. Holzer analysis is the original method developed for engine torsional vibration analysis which has been used since World War II. With the advent of computers, impedance modeling and transfer matrices become popular. Time domain techniques use time as the independent variable. A

time domain excitation torque is applied to the crankshaft model at each cylinder. The dynamic response of the cranktrain is then computed as a function of time. This task is usually performed using a commercial package. Because all the differential equations are solved by numerical integration, the computational cost is much higher than those for ordal superposition methods. Time domain techniques can be applied to transient simulation, while order domain techniques are suitable for quasi steady state vibration simulation. Order domain techniques has been proven to be the best tool for engine torsional vibration simulation by many researchers, as the combustion events and crankshaft rotation are repeated cycle-by-cycle.

In this study, transfer matrix method is used to investigate the torsional vibration characteristics of the crankshaft system [56]. The system is analyzed at discrete frequencies corresponding to half and full engine orders at a given speed. Engine orders ½ through 12^{th} orders are included in the analysis. The angular dynamic responses are expressed as a series of sinusoidal and cosine terms. These terms have the same frequencies as the input excitation torque. At each frequency, single order excitations are calculated first and then results are superposed to obtain the synthesized vibration characteristics.

The procedure for solving the crankshaft dynamic equation using transfer matrix method is summarized below.

- Zero applied torque is assumed as one of the boundary conditions at each end of the system.
- System matrix is calculated by successively multiplying the transfer matrices representing the dynamics of each single element. The system matrix has the same size as an individual element matrix.
- Reduced set of equations is solved for the unknown displacement boundary conditions at each end of the system.
- Intermediate states are then calculated by successive multiplication of the element matrices starting from either end of the system.

For torsional vibration simulations, a code is written in MATLAB language and given in Appendix A. Tables 2.2-2.4, along with the cylinder gas pressure values are used as inputs to the torsional vibration simulation.

2.5.1. Torsional Vibration Angle Amplitudes at Crankshaft Front End

Results obtained for crankshaft front end torsional vibration angle amplitudes in order by order form are given in Tables 2.6 and 2.7 for 7.3 L engine and in Tables 2.8 and 2.9 for 9.0 L engine with and without TV damper cases, respectively. The syntheses of all harmonics up to the 12^{th} order are given in Figures 2.5-2.13 for 7.3 L engine and in Figures 2.14-2.20 for 9.0 L engine.

The permissible level for the single order crankshaft front end amplitudes is 0.2°. The front end amplitudes of the engine without damper make obvious that a TV damper must be used for 7.3 L engine because the 6^{th} order amplitude is approximately three times larger than the recommended limit at 2220 rpm and 2400 rpm engine speeds. From Figures 2.10 and 2.11 it is seen that TV damper plays an important role on front end torsional vibration at these engine speeds. Similarly, for 9.0 L engine, the 6^{th} order amplitude reaches to 0.27° at 2200 rpm which is again larger than the recommended limit. With the inclusion of TV damper to crankshaft system this amplitude reduces to 0.15°. From Figures 2.14-2.20, it is seen that TV damper has the biggest effect on front end torsional vibration at 2200 rpm engine speed. All the single order amplitudes are below the permissible limit with the proposed TV dampers for both engines.

Table 2.6. Crankshaft front end torsional vibration amplitudes for 7.3 L engine w/o TV damper

Order No	**Front end torsional vibration amplitudes (degree) (7.3 L engine w/o damper)**						
	1200 rpm	**1480 rpm**	**1600 rpm**	**1700 rpm**	**1850 rpm**	**2220 rpm**	**2400 rpm**
0.5	0.043454	0.041470	0.042091	0.042423	0.042571	0.045076	0.047263
1.0	0.003139	0.002672	0.002603	0.002543	0.002443	0.002334	0.002323
1.5	0.151607	0.144869	0.147330	0.148811	0.149928	0.160853	0.170006
2.0	0.001174	0.000769	0.000647	0.000543	0.000387	0.000096	0.000003
2.5	0.047887	0.046435	0.047581	0.048392	0.049316	0.054753	0.059049
3.0	0.157317	0.031426	0.001047	0.019833	0.043225	0.081364	0.095974
3.5	0.036162	0.035988	0.037384	0.038506	0.040095	0.047704	0.053790
4.0	0.000006	0.000533	0.000836	0.001127	0.001636	0.003673	0.005398
4.5	0.067785	0.070381	0.074842	0.078849	0.085471	0.117951	0.149208
5.0	0.000417	0.001117	0.001577	0.002051	0.002965	0.007930	0.014366
5.5	0.018999	0.020960	0.023131	0.025324	0.029610	0.060482	0.126433
6.0	0.050144	0.075867	0.092703	0.110298	0.147886	0.612130	0.651143
6.5	0.013675	0.016736	0.019860	0.023651	0.033772	0.081017	0.032409
7.0	0.000848	0.002084	0.003282	0.005043	0.011851	0.010891	0.007869
7.5	0.026401	0.039198	0.055309	0.085095	0.207008	0.031460	0.020618
8.0	0.000924	0.002902	0.006192	0.015239	0.009479	0.003933	0.003590
8.5	0.007620	0.017129	0.041464	0.028840	0.010487	0.003433	0.002443
9.0	0.032670	0.134727	0.138600	0.065591	0.034941	0.016920	0.014117
9.5	0.006324	0.025597	0.008762	0.005055	0.002886	0.001198	0.000847
10.0	0.001203	0.003272	0.001868	0.001474	0.001209	0.001096	0.001164
10.5	0.016510	0.010466	0.005780	0.004047	0.002627	0.001140	0.000733
11.0	0.001866	0.000917	0.000718	0.000640	0.000582	0.000607	0.000682
11.5	0.008745	0.001025	0.000662	0.000489	0.000324	0.000116	0.000046
12.0	0.024164	0.004110	0.003046	0.002511	0.001995	0.001487	0.001444

Table 2.7. Crankshaft front end torsional vibration amplitudes for 7.3 L engine with TV damper

Order No	Front end torsional vibration amplitudes (degree) (7.3 L engine with damper)						
	1200 rpm	1480 rpm	1600 rpm	1700 rpm	1850 rpm	2220 rpm	2400 rpm
0.5	0.040652	0.038790	0.039379	0.039699	0.039858	0.042276	0.044376
1.0	0.002947	0.002519	0.002460	0.002407	0.002320	0.002239	0.002241
1.5	0.143861	0.138972	0.142129	0.144298	0.146635	0.161500	0.173404
2.0	0.001133	0.000758	0.000668	0.000547	0.000397	0.000105	0.000003
2.5	0.0472926	0.047668	0.049902	0.051805	0.054740	0.068963	0.081134
3.0	0.160462	0.034235	0.001185	0.023313	0.054443	0.131736	0.180766
3.5	0.038545	0.042776	0.047498	0.052347	0.061742	0.098412	0.096746
4.0	0.000007	0.000720	0.001263	0.001899	0.003230	0.005234	0.005332
4.5	0.083282	0.113953	0.140964	0.161736	0.158365	0.097401	0.087909
5.0	0.000573	0.002206	0.003196	0.003531	0.003484	0.004134	0.004976
5.5	0.030257	0.041229	0.034369	0.028284	0.022568	0.018680	0.018299
6.0	0.094446	0.108127	0.091564	0.083176	0.077100	0.078177	0.079029
6.5	0.028208	0.016373	0.013773	0.012586	0.011545	0.010133	0.009236
7.0	0.001526	0.001469	0.001641	0.001838	0.002172	0.003017	0.003355
7.5	0.035333	0.020436	0.019156	0.018384	0.017016	0.012919	0.011009
8.0	0.000912	0.001090	0.001286	0.001452	0.001656	0.002025	0.002209
8.5	0.005746	0.004191	0.003950	0.003680	0.003160	0.002043	0.001660
9.0	0.019248	0.017206	0.016822	0.016038	0.014348	0.011141	0.010360
9.5	0.003877	0.002257	0.002021	0.001790	0.001441	0.000853	0.000664
10.0	0.000416	0.000572	0.000627	0.000658	0.000689	0.000832	0.000970
10.5	0.003983	0.002899	0.002464	0.002113	0.001651	0.000917	0.000650
11.0	0.000270	0.000339	0.000360	0.000374	0.000394	0.000517	0.000646
11.5	0.000728	0.000460	0.000373	0.000311	0.000233	0.000105	0.000047
12.0	0.002933	0.002116	0.001874	0.001706	0.001514	0.001429	0.001611

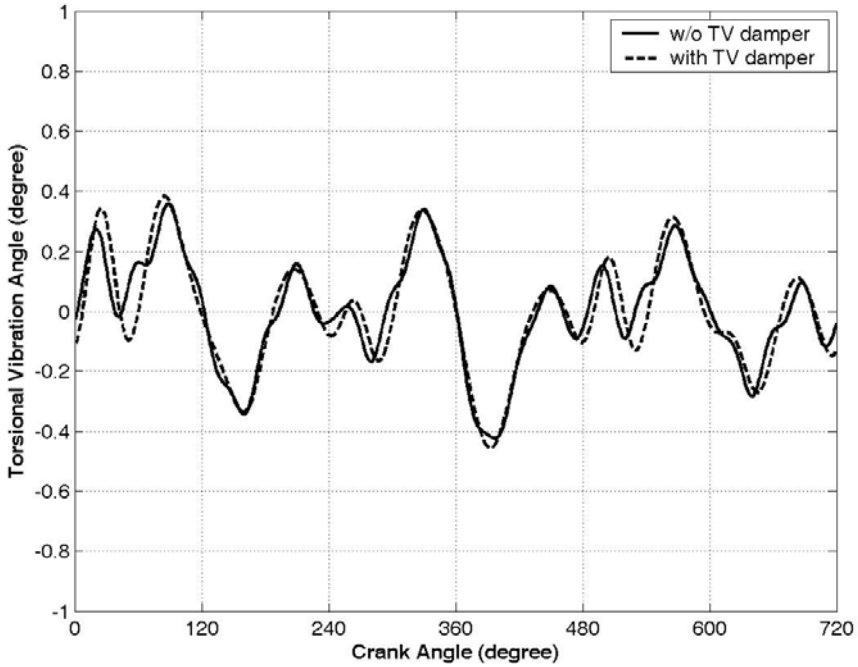

Figure 2.5. Crankshaft front end torsional vibration at 1200 rpm for 7.3L engine (with and w/o TV damper)

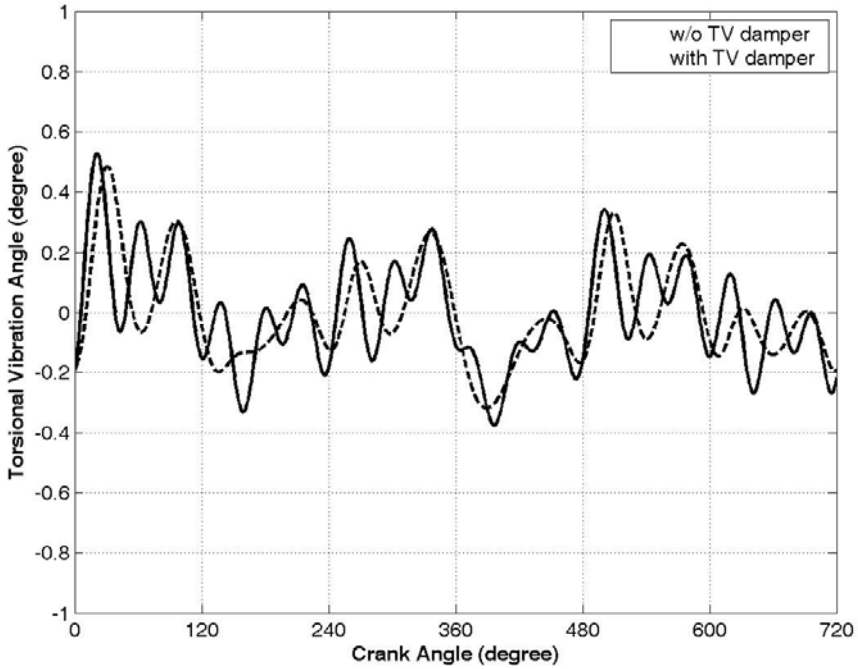

Figure 2.6. Crankshaft front end torsional vibration at 1480 rpm for 7.3L engine (with and w/o TV damper)

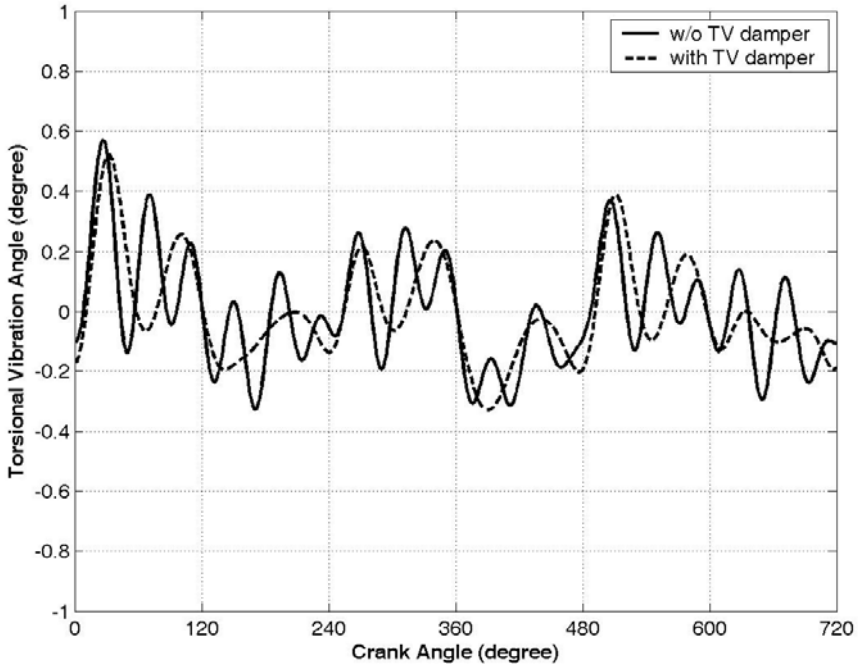

Figure 2.7. Crankshaft front end torsional vibration at 1600 rpm for 7.3L engine (with and w/o TV damper)

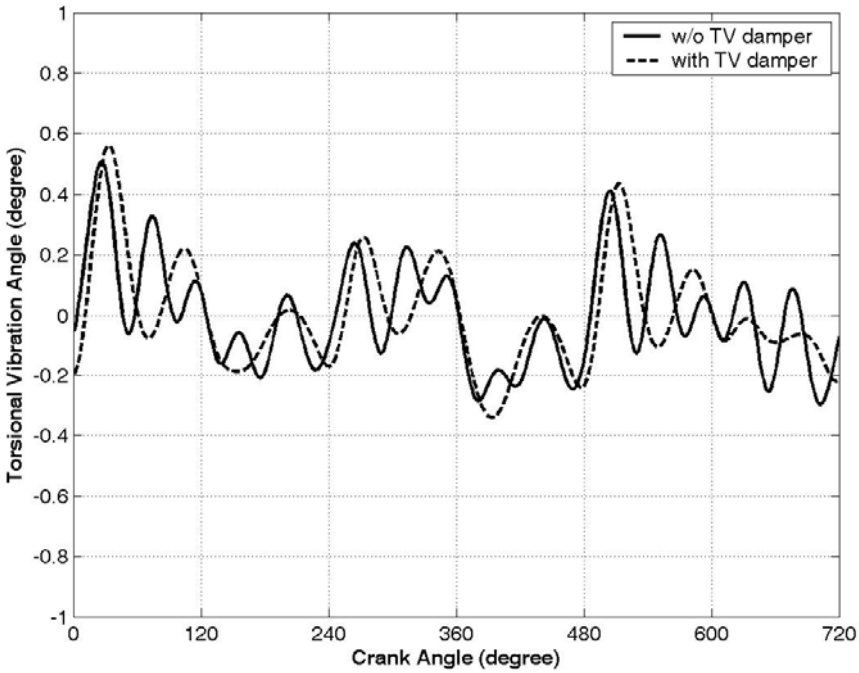

Figure 2.8. Crankshaft front end torsional vibration at 1700 rpm for 7.3L engine (with and w/o TV damper)

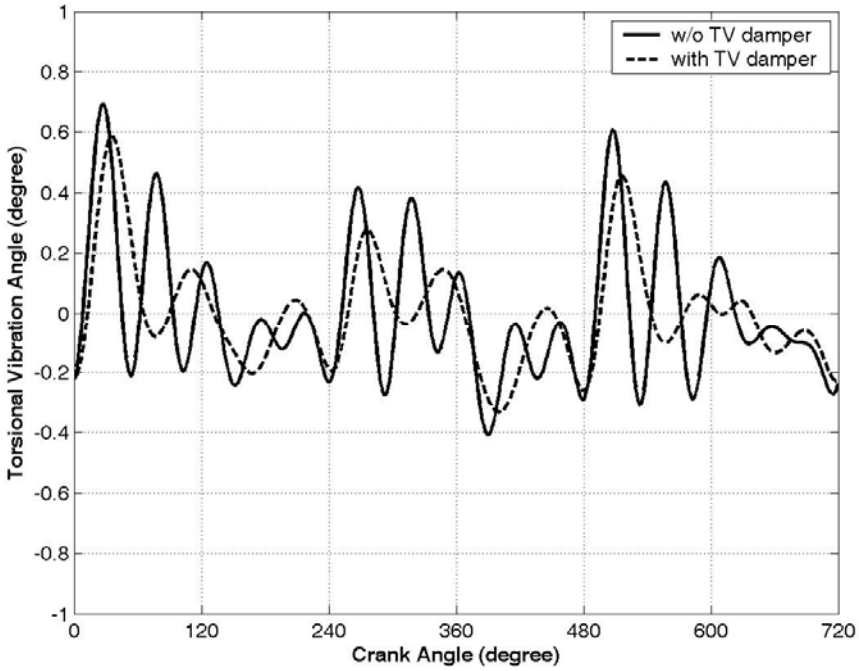

Figure 2.9. Crankshaft front end torsional vibration at 1850 rpm for 7.3L engine (with and w/o TV damper)

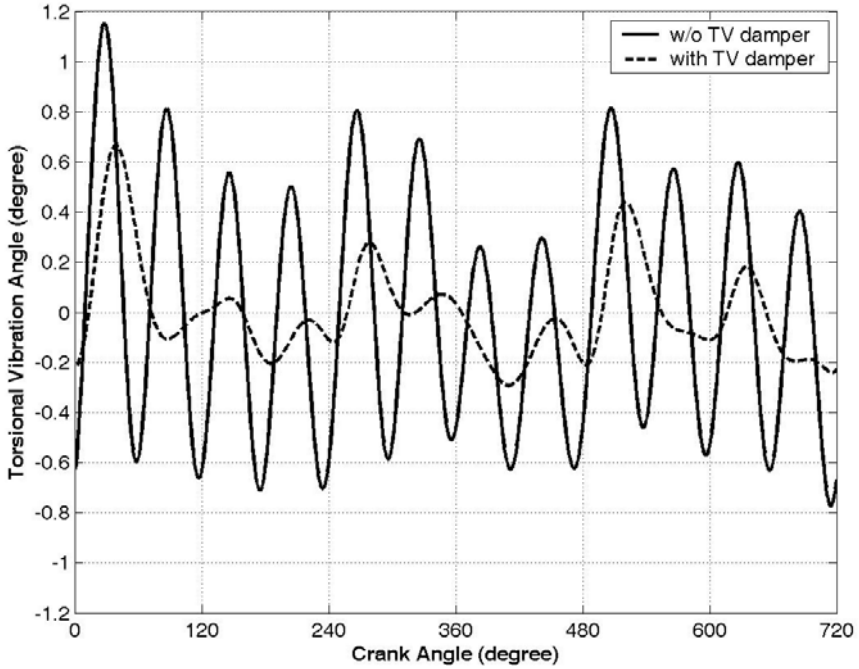

Figure 2.10. Crankshaft front end torsional vibration at 2220 rpm for 7.3L engine (with and w/o TV damper)

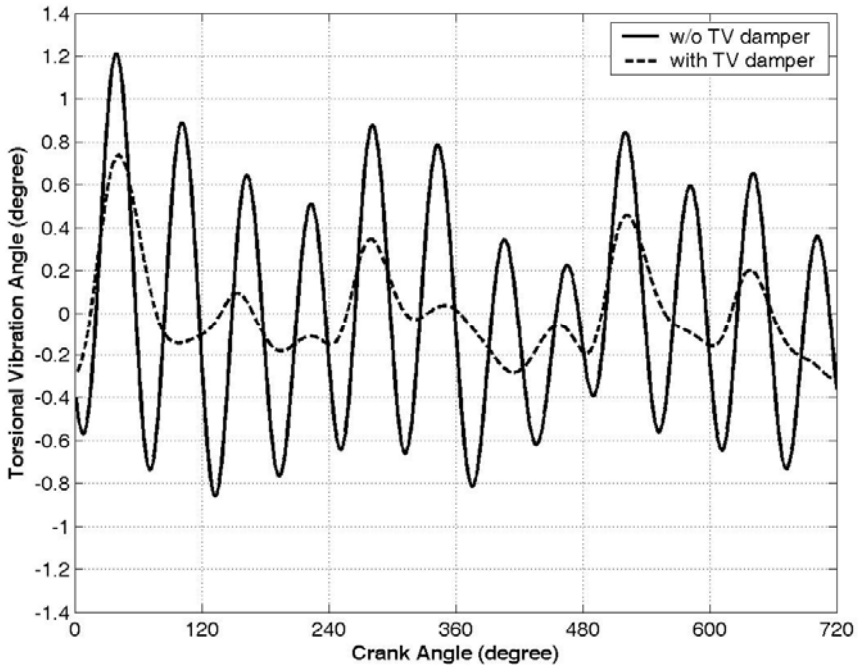

Figure 2.11. Crankshaft front end torsional vibration at 2400 rpm for 7.3L engine (with and w/o TV damper)

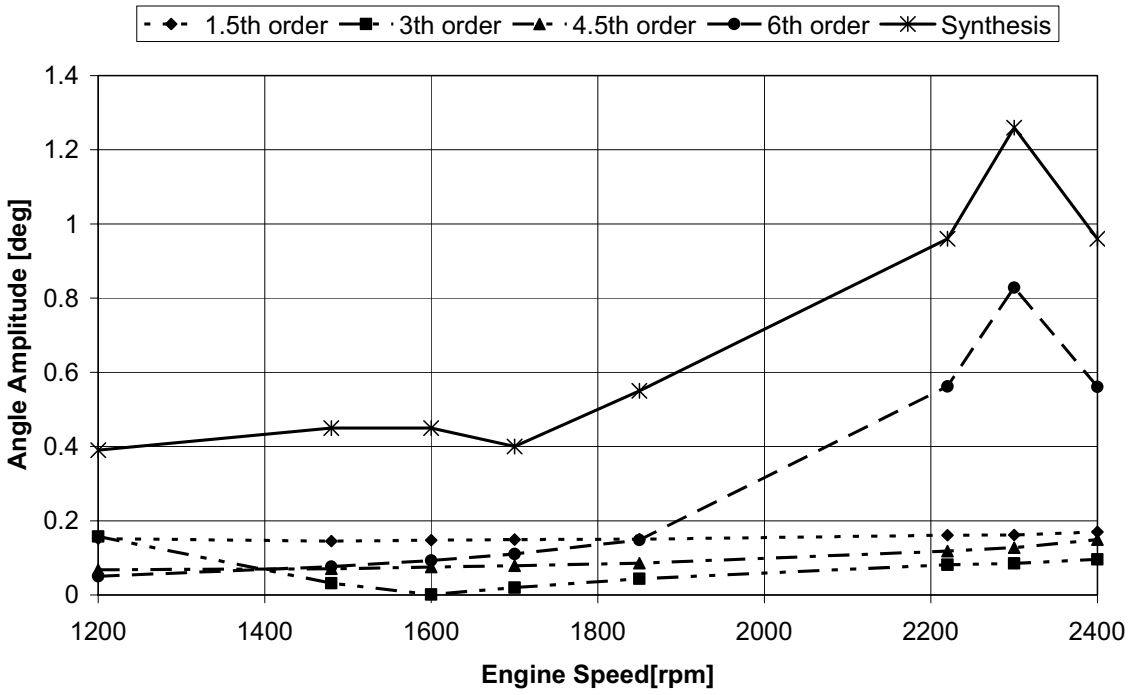

Figure 2.12. Torsional vibration angle amplitudes at crankshaft front end for 7.3 L engine w/o TV damper

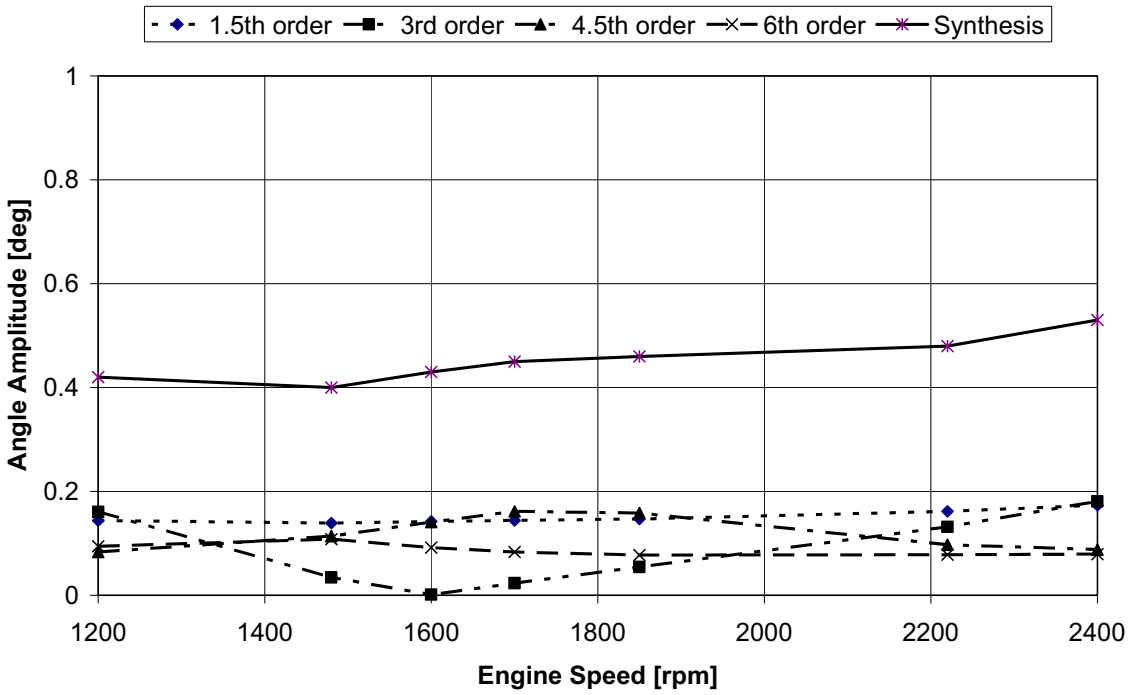

Figure 2.13. Torsional vibration angle amplitudes at crankshaft front end for 7.3 L engine with TV damper

Table 2.8. Crankshaft front end torsional vibration amplitudes for 9.0 L engine w/o TV damper

Order No	Front end torsional vibration amplitudes (degree) (9.0 L engine w/o damper)						
	800 rpm	1000 rpm	1200 rpm	1350 rpm	1675 rpm	2000 rpm	2200 rpm
0.5	0.036226	0.051089	0.055025	0.057692	0.058618	0.058059	0.051710
1.0	0.003093	0.003814	0.003818	0.003800	0.003459	0.003139	0.002550
1.5	0.116259	0.168513	0.187164	0.198722	0.204282	0.203747	0.178659
2.0	0.001190	0.001461	0.001339	0.001189	0.000735	0.000323	0.000078
2.5	0.035560	0.051863	0.058038	0.060481	0.062802	0.065351	0.060185
3.0	0.444790	0.333066	0.178450	0.092292	0.018462	0.069323	0.069618
3.5	0.026749	0.038586	0.042716	0.043646	0.045968	0.049854	0.049534
4.0	0.000399	0.000307	0.000006	0.000287	0.001084	0.002260	0.003127
4.5	0.049426	0.070347	0.076906	0.077065	0.084285	0.098428	0.109302
5.0	0.000148	0.000057	0.000415	0.000725	0.001752	0.003628	0.005797
5.5	0.013480	0.018819	0.020217	0.020204	0.023639	0.031454	0.042819
6.0	0.000311	0.030134	0.050191	0.059874	0.091174	0.153552	0.273510
6.5	0.009454	0.012848	0.013628	0.013729	0.018264	0.033345	0.083380
7.0	0.000088	0.000368	0.000714	0.001045	0.002870	0.012833	0.019562
7.5	0.017294	0.022737	0.023699	0.025809	0.046116	0.137792	0.051171
8.0	0.000134	0.000400	0.000718	0.001094	0.004537	0.006889	0.004566
8.5	0.004774	0.005982	0.006039	0.007047	0.025703	0.007363	0.004476
9.0	0.012482	0.020083	0.022492	0.032037	0.130047	0.024882	0.018724
9.5	0.003556	0.004198	0.004209	0.005982	0.008644	0.002058	0.001440
10.0	0.000175	0.000406	0.000641	0.001498	0.001709	0.000939	0.000982
10.5	0.007313	0.008594	0.007796	0.017611	0.005158	0.001946	0.001382
11.0	0.000185	0.000496	0.000663	0.002028	0.000638	0.000492	0.000495
11.5	0.002260	0.002735	0.003073	0.002391	0.000560	0.000257	0.000162
12.0	0.008929	0.014063	0.022306	0.005141	0.002673	0.001875	0.001203

Table 2.9. Crankshaft front end torsional vibration amplitudes for 9.0 L engine with TV damper

Order No	Front end torsional vibration amplitudes (degree) (9.0 L engine with damper)						
	800 rpm	1000 rpm	1200 rpm	1350 rpm	1675 rpm	2000 rpm	2200 rpm
0.5	0.034522	0.048585	0.052276	0.054792	0.055672	0.055177	0.049174
1.0	0.002937	0.003625	0.003633	0.003621	0.003309	0.003019	0.002462
1.5	0.110643	0.160868	0.179417	0.191229	0.198691	0.201066	0.178301
2.0	0.001138	0.001405	0.001298	0.001162	0.000735	0.000334	0.000083
2.5	0.034203	0.050427	0.057275	0.060549	0.065664	0.072820	0.070286
3.0	0.431419	0.328684	0.180481	0.095661	0.020618	0.084647	0.087875
3.5	0.026227	0.038843	0.044699	0.047491	0.055496	0.063084	0.060922
4.0	0.000397	0.000317	0.000006	0.000332	0.001371	0.002727	0.003580
4.5	0.049988	0.075192	0.088961	0.094642	0.104622	0.111297	0.117402
5.0	0.000153	0.000064	0.000507	0.000918	0.002062	0.003875	0.005772
5.5	0.014302	0.021978	0.025519	0.025221	0.026396	0.031318	0.036306
6.0	0.000340	0.036795	0.063218	0.071769	0.097091	0.133023	0.154988
6.5	0.010731	0.016166	0.016659	0.015740	0.018365	0.020917	0.020000
7.0	0.000103	0.000465	0.000839	0.001152	0.002615	0.004075	0.004393
7.5	0.021118	0.028279	0.026797	0.027363	0.034433	0.024746	0.019617
8.0	0.000168	0.000483	0.000785	0.001108	0.002285	0.002168	0.002281
8.5	0.006045	0.006981	0.006374	0.006660	0.006539	0.003253	0.002594
9.0	0.015721	0.022709	0.022781	0.026855	0.024097	0.013234	0.011937
9.5	0.004399	0.004611	0.004016	0.004053	0.002608	0.001228	0.000983
10.0	0.000211	0.000433	0.000555	0.000707	0.000707	0.000607	0.000707
10.5	0.008591	0.008898	0.005748	0.004753	0.002571	0.001336	0.001041
11.0	0.000211	0.000405	0.000376	0.000353	0.000358	0.000354	0.000388
11.5	0.002525	0.002576	0.001159	0.000581	0.000342	0.000193	0.000132
12.0	0.009754	0.012183	0.004883	0.001765	0.001739	0.001459	0.001018

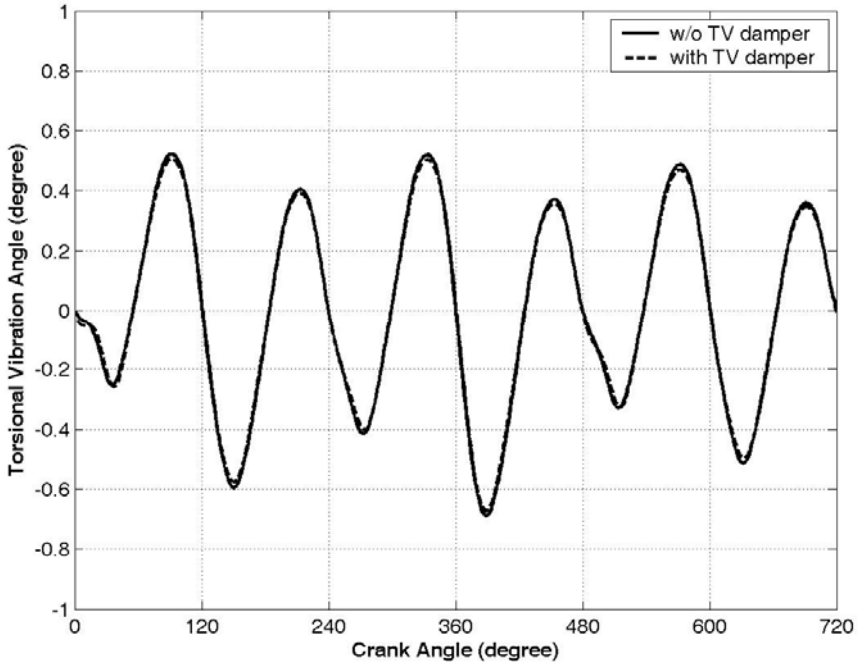

Figure 2.14. Crankshaft front end torsional vibration at 800 rpm for 9.0L engine (with and w/o TV damper)

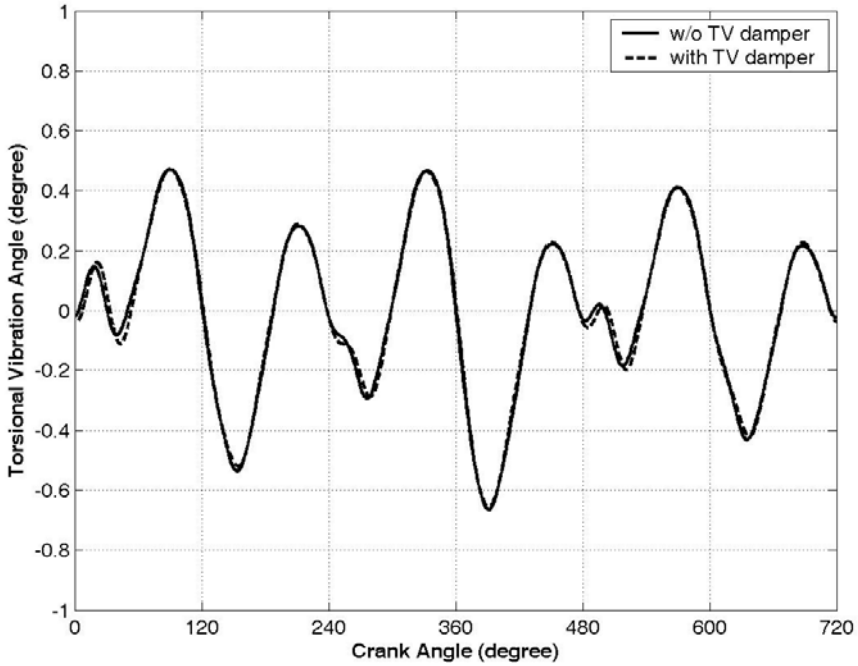

Figure 2.15. Crankshaft front end torsional vibration at 1000 rpm for 9.0L engine (with and w/o TV damper)

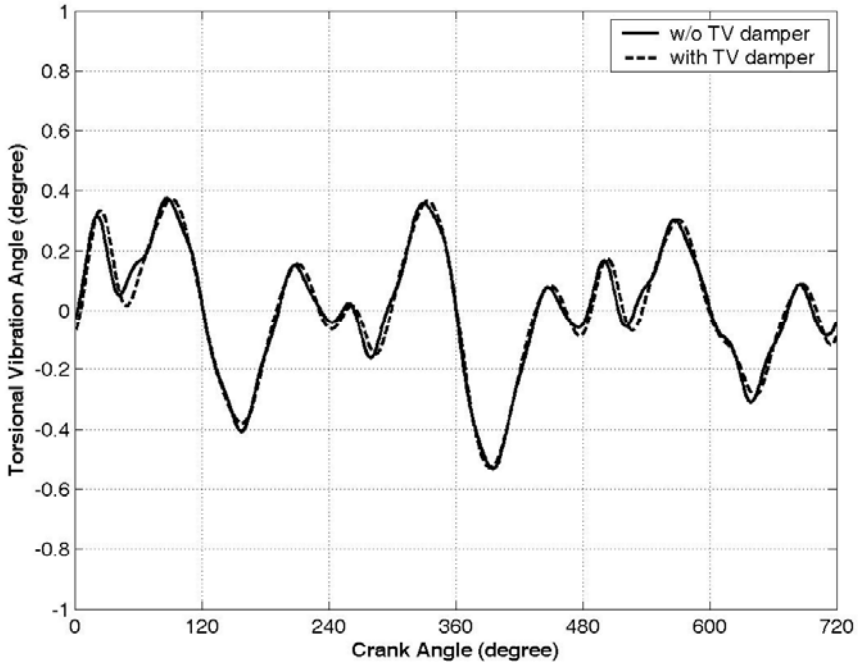

Figure 2.16. Crankshaft front end torsional vibration at 1200 rpm for 9.0L engine (with and w/o TV damper)

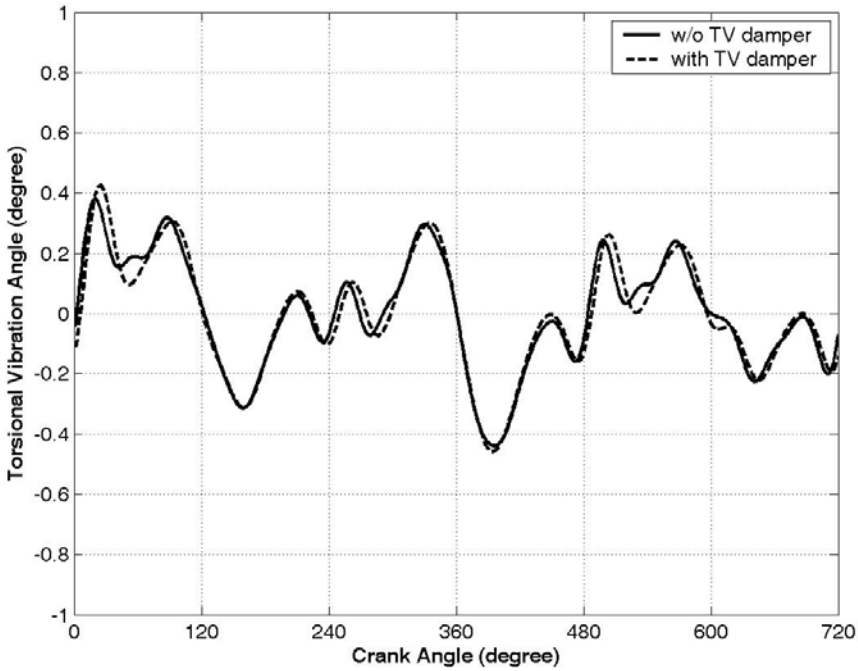

Figure 2.17. Crankshaft front end torsional vibration at 1350 rpm for 9.0L engine (with and w/o TV damper)

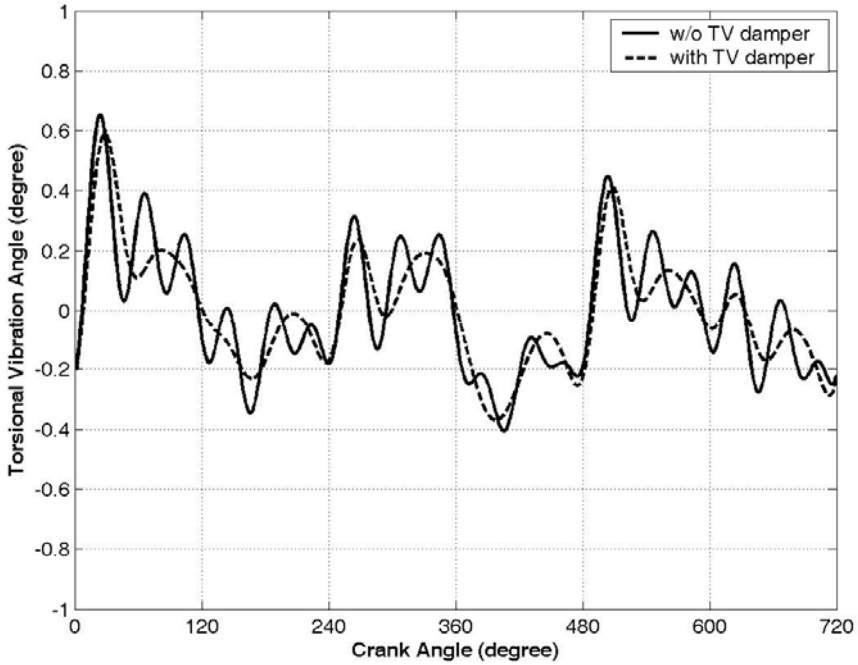

Figure 2.18. Crankshaft front end torsional vibration at 1675 rpm for 9.0L engine (with and w/o TV damper)

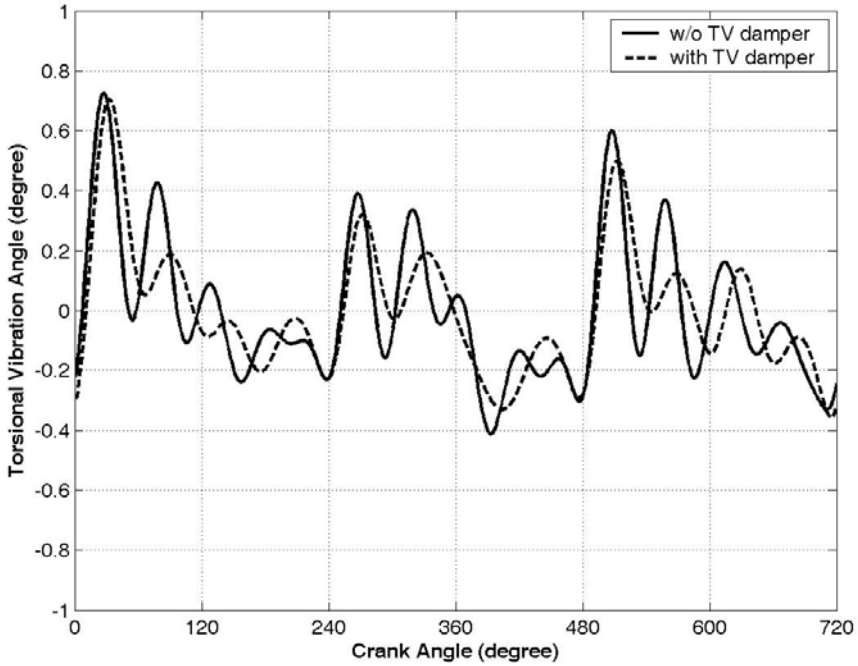

Figure 2.19. Crankshaft front end torsional vibration at 2000 rpm for 9.0L engine (with and w/o TV damper)

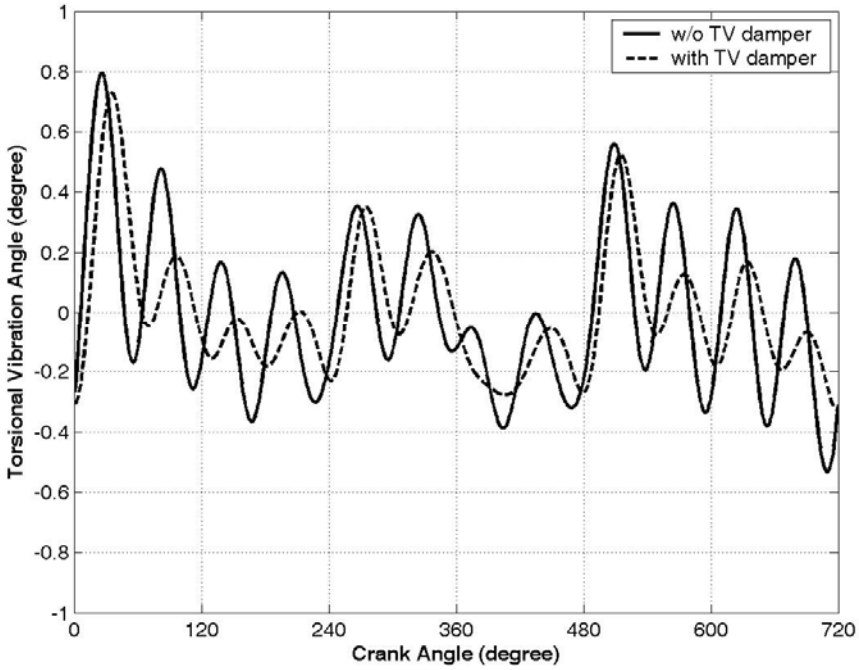

Figure 2.20. Crankshaft front end torsional vibration at 2200 rpm for 9.0L engine (with and w/o TV damper)

2.5.2. Torsional Vibration Stress Amplitudes

The synthesized torsional vibration stress amplitudes (related to the crankpin diameter) are plotted in Figure 2.21 for 7.3 L engine without TV damper and in Figure 2.22 for 7.3 L engine with TV damper. The stresses are calculated at each shaft between the crank throws. According to calculations maximum torsional vibration stress amplitude occurs at the shaft between throw 4 and 5 and it reaches to 100 MPa at 2300 rpm for the w/o damper case. As can be seen from Figure 2.22, vibration stress amplitude at 2300 rpm is reduced from 100 MPa to 40 MPa level with the inclusion of TV damper. These stress values will be used in Chapter 3 while performing the classical crankshaft stress analysis for 7.3 L engine.

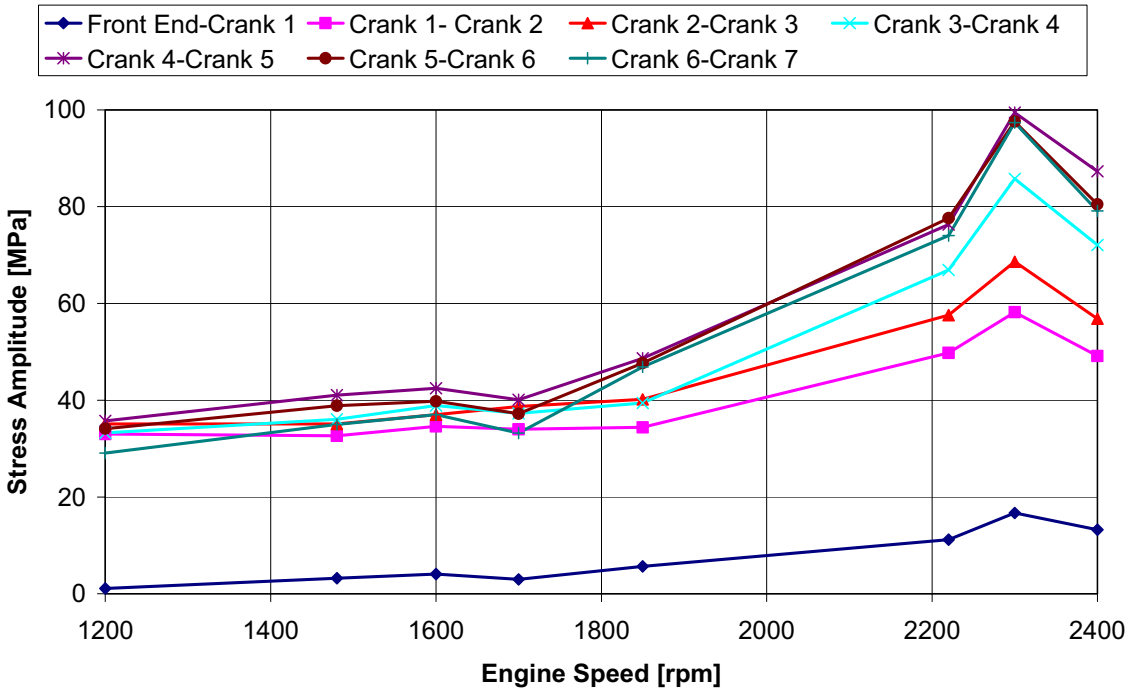

Figure 2.21. Torsional vibration stress amplitudes in crankshaft related to the crank pin diameter (7.3 L engine without damper)

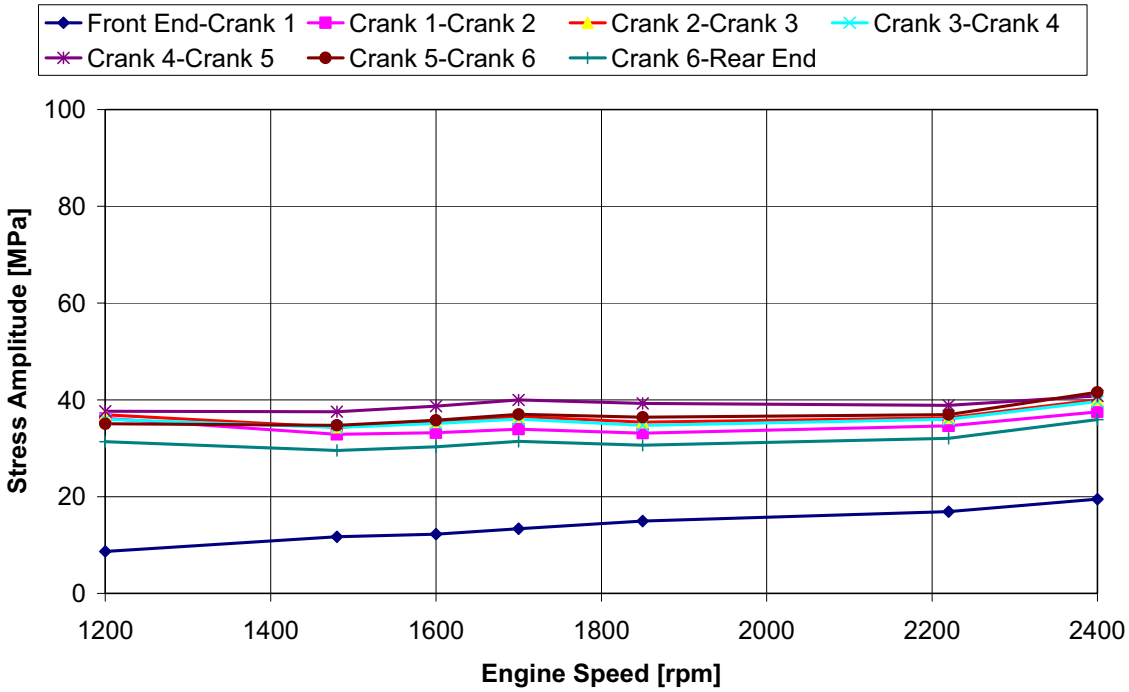

Figure 2.22. Torsional vibration stress amplitudes in crankshaft related to the crank pin diameter (7.3 L engine with damper)

2.5.3. Torsional Vibration Measurement

The comparison of calculations and measurements is a decisive quality criterion in the CAE environment. The torsional vibrations on the front end are evaluated by AVL [57] for the 7.3 L engine crankshaft in the high speed range where flywheel runs smoothly. On a test bed installation the torsional dynamics of the engine is superimposed by the torsional dynamics of the arrangement engine – coupling – dynamometer. The layout of the coupling stiffness typically produces a resonance in the speed range between starter speed and idle speed. The torsional dynamics of the engine can be furthermore splitted into the engine speed irregularity and the torsional vibration of the crankshaft. This means that the measured signal at the front end of the engines superimposed by the coupling resonance, the engine speed irregularity and the torsion of the crankshaft. Arrangements with coupling resonance's close to idle speed result in an increased speed irregularity which is not coming from the engine itself. Engine speed irregularities are high at full load conditions in the low to medium speed range. Due to the big inertia of the flywheel, the amplitudes of the speed irregularity are small compared to the torsion amplitudes of the crankshaft in the medium and upper engine speed range. This is the relevant speed range for the evaluation of the viscous damper performance. A Fourier analysis of the front end angular movement gives then the amplitudes of the interesting harmonic orders.

Calculations are performed up to the rated speed. The results obtained are shown in Figure 2.23 to Figure 2.27. As it is explained in above paragraph, the 3^{rd} order vibration amplitude shows a significant increase in the lower speed range which can be seen from Figure 2.24. This is a cyclic speed variation, which can be influenced only by the total inertia of the cranktrain and thus mainly by the flywheel and clutch size. Calculated and measured data can be compared considering the fact that the calculation simulates an infinite weak coupling between engine and brake, thus no coupling resonance occurs at low engine speed. As can be seen from Figure 2.23, calculated and experimental results for torsional vibration amplitude show good correlation at the engine speed range of 1200 rpm to 2400 rpm.

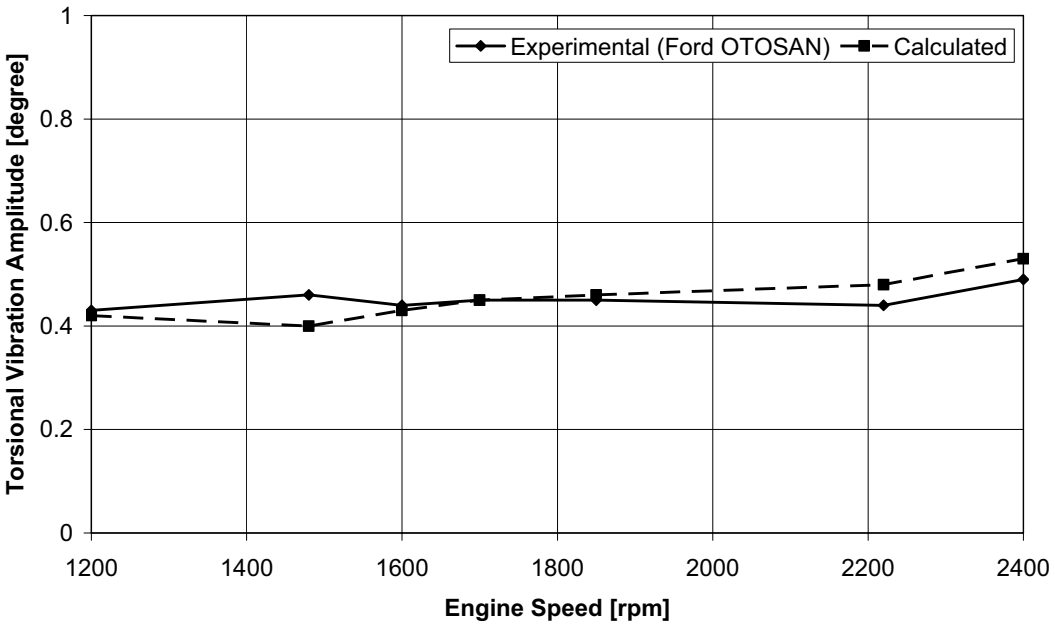

Figure 2.23. Total amplitude of crankshaft torsion vibration – Comparison of experimental and calculated data

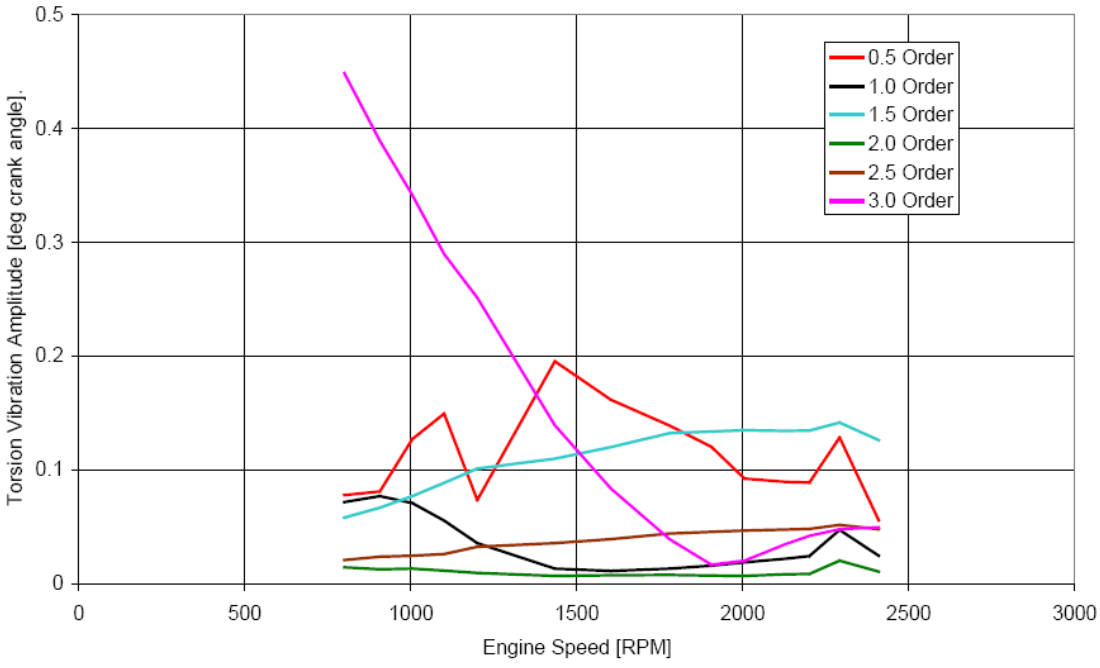

Figure 2.24. Measured harmonic orders - 0.5th order to 3rd order [57]

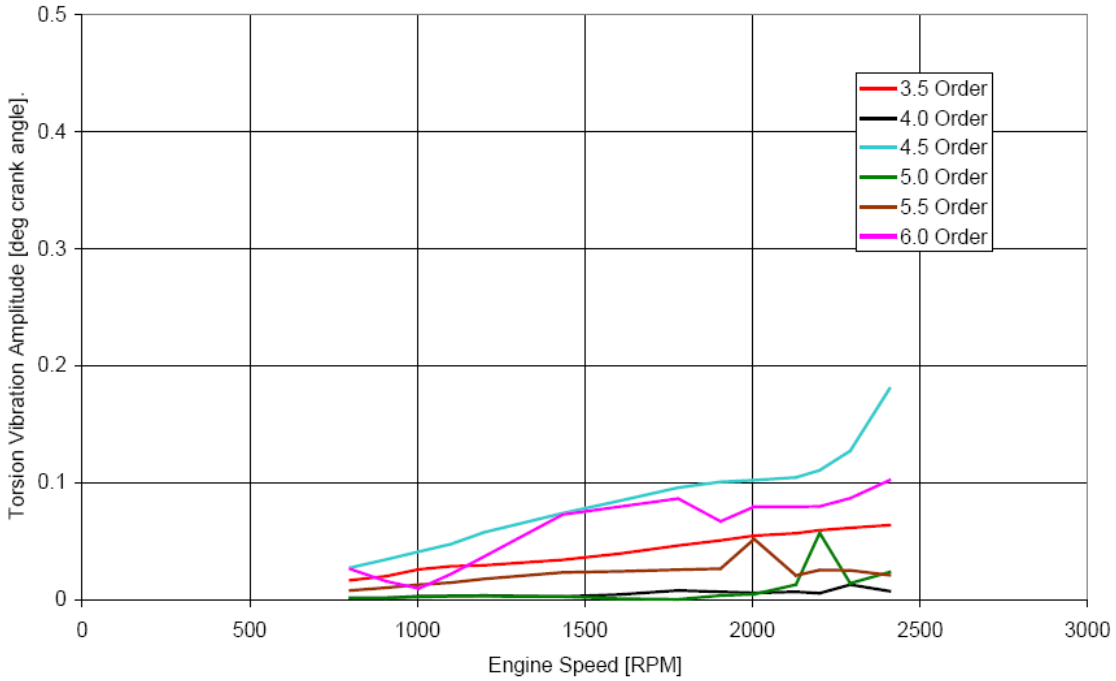

Figure 2.25. Measured harmonic orders - 3.5th order to 6th order [57]

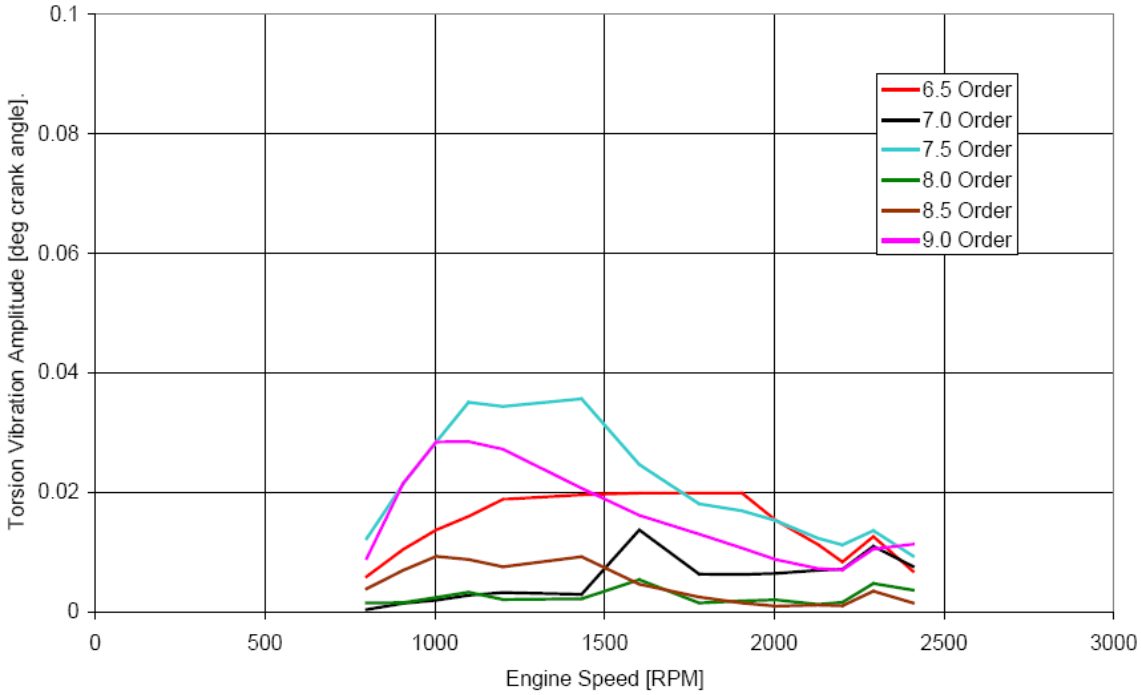

Figure 2.26. Measured harmonic orders - 6.5th order to 9th order [57]

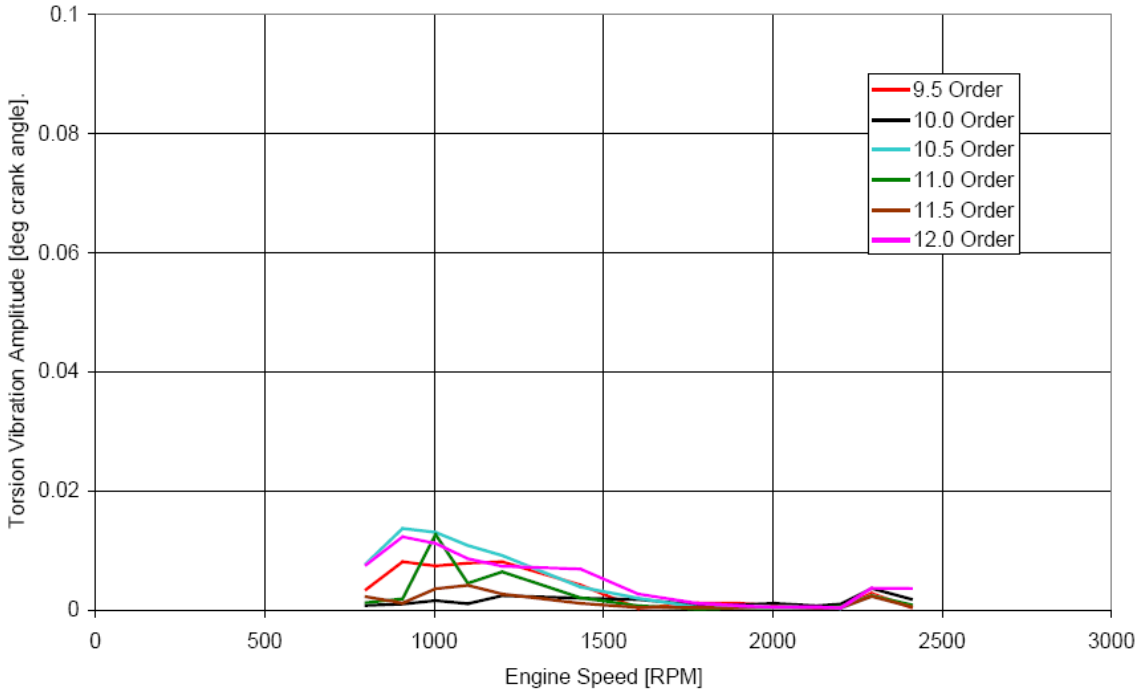

Figure 2.27. Measured harmonic orders - 9.5th order to 12th order [57]

2.6. Torsional Vibration Sensitivity Analyses

In this part of the study, the effect of stiffness, damping coefficient, ring inertia and hub inertia change of the TV damper on natural frequencies and torsional vibration amplitudes at the crankshaft front end are investigated for the crankshaft system of the 9.0 L engine. Effect of cylinder misfire on forced torsional vibration of the crankshaft system is also discussed.

2.6.1. Effect of TV Damper Specifications on Torsional Vibration

A standard viscous damper with fan blades with an outer diameter of 310 mm and a width of 32 mm is used with the following main specifications for the 9.0 L engine:

Inertia of the ring : 0.127 kgm^2

Inertia of the housing : 0.056 kgm^2

Viscosity of the silicon oil : 0.15 m^2/s at 80 ^oC

Torsional stiffness : 69500 Nm/rad

Relative damping : 73.67 Nms/rad

For 9.0 L engine crankshaft system with and without TV damper, the natural frequencies for the first three modes are given in Table 2.10. The effect of altering the stiffness, ring inertia and hub inertia of the TV damper on first two natural frequencies are given in Tables 2.11-2.13 and they are plotted in Figures 2.28-2.30.

Table 2.10. Natural frequencies of the 9.0 L engine crankshaft system

	ω_1	ω_2	ω_3
9.0 L engine crankshaft system w/o damper	1549 rad/sec (14795 rpm)	4356 rad/sec (41598 rpm)	7236 rad/sec (69103 rpm)
9.0 L engine crankshaft system with damper	684 rad/sec (6534 rpm)	1495 rad/sec (14278 rpm)	3972 rad/sec (37930 rpm)

Table 2.11. Effect of TV damper torsional stiffness change on natural frequencies of the 9.0L engine crankshaft system

	Torsional stiffness (Nm/rad)						
	-30% (48650)	-20% (55600)	-10% (62550)	0% (69500)	10% (76450)	20% (83400)	30% (90350)
Mode 1 (rad/sec)	591	625	656	684	710	733	754
Mode 2 (rad/sec)	1452	1466	1480	1495	1511	1526	1542

Table 2.12. Effect of TV damper hub inertia change on natural frequencies of the 9.0 L engine crankshaft system

	Hub inertia (kgm^2)						
	-30% (0.0392)	-20% (0.0448)	-10% (0.0504)	0% (0.056)	10% (0.0616)	20% (0.0672)	30% (0.0728)
Mode 1 (rad/sec)	685.1	684.8	684.5	684.2	684	683.7	683.4
Mode 2 (rad/sec)	1544	1527	1511	1495	1480	1465	1450

Table 2.13. Effect of TV damper ring inertia change on natural frequencies of the 9.0 L engine crankshaft system

	Ring inertia (kgm^2)						
	-30% (0.0889)	-20% (0.1016)	-10% (0.1143)	00% (0.127)	10% (0.1397)	20% (0.1524)	30% (0.1651)
Mode 1 (rad/sec)	804	757	718	684	655	630	607
Mode 2 (rad/sec)	1513	1505	1499	1495	1492	1489	1487

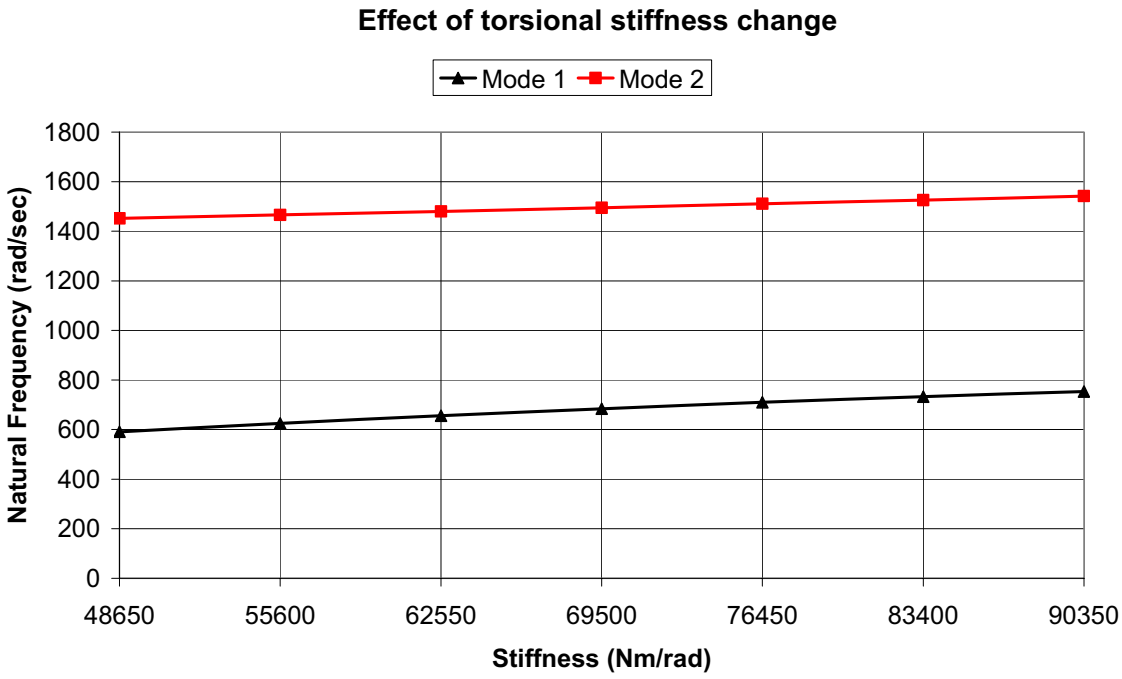

Figure 2.28. Effect of torsional stiffness change on natural frequencies

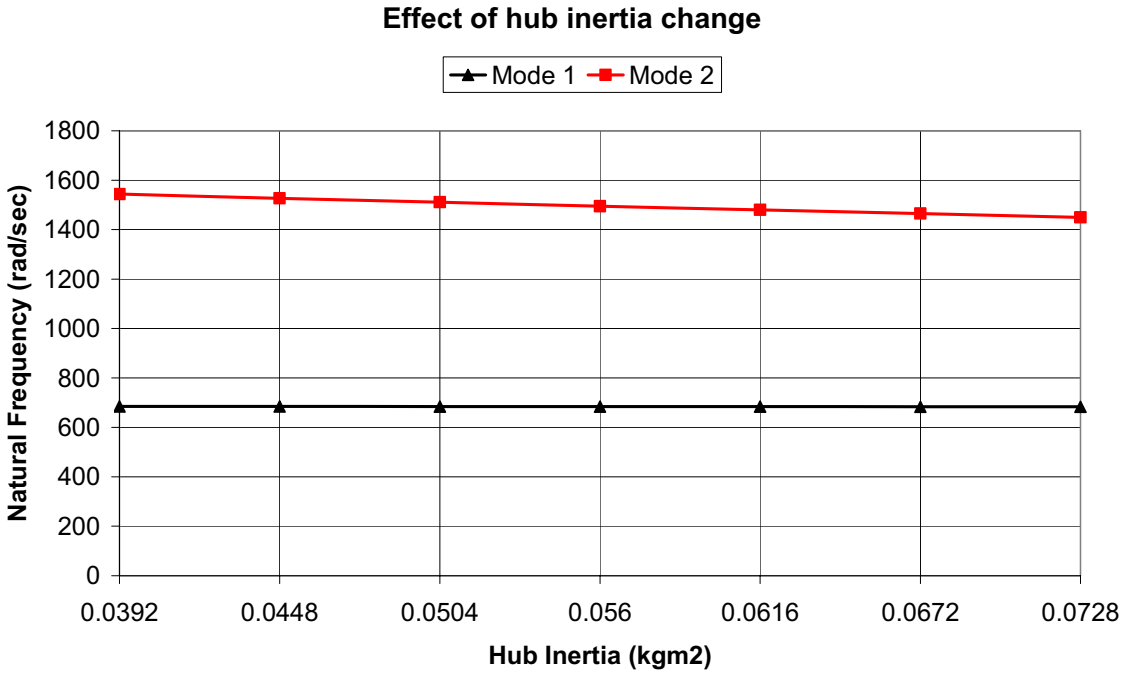

Figure 2.29. Effect of hub inertia change on natural frequencies

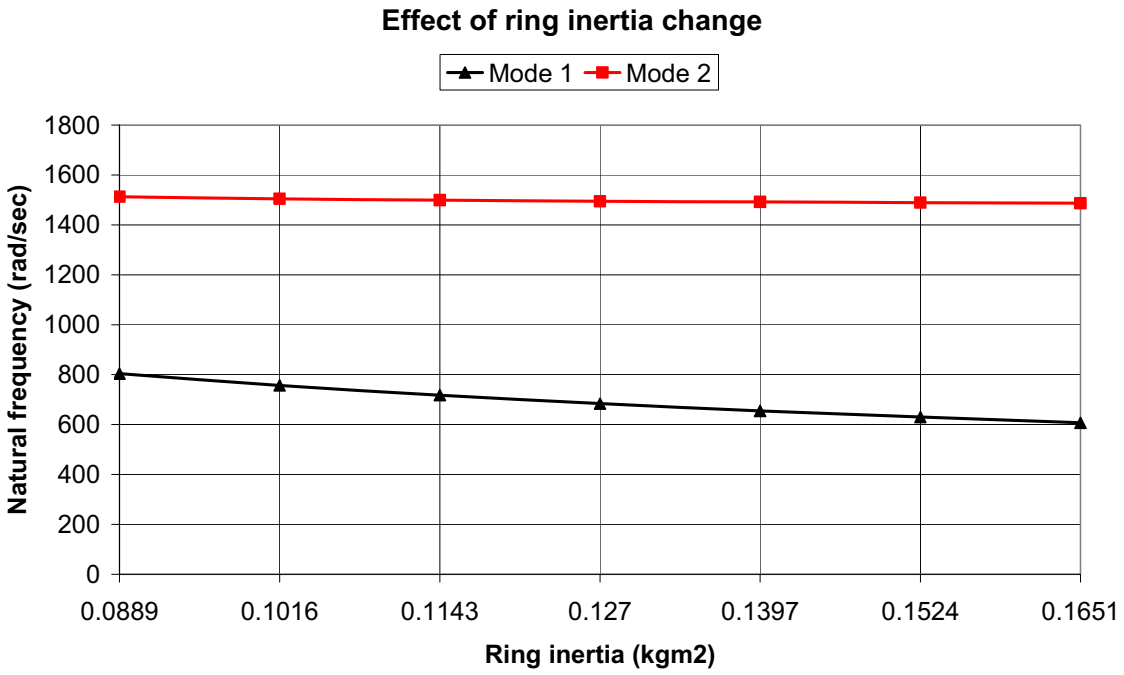

Figure 2.30. Effect of ring inertia change on natural frequencies

Effect of TV damper stiffness, damping coefficient, hub inertia and ring inertia changes on front end torsional vibration amplitudes are given in Tables 2.14-2.17 for the first eighteen orders (0.5, 1.0, 1.5, …,8.0) at the engine speed of 2200 rpm. The syntheses of all harmonics up to the 12th order for each case are given in Figures 2.31-2.34. It can be seen from the figures that as the torsional stiffness and damping coefficient values of the TV damper increases, torsional vibration angle amplitude at the crankshaft front end decreases. It can also be seen that hub and ring inertias of the TV damper has little effect on front end torsional vibration characteristics for this specific engine speed.

A more detailed analysis of the effect of TV damper stiffness and damping coefficients on crankshaft stresses is given in Chapter 4.

Table 2.14. Crankshaft front end torsional vibration amplitudes at 2200 rpm for first 16 orders with various torsional stiffness values of the TV damper

Order No	TV Damper Torsional Stiffness (Nm/rad)						
	-30% (48650)	-20% (55600)	-10% (62550)	0% (69500)	10% (76450)	20% (83400)	30% (90350)
	Front end torsional vibration angle amplitudes (degree)						
0.5	0.049157	0.049164	0.049170	0.049174	0.049178	0.049181	0.049184
1.0	0.002460	0.002461	0.002461	0.002462	0.002463	0.002463	0.002463
1.5	0.178275	0.178285	0.178294	0.178301	0.178307	0.178312	0.178316
2.0	0.000083	0.000083	0.000083	0.000083	0.000083	0.000083	0.000083
2.5	0.068269	0.069140	0.069824	0.070286	0.070547	0.070656	0.070661
3.0	0.081416	0.083242	0.085456	0.087875	0.090250	0.092344	0.094006
3.5	0.057975	0.058528	0.059481	0.060922	0.062918	0.065495	0.068602
4.0	0.003658	0.003620	0.003593	0.003580	0.003585	0.003613	0.003671
4.5	0.127968	0.124329	0.120794	0.117402	0.114201	0.111247	0.108607
5.0	0.006639	0.006340	0.006051	0.005772	0.005503	0.005246	0.005000
5.5	0.043038	0.040696	0.038452	0.036306	0.034259	0.032311	0.030461
6.0	0.177595	0.170150	0.162589	0.154988	0.147415	0.139934	0.132596
6.5	0.021211	0.020865	0.020460	0.020000	0.019484	0.018920	0.018313
7.0	0.004426	0.004423	0.004412	0.004393	0.004365	0.004327	0.004279
7.5	0.019358	0.019458	0.019545	0.019617	0.019671	0.019703	0.019712
8.0	0.002237	0.002252	0.002266	0.002281	0.002294	0.002307	0.002319

Table 2.15. Crankshaft front end torsional vibration amplitudes at 2200 rpm for first 16 orders with various damping coefficients of the TV damper

Order No	TV Damper Damping Coefficient (Nms/rad)						
	-30% (51.569)	**-20% (58.936)**	**-10% (66.303)**	**0% (73.67)**	**10% (81.037)**	**20% (88.404)**	**30% (95.771)**
	Front end torsional vibration angle amplitudes (degree)						
0.5	0.049174	0.049174	0.049174	0.049174	0.049174	0.049175	0.049175
1.0	0.002462	0.002462	0.002462	0.002462	0.002462	0.002462	0.002462
1.5	0.178299	0.178299	0.178300	0.178301	0.178301	0.178303	0.178304
2.0	0.000084	0.000083	0.000083	0.000083	0.000083	0.000083	0.000083
2.5	0.071896	0.071247	0.070717	0.070286	0.069933	0.069643	0.069402
3.0	0.088890	0.088416	0.088098	0.087875	0.087715	0.087596	0.087506
3.5	0.053955	0.056751	0.059040	0.060922	0.062475	0.063766	0.064847
4.0	0.003034	0.003222	0.003405	0.003580	0.003746	0.003902	0.004049
4.5	0.101645	0.106635	0.111913	0.117402	0.123039	0.128771	0.134555
5.0	0.005253	0.005412	0.005586	0.005772	0.005968	0.006173	0.006384
5.5	0.036259	0.036219	0.036238	0.036306	0.036414	0.036555	0.036721
6.0	0.178817	0.169543	0.161676	0.154988	0.149283	0.144399	0.140204
6.5	0.025274	0.023117	0.021396	0.020000	0.018848	0.017890	0.017083
7.0	0.005412	0.005012	0.004676	0.004393	0.004153	0.003947	0.003770
7.5	0.022877	0.021675	0.020590	0.019617	0.018748	0.017973	0.017281
8.0	0.002548	0.002454	0.002365	0.002281	0.002202	0.002130	0.002062

Table 2.16. Crankshaft front end torsional vibration amplitudes at 2200 rpm for first 16 orders with various hub inertia values of the TV damper

Order No	TV Damper Hub Inertia (kgm^2)						
	-30% (0.0392)	**-20% (0.0448)**	**-10% (0.0504)**	**0% (0.056)**	**10% (0.0616)**	**20% (0.0672)**	**30% (0.0728)**
	Front end torsional vibration angle amplitudes (degree)						
0.5	0.049393	0.049320	0.049247	0.049174	0.049102	0.049030	0.048958
1.0	0.002469	0.002467	0.002464	0.002462	0.002460	0.002457	0.002455
1.5	0.178328	0.178319	0.178310	0.178301	0.178292	0.178283	0.178274
2.0	0.000083	0.000083	0.000083	0.000083	0.000083	0.000083	0.000084
2.5	0.069458	0.069732	0.070008	0.070286	0.070566	0.070848	0.071133
3.0	0.085921	0.086563	0.087214	0.087875	0.088546	0.089226	0.089917
3.5	0.058943	0.059590	0.060249	0.060922	0.061608	0.062308	0.063022
4.0	0.003427	0.003477	0.003528	0.003580	0.003633	0.003688	0.003744
4.5	0.111022	0.113096	0.115222	0.117402	0.119634	0.121917	0.124251
5.0	0.005401	0.005523	0.005646	0.005772	0.005899	0.006026	0.006153
5.5	0.034150	0.034900	0.035622	0.036306	0.036942	0.037520	0.038029
6.0	0.152560	0.153884	0.154702	0.154988	0.154733	0.153945	0.152649
6.5	0.021170	0.020840	0.020446	0.020000	0.019510	0.018992	0.018455
7.0	0.004871	0.004712	0.004551	0.004393	0.004238	0.004088	0.003942
7.5	0.022032	0.021188	0.020382	0.019617	0.018890	0.018201	0.017550
8.0	0.002554	0.002458	0.002366	0.002281	0.002200	0.002124	0.002052

Table 2.17. Crankshaft front end torsional vibration amplitudes at 2200 rpm for first 16 orders with various ring inertia values of the TV damper

Order No	TV Damper Ring Inertia (kgm^2)						
	-30% (0.0889)	**-20% (0.1016)**	**-10% (0.1143)**	**0% (0.127)**	**10% (0.1397)**	**20% (0.1524)**	**30% (0.1651)**
	Front end torsional vibration angle amplitudes (degree)						
0.5	0.049695	0.049521	0.049347	0.049174	0.049002	0.048829	0.048657
1.0	0.002482	0.002475	0.002469	0.002462	0.002455	0.002448	0.002442
1.5	0.178396	0.178366	0.178334	0.178301	0.178266	0.178229	0.178190
2.0	0.000082	0.000082	0.000083	0.000083	0.000084	0.000084	0.000085
2.5	0.067356	0.068332	0.069326	0.070286	0.071130	0.071754	0.072039
3.0	0.085853	0.087367	0.088149	0.087875	0.086429	0.083999	0.081002
3.5	0.067287	0.066371	0.064037	0.060922	0.057720	0.054868	0.052522
4.0	0.004436	0.004132	0.003830	0.003580	0.003388	0.003246	0.003142
4.5	0.150074	0.135282	0.124706	0.117402	0.112362	0.108840	0.106335
5.0	0.007118	0.006453	0.006038	0.005772	0.005596	0.005478	0.005395
5.5	0.040944	0.038533	0.037136	0.036306	0.035808	0.035509	0.035335
6.0	0.155699	0.154165	0.154186	0.154988	0.156164	0.157499	0.158875
6.5	0.018698	0.019107	0.019555	0.020000	0.020421	0.020815	0.021177
7.0	0.004053	0.004173	0.004288	0.004393	0.004488	0.004573	0.004649
7.5	0.018288	0.018783	0.019227	0.019617	0.019957	0.020255	0.020516
8.0	0.002156	0.002204	0.002245	0.002281	0.002311	0.002337	0.002359

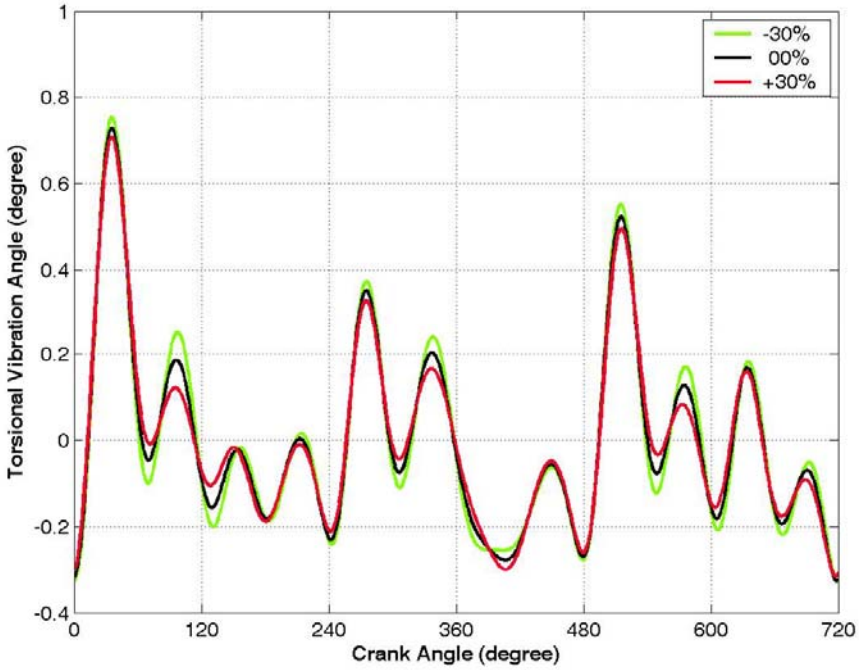

Figure 2.31. Effect of torsional stiffness change on front end torsional vibration at 2200 rpm engine speed

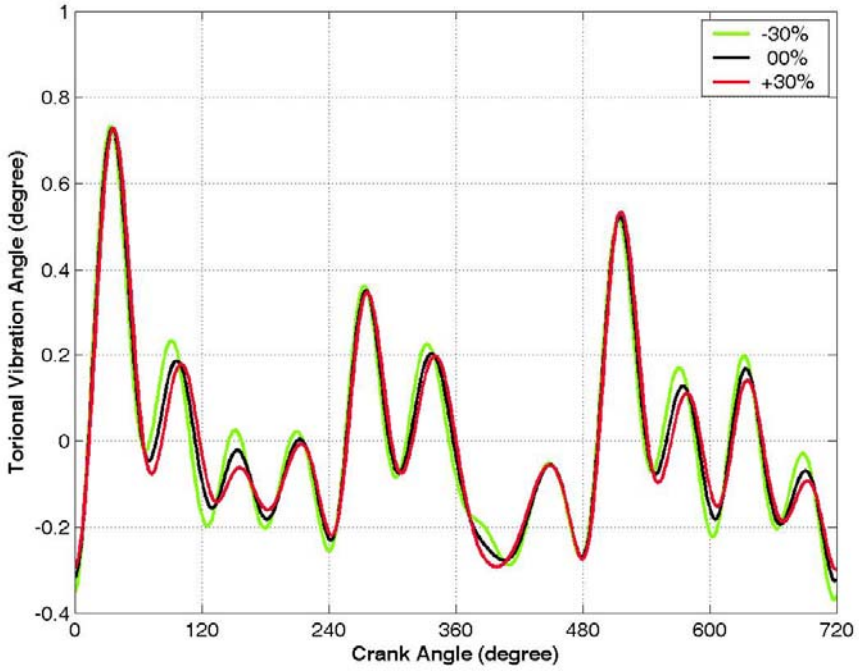

Figure 2.32. Effect of damping coefficient change on front end torsional vibration at 2200 rpm engine speed

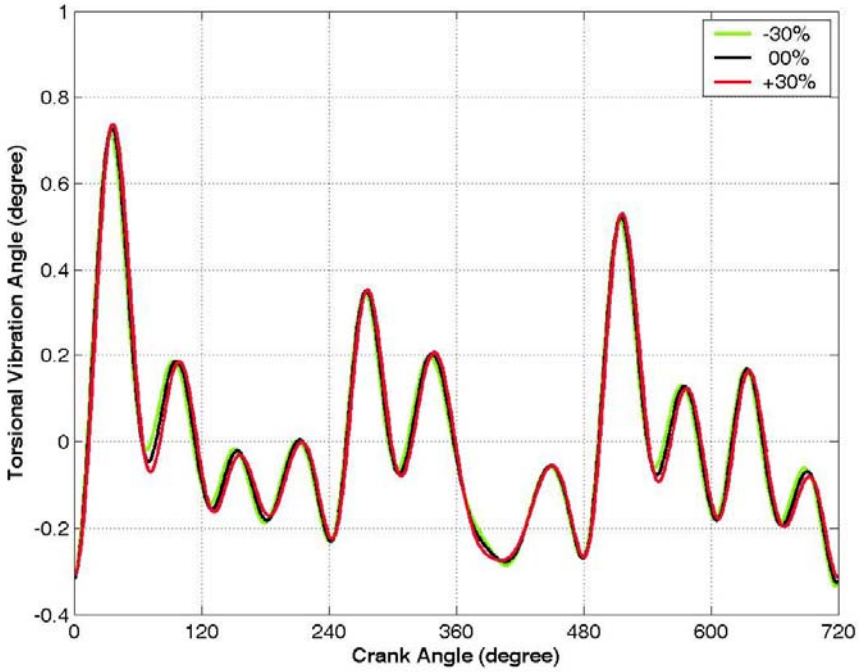

Figure 2.33. Effect of hub inertia change on front end torsional vibration at 2200 rpm engine speed

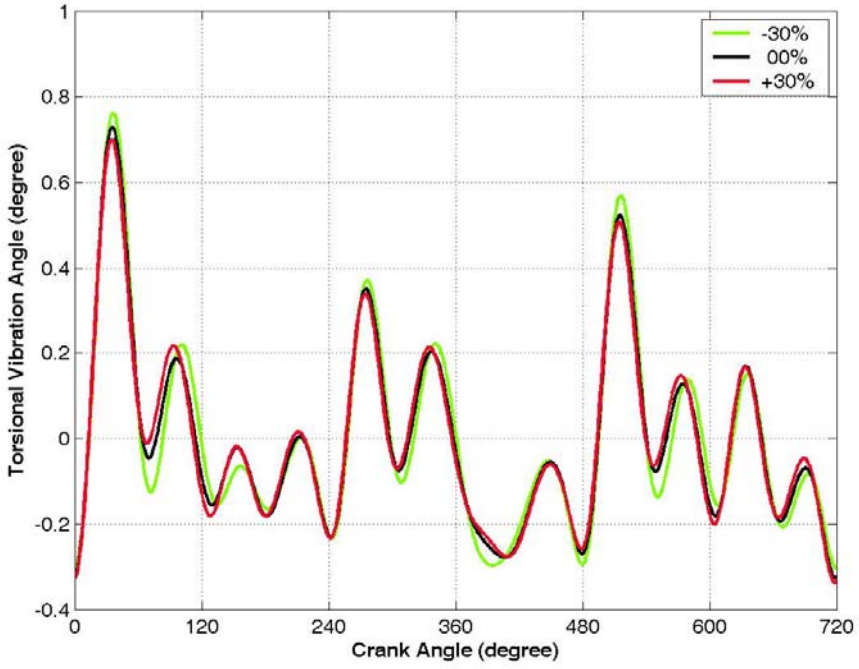

Figure 2.34. Effect of ring inertia change on front end torsional vibration at 2200 rpm engine speed

2.6.2. Effect of Cylinder Misfire on Forced Torsional Vibration

Misfiring cylinder is a cylinder with a cylinder gas pressure curve peak pressure that is significantly lower than the normal one. Common causes of misfire are faulty fuel injectors, faulty valves and faulty piston rings. A misfiring cylinder in an internal combustion engine results in decreased engine performance, increased exhaust emissions and increased cranktrain noise and vibration. In this part of the study, the effect of cylinder misfire on front end torsional vibration characteristics is investigated for 20%, 50% and 80% misfire conditions. For 20% misfire, peak firing pressure (PFP) of a specific cylinder decreases by 20%, for 50% misfire, PFP decreases by 50% and so on. Analyses are carried at an engine speed of 2000 rpm and the results are given in Figures 2.35-2.40. From these figures it is seen that as the misfire ratio increases, torsional vibration angle amplitude at crankshaft front end increases gradually.

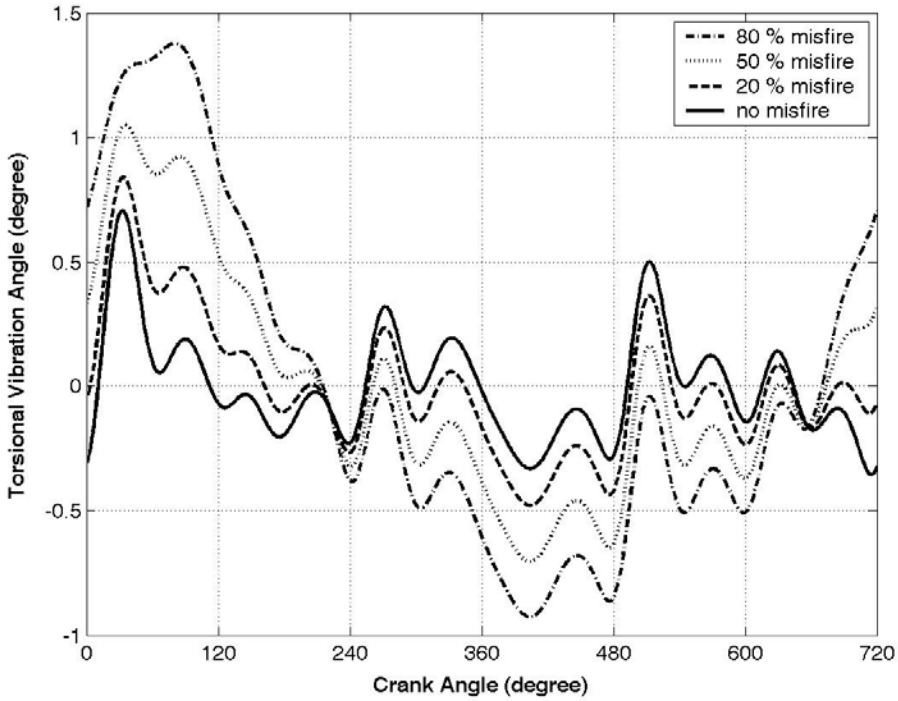

Figure 2.35. Front end torsional vibration when cylinder # 1 misfires at 2000 rpm

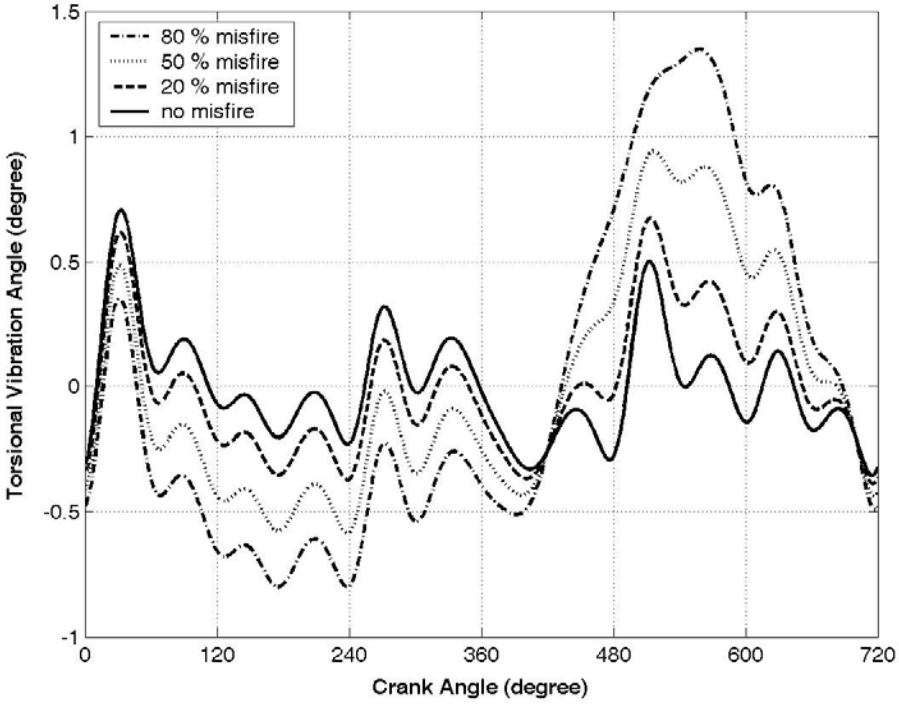

Figure 2.36. Front end torsional vibration when cylinder # 2 misfires at 2000 rpm

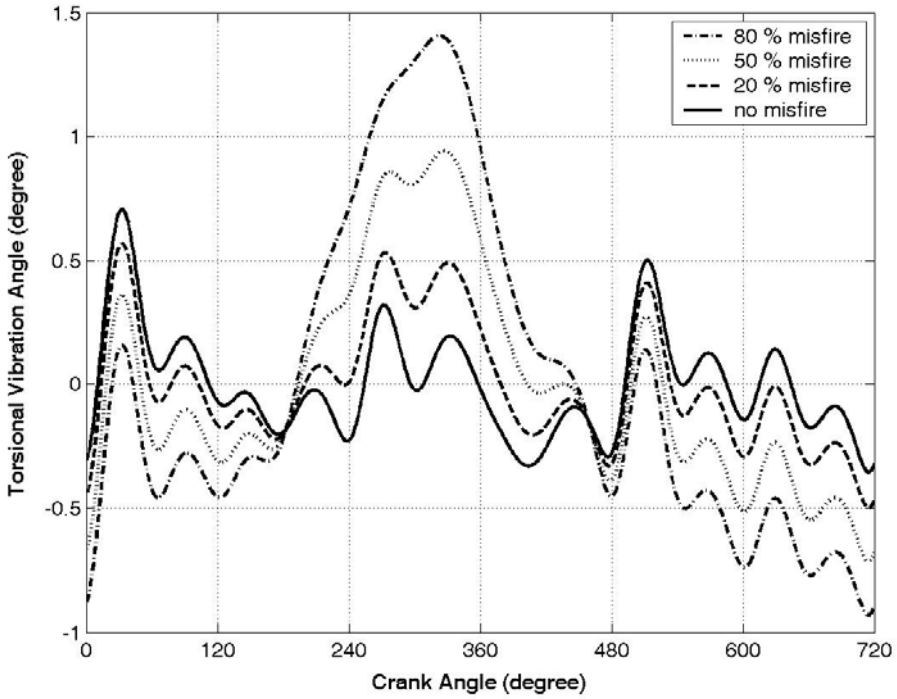

Figure 2.37. Front end torsional vibration when cylinder # 3 misfires at 2000 rpm

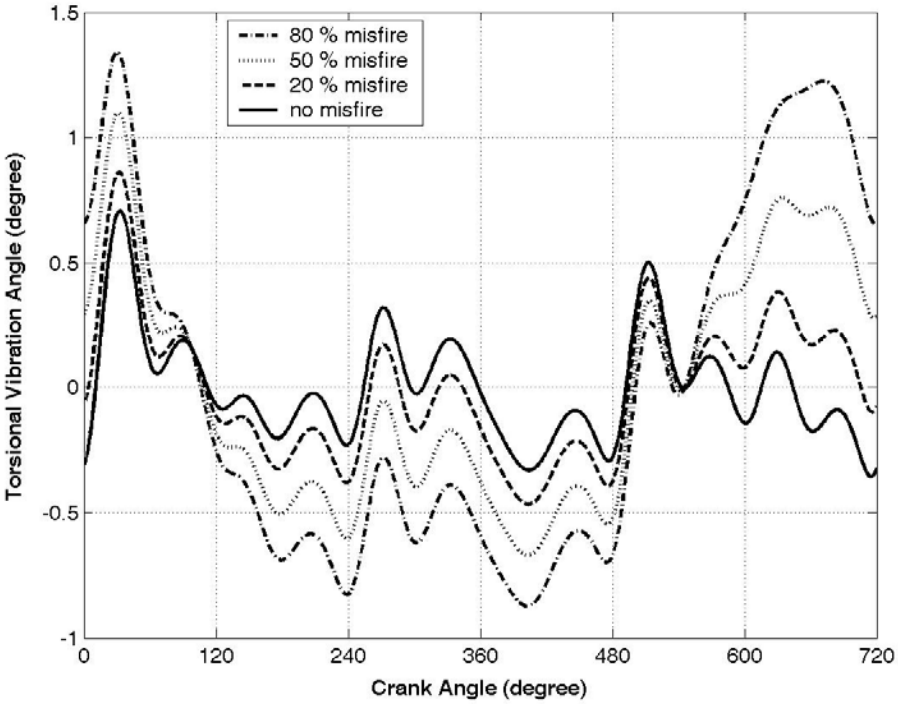

Figure 2.38. Front end torsional vibration when cylinder # 4 misfires at 2000 rpm

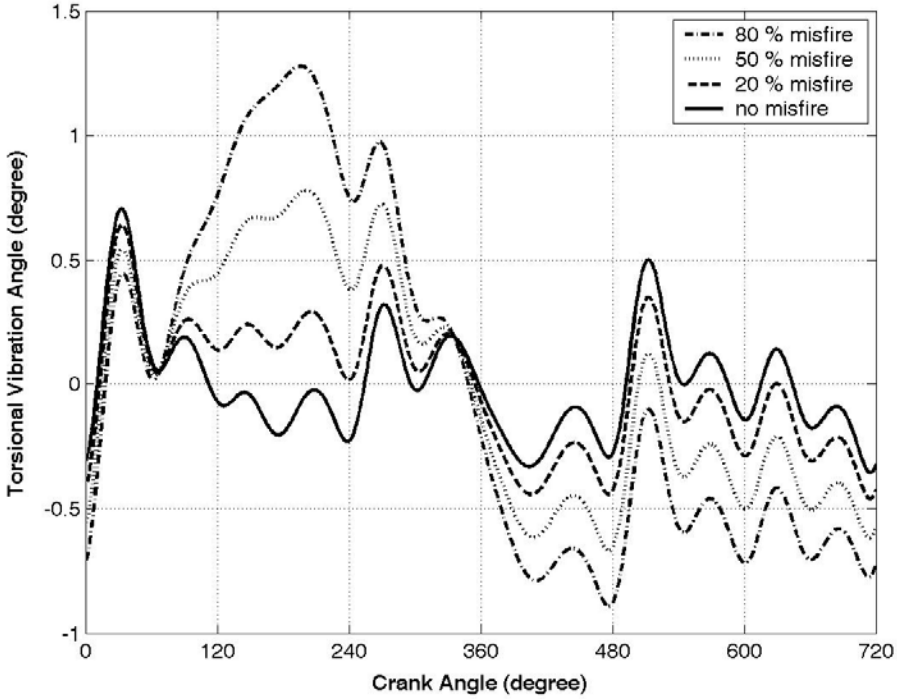

Figure 2.39. Front end torsional vibration when cylinder # 5 misfires at 2000 rpm

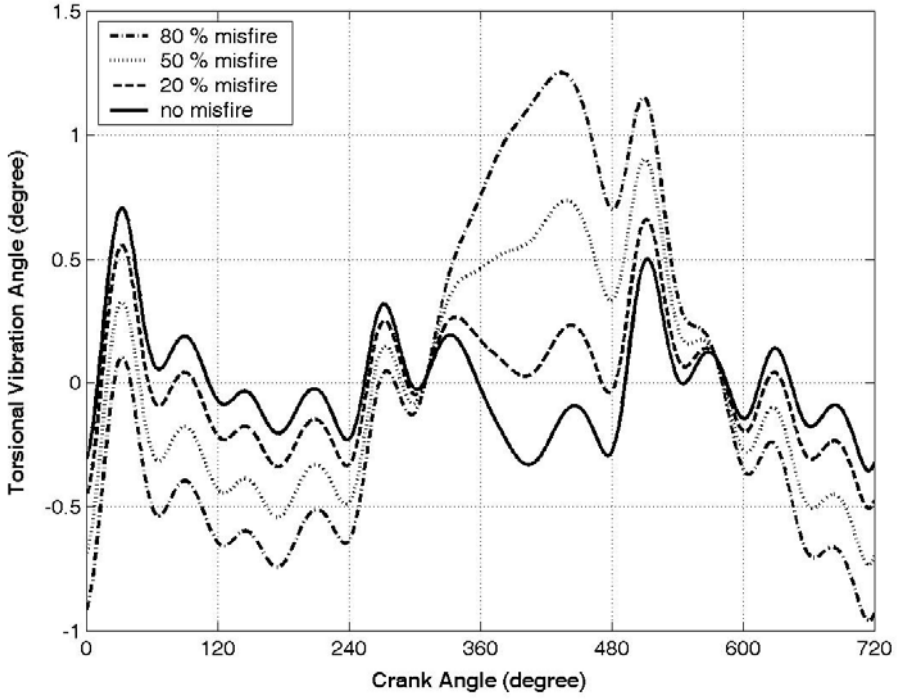

Figure 2.40. Front end torsional vibration when cylinder # 6 misfires at 2000 rpm

3. CLASSICAL FORCE AND STRESS ANALYSIS OF CRANKSHAFT SYSTEM

3.1. Introduction

Due to geometric complexity of a crankshaft and its bearings along with complexity of loading, calculation of stresses in this component is difficult. Since 1960's calculation procedures have been developed to determine safety factors [30]. These procedures have undergone continuous refinement through theoretical and experimental investigations. Following points are considered in the analyses:

- Stress concentration at the most stressed region of the crankshaft with the aid of stress concentration coefficients,
- Equivalent stress resulting from bending and torsion (using nominal stresses),
- Endurance limit of the component.

The necessary load data for the evaluation of nominal stresses are bending and torsional vibration moments and compression forces. Gas and mass forces are considered for the computation of nominal stresses. The procedure is explained in the following sections.

3.2. Force Analysis of Crankshaft System

The forces in an internal combustion engine may be divided into two categories. First one is the pressure forces which are determined by gas pressure inside the cylinders. The second one is the inertia forces which are caused by the acceleration and deceleration of moving engine components. Inertia forces and moments depend only on the engine speed while pressure forces and moments depend mainly on the load applied to the engine. There are also gravitational forces but they are negligible compared to gas pressure and inertia forces.

3.2.1. Pressure Forces

Gas pressure forces in cylinders are acting on piston head, cylinder head and on side walls of cylinder. The gas pressure force is equal to:

$$F_P = \frac{\pi D^2}{4} \cdot P(\theta) \tag{3.1}$$

where D is cylinder diameter, $P(\theta)$ is the difference between gas pressure inside the cylinder and pressure in the crankcase. The gas forces are transmitted to crankshaft through piston and connecting rod. The gas pressure force mainly depends on the maximum combustion pressure and this depends on the compression ratio, compression end pressure, combustion process, mixture and the load of the engine.

3.2.2. Inertia Forces

Inertia forces are oriented in opposite direction of acceleration. To determine inertia forces, the masses and the centers of gravities of moving parts must be known. To determine the mass and the center of gravity of complicated parts, they can be dissected into simple geometric parts or a CAD program may be used to calculate them. In this study Pro ENGINEER is used to calculate masses and centers of gravities of all crank throws and all parts in the system.

Moving engine parts carry out following motions:

- Crank throw and the part of the connecting rod near the piston rotate around the crankshaft axis,
- Piston and the part of the connecting rod near the piston have a reciprocating motion,
- Middle part of the connecting rod with the center of gravity has a revolution path similar to an ellipse.

The moment of inertia is a function of both mass and position and therefore in the case of a crank-slider mechanism where the geometry changes the moment of inertia will also vary. Therefore, inertia forces are investigated in three parts: inertia force of the connecting rod, inertia force of the rotating parts, inertia force of the reciprocating parts.

3.2.2.1. Inertia Force of the Connecting Rod

The connecting rod has a planar motion. Describing the motion of the connecting rod is more complex then the other parts of the crank-slider mechanism since it undertakes both translational and rotational motion. In order to obtain the inertia forces produced by the connecting rod, this motion can be considered as resulting from the translation of its center of gravity and a rotation about this center.

Since the whole connecting rod translates according to the translation of its center of gravity, the inertia force determined by this motion will be:

$$F_{i_{cr}} = -m_{cr}\, a_{G_{cr}} \tag{3.2}$$

Rotational motion of the connecting rod around its center of gravity produces a normal force dF_N and a tangential force dF_T on the infinitesimal element dm. Integrating for the whole con-rod, the resultant of these forces are zero since they represent the static moment around the center of gravity.

$$F_{i_{N_{cr}}} = -\omega_{cr}^{\,2} \int_{con-rod} x\, dm = 0 \tag{3.3}$$

$$F_{i_{T_{cr}}} = -\alpha_{cr} \int_{con-rod} x\, dm = 0 \tag{3.4}$$

The resultant tangential force is zero but tangential forces acting on the mass elements of the connecting rod yield a turning moment about the center of gravity:

$$M_{i_{T_{cr}}} = -\alpha_{cr} \int_{con-rod} x^2\, dm = -I_{cr}\, \alpha_{cr} \tag{3.5}$$

where I_{cr} represents the mass moment of inertia of the connecting rod about its center of gravity.

Thus on the connecting rod, an inertia force corresponding to the translational motion of the center of gravity and a moment corresponding to the rotation about this center act.

The same result may be obtained considering an equivalent system of two concentrated masses, m_A and m_B, located at the piston and crank pin side respectively. For a dynamically equivalent model of the connecting rod, three requirements must be satisfied:

1. The total mass of the model must be equal to that of the original body.
2. The center of gravity must be the same as for the original body.
3. The moment of inertia must be equal to that of the original body.

So, the conditions that must be fulfilled by this system in order to be dynamically equivalent to the real con-rod can be expressed by the following equations:

$$m_A + m_B = m_{cr} \tag{3.6}$$

$$x_A\, m_A = x_B\, m_B \tag{3.7}$$

$$x_A^{\,2}\, m_A + x_B^{\,2}\, m_B = I_{cr} \tag{3.8}$$

This is a system of three equations with four unknowns: m_A, m_B, x_A, x_B and consequently has infinitely many solutions. An exact dynamic model may be constructed using two point masses. For general connecting rod designs only one of these point masses may be placed at either joint, thus the motion of the other will not be a pure rotation or translation. Our interest is to place the two masses exactly in the articulations of the con-rod with the piston pin and with the crankpin. Placing the concentrated masses in these positions leaves in only two unknowns: the masses themselves. Now we have a system of three equations with two unknowns. In order to solve it, one equation should be eliminated. A common approximation is to consider a statically equivalent model in which the last

requirement is not fulfilled. That is the conservation of mass and position of center of gravity are respected and conservation of the mass moment of inertia is neglected. Proceeding in this manner an error is introduced which depends upon the difference between the mass moment of inertia of two-mass system and the real con-rod. In order to avoid this error a correction couple should be considered:

$$\Delta M_{cr} = m_{cr}\,\alpha\left(I_{cr} - I_{eq}\right) \tag{3.9}$$

where $I_{eq}=m_{cr\_tr}\,l_A^2+m_{cr\_r}\,l_B^2$.

Detailed error analysis of the statically equivalent model compared to dynamically equivalent model and distributed models including manufacturing tolerances are given in [58]. According to this study, the error associated with this approximation is small for medium speed 6 cylindered in-line engines.

3.2.2.2. Inertia Forces of the Rotating Parts

In order to determine the forces acting on the elements of the crank, one should integrate for the whole volume of the part. Thus, for the crank web:

$$F_{i_{web}} = \omega^2 \int_{web} r_x\, dm \tag{3.10}$$

The integral in (3.10) represents the static moment of the crank-web and may be expressed as the product of total mass of the web and the distance from its center of gravity to the axis of rotation:

$$S_{web} = \int_{web} r_x\, dm = m_{web}\, r_{G_{web}} \tag{3.11}$$

Then the inertia force of the crank-web may be expressed as:

$$F_{i_{web}} = m_{web}\, r_{G_{web}}\, \omega^2 \tag{3.12}$$

In the same manner, the inertia forces of the crank-pin, counterweight and rotating part of the connecting rod are:

$$F_{i_{cp}} = m_{cp}\, r\, \omega^2 \tag{3.13}$$

$$F_{i_{cw}} = m_{cw}\, r_{G_{cw}}\, \omega^2 \tag{3.14}$$

$$F_{i_{cr-r}} = m_{cr-r}\, r\, \omega^2 \tag{3.15}$$

Denoting the rotating mass that consists of the mass of the crank pin, the crank webs, and rotating part of the mass of the connecting rod, as m_R, the rotating inertia force for each cylinder can be written as:

$$F_{i_R} = m_R \cdot r_R \cdot \omega^2 \tag{3.16}$$

where r_R represents the distance from the crankshaft center of rotation to the center of gravity of the rotating mass.

3.2.2.3. Inertia Forces of the Reciprocating Parts

Denoting the reciprocating mass, consisting of mass of the piston, piston rings, piston pin, and reciprocating part of the mass of the connecting rod by m_{TR}, the reciprocating inertia force is:

$$F_{i_{TR}} = -m_{TR}\, a_p \tag{3.17}$$

where a_p is the piston acceleration and given in full form by equation (1.14) and in simplified form by equation (1.15).

3.2.3. Force Resolution at the Crank Train and Main Bearing Forces

The forces acting on the crankshaft assembly are shown schematically on Figure 3.1. The total force acting along the cylinder axis is:

$$F_{TOT} = F_P + F_{i_{TR}} \tag{3.18}$$

Total force, F_{TOT}, decomposes in a component F_{CR} along the con-rod axis and a component F_N normal to the cylinder axis. The values of these forces are given by:

$$F_{CR} = \frac{F_{TOT}}{\cos\beta} = \frac{F_{TOT}}{\sqrt{1-\lambda^2 \sin^2\theta}} \tag{3.19}$$

$$F_N = F_{TOT} \cdot \tan\beta = F_{TOT} \cdot \frac{\lambda \cdot \sin\theta}{\sqrt{1-\lambda^2 \sin^2\theta}} \tag{3.20}$$

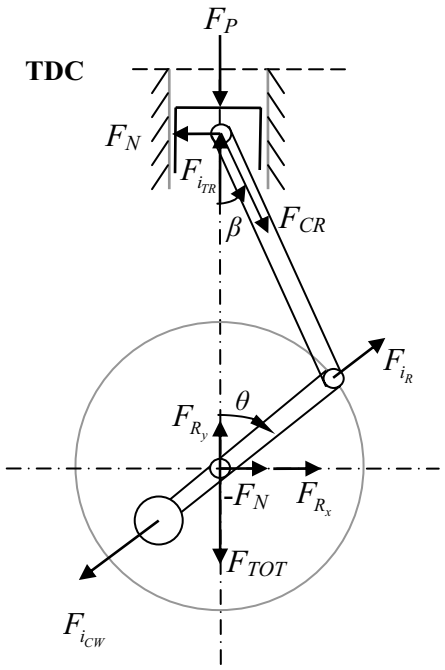

Figure 3.1. Forces acting on crankshaft assembly

If the rotating inertia forces are transformed to the crankshaft axis, following equations are obtained.

$$F_{R_X} = \left(F_{i_R} - F_{CW}\right) \cdot \sin\theta \tag{3.21}$$

$$F_{R_Y} = \left(F_{i_R} - F_{CW}\right) \cdot \cos\theta \tag{3.22}$$

The loading on the main bearings is statically and dynamically indeterminate, but the loading of a main bearing is mostly determined by the forces acting on two adjacent cranks and almost not influenced by forces acting on more distant cranks. So as a reasonable approximation, the forces acting on a main bearing may be calculated taking into account only the forces acting on the adjacent cranks, considering each crank as a statically determined element. The main bearing loads are shown in Figure 3.2.

If all of the forces on a cylinder are transformed to the intersection of cylinder axis and crankshaft rotation axis, following equations are obtained.

$$F_{X_j} = -F_{N_j} + F_{R_X} \tag{3.23}$$

$$F_{Y_j} = F_{TOT_j} - F_{R_Y} \tag{3.24}$$

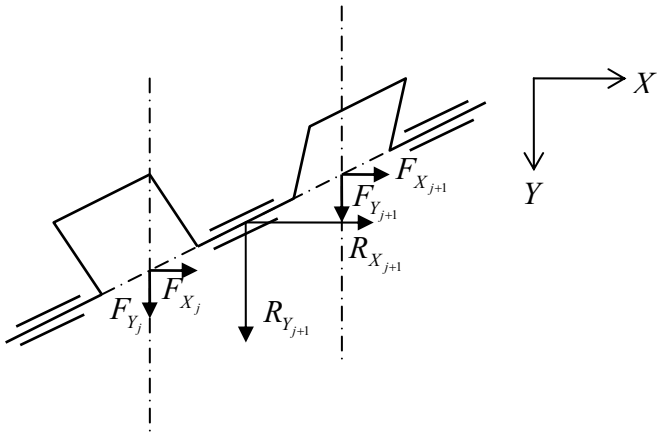

Figure 3.2. Forces acting on main bearings

Then main bearing loads in *x* and *y*-directions are calculated as:

$$R_{X_{j+1}} = \frac{1}{2} \cdot \left(F_{X_j} + F_{X_{j+1}} \right) \tag{3.25}$$

$$R_{Y_{j+1}} = \frac{1}{2} \cdot \left(F_{Y_j} + F_{Y_{j+1}} \right) \tag{3.26}$$

The magnitude of the main bearing load is:

$$R_{j+1} = \sqrt{R^2{}_{X_{j+1}} + R^2{}_{Y_{j+1}}} \tag{3.27}$$

Based on this formulation, main bearing loads are calculated for 7.3 L in-line six cylinder diesel engine with the following specifications:

Bore diameter	: 112 mm
Stroke	: 124 mm
Swept volume	: 7.3 L
Peak firing pressure	: 180 bar
Connecting rod length	: 222 mm
Cylinder spacing	: 134 mm
Mass of complete piston	: 2.79 kg
Connecting rod reciprocating mass	: 0.77 kg
Reciprocating mass (total per cylinder)	: 3.55 kg
Connecting rod rotating mass	: 1.89 kg
Unbalance of crank throw	: 207.7 kg.mm
Unbalance of counterweight	: 102.4 kg.mm

Same crankshaft is also modeled in ADAMS/Engine environment using rigid crankshaft model to see the accuracy of the analytical formulation. Analyses are carried out at an engine speed of 2400 rpm. Comparison of the analytical results with the ADAMS's results for crankshaft main bearings in engine cross and vertical directions are given in Figures 3.3-3.9.

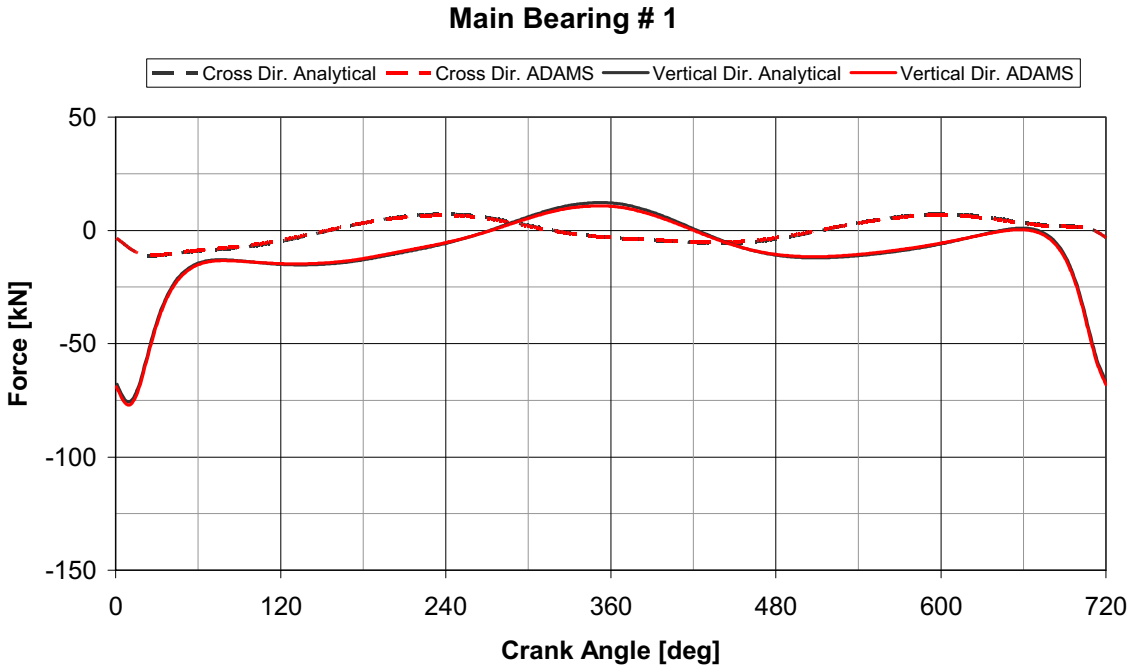

Figure 3.3. Comparison of forces acting on main bearing #1

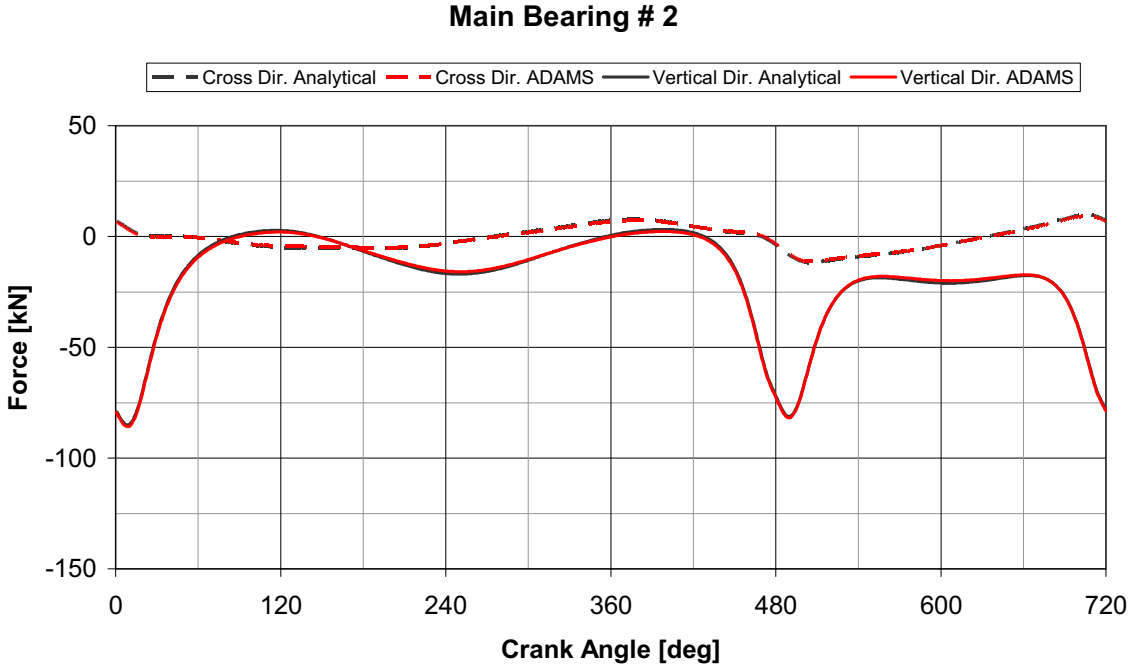

Figure 3.4. Comparison of forces acting on main bearing #2

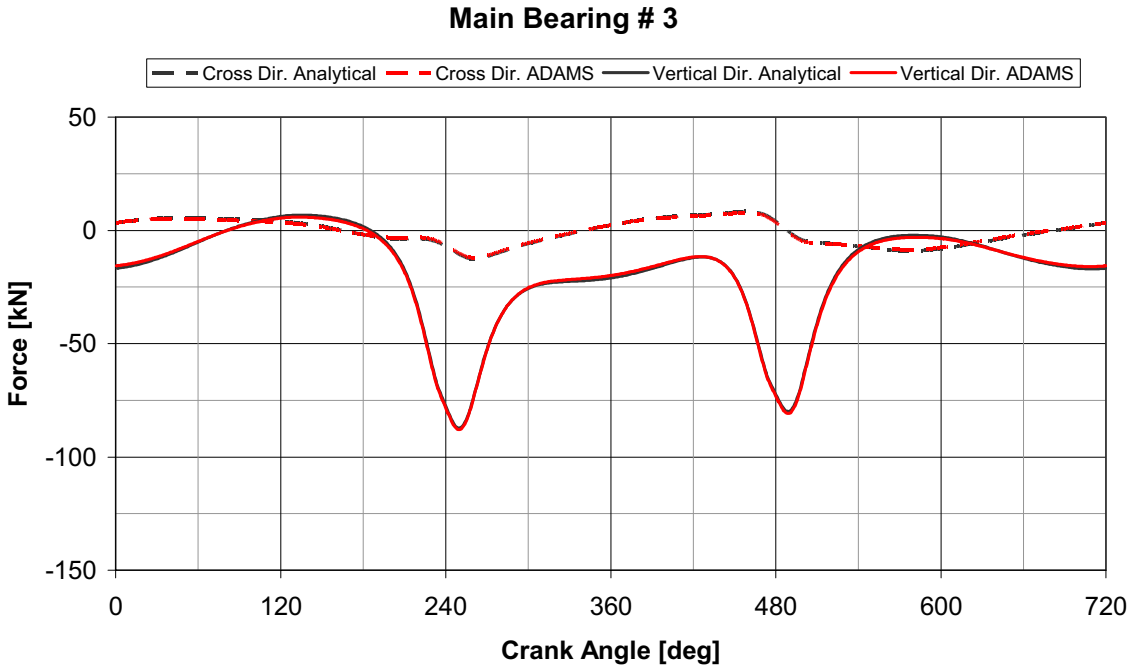

Figure 3.5. Comparison of forces acting on main bearing #3

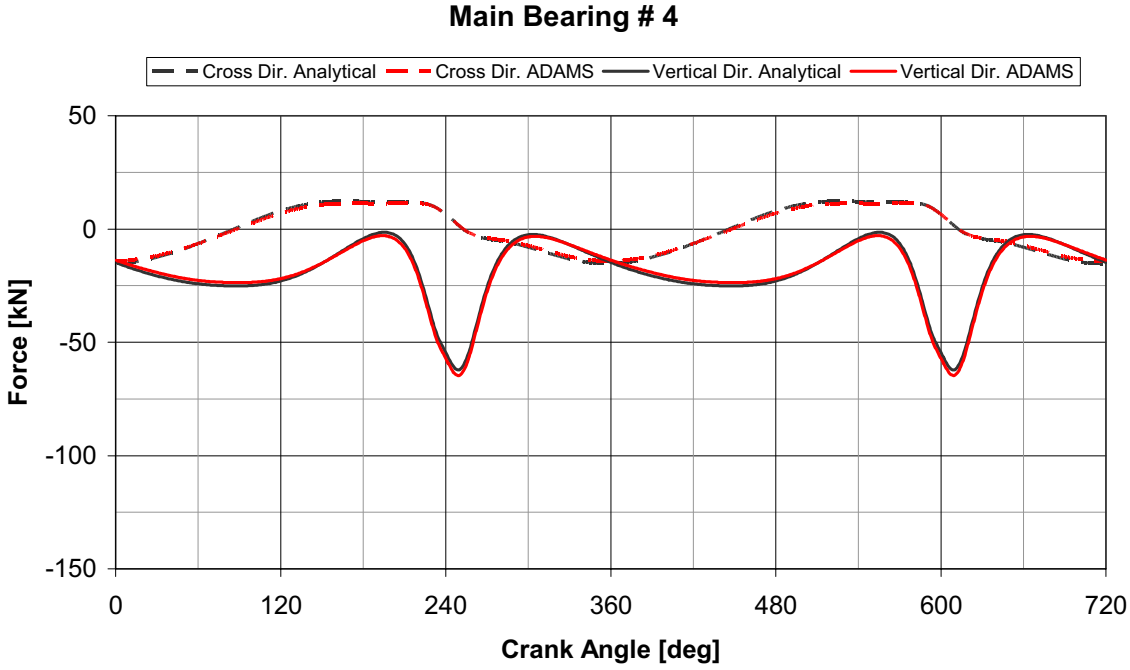

Figure 3.6. Comparison of forces acting on main bearing #4

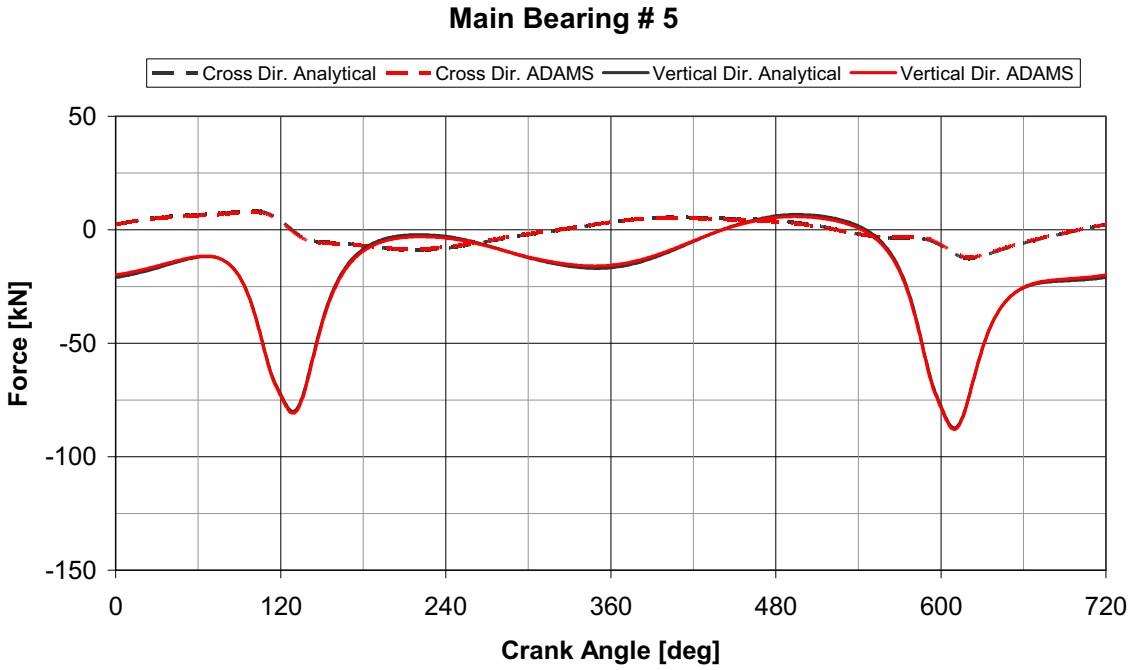

Figure 3.7. Comparison of forces acting on main bearing #5

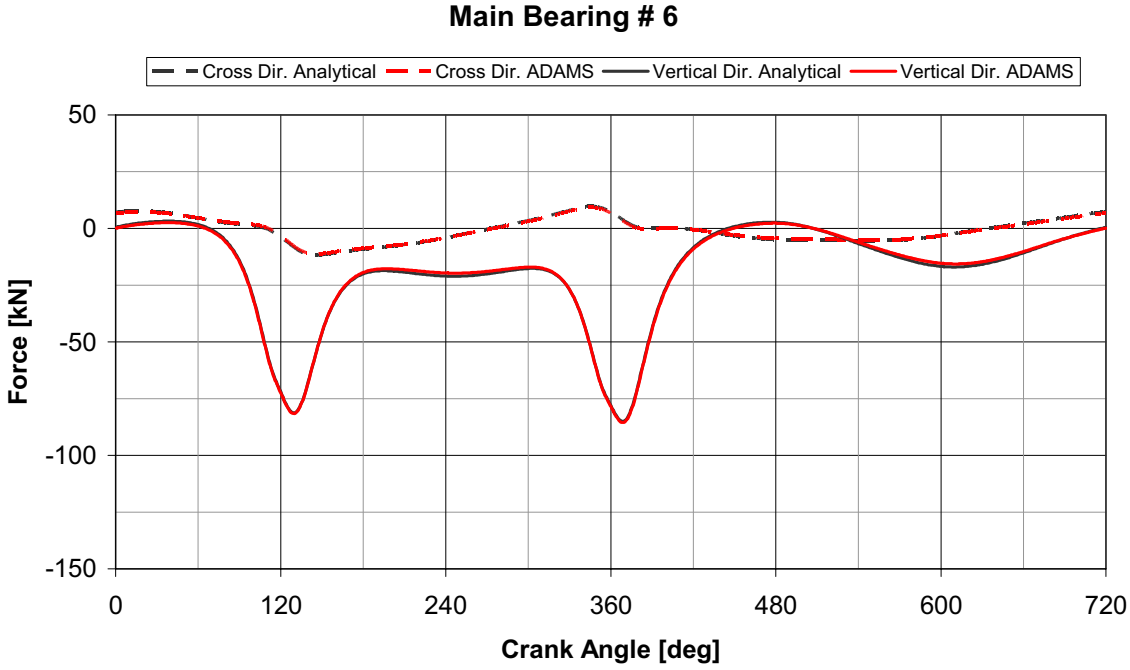

Figure 3.8. Comparison of forces acting on main bearing #6

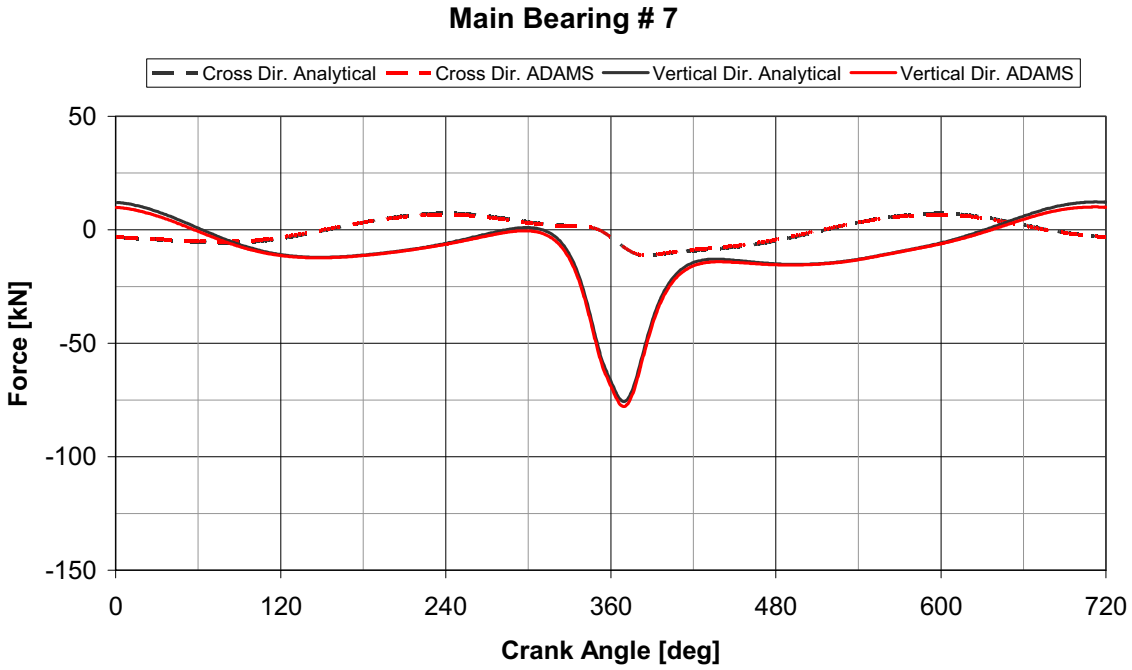

Figure 3.9. Comparison of forces acting on main bearing #7

3.3. Stress Analysis of Crankshaft System

The principle is based on the computation of stresses in the web cross section. By using stress concentration factors, the local stress values in the fillet radius are determined [59].

3.3.1. Nominal Stresses due to Bending Moments and Radial Forces

The nominal stress amplitudes and the nominal mean stresses which are determined from the maximum and minimum bending moment and the according radial forces are related to the crank web cross section area passing from the crankpin fillet to the main journal fillet as shown in Figure 3.10 (Projection of the cross-section A-A on a plane which is perpendicular to the crank throw direction). Consequently the nominal stresses are obtained from the following formulas:

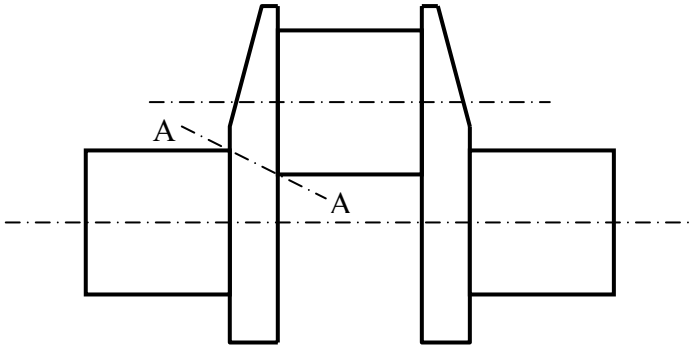

Figure 3.10. Crankthrow and cross section A-A for crankshaft stress analysis

$$\sigma_{BN} = \frac{M_B}{Z} = F \cdot \frac{d}{Z} \tag{3.28}$$

$$\sigma_{QN} = \frac{F}{A} \tag{3.29}$$

where

σ_{BN}	: nominal bending stress related to the normal crank web cross- section
σ_{QN}	: nominal tensile or compressive stress in the normal crank web cross section due to radial forces in the crank web
$M_B = F \cdot d$	: bending moment in the center of the crank web due to the bearing force component L
F	: bearing force component acting in the crank throw direction
Z, A	: sectional modulus and cross section area of the projected web cross section respectively
d	: axial distance between bearing center and web center.

It should be noticed that the bearing force component F is equal with the radial force in the web. In the evaluation of the bearing force components F the following forces are taken into account:

- Gas forces according to cylinder pressure diagram.
- Reciprocating inertia forces due to piston and connecting rod reciprocating portion.
- Centrifugal forces due to the connecting rod rotating portion, crankpin, crank webs and due to the counterweights.

To ascertain the stress amplitudes and the mean stresses in each fillet, the bending moments in the center of each crank web as well as the radial forces are computed for a complete load cycle. These computations are based on a statically determinate support of each crank throw.

In order to provide the necessary data for the evaluation of the maximum and minimum fillet stresses, computations of bearing loads should be carried out for a complete load cycle at different engine operating conditions.

3.3.2. Actual Fillet Stresses due to Bending Moments and Radial Forces

With the applied calculation method for the evaluation of fillet stresses, based on the stress concentration factors the actual maximum fillet stresses are obtained from the following formulas:

Crankpin fillet:

$$\sigma_c = \alpha \cdot \sigma_{BN} \tag{3.30}$$

Main journal fillet:

$$\sigma_j = \beta_B \cdot \sigma_{BN} + \beta_Q \cdot \sigma_{QN} \tag{3.31}$$

where

σ_c, σ_j : maximum stress in crankpin and main journal fillets respectively

α : stress concentration factor for the crankpin fillet

β_B, β_Q : stress concentration factors for the main journal fillet

In order to ascertain the maximum and minimum fillet stresses and then the fillet stress amplitudes and the mean fillet stresses, above fillet stress calculations have to be carried out for a complete load cycle. With the maximum and minimum fillet stresses (σ_{max} , σ_{min}) occurring during one load cycle, the stress amplitude and the mean stress for this operating condition are obtained from the following formulas:

$$\sigma_a = \frac{\sigma_{\max} - \sigma_{\min}}{2} \tag{3.32}$$

$$\sigma_m = \frac{\sigma_{\max} + \sigma_{\min}}{2} \tag{3.33}$$

3.3.3. Combined Stresses for Bending and Torsion

For a cursory evaluation of a crankshaft design e.g. in an early design stage when a torsional vibration calculation and consequently torsional stresses are not yet available, the safety factors are determined only with the bending stresses according to chapter 3.3.2. In this level of computations the additional torsional stresses are roughly taken into account by the assessment of accordingly high required safety factors which include an allowance for the additional torsional stresses and which are available from experience. In a final level of computations, however, a more precise evaluation of torsional stresses has to be performed.

Evaluation of the effect of additional torsional stresses is based on combined stresses due to bending and due to torsion which in general are determined according to the energy of distortion theory.

$$\sigma_C = \sqrt{\left(\sigma_a\right)^2 + 3 \cdot \left(C \cdot \sigma_T\right)^2} \tag{3.34}$$

where

σ_C : combined stress

σ_a : fillet stress amplitude due to bending according to chapter 3.3.2

σ_T : fillet stress amplitude due to torsion (nominal torsional stress amplitude in the crankpin or main journal times stress concentration factor in torsion).

In this evaluation of combined stress amplitude it is assumed that the maximum and minimum bending stresses occur simultaneously with the maximum and minimum torsional stresses. This assumption is probably too extreme which tends to yield higher than actual combined stresses.

In general the coefficient C in above formula for the combined stress is set equal unity (C = 1). This assessment is correct if the bending fatigue strength is $\sqrt{3}$ times the fatigue strength in torsion. If the actual ratio of these fatigue strengths should considerably differ from this figure, a correction of the torsional stresses has to be performed by the introduction of

$$C = \frac{\sigma_{fB}}{\sqrt{3} \cdot \sigma_{fT}} \tag{3.35}$$

where σ_{fB} and σ_{fT} are the actual fatigue strength data in bending and torsion.

3.3.4. Stress Concentration Factors

For a first assessment of crankshaft strength the stress concentration factors can be calculated according to the FVV (“Forschungsvereinigung Verbrennungskraftmaschinen”, European Automotive Industry) method. This method is derived from measurements on cranks with simple rectangular crank webs. The final strength analysis is usually performed with stress concentration factors determined by a FEM calculation.

3.3.5. Results

The main dimensions of the crankshaft as well as stress concentration factors for bending and torsion, each for both the crank pin and the main journal fillet are given in Table 3.1. These data are for 7.3 L in-line six cylinder diesel engine crankshaft [60].

Torsional vibration analysis for 7.3 L engine crankshaft system is carried out at Chapter 2 of the thesis. Torsional vibration stress amplitudes at various sections of the crankshaft are given in Tables 3.2 and 3.3 referred to the crank pin and main journal diameter, respectively. These stress amplitudes are taken into account for the evaluation of the combined stresses.

Table 3.1. Crankshaft dimensions and stress concentration factors [60]

	Unit	Value
Total web thickness	mm	28.50
Maximum web width	mm	111.00
Crankpin diameter	mm	77.00
Web width at crankpin	mm	111.00
Minimum fillet radius at crankpin	mm	2.50
Main journal diameter	mm	88.00
Web width at main journal	mm	106.00
Minimum fillet radius at main journal	mm	2.50
Stress concentration factor – bending - crankpin	-	2.37
Stress concentration factor – bending – main journal	-	2.83
Stress concentration factor – torsion - crankpin	-	2.80
Stress concentration factor – bending – main journal	-	3.08
Stress concentration factor – radial force	-	1.30

Table 3.2. Torsional Vibration Stress Amplitudes referred to the crank pin diameter

	1200 rpm	1480 rpm	1600 rpm	1700 rpm	1850 rpm	2220 rpm	2400 rpm
Front End -Crank 1	8.67	11.69	12.26	13.35	14.95	16.90	19.28
Crank1-Crank2	36.17	32.90	33.21	33.96	33.11	34.62	37.51
Crank2-Crank3	36.92	34.37	35.45	36.59	35.39	36.30	40.04
Crank3-Crank4	35.98	34.33	35.16	36.03	34.75	35.97	39.67
Crank4-Crank5	37.65	37.56	38.73	40.00	39.28	38.88	40.83
Crank5-Crank6	35.06	34.74	35.78	37.02	36.40	36.96	41.56
Crank6-Rear End	31.36	29.57	30.32	31.40	30.61	32.04	35.92

Table 3.3. Torsional Vibration Stress Amplitudes referred to the main pin diameter

	1200 rpm	1480 rpm	1600 rpm	1700 rpm	1850 rpm	2220 rpm	2400 rpm
Front End -Crank 1	5.81	7.83	8.21	8.94	10.02	11.32	12.91
Crank1-Crank2	24.23	22.04	22.25	22.75	22.18	23.20	25.13
Crank2-Crank3	24.74	23.03	23.75	24.52	23.71	24.32	26.83
Crank3-Crank4	24.11	23.00	23.56	24.14	23.28	24.10	26.58
Crank4-Crank5	25.23	25.17	25.95	26.80	26.32	26.05	27.36
Crank5-Crank6	23.49	23.28	23.97	24.80	24.39	24.76	27.85
Crank6-Rear End	21.01	19.81	20.31	21.04	20.51	21.47	24.07

Actual torsional vibration stress amplitudes at the crankpin and main journal fillets can be found using stress concentration factors for torsion given in Table 3.1. Actual stress amplitudes and mean stresses at crank pin and main pin fillets due to bending moments and radial forces are given in Table 3.4. Combined stresses at fillets of the webs can be found using Equation (3.34). Equivalent stresses at crank pin and main pin fillets of the webs are given in Tables 3.5 and 3.6. From these tables it is seen that, maximum combined stress amplitude and maximum mean stresses occur at web 11 and web 8 at 2400 rpm which is the rated speed for this engine. It is also seen that, main pin fillet location is more critical than crank pin fillet location.

Table 3.4. Actual fillet stresses due to bending moments and radial forces

ω [rpm]	Webs with counterweights				Webs w/o counterweights			
	Crankpin fillet		Main pin fillet		Crankpin fillet		Main pin fillet	
	Amp. [Mpa]	Mean [Mpa]	Amp. [Mpa]	Mean [Mpa]	Amp. [Mpa]	Mean [Mpa]	Amp. [Mpa]	Mean [Mpa]
1200	216.6	185.3	276.2	-236.3	216.6	178.0	276.2	-226.9
1480	203.7	167.0	259.7	-212.8	203.7	156.1	259.7	-199.0
1600	205.6	165.5	262.1	-211.1	205.6	152.7	262.1	-194.7
1700	206.3	163.4	263.1	-208.3	206.3	149.0	263.1	-189.9
1850	205.7	158.3	262.3	-201.8	205.7	141.3	262.3	-180.1
2220	214.6	153.5	273.6	-195.7	214.6	128.8	273.6	-164.2
2400	223.6	154.4	285.1	-196.9	223.6	125.7	285.1	-160.3

Table 3.5. Combined stresses at the crank pin fillet of the webs

	2400 rpm		2220 rpm		1850 rpm		1700 rpm		1600 rpm		1480 r
	Amp.	Mean	Amp.	Mean	Amp.	Mean	Amp.	Mean	Amp.	Mean	Amp.
Web1	242.4	155.5	229.7	154.0	218.1	158.6	216.2	163.8	214.0	165.8	211.4
Web2	288.3	169.3	272.5	168.6	261.0	173.8	264.0	178.7	261.2	180.8	258.8
Web3	288.3	143.6	272.5	146.6	261.0	158.4	264.0	165.6	261.2	169.2	258.8
Web4	296.2	134.0	277.6	137.5	267.9	153.2	272.1	160.7	268.0	164.3	263.2
Web5	296.2	161.2	277.6	160.8	267.9	169.1	272.1	174.2	268.0	176.2	263.2
Web6	295.0	167.6	276.6	166.6	265.9	168.7	270.3	172.3	267.1	173.9	263.1
Web7	295.0	167.6	276.6	166.6	265.9	168.7	270.3	172.3	267.1	173.9	263.1
Web8	298.7	172.3	285.7	167.4	280.4	165.7	283.2	170.0	278.5	172.0	273.3
Web9	298.7	147.2	285.7	145.1	280.4	149.5	283.2	156.2	278.5	159.7	273.3
Web10	301.0	130.7	279.6	134.9	271.1	144.2	273.5	151.6	269.0	155.4	264.3
Web11	301.0	158.5	279.6	158.6	271.1	160.9	273.5	165.8	269.0	168.0	264.3
Web12	283.5	157.3	265.0	157.2	253.7	162.0	256.4	167.1	252.8	169.4	249.1

Table 3.6. Combined stresses at the main pin fillet of the webs

	2400 rpm		**2220 rpm**		**1850 rpm**		**1700 rpm**		**1600 rpm**		**1480 r**	
	Amp.	Mean	Amp.	Mean	Amp.	Mean	Amp.	Mean	Amp.	Mean	Amp.	
Web1	293.3	197.3	280.2	195.9	267.7	201.9	267.3	208.5	265.8	211.2	263.0	
Web2	315.0	203.4	300.3	202.3	287.7	208.6	289.7	215.0	287.8	217.8	285.1	
Web3	315.0	168.2	300.2	172.1	287.7	187.7	289.7	197.2	287.8	202.0	285.1	
Web4	319.0	163.9	302.8	168.0	291.2	185.3	293.8	195.0	291.2	199.8	287.3	
Web5	319.0	199.8	302.8	198.8	291.2	206.5	293.8	213.0	291.2	215.7	287.3	
Web6	318.4	202.6	302.3	201.4	290.2	206.3	292.9	212.2	290.7	214.7	287.2	
Web7	318.4	202.6	302.3	201.4	290.2	206.3	292.9	212.2	290.7	214.7	287.2	
Web8	320.2	204.8	306.9	201.8	297.5	205.0	299.4	211.2	296.4	213.9	292.3	
Web9	320.2	169.9	306.8	171.4	297.5	183.7	299.4	193.0	296.4	197.8	292.4	
Web10	321.5	162.4	303.8	166.8	292.8	181.4	294.5	191.0	291.7	195.9	287.9	
Web11	321.5	198.6	303.8	197.9	292.8	202.9	294.5	209.3	291.7	212.1	287.8	
Web12	312.7	198.1	296.6	197.3	284.2	203.4	286.0	209.9	283.6	212.7	280.4	

In traditional stress analyses, some simplifications are made regarding the calculation of crankshaft system forces and stresses.

- Crankshaft is assumed to be a rigid structure and analyses are based on each single crank throw. Therefore, statically determinate system is used for the crankshaft system boundary conditions, the connection of crankshaft to bearings.
- No bending vibration effect is considered which can lead considerable errors for the crankshaft systems with heavy flywheels.
- Connecting rod mass is partitioned into two masses, one rotating with the crankshaft and other reciprocating with the piston.
- Bearings are considered as only constraining parts and hydrodynamic oil film pressure in the bearings are not considered.
- Flywheel gyroscopic effects are not considered.
- Maximum torsional and bending stresses are assumed to occur at the same time.

These simplifications affect the accuracy of the obtained stresses at the main bearing and pin bearing fillet locations. In the next chapter, an advanced crankshaft dynamic analysis is introduced which eliminates the above deficiencies and takes into account axial, bending and torsional vibrations of the crankshaft.

4. DYNAMIC ANALYSIS OF CRANKSHAFT SYSTEM USING ADAMS

4.1. Introduction

Simple analytical crankshaft stress calculations are based on superposition of torsional and bending loading. Make some approximations, and use tabulated empirical formulas; their accuracy is limited. Moreover, they do not consider the effect of bending and axial vibrations of the crankshaft, and flywheel gyroscopic effects. More detailed calculation methods are needed to achieve more accurate results, which allow a design that is nearer to the mechanical limit.

With increasing power of modern computers, the use of simulation in development stage has increased. However, it is necessary to evaluate the efficiency of the different CAE tools and to check which kind of simulation matches the design target best. Often, combinations of different simulation techniques are used to get better results. A good example is the combination of nonlinear Multibody System Simulation (MSS) with linear Finite Element Analysis (FEA). The global dynamics of continuous structures, represented by a large number of degrees of freedom is reduced, using FEA. The global dynamics of several parts, interacting with each other then become possible to be calculated by MSS. A typical example for such a simulation is the interaction between rotating crankshaft and engine block. Besides the structural deformations of crankshaft, the influence of the gyroscopic effects, caused by the rotation of crankshaft and flywheel, is considered combining FEA and MSS. Nonlinear hydrodynamics of bearings is taken into consideration.

In this study ADAMS/Engine is used to account for the interaction of crankshaft system components with each other and MSC/Nastran is used to include crankshaft flexibility into analyses. With the usage of a finite element program, the large number of degree of freedoms of a flexible structure can considerably be reduced and be used in the dynamic analysis. In this study mesh reduction of the crankshaft system is performed using “Component Mode Synthesis” technique.

In subsequent sections, details of modeling crankshaft system in ADAMS environment are introduced first. Then, dynamic analysis of the crankshaft system, which represents the calculation of forces, displacements and stresses on the crankshaft over a complete engine cycle (two revolutions of the crankshaft) under steady state conditions, is studied using ADAMS/Engine taking coupled axial, torsional and bending vibrations into consideration through beam and flexible crankshaft models. Effects of crankshaft system components on the stress and vibration characteristics of the crankshaft are investigated.

4.2. Modeling Crankshaft System Using ADAMS

4.2.1. Crankshaft Model Descriptions in ADAMS

A crankshaft consists of four kinds of parts: main pin, crank pin, web and shaft sections. In ADAMS, main parts, pin parts and shaft sections are represented simply as cylinders defined by their diameter and length. The Figures 4.1 and 4.2 show the inner design scheme of the crankshaft and the geometry of web parts, respectively [61].

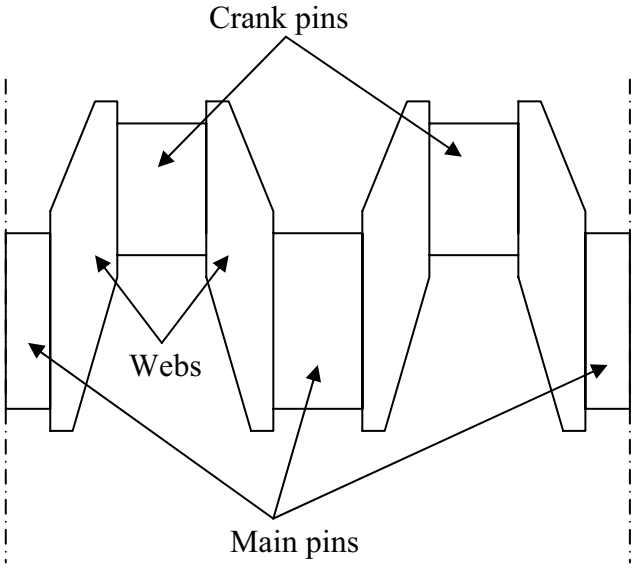

Figure 4.1. Crankshaft design scheme [61]

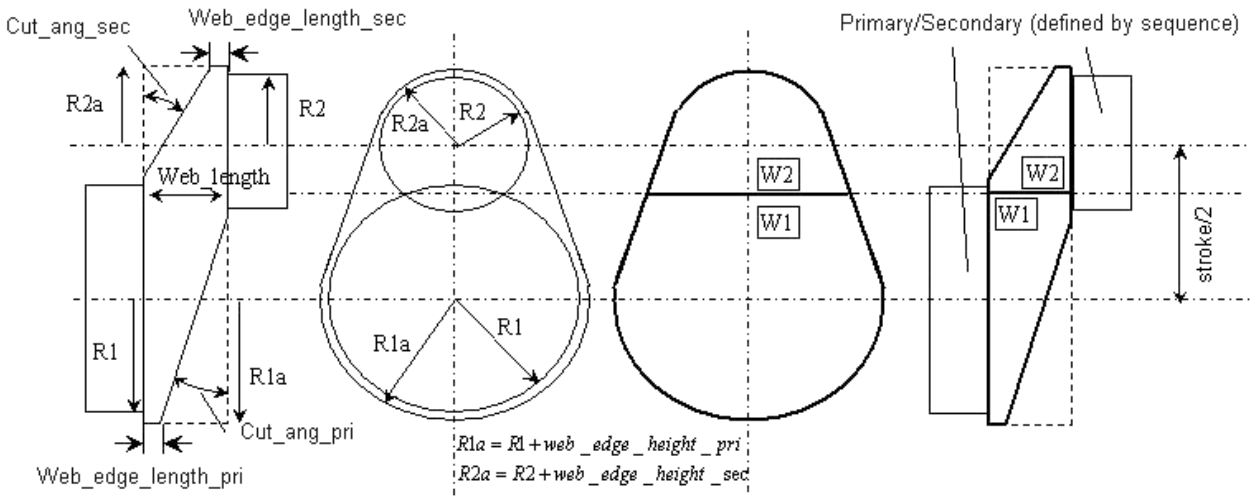

Figure 4.2. Geometry of web parts [61]

In ADAMS/Engine, a crankshaft can be modeled in four different ways:

- Rigid crankshaft
- Torsional-flexible crankshaft
- Beam crankshaft
- Flexible crankshaft

Rigid, torsional-flexible and beam crankshaft models are available in ADAMS/Engine libraries. Flexible crankshaft model should be created using an additional finite element program such as NASTRAN together with ADAMS/Engine.

Rigid crankshaft model is mainly used for balancing purposes. To get a first idea about the dynamics it is often sufficient to know about the free forces and reaction torques of a new cranktrain design. For this, a simple model that uses a rigid crankshaft, connected to main bearings and connecting rods, is used. Due to the low number of degrees of freedom it is expected to be very fast. Rigid crankshaft model of ADAMS/Engine is shown in Figure 4.3.

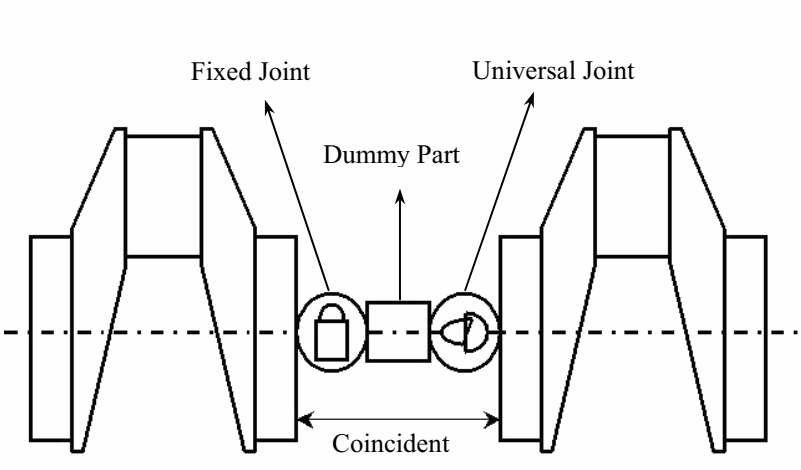

Figure 4.3. Rigid crankshaft model, [61]

Torsional-flexible crankshaft model is used to investigate torsional vibrations. Each throw is modeled as one rigid part and springs are used between each throw to represent the torsional stiffness of them. This is possible without changing the topology of the model by using a different modeling option on the crankshaft element. The already defined data for rigid crankshaft are inherited to this model and the additional data for the stiffness and damping of the shaft is automatically calculated based on geometry and material data. Without high vitality FE models of the crankshaft it is not possible to determine the component stresses to the highest level of accuracy, but it is noteworthy that even with the rigid body based models with compliant connections it is possible to make comparative analysis very well. Also, the investigation of rotational vibrations and the effects of a torsional vibration damper with respect to the stresses can be performed with this model since it is possible to easily activate such a damper. Torsional-flexible crankshaft model is shown in Figure 4.4.

Beam crankshaft model is used to represent the torsional and bending stiffness of the crankshaft. For the calculation of the bending stresses and bearing loads it is required to increase the level of refinement such that beam elements are connecting the parts representing the main pin, web and crank pin. The stiffness and damping of the beams are calculated based on the geometry and material data of the crankshaft. Beam crankshaft model is given in Figure 4.5.

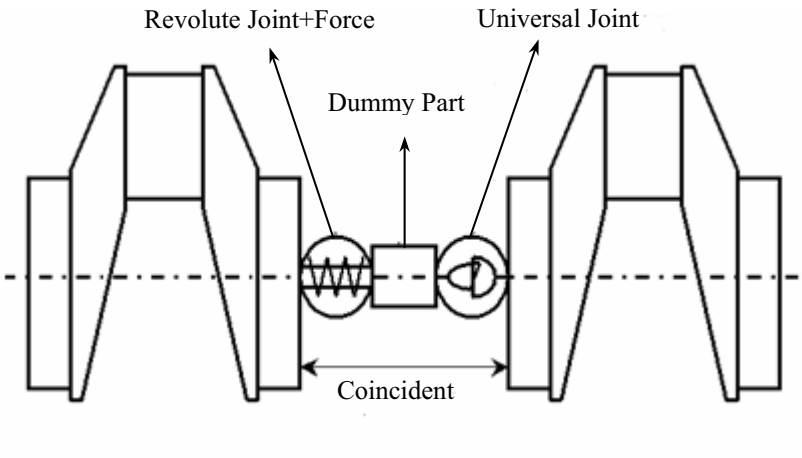

Figure 4.4. Torsional-flexible crankshaft model, [61]

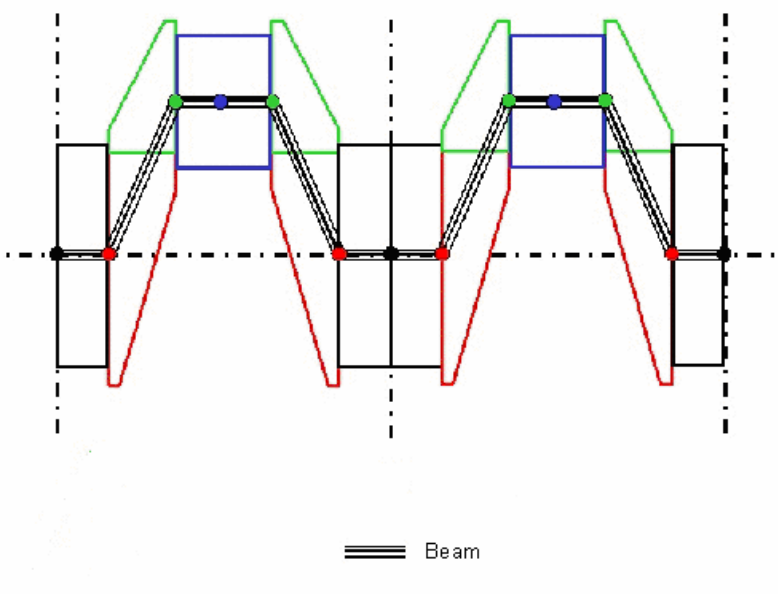

Figure 4.5. Beam crankshaft model, [61]

Flexible crankshaft model represents the next higher level of refinement. It is perfect to deliver highly accurate boundary conditions for detailed stress analysis. With this model it is possible to find the stresses at the critical locations of the crankshaft like the fillets. Figure 4.6 shows the flexible crankshaft which is obtained in MSC.Nastran, and transferred to ADAMS. To obtain this model Component Mode Synthesis (CMS) technique is used which is explained in the next section. The main advantage of this technique is that very large finite element structures can be modeled with much smaller number of modal degrees of freedom.

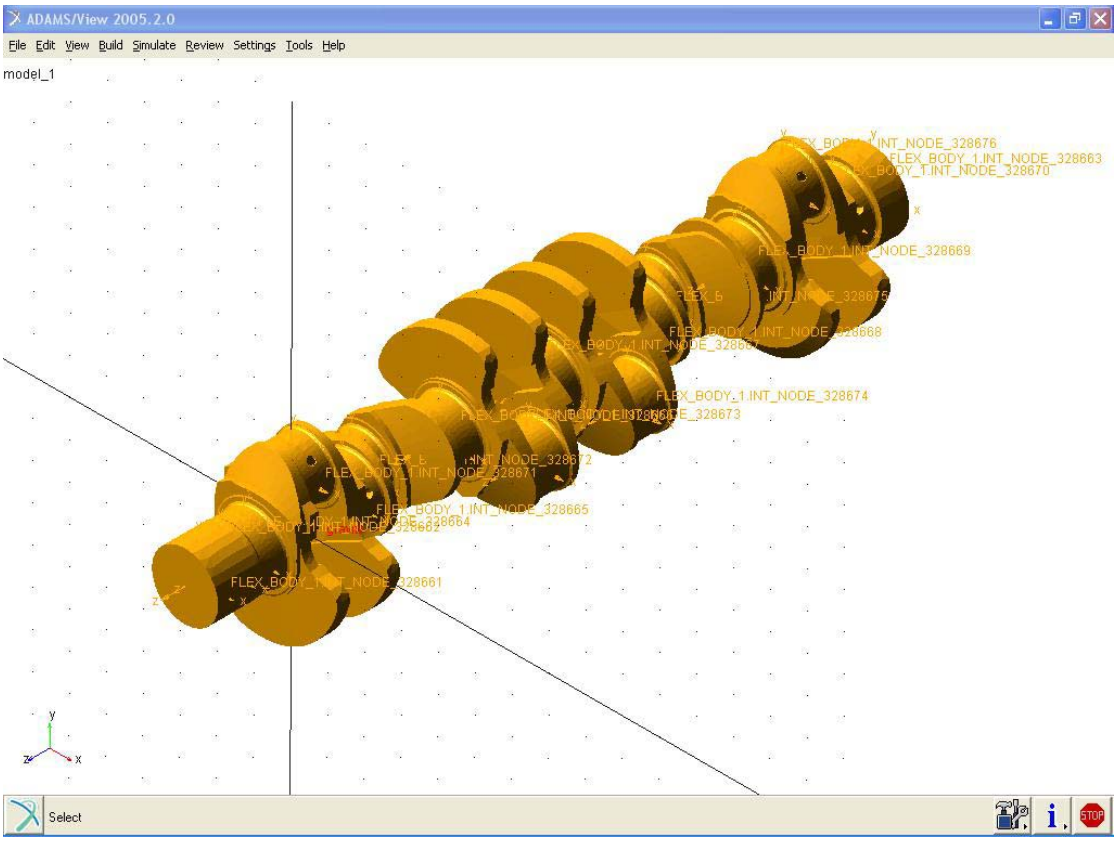

Figure 4.6. Flexible crankshaft model

4.2.2. Theory of Implementing Flexible Bodies in ADAMS

The single most important assumption behind the flexible body is that only small, linear body deformations relative to a local reference frame is considered, while that local reference frame is undergoing large, non-linear global motion [62].

The discretization of a flexible component into a finite element model represents the infinite number of DOF with a finite, but very large number of finite element DOF. The linear deformations of the nodes of this finite element mode, **u**, can be approximated as a linear combination of a smaller number of shape vectors (or mode shapes), ϕ.

$$\mathbf{u} = \sum_{i=1}^{M} \phi_i \cdot q_i \tag{4.1}$$

where M is the number of mode shape and q_i, are the modal coordinates.

Equation (4.1) can be shown in matrix form as

$$\mathbf{u} = \mathbf{\Phi} \cdot \mathbf{q} \tag{4.2}$$

where **q** is the vector of modal coordinates and **Φ** is the shape function matrix that is result of finite element analysis and used for transformation from small set of modal coordinates , **q**, to the larger set of physical coordinates, **u**.

The basic premise of modal superposition is that the deformation behavior of a component with a very large number of nodal DOF can be captured with a much smaller number of modal DOF. This reduction in DOF is referred as modal truncation. For reduction of finite element models, the Craig-Bampton method is used.

4.2.2.1. Component Mode Synthesis—The Craig-Bampton Method. Elastic body contains two types of nodes, interface nodes where forces and boundary conditions interact with the finite element structure during multibody system simulation (MSS), and interior nodes. In MSS the position of elastic body is computed by superposing its rigid body motion and elastic deformation. In ADAMS, this is performed using "Component Mode Synthesis" technique based on Craig-Bampton method [63, 64]. The system DOFs are partitioned into boundary DOF, $\mathbf{u}_B$, and interior DOF, $\mathbf{u}_I$. Two sets of mode shapes are defined, as follows:

Constraint modes: These modes are static shapes obtained by giving each boundary DOF a unit displacement while holding all other boundary DOF fixed. The basis of constraint modes completely spans all possible motions of the boundary DOFs, with a one-to-one correspondence between the modal coordinates of the constraint modes and the displacement in the corresponding boundary DOF, $\mathbf{q}_C = \mathbf{u}_B$. As an example, Figure 4.7 shows two constraint modes for the left end of a beam that has attachment points at the two ends. The figure on the left shows the constraint mode corresponding to a unit translation while the figure on the right corresponds to a unit rotation

Fixed-boundary normal modes: These modes are obtained by fixing the boundary DOF and solving an eigenvalue problem. There are as many fixed-boundary normal modes as the user desires. These modes define the modal expansion of the interior DOF. The quality of this modal expansion is proportional to the number of modes retained by the user. As an example Figure 4.8 shows two fixed-boundary normal modes for a beam that has attachment points at the two ends.

Figure 4.7. Two constraint modes for the left end of a beam that has attachment points at the two ends

Figure 4.8. Two fixed-boundary normal modes for a beam that has attachment points at the two ends

The modal transformation between the physical DOF and the Craig-Bampton modes and their modal coordinates is described by the following equation:

$$\mathbf{u} = \begin{Bmatrix} \mathbf{u}_B \\ \mathbf{u}_I \end{Bmatrix} = \begin{bmatrix} \mathbf{I} & \mathbf{0} \\ \boldsymbol{\Phi}_{IC} & \boldsymbol{\Phi}_{IN} \end{bmatrix} \cdot \begin{Bmatrix} \mathbf{q}_C \\ \mathbf{q}_N \end{Bmatrix} \tag{4.3}$$

where $\mathbf{u}_B$ is the column vector of boundary DOF and $\mathbf{u}_I$ is the column vector of interior DOF. $\mathbf{I}$, $\mathbf{0}$ are identity and zero matrices, respectively. $\boldsymbol{\Phi}_{IC}$ is the matrix of physical displacements of the interior DOF in the constraint modes. $\boldsymbol{\Phi}_{IN}$ is the matrix of physical displacements of the interior DOF in the normal modes. $\mathbf{q}_C$ is the column vector of modal coordinates of the constraint modes. $\mathbf{q}_N$ is the column vector of modal coordinates of the fixed-boundary normal modes.

The generalized stiffness and mass matrices corresponding to the Craig-Bampton modal basis are obtained via a modal transformation. The stiffness transformation is

$$\hat{\mathbf{K}} = \boldsymbol{\Phi}^T \mathbf{K} \boldsymbol{\Phi} = \begin{bmatrix} \mathbf{I} & \mathbf{0} \\ \boldsymbol{\Phi}_{IC} & \boldsymbol{\Phi}_{IN} \end{bmatrix}^T \begin{bmatrix} \mathbf{K}_{BB} & \mathbf{K}_{BI} \\ \mathbf{K}_{IB} & \mathbf{K}_{II} \end{bmatrix} \begin{bmatrix} \mathbf{I} & \mathbf{0} \\ \boldsymbol{\Phi}_{IC} & \boldsymbol{\Phi}_{IN} \end{bmatrix} = \begin{bmatrix} \hat{\mathbf{K}}_{CC} & \mathbf{0} \\ \mathbf{0} & \hat{\mathbf{K}}_{NN} \end{bmatrix} \tag{4.4}$$

and the mass transformation is

$$\hat{\mathbf{M}} = \boldsymbol{\Phi}^T \mathbf{M} \boldsymbol{\Phi} = \begin{bmatrix} \mathbf{I} & \mathbf{0} \\ \boldsymbol{\Phi}_{IC} & \boldsymbol{\Phi}_{IN} \end{bmatrix}^T \begin{bmatrix} \mathbf{M}_{BB} & \mathbf{M}_{BI} \\ \mathbf{M}_{IB} & \mathbf{M}_{II} \end{bmatrix} \begin{bmatrix} \mathbf{I} & \mathbf{0} \\ \boldsymbol{\Phi}_{IC} & \boldsymbol{\Phi}_{IN} \end{bmatrix} = \begin{bmatrix} \hat{\mathbf{M}}_{CC} & \hat{\mathbf{M}}_{NC} \\ \hat{\mathbf{M}}_{CN} & \hat{\mathbf{M}}_{NN} \end{bmatrix} \tag{4.5}$$

where the subscripts *I*, *B*, *N* and *C* denote internal DOF, boundary DOF, normal mode and constraint mode, respectively. The caret on $\hat{\mathbf{M}}$ and $\hat{\mathbf{K}}$ denotes that this is generalized mass and stiffness.

Equations (4.4) and (4.5) have the following properties:

- Submatrices $\hat{\mathbf{M}}_{NN}$ and $\hat{\mathbf{K}}_{NN}$ are diagonal matrices because they are associated with eigenvectors.
- Matrix $\hat{\mathbf{K}}$ is block diagonal. There is no stiffness coupling between the constraint modes and fixed-boundary normal modes.
- Matrix $\hat{\mathbf{M}}$ is not block diagonal because there is an inertia coupling between the constraint modes and the fixed-boundary normal modes.

4.2.2.2. Mode Shape Orthonormalization. The Craig-Bampton method is a powerful method for tailoring the modal basis to capture both the desired attachment effects and the desired level of dynamic content. However, the raw Craig-Bampton modal basis has certain deficiencies that make it unsuitable for direct use in a dynamic system simulation. These are:

- Embedded in the Craig-Bampton constraint modes are 6 rigid body DOF which must be eliminated before the ADAMS analysis because ADAMS provides its own large-motion rigid body DOF.

- The Craig-Bampton constraint modes are the result of a static condensation. Consequently, these modes do not advertise the dynamic frequency content that they must contribute to the flexible body. Successful simulation of a non-linear system with unknown frequency content is unlikely.

- Craig-Bampton constraint modes cannot be disabled because to do so would be equivalent to applying a constraint on the system.

The problems mentioned above can be easily resolved by applying a simple mathematical operation on the Craig-Bampton modes. The Craig-Bampton constrained modes are not an orthogonal set of modes, as evidenced by the fact that their generalized mass and stiffness matrices $\hat{\mathbf{K}}$ and $\hat{\mathbf{M}}$, encountered in Equations (4.4) and (4.5), are not diagonal. To obtain decoupled set of modes, constrained modes and normal modes are orthogonalized by solving a generalized eigenvalue problem,

$$\hat{\mathbf{K}}\mathbf{q} = \lambda\hat{\mathbf{M}}\mathbf{q} \tag{4.6}$$

Eigenvectors obtained from Equation (6.6) is arranged in a transformation matrix $\mathbf{N}$ which transforms the Craig-Bampton modal basis to an equivalent orthogonal basis with modal coordinates $\mathbf{q}^*$.

$$\mathbf{N}\cdot\mathbf{q}^* = \mathbf{q} \tag{4.7}$$

As a result flexible body deformation can be expressed as:

$$\mathbf{u} = \mathbf{\Phi}\cdot\mathbf{q} = \mathbf{\Phi}\cdot\mathbf{N}\cdot\mathbf{q}^* = \mathbf{\Phi}^*\cdot\mathbf{q}^* \tag{4.8}$$

where $\mathbf{\Phi}^*$ is the matrix of orthogonalized Craig-Bampton modes.

The orthogonalized Craig-Bampton modes are not eigenvectors of the original system. They are eigenvectors of the Craig-Bampton representation of the system and as such have a natural frequency associated with them.

Each orthogonalized mode of the crankshaft corresponds with a stress distribution called modal stress. The resulting stress state of the crankshaft is calculated by a linear combination of modal stresses.

$$\boldsymbol{\sigma} = \mathbf{\Phi}^{\sigma}\cdot\mathbf{N}\cdot\mathbf{q}^* \tag{4.9}$$

where $\mathbf{\Phi}^{\sigma}$ contains the modal stresses according to the deformation modes in matrix $\mathbf{\Phi}$.

4.2.3. Bearing Types in ADAMS

Modeling and simulation of the plain journal bearings of the crankshaft have great effect on dynamic behavior of the crankshaft and it is an essential part of an accurate dynamic stress calculation. Sliding bearings are used in the case of a six cylinder in-line diesel engine. A sliding bearing is described as a sleeve around a pin with a lubricating fluid. The lubricant is supplied with a suitable slot. Tangential and radial motion in combination with a wedged gap generate a pressure in oil film in the sliding bearing. Bearing loading is periodical and a pin center comes through a bearing trajectory.

Assuming an incompressible fluid (Newton's fluid) with a constant viscosity in a laminar lubricating flow, an equation describing the force equilibrium in a differential fluid element can be established. This equation is also known as the Navier-Stokes equation and can be written as:

$$\rho \mathbf{w}\left(\nabla \mathbf{w}\right) = -\nabla \mathbf{p} + \eta \nabla^2 \mathbf{w} + \rho \mathbf{g} \tag{4.10}$$

where $\rho \mathbf{w}\left(\nabla \mathbf{w}\right)$ denotes specific inertia forces, $\nabla \mathbf{p}$ specific pressure forces, $\eta \nabla^2 \mathbf{w}$ specific viscosity forces, $\rho \mathbf{g}$ specific mass forces and $\mathbf{w}$ the velocity vector of the fluid element.

Making several reasonable assumptions and applying appropriate transformations and boundary conditions, Equation (4.10) can be rewritten to the form of:

$$\frac{\partial^2 \Pi}{\partial \varphi^2} + \left(\frac{D}{B}\right)^2 \cdot \frac{\partial^2 \Pi}{\partial Z^2} + a\left(\varphi, Z\right) \cdot \Pi = b\left(\varphi, Z\right) \tag{4.11}$$

which is also known as Reynold's differential equation. Π denotes a transformed pressure distribution, φ and Z are the coordinates in circumference and width direction, D/B a form factor and a and b are position-dependent coefficients. Equation (4.11), which is the form

of a partial elliptic differential equation, can not be solved analytically. However, it can be solved numerically using an iterative algorithm as it is done in the HD subroutine.

The implementation of this oil film model into ADAMS is done by a GFORCE-Subroutine (GFOSUB). The parameters that are needed by the subroutine are the rotational speed of the crankshaft, position and velocity vector of journal against the bearing shell at each bearing side to consider an inclined position of the crankshaft inside the bearing shell. To keep track of the actual bearing state, two initially coincident markers (shell and journal) are placed at each bearing side.

When modeling hydrodynamic bearings in ADAMS, one can choose to include or exclude misalignment effects by using the following methods [61]:

- Two-dimensional method (neglecting misalignment) - An empirical analytical equation is used. This approach, which is similar to impedance method, is the most efficient way to model hydrodynamic bearings.

- Three-dimensional method (accounting for misalignment) - The Reynolds equation must be solved explicitly. To keep the simulation effort in a reasonable range, the hydrodynamic solution is decoupled from the dynamic solution of ADAMS/Solver. The Reynolds equation is solved for several bearing working conditions (about 60 eccentricities and 60 misalignment angles) prior to the dynamic analysis. The results are stored in hydrodynamic databases representing the dimensionless bearing reactions (forces and force-attachment coordinates) to dimensionless states (eccentricity and misalignment value). During the dynamic solution, ADAMS/Solver subroutines do the database access and the necessary analytical steps (coordinate transformations, and so on). The process is shown in Figure 4.9, [65].

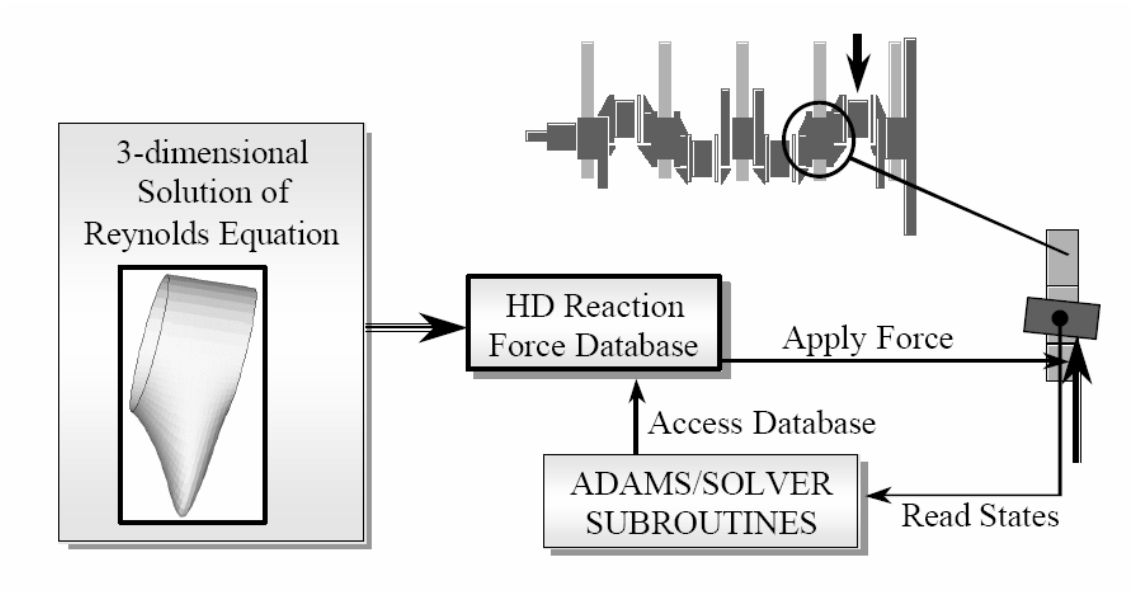

Figure 4.9. Process of modeling 3D Hydrodynamic Bearing in ADAMS/Engine, [65]

4.2.4. Modeling Torsional Vibration Damper

Torsional vibration (TV) damper is used for reducing the torsional vibration angle and stress amplitudes at the crankshaft. In ADAMS/Engine a TV damper can be modeled in three different ways. These are [61]

- Linear TV damper
- Rubber TV damper
- Viscous TV damper

A linear torsional damper consists of two masses: an inner mass (hub part) and an outer mass (ring part), connected with a revolute joint. The hub part is constrained with a fixed joint at the attachment part. The force (torque) from one part to another is transmitted through a force element, an element-like spring damper, as shown in the figure that follows. The stiffness and damping of this force element determine the transfer behavior of the element. Schematic representation of Linear TV damper is shown in Figure 4.10.

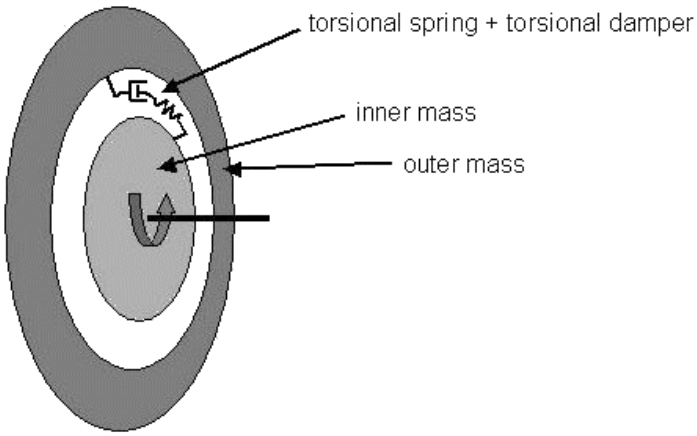

Figure 4.10. Linear TV Damper with implemented force element [61]

A rubber torsional damper consists of two parts (masses), a ring part (mass), and a hub part (mass), connected together with a revolute joint. The hub part is constrained with a fixed joint at the attachment part. The force (torque) between the hub and the ring is transmitted through a combination of a single-component torque and a transfer function. The total transfer behavior of the component is determined through a model of four spring components and three damping components arranged as shown in Figure 4.11. The displacement dependency is defined in a spline entered in a torque table. K_0 is the derivative of the static torque-displacement relationship at zero angular displacement. One can specify K_2-K_4 and C_2-C_4 or let ADAMS/Engine calculate these parameters to fit the constant loss angle you define for the dynamic stiffness. The dynamic stiffness is the stiffness curve at zero displacement [61].

A viscous torsional-vibration damper (or hydro torsional damper) consists of two parts (masses), a ring part (mass), and a hub part (mass), connected together with a revolute joint. The hub part is constrained with a fixed joint at the attachment part. The force (torque) from the one part to another is transmitted through a liquid of high viscosity (silicon oil). Cross section of a viscous TV damper is shown in Figure 4.12 [61].

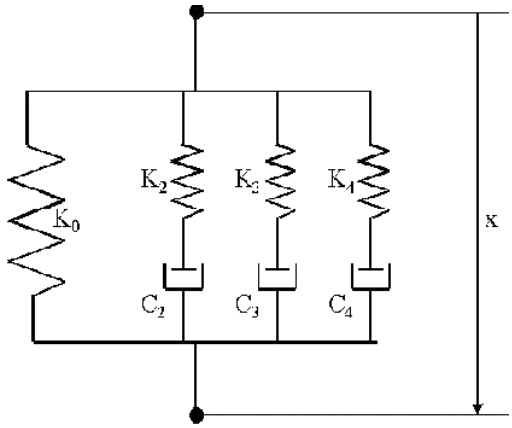

Figure 4.11. Extended Poynting-Thomson model of force component implemented in rubber TV damper [61]

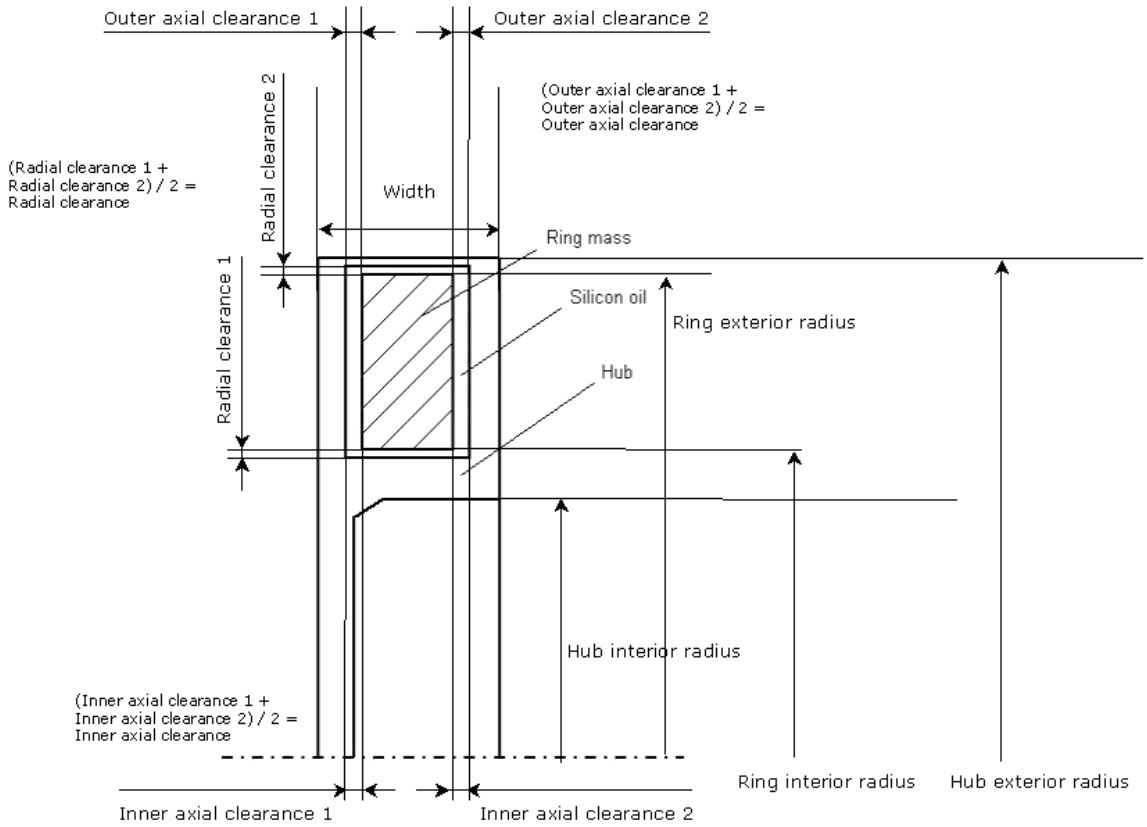

Figure 4.12. Cross-section of viscous TV damper [61]

4.2.5. Modeling Flywheel

A flywheel is an energy storage device. It absorbs mechanical energy by increasing its angular velocity and delivers energy by decreasing its angular velocity. It is used to smooth the flow of energy between a power source and its load. In ADAMS/Engine a flywheel can be modeled in three different ways. These are [61]:

- Single-mass flywheel
- Linear dual-mass flywheel
- Dual-mass flywheel

A single-mass flywheel is a part constrained with a fixed joint. Schematic representation of a single mass flywheel is given in Figure 4.13. A linear dual-mass flywheel consists of two parts connected with a revolute joint. Primary part is constrained with a fixed joint at the attachment part. Secondary part (wheel part) can be connected another part. The force (torque) from one part to another is transmitted over spring damper element. The stiffness and the damping between the wheels work linearly.

A dual-mass flywheel consists of two parts: a primary and a secondary part connected together with a revolute joint. The primary part is constrained with a fixed joint at the attachment part. Secondary part (wheel part) can be connected to another part. The force (torque) from the one part to another is transmitted over an arc spring. At the outer radius of the arc spring there is a friction contact to the secondary mass (see Figure 4.14).

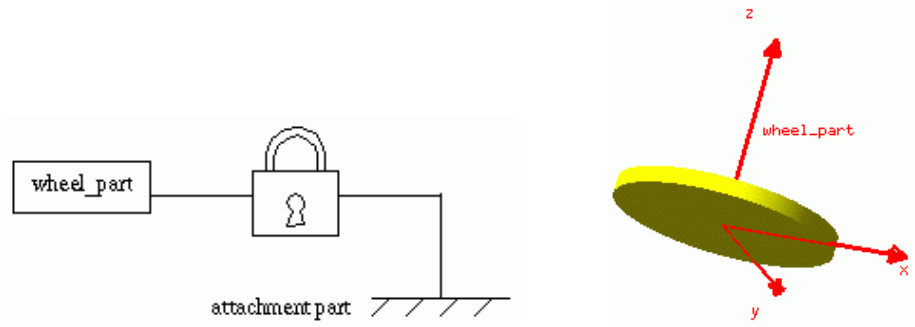

Figure 4.13. Schematic representation of a single-mass flywheel [61]

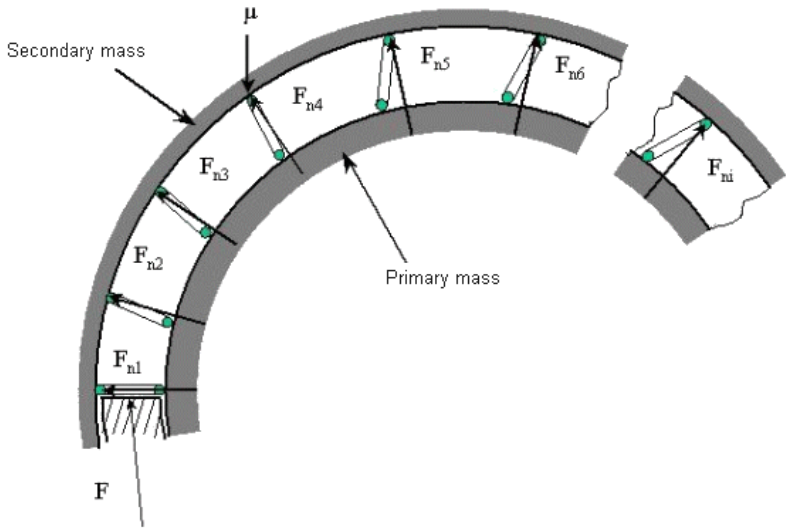

Figure 4.14. Geometry of a dual-mass flywheel [61]

4.2.6. Cranktrain Model

A cranktrain consists of a crankshaft, an engine block, pistons, connecting rods, piston pins, a flywheel and a torsional vibration damper. The connection between rotating components is enabled by bearings: main journal bearings, crank pin bearings and piston pin bearings. The behavior of the bearings depends on several parameters. For example, the oil has an important influence on hydrodynamic bearings. Besides the impact of the oil-supply pressure, there is high sensitivity to the viscosity of the oil. The viscosity depends on the oil temperature, which in turn depends on the engine speed. Also, the behavior of the torsional damper changes with the temperature, which is also dependent on the engine speed. The flywheel and the torsional damper are fixed to the crankshaft. The drive end of the cranktrain may be connected to a test rig. The cranktrain test rig always consists of a dyno that delivers an applied rotation. To represent a simple linear drivetrain model, you can place up to three interim parts and up to four rotational spring-damper connectors between the applied rotation and the crankshaft or flywheel. A gas force acts on each piston, and the related reaction gas force acts between the piston and the block. Schematic representation of a cranktrain model is shown in Figure 4.15. The procedure for dynamic analysis of a cranktrain is outlined in Figure 4.16 [66].

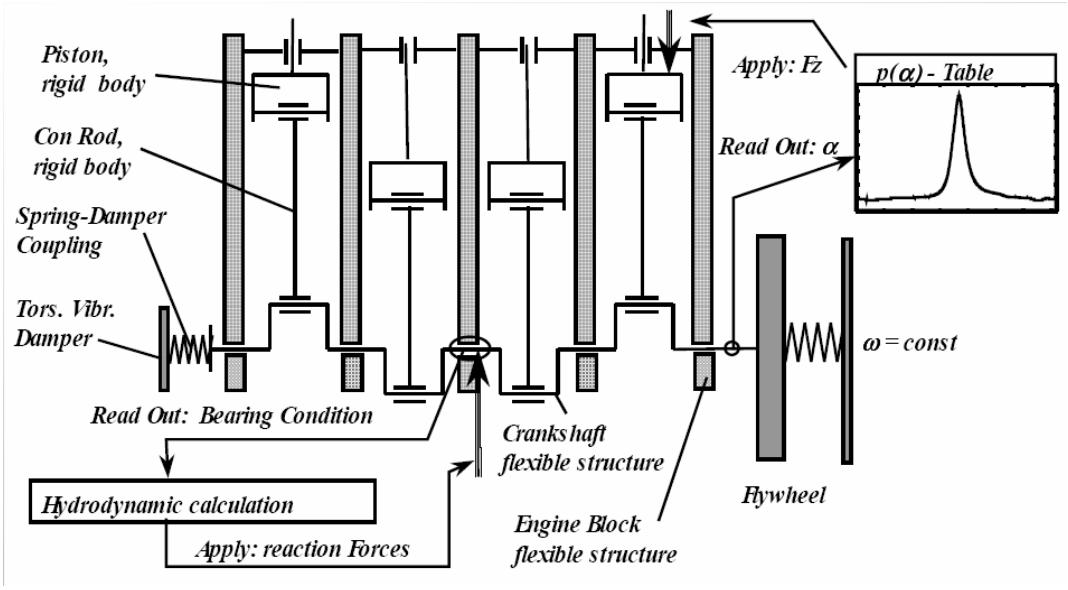

Figure 4.15. Schematic representation of a cranktrain model, [66]

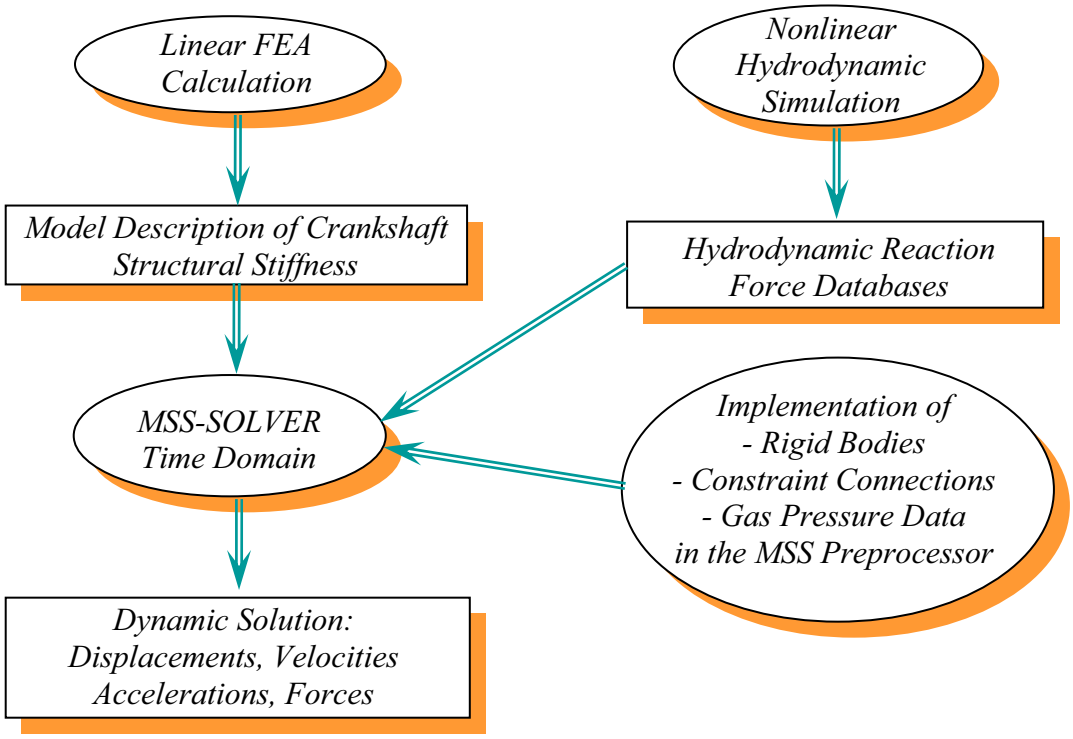

Figure 4.16. Cranktrain dynamic analysis procedure, [66]

4.3. Model Descriptions

Crankshaft system of an internal combustion engine consists of various parts such as crankshaft, piston, connecting rod, flywheel and torsional vibration damper. To predict the dynamic stresses of the crankshaft correctly, the crankshaft system should be considered as a whole. Dynamic analyses are carried out for a 7.3 L in-line six cylinder heavy duty diesel engine crankshaft system. The data for the engine are tabulated in Table 1.1. The crankshaft configuration of the 7.3 L engine is shown in Figure 4.17.

As mentioned in previous section, for determination of main bearing forces, a crankshaft may be modeled as rigid, beam or flexible structure. In rigid model, no vibration effects are considered which can lead considerable errors if vibration effects have major role on the system (like in multithrow crankshafts). Moreover, rigid model assumes crankshaft to be statically determinate that is reaction force of any given bearing depends on the load exerted on the throws adjacent to that bearing. Main bearing forces for 7.3 L engine using rigid crankshaft model was given previously in Chapter 3 while describing the traditional crankshaft force analysis.

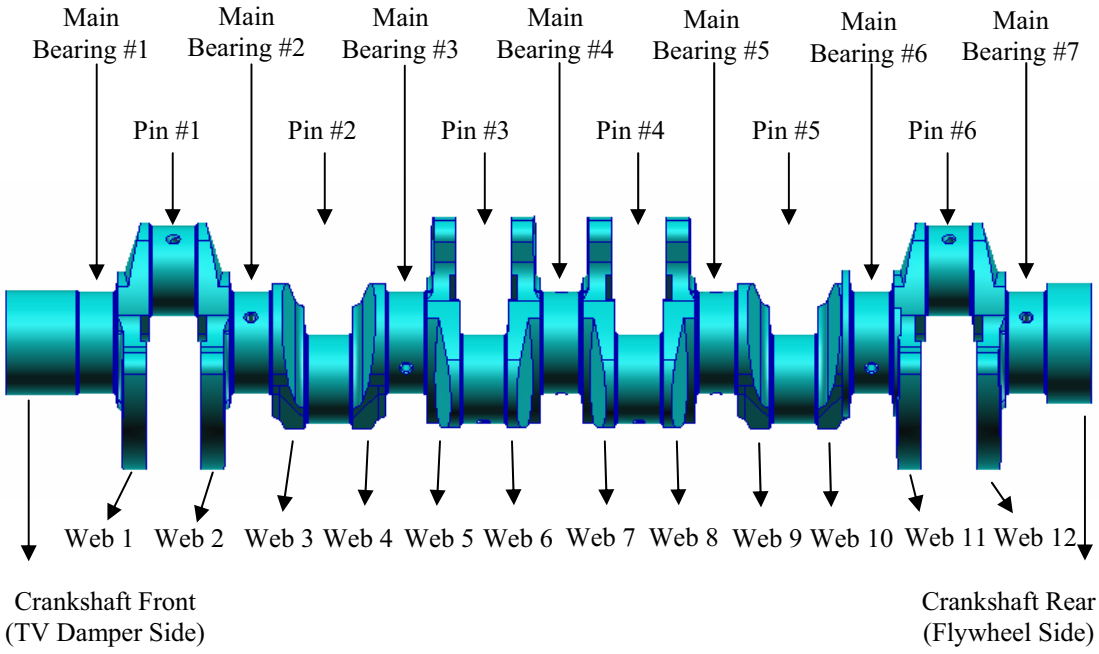

Figure 4.17. Location of main bearings, pins and webs

For realistic crankshaft force and stress analysis coupled axial, torsional and bending vibrations must be taken into consideration which is the case for beam and flexible crankshaft models. Additionally, beam and flexible crankshaft models assumes the crankshaft to be statically indeterminate that is the load exerted on a throw affects all of the bearings. Therefore, beam and flexible crankshaft models are used to obtain main bearing loads and to determine the stresses through the crankshaft.

The position and value of counterweights and web geometry for beam crankshaft model are given in Tables 4.1 and 4.2, respectively.

Table 4.1. 7.3 L engine crankshaft counterweight positions and masses

Number	Effective Radius (mm)	Mass (kg)	Angle (^{o})	Axial Offset
1	62	1.651613	-210	0
2	62	1.651613	-210	0
3	-	-	-	-
4	-	-	-	-
5	62	1.651613	-30	0
6	62	1.651613	-30	0
7	62	1.651613	-30	0
8	62	1.651613	-30	0
9	-	-	-	-
10	-	-	-	-
11	62	1.651613	-210	0
12	62	1.651613	-210	0

Table 4.2. 7.3 L engine crankshaft web geometry

Web No	Cut Angle Primary (^{o})	Edge Height Primary (mm)	Edge Length Primary (mm)	Cut Angle Secondary (^{o})	Edge Height Secondary (mm)	Edge Length Secondary (mm)
1-12	17.58	7.125	7.125	20.73	7.125	7.125

Details of modeling a flexible part in ADAMS are explained in subsection 4.2.2. Finite element model of the 7.3 L engine crankshaft is obtained using the commercial code MSC.Nastran and is shown in Figure 4.18. This model is characterized by approximately 300 000 ten-node tetrahedral elements and 500 000 nodes. The modal model of the crankshaft is developed with 32 boundary degrees of freedom associated with 16 interface nodes. The constrained modes obtained from static analysis correspond to these DOFs. Flexible crankshaft model is obtained through modal synthesis considering the first 40 fixed boundary normal modes. Therefore flexible crankshaft model is characterized by 72 DOFs. Two crankshaft models, with oil holes and without oil holes, are considered to see the effect of oil holes on crankshaft stresses. Modal frequencies of these models are given in Table 4.3 for the first 10 modes. Flexible crankshaft model for the crankshaft with oil holes is shown in Figure 4.19. This model is exported to ADAMS environment and, dynamic force and stress analyses are carried out.

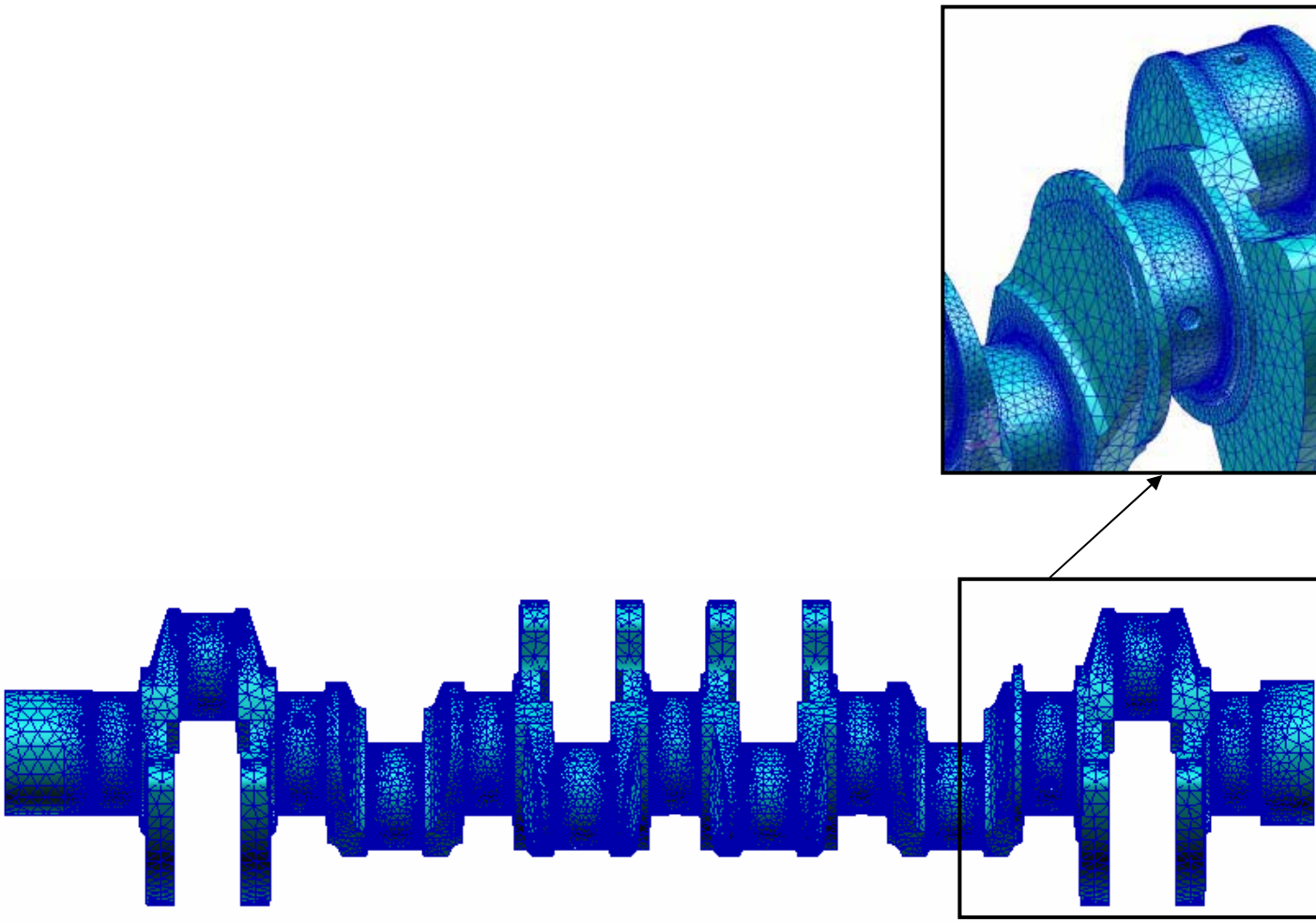

Figure 4.18. Crankshaft finite element model

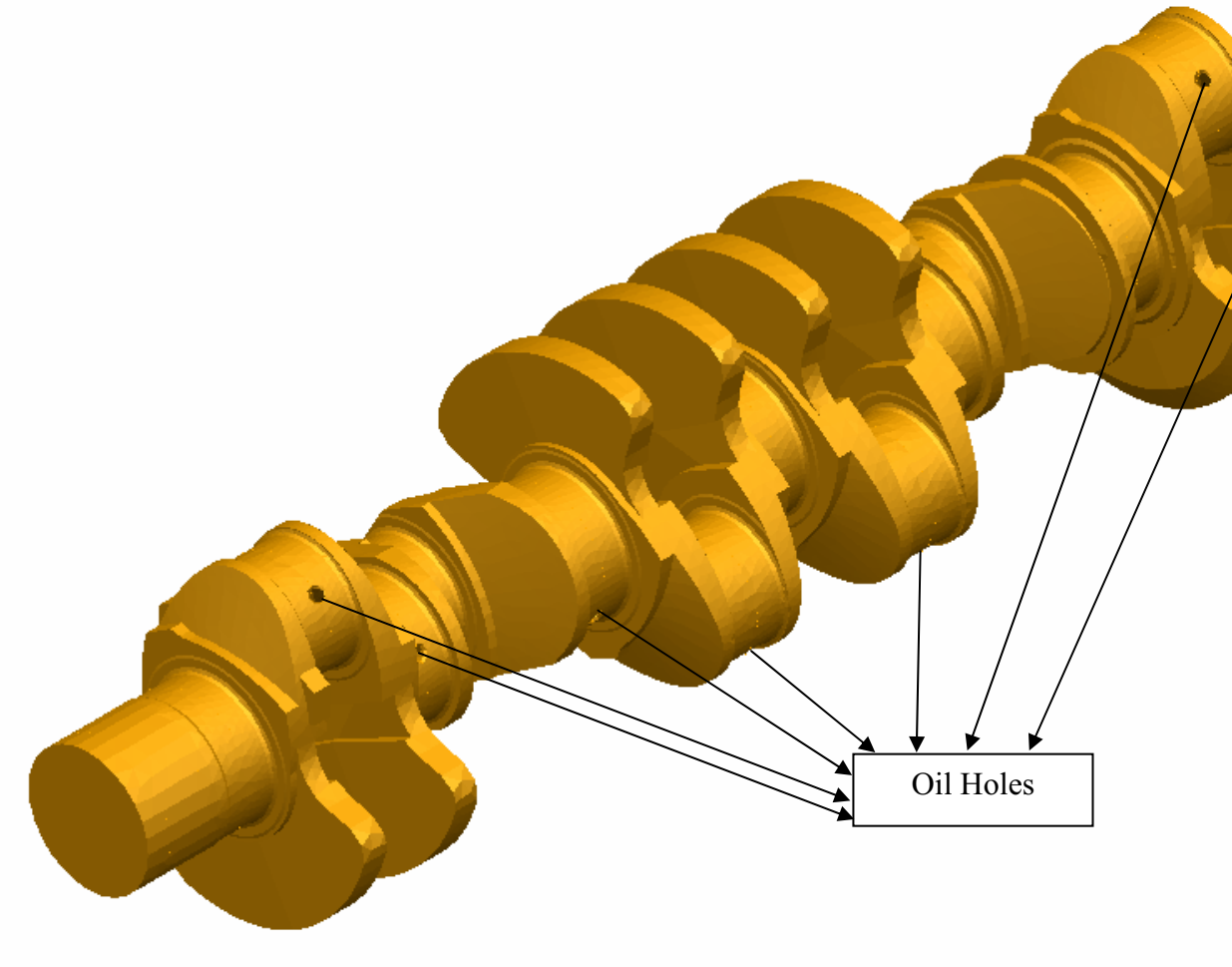

Figure 4.19. Flexible crankshaft model for the crankshaft with oil holes

Table 4.3. Modal frequencies of the 7.3 L engine crankshaft

Number	**Nastran FE-Model (w/o oil holes)** Frequency [Hz]	**Nastran FE-Model (with oil holes)** Frequency [Hz]
Mode 1 (1st bending vibration)	156.1	155.7
Mode 2 (1st bending vibration)	180.5	180.5
Mode 3 (2nd bending vibration)	418.7	419.1
Mode 4 (2nd bending vibration)	451.3	451.1
Mode 5 (1st axial vibration)	516.1	515.8
Mode 6 (1st torsional vibration)	581.7	584.1
Mode 7 (3rd bending vibration)	744.5	745.4
Mode 8 (3rd bending vibration)	817.0	815.3
Mode 9 (2nd torsional vibration)	958.4	958.6
Mode 10 (4th bending vibration)	1142.5	1142.2

Flywheel and TV damper specifications are as follows:

Flywheel mass (including clutch) : 65.65 kg

Flywheel principle moments of inertia : I1=0.896 kgm^2

I2=0.896 kgm^2

I3=1.793 kgm^2

Mass of TV damper ring : 4.94 kg

Mass of TV damper housing : 6.86 kg

Moment of inertia of the ring : 0.127 kgm2

Moment of inertia of housing : 0.056 kgm2

Torsional stiffness of TV Damper : 125000 Nm/rad

Damping coefficient of TV damper : 95 Nms/rad

The cranktrain models obtained for 7.3 L engine with beam and flexible crankshafts are given in Figures 4.20 and 4.21.

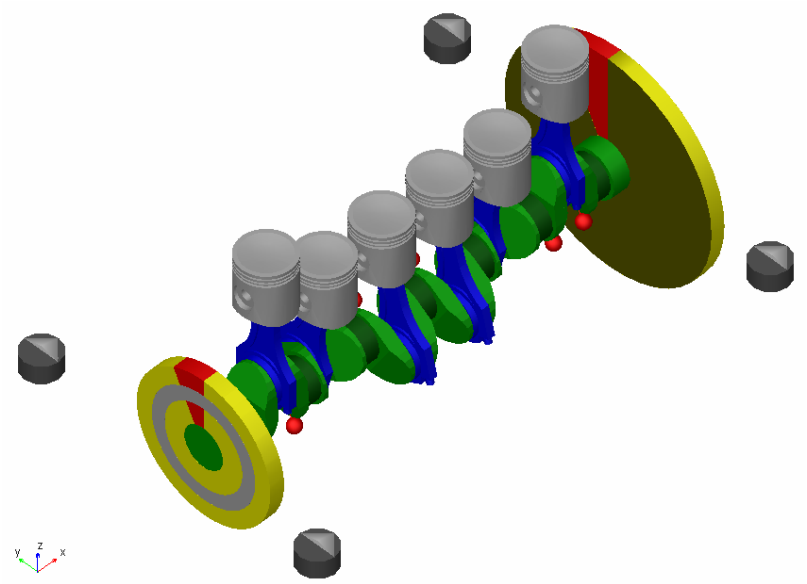

Figure 4.20. Cranktrain model for beam crankshaft

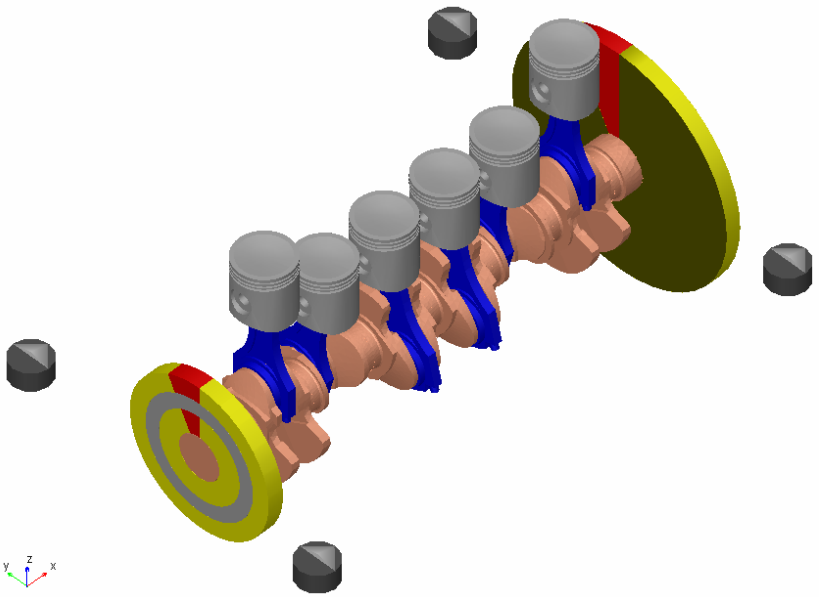

Figure 4.21. Cranktrain model for flexible crankshaft

4.4. Crankshaft Main Bearing Loads

Crankshafts of internal combustion engines are subjected to complex forces and torques which vary continuously with location and time. These forces are the ones that are coming from cylinder gas pressure and inertial effects of rotating and reciprocating components of the crankshaft system. The cylinder gas pressure force acting on the piston head is transmitted to the crankpin through the connecting rod assembly. The radial component of the transmitted force causes crankshaft to bend and transmitted to the engine block at main bearing locations. The tangential component of the transmitted force, on the other hand, is used to rotate the crankshaft.

The gas pressure variations inside the cylinders with respect to crank angle for 7.3 L engine at various engine speeds are obtained using AVL/Boost engine cycle calculation program which simulates the thermodynamic processes in the engine taking into account one dimensional gas dynamics in the intake and exhaust systems and given in Figure 4.22 [67].

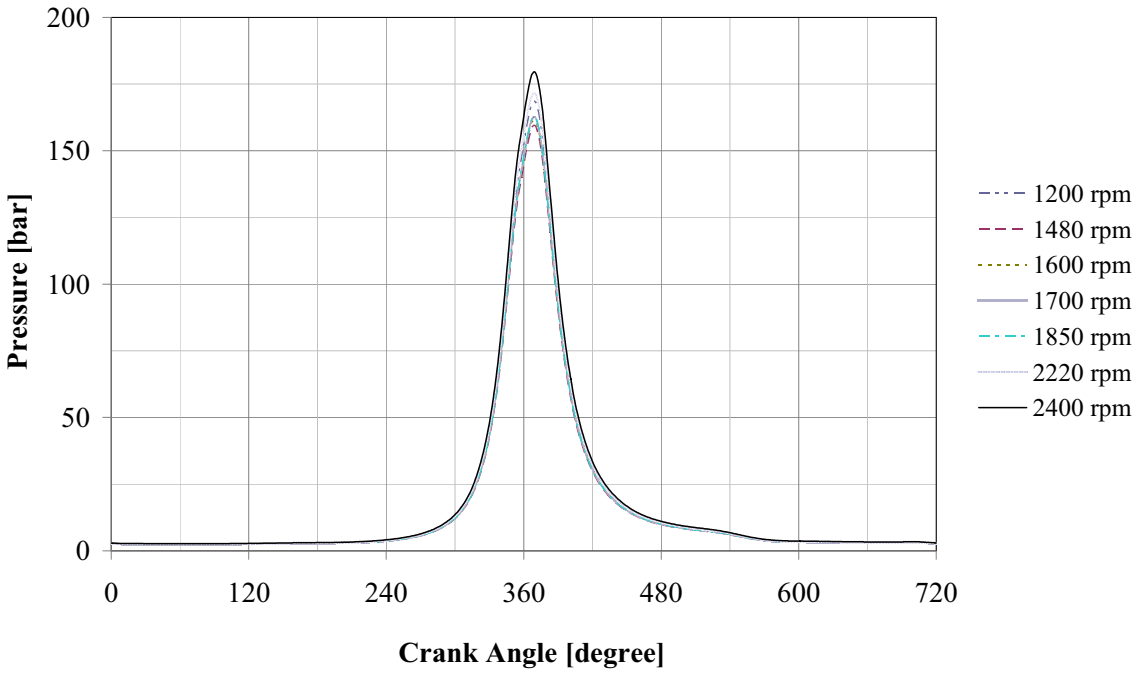

Figure 4.22. Gas pressure curves at different engine speeds for 7.3 L engine

Implementation of boundary conditions at the main bearing locations is another important aspect for the dynamic analysis of crankshaft system. In this study hydrodynamic bearing models of ADAMS/Engine are used to model the bearings.

Dynamic force analyses are carried out at the rated engine speed of 2400 rpm under full load which is the most critical loading condition for beam and flexible crankshaft models. The results are compared to AVL/Excite results which use an Elasto-Hydro-Dynamic (EHD) approach to model the main bearings [68] and are given in Figures 4.23-4.43. EHD approach takes into account the backward influence of the local deformations of the crank pins and shells on the oil pressure distribution. EHD approaches lead to performance disadvantages due to the fact that the Reynolds Differential Equation has to be solved for a large number of degrees of freedom in a closed loop with the dynamic equations of motions of the dynamic system.

In Figures 4.23 and 4.43, it can be seen that hydrodynamic approaches that decouple the hydrodynamic behavior from the structural dynamic behavior, either with beam crank or flexible crank are sufficient to determine forces on bearings and their influence on the cranktrain subsystem. It can also be seen that maximum main bearing loads occur at bearings # 2 and # 6 where bending vibration effects of TV damper and flywheel take an important role. Maximum bearing force at bearing # 2 is due to firing of cylinder 1 and maximum bearing force at bearing # 6 is caused by firing of cylinder 6.

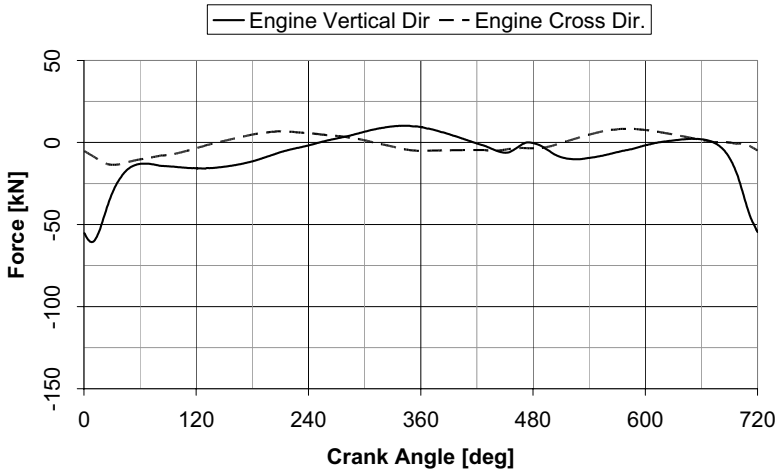

Figure 4.23. Forces acting on main bearing #1, beam crankshaft model

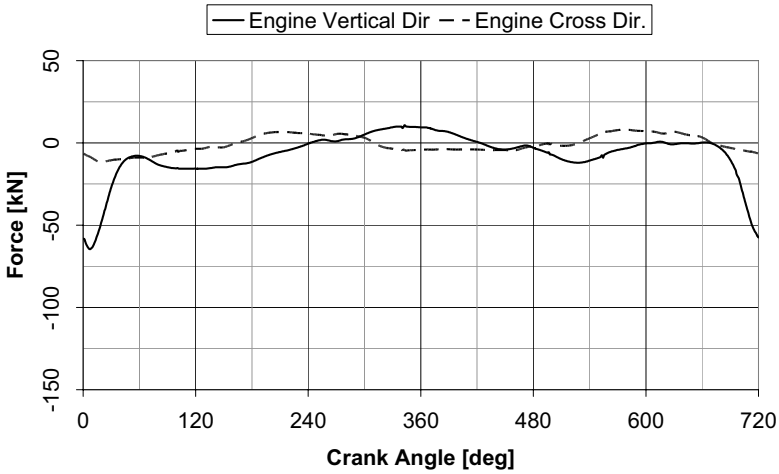

Figure 4.24. Forces acting on main bearing #1, flexible crankshaft model

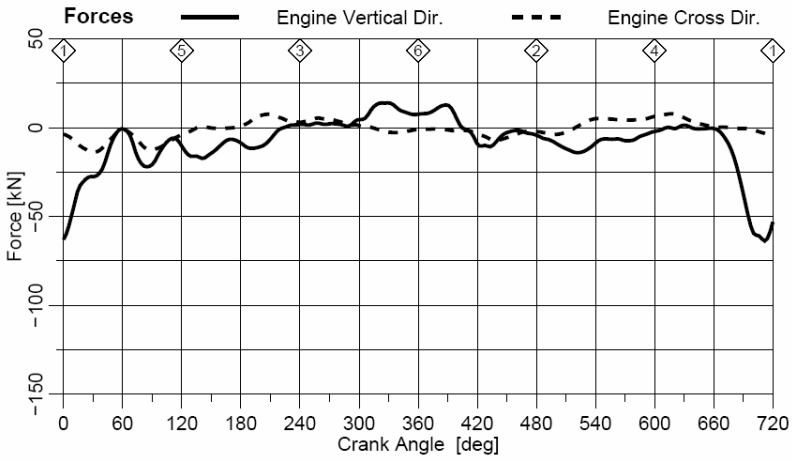

Figure 4.25. Forces acting on main bearing #1, (AVL/Excite)

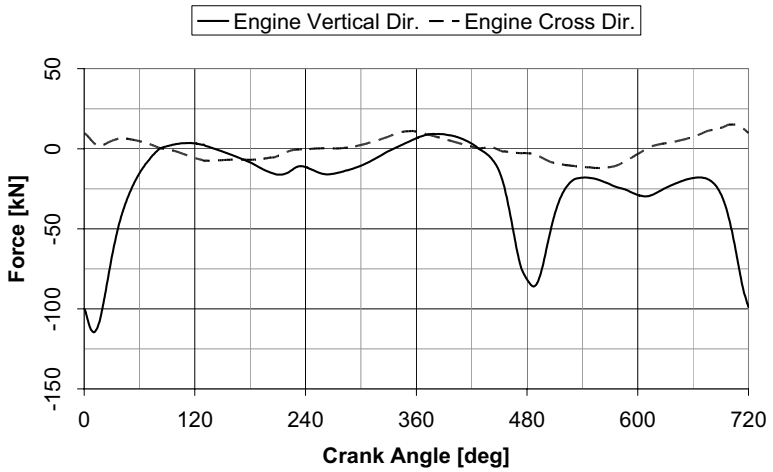

Figure 4.26. Forces acting on main bearing #2, beam crankshaft model

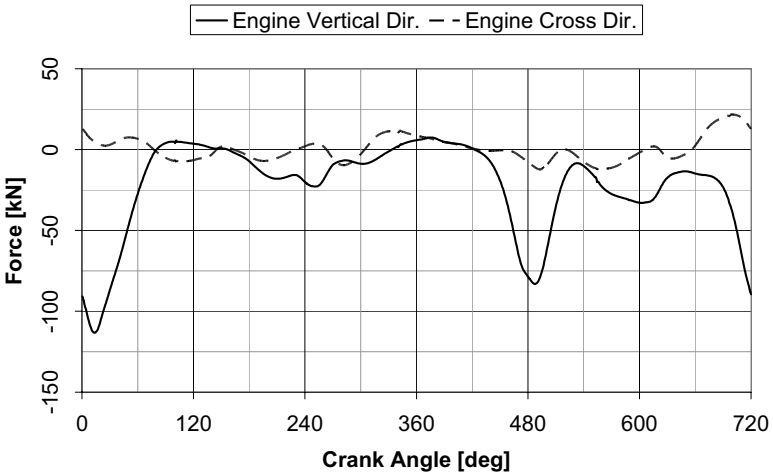

Figure 4.27. Forces acting on main bearing #2, flexible crankshaft model

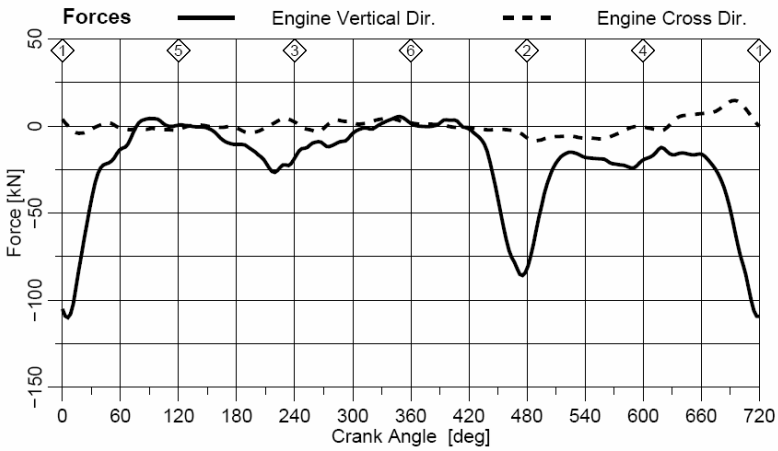

Figure 4.28. Forces acting on main bearing #2, (AVL/Excite)

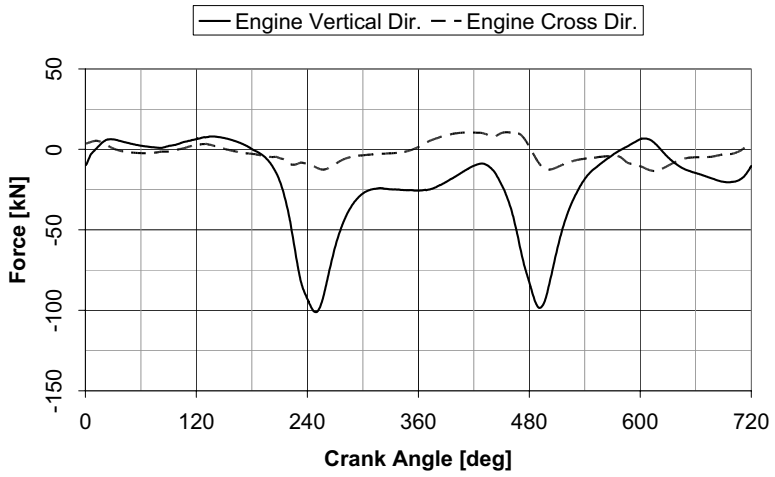

Figure 4.29. Forces acting on main bearing #3, beam crankshaft model

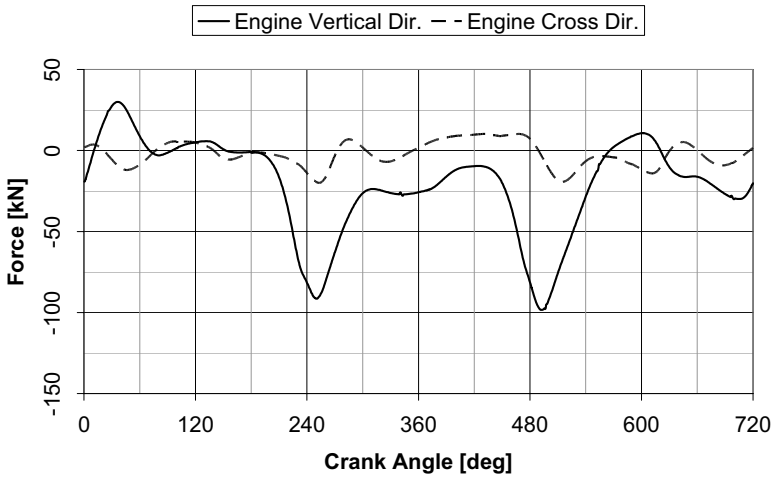

Figure 4.30. Forces acting on main bearing #3, flexible crankshaft model

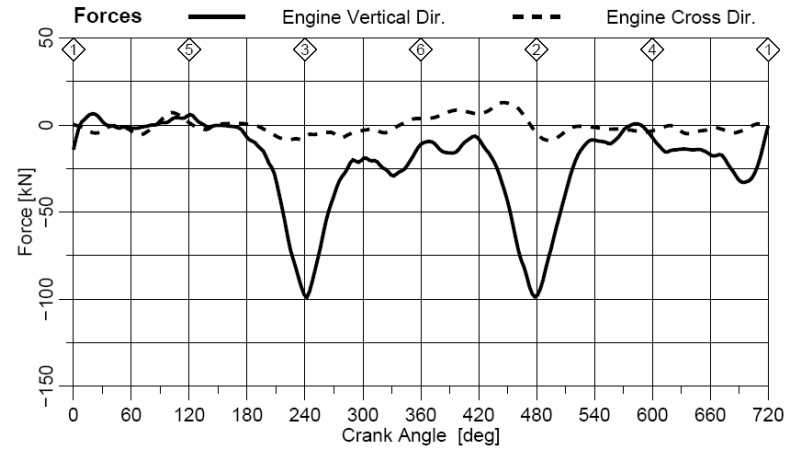

Figure 4.31. Forces acting on main bearing #3, (AVL/Excite)

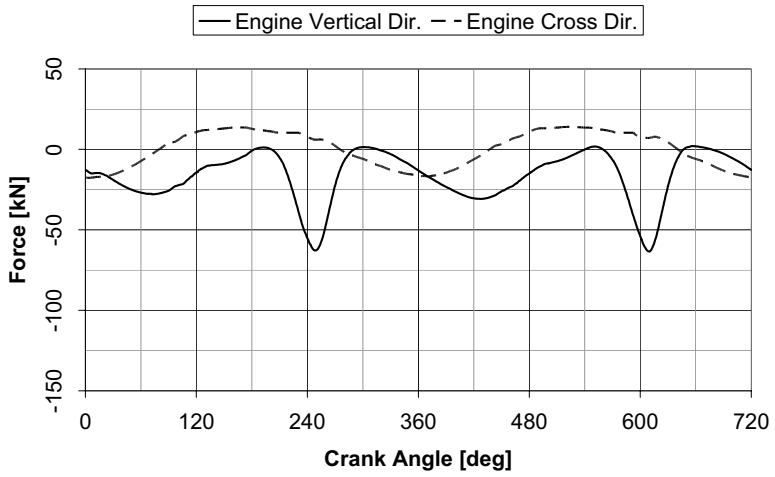

Figure 4.32. Forces acting on main bearing #4, beam crankshaft model

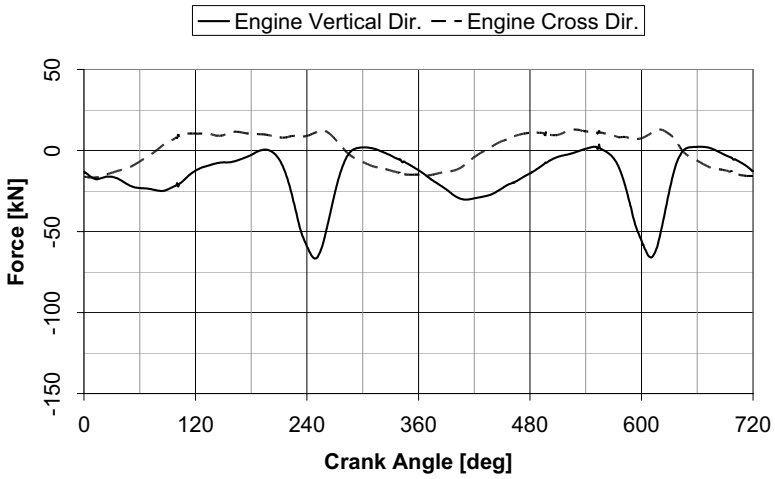

Figure 4.33. Forces acting on main bearing #4, flexible crankshaft model

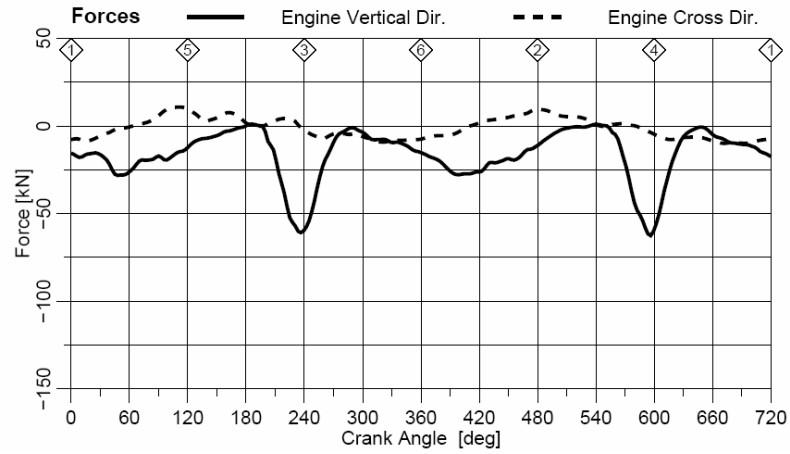

Figure 4.34. Forces acting on main bearing #4, (AVL/Excite)

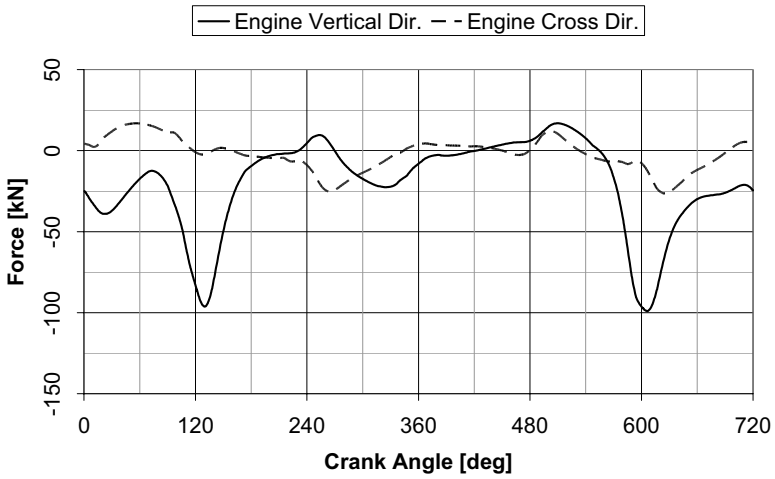

Figure 4.35. Forces acting on main bearing #5, beam crankshaft model

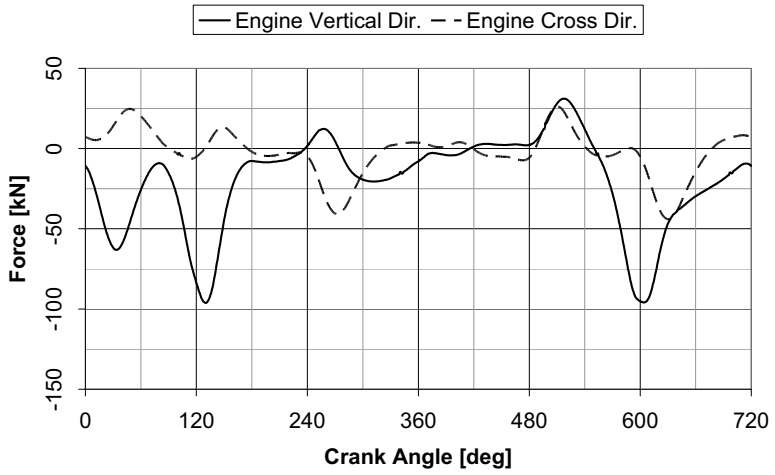

Figure 4.36. Forces acting on main bearing #5, flexible crankshaft model

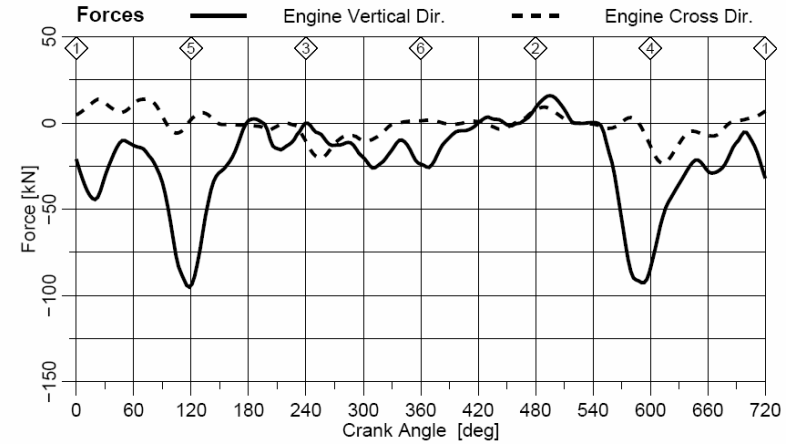

Figure 4.37. Forces acting on main bearing #5, (AVL/Excite)

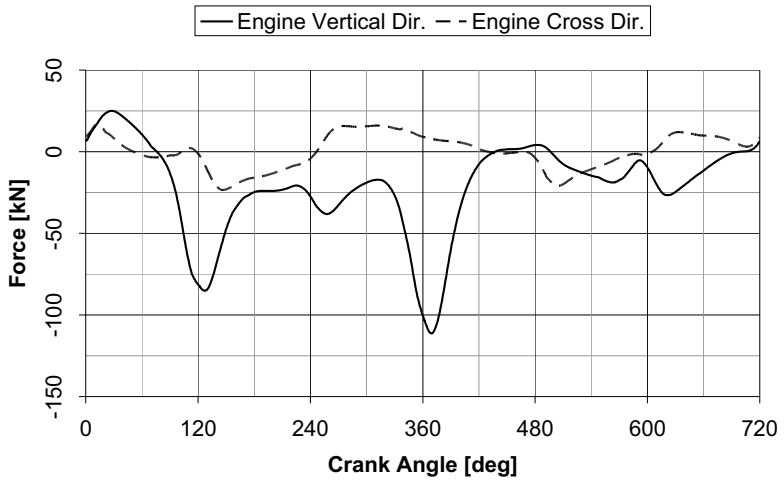

Figure 4.38. Forces acting on main bearing #6, beam crankshaft model

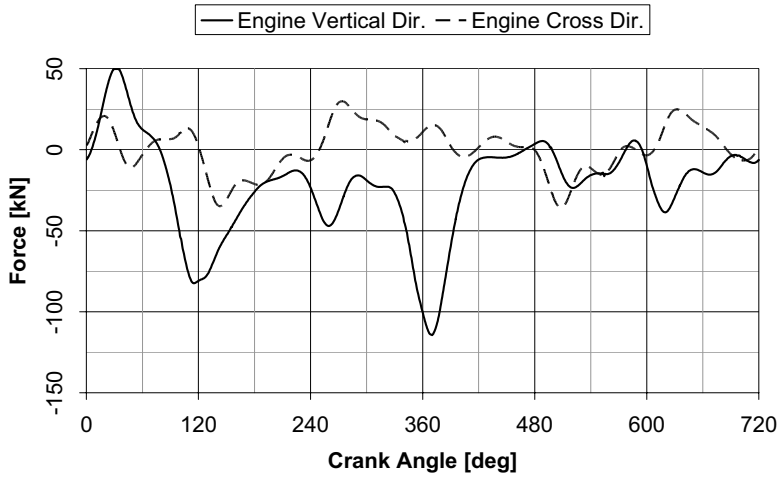

Figure 4.39. Forces acting on main bearing #6, flexible crankshaft model

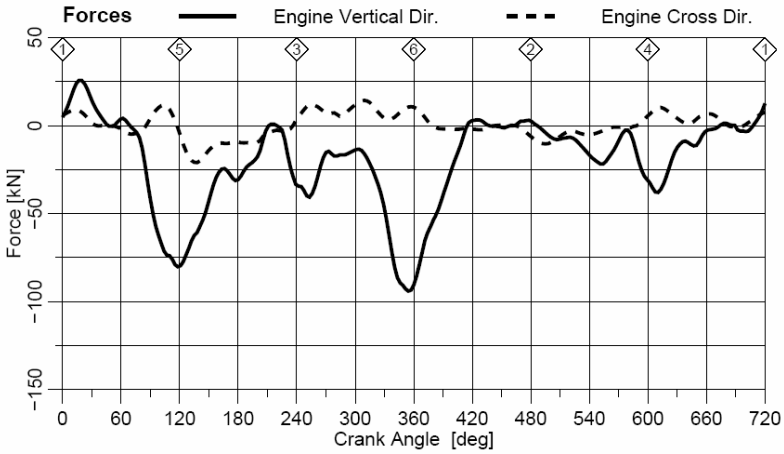

Figure 4.40. Forces acting on main bearing #6, (AVL/Excite)

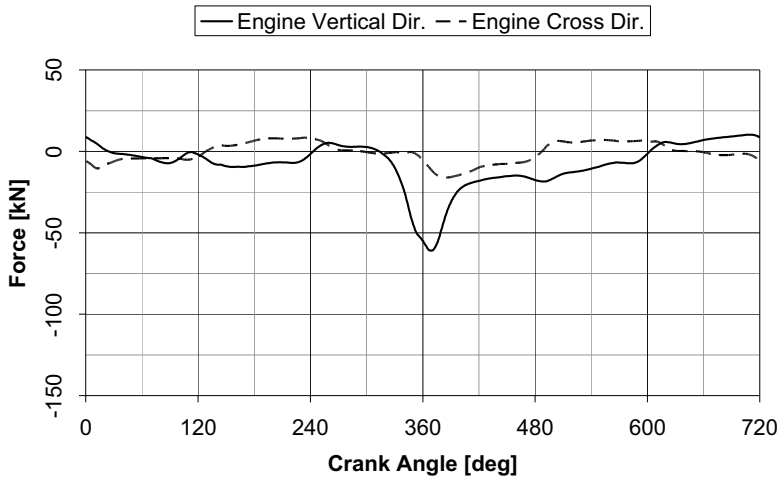

Figure 4.41. Forces acting on main bearing #7, beam crankshaft model

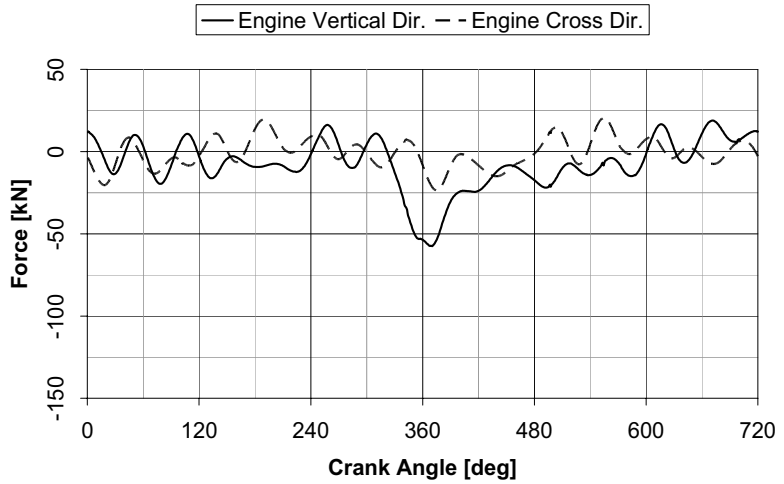

Figure 4.42. Forces acting on main bearing #7, flexible crankshaft model

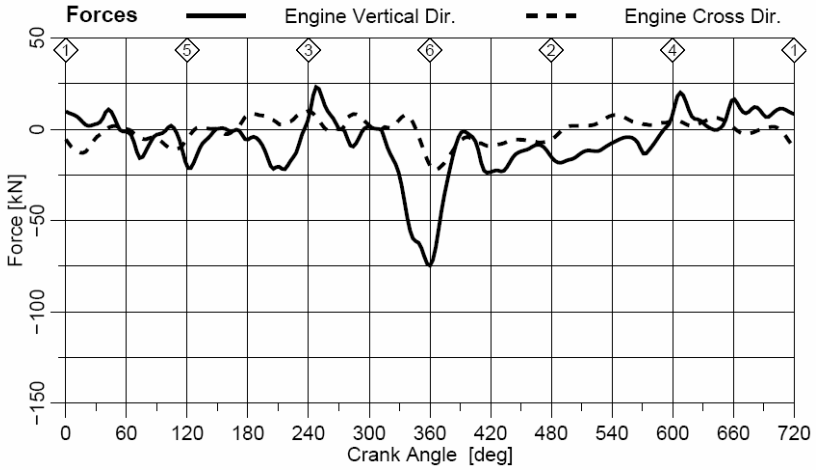

Figure 4.43. Forces acting on main bearing #7, (AVL/Excite)

4.5. Dynamic Stress Analyses

Stress analyses are carried using beam crankshaft and flexible crankshaft models. Using beam model nominal stresses at each web of the crankshaft are calculated. These results give an idea on most stressed regions of the crankshaft. If the stress concentration factors at main pin and crankpin fillets are known, actual fillet stresses for bending and torsion can be calculated. Flexible crankshaft model is good to get accurate boundary conditions for detailed stress analysis. With this model it is possible to find stresses at critical locations of the crankshaft such as crankshaft fillets.

4.5.1. Beam Crankshaft Model

For beam crankshaft model, torque at the connection points of main pins and webs and web bending moments are determined first. These locations are shown in Figure 4.44 for first two crank throws. Bending and shear stresses are calculated at each web and pin center. Torsional stresses are calculated at the connection points between main pins and webs.

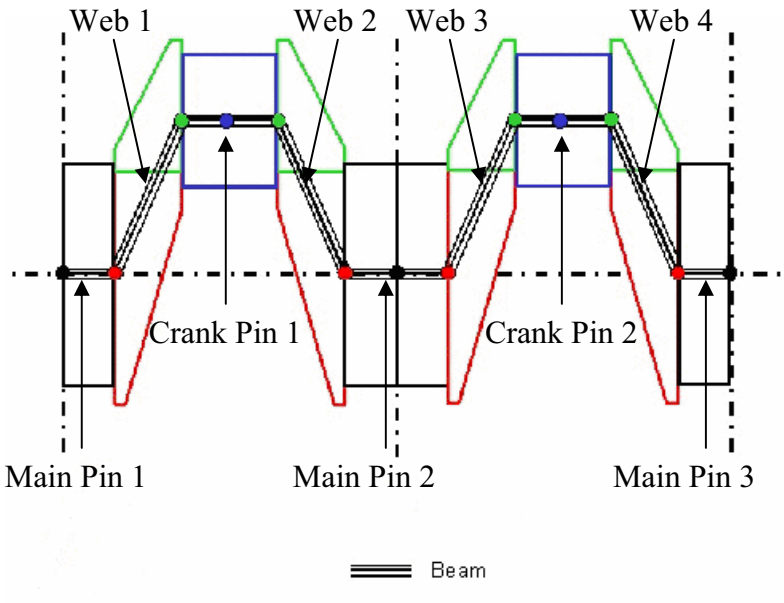

Figure 4.44. Locations of main pin, crank pin and webs for beam crankshaft model, [61]

The results for beam crankshaft model are given in Appendix B. The most critical region of the crankshaft is Web 12 where maximum bending stress reaches 143 MPa. Second critical region is Web 1. At this web maximum bending stress reads 138 MPa. Torsional stresses do not reach high values for 7.3 L engine crankshaft. Maximum torsional, bending and shear stresses at each web of beam crankshaft model is given in Table 4.4

Table 4.4. Maximum stresses for beam crankshaft model

	Maximum Torsional Stress (MPa)	Maximum Bending Stress (MPa)	Maximum Shear Stress (MPa)
Web #1	6.8	137.9	9.8
Web #2	37.2	43.3	16.7
Web #3	37.2	42.8	11.2
Web #4	41.6	44.1	15.9
Web #5	41.6	43.2	14.4
Web #6	36.8	92.6	12.2
Web #7	36.8	92.4	11.5
Web #8	41.7	57.6	15.2
Web #9	41.7	50.2	13.7
Web #10	38.4	54.3	13.1
Web #11	38.4	42.2	16.2
Web #12	33.5	142.8	11.0

4.5.2. Flexible Crankshaft Model

When flexible crankshaft model is used, crankshafts with and without oil holes are considered to see effects of oil holes on crankshaft stresses. Oil holes bore diameters are 8 mm and fillet radii are 3 mm. To see the effect of torsional vibration damper on crankshaft stresses, analyses are performed with and without torsional vibration damper. A linear torsional vibration damper, the specifications of which are given in section 4.3, is used when a TV damper is included into the analyses.

The most critical web is found to be the 12th web which is the one near the flywheel. Dynamic stress results at main journal and crank pin fillets of this web are given in Figures 4.45-4.68 for the cases mentioned above.

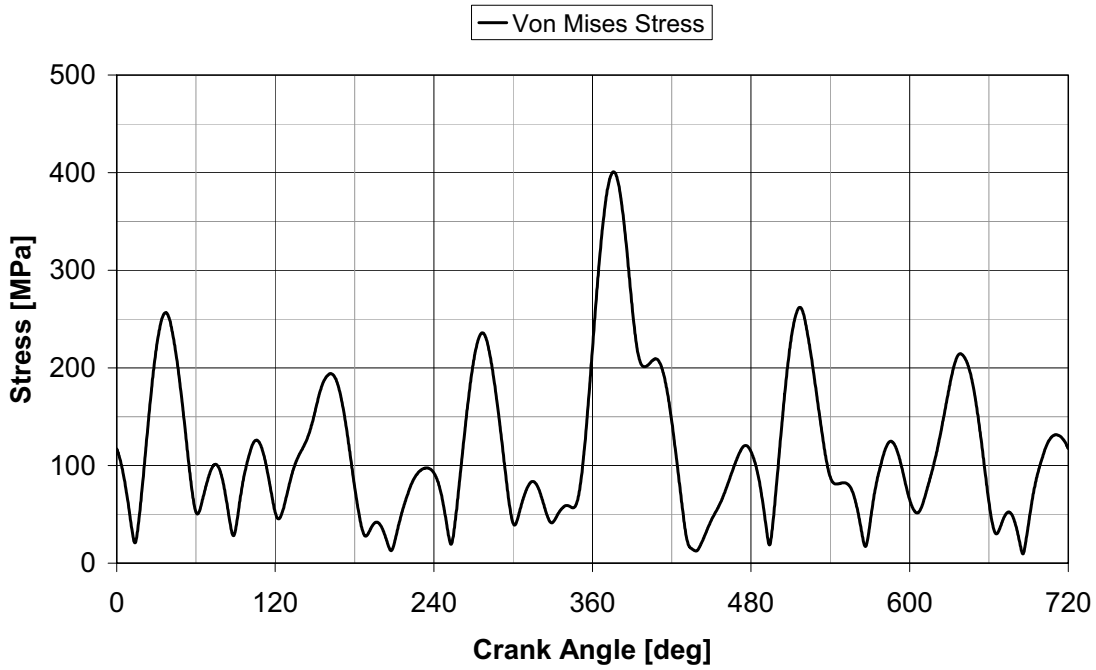

Figure 4.45. Time history of Von Mises stress at Web #12, fillet to main journal (no oil holes, without TV damper)

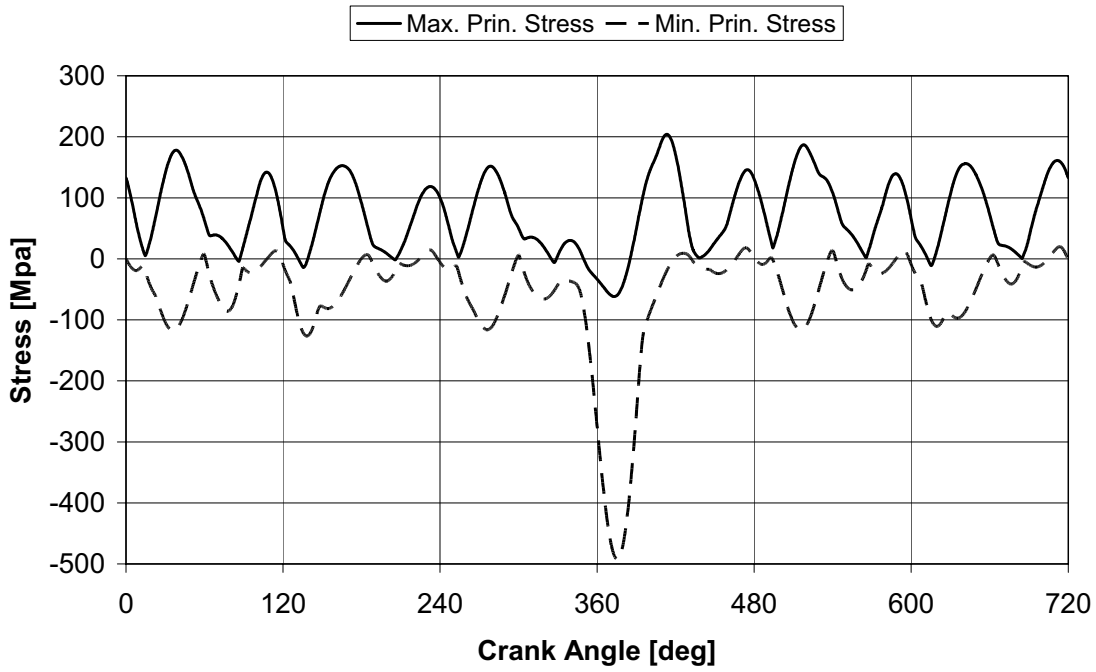

Figure 4.46. Time history of maximum and minimum principle stresses at Web #12, fillet to main journal (no oil holes, without TV damper)

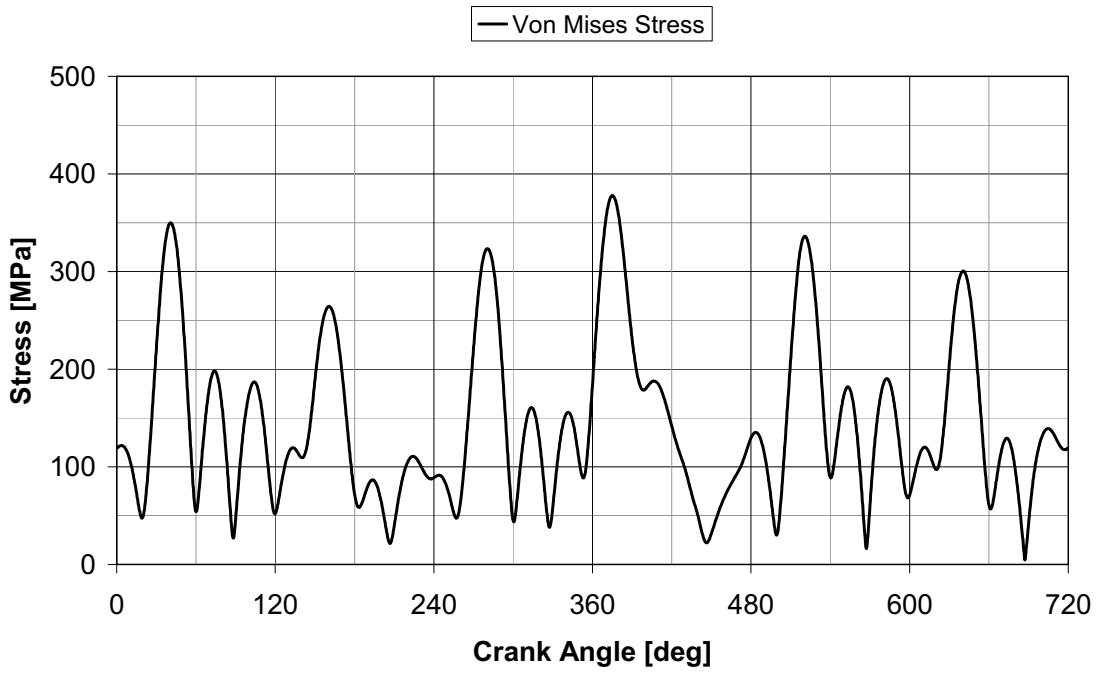

Figure 4.47. Time history of Von Mises stress at Web #12, fillet to crank pin (no oil holes, without TV damper)

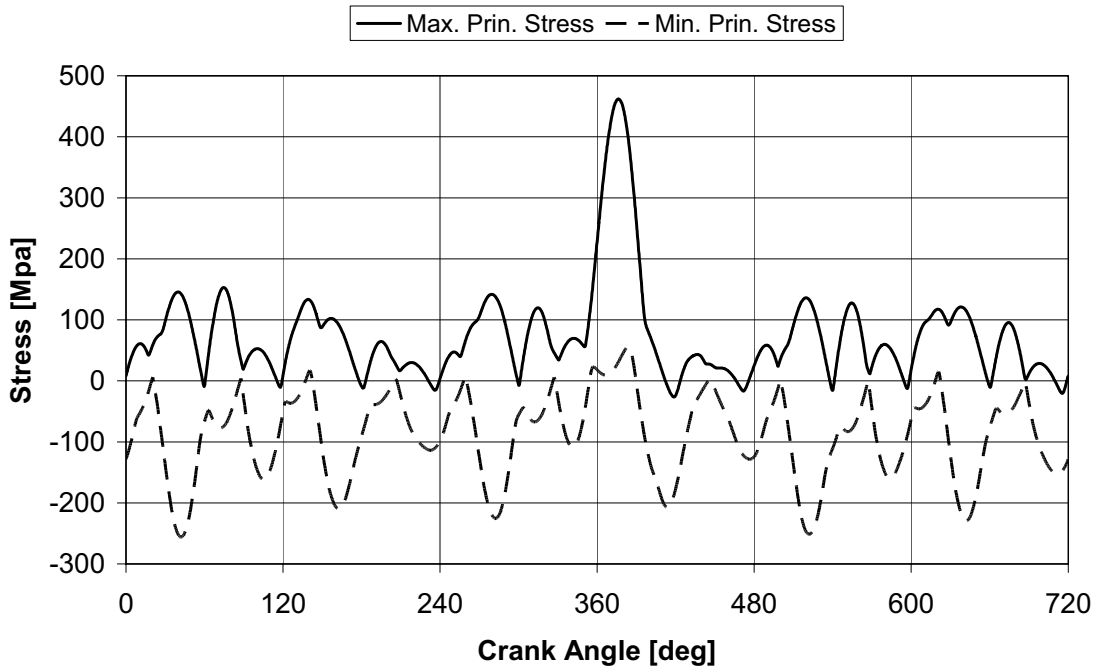

Figure 4.48. Time history of maximum and minimum principle stresses at Web #12, fillet to crank pin (no oil holes, without TV damper)

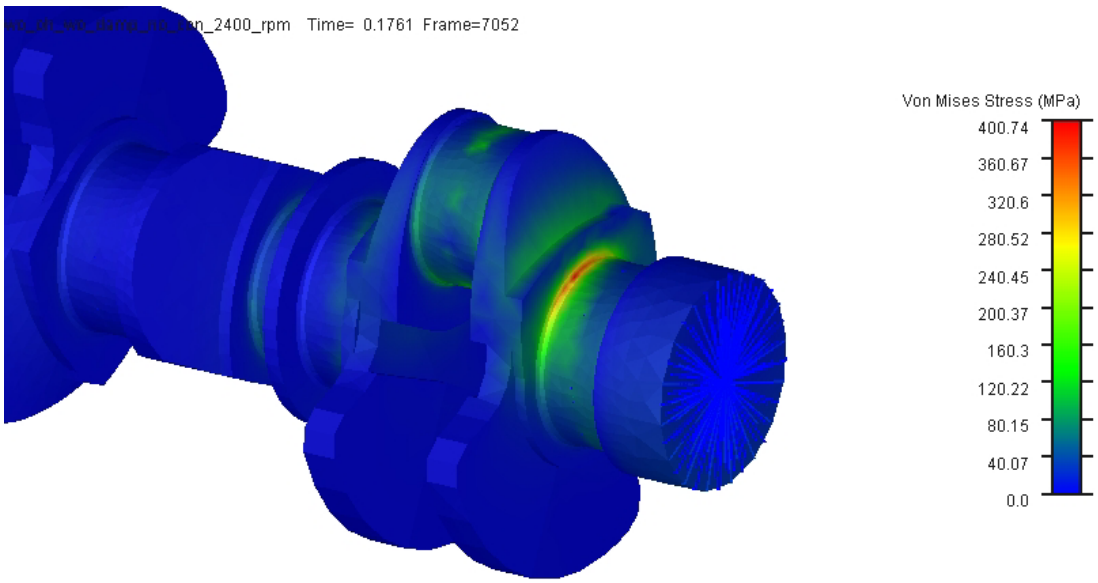

Figure 4.49. Stress state at Web #12, fillet to main journal (no oil holes, without TV damper)

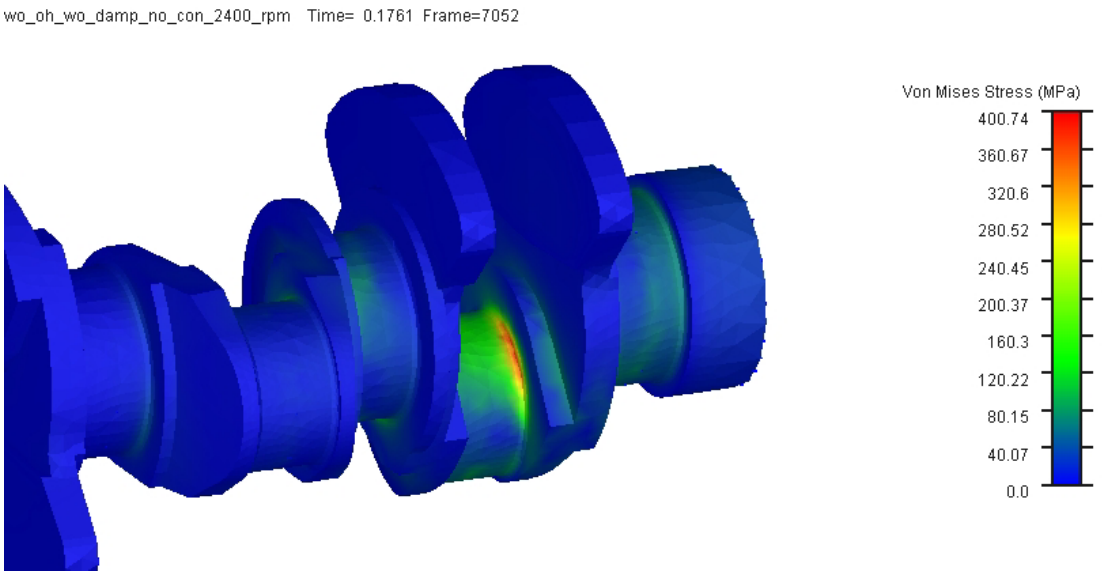

Figure 4.50. Stress state at Web #12, fillet to crank pin (no oil holes, without TV damper)

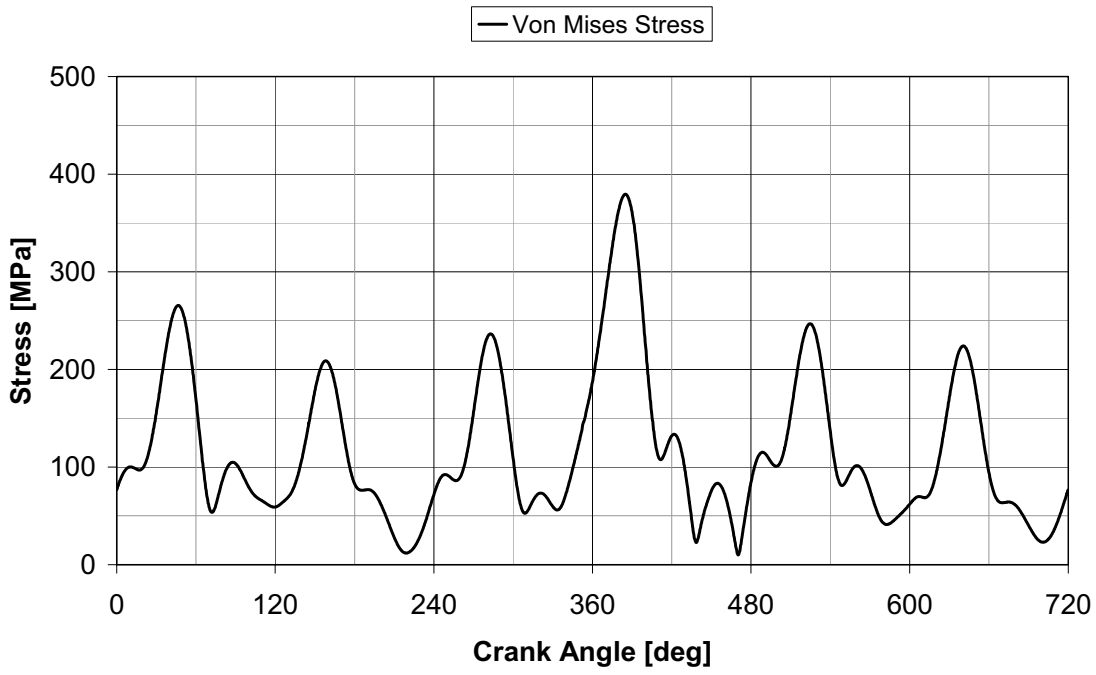

Figure 4.51. Time history of Von Mises stress at Web #12, fillet to main journal (no oil holes, with TV damper)

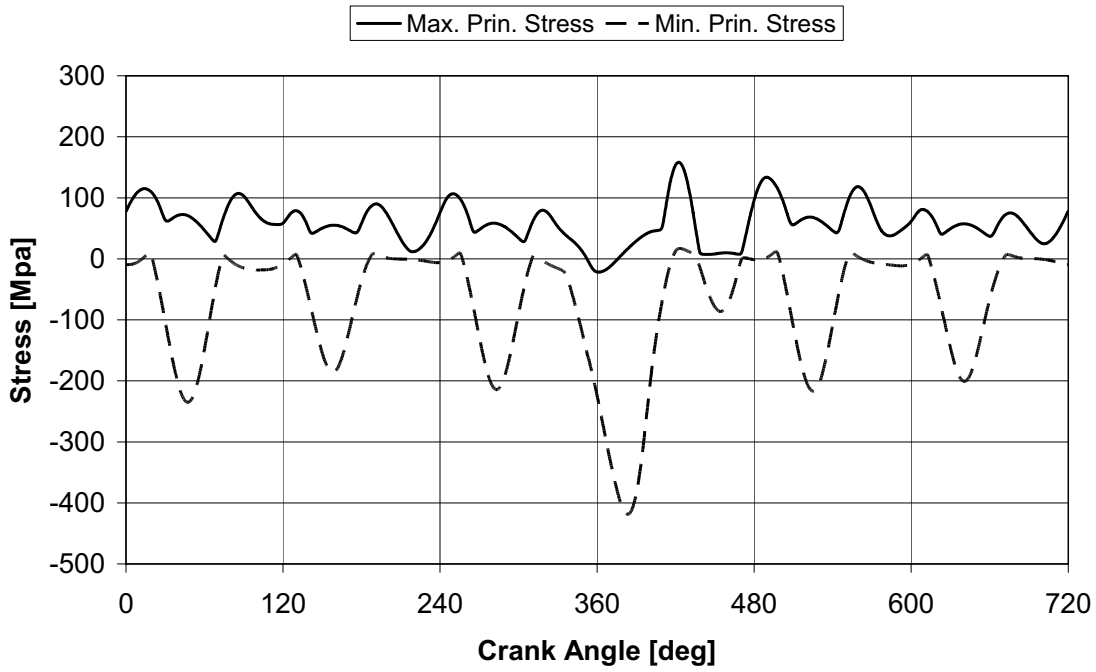

Figure 4.52. Time history of maximum and minimum principle stresses at Web #12, fillet to main journal (no oil holes, with TV damper)

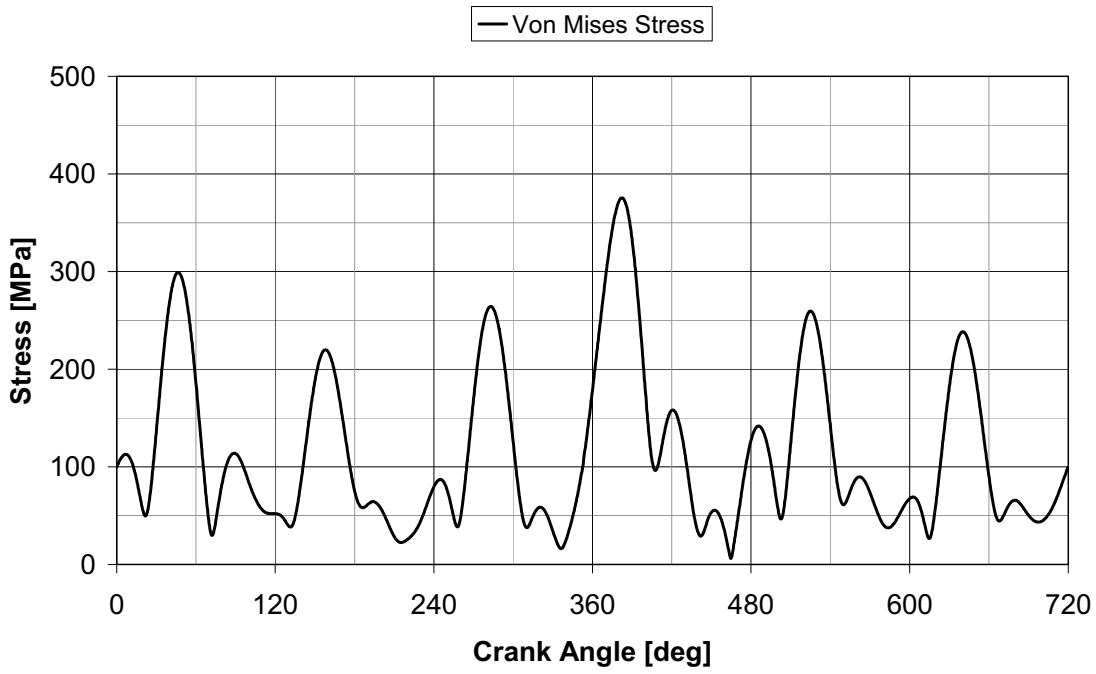

Figure 4.53. Time history of Von Mises stress at Web #12, fillet to crank pin (no oil holes, with TV damper)

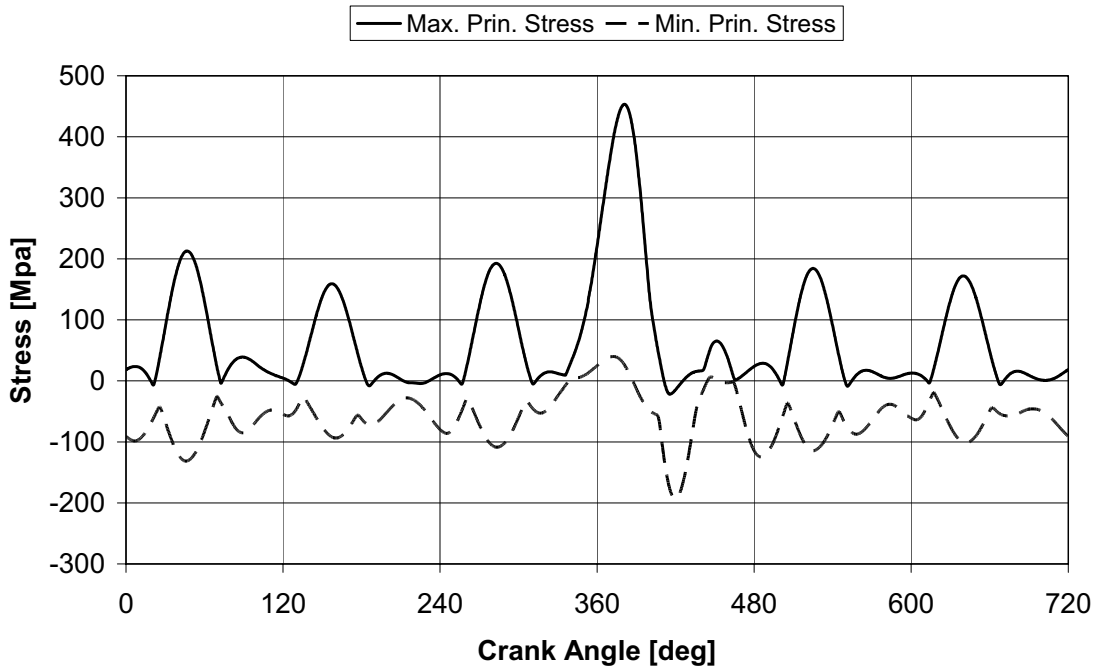

Figure 4.54. Time history of maximum and minimum principle stresses at Web #12, fillet to crank pin (no oil holes, with TV damper)

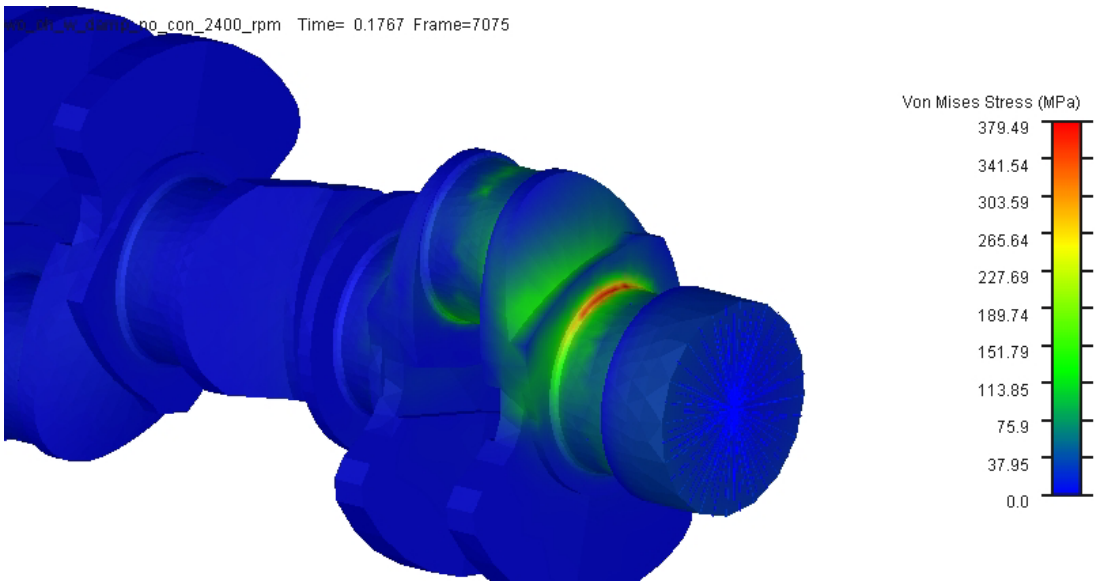

Figure 4.55. Stress state at Web #12, fillet to main journal 7 (no oil holes, with TV damper)

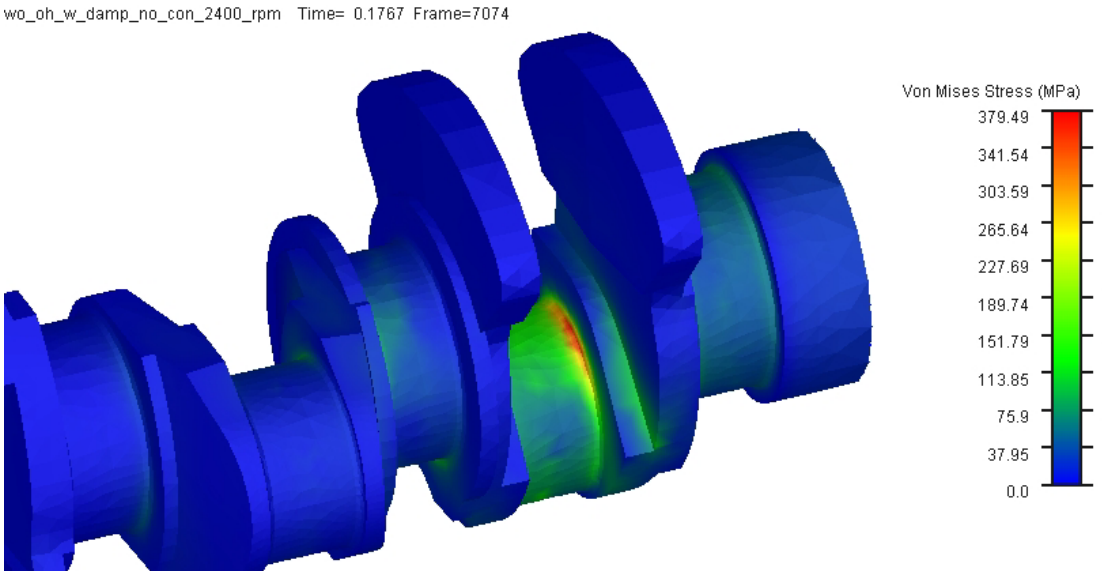

Figure 4.56. Stress state at Web #12, fillet to crank pin (no oil holes, with TV damper)

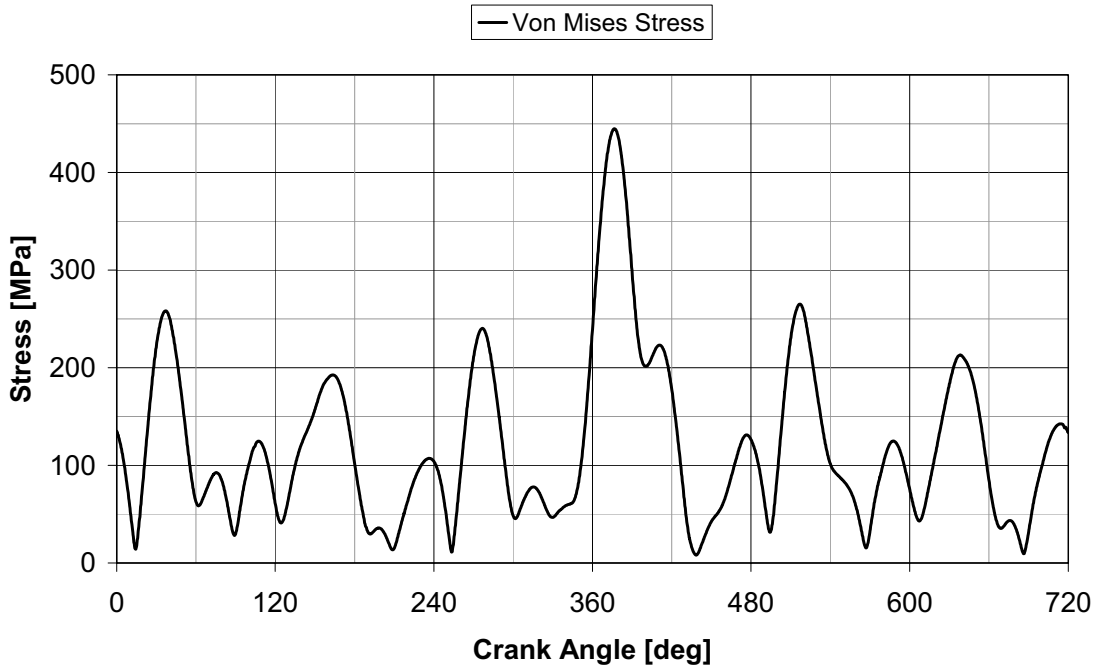

Figure 4.57. Time history of Von Mises stress at Web #12, fillet to main journal (with oil holes, without TV damper)

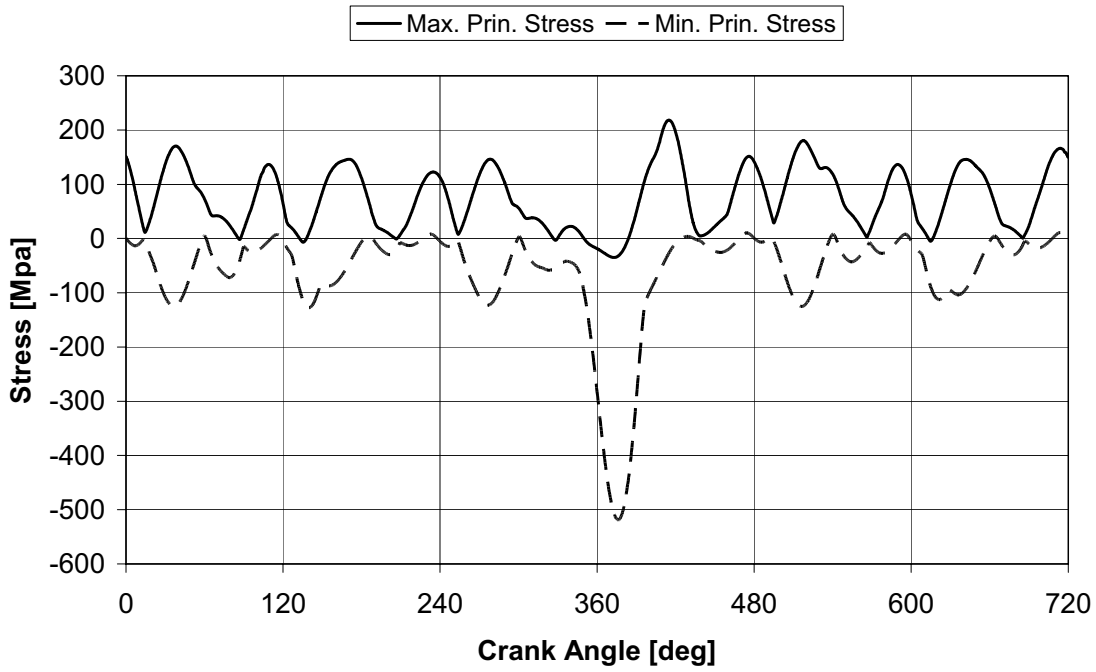

Figure 4.58. Time history of maximum and minimum principle stresses at Web #12, fillet to main journal (with oil holes, without TV damper)

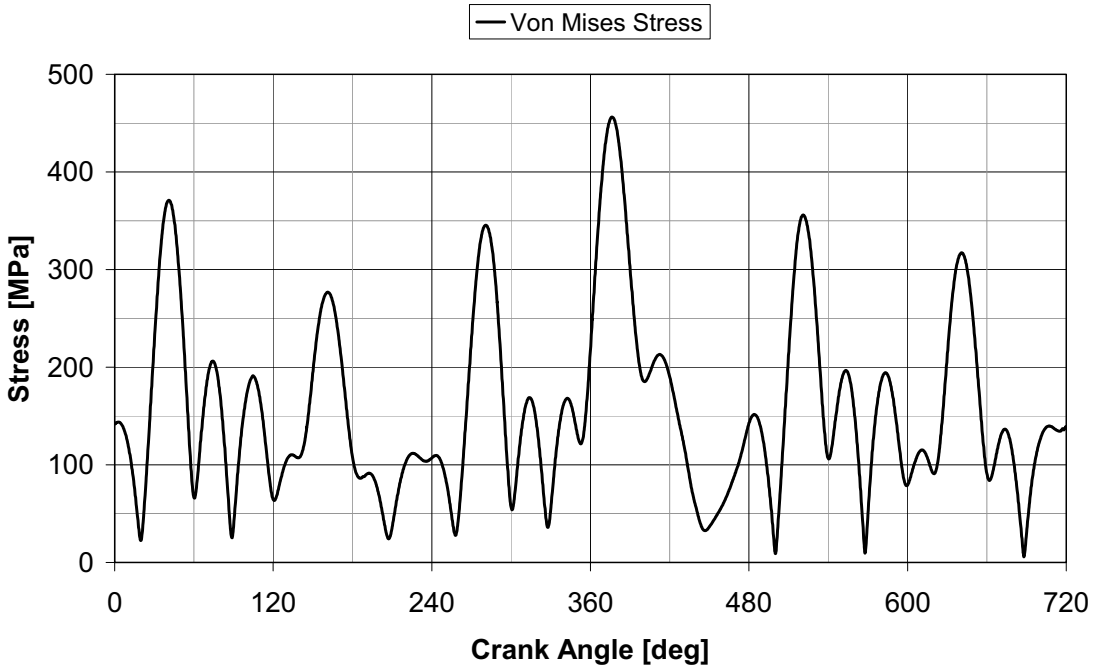

Figure 4.59. Time history of Von Mises stress at Web #12, fillet to crank pin (with oil holes, without TV damper)

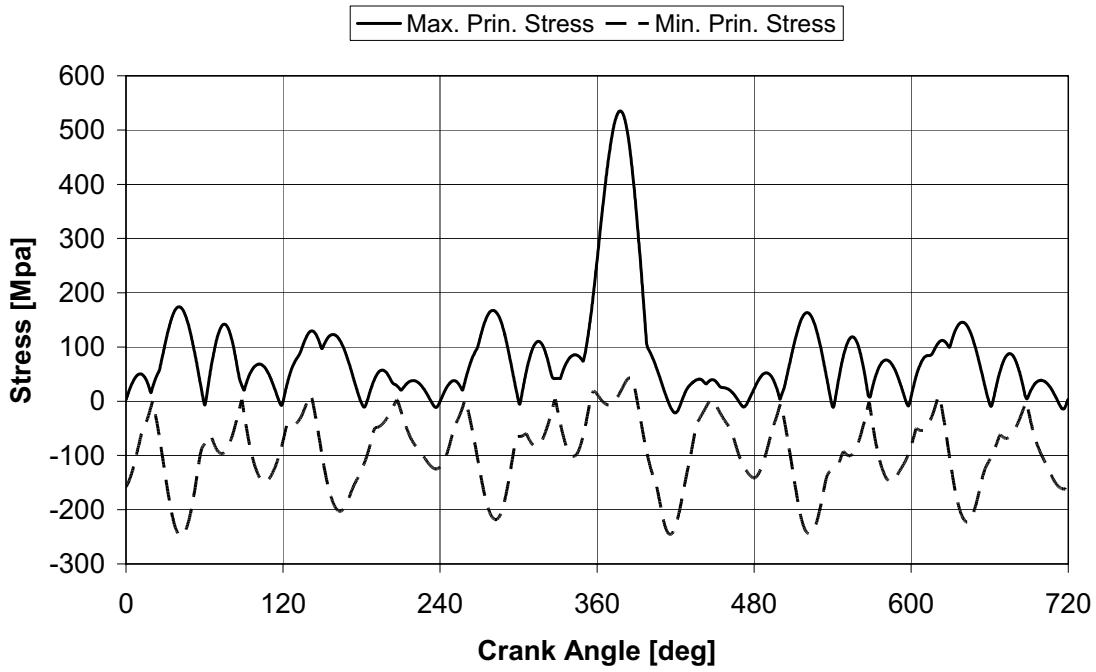

Figure 4.60. Time history of maximum and minimum principle stresses at Web #12, fillet to crank pin (with oil holes, without TV damper)

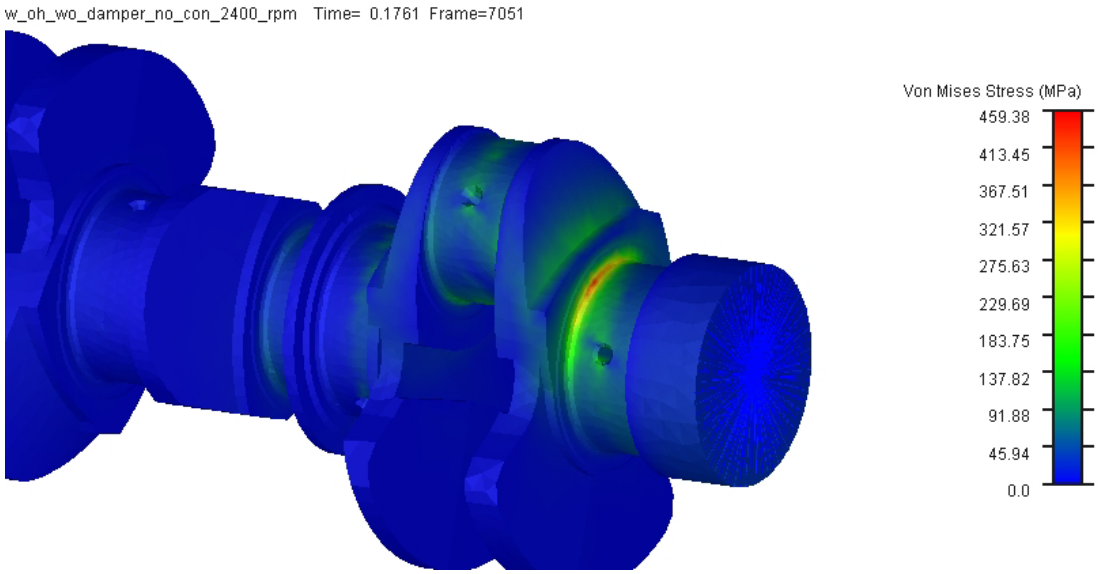

Figure 4.61. Stress state at Web #12, fillet to main journal (with oil holes, without TV damper)

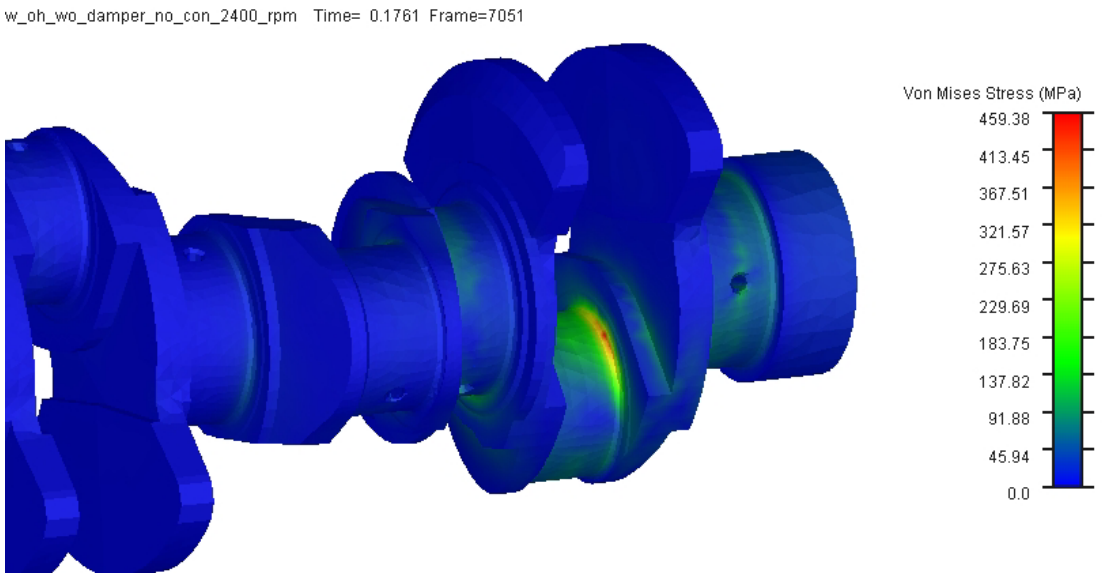

Figure 4.62. Stress state at Web #12, fillet to crank pin (with oil holes, without TV damper)

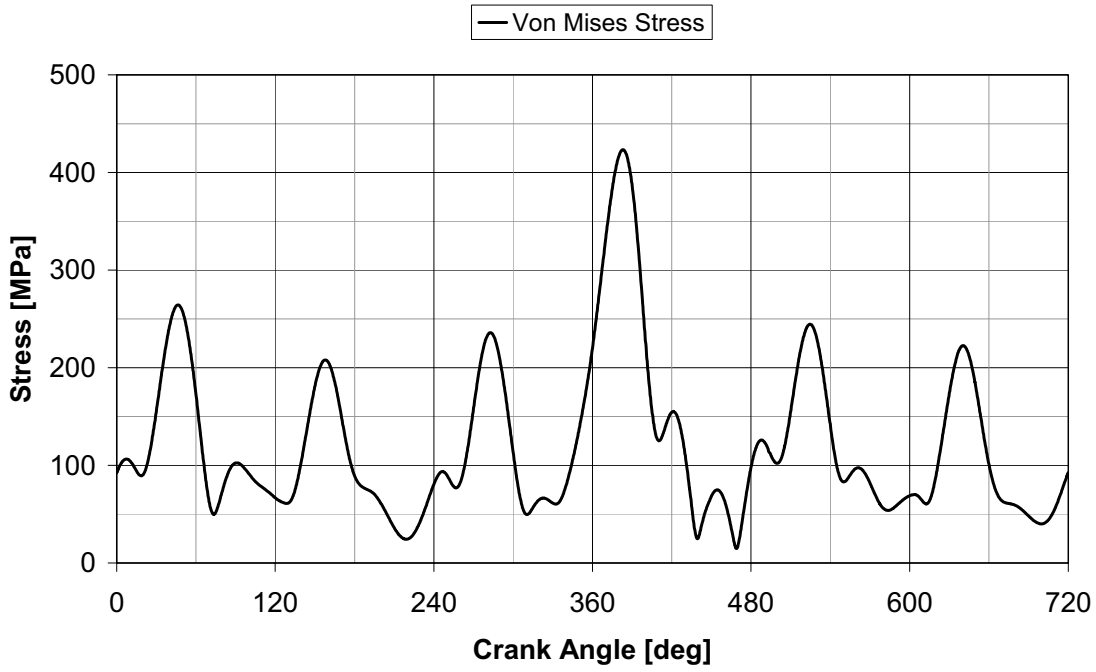

Figure 4.63. Time history of Von Mises stress at Web #12, fillet to main journal (with oil holes, with TV damper)

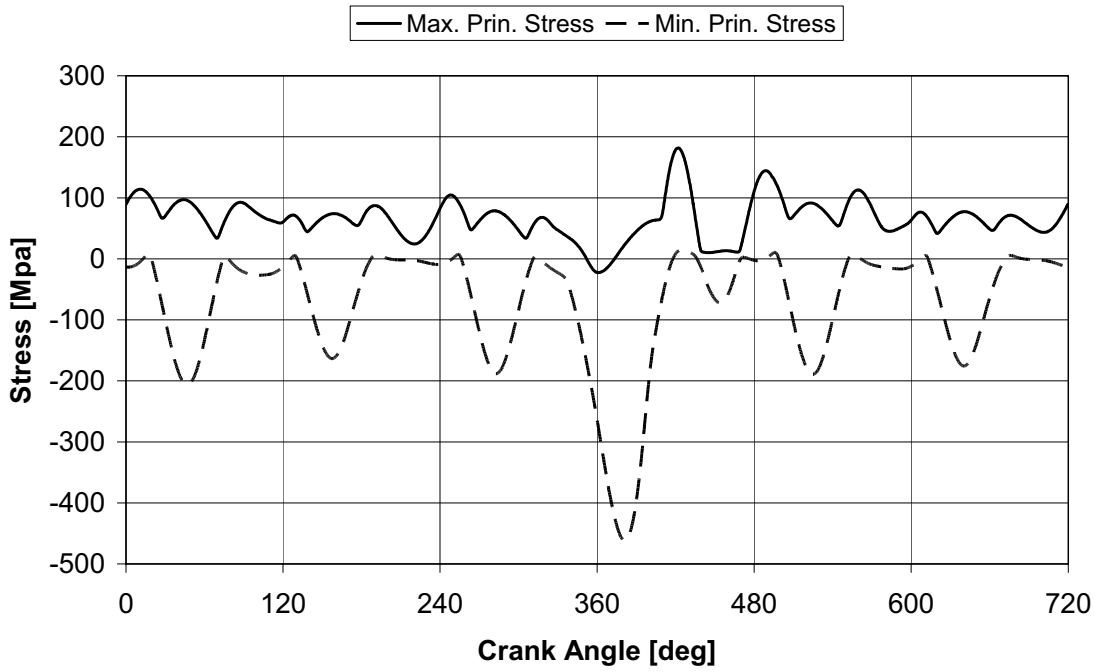

Figure 4.64. Time history of maximum and minimum principle stresses at Web #12, fillet to main journal (with oil holes, with TV damper)

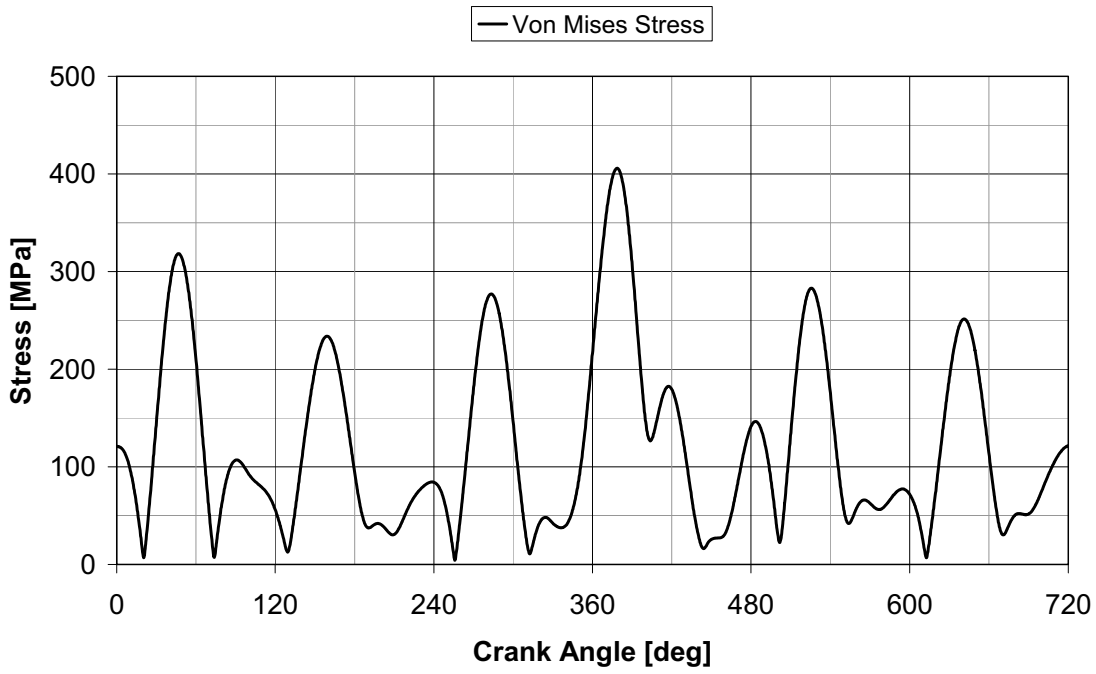

Figure 4.65. Time history of Von Mises stress at Web #12, fillet to crank pin (with oil holes, with TV damper)

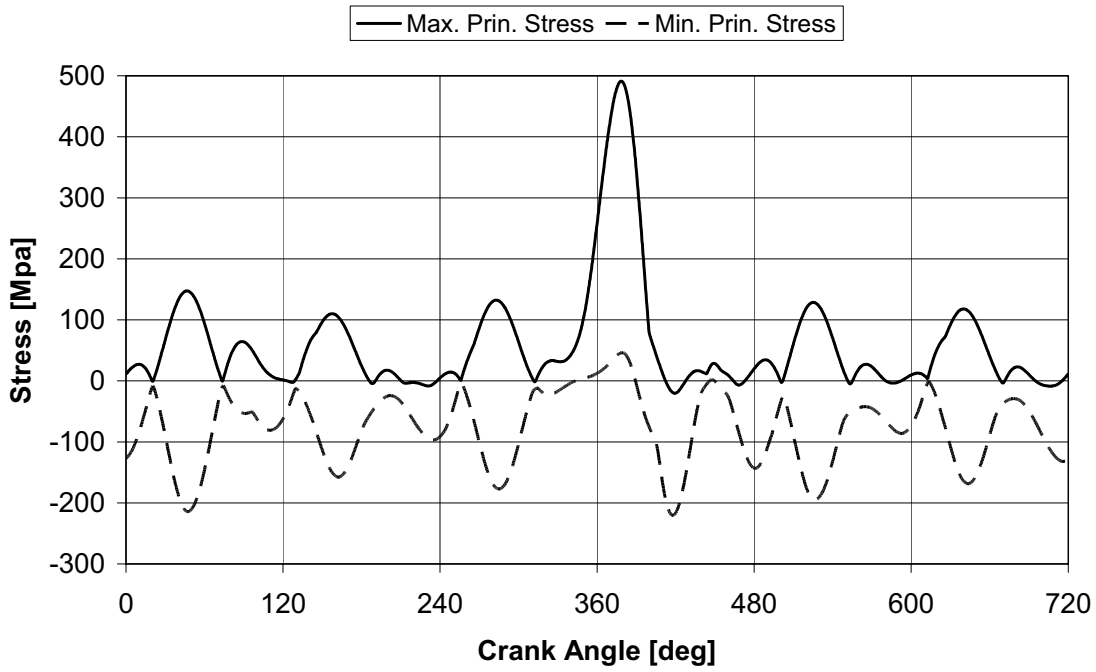

Figure 4.66. Time history of maximum and minimum principle stresses at Web #12, fillet to crank pin (with oil holes, with TV damper)

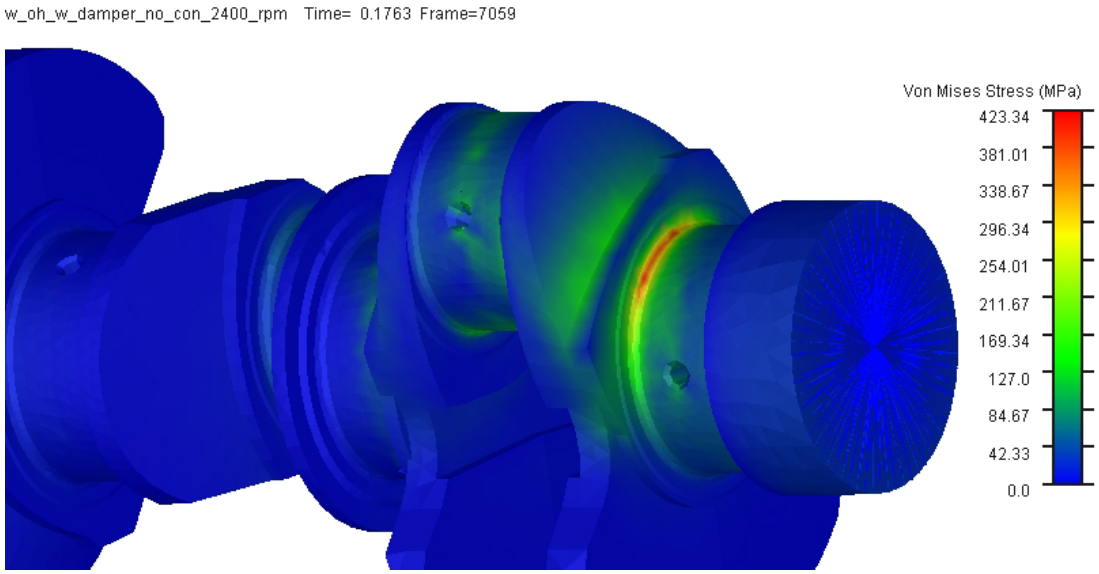

Figure 4.67. Stress state at Web #12, fillet to main journal (with oil holes, with TV damper)

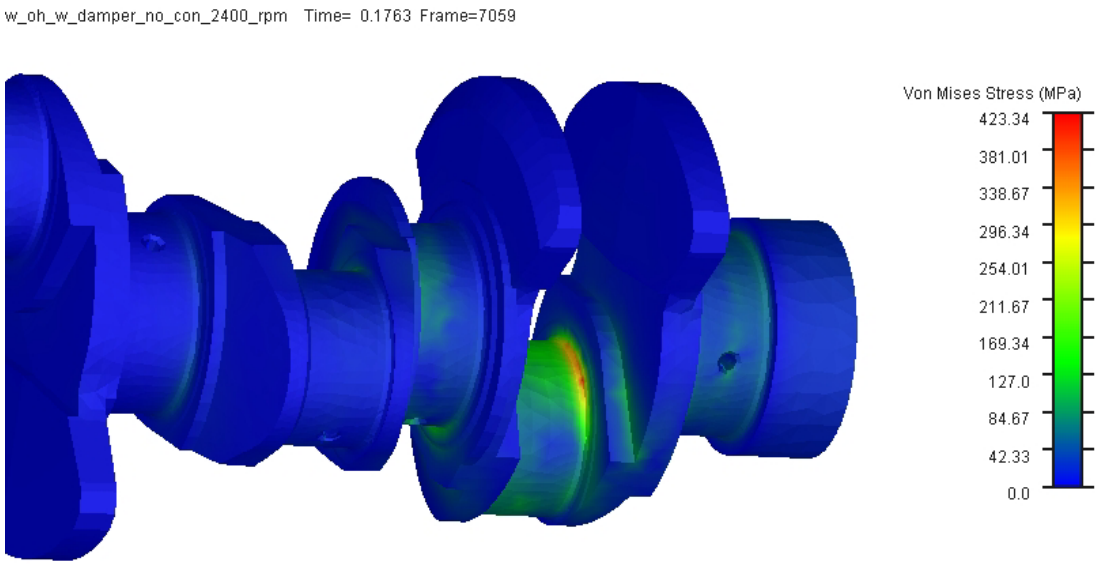

Figure 4.68. Stress state at Web #12, fillet to crank pin (with oil holes, with TV damper)

From Figures 4.45 to 4.68, following results can be drawn: Maximum Von Mises stress on the crankshaft with oil holes and without TV damper is 459.4 MPa and it occurs at crank pin fillet. For the same crankshaft with TV damper, the maximum stress reduces to 423.3 MPa and it occurs at main pin fillet. Maximum von Mises stress of the crankshaft without oil holes and TV damper is 400.7 MPa and it occurs at the main pin fillet. For the same crankshaft with TV damper, the maximum stress reduces to 379.5 MPa and it occurs at main pin fillet. For all cases, maximum stresses occur during firing of cylinder # 6 when cylinder 6 is nearly at top dead center position and the load tends to bend the crankshaft. Therefore, maximum stresses occur as a result of bending. Other five peaks seen in Figures 4.45 to 4.68 are the result of torsional vibration of the crankshaft. The effect of TV damper on dynamic stresses can clearly be seen in Figures 4.51-4.56 for crankshaft without oil holes and in Figures 4.63-4.68 for crankshaft with oil holes. Stress amplitudes reduce with the addition of TV damper. Oil holes reduce the effective area and are close to fillet regions. As can be seen from Figures 4.57-4.68, crankshaft with oil holes has higher stresses than the one without oil holes. A separate attention must be given to oil holes in the design stage of the crankshaft and they must be included into analyses.

4.5.3. Effect of TV Damper Stiffness and Damping on Crankshaft Stress

Effects of stiffness and damping values of the TV damper on crankshaft stresses are investigated using the flexible crankshaft model with oil holes and the results are plotted in Figures 4.69 - 4.74. Maximum Von Mises stress change at main pin and crank pin fillets of Web #12 with respect to stiffness and damping values of the TV damper is given in Tables 4.5 and 4.6, respectively.

As can be seen from Figures 4.69 to 4.74, stiffness and damping value changes of the TV damper have little influence on maximum Von Mises stress at main pin and crank pin fillets because maximum Von Mises stress occurs due to bending but not torsion for this specific engine. Peak values of Von Mises stress increase due to contribution of cylinder 5 and 4 and decrease due to contribution of cylinder 2 as the stiffness value of the TV damper increases. From Tables 4.4 and 4.5, it is seen that roughly an optimum value of stiffness and damping values of the TV damper exists and these optimum values are approximately 100000 Nm/rad for stiffness and 75 Nms/rad for damping.

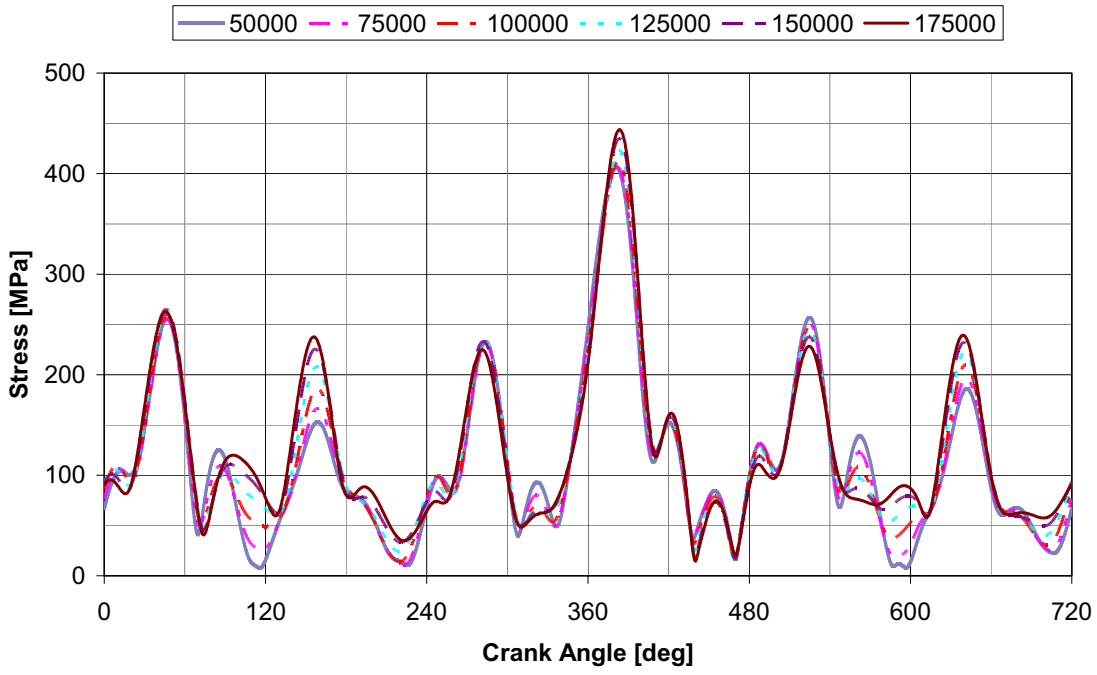

Figure 4.69. Time history of Von Mises stress at Web #12 for different torsional stiffness values of the damper (Node 273404), fillet to main journal 7

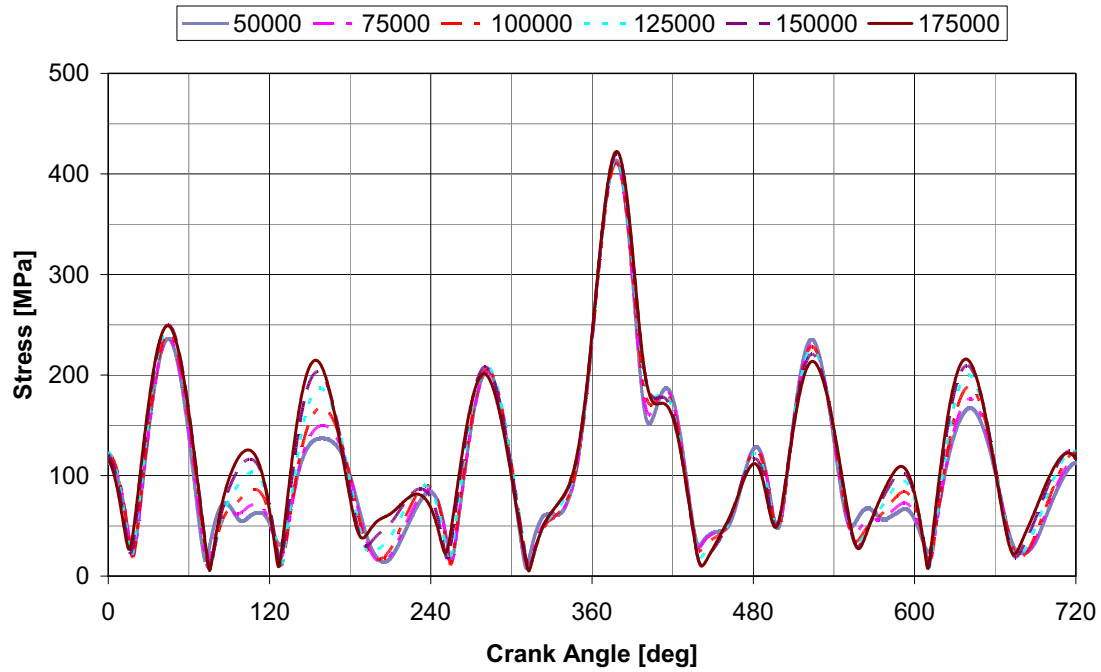

Figure 4.70. Time history of Von Mises stress at Web #12 for different torsional stiffness values of the damper (Node 273514), fillet to main journal 7

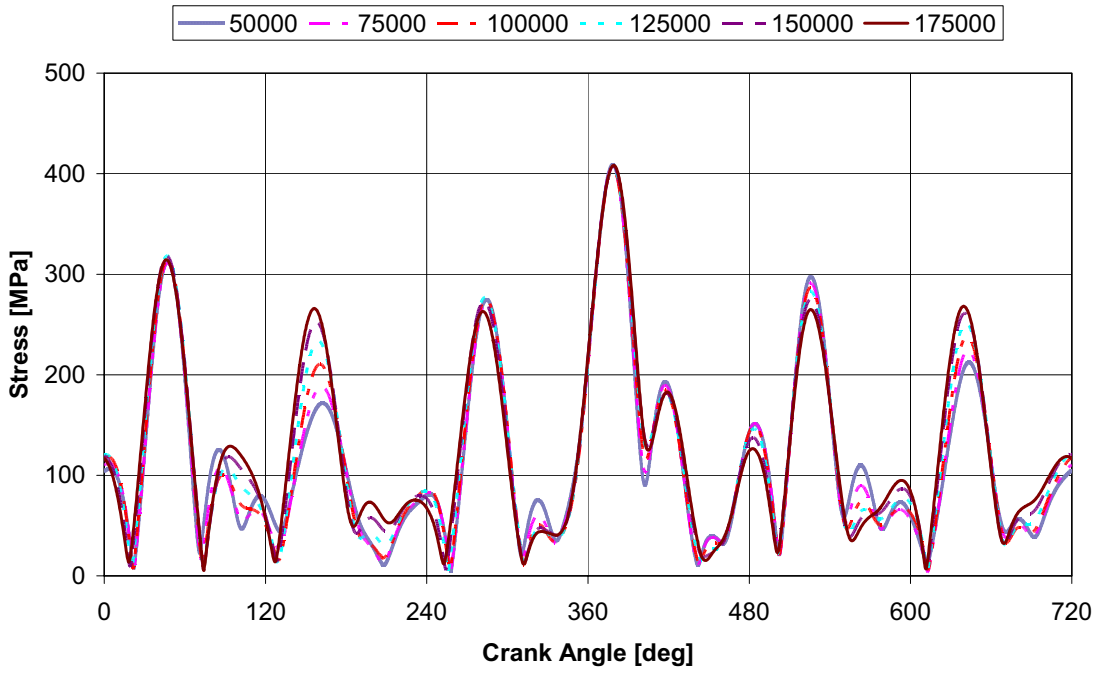

Figure 4.71. Time history of Von Mises stress at Web #12 for different torsional stiffness values of the damper (Node 277307), fillet to crank pin

Table 4.5. Maximum Von Mises stress change at main pin and crank pin fillets of Web #12 with respect to stiffness of the TV damper (damping coefficient : 95 Nms/rad)

Stiffness (Nm/rad)	Main Pin Fillet (Node 273404) (MPa)	Main Pin Fillet (Node 273514) (MPa)	Crank Pin Fillet (Node 277307) (MPa)
50000	406.59	413.60	408.29
75000	406.71	411.61	406.58
100000	412.23	410.91	404.51
125000	423.34	414.51	405.85
150000	435.21	419.86	407.76
175000	443.72	422.42	408.37

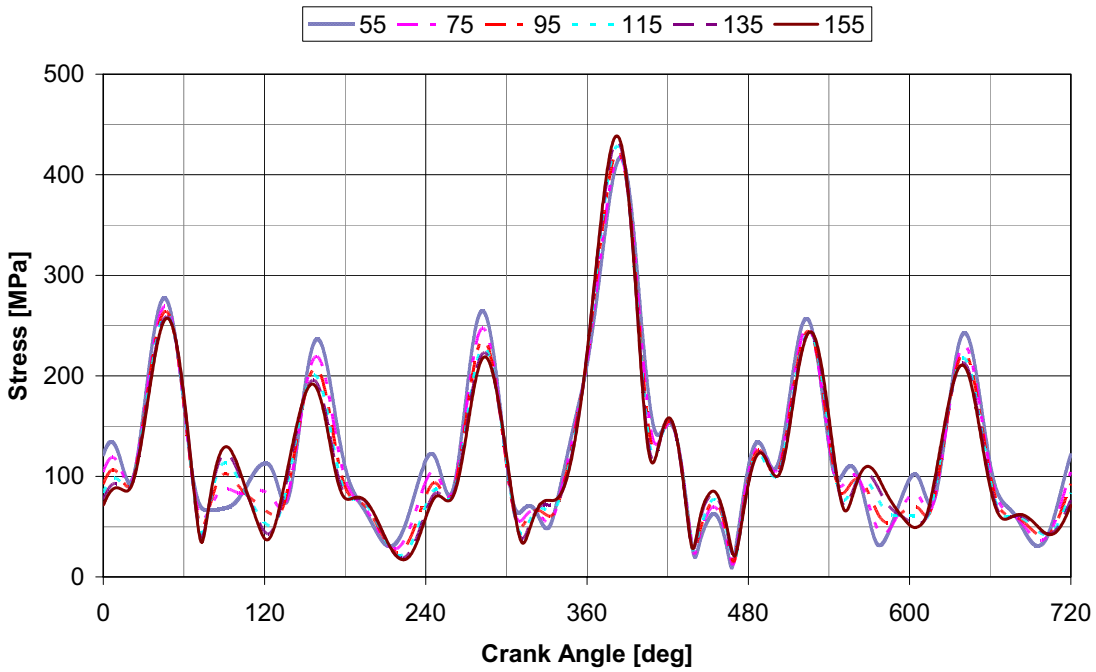

Figure 4.72. Time history of Von Mises stress at Web #12 for different damping values of the damper (Node 273404), fillet to main journal 7

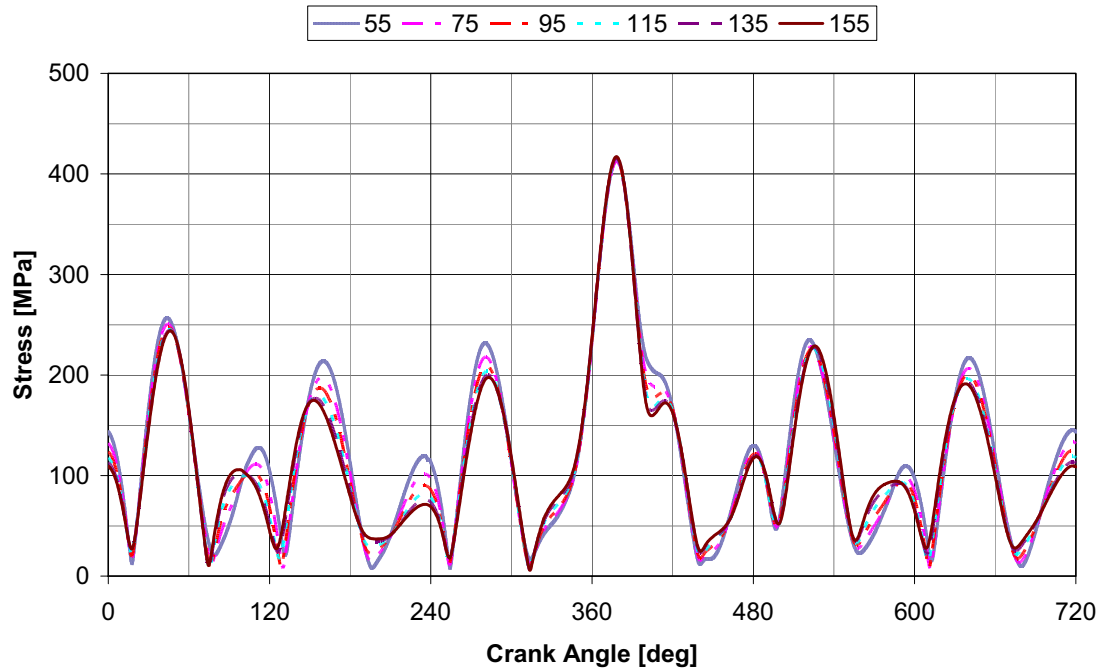

Figure 4.73. Time history of Von Mises stress at Web #12 for different damping values of the damper (Node 273514), fillet to main journal 7

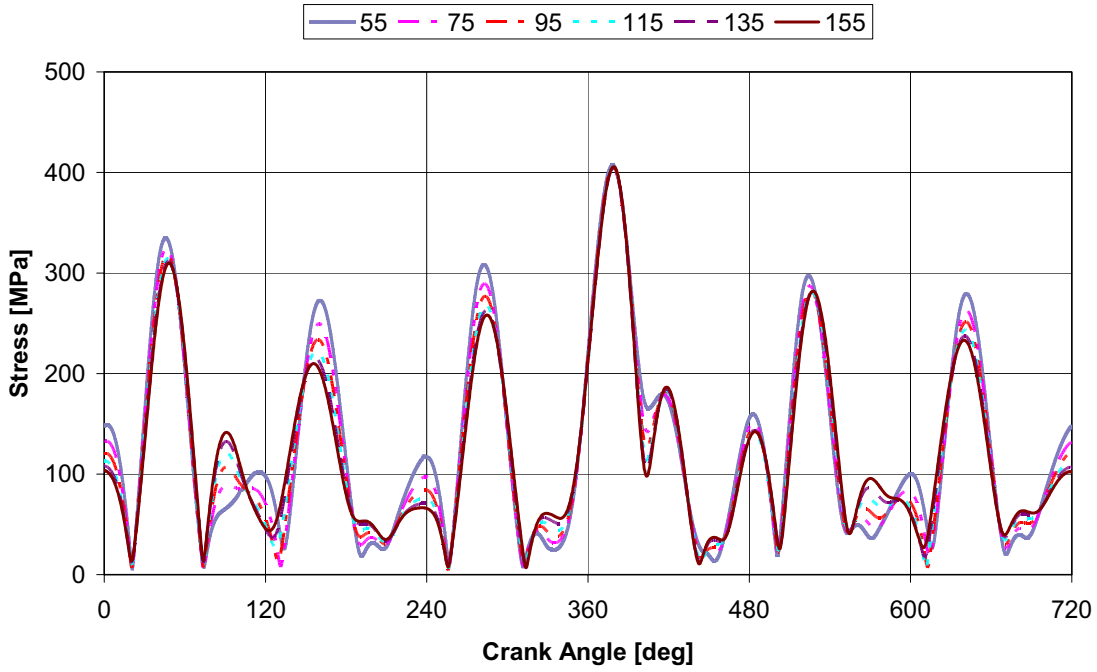

Figure 4.74. Time history of Von Mises stress at Web #12 for different damping values of the damper (Node 277307), fillet to crankpin

Table 4.6. Maximum Von Mises stress change at main pin and crank pin fillets of Web 12 with respect to damping coefficient of the TV damper (stiffness : 125000 Nm/rad)

Damping (Nms/rad)	Main Pin Fillet (Node 273404) (MPa)	Main Pin Fillet (Node 273514) (MPa)	Crank Pin Fillet (Node 277307) (MPa)
55	417.16	414.09	407.07
75	418.16	412.48	404.02
95	423.34	414.51	405.85
115	428.63	415.41	405.29
135	433.08	415.70	404.55
155	438.66	417.16	405.66

4.6. Oil Film Thickness Analysis

Oil film thicknesses at the main bearings are calculated using two and three dimensional hydrodynamic bearing models. The oil film characteristics are chosen for SAE 10W-40, where oil density is 900 kg/mm^3. Dynamic viscosity change of oil with respect to temperature is given in Table 4.7. The other characteristic input data for the analysis are given in Table 4.8.

The analyses are carried out for the full load operating condition (18 MPa) at rated engine speed (2400 rpm) and obtained results for the minimum oil film thicknesses and orbital curves for the main bearings are given in Figures 4.75 – 4.102. Minimum oil film thickness occurs in bearing # 5 when main bearings are modeled using 2D Hydrodynamic approach and it is 2.5 μm. When main bearings are modeled using 3D Hydrodynamic approach, minimum oil film thickness occurs at main bearings # 5 and # 6 and it is roughly 3 μm.

Table 4.7. Dynamic viscosity change of SAE 10W-40 oil with respect to temperature

Temperature [°C]	Viscosity [Pas]
0	1.091652
10	0.468550
20	0.232975
30	0.129544
40	0.078575
50	0.051062
60	0.035081
70	0.025223
80	0.018832
90	0.014512
100	0.011486
110	0.009300
120	0.007680
130	0.006451
140	0.005500
150	0.004750
160	0.004150
170	0.003663
180	0.003262
190	0.002929
200	0.002650

Table 4.8. Input data for oil film thickness calculation

Parameter	**Value**
Bearing width	30 mm
Bearing diameter	88 mm
Radial clearance	41.0 μm
Oil supply pressure	4.5 bar

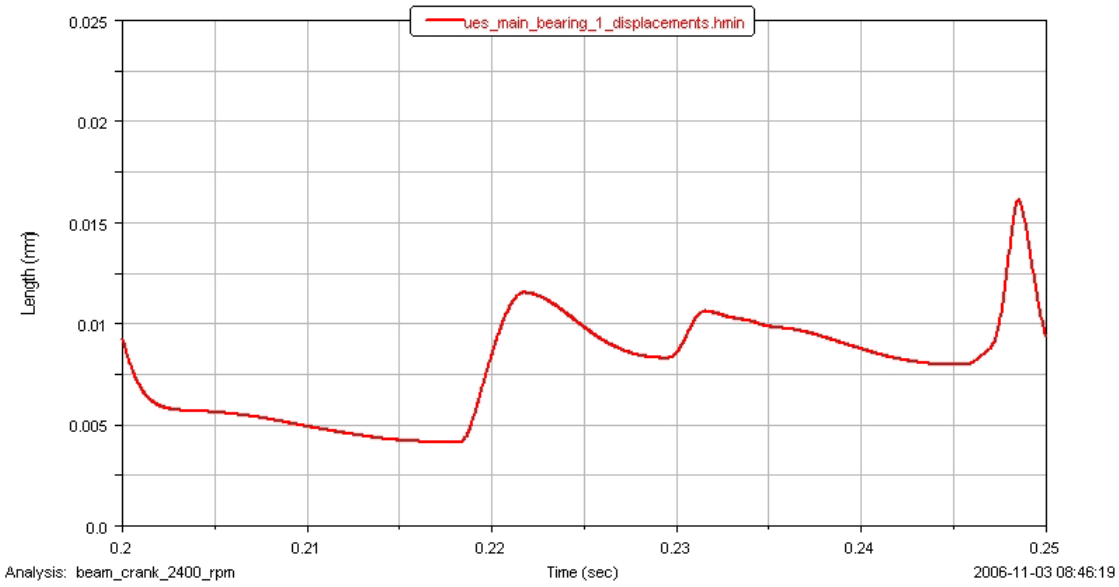

Figure 4.75. Minimum oil film thickness for main bearing #1 using 2D Hydrodynamic model

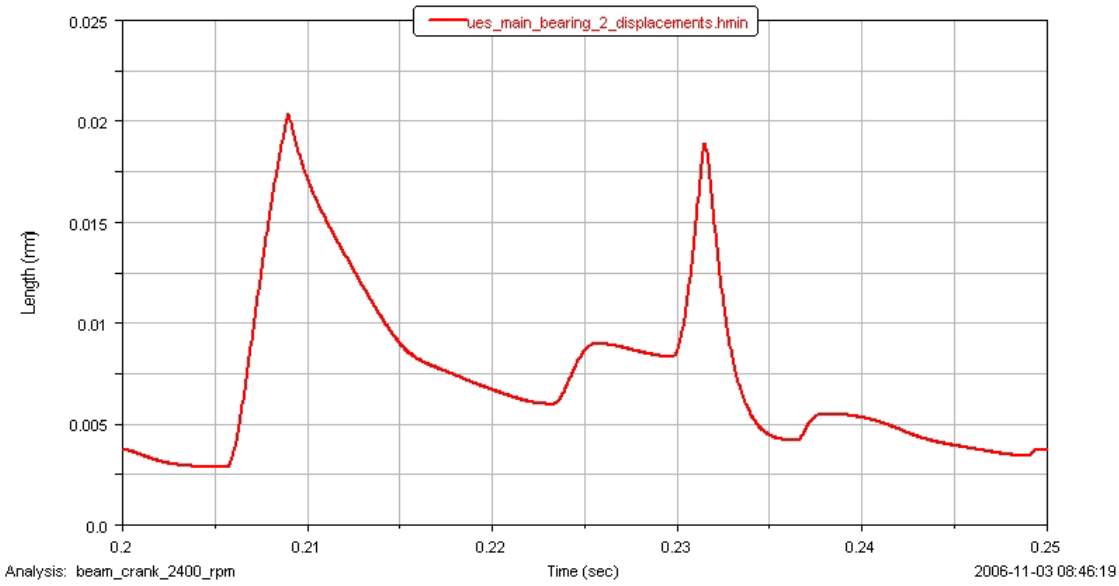

Figure 4.76. Minimum oil film thickness for main bearing #2 using 2D Hydrodynamic model

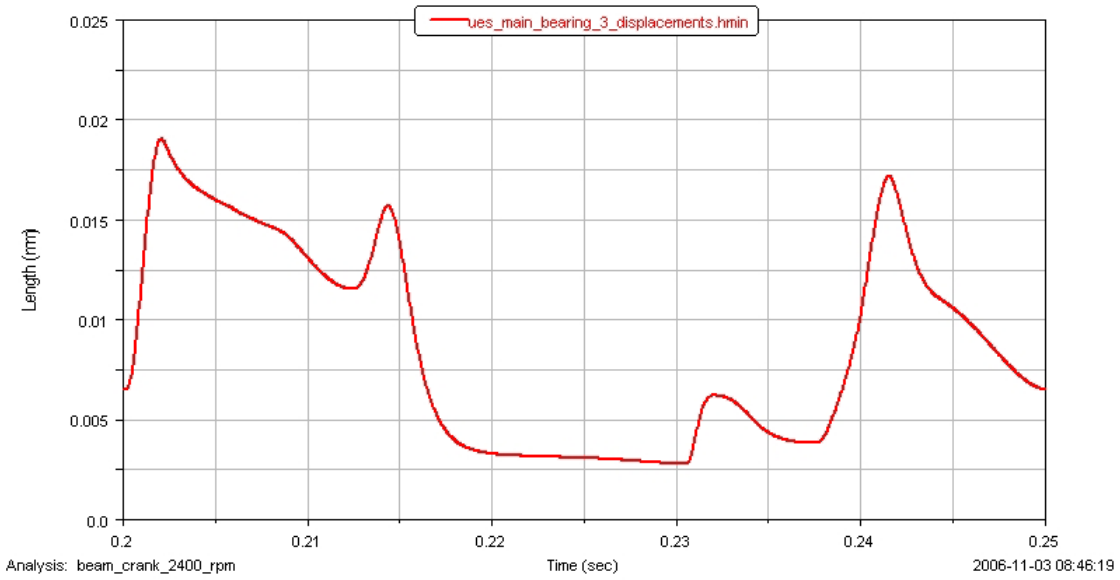

Figure 4.77. Minimum oil film thickness for main bearing #3 using 2D Hydrodynamic model

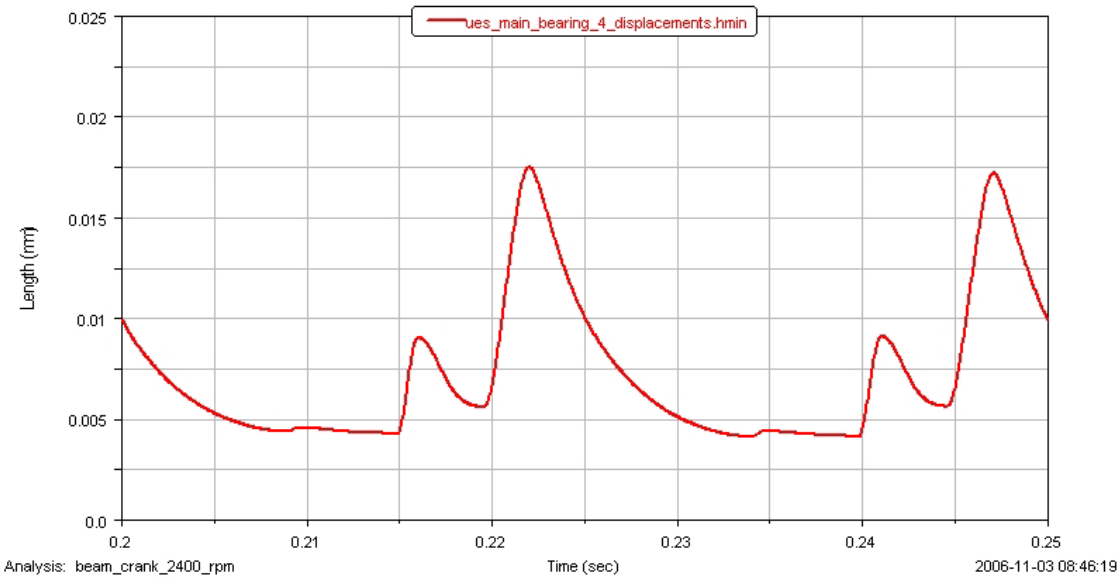

Figure 4.78. Minimum oil film thickness for main bearing #4 using 2D Hydrodynamic model

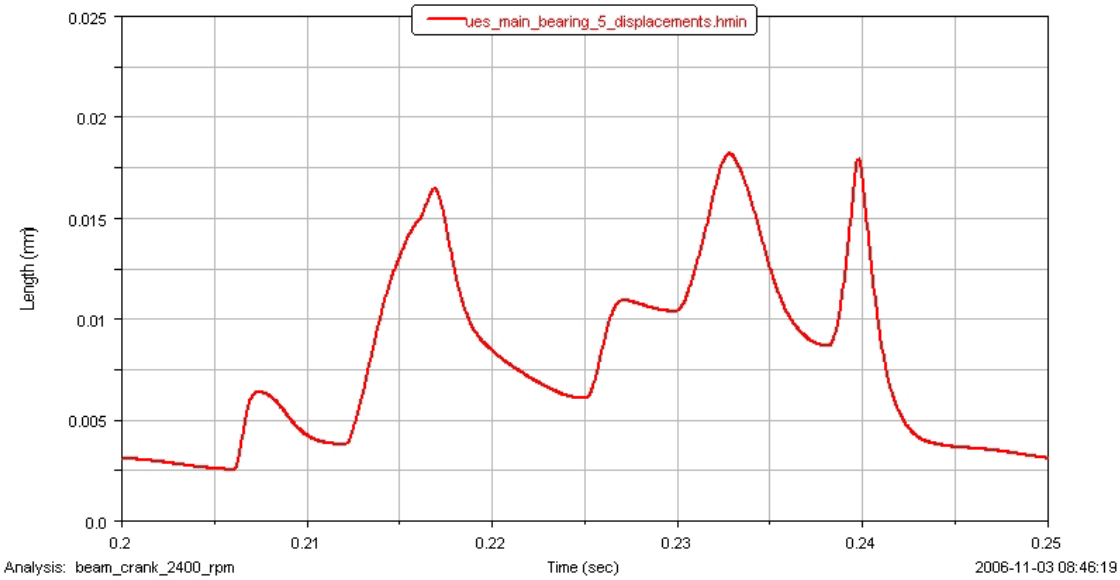

Figure 4.79. Minimum oil film thickness for main bearing #5 using 2D Hydrodynamic model

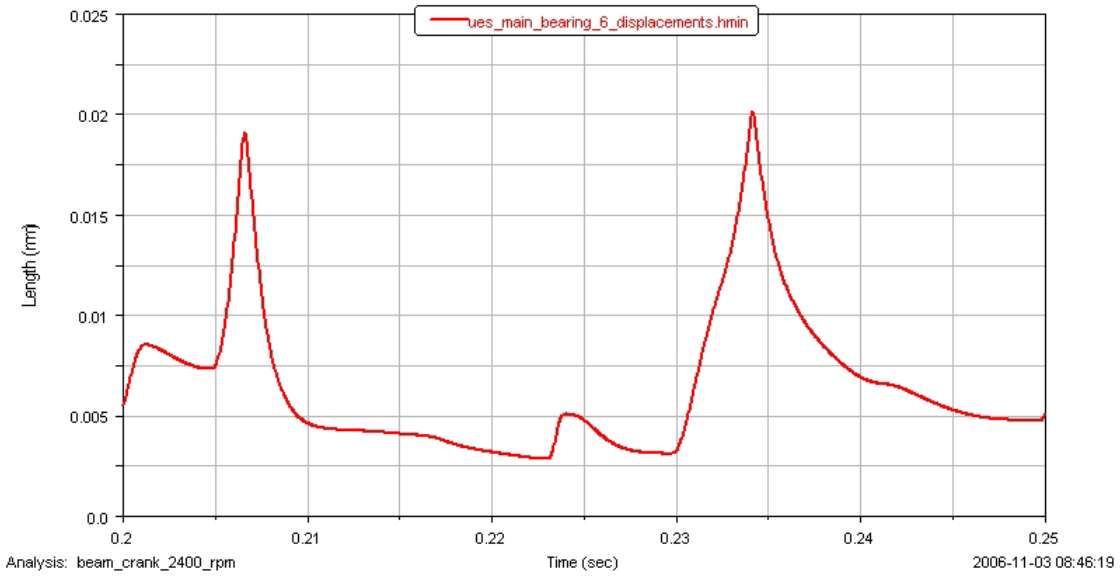

Figure 4.80. Minimum oil film thickness for main bearing #6 using 2D Hydrodynamic model

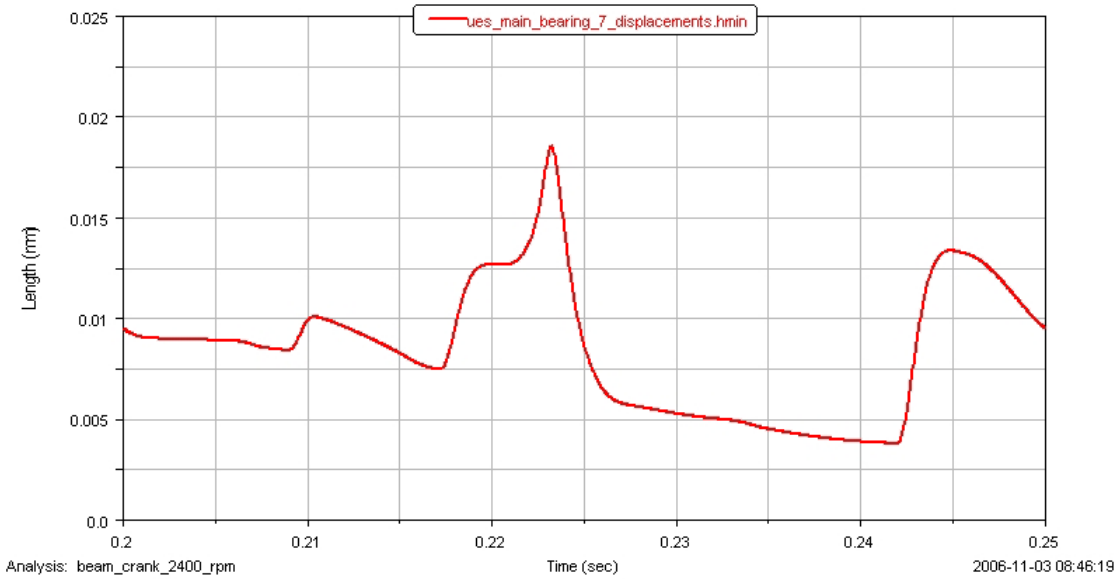

Figure 4.81. Minimum oil film thickness for main bearing #7 using 2D Hydrodynamic model

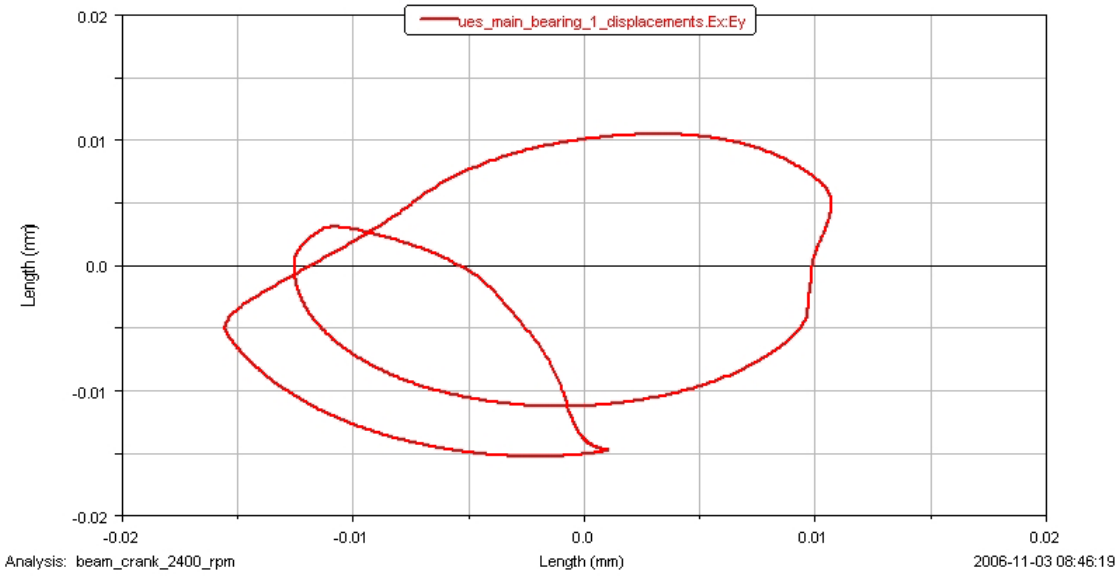

Figure 4.82. Orbital curve for main bearing #1 using 2D Hydrodynamic model

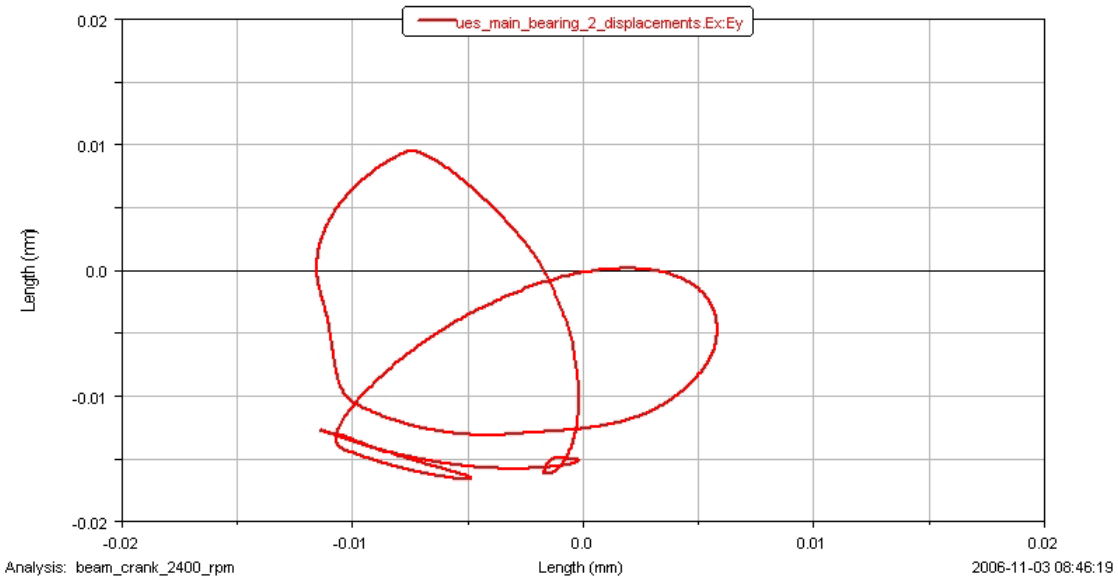

Figure 4.83. Orbital curve for main bearing #2 using 2D Hydrodynamic model

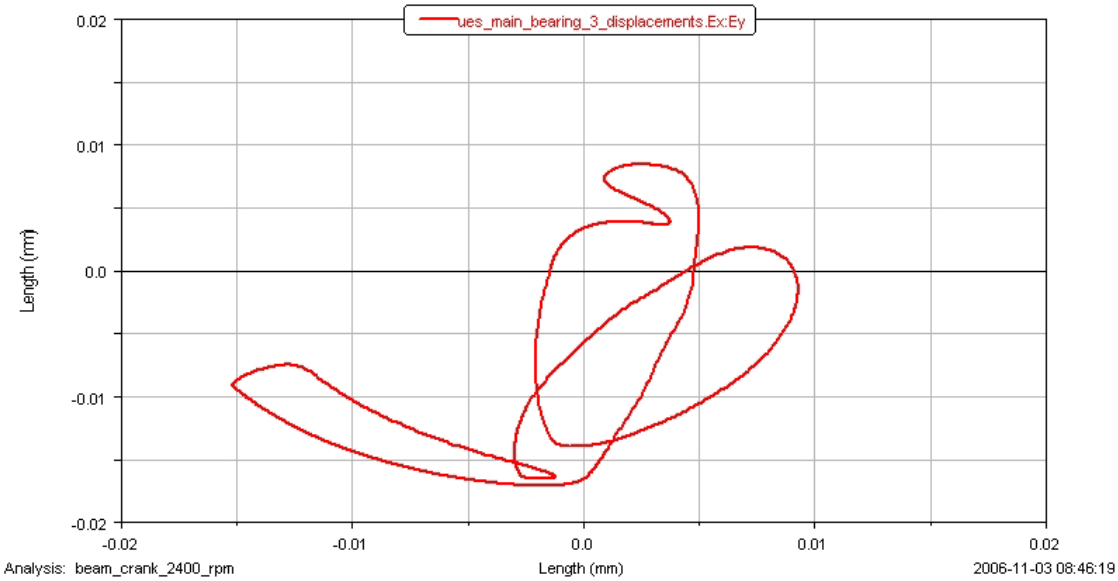

Figure 4.84. Orbital curve for main bearing #3 using 2D Hydrodynamic model

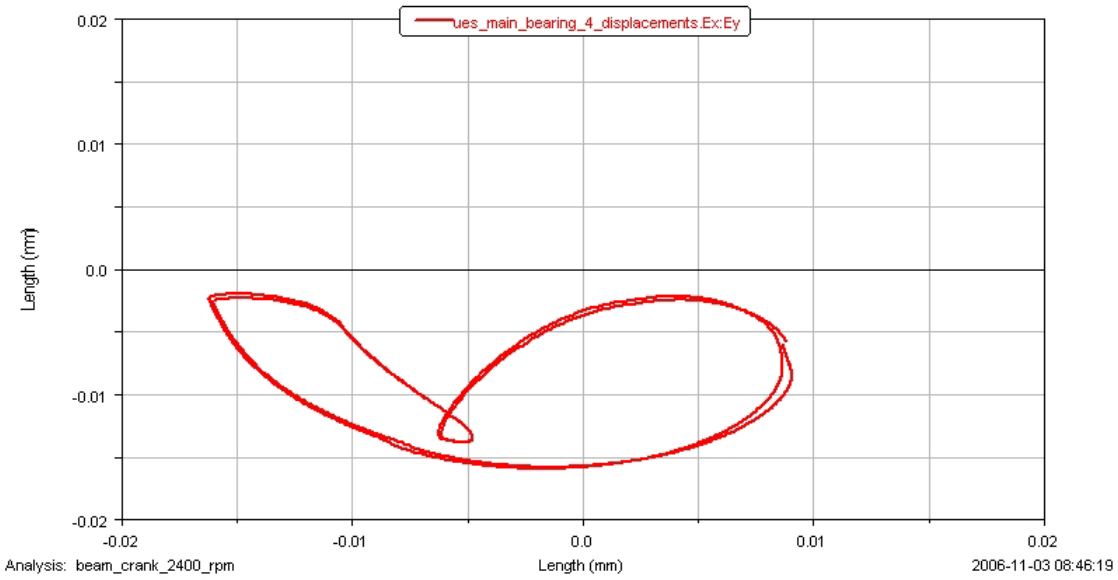

Figure 4.85. Orbital curve for main bearing #4 using 2D Hydrodynamic model

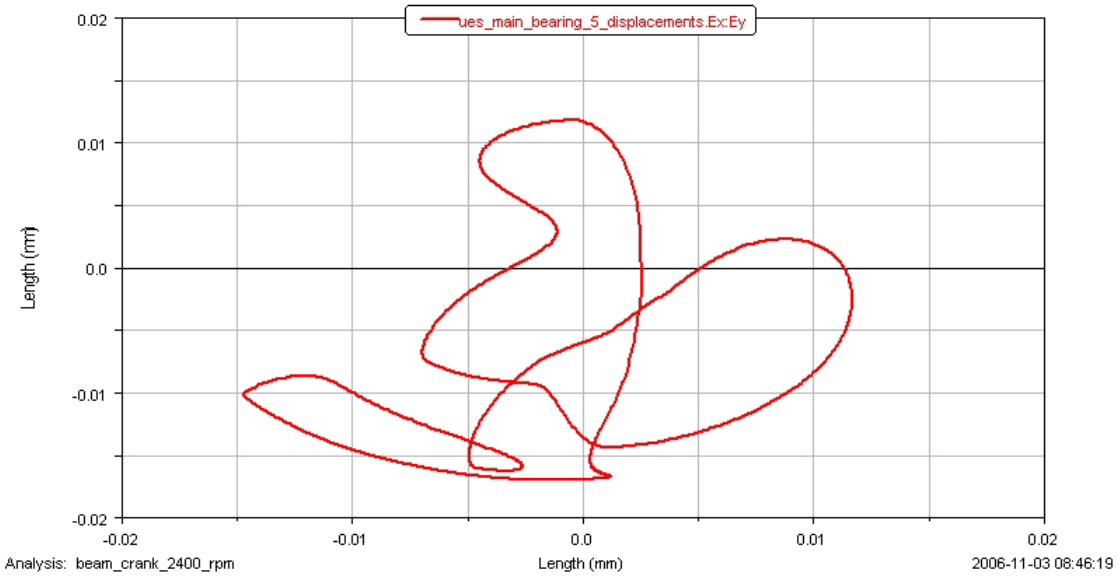

Figure 4.86. Orbital curve for main bearing #5 using 2D Hydrodynamic model

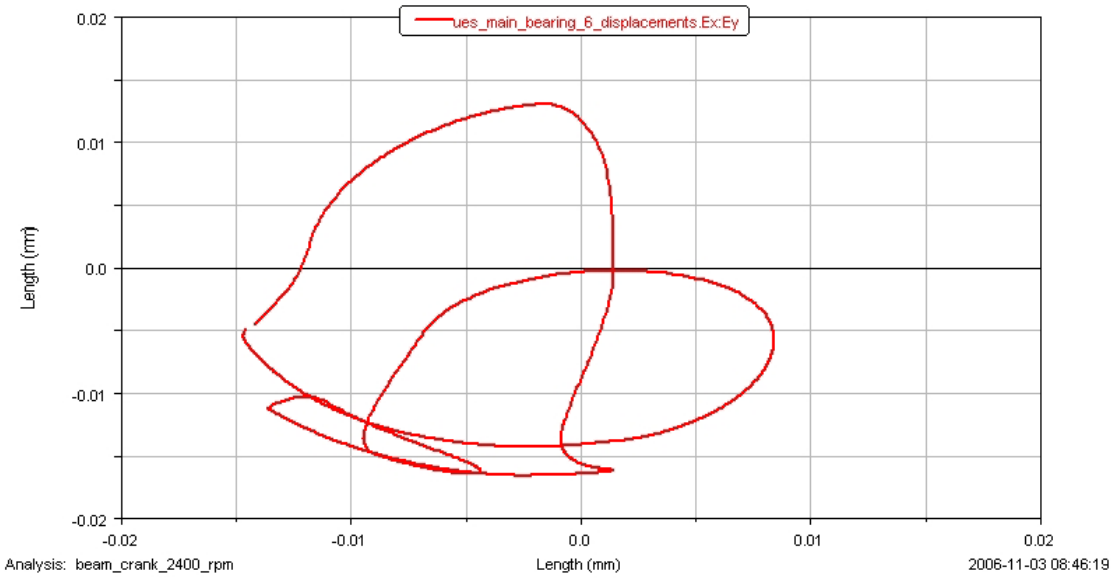

Figure 4.87. Orbital curve for main bearing #6 using 2D Hydrodynamic model

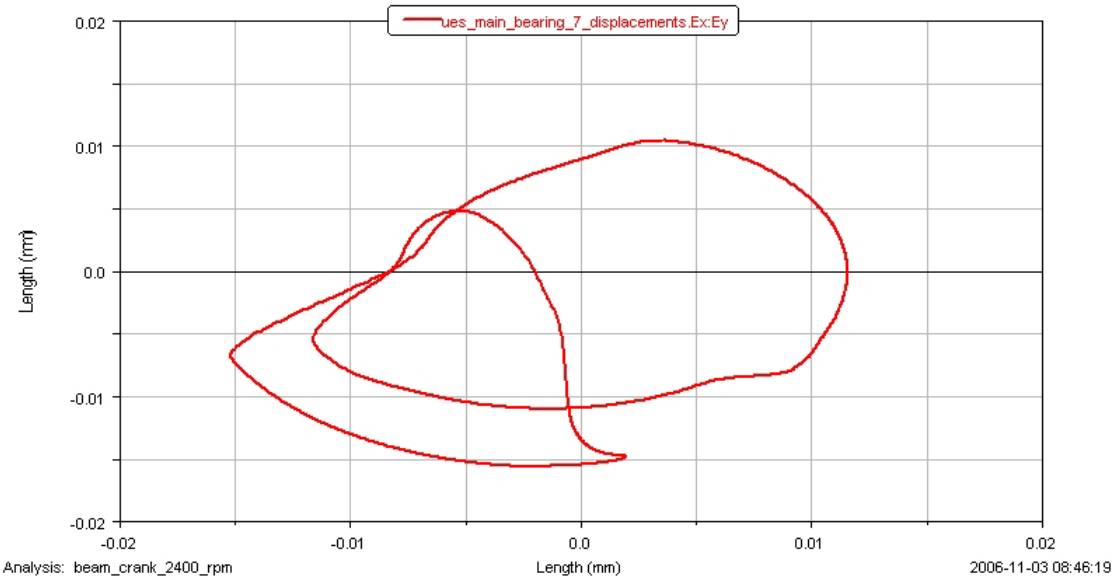

Figure 4.88. Orbital curve for main bearing #7 using 2D Hydrodynamic model

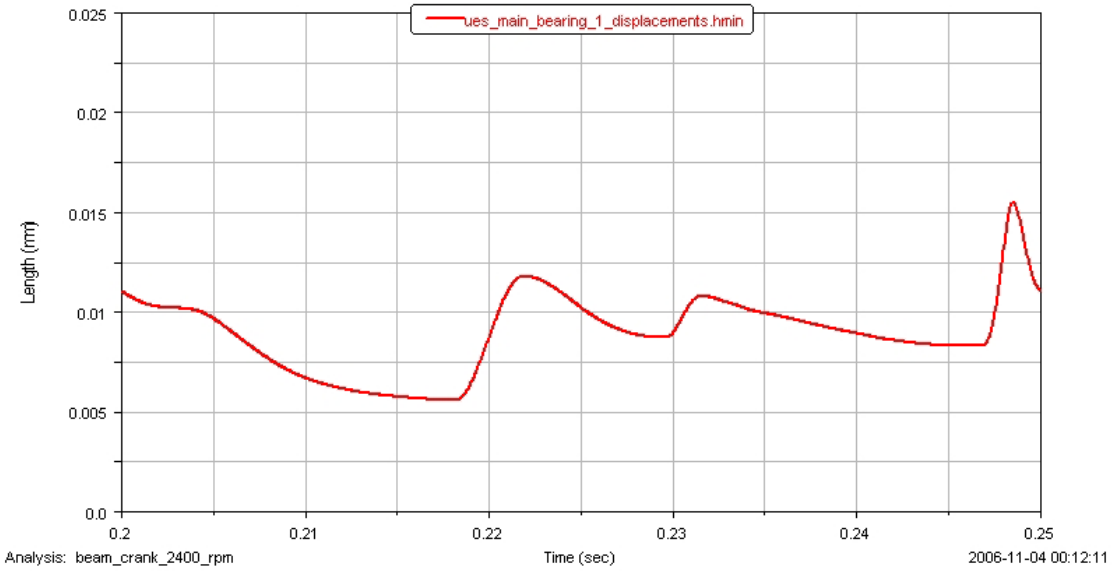

Figure 4.89. Minimum oil film thickness for main bearing #1 using 3D Hydrodynamic model

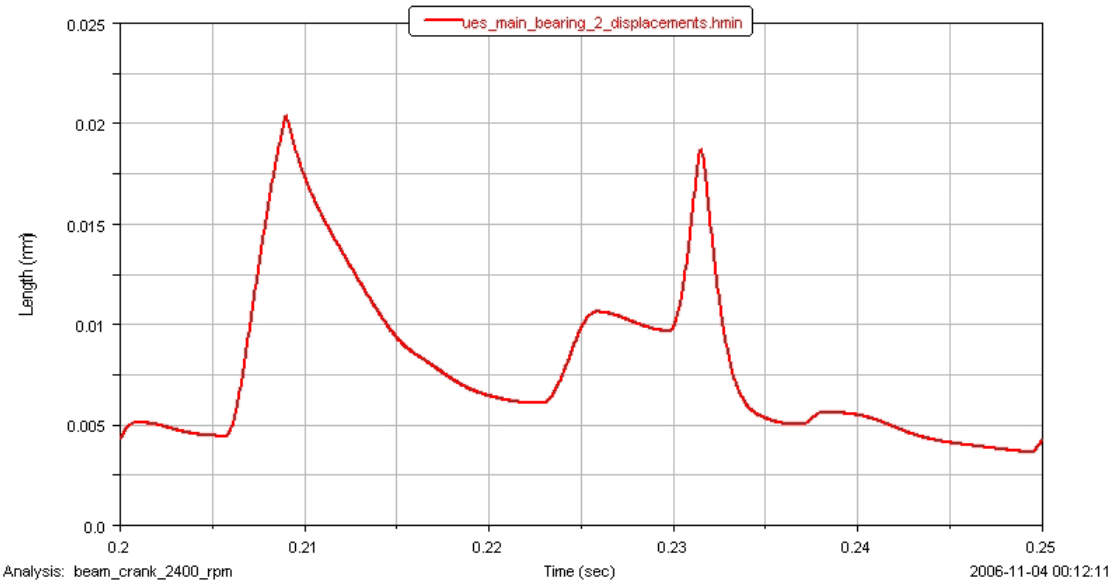

Figure 4.90. Minimum oil film thickness for main bearing #2 using 3D Hydrodynamic model

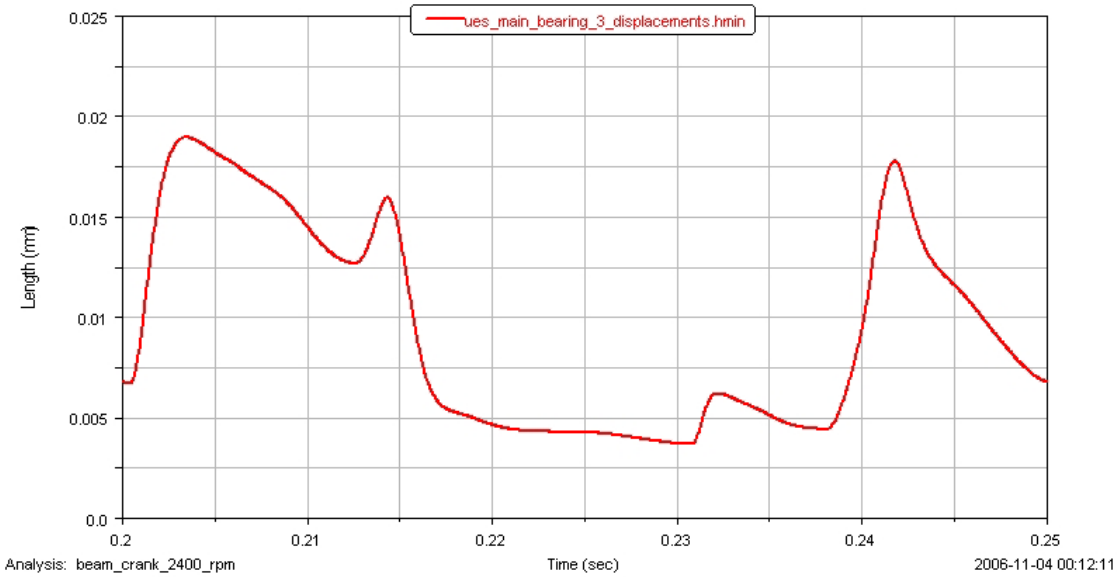

Figure 4.91. Minimum oil film thickness for main bearing #3 using 3D Hydrodynamic model

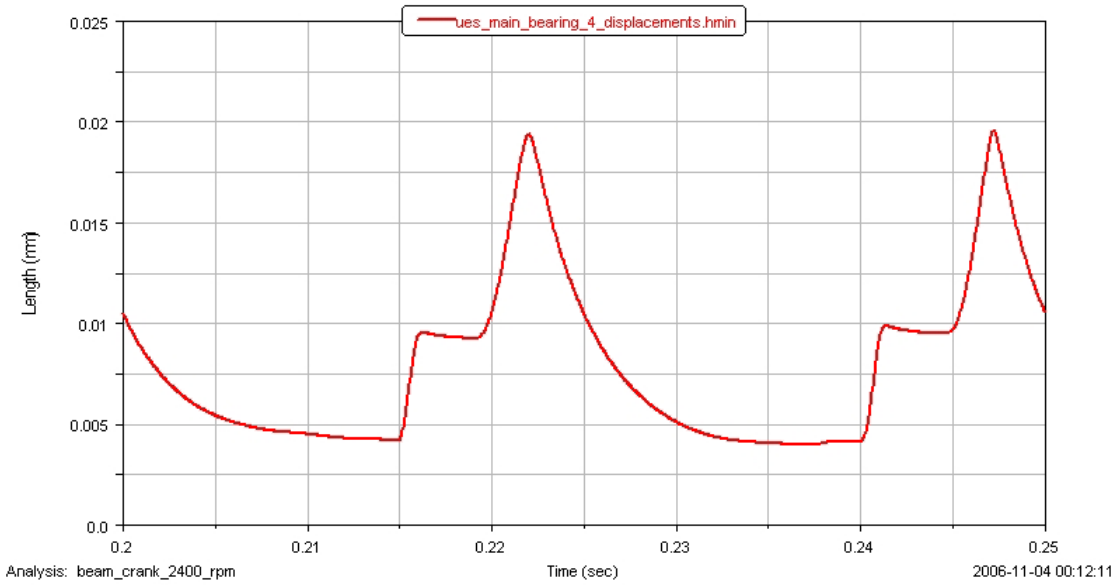

Figure 4.92. Minimum oil film thickness for main bearing #4 using 3D Hydrodynamic model

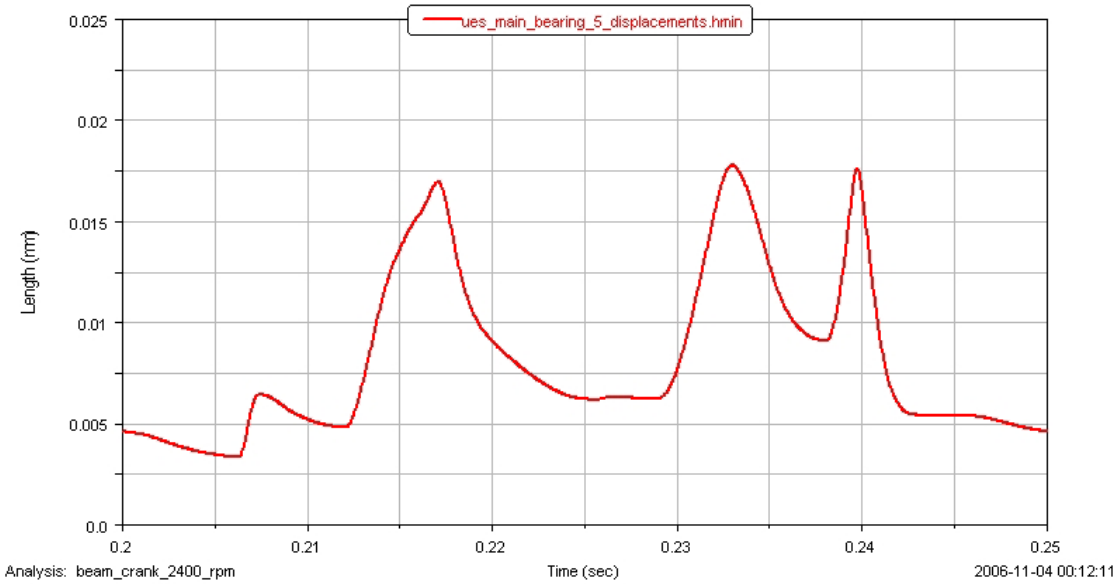

Figure 4.93. Minimum oil film thickness for main bearing #5 using 3D Hydrodynamic model

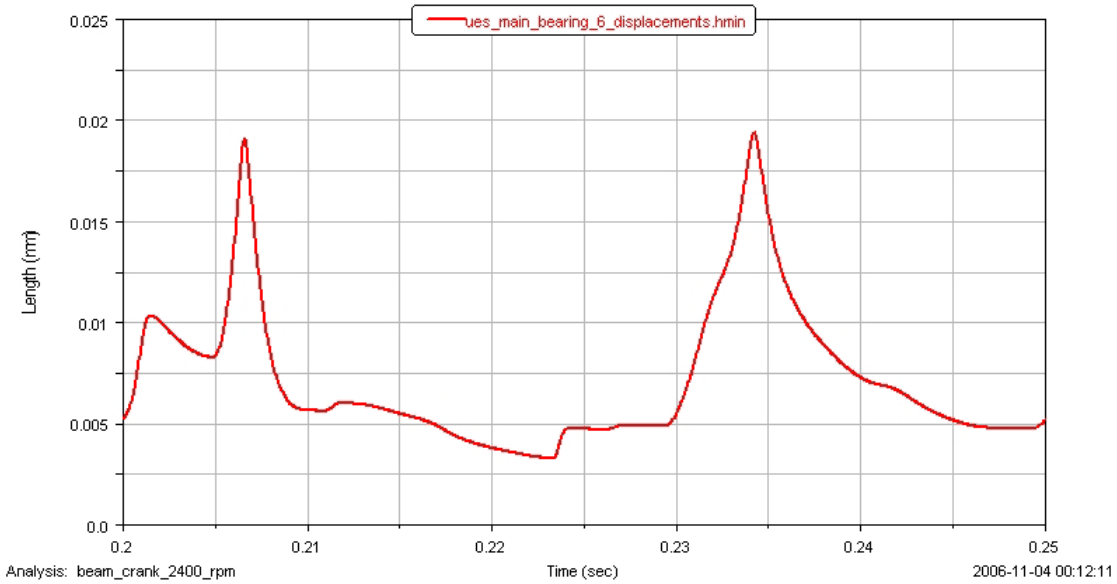

Figure 4.94. Minimum oil film thickness for main bearing #6 using 3D Hydrodynamic model

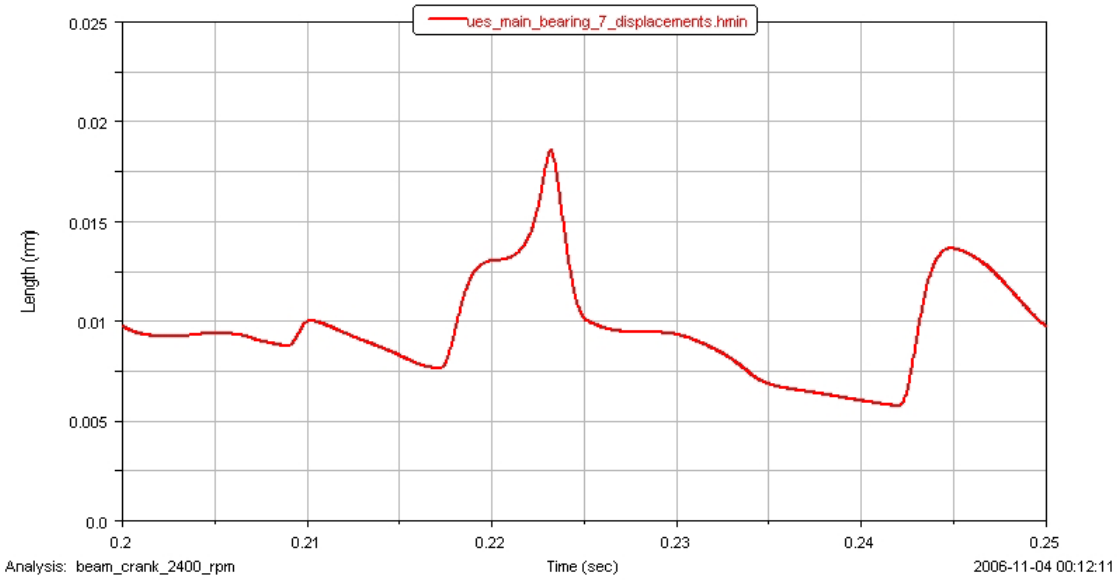

Figure 4.95. Minimum oil film thickness for main bearing #7 using 3D Hydrodynamic model

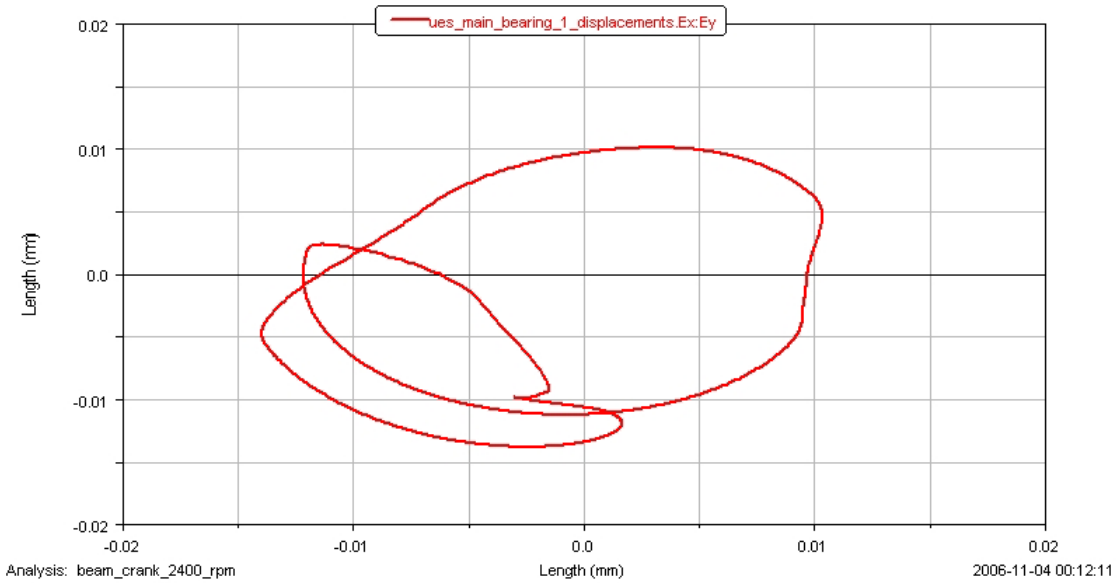

Figure 4.96. Orbital curve for main bearing #1 using 3D Hydrodynamic model

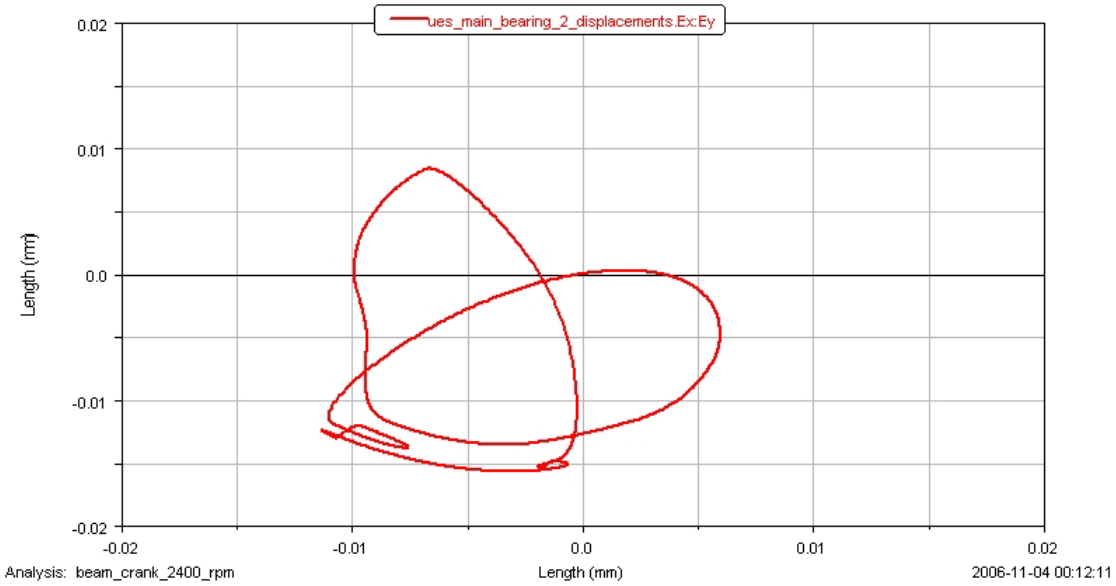

Figure 4.97. Orbital curve for main bearing #2 using 3D Hydrodynamic model

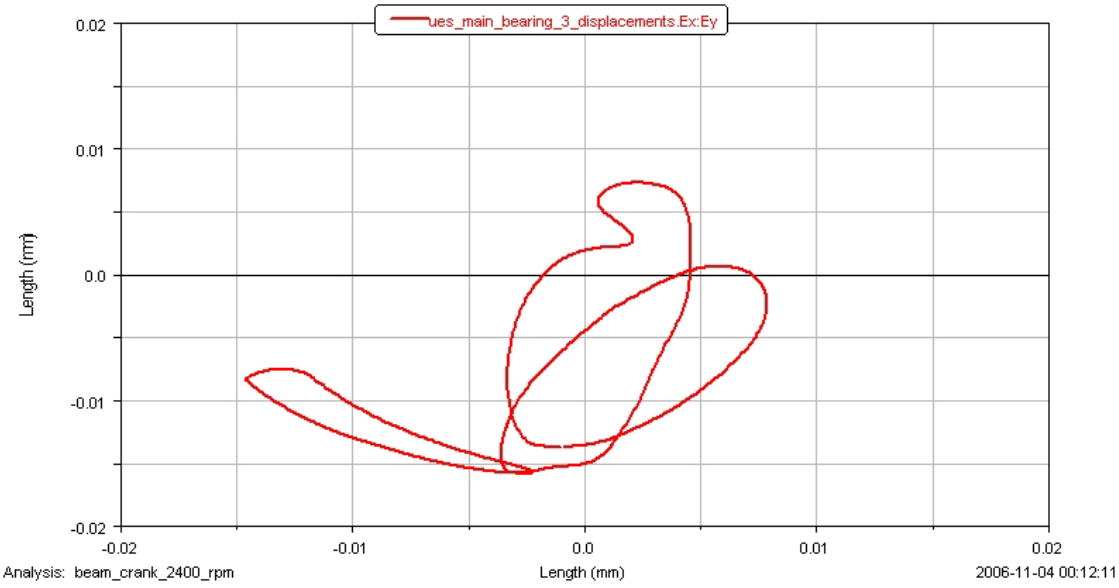

Figure 4.98. Orbital curve for main bearing #3 using 3D Hydrodynamic model

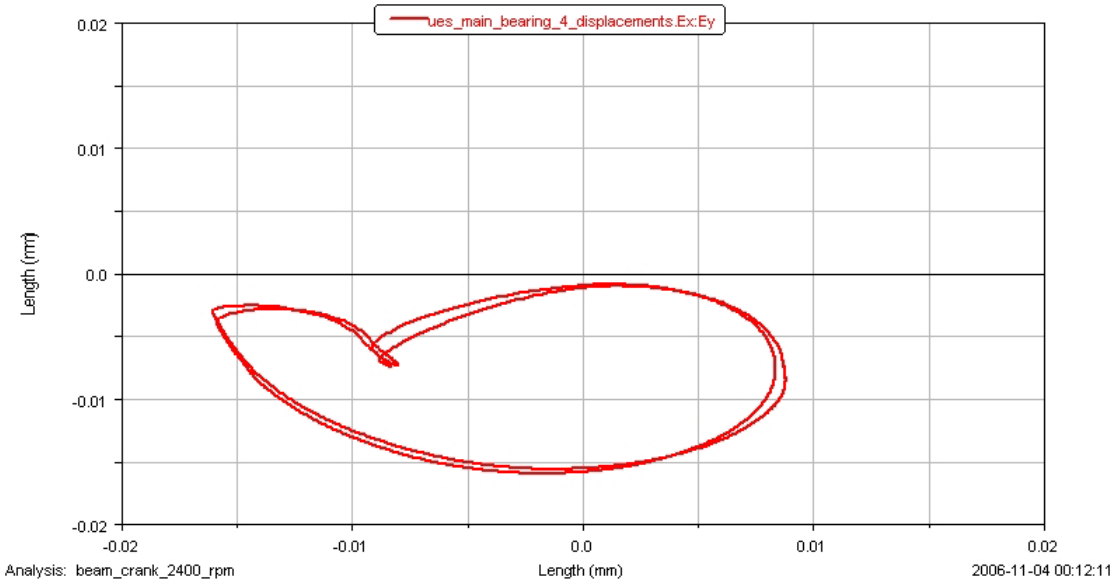

Figure 4.99. Orbital curve for main bearing #4 using 3D Hydrodynamic model

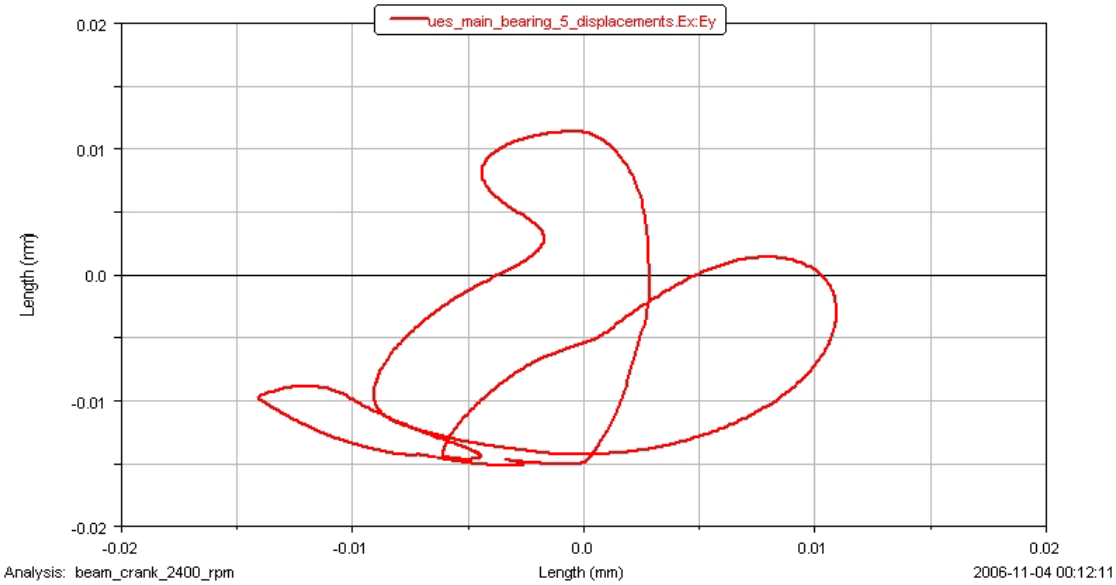

Figure 4.100. Orbital curve for main bearing #5 using 3D Hydrodynamic model

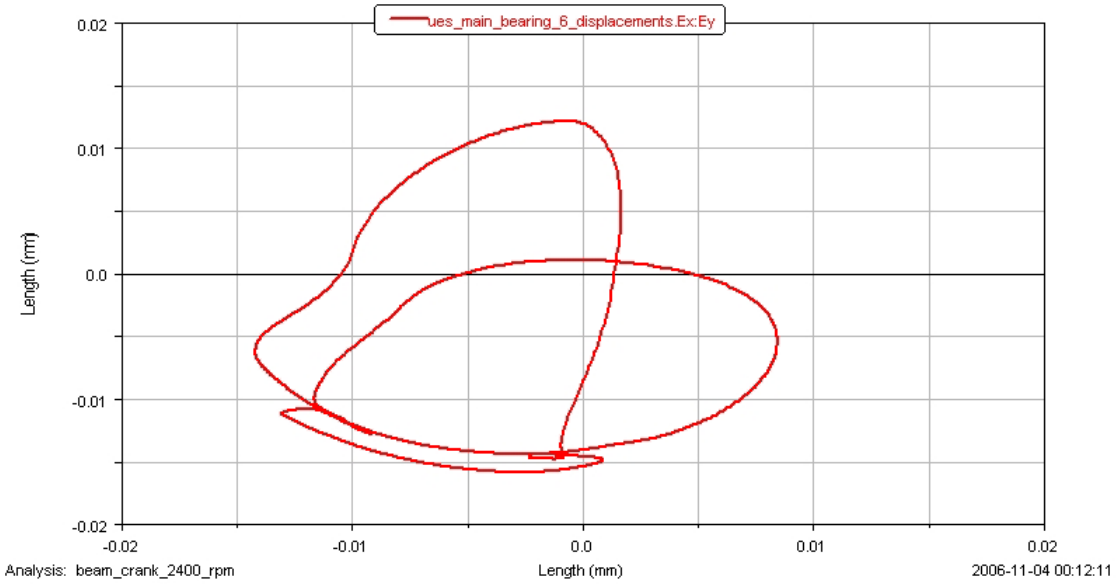

Figure 4.101. Orbital curve for main bearing #6 using 3D Hydrodynamic model

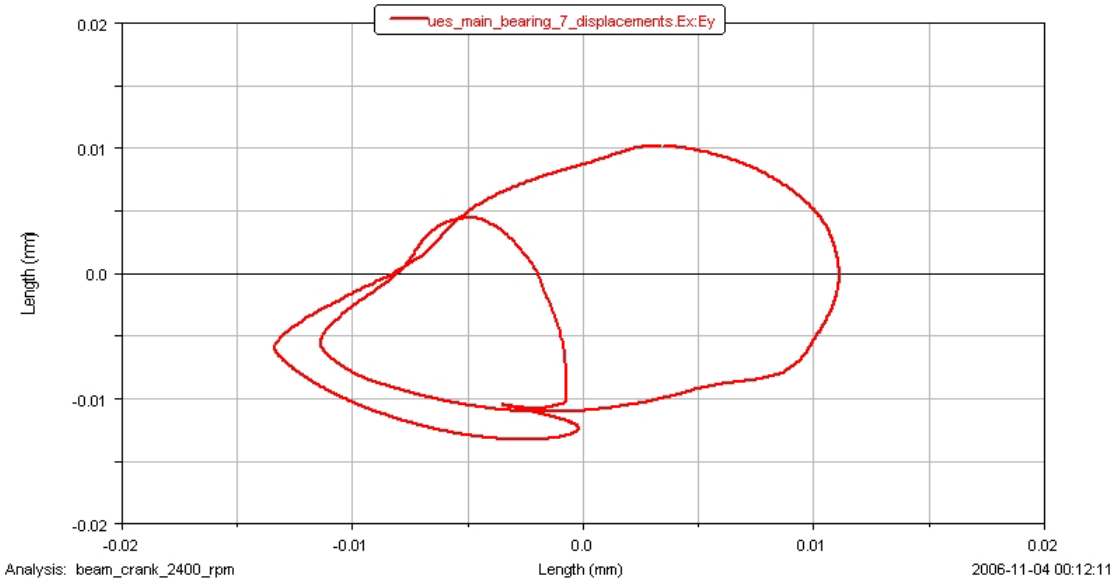

Figure 4.102. Orbital curve for main bearing #7 using 3D Hydrodynamic model

5. COUNTERWEIGHT CONFIGURATION ANALYSIS

5.1. Introduction

It is an important design criterion to decrease the weight of the internal combustion engines. It is achieved only if adequate component strength can be satisfied. The crankshaft system contributes significantly to the overall engine weight. Especially from the strength point of view the position and mass of counterweights are important, so optimizing the design is desirable. Bearing life is another important design criterion. The life of the bearings depends on the maximum and average bearing loads, [69]. So, obtaining the bearing load as a function of counterweight balancing rate is important.

In this part of the study, counterweight mass and position analysis of the crankshaft system of Ford Otosan 9.0 L in-line 6-cylinder **H**eavy **D**uty **D**iesel engine is presented. Bearing reaction forces and bending stresses on the crankshaft system of 9.0 L engine are calculated for different counterweight configurations with the current settings for TV damper and flywheel. The data for the engine are given in Table 1.1. Flywheel and TV damper specifications are as follows:

Flywheel mass	: 47.84 kg
Flywheel principle moments of inertia	: I_1=7.96E+5 kgmm^2
	I_2=7.97E+5 kgmm^2
	I_3=1.57E+9 kgmm^2
Mass of the TV damper ring	: 4.94 kg
Mass of the TV damper housing	: 6.86 kg
Moment of inertia of the ring	: 0.127 kgm^2
Moment of inertia of housing	: 0.0559 kgm^2
Torsional stiffness of TV Damper	: 69500 Nm/rad
Damping coefficient of TV damper	: 73.67 Nms/rad

The 9.0 L engine crankshaft has 8 counterweights at crank webs 1, 2, 5, 6, 7, 8, 11 and 12. 3D solid model of the crankshaft and its schematic representetation are shown in Figure 5.1 and 5.2. The static unbalance of each crank throw for this arrangement has been determined on the basis of the CAD mass properties of the different cranks (with and w/o counterweights) using Pro/Engineer and is given in Table 5.1. The balancing system data for the crank train are given in Table 5.2.

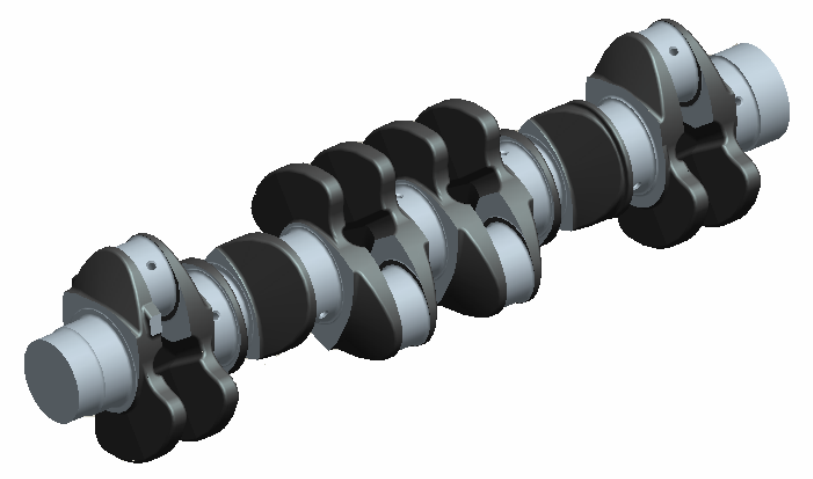

Figure 5.1. 3D solid model of the 9.0 L engine crankshaft

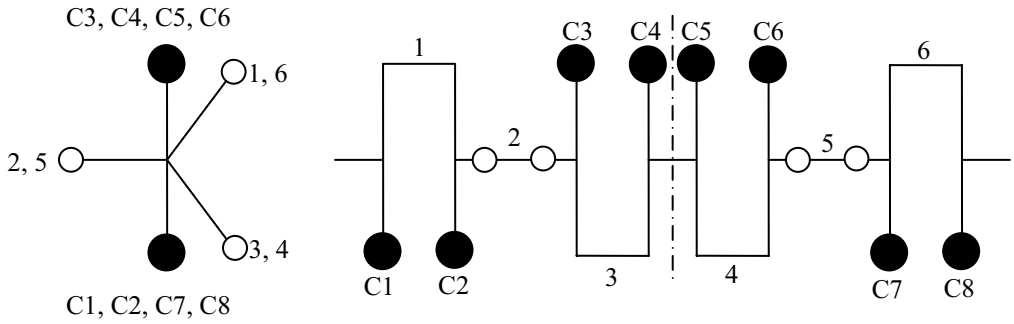

Fig. 5.2. Eight counterweight arrangement of the 9.0 L engine crankshaft

Table 5.1. CAD mass properties of the crank throws

	Throw 1	Throw 2	Throw 3	Throw 4	Throw 5	Throw 6
Mass (kg)	12.5	9.25	12.5	12.5	9.28	12.55
CG position from crank rotation axis	12.423	31.435	11.967	11.966	31.027	11.702
Static Unbalance (kgmm)	155.265	290.767	149.734	149.734	287.871	146.856

Table 5.2. Balancing system data

Crank radius	mm	72
Connecting rod length	mm	239
Mass of complete piston	kg	3.42
Connecting rod reciprocating mass	kg	0.92
Reciprocating mass (total per cylinder)	kg	4.32
Connecting rod rotating mass	kg	2.01

Using the 3D solid model of the crankshaft and the data in Tables 1.1, 5.1 and 5.2, rigid, beam and elastic 3D solid crankshaft models are obtained. 3D solid crankshaft model of 9.0 L engine is obtained in MSC.Nastran using modal superposition technique and exported to ADAMS. Model of the crankshaft system that is obtained in ADAMS/Engine is shown in Figure 5.3.

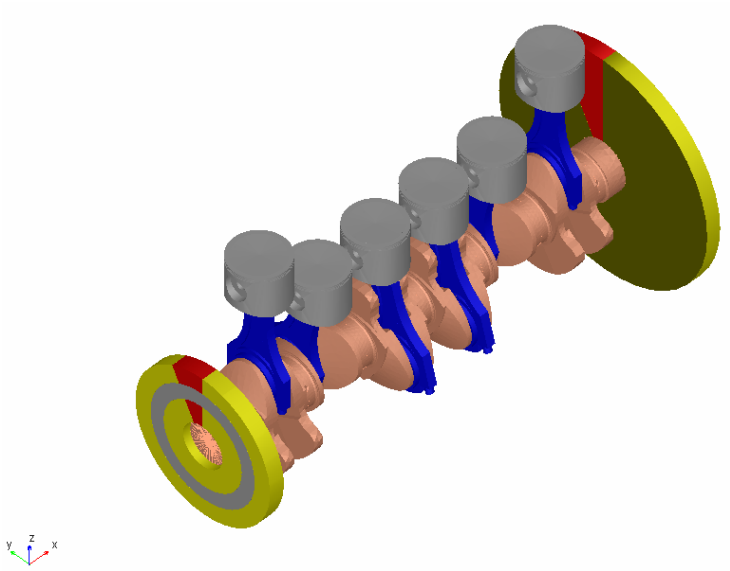

Figure 5.3. Model of the crankshaft system

5.2. Forces Acting on Crankshaft System and Balancing

The forces in an internal combustion engine may be divided into two main parts: pressure forces and inertia forces.

Inertia forces are oriented in a direction opposite to the acceleration. To determine inertia forces, the masses and the center of gravity of the moving parts must be known. In this study, all of the parts in the crankshaft system are first modeled using Computer Aided Design (CAD) software Pro/Engineer. Then this models are used to calculate the mass and center of gravity of all crank throws and all of the parts in the crankshaft system.

The rotating inertia force for each cylinder can be written in vector notation as:

$$\vec{F}_{iR,j} = m_R \cdot r_R \cdot \omega^2 \cdot \left(-\sin\theta_j\,\hat{\mathbf{j}} + \cos\theta_j\,\hat{\mathbf{k}}\right) \tag{5.1}$$

where m_R is the rotating mass that consists of the mass of the crank pin, the crank webs and rotating part of the mass of the connecting rod, r_R is the distance from the crankshaft center of rotation to the center of gravity of the rotating mass, ω is the angular velocity of

the crankshaft, and θ_j is the angular position of each crank throw with respect to TDC position. If there are two counterweights per crank throw, each counterweight force is given by, [48]

$$\vec{F}_{CW\,i,j} = -m_{CW\,i,j} \cdot r_{CW\,i,j} \cdot \omega^2 \cdot \left[-\sin\left(\theta_j + \gamma_{i,j}\right)\hat{\mathbf{j}} + \cos\left(\theta_j + \gamma_{i,j}\right)\hat{\mathbf{k}} \right], \qquad \begin{matrix} i = 1,2 \\ j = 1,2,...,6 \end{matrix} \tag{5.2}$$

where $\gamma_{i,j}$ is the offset angle of counterweight mass from 180 degree opposite of crank throw ‘‘ j ’’. There are two counterweights per throw. “ i ” denotes the counterweight number. For complete balancing of each crank (K=100%)

$$\left(m_{CW1,j} \cdot r_{CW1,j} + m_{CW2,j} \cdot r_{CW2,j}\right) = m_R \cdot r_R\,, \qquad j = 1, 2, \ldots, 6 \tag{5.3}$$

The counterweight size that is required to accomplish an assessed balancing rate is:

$$U_{CW} = \frac{K \cdot \left(U_{Crank\_throw} + m_{cr-r} \cdot r\right) \cdot \cos\gamma}{2} \tag{5.4}$$

where U_{CW} is the static unbalance of each counterweight, U_{Crank_throw} is the static unbalance of each crank throw, $m_{cr\text{-}r}$ is the mass of connecting rod rotating portion, r is the crank radius and K is the balancing rate of the internal couple due to rotating forces. From this formula follows the balancing rate for a given crankshaft and a given counterweight size with:

$$K = \frac{2 \cdot U_{CW}}{\left(U_{Crank\_throw} + m_{cr-r} \cdot r\right) \cdot \cos\gamma} \tag{5.5}$$

For the standard six-cylinder engine crankshaft with three pairs of crank-throws disposed at angles of 120 degrees that are arranged symmetrical to the crankshaft center, rotating forces, and first and second order reciprocating forces are naturally balanced and no crankshaft counterweights would be required. This can be explained by the first and second order vector stars shown in Figure 5.4. The six-cylinder crankshaft generates

rotating and first and second order reciprocating couples in each crankshaft half, which balance each other but which result in an internal bending moment. Also at high speeds, the two equally directed crank throws No. 3 and No. 4 yield a high rotating load on the center main bearing. As a result, crankshaft counterweights are used to reduce internal couples and rotating bearing loads in particular on the center main bearing.

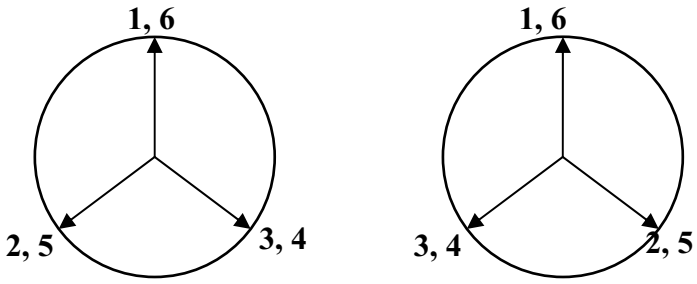

Figure 5.4. First and second order vector stars

The rotating inertia force of each cylinder is usually offset at least partially by counterweights placed on the opposite side of each crank. In general, the counterweights are designed for a balancing rate between 50% and 100% of the internal couple.

The gas forces in the cylinders are acting on the piston head, the cylinder head and on the side walls of the cylinder. This force is equal to:

$$\vec{F}_{p,j} = -\frac{\pi D^2}{4} \cdot \left[P_{cyl,j}(\theta) - P_{cc,j}(\theta) \right] \hat{\mathbf{k}} \tag{5.6}$$

where D is cylinder diameter, P_{cyl} is the gas pressure in the cylinder and P_{cc} is the pressure in the crankcase. The gas forces are transmitted to the crankshaft through the piston and connecting rod.

Cylinder pressure curves for 9.0 L engine on full load at different engine speeds are given in Figure 5.5 which are obtained using AVL/Boost software program.

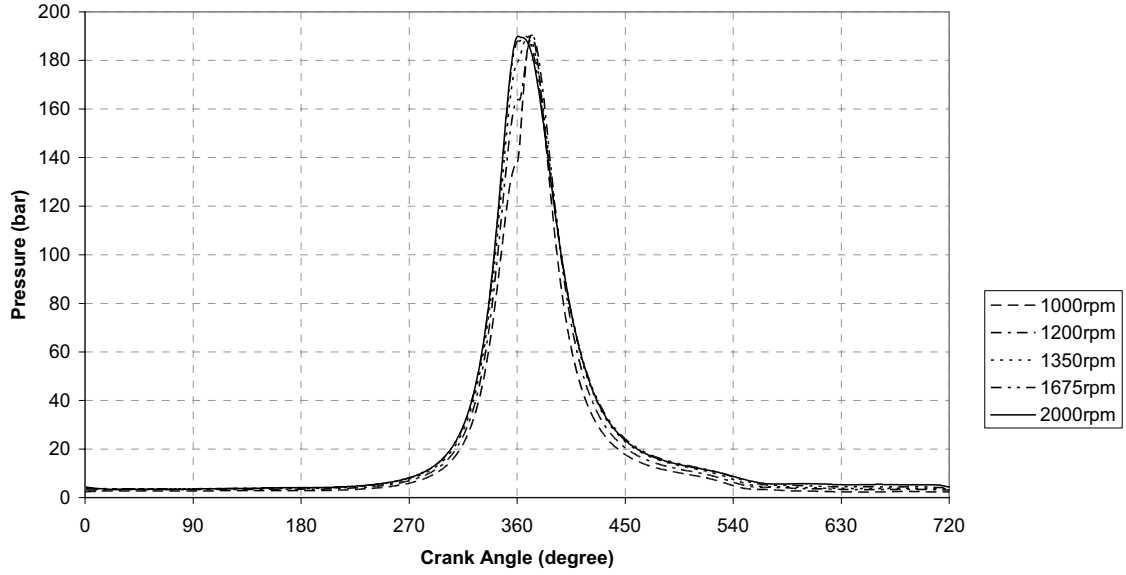

Figure 5.5. Gas pressure values at different engine speeds for the 9.0 L engine

5.3. Main Bearing Loads: Comparison of Crankshaft Models

Main bearing loads are calculated using ADAMS's rigid, beam and 3D solid crankshaft models and compared. In rigid model, no vibration effects are considered which can lead to considerable errors if vibration effects have a major role on the system (like in multithrow crankshafts). To consider vibration effects beam crankshaft model is used and main bearing loads and bending stresses at webs are calculated. Rigid model assumes crankshaft to be statically determinate and reaction force of any given bearing depends on the load exerted on the throws adjacent to that bearing. Beam model assumes the crankshaft to be statically indeterminate and the load exerted on a throw affects all bearings. Analyses are carried out at an engine speed range of 1000 to 2000 rpm. A more sophisticated 3D solid hybrid model that combines FE with ADAMS is used to check the results obtained by beam model.

Maximum main bearing load occurs at bearing number two at an engine speed of 1000 rpm, therefore results are plotted in Figures 5.6-5.12 for 1000 rpm only. Rigid crankshaft model overestimates the maximum main bearing load at bearings 1 and 7 with respect to beam and flexible crankshaft models. However it underestimates the maximum main bearing load at other bearings. For example at bearing 2, beam model gives a maximum main bearing load that is 50% more than that of rigid model's because the beam model assumes the crankshaft to be statically indeterminate and considers bending vibrations. Maximum main bearing load difference of beam and 3D solid models is approximately 5%. Main bearing loads for beam and 3D solid crankshaft models are generally in good agreement. In bearings 3, 5 and 6, 3D solid model gives larger bearing loads at firing positions of the cylinders that are not adjacent to bearing. Because obtaining elastic 3D solid models for different counterweight configurations is difficult and time consuming, and beam model gives equally valid results, beam model is used in the rest of the work to study the effect of counterweight configuration on main bearing loads and crankshaft bending stresses.

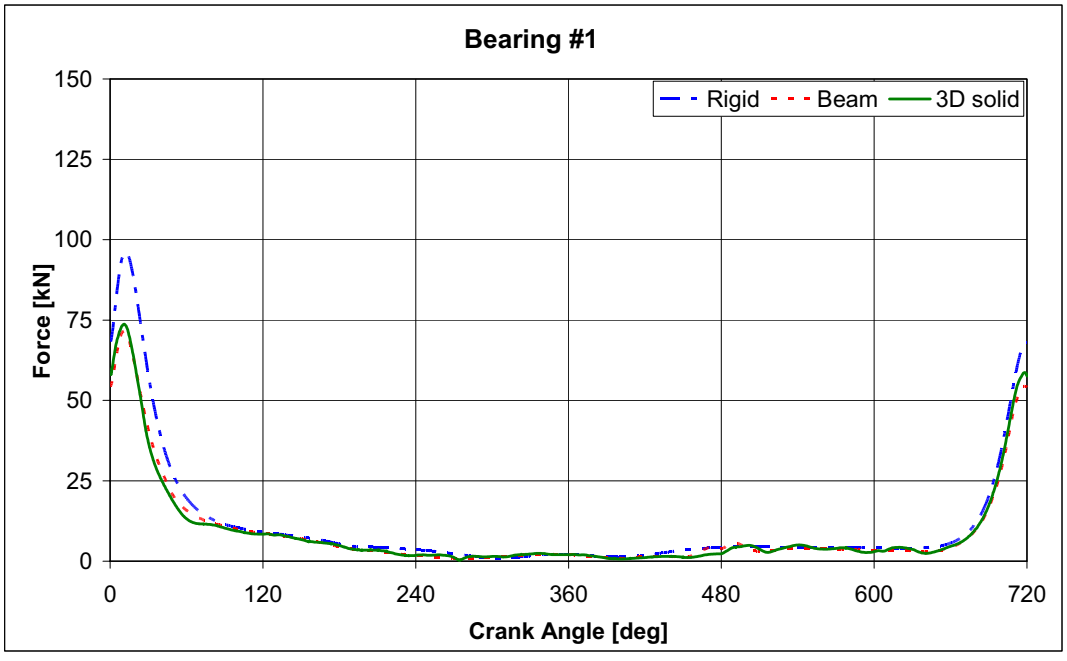

Figure 5.6. Forces acting on main bearing #1 for rigid, beam and 3D solid crankshaft models at 1000 rpm engine speed

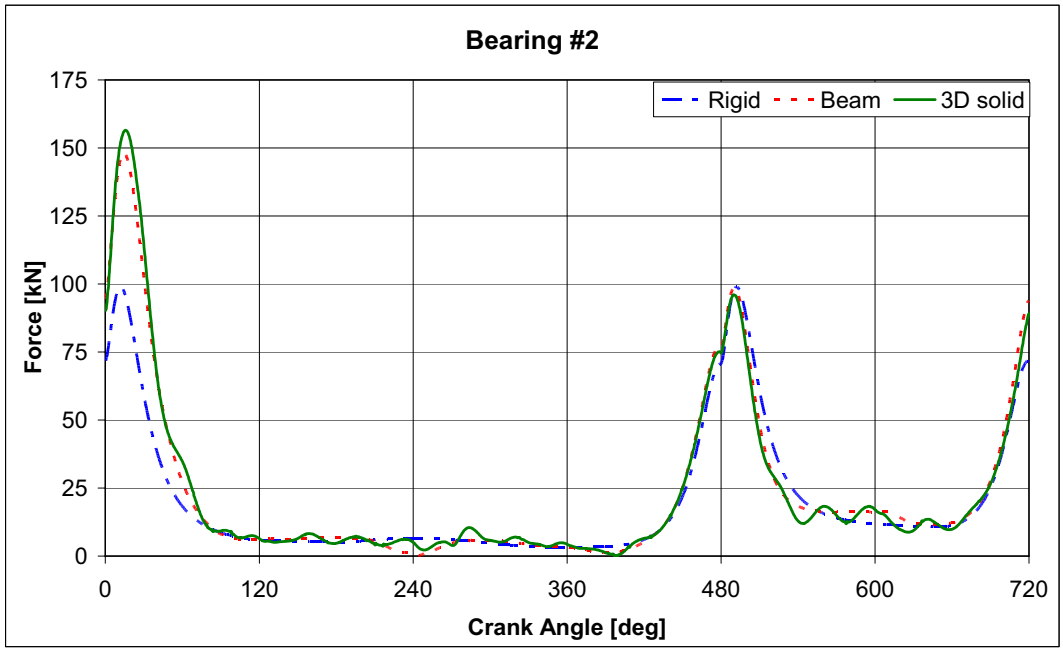

Figure 5.7. Forces acting on main bearing #2 for rigid, beam and 3D solid crankshaft models at 1000 rpm engine speed

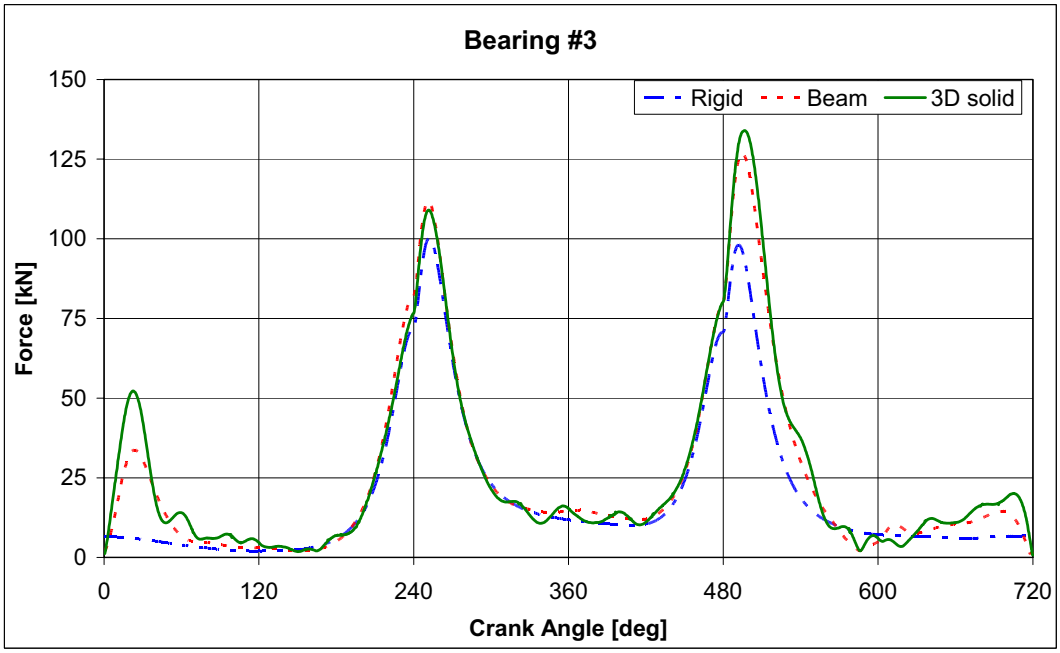

Figure 5.8. Forces acting on main bearing #3 for rigid, beam and 3D solid crankshaft models at 1000 rpm engine speed

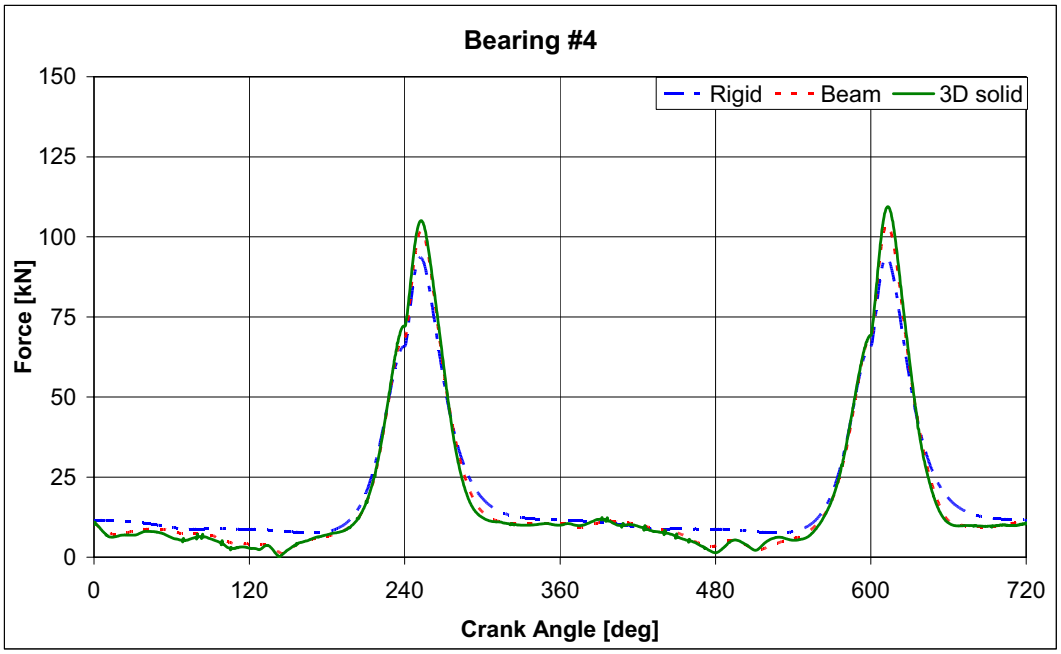

Figure 5.9. Forces acting on main bearing #4 for rigid, beam and 3D solid crankshaft models at 1000 rpm engine speed

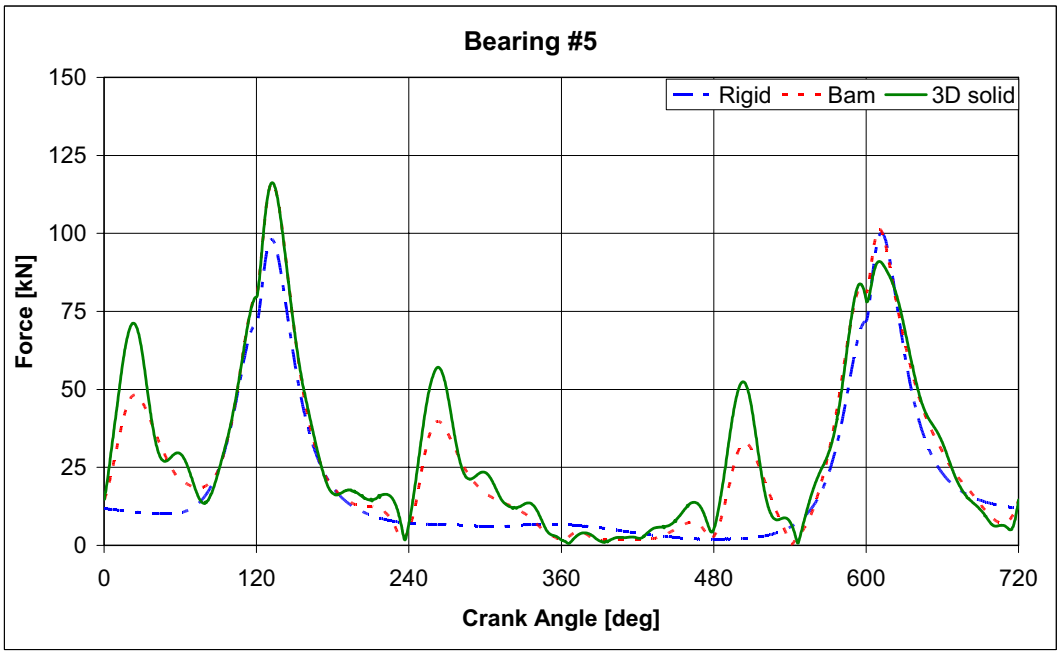

Figure 5.10. Forces acting on main bearing #5 for rigid, beam and 3D solid crankshaft models at 1000 rpm engine speed

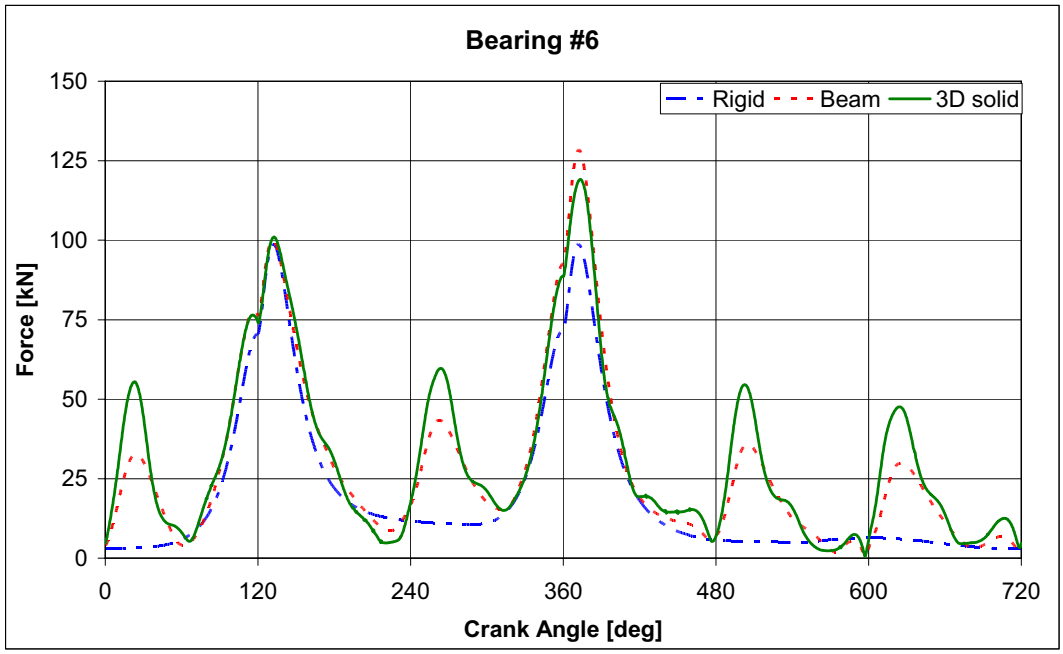

Figure 5.11. Forces acting on main bearing #6 for rigid, beam and 3D solid crankshaft models at 1000 rpm engine speed

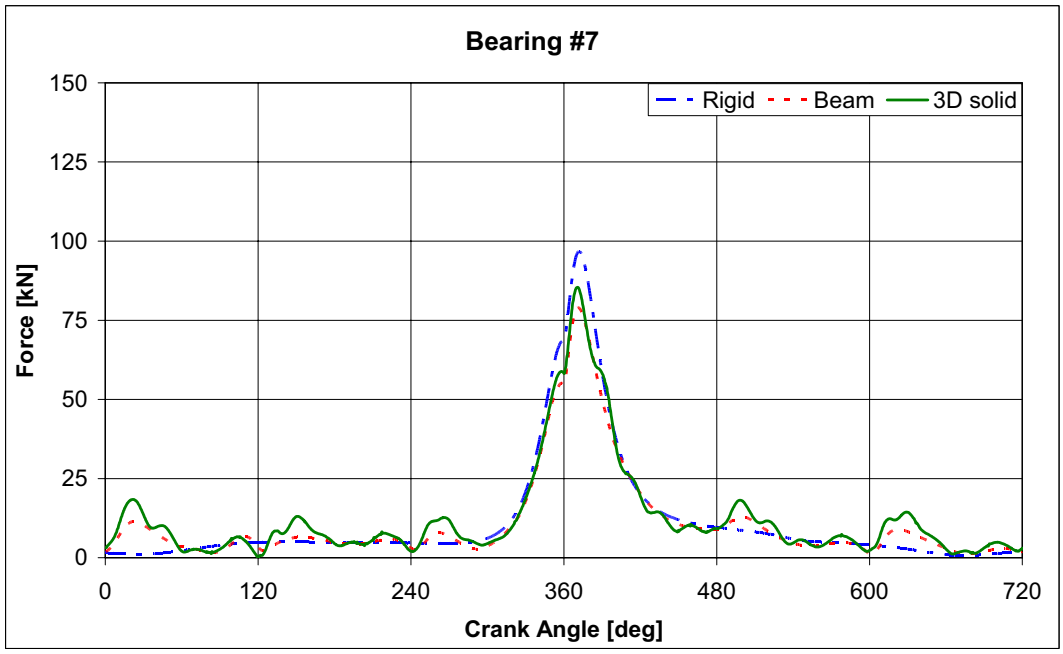

Figure 5.12. Forces acting on main bearing #7 for rigid, beam and 3D solid crankshaft models at 1000 rpm engine speed

5.4. Effect of counterweight configuration on main bearing load and crankshaft bending stress

The effect of counterweight arrangement on bearing forces and crankshaft bending stresses is investigated using beam model for the following cases:

- No counterweights, $K = 0\%$
- 12 counterweights with $K = 50\%,\ \gamma = 0^{o}$ and $K = 100\%,\ \gamma = 0^{o}$
- 8 counterweights with $K = 50\%,\ \gamma = 30^{o}$ and $K = 100\%,\ \gamma = 30^{o}$

5.4.1. Twelve counterweighs, $\gamma = 0°$, K=0%, K=50% and K=100%

In this configuration, counterweights are placed on opposite sides of all webs. Counterweight static unbalance is calculated using Equation (5.5) for K = 50% and K = 100% balancing rates. Maximum and average main bearing loads are calculated using the beam crankshaft model considering inertial and gas pressure forces and are plotted in Figures 5.13-5.26 as function of crankshaft angular velocity and balancing rate.

As can be seen from the figures, maximum bearing load increases with increasing balancing rate. This behavior can be explained as follows: For six cylinder in-line engine crankshafts, the rotating inertia force and first harmonic component of the reciprocating inertia force are in-phase and add in the direction of the cylinder. The pressure force is almost maximum at top dead center position where the reciprocating inertia force and the component of the rotating inertia force in cylinder direction are also at maximum levels. Because the pressure and inertia forces are opposite in-sign, they subtract from each other which increases the maximum bearing load at high balancing rates. On the other hand, average bearing force increases with decreasing balancing rate. Maximum main bearing load occurs at bearing number two at engine speed of 1000 rpm and average main bearing load of bearing 6 is larger than other bearings' average loads because bending vibrations of damper and flywheel occur. At main bearings 3, 4 and 5, where the influence of damper and flywheel bending vibrations is minimal, only torsional vibration occurs and their loads are less.

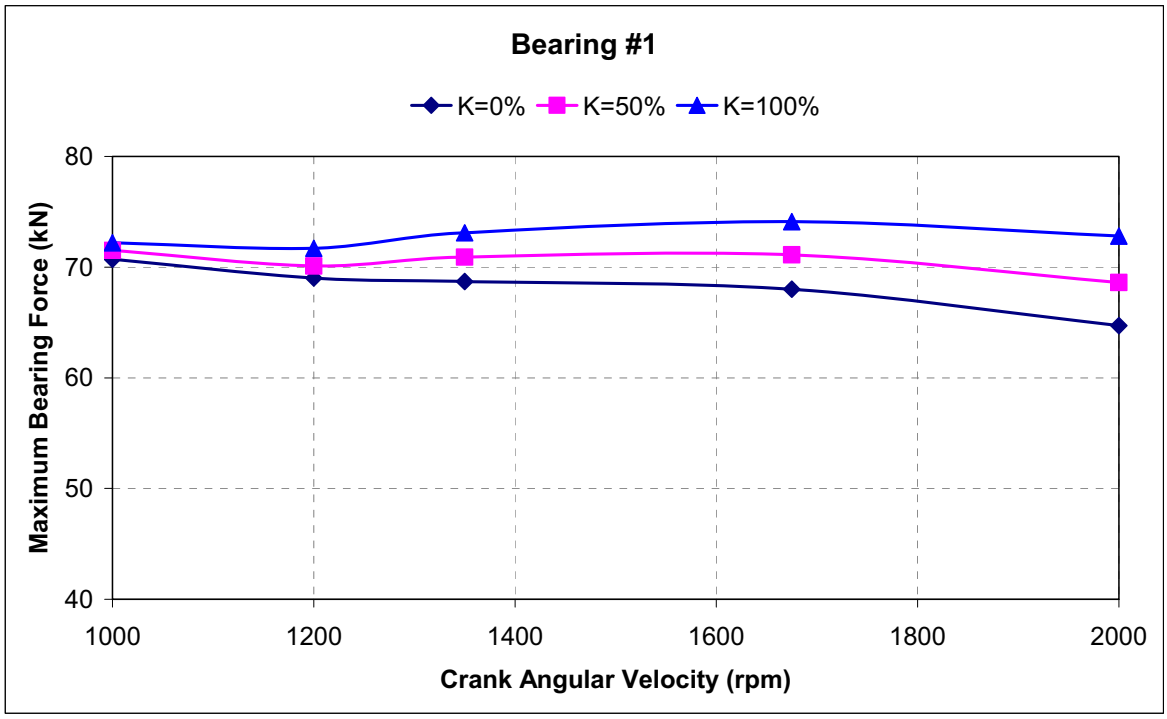

Figure 5.13. Maximum bearing forces at bearing #1 for twelve-counterweight configurations

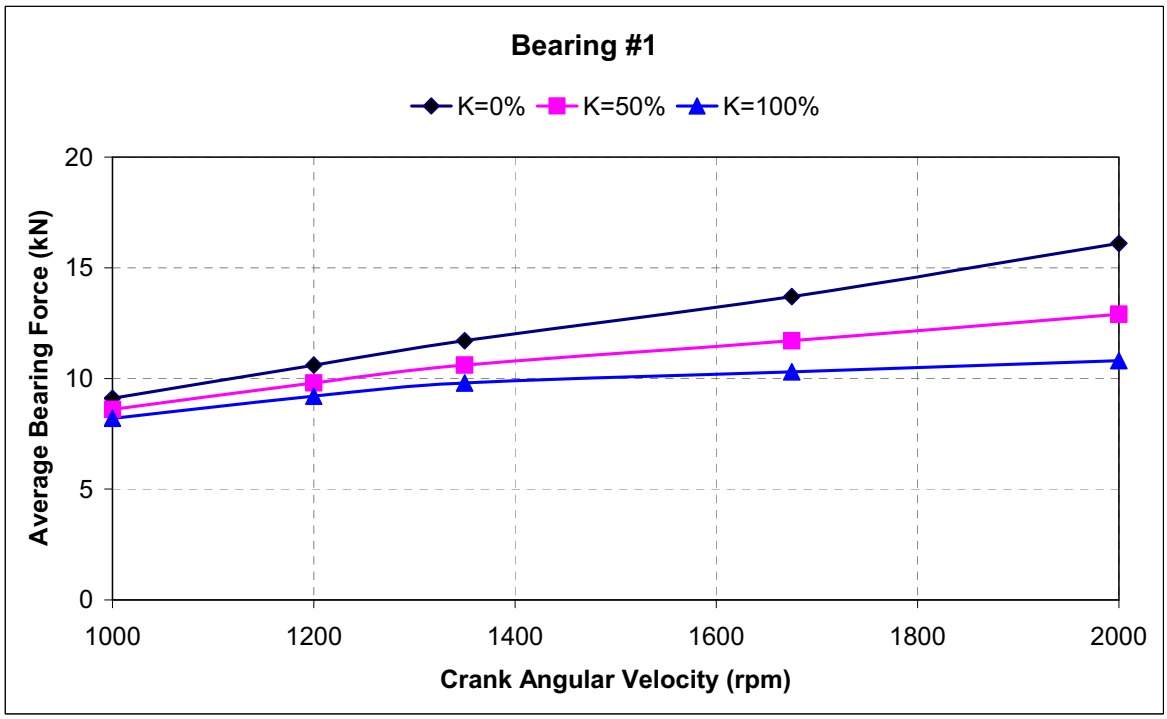

Figure 5.14. Average bearing forces at bearing #1 for twelve-counterweight configurations

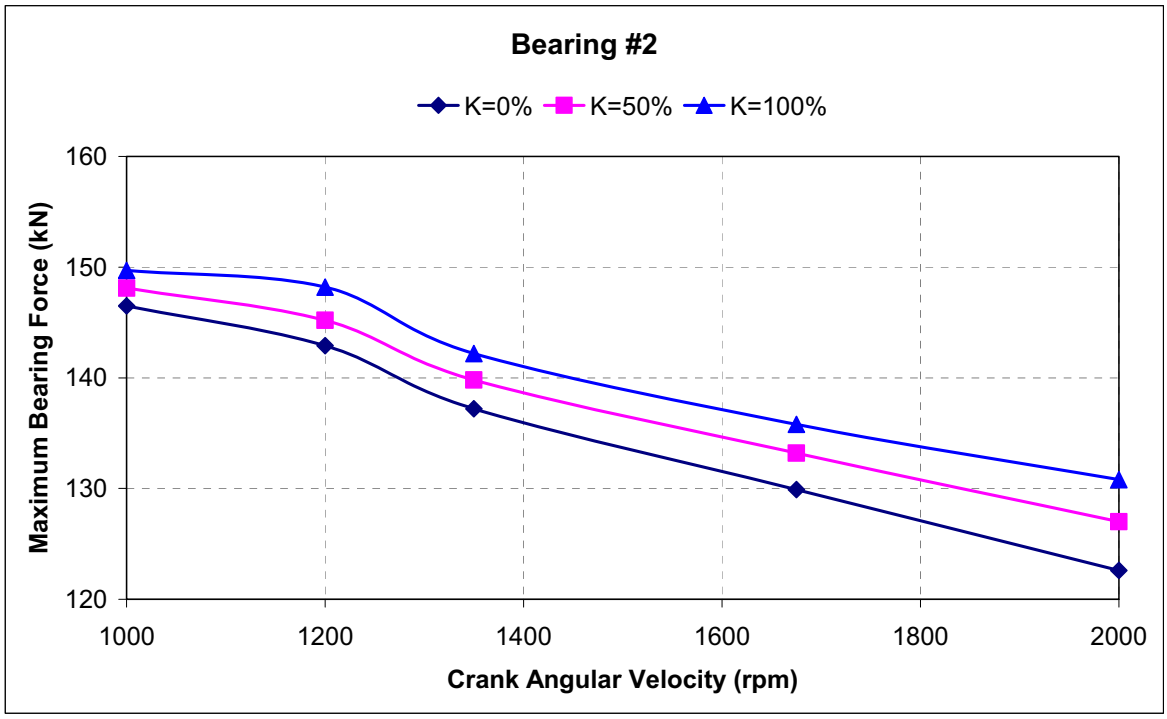

Figure 5.15. Maximum bearing forces at bearing #2 for twelve-counterweight configurations

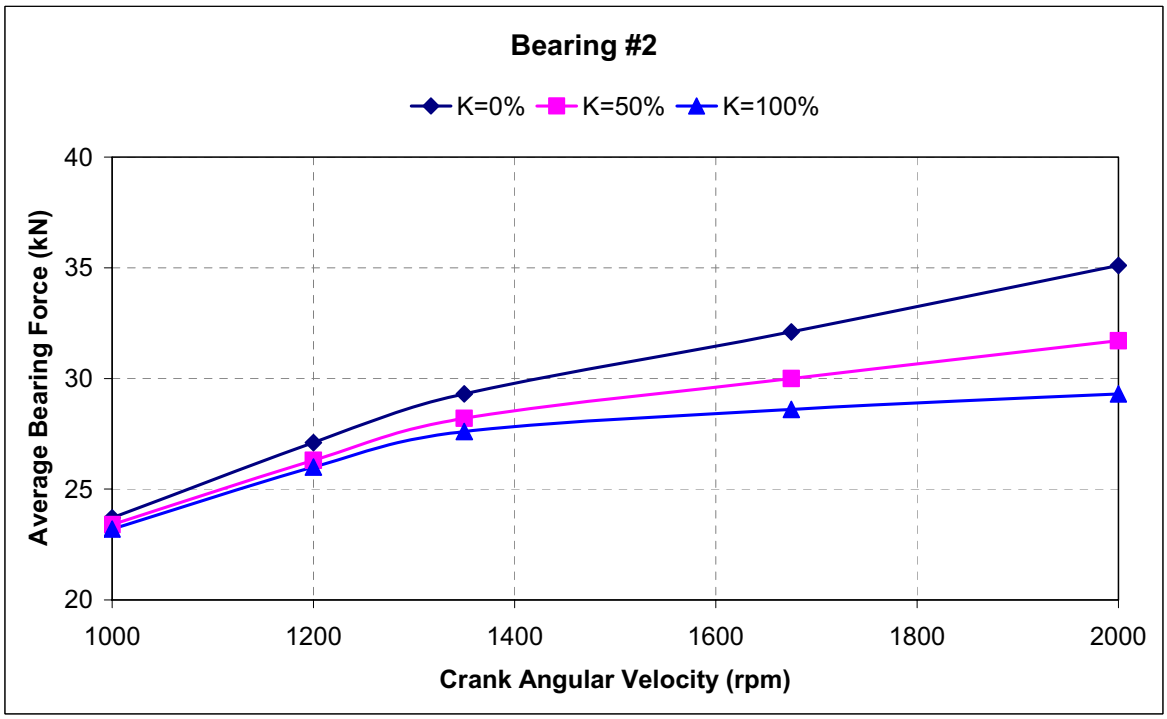

Figure 5.16. Average bearing forces at bearing #2 for twelve-counterweight configurations

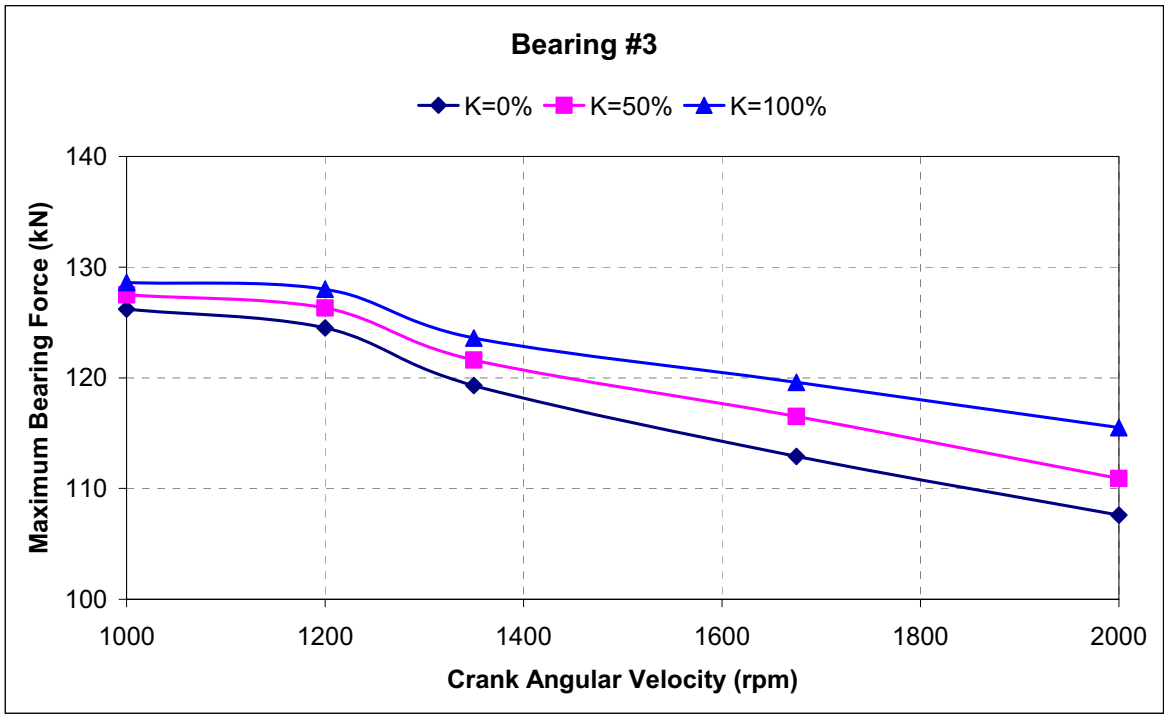

Figure 5.17. Maximum bearing forces at bearing #3 for twelve-counterweight configurations

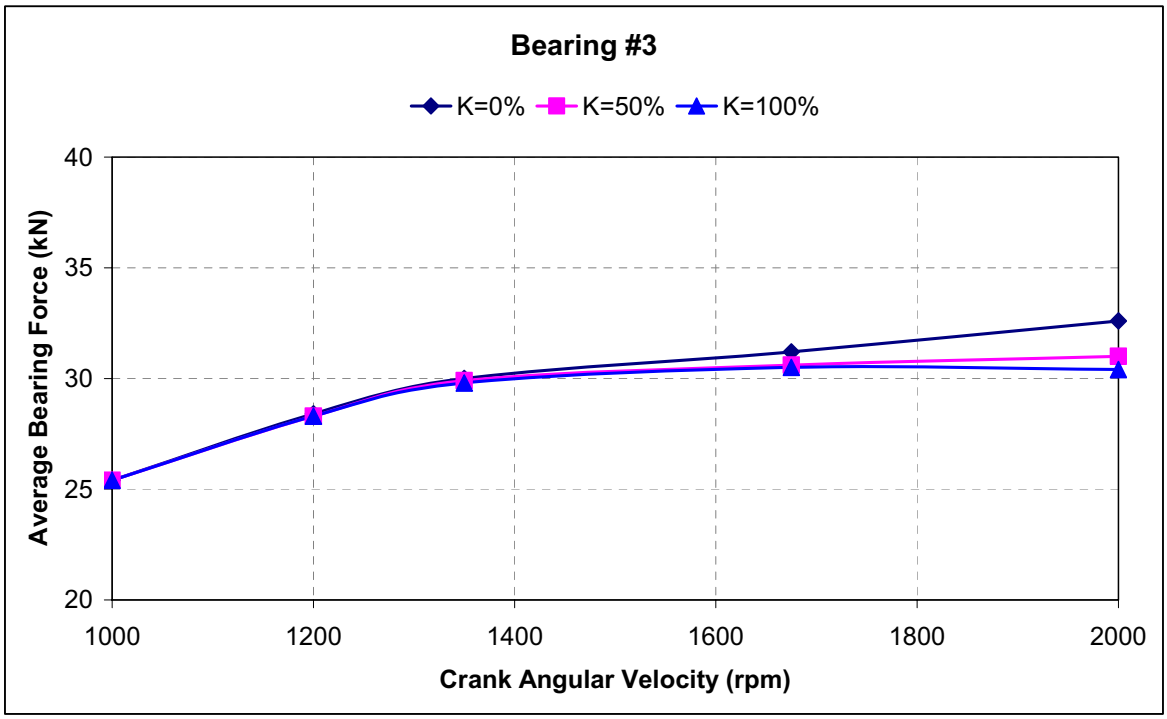

Figure 5.18. Average bearing forces at bearing #3 for twelve-counterweight configurations

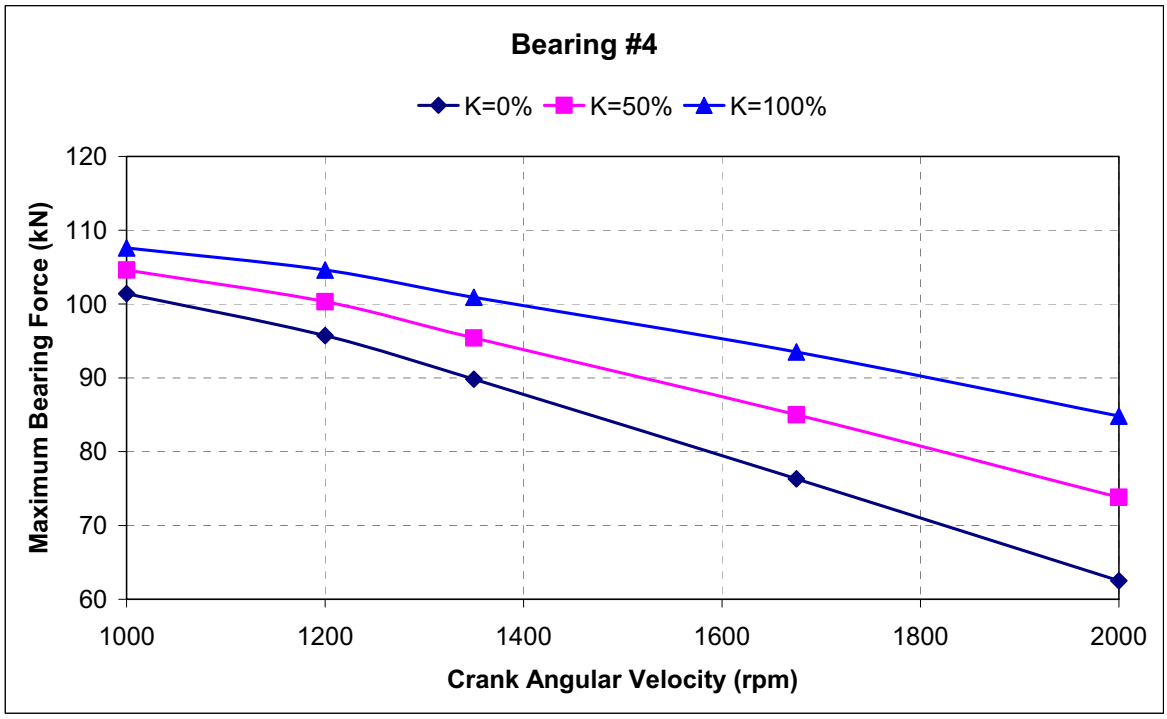

Figure 5.19. Maximum bearing forces at bearing #4 for twelve-counterweight configurations

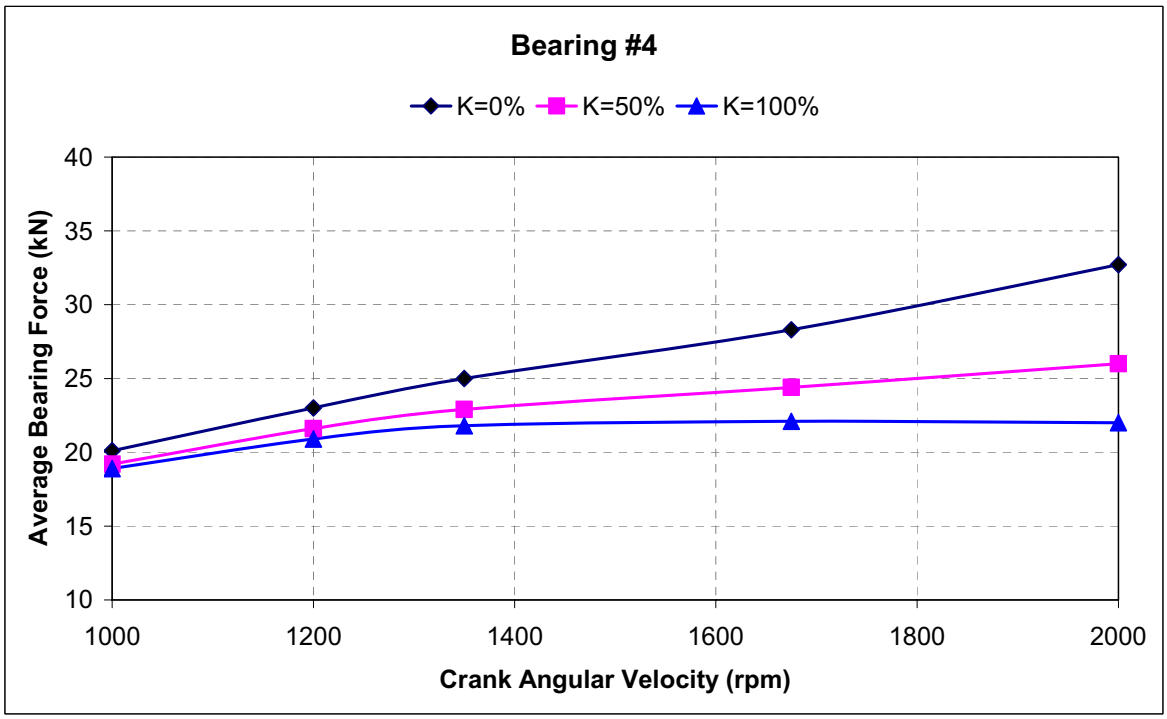

Figure 5.20. Average bearing forces at bearing #4 for twelve-counterweight configurations

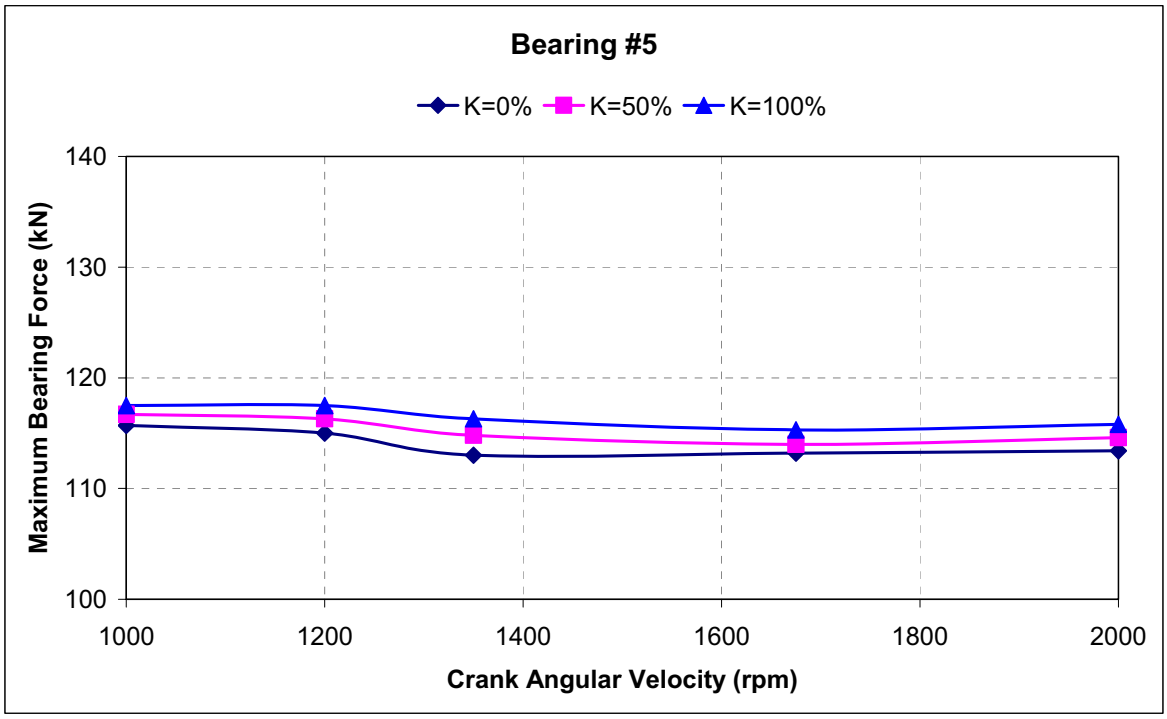

Figure 5.21. Maximum bearing forces at bearing #5 for twelve-counterweight configurations

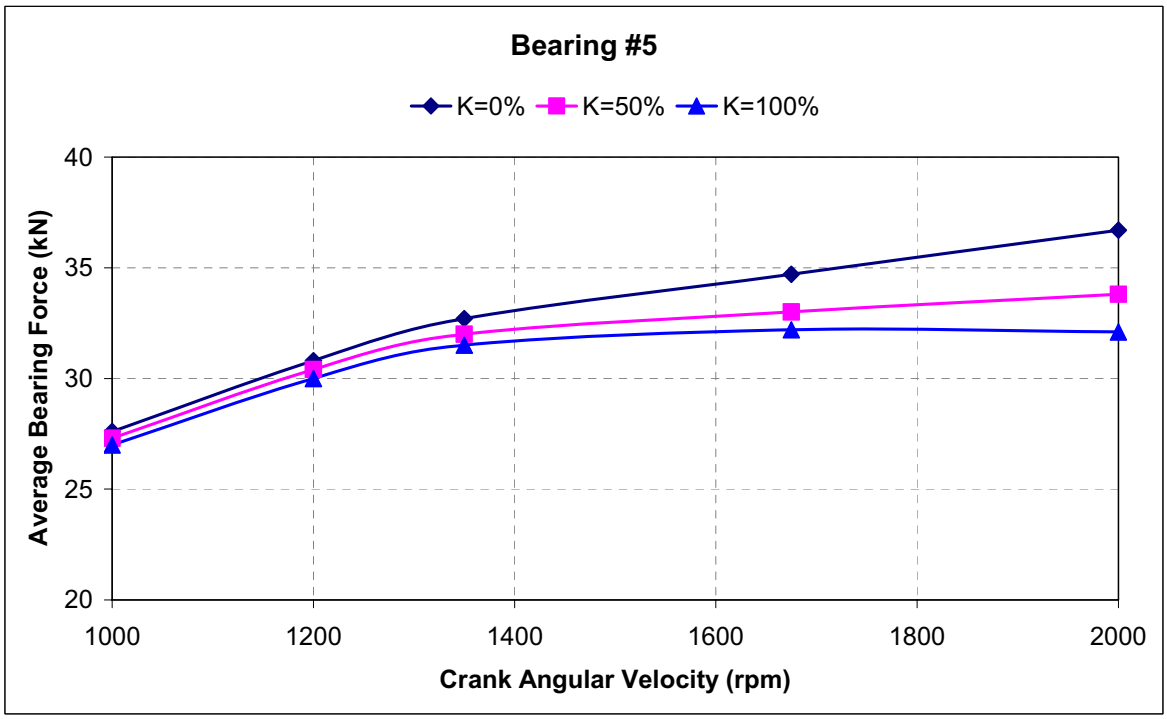

Figure 5.22. Average bearing forces at bearing #5 for twelve-counterweight configurations

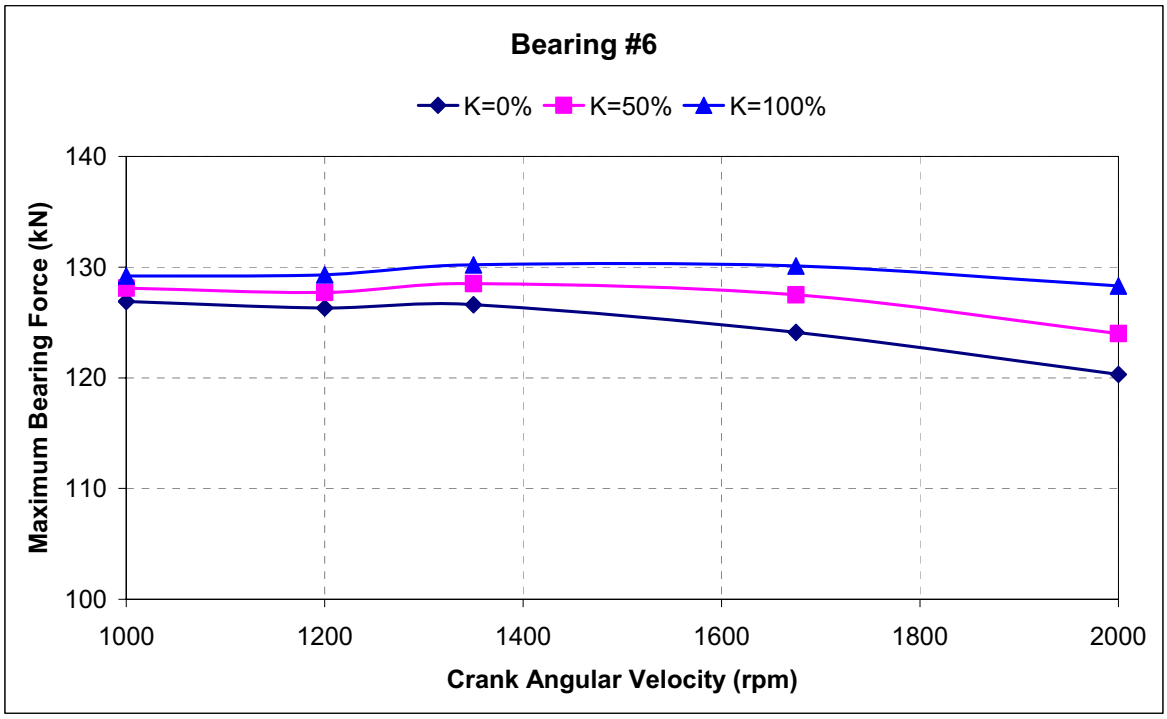

Figure 5.23. Maximum bearing forces at bearing #6 for twelve-counterweight configurations

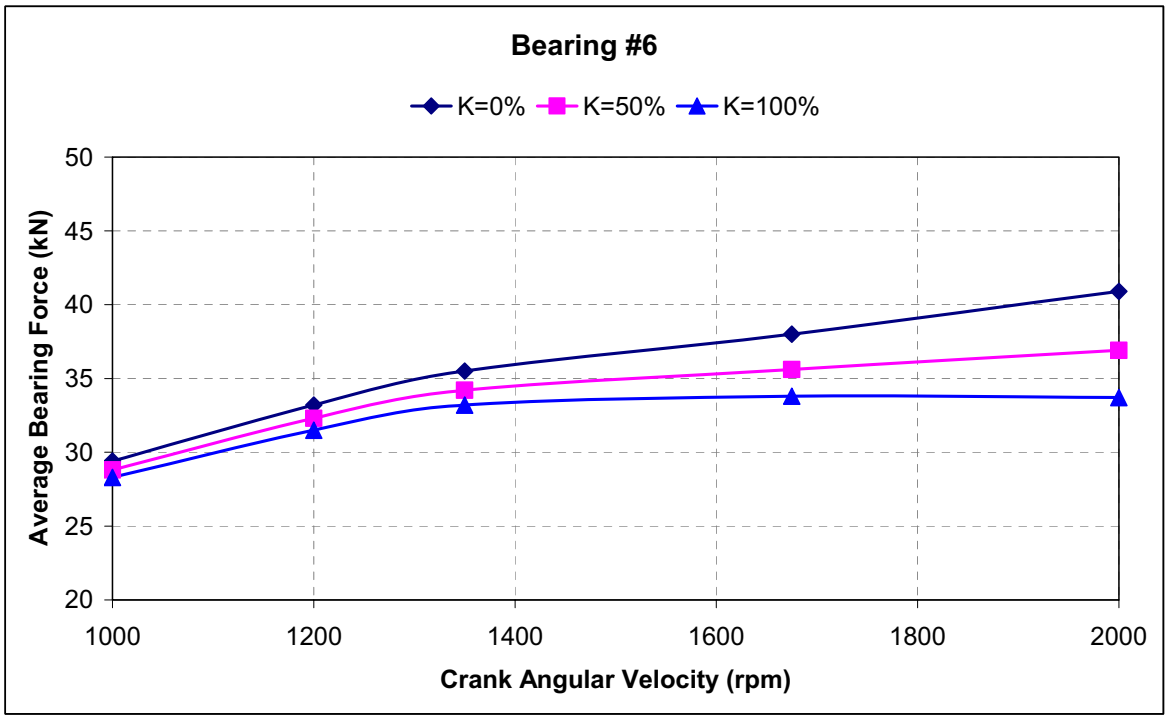

Figure 5.24. Average bearing forces at bearing #6 for twelve-counterweight configurations

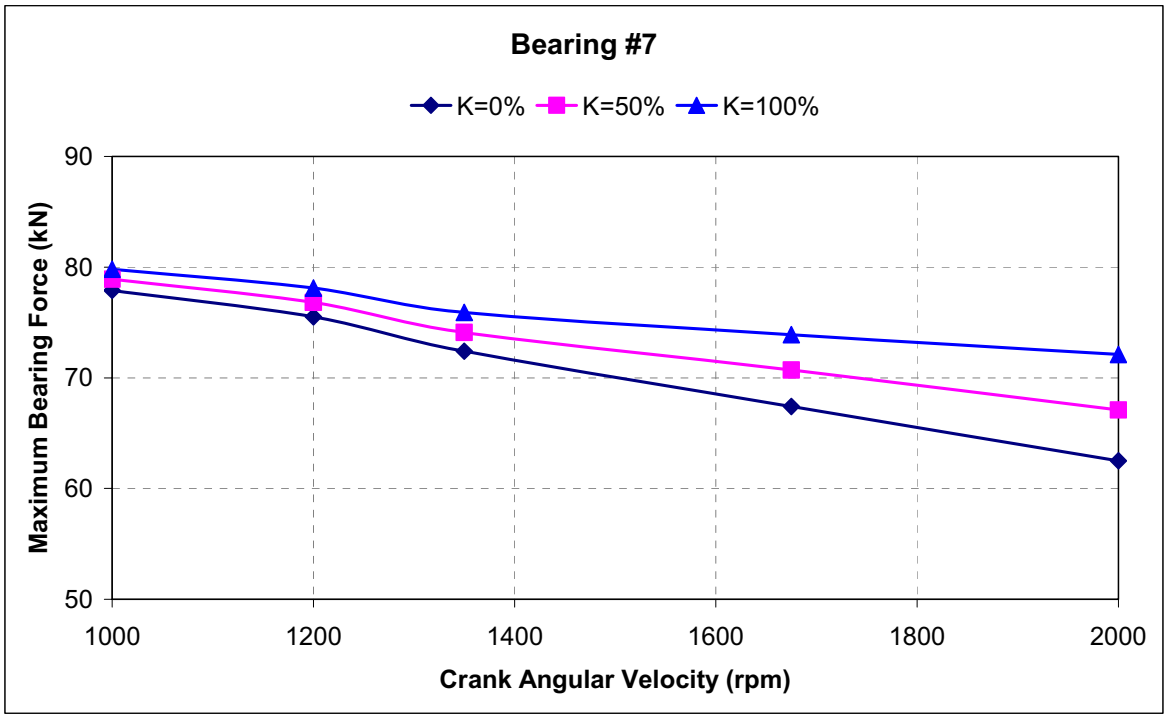

Figure 5.25. Maximum bearing forces at bearing #7 for twelve-counterweight configurations

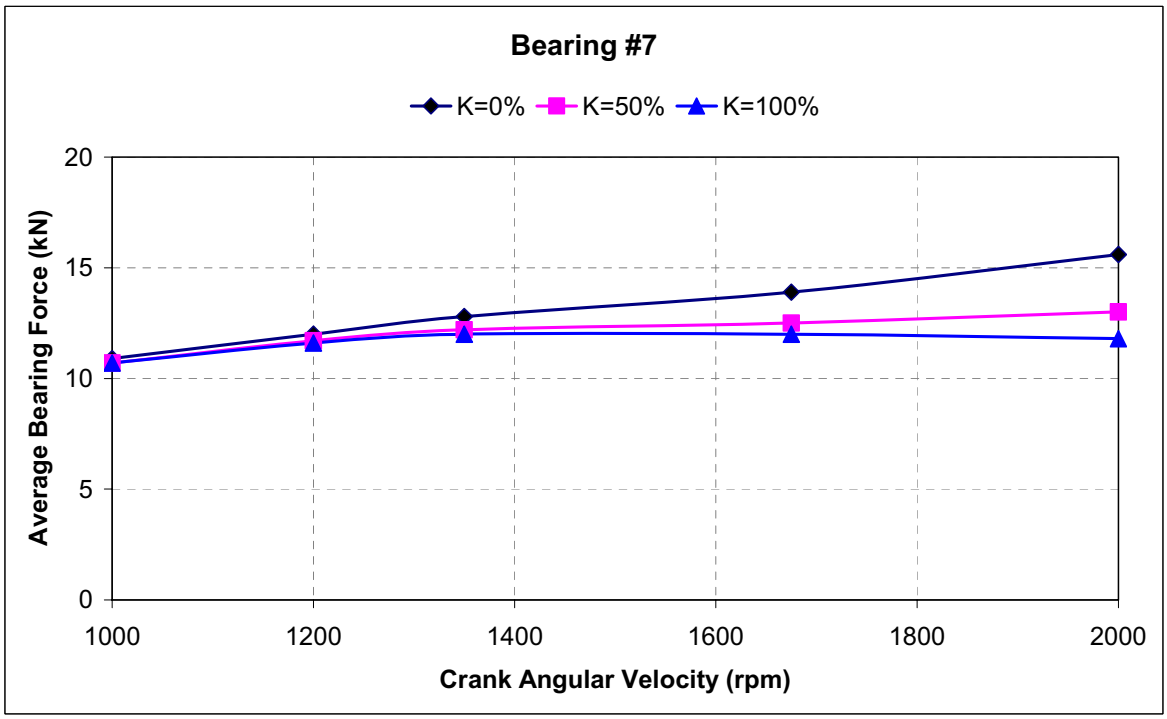

Figure 5.26. Average bearing forces at bearing #7 for twelve-counterweight configurations

Maximum bending stresses at each web for beam crankshaft model are given in Tables 5.3-5.5. As can be seen from the tables, maximum bending stress occurs at webs 1 and 12. Since maximum bearing force for K=100% case is higher than K=50% and K=0% cases, maximum bending stress for K=100% case is slightly higher than K=50% and K=0% cases.

Table 5.3. Maximum bending stresses for no counterweight configuration, *K*=0%

	Maximum Bending Stress (MPa)				
	1000 rpm	**1200 rpm**	**1350 rpm**	**1675 rpm**	**2000 rpm**
Web #1	135.9	133.4	136.5	135	127.8
Web #2	40.6	47.8	51.4	50.3	46
Web #3	44.5	50.2	53.9	52.4	47.3
Web #4	46.9	48.9	49.2	47.6	47.8
Web #5	48.6	51.5	51.1	51.8	53.1
Web #6	88.3	87.1	85.7	83.3	80.4
Web #7	78.9	78.6	80.2	80.7	80.4
Web #8	82.2	79.9	74.5	66.1	57
Web #9	72.8	70.9	66.1	59	51.3
Web #10	77.6	74.2	68.3	58.9	48.6
Web #11	67.4	64.3	58.9	50.1	42
Web #12	145.7	141.7	144.2	140.3	131.8

Table 5.4. Maximum bending stresses for twelve-counterweight configuration with K=50%

	Maximum Bending Stress (MPa)				
	1000 rpm	**1200 rpm**	**1350 rpm**	**1675 rpm**	**2000 rpm**
Web #1	138.4	136.8	140.9	141.2	135.9
Web #2	41.9	49.5	53.5	53.6	50.5
Web #3	45.8	52	56.1	55.9	52.2
Web #4	46.3	47.8	51.2	50.6	46.5
Web #5	47.6	49.9	49.2	48.7	48.4
Web #6	88.6	87.5	86.1	83.8	81.2
Web #7	79.4	79.	80.9	81.8	81.7
Web #8	83.6	81.9	76.8	69.4	61.5
Web #9	74	72.5	68.1	61.7	55
Web #10	79	76.1	70.7	62.4	53.4
Web #11	68.6	66	61	53.2	44.7
Web #12	147.8	144.8	148.4	146.6	140.1

Table 5.5. Maximum bending stresses for twelve-counterweight configuration with K=100%

	Maximum Bending Stress (MPa)				
	1000 rpm	**1200 rpm**	**1350 rpm**	**1675 rpm**	**2000 rpm**
Web #1	140.6	140.0	145.0	147.3	143.8
Web #2	43	51.2	55.6	56.7	54.8
Web #3	47.1	53.7	58.3	59.1	56.7
Web #4	45.6	49	53.1	53.4	50.3
Web #5	47.4	48.5	48.4	49	48.2
Web #6	88.8	87.7	86.4	84.3	81.9
Web #7	79.8	79.8	81.6	82.7	83
Web #8	84.9	83.7	79	72.5	65.8
Web #9	75.1	74	69.9	64.3	58.5
Web #10	80.4	78	73	65.8	58
Web #11	69.8	67.7	63.1	56.2	48.7
Web #12	149.9	147.8	152.3	152.7	148.4

5.4.2. Eight counterweights, $\gamma = 30^{o}$, *K*=50% and *K*=100%

Eight-counterweight configuration shows the same trend as the twelve-counterweight configuration for maximum and average bearing forces: maximum bearing force increases with increasing balancing rate whereas average bearing force increases with decreasing balancing rate. Maximum and average bearing forces for $\gamma = 30^{o}$, *K*=50% and *K*=100% counterweight configurations are calculated for beam crankshaft model considering inertial and gas pressure forces and given in Figures 5.27-5.40.

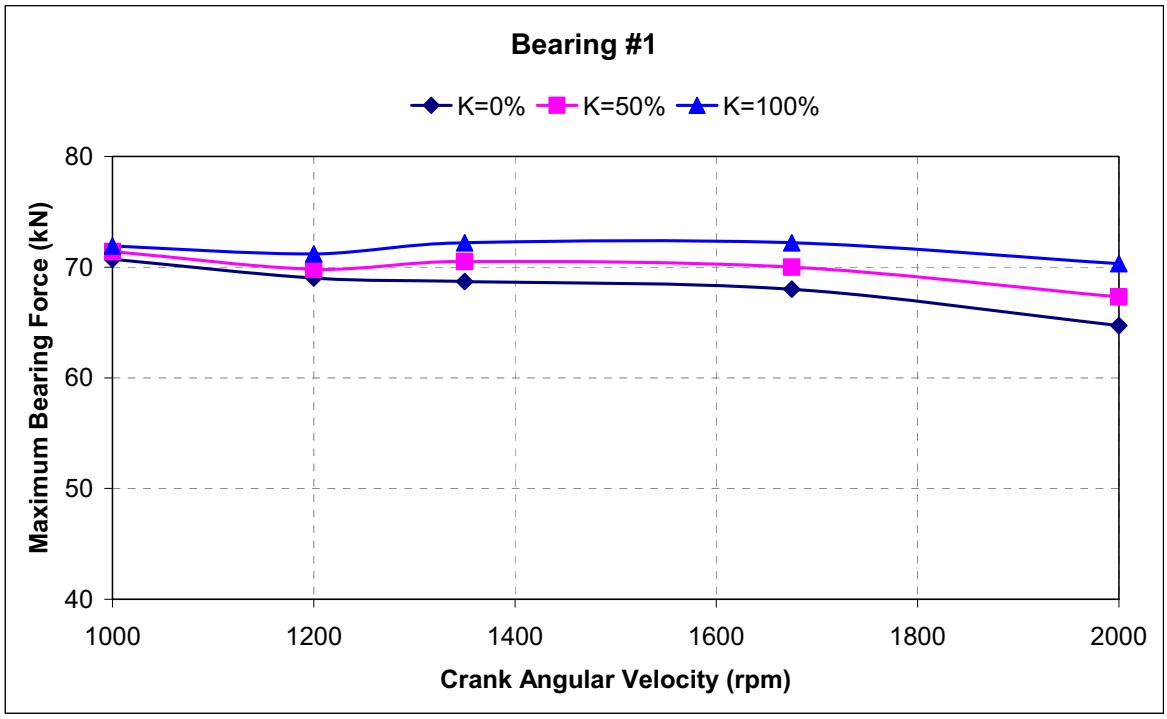

Figure 5.27. Maximum bearing forces at bearing #1 for eight-counterweight configurations

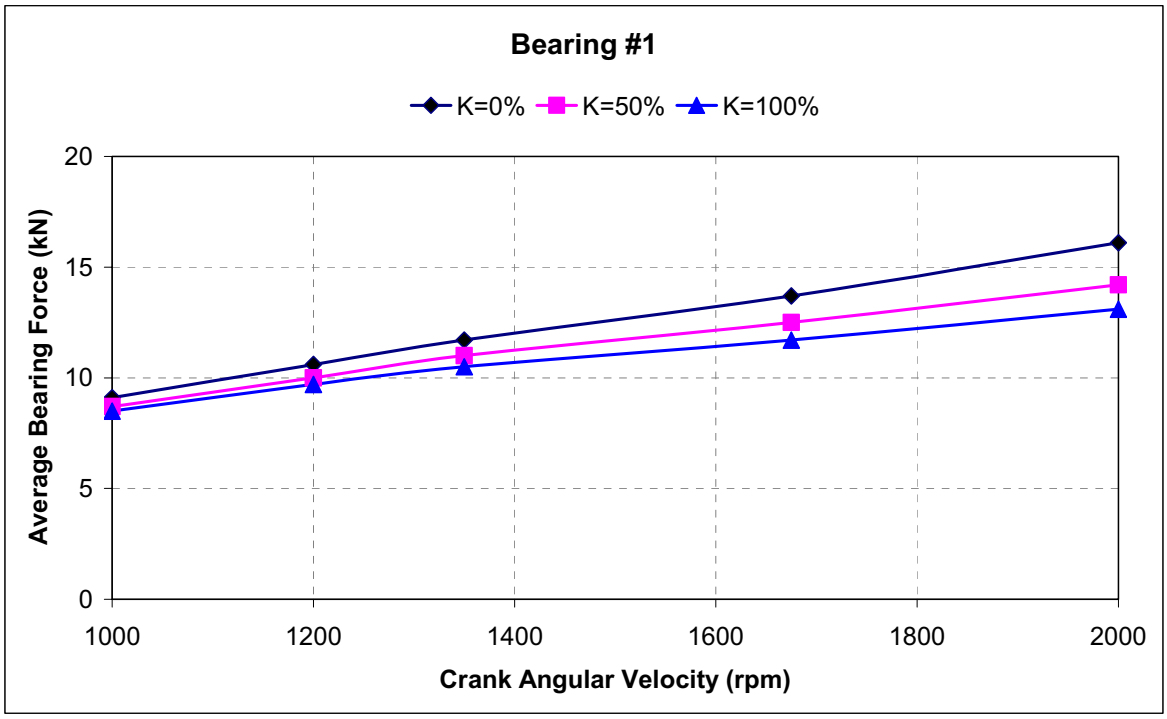

Figure 5.28. Average bearing forces at bearing #1 for eight-counterweight configurations

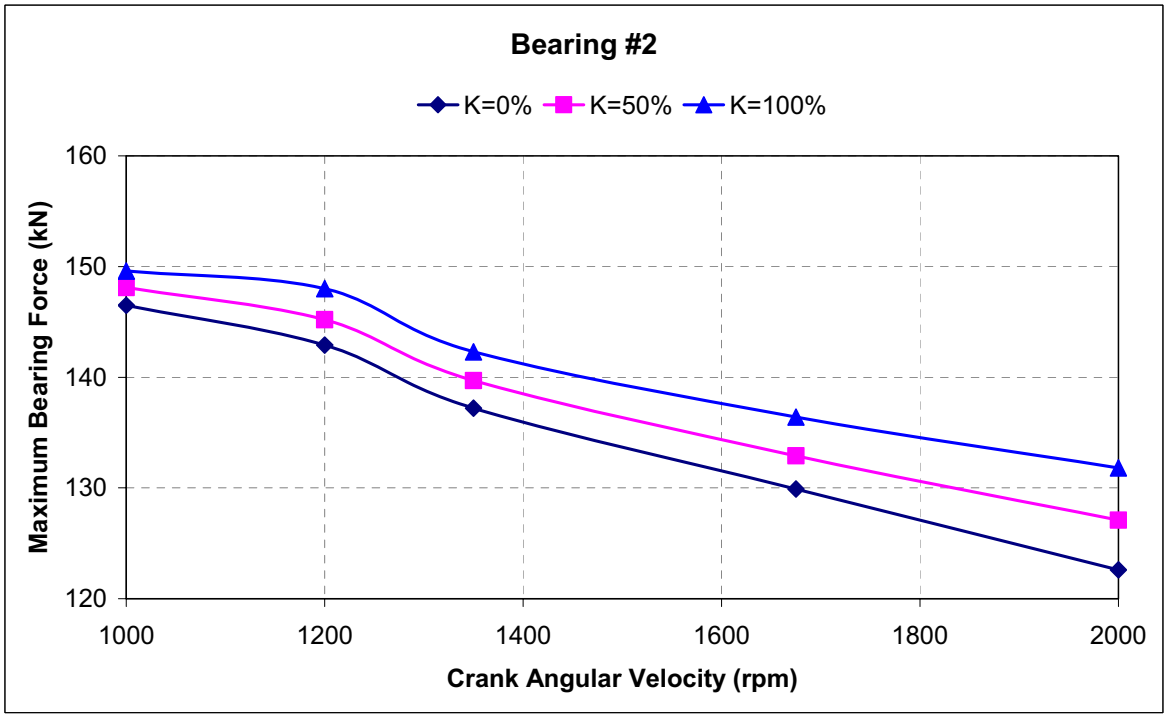

Figure 5.29. Maximum bearing forces at bearing #2 for eight-counterweight configurations

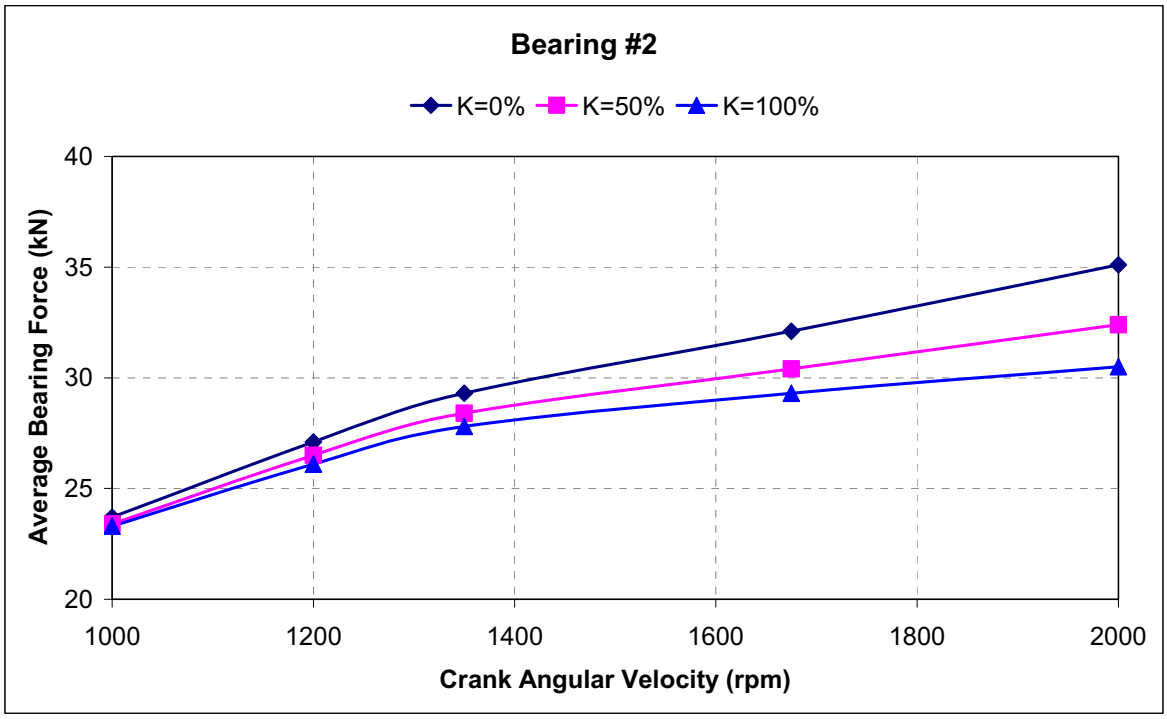

Figure 5.30. Average bearing forces at bearing #2 for eight-counterweight configurations

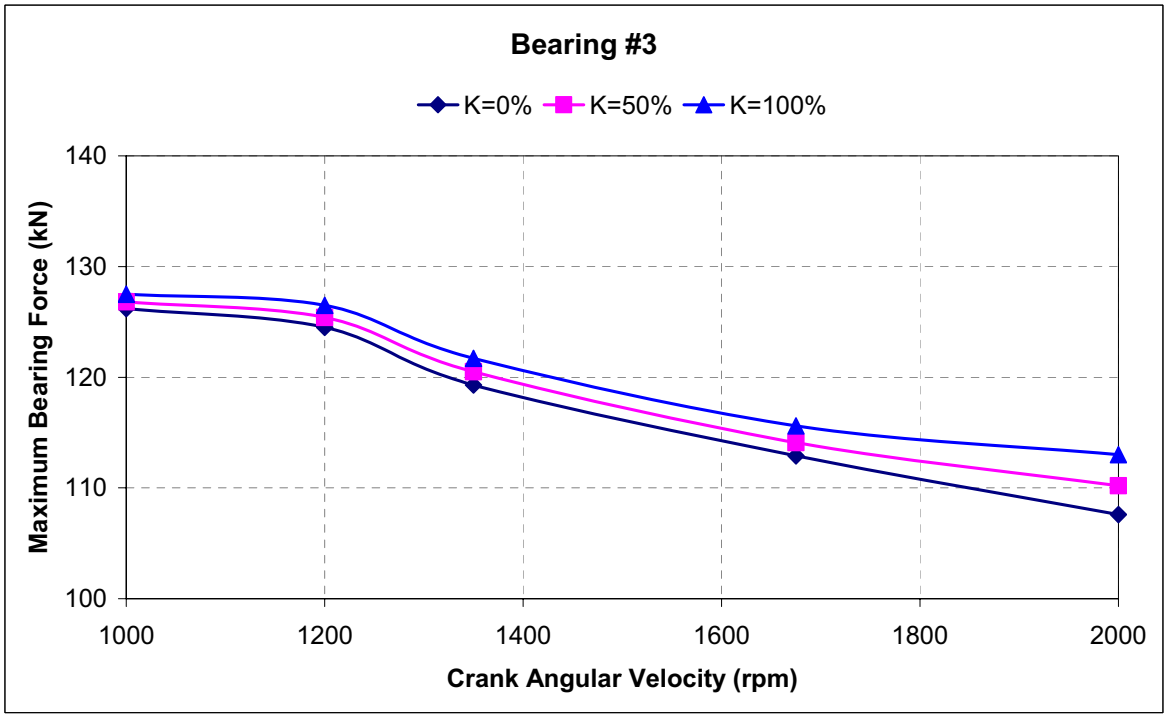

Figure 5.31. Maximum bearing forces at bearing #3 for eight-counterweight configurations

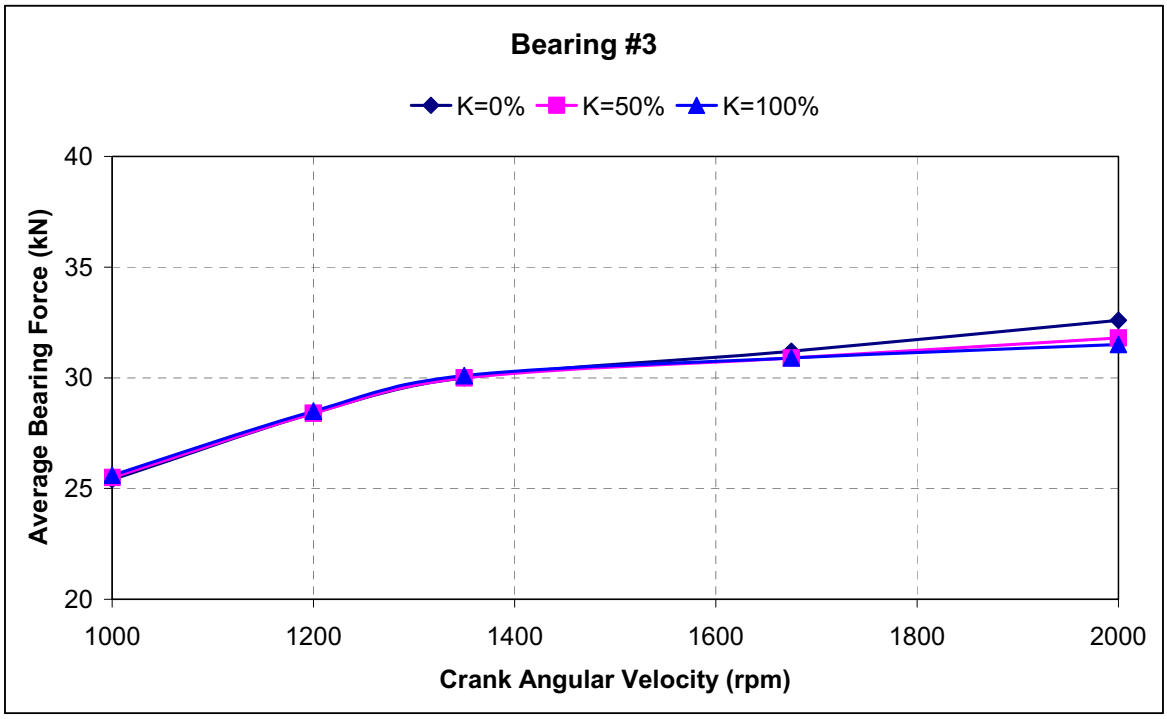

Figure 5.32. Average bearing forces at bearing #3 for eight-counterweight configurations

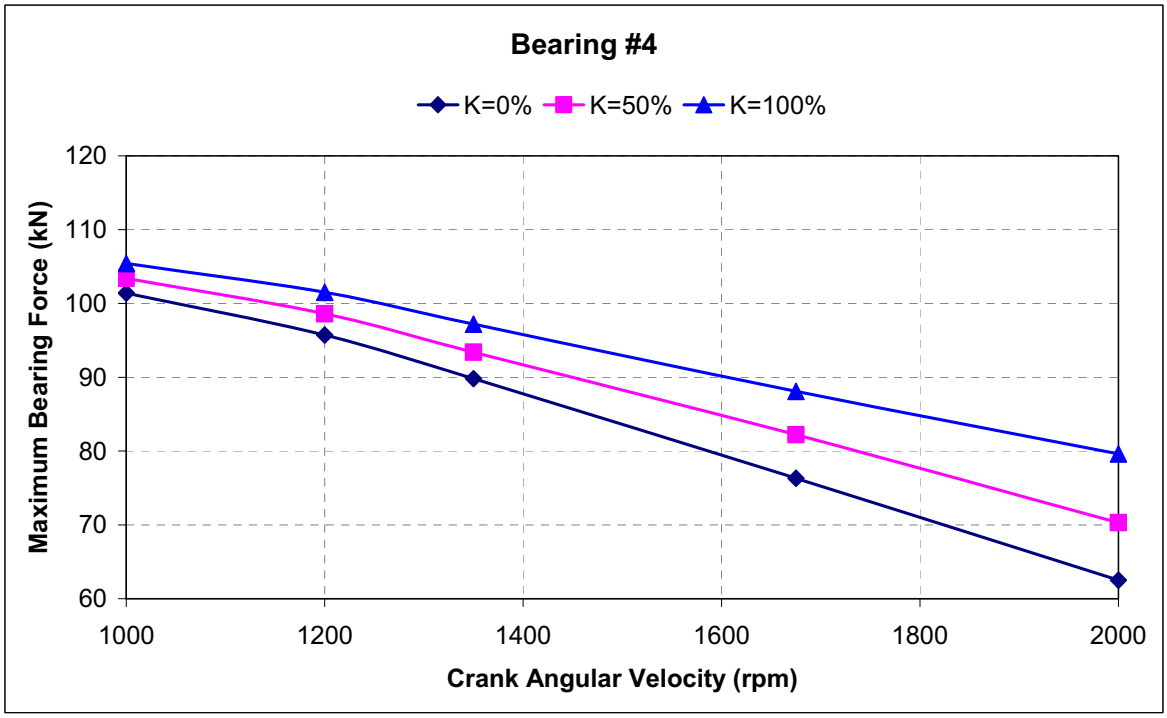

Figure 5.33. Maximum bearing forces at bearing #4 for eight-counterweight configurations

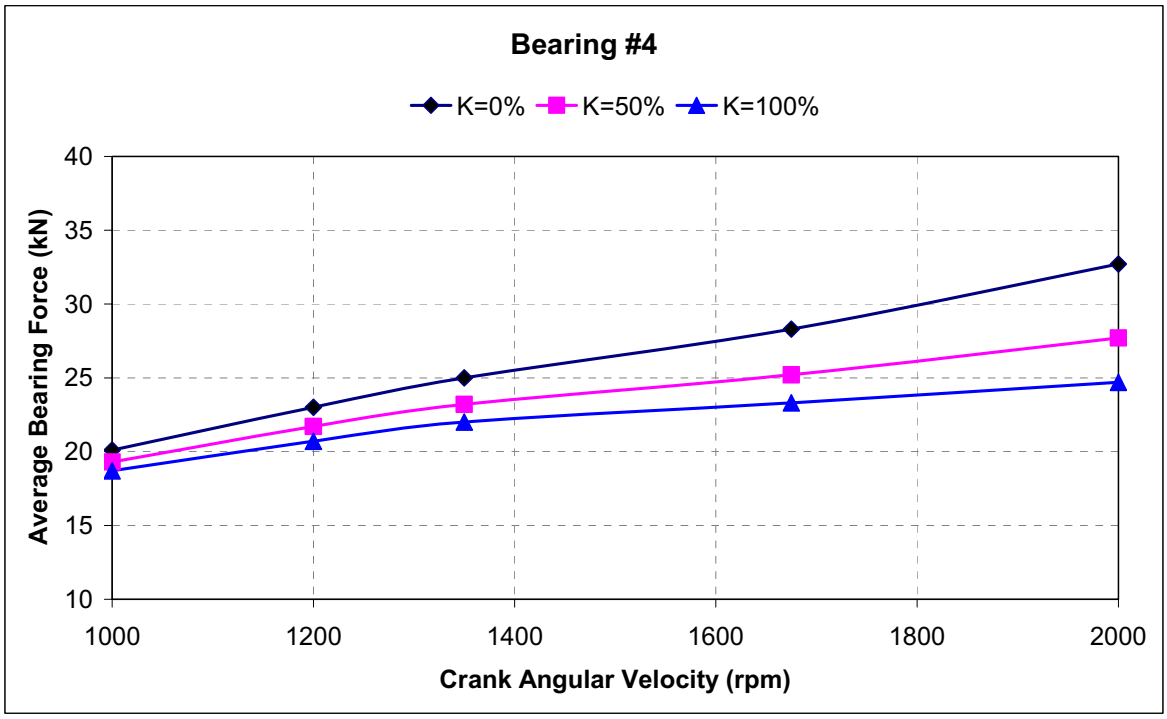

Figure 5.34. Average bearing forces at bearing #4 for eight-counterweight configurations

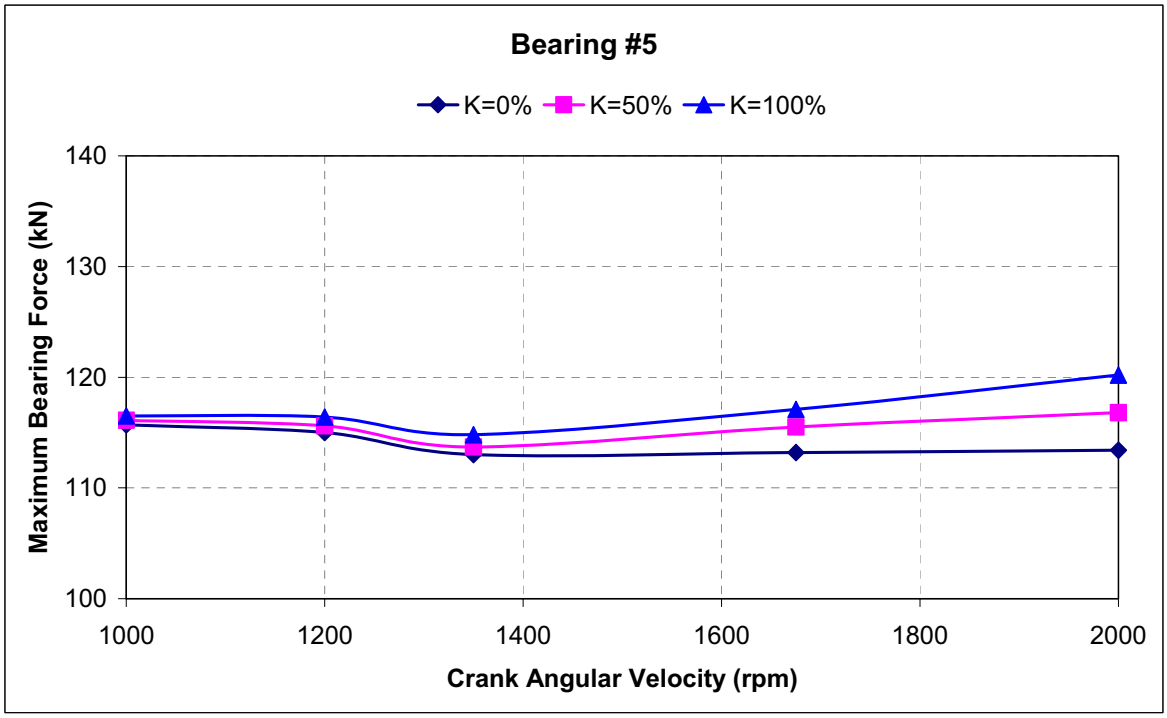

Figure 5.35. Maximum bearing forces at bearing #5 for eight-counterweight configurations

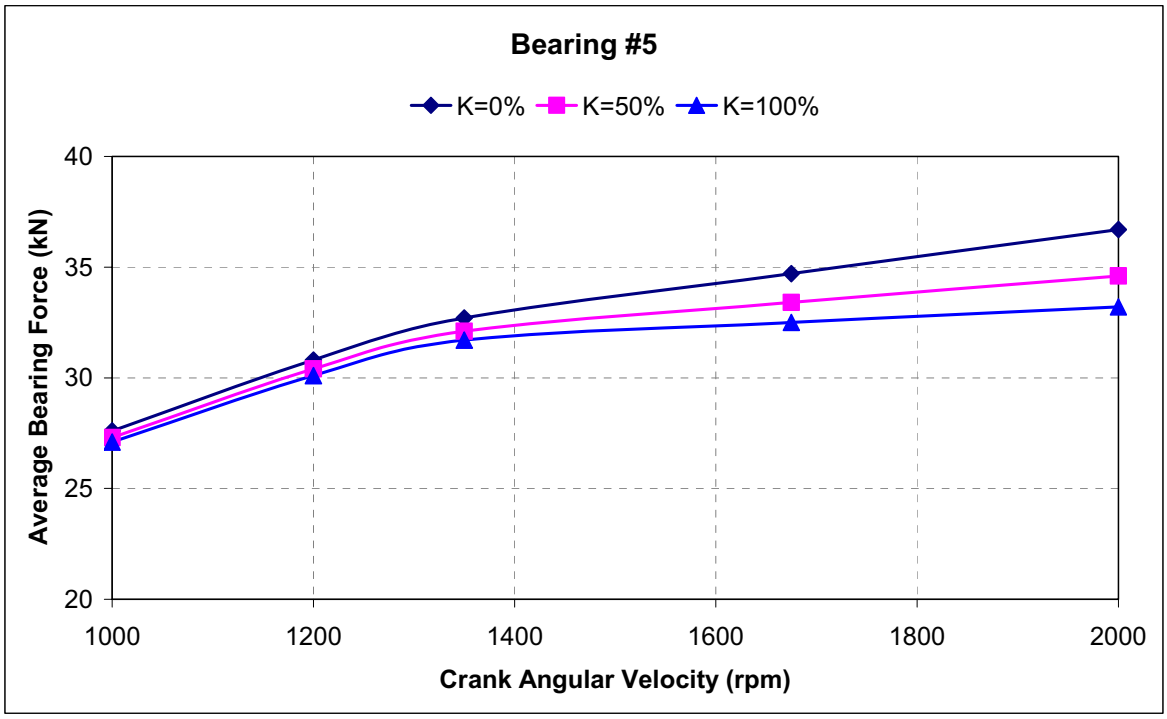

Figure 5.36. Average bearing forces at bearing #5 for eight-counterweight configurations

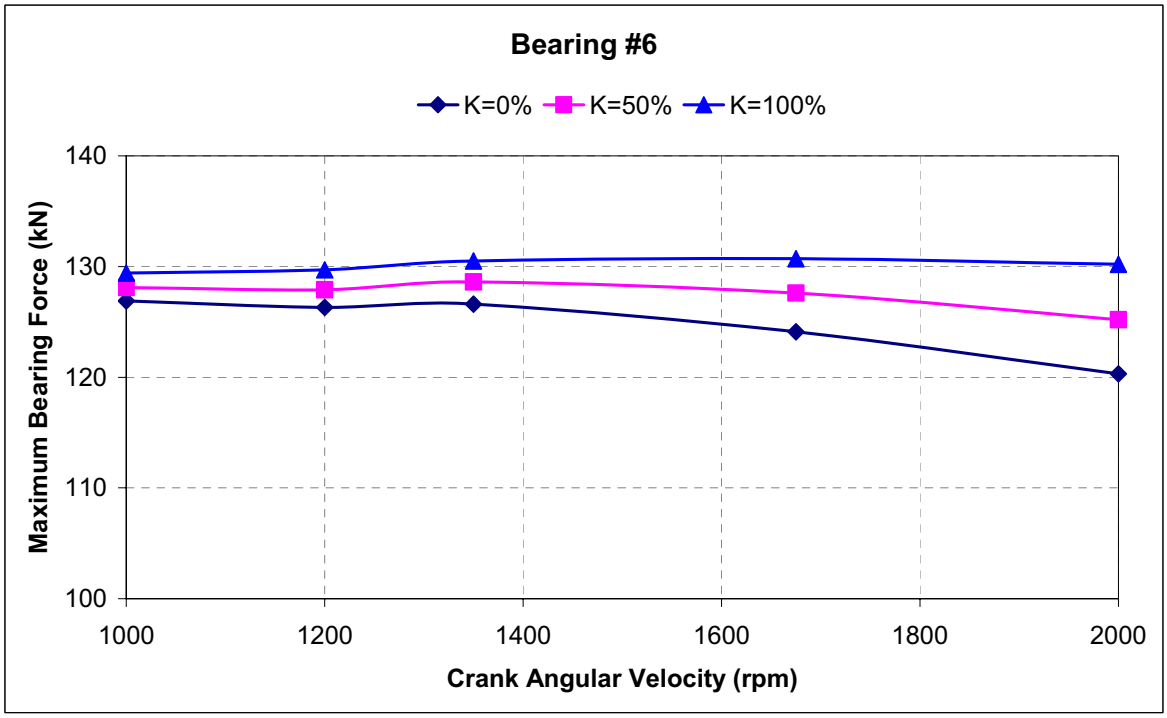

Figure 5.37. Maximum bearing forces at bearing #6 for eight-counterweight configurations

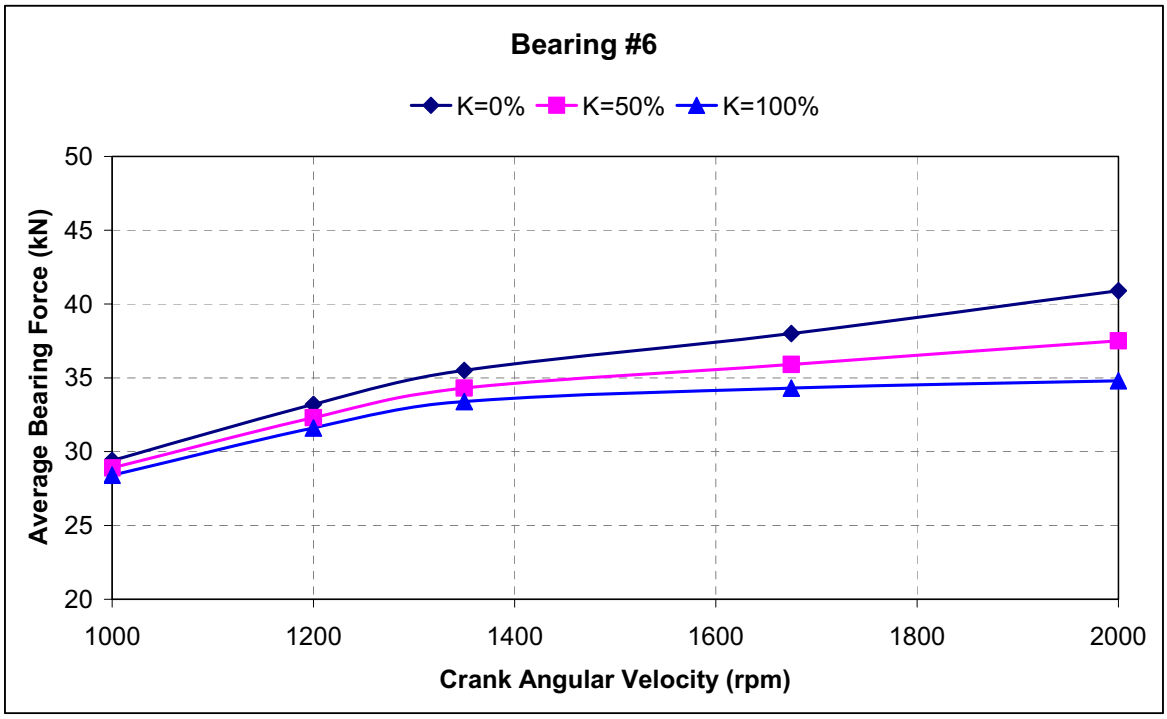

Figure 5.38. Average bearing forces at bearing #6 for eight-counterweight configurations

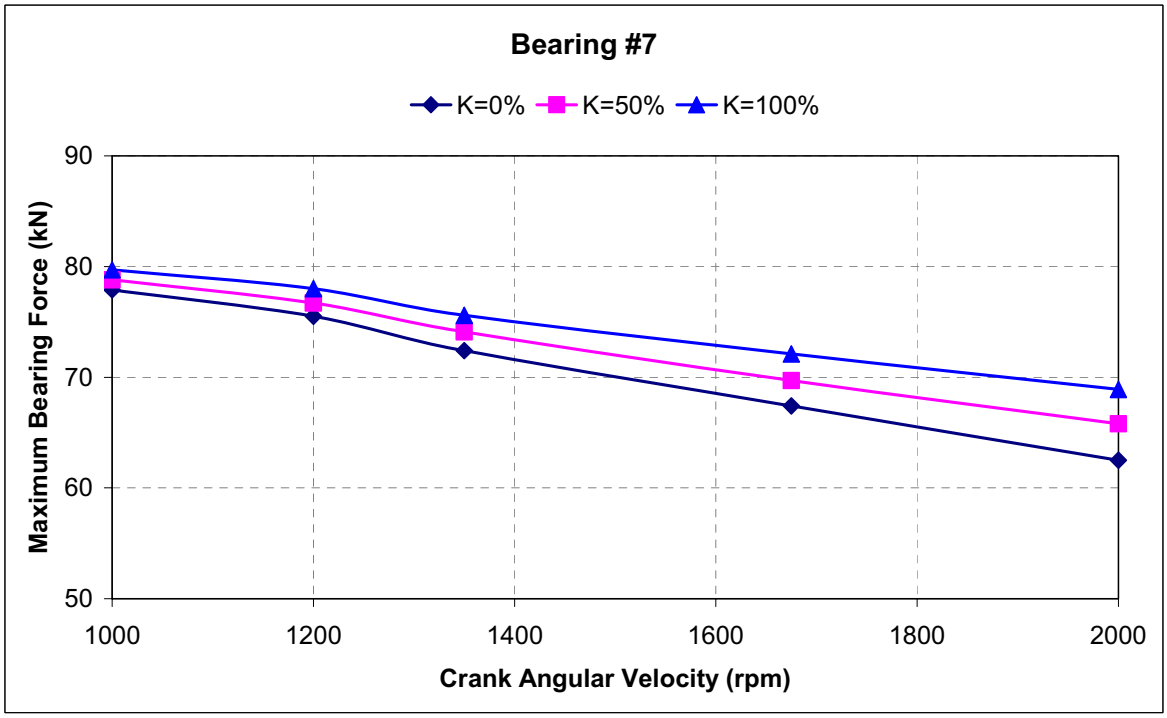

Figure 5.39. Maximum bearing forces at bearing #7 for eight-counterweight configurations

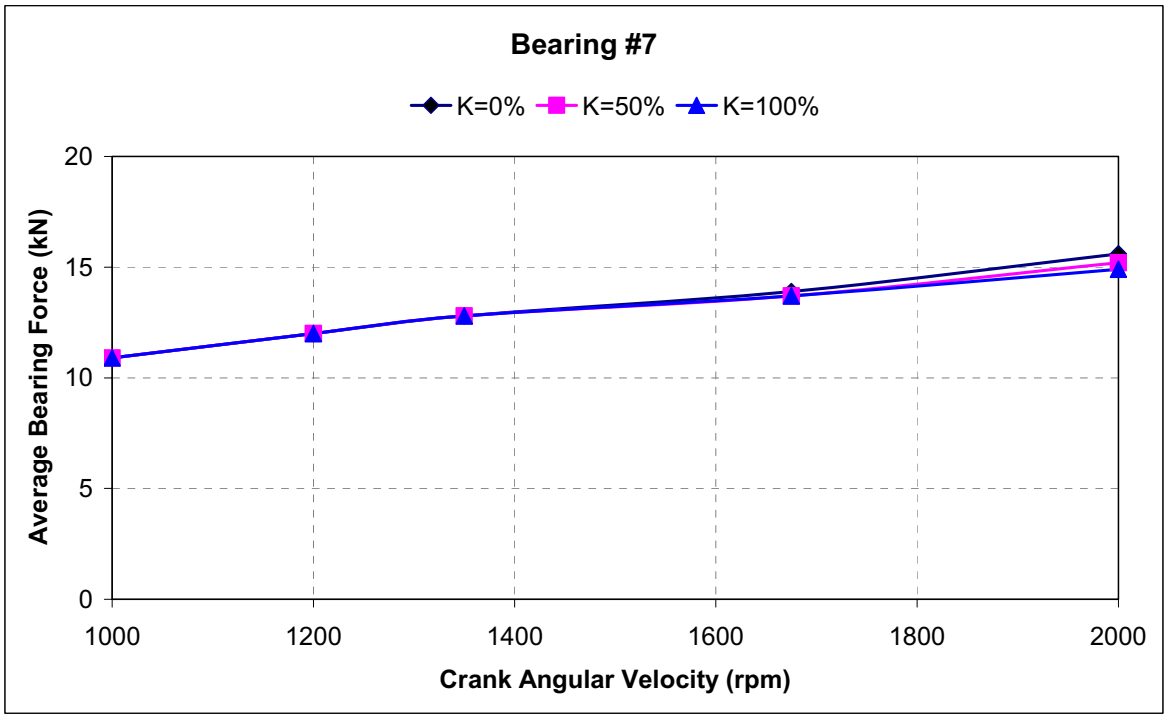

Figure 5.40. Average bearing forces at bearing #7 for eight-counterweight configurations

Maximum bending stresses for two crankshaft configurations are given in Tables 5.6 and 5.7. When compared to 12 counterweights with $\gamma = 0^{o}$ and K=50% and K=100% configurations, the maximum bending stresses for 8 counterweights with $\gamma = 30^{o}$, K=50% and K=100% configurations are smaller due to lower counterweight mass.

Table 5.6. Maximum bending stress for eight counterweights, $\gamma = 30^{o}$, K=50% counterweight configuration

	Maximum Bending Stress (MPa)				
	1000 rpm	**1200 rpm**	**1350 rpm**	**1675 rpm**	**2000 rpm**
Web #1	137.6	135.7	139.3	139.0	133.0
Web #2	41.1	48.4	52.2	51.6	47.7
Web #3	44.7	50.5	54.3	53	48.2
Web #4	47	49	49.4	47.9	47.7
Web #5	48.2	50.9	50.4	50.6	51.2
Web #6	88.4	87.3	85.8	83.5	80.7
Web #7	79.2	78.9	80.6	81.3	81
Web #8	82.8	80.8	75.4	67.5	58.8
Web #9	73	71.1	66.3	59.2	51.5
Web #10	77.9	74.6	68.8	59.6	49.4
Web #11	67.9	65	59.7	51.3	41.9
Web #12	147.1	143.8	147.1	144.5	137.2

Table 5.7. Maximum bending stress for eight counterweights, $\gamma = 30^{o}$, K=100% counterweight configuration

	Maximum Bending Stress (MPa)				
	1000 rpm	**1200 rpm**	**1350 rpm**	**1675 rpm**	**2000 rpm**
Web #1	139.1	137.9	142.2	142.9	138.1
Web #2	41.2	48.5	52.3	51.8	47.9
Web #3	44.8	50.6	54.3	53.1	48.3
Web #4	47.1	49	49.5	48	47.7
Web #5	48.2	50.9	50.3	50.4	51
Web #6	88.5	87.3	85.9	83.5	80.7
Web #7	79.2	79	80.6	81.3	81.2
Web #8	82.9	80.9	75.6	67.7	59.1
Web #9	73	71.2	66.4	59.2	51.5
Web #10	78	74.7	68.9	59.7	49.6
Web #11	68	65.1	59.9	51.5	42.2
Web #12	148.6	146.0	149.8	148.8	143.1

6. SUMMARY AND CONCLUSIONS

In this study, dynamic analysis of the crankshaft system of an inline 6-cylinder diesel engine is carried out using finite elements and multibody dynamics considering the flexibility of the crankshaft and effect of crankshaft system components. Coupled axial, bending and torsional vibrations of the crankshaft system are taken into account. Effect of each part of the crankshaft system on the crankshaft dynamic stress and vibration characteristics is determined. For the numerical analysis of the crankshaft system, Msc.Nastran, Msc.Adams (Automatic Dynamic Analysis of Mechanical Systems) and MATLAB software programs are used.

Torsional vibration analyses are carried out for 7.3 L and 9.0 L engines with and without TV dampers and torsional vibration amplitudes at the crankshaft front and rear ends for the crankshaft systems are calculated. For this purpose, a torsional vibration analysis program is written in MATLAB. The analyses are carried out for specific TV dampers which are currently used in these engines but effect of any TV damper on torsional vibration characteristics may be determined with this particular program.The sixth order front end vibration amplitude that is the critical one is reduced with the proposed TV dampers. The calculation results are verified by experimental results available for 7.3 L engine crankshaft. Effect of cylinder misfire on front end torsional vibration characteristics is also investigated for 20%, 50% and 80% misfire conditions. It is seen that as the misfire ratio increases, torsional vibration angle amplitude at crankshaft front end increases gradually.

For crankshaft stress calculations, traditional methods based on simple superposition of torsional and bending stresses are state of art. This type of analysis is carried out at Chapter 3. First, main bearing reaction forces are obtained assuming crankshaft as a statically determinate system: Each main bearing force is the resultant of forces coming from two adjacent throws. The results are compared to the results obtained using rigid crankshaft model of ADAMS and found to be satisfactory. Nominal stresses due to bending moments and radial forces are calculated at the webs of the crankshaft. Actual fillet stresses are calculated using stress concentration factors and equivalent stresses are

determined using distortion energy. It is seen that web 8 and web 11 are the most critical webs and maximum stresses occur at an engine speed of 2400 rpm. It is also seen that, main pin fillet location is more critical than crank pin fillet location.

In traditional force and stress analyses, some simplifications are made in calculation of crankshaft system forces and stresses. Crankshaft is assumed to be a rigid structure and analyses are based on each single crank throw. Maximum torsional and bending stresses are assumed to occur at the same time. Hydrodynamic oil pressures in bearings are not considered and bearings are treated as constraining elements. No bending vibration effect is considered. Connecting rod mass is partitioned into two masses, one rotating with the crankshaft and other reciprocating with the piston. Because of aforementioned assumptions, some error is introduced into the analyses. To overcome these deficiencies, an advanced method is introduced in Chapter 4 for dynamic analysis of crankshaft system.

The dynamic analyses are carried out using beam and flexible crankshaft models. Beam crankshaft model is supplied by the ADAMS/Engine. The flexible crankshaft model is obtained using MSC.Nastran and transferred to ADAMS. Hydrodynamic bearing models supplied by ADAMS/Engine are used in the analyses. The aim of this part is to calculate main bearing forces, to calculate dynamic stresses and to determine the critical areas of loading for the crankshaft system of 7.3 L NHDD engine using Finite Elements and Multibody Dynamics simultaneously.

First, main bearing forces are calculated for beam and flexible crankshaft models. Comparing the results obtained by ADAMS/Engine to the results obtained by AVL/Excite, it can be concluded that hydrodynamic approaches that decouple the hydrodynamic behavior from the structural dynamic behavior, either with beam crank or flexible crank model are sufficient to determine the forces in bearings. It is seen that maximum main bearing loads occur at bearing # 2 due to firing of cylinder 1 and at bearing # 6 due to firing of cylinder 6.

Second, dynamic stress analyses are carried out for beam and flexible crankshaft models at the rated engine speed, 2400 rpm under full load (18 Mpa) which is the most critical loading condition. At this engine speed, main torque and web bending moments are

calculated for beam crankshaft model. Then bending and shear stresses are determined at each web center. Torsional stresses are also calculated at the connection points between main pins and webs. It is seen that most critical region of the crankshaft is Web 12 where maximum bending stress reaches a maximum value of 143 MPa. In flexible crankshaft analysis, two crankshaft models, with and without oil holes are considered to see the effect of oil holes on crankshaft stresses. The load torque is directly applied to the flywheel. To see the effect of torsional vibration damper on crankshaft stresses, all analyses mentioned above are performed with and without vibration damper. The most critical web was found to be web 12 which is the one near the flywheel. It is seen that maximum von Mises stress of the crankshaft with oil holes and without damper case is 459.4 MPa and it occurs at crank pin fillet. For the same crankshaft with damper, the maximum stress reduces to 423.3 MPa and it occurs at the main pin fillet. Similarly, maximum von Mises stress of the crankshaft without oil holes and damper case is 400.7 MPa and it occurs at the main pin fillet. For the same crankshaft with damper, the maximum stress reduces to 379.5 MPa and it occurs at main pin fillet. It is seen that for all cases, maximum stresses occur during firing of cylinder # 6 when cylinder 6 is nearly at top dead center position and the load tends to bend the crankshaft which show that maximum stresses occur as a result of bending.

Oil film thickness analyses are also carried out. The most critical loading condition is considered. For all main bearings the minimum oil film thickness is higher then the permissible limit of 1 μm. It is seen that, although HD approaches that decouple the hydrodynamic behavior from the structural dynamic behavior do not deliver quantitative accurate pin orbital curves, they are absolutely sufficient to determine the forces in the bearing and their influence on the cranktrain subsystem.

Traditional and advanced crankshaft stress analysis show that although static crankshaft analysis assume the maximum bending and torsional stresses occur simultaneosly, bending vibrations and gyroscopic effects could become an issue with heavy flywheels. The main advantages of the advanced crankshaft dynamic analysis are as follows:

- Finite element and multibody dynamic programs are used together to include crankshaft flexibility and interaction of crankshaft system components with each other into the analysis.

- All of axial, bending and torsional vibrations of the crankshaft are taken into account.

- Hydrodynamic effects in bearing locations are considered.

- Flywheel and TV damper, that have critical roles in bending and torsional vibrations of the crankshaft system, are included in modeling the crankshaft system.

- Static and dynamic effects, and non-constant moment of inertias are considered. Quasi static crank train simulation is replaced by full dynamic analysis.

- All analyses can be performed in reasonable time for whole speed range.

- Dynamic force and stress analyses can be carried out in the same environment so that transferring data from one software to other and possible transfer errors are avoided.

In Chapter 5, the effect of counterweight configuration on bearing load and bending stress is investigated for a 9.0 L in-line 6-cylinder diesel engine crankshaft system in the presence of inertial and gas pressure forces. Five different counterweight configurations are studied in the analyses: no counterweights, 12-counterweights with K= 50% and 100%, and 8-counterweights with 30° counterweight angle, and K=50% and 100%. Analyses are carried out at an engine speed range of 1000 to 2000 rpm.

First, 3D solid model of the crankshaft is obtained using Pro/Engineer and MSC.Nastran. The crankshaft is also modeled using rigid and beam models of ADAMS/Engine. Main bearing loads are obtained for the models using ADAMS, and the results are compared to each other. It is seen that main bearing loads for beam and elastic

3D solid crankshaft models are in good agreement. As a result, because obtaining elastic 3D solid models for different counterweight configurations is difficult and time consuming, beam model is used in this work to study the effect of counterweight configuration on main bearing loads and crankshaft bending stresses.

Using beam model of ADAMS/Engine, main bearing reaction loads are obtained for no counterweight configuration, and twelve-counterweight configurations with 50% and 100% balancing rates. It is observed that maximum bearing reaction force increases with increasing balancing rate. Average bearing loads and maximum web bending stresses are also calculated. Maximum web bending stress is higher for 100% balancing rate than for 50% and 0% balancing rates. On the other hand, as the balancing rate increases, the average bearing load decreases due to lower inertia force.

Similarly, maximum and average bearing loads and bending stresses are calculated for eight-counterweight configuration with a counterweight angle of 30°. In the case of maximum and average bearing forces, eight-counterweight configurations shows the same trend as that of twelve-counterweight configurations: the maximum bearing load decreases with decreasing balancing rate, whereas average bearing load increases with decreasing balancing rate. In the case of eight-counterweight configurations with K=50% and 100%, the maximum bending stress is smaller when compared to twelve-counterweight configurations with K=50% and 100%, respectively.

It is observed that for this specific 9.0 L engine, which has a peak firing pressure of 190 bar and rated speed of 2200 rpm, inertial forces are less important than gas pressure forces for the design of the crankshaft. Addition of counterweights increases maximum bearing load but decreases average bearing load as shown in Figures 13-26. Maximum bearing load determines maximum stress and its location on the crankshaft; on the other hand, average bearing load directly affects bearing life. Therefore, selection of best counterweight configuration should be made considering both maximum and average bearing loads.

With this study, a general procedure is obtained for the dynamic stress and vibration analyses of crankshaft system of internal combustion engines and for the determination of

effects of crankshaft system components on the dynamic stress and vibration characteristics of the crankshaft. With the proposed method, the time required from conceptual design to development process reduces and the amount of engine testing, which accounts for a considerable cost, diminishes.

This dissertation demonstrated the usage of finite elements and multi body system simulation programs together for dynamic analysis of diesel engine crankshaft system. Based on the results of this study, the author suggests the following recommendations to be considered for future study.

Elasto-hydrodynamic bearing approach that considers the backward influence of the structural deformation of the crankshaft and bearing cap on the local oil film pressure distribution can be used to model the bearings. This approach is important looking at the bearings themselves and evaluating their durability in detail.

Boundary conditions should be investigated carefully, not only for stress issues, but also for questions concerning friction and wearout and for NVH. Further studies are necessary to optimize the interaction of the CAE programs. Experiments should be carried out to validate the new technology.

Time history of stresses that are obtained at crankpin and main pin fillet regions can be used in fatigue life calculations and otimization of the crankshaft can be performed using commercial programs like FEMFAT, ANSYS and MSC.FATIGUE.

Engine block can also be modeled as a flexible structure. By this way effect of deformation of cylinder block on main bearing loads and crankshaft stresses can be evaluated.

APPENDIX A
MATLAB CODE FOR TORSIONAL VIBRATION ANALYSIS

```
function yasin()

load data2400.txt
pgt=data2400;
clear data2400

omega=2400*pi/30;
mrec=3.55;
r=0.062;
L=0.222;
D=0.112;
n=length(pgt);

lambda=r/L;

theta=1:720;
theta=theta*pi/180;

for i=1:n
   ptgt(i)=pgt(i)*(sin(theta(i))+(lambda*sin(theta(i))*cos(theta(i))/(sqrt(1-
lambda^2*sin(theta(i))*sin(theta(i))))));
end

Aop=0;
for i=1:n
   Aop=Aop+ptgt(i);
end
Aop=Aop/720;

k=24;
Ap=zeros(k,1);
for j=1:k
   for i=1:n
      Ap(j)=Ap(j)+(ptgt(i)*cos(i*(j/2)*pi/180));
   end
end
Ap=Ap/360;

Bp=zeros(k,1);
for j=1:k
   for i=1:n
      Bp(j)=Bp(j)+(ptgt(i)*sin(i*(j/2)*pi/180));
   end
end
Bp=Bp/360;


ptgtcor=zeros(n,1);
for i=1:n
   for j=1:k
      ptgtcor(i)=ptgtcor(i)+(Ap(j)*cos((j/2)*i*pi/180)+Bp(j)*sin((j/2)*i*pi/180));
   end
end
ptgtcor=ptgtcor+Aop;
```

```
BI(1)=((lambda/4)+(lambda^3/16)+(15*lambda^5/512));
BI(2)=((-0.5)-(lambda^4/32)-(lambda^6/32));
BI(3)=((-3*lambda/4)-(9*lambda^3/32)-(81*lambda^5/512));
BI(4)=(-(lambda^2/4)-(lambda^4/8)-(lambda^6/16));
BI(5)=((5*lambda^3/32)+(75*lambda^5/512));
BI(6)=((3*lambda^4/32)+(3*lambda^6/32));
BI=BI*4*mrec*r*omega^2/(pi*D^2);

%For cylinder 1

T1Re(1)=(pi*D^2*r/4)*(Ap(1)*cos(0)-Bp(1)*sin(0));
T1Re(2)=(pi*D^2*r/4)*(Ap(2)*cos(0)-(Bp(2)+BI(1))*sin(0));
T1Re(3)=(pi*D^2*r/4)*(Ap(3)*cos(0)-Bp(3)*sin(0));
T1Re(4)=(pi*D^2*r/4)*(Ap(4)*cos(0)-(Bp(4)+BI(2))*sin(0));
T1Re(5)=(pi*D^2*r/4)*(Ap(5)*cos(0)-Bp(5)*sin(0));
T1Re(6)=(pi*D^2*r/4)*(Ap(6)*cos(0)-(Bp(6)+BI(3))*sin(0));
T1Re(7)=(pi*D^2*r/4)*(Ap(7)*cos(0)-Bp(7)*sin(0));
T1Re(8)=(pi*D^2*r/4)*(Ap(8)*cos(0)-(Bp(8)+BI(4))*sin(0));
T1Re(9)=(pi*D^2*r/4)*(Ap(9)*cos(0)-Bp(9)*sin(0));
T1Re(10)=(pi*D^2*r/4)*(Ap(10)*cos(0)-(Bp(10)+BI(5))*sin(0));
T1Re(11)=(pi*D^2*r/4)*(Ap(11)*cos(0)-Bp(11)*sin(0));
T1Re(12)=(pi*D^2*r/4)*(Ap(12)*cos(0)-(Bp(12)+BI(6))*sin(0));
T1Re(13)=(pi*D^2*r/4)*(Ap(13)*cos(0)-Bp(13)*sin(0));
T1Re(14)=(pi*D^2*r/4)*(Ap(14)*cos(0)-Bp(14)*sin(0));
T1Re(15)=(pi*D^2*r/4)*(Ap(15)*cos(0)-Bp(15)*sin(0));
T1Re(16)=(pi*D^2*r/4)*(Ap(16)*cos(0)-Bp(16)*sin(0));
T1Re(17)=(pi*D^2*r/4)*(Ap(17)*cos(0)-Bp(17)*sin(0));
T1Re(18)=(pi*D^2*r/4)*(Ap(18)*cos(0)-Bp(18)*sin(0));
T1Re(19)=(pi*D^2*r/4)*(Ap(19)*cos(0)-Bp(19)*sin(0));
T1Re(20)=(pi*D^2*r/4)*(Ap(20)*cos(0)-Bp(20)*sin(0));
T1Re(21)=(pi*D^2*r/4)*(Ap(21)*cos(0)-Bp(21)*sin(0));
T1Re(22)=(pi*D^2*r/4)*(Ap(22)*cos(0)-Bp(22)*sin(0));
T1Re(23)=(pi*D^2*r/4)*(Ap(23)*cos(0)-Bp(23)*sin(0));
T1Re(24)=(pi*D^2*r/4)*(Ap(24)*cos(0)-Bp(24)*sin(0));

T1Im(1)=-(pi*D^2*r/4)*(Ap(1)*sin(0)+Bp(1)*cos(0));
T1Im(2)=-(pi*D^2*r/4)*(Ap(2)*sin(0)+(Bp(2)+BI(1))*cos(0));
T1Im(3)=-(pi*D^2*r/4)*(Ap(3)*sin(0)+Bp(3)*cos(0));
T1Im(4)=-(pi*D^2*r/4)*(Ap(4)*sin(0)+(Bp(4)+BI(2))*cos(0));
T1Im(5)=-(pi*D^2*r/4)*(Ap(5)*sin(0)+Bp(5)*cos(0));
T1Im(6)=-(pi*D^2*r/4)*(Ap(6)*sin(0)+(Bp(6)+BI(3))*cos(0));
T1Im(7)=-(pi*D^2*r/4)*(Ap(7)*sin(0)+Bp(7)*cos(0));
T1Im(8)=-(pi*D^2*r/4)*(Ap(8)*sin(0)+(Bp(8)+BI(4))*cos(0));
T1Im(9)=-(pi*D^2*r/4)*(Ap(9)*sin(0)+Bp(9)*cos(0));
T1Im(10)=-(pi*D^2*r/4)*(Ap(10)*sin(0)+(Bp(10)+BI(5))*cos(0));
T1Im(11)=-(pi*D^2*r/4)*(Ap(11)*sin(0)+Bp(11)*cos(0));
T1Im(12)=-(pi*D^2*r/4)*(Ap(12)*sin(0)+(Bp(12)+BI(6))*cos(0));
T1Im(13)=-(pi*D^2*r/4)*(Ap(13)*sin(0)+Bp(13)*cos(0));
T1Im(14)=-(pi*D^2*r/4)*(Ap(14)*sin(0)+Bp(14)*cos(0));
T1Im(15)=-(pi*D^2*r/4)*(Ap(15)*sin(0)+Bp(15)*cos(0));
T1Im(16)=-(pi*D^2*r/4)*(Ap(16)*sin(0)+Bp(16)*cos(0));
T1Im(17)=-(pi*D^2*r/4)*(Ap(17)*sin(0)+Bp(17)*cos(0));
T1Im(18)=-(pi*D^2*r/4)*(Ap(18)*sin(0)+Bp(18)*cos(0));
T1Im(19)=-(pi*D^2*r/4)*(Ap(19)*sin(0)+Bp(19)*cos(0));
T1Im(20)=-(pi*D^2*r/4)*(Ap(20)*sin(0)+Bp(20)*cos(0));
T1Im(21)=-(pi*D^2*r/4)*(Ap(21)*sin(0)+Bp(21)*cos(0));
T1Im(22)=-(pi*D^2*r/4)*(Ap(22)*sin(0)+Bp(22)*cos(0));
T1Im(23)=-(pi*D^2*r/4)*(Ap(23)*sin(0)+Bp(23)*cos(0));
T1Im(24)=-(pi*D^2*r/4)*(Ap(24)*sin(0)+Bp(24)*cos(0));
```

```
%For cylinder 2

T2Re(1)=(pi*D^2*r/4)*(Ap(1)*cos((8*pi/3)*0.5)-Bp(1)*sin((8*pi/3)*0.5));
T2Re(2)=(pi*D^2*r/4)*(Ap(2)*cos(8*pi/3)-(Bp(2)+BI(1))*sin(8*pi/3));
T2Re(3)=(pi*D^2*r/4)*(Ap(3)*cos((8*pi/3)*1.5)-Bp(3)*sin((8*pi/3)*1.5));
T2Re(4)=(pi*D^2*r/4)*(Ap(4)*cos((8*pi/3)*2)-(Bp(4)+BI(2))*sin((8*pi/3)*2));
T2Re(5)=(pi*D^2*r/4)*(Ap(5)*cos((8*pi/3)*2.5)-Bp(5)*sin((8*pi/3)*2.5));
T2Re(6)=(pi*D^2*r/4)*(Ap(6)*cos((8*pi/3)*3)-(Bp(6)+BI(3))*sin((8*pi/3)*3));
T2Re(7)=(pi*D^2*r/4)*(Ap(7)*cos((8*pi/3)*3.5)-Bp(7)*sin((8*pi/3)*3.5));
T2Re(8)=(pi*D^2*r/4)*(Ap(8)*cos((8*pi/3)*4)-(Bp(8)+BI(4))*sin((8*pi/3)*4));
T2Re(9)=(pi*D^2*r/4)*(Ap(9)*cos((8*pi/3)*4.5)-Bp(9)*sin((8*pi/3)*4.5));
T2Re(10)=(pi*D^2*r/4)*(Ap(10)*cos((8*pi/3)*5)-(Bp(10)+BI(5))*sin((8*pi/3)*5));
T2Re(11)=(pi*D^2*r/4)*(Ap(11)*cos((8*pi/3)*5.5)-Bp(11)*sin((8*pi/3)*5.5));
T2Re(12)=(pi*D^2*r/4)*(Ap(12)*cos((8*pi/3)*6)-(Bp(12)+BI(6))*sin((8*pi/3)*6));
T2Re(13)=(pi*D^2*r/4)*(Ap(13)*cos((8*pi/3)*6.5)-Bp(13)*sin((8*pi/3)*6.5));
T2Re(14)=(pi*D^2*r/4)*(Ap(14)*cos((8*pi/3)*7)-Bp(14)*sin((8*pi/3)*7));
T2Re(15)=(pi*D^2*r/4)*(Ap(15)*cos((8*pi/3)*7.5)-Bp(15)*sin((8*pi/3)*7.5));
T2Re(16)=(pi*D^2*r/4)*(Ap(16)*cos((8*pi/3)*8)-Bp(16)*sin((8*pi/3)*8));
T2Re(17)=(pi*D^2*r/4)*(Ap(17)*cos((8*pi/3)*8.5)-Bp(17)*sin((8*pi/3)*8.5));
T2Re(18)=(pi*D^2*r/4)*(Ap(18)*cos((8*pi/3)*9)-Bp(18)*sin((8*pi/3)*9));
T2Re(19)=(pi*D^2*r/4)*(Ap(19)*cos((8*pi/3)*9.5)-Bp(19)*sin((8*pi/3)*9.5));
T2Re(20)=(pi*D^2*r/4)*(Ap(20)*cos((8*pi/3)*10)-Bp(20)*sin((8*pi/3)*10));
T2Re(21)=(pi*D^2*r/4)*(Ap(21)*cos((8*pi/3)*10.5)-Bp(21)*sin((8*pi/3)*10.5));
T2Re(22)=(pi*D^2*r/4)*(Ap(22)*cos((8*pi/3)*11)-Bp(22)*sin((8*pi/3)*11));
T2Re(23)=(pi*D^2*r/4)*(Ap(23)*cos((8*pi/3)*11.5)-Bp(23)*sin((8*pi/3)*11.5));
T2Re(24)=(pi*D^2*r/4)*(Ap(24)*cos((8*pi/3)*12)-Bp(24)*sin((8*pi/3)*12));

T2Im(1)=-(pi*D^2*r/4)*(Ap(1)*sin((8*pi/3)*0.5)+Bp(1)*cos((8*pi/3)*0.5));
T2Im(2)=-(pi*D^2*r/4)*(Ap(2)*sin(8*pi/3)+(Bp(2)+BI(1))*cos(8*pi/3));
T2Im(3)=-(pi*D^2*r/4)*(Ap(3)*sin((8*pi/3)*1.5)+Bp(3)*cos((8*pi/3)*1.5));
T2Im(4)=-(pi*D^2*r/4)*(Ap(4)*sin((8*pi/3)*2)+(Bp(4)+BI(2))*cos((8*pi/3)*2));
T2Im(5)=-(pi*D^2*r/4)*(Ap(5)*sin((8*pi/3)*2.5)+Bp(5)*cos((8*pi/3)*2.5));
T2Im(6)=-(pi*D^2*r/4)*(Ap(6)*sin((8*pi/3)*3)+(Bp(6)+BI(3))*cos((8*pi/3)*3));
T2Im(7)=-(pi*D^2*r/4)*(Ap(7)*sin((8*pi/3)*3.5)+Bp(7)*cos((8*pi/3)*3.5));
T2Im(8)=-(pi*D^2*r/4)*(Ap(8)*sin((8*pi/3)*4)+(Bp(8)+BI(4))*cos((8*pi/3)*4));
T2Im(9)=-(pi*D^2*r/4)*(Ap(9)*sin((8*pi/3)*4.5)+Bp(9)*cos((8*pi/3)*4.5));
T2Im(10)=-(pi*D^2*r/4)*(Ap(10)*sin((8*pi/3)*5)+(Bp(10)+BI(5))*cos((8*pi/3)*5));
T2Im(11)=-(pi*D^2*r/4)*(Ap(11)*sin((8*pi/3)*5.5)+Bp(11)*cos((8*pi/3)*5.5));
T2Im(12)=-(pi*D^2*r/4)*(Ap(12)*sin((8*pi/3)*6)+(Bp(12)+BI(6))*cos((8*pi/3)*6));
T2Im(13)=-(pi*D^2*r/4)*(Ap(13)*sin((8*pi/3)*6.5)+Bp(13)*cos((8*pi/3)*6.5));
T2Im(14)=-(pi*D^2*r/4)*(Ap(14)*sin((8*pi/3)*7)+Bp(14)*cos((8*pi/3)*7));
T2Im(15)=-(pi*D^2*r/4)*(Ap(15)*sin((8*pi/3)*7.5)+Bp(15)*cos((8*pi/3)*7.5));
T2Im(16)=-(pi*D^2*r/4)*(Ap(16)*sin((8*pi/3)*8)+Bp(16)*cos((8*pi/3)*8));
T2Im(17)=-(pi*D^2*r/4)*(Ap(17)*sin((8*pi/3)*8.5)+Bp(17)*cos((8*pi/3)*8.5));
T2Im(18)=-(pi*D^2*r/4)*(Ap(18)*sin((8*pi/3)*9)+Bp(18)*cos((8*pi/3)*9));
T2Im(19)=-(pi*D^2*r/4)*(Ap(19)*sin((8*pi/3)*9.5)+Bp(19)*cos((8*pi/3)*9.5));
T2Im(20)=-(pi*D^2*r/4)*(Ap(20)*sin((8*pi/3)*10)+Bp(20)*cos((8*pi/3)*10));
T2Im(21)=-(pi*D^2*r/4)*(Ap(21)*sin((8*pi/3)*10.5)+Bp(21)*cos((8*pi/3)*10.5));
T2Im(22)=-(pi*D^2*r/4)*(Ap(22)*sin((8*pi/3)*11)+Bp(22)*cos((8*pi/3)*11));
T2Im(23)=-(pi*D^2*r/4)*(Ap(23)*sin((8*pi/3)*11.5)+Bp(23)*cos((8*pi/3)*11.5));
T2Im(24)=-(pi*D^2*r/4)*(Ap(24)*sin((8*pi/3)*12)+Bp(24)*cos((8*pi/3)*12));


%For cylinder 3

T3Re(1)=(pi*D^2*r/4)*(Ap(1)*cos((4*pi/3)*0.5)-Bp(1)*sin((4*pi/3)*0.5));
T3Re(2)=(pi*D^2*r/4)*(Ap(2)*cos(4*pi/3)-(Bp(2)+BI(1))*sin(4*pi/3));
T3Re(3)=(pi*D^2*r/4)*(Ap(3)*cos((4*pi/3)*1.5)-Bp(3)*sin((4*pi/3)*1.5));
```

```
T3Re(4)=(pi*D^2*r/4)*(Ap(4)*cos((4*pi/3)*2)-(Bp(4)+BI(2))*sin((4*pi/3)*2));
T3Re(5)=(pi*D^2*r/4)*(Ap(5)*cos((4*pi/3)*2.5)-Bp(5)*sin((4*pi/3)*2.5));
T3Re(6)=(pi*D^2*r/4)*(Ap(6)*cos((4*pi/3)*3)-(Bp(6)+BI(3))*sin((4*pi/3)*3));
T3Re(7)=(pi*D^2*r/4)*(Ap(7)*cos((4*pi/3)*3.5)-Bp(7)*sin((4*pi/3)*3.5));
T3Re(8)=(pi*D^2*r/4)*(Ap(8)*cos((4*pi/3)*4)-(Bp(8)+BI(4))*sin((4*pi/3)*4));
T3Re(9)=(pi*D^2*r/4)*(Ap(9)*cos((4*pi/3)*4.5)-Bp(9)*sin((4*pi/3)*4.5));
T3Re(10)=(pi*D^2*r/4)*(Ap(10)*cos((4*pi/3)*5)-(Bp(10)+BI(5))*sin((4*pi/3)*5));
T3Re(11)=(pi*D^2*r/4)*(Ap(11)*cos((4*pi/3)*5.5)-Bp(11)*sin((4*pi/3)*5.5));
T3Re(12)=(pi*D^2*r/4)*(Ap(12)*cos((4*pi/3)*6)-(Bp(12)+BI(6))*sin((4*pi/3)*6));
T3Re(13)=(pi*D^2*r/4)*(Ap(13)*cos((4*pi/3)*6.5)-Bp(13)*sin((4*pi/3)*6.5));
T3Re(14)=(pi*D^2*r/4)*(Ap(14)*cos((4*pi/3)*7)-Bp(14)*sin((4*pi/3)*7));
T3Re(15)=(pi*D^2*r/4)*(Ap(15)*cos((4*pi/3)*7.5)-Bp(15)*sin((4*pi/3)*7.5));
T3Re(16)=(pi*D^2*r/4)*(Ap(16)*cos((4*pi/3)*8)-Bp(16)*sin((4*pi/3)*8));
T3Re(17)=(pi*D^2*r/4)*(Ap(17)*cos((4*pi/3)*8.5)-Bp(17)*sin((4*pi/3)*8.5));
T3Re(18)=(pi*D^2*r/4)*(Ap(18)*cos((4*pi/3)*9)-Bp(18)*sin((4*pi/3)*9));
T3Re(19)=(pi*D^2*r/4)*(Ap(19)*cos((4*pi/3)*9.5)-Bp(19)*sin((4*pi/3)*9.5));
T3Re(20)=(pi*D^2*r/4)*(Ap(20)*cos((4*pi/3)*10)-Bp(20)*sin((4*pi/3)*10));
T3Re(21)=(pi*D^2*r/4)*(Ap(21)*cos((4*pi/3)*10.5)-Bp(21)*sin((4*pi/3)*10.5));
T3Re(22)=(pi*D^2*r/4)*(Ap(22)*cos((4*pi/3)*11)-Bp(22)*sin((4*pi/3)*11));
T3Re(23)=(pi*D^2*r/4)*(Ap(23)*cos((4*pi/3)*11.5)-Bp(23)*sin((4*pi/3)*11.5));
T3Re(24)=(pi*D^2*r/4)*(Ap(24)*cos((4*pi/3)*12)-Bp(24)*sin((4*pi/3)*12));

T3Im(1)=-(pi*D^2*r/4)*(Ap(1)*sin((4*pi/3)*0.5)+Bp(1)*cos((4*pi/3)*0.5));
T3Im(2)=-(pi*D^2*r/4)*(Ap(2)*sin(4*pi/3)+(Bp(2)+BI(1))*cos(4*pi/3));
T3Im(3)=-(pi*D^2*r/4)*(Ap(3)*sin((4*pi/3)*1.5)+Bp(3)*cos((4*pi/3)*1.5));
T3Im(4)=-(pi*D^2*r/4)*(Ap(4)*sin((4*pi/3)*2)+(Bp(4)+BI(2))*cos((4*pi/3)*2));
T3Im(5)=-(pi*D^2*r/4)*(Ap(5)*sin((4*pi/3)*2.5)+Bp(5)*cos((4*pi/3)*2.5));
T3Im(6)=-(pi*D^2*r/4)*(Ap(6)*sin((4*pi/3)*3)+(Bp(6)+BI(3))*cos((4*pi/3)*3));
T3Im(7)=-(pi*D^2*r/4)*(Ap(7)*sin((4*pi/3)*3.5)+Bp(7)*cos((4*pi/3)*3.5));
T3Im(8)=-(pi*D^2*r/4)*(Ap(8)*sin((4*pi/3)*4)+(Bp(8)+BI(4))*cos((4*pi/3)*4));
T3Im(9)=-(pi*D^2*r/4)*(Ap(9)*sin((4*pi/3)*4.5)+Bp(9)*cos((4*pi/3)*4.5));
T3Im(10)=-(pi*D^2*r/4)*(Ap(10)*sin((4*pi/3)*5)+(Bp(10)+BI(5))*cos((4*pi/3)*5));
T3Im(11)=-(pi*D^2*r/4)*(Ap(11)*sin((4*pi/3)*5.5)+Bp(11)*cos((4*pi/3)*5.5));
T3Im(12)=-(pi*D^2*r/4)*(Ap(12)*sin((4*pi/3)*6)+(Bp(12)+BI(6))*cos((4*pi/3)*6));
T3Im(13)=-(pi*D^2*r/4)*(Ap(13)*sin((4*pi/3)*6.5)+Bp(13)*cos((4*pi/3)*6.5));
T3Im(14)=-(pi*D^2*r/4)*(Ap(14)*sin((4*pi/3)*7)+Bp(14)*cos((4*pi/3)*7));
T3Im(15)=-(pi*D^2*r/4)*(Ap(15)*sin((4*pi/3)*7.5)+Bp(15)*cos((4*pi/3)*7.5));
T3Im(16)=-(pi*D^2*r/4)*(Ap(16)*sin((4*pi/3)*8)+Bp(16)*cos((4*pi/3)*8));
T3Im(17)=-(pi*D^2*r/4)*(Ap(17)*sin((4*pi/3)*8.5)+Bp(17)*cos((4*pi/3)*8.5));
T3Im(18)=-(pi*D^2*r/4)*(Ap(18)*sin((4*pi/3)*9)+Bp(18)*cos((4*pi/3)*9));
T3Im(19)=-(pi*D^2*r/4)*(Ap(19)*sin((4*pi/3)*9.5)+Bp(19)*cos((4*pi/3)*9.5));
T3Im(20)=-(pi*D^2*r/4)*(Ap(20)*sin((4*pi/3)*10)+Bp(20)*cos((4*pi/3)*10));
T3Im(21)=-(pi*D^2*r/4)*(Ap(21)*sin((4*pi/3)*10.5)+Bp(21)*cos((4*pi/3)*10.5));
T3Im(22)=-(pi*D^2*r/4)*(Ap(22)*sin((4*pi/3)*11)+Bp(22)*cos((4*pi/3)*11));
T3Im(23)=-(pi*D^2*r/4)*(Ap(23)*sin((4*pi/3)*11.5)+Bp(23)*cos((4*pi/3)*11.5));
T3Im(24)=-(pi*D^2*r/4)*(Ap(24)*sin((4*pi/3)*12)+Bp(24)*cos((4*pi/3)*12));


%For cylinder 4

T4Re(1)=(pi*D^2*r/4)*(Ap(1)*cos((10*pi/3)*0.5)-Bp(1)*sin((10*pi/3)*0.5));
T4Re(2)=(pi*D^2*r/4)*(Ap(2)*cos(10*pi/3)-(Bp(2)+BI(1))*sin(10*pi/3));
T4Re(3)=(pi*D^2*r/4)*(Ap(3)*cos((10*pi/3)*1.5)-Bp(3)*sin((10*pi/3)*1.5));
T4Re(4)=(pi*D^2*r/4)*(Ap(4)*cos((10*pi/3)*2)-(Bp(4)+BI(2))*sin((10*pi/3)*2));
T4Re(5)=(pi*D^2*r/4)*(Ap(5)*cos((10*pi/3)*2.5)-Bp(5)*sin((10*pi/3)*2.5));
T4Re(6)=(pi*D^2*r/4)*(Ap(6)*cos((10*pi/3)*3)-(Bp(6)+BI(3))*sin((10*pi/3)*3));
T4Re(7)=(pi*D^2*r/4)*(Ap(7)*cos((10*pi/3)*3.5)-Bp(7)*sin((10*pi/3)*3.5));
T4Re(8)=(pi*D^2*r/4)*(Ap(8)*cos((10*pi/3)*4)-(Bp(8)+BI(4))*sin((10*pi/3)*4));
T4Re(9)=(pi*D^2*r/4)*(Ap(9)*cos((10*pi/3)*4.5)-Bp(9)*sin((10*pi/3)*4.5));
```

```
T4Re(10)=(pi*D^2*r/4)*(Ap(10)*cos((10*pi/3)*5)-(Bp(10)+BI(5))*sin((10*pi/3)*5));
T4Re(11)=(pi*D^2*r/4)*(Ap(11)*cos((10*pi/3)*5.5)-Bp(11)*sin((10*pi/3)*5.5));
T4Re(12)=(pi*D^2*r/4)*(Ap(12)*cos((10*pi/3)*6)-(Bp(12)+BI(6))*sin((10*pi/3)*6));
T4Re(13)=(pi*D^2*r/4)*(Ap(13)*cos((10*pi/3)*6.5)-Bp(13)*sin((10*pi/3)*6.5));
T4Re(14)=(pi*D^2*r/4)*(Ap(14)*cos((10*pi/3)*7)-Bp(14)*sin((10*pi/3)*7));
T4Re(15)=(pi*D^2*r/4)*(Ap(15)*cos((10*pi/3)*7.5)-Bp(15)*sin((10*pi/3)*7.5));
T4Re(16)=(pi*D^2*r/4)*(Ap(16)*cos((10*pi/3)*8)-Bp(16)*sin((10*pi/3)*8));
T4Re(17)=(pi*D^2*r/4)*(Ap(17)*cos((10*pi/3)*8.5)-Bp(17)*sin((10*pi/3)*8.5));
T4Re(18)=(pi*D^2*r/4)*(Ap(18)*cos((10*pi/3)*9)-Bp(18)*sin((10*pi/3)*9));
T4Re(19)=(pi*D^2*r/4)*(Ap(19)*cos((10*pi/3)*9.5)-Bp(19)*sin((10*pi/3)*9.5));
T4Re(20)=(pi*D^2*r/4)*(Ap(20)*cos((10*pi/3)*10)-Bp(20)*sin((10*pi/3)*10));
T4Re(21)=(pi*D^2*r/4)*(Ap(21)*cos((10*pi/3)*10.5)-Bp(21)*sin((10*pi/3)*10.5));
T4Re(22)=(pi*D^2*r/4)*(Ap(22)*cos((10*pi/3)*11)-Bp(22)*sin((10*pi/3)*11));
T4Re(23)=(pi*D^2*r/4)*(Ap(23)*cos((10*pi/3)*11.5)-Bp(23)*sin((10*pi/3)*11.5));
T4Re(24)=(pi*D^2*r/4)*(Ap(24)*cos((10*pi/3)*12)-Bp(24)*sin((10*pi/3)*12));

T4Im(1)=-(pi*D^2*r/4)*(Ap(1)*sin((10*pi/3)*0.5)+Bp(1)*cos((10*pi/3)*0.5));
T4Im(2)=-(pi*D^2*r/4)*(Ap(2)*sin(10*pi/3)+(Bp(2)+BI(1))*cos(10*pi/3));
T4Im(3)=-(pi*D^2*r/4)*(Ap(3)*sin((10*pi/3)*1.5)+Bp(3)*cos((10*pi/3)*1.5));
T4Im(4)=-(pi*D^2*r/4)*(Ap(4)*sin((10*pi/3)*2)+(Bp(4)+BI(2))*cos((10*pi/3)*2));
T4Im(5)=-(pi*D^2*r/4)*(Ap(5)*sin((10*pi/3)*2.5)+Bp(5)*cos((10*pi/3)*2.5));
T4Im(6)=-(pi*D^2*r/4)*(Ap(6)*sin((10*pi/3)*3)+(Bp(6)+BI(3))*cos((10*pi/3)*3));
T4Im(7)=-(pi*D^2*r/4)*(Ap(7)*sin((10*pi/3)*3.5)+Bp(7)*cos((10*pi/3)*3.5));
T4Im(8)=-(pi*D^2*r/4)*(Ap(8)*sin((10*pi/3)*4)+(Bp(8)+BI(4))*cos((10*pi/3)*4));
T4Im(9)=-(pi*D^2*r/4)*(Ap(9)*sin((10*pi/3)*4.5)+Bp(9)*cos((10*pi/3)*4.5));
T4Im(10)=-(pi*D^2*r/4)*(Ap(10)*sin((10*pi/3)*5)+(Bp(10)+BI(5))*cos((10*pi/3)*5));
T4Im(11)=-(pi*D^2*r/4)*(Ap(11)*sin((10*pi/3)*5.5)+Bp(11)*cos((10*pi/3)*5.5));
T4Im(12)=-(pi*D^2*r/4)*(Ap(12)*sin((10*pi/3)*6)+(Bp(12)+BI(6))*cos((10*pi/3)*6));
T4Im(13)=-(pi*D^2*r/4)*(Ap(13)*sin((10*pi/3)*6.5)+Bp(13)*cos((10*pi/3)*6.5));
T4Im(14)=-(pi*D^2*r/4)*(Ap(14)*sin((10*pi/3)*7)+Bp(14)*cos((10*pi/3)*7));
T4Im(15)=-(pi*D^2*r/4)*(Ap(15)*sin((10*pi/3)*7.5)+Bp(15)*cos((10*pi/3)*7.5));
T4Im(16)=-(pi*D^2*r/4)*(Ap(16)*sin((10*pi/3)*8)+Bp(16)*cos((10*pi/3)*8));
T4Im(17)=-(pi*D^2*r/4)*(Ap(17)*sin((10*pi/3)*8.5)+Bp(17)*cos((10*pi/3)*8.5));
T4Im(18)=-(pi*D^2*r/4)*(Ap(18)*sin((10*pi/3)*9)+Bp(18)*cos((10*pi/3)*9));
T4Im(19)=-(pi*D^2*r/4)*(Ap(19)*sin((10*pi/3)*9.5)+Bp(19)*cos((10*pi/3)*9.5));
T4Im(20)=-(pi*D^2*r/4)*(Ap(20)*sin((10*pi/3)*10)+Bp(20)*cos((10*pi/3)*10));
T4Im(21)=-(pi*D^2*r/4)*(Ap(21)*sin((10*pi/3)*10.5)+Bp(21)*cos((10*pi/3)*10.5));
T4Im(22)=-(pi*D^2*r/4)*(Ap(22)*sin((10*pi/3)*11)+Bp(22)*cos((10*pi/3)*11));
T4Im(23)=-(pi*D^2*r/4)*(Ap(23)*sin((10*pi/3)*11.5)+Bp(23)*cos((10*pi/3)*11.5));
T4Im(24)=-(pi*D^2*r/4)*(Ap(24)*sin((10*pi/3)*12)+Bp(24)*cos((10*pi/3)*12));


%For cylinder 5

T5Re(1)=(pi*D^2*r/4)*(Ap(1)*cos((2*pi/3)*0.5)-Bp(1)*sin((2*pi/3)*0.5));
T5Re(2)=(pi*D^2*r/4)*(Ap(2)*cos(2*pi/3)-(Bp(2)+BI(1))*sin(2*pi/3));
T5Re(3)=(pi*D^2*r/4)*(Ap(3)*cos((2*pi/3)*1.5)-Bp(3)*sin((2*pi/3)*1.5));
T5Re(4)=(pi*D^2*r/4)*(Ap(4)*cos((2*pi/3)*2)-(Bp(4)+BI(2))*sin((2*pi/3)*2));
T5Re(5)=(pi*D^2*r/4)*(Ap(5)*cos((2*pi/3)*2.5)-Bp(5)*sin((2*pi/3)*2.5));
T5Re(6)=(pi*D^2*r/4)*(Ap(6)*cos((2*pi/3)*3)-(Bp(6)+BI(3))*sin((2*pi/3)*3));
T5Re(7)=(pi*D^2*r/4)*(Ap(7)*cos((2*pi/3)*3.5)-Bp(7)*sin((2*pi/3)*3.5));
T5Re(8)=(pi*D^2*r/4)*(Ap(8)*cos((2*pi/3)*4)-(Bp(8)+BI(4))*sin((2*pi/3)*4));
T5Re(9)=(pi*D^2*r/4)*(Ap(9)*cos((2*pi/3)*4.5)-Bp(9)*sin((2*pi/3)*4.5));
T5Re(10)=(pi*D^2*r/4)*(Ap(10)*cos((2*pi/3)*5)-(Bp(10)+BI(5))*sin((2*pi/3)*5));
T5Re(11)=(pi*D^2*r/4)*(Ap(11)*cos((2*pi/3)*5.5)-Bp(11)*sin((2*pi/3)*5.5));
T5Re(12)=(pi*D^2*r/4)*(Ap(12)*cos((2*pi/3)*6)-(Bp(12)+BI(6))*sin((2*pi/3)*6));
T5Re(13)=(pi*D^2*r/4)*(Ap(13)*cos((2*pi/3)*6.5)-Bp(13)*sin((2*pi/3)*6.5));
T5Re(14)=(pi*D^2*r/4)*(Ap(14)*cos((2*pi/3)*7)-Bp(14)*sin((2*pi/3)*7));
T5Re(15)=(pi*D^2*r/4)*(Ap(15)*cos((2*pi/3)*7.5)-Bp(15)*sin((2*pi/3)*7.5));
```

```
T5Re(16)=(pi*D^2*r/4)*(Ap(16)*cos((2*pi/3)*8)-Bp(16)*sin((2*pi/3)*8));
T5Re(17)=(pi*D^2*r/4)*(Ap(17)*cos((2*pi/3)*8.5)-Bp(17)*sin((2*pi/3)*8.5));
T5Re(18)=(pi*D^2*r/4)*(Ap(18)*cos((2*pi/3)*9)-Bp(18)*sin((2*pi/3)*9));
T5Re(19)=(pi*D^2*r/4)*(Ap(19)*cos((2*pi/3)*9.5)-Bp(19)*sin((2*pi/3)*9.5));
T5Re(20)=(pi*D^2*r/4)*(Ap(20)*cos((2*pi/3)*10)-Bp(20)*sin((2*pi/3)*10));
T5Re(21)=(pi*D^2*r/4)*(Ap(21)*cos((2*pi/3)*10.5)-Bp(21)*sin((2*pi/3)*10.5));
T5Re(22)=(pi*D^2*r/4)*(Ap(22)*cos((2*pi/3)*11)-Bp(22)*sin((2*pi/3)*11));
T5Re(23)=(pi*D^2*r/4)*(Ap(23)*cos((2*pi/3)*11.5)-Bp(23)*sin((2*pi/3)*11.5));
T5Re(24)=(pi*D^2*r/4)*(Ap(24)*cos((2*pi/3)*12)-Bp(24)*sin((2*pi/3)*12));

T5Im(1)=-(pi*D^2*r/4)*(Ap(1)*sin((2*pi/3)*0.5)+Bp(1)*cos((2*pi/3)*0.5));
T5Im(2)=-(pi*D^2*r/4)*(Ap(2)*sin(2*pi/3)+(Bp(2)+BI(1))*cos(2*pi/3));
T5Im(3)=-(pi*D^2*r/4)*(Ap(3)*sin((2*pi/3)*1.5)+Bp(3)*cos((2*pi/3)*1.5));
T5Im(4)=-(pi*D^2*r/4)*(Ap(4)*sin((2*pi/3)*2)+(Bp(4)+BI(2))*cos((2*pi/3)*2));
T5Im(5)=-(pi*D^2*r/4)*(Ap(5)*sin((2*pi/3)*2.5)+Bp(5)*cos((2*pi/3)*2.5));
T5Im(6)=-(pi*D^2*r/4)*(Ap(6)*sin((2*pi/3)*3)+(Bp(6)+BI(3))*cos((2*pi/3)*3));
T5Im(7)=-(pi*D^2*r/4)*(Ap(7)*sin((2*pi/3)*3.5)+Bp(7)*cos((2*pi/3)*3.5));
T5Im(8)=-(pi*D^2*r/4)*(Ap(8)*sin((2*pi/3)*4)+(Bp(8)+BI(4))*cos((2*pi/3)*4));
T5Im(9)=-(pi*D^2*r/4)*(Ap(9)*sin((2*pi/3)*4.5)+Bp(9)*cos((2*pi/3)*4.5));
T5Im(10)=-(pi*D^2*r/4)*(Ap(10)*sin((2*pi/3)*5)+(Bp(10)+BI(5))*cos((2*pi/3)*5));
T5Im(11)=-(pi*D^2*r/4)*(Ap(11)*sin((2*pi/3)*5.5)+Bp(11)*cos((2*pi/3)*5.5));
T5Im(12)=-(pi*D^2*r/4)*(Ap(12)*sin((2*pi/3)*6)+(Bp(12)+BI(6))*cos((2*pi/3)*6));
T5Im(13)=-(pi*D^2*r/4)*(Ap(13)*sin((2*pi/3)*6.5)+Bp(13)*cos((2*pi/3)*6.5));
T5Im(14)=-(pi*D^2*r/4)*(Ap(14)*sin((2*pi/3)*7)+Bp(14)*cos((2*pi/3)*7));
T5Im(15)=-(pi*D^2*r/4)*(Ap(15)*sin((2*pi/3)*7.5)+Bp(15)*cos((2*pi/3)*7.5));
T5Im(16)=-(pi*D^2*r/4)*(Ap(16)*sin((2*pi/3)*8)+Bp(16)*cos((2*pi/3)*8));
T5Im(17)=-(pi*D^2*r/4)*(Ap(17)*sin((2*pi/3)*8.5)+Bp(17)*cos((2*pi/3)*8.5));
T5Im(18)=-(pi*D^2*r/4)*(Ap(18)*sin((2*pi/3)*9)+Bp(18)*cos((2*pi/3)*9));
T5Im(19)=-(pi*D^2*r/4)*(Ap(19)*sin((2*pi/3)*9.5)+Bp(19)*cos((2*pi/3)*9.5));
T5Im(20)=-(pi*D^2*r/4)*(Ap(20)*sin((2*pi/3)*10)+Bp(20)*cos((2*pi/3)*10));
T5Im(21)=-(pi*D^2*r/4)*(Ap(21)*sin((2*pi/3)*10.5)+Bp(21)*cos((2*pi/3)*10.5));
T5Im(22)=-(pi*D^2*r/4)*(Ap(22)*sin((2*pi/3)*11)+Bp(22)*cos((2*pi/3)*11));
T5Im(23)=-(pi*D^2*r/4)*(Ap(23)*sin((2*pi/3)*11.5)+Bp(23)*cos((2*pi/3)*11.5));
T5Im(24)=-(pi*D^2*r/4)*(Ap(24)*sin((2*pi/3)*12)+Bp(24)*cos((2*pi/3)*12));


%For cylinder 6

T6Re(1)=(pi*D^2*r/4)*(Ap(1)*cos((2*pi)*0.5)-Bp(1)*sin((2*pi)*0.5));
T6Re(2)=(pi*D^2*r/4)*(Ap(2)*cos(2*pi)-(Bp(2)+BI(1))*sin(2*pi));
T6Re(3)=(pi*D^2*r/4)*(Ap(3)*cos((2*pi)*1.5)-Bp(3)*sin((2*pi)*1.5));
T6Re(4)=(pi*D^2*r/4)*(Ap(4)*cos((2*pi)*2)-(Bp(4)+BI(2))*sin((2*pi)*2));
T6Re(5)=(pi*D^2*r/4)*(Ap(5)*cos((2*pi)*2.5)-Bp(5)*sin((2*pi)*2.5));
T6Re(6)=(pi*D^2*r/4)*(Ap(6)*cos((2*pi)*3)-(Bp(6)+BI(3))*sin((2*pi)*3));
T6Re(7)=(pi*D^2*r/4)*(Ap(7)*cos((2*pi)*3.5)-Bp(7)*sin((2*pi)*3.5));
T6Re(8)=(pi*D^2*r/4)*(Ap(8)*cos((2*pi)*4)-(Bp(8)+BI(4))*sin((2*pi)*4));
T6Re(9)=(pi*D^2*r/4)*(Ap(9)*cos((2*pi)*4.5)-Bp(9)*sin((2*pi)*4.5));
T6Re(10)=(pi*D^2*r/4)*(Ap(10)*cos((2*pi)*5)-(Bp(10)+BI(5))*sin((2*pi)*5));
T6Re(11)=(pi*D^2*r/4)*(Ap(11)*cos((2*pi)*5.5)-Bp(11)*sin((2*pi)*5.5));
T6Re(12)=(pi*D^2*r/4)*(Ap(12)*cos((2*pi)*6)-(Bp(12)+BI(6))*sin((2*pi)*6));
T6Re(13)=(pi*D^2*r/4)*(Ap(13)*cos((2*pi)*6.5)-Bp(13)*sin((2*pi)*6.5));
T6Re(14)=(pi*D^2*r/4)*(Ap(14)*cos((2*pi)*7)-Bp(14)*sin((2*pi)*7));
T6Re(15)=(pi*D^2*r/4)*(Ap(15)*cos((2*pi)*7.5)-Bp(15)*sin((2*pi)*7.5));
T6Re(16)=(pi*D^2*r/4)*(Ap(16)*cos((2*pi)*8)-Bp(16)*sin((2*pi)*8));
T6Re(17)=(pi*D^2*r/4)*(Ap(17)*cos((2*pi)*8.5)-Bp(17)*sin((2*pi)*8.5));
T6Re(18)=(pi*D^2*r/4)*(Ap(18)*cos((2*pi)*9)-Bp(18)*sin((2*pi)*9));
T6Re(19)=(pi*D^2*r/4)*(Ap(19)*cos((2*pi)*9.5)-Bp(19)*sin((2*pi)*9.5));
T6Re(20)=(pi*D^2*r/4)*(Ap(20)*cos((2*pi)*10)-Bp(20)*sin((2*pi)*10));
T6Re(21)=(pi*D^2*r/4)*(Ap(21)*cos((2*pi)*10.5)-Bp(21)*sin((2*pi)*10.5));
```

```
T6Re(22)=(pi*D^2*r/4)*(Ap(22)*cos((2*pi)*11)-Bp(22)*sin((2*pi)*11));
T6Re(23)=(pi*D^2*r/4)*(Ap(23)*cos((2*pi)*11.5)-Bp(23)*sin((2*pi)*11.5));
T6Re(24)=(pi*D^2*r/4)*(Ap(24)*cos((2*pi)*12)-Bp(24)*sin((2*pi)*12));

T6Im(1)=-(pi*D^2*r/4)*(Ap(1)*sin((2*pi)*0.5)+Bp(1)*cos((2*pi)*0.5));
T6Im(2)=-(pi*D^2*r/4)*(Ap(2)*sin(2*pi)+(Bp(2)+BI(1))*cos(2*pi));
T6Im(3)=-(pi*D^2*r/4)*(Ap(3)*sin((2*pi)*1.5)+Bp(3)*cos((2*pi)*1.5));
T6Im(4)=-(pi*D^2*r/4)*(Ap(4)*sin((2*pi)*2)+(Bp(4)+BI(2))*cos((2*pi)*2));
T6Im(5)=-(pi*D^2*r/4)*(Ap(5)*sin((2*pi)*2.5)+Bp(5)*cos((2*pi)*2.5));
T6Im(6)=-(pi*D^2*r/4)*(Ap(6)*sin((2*pi)*3)+(Bp(6)+BI(3))*cos((2*pi)*3));
T6Im(7)=-(pi*D^2*r/4)*(Ap(7)*sin((2*pi)*3.5)+Bp(7)*cos((2*pi)*3.5));
T6Im(8)=-(pi*D^2*r/4)*(Ap(8)*sin((2*pi)*4)+(Bp(8)+BI(4))*cos((2*pi)*4));
T6Im(9)=-(pi*D^2*r/4)*(Ap(9)*sin((2*pi)*4.5)+Bp(9)*cos((2*pi)*4.5));
T6Im(10)=-(pi*D^2*r/4)*(Ap(10)*sin((2*pi)*5)+(Bp(10)+BI(5))*cos((2*pi)*5));
T6Im(11)=-(pi*D^2*r/4)*(Ap(11)*sin((2*pi)*5.5)+Bp(11)*cos((2*pi)*5.5));
T6Im(12)=-(pi*D^2*r/4)*(Ap(12)*sin((2*pi)*6)+(Bp(12)+BI(6))*cos((2*pi)*6));
T6Im(13)=-(pi*D^2*r/4)*(Ap(13)*sin((2*pi)*6.5)+Bp(13)*cos((2*pi)*6.5));
T6Im(14)=-(pi*D^2*r/4)*(Ap(14)*sin((2*pi)*7)+Bp(14)*cos((2*pi)*7));
T6Im(15)=-(pi*D^2*r/4)*(Ap(15)*sin((2*pi)*7.5)+Bp(15)*cos((2*pi)*7.5));
T6Im(16)=-(pi*D^2*r/4)*(Ap(16)*sin((2*pi)*8)+Bp(16)*cos((2*pi)*8));
T6Im(17)=-(pi*D^2*r/4)*(Ap(17)*sin((2*pi)*8.5)+Bp(17)*cos((2*pi)*8.5));
T6Im(18)=-(pi*D^2*r/4)*(Ap(18)*sin((2*pi)*9)+Bp(18)*cos((2*pi)*9));
T6Im(19)=-(pi*D^2*r/4)*(Ap(19)*sin((2*pi)*9.5)+Bp(19)*cos((2*pi)*9.5));
T6Im(20)=-(pi*D^2*r/4)*(Ap(20)*sin((2*pi)*10)+Bp(20)*cos((2*pi)*10));
T6Im(21)=-(pi*D^2*r/4)*(Ap(21)*sin((2*pi)*10.5)+Bp(21)*cos((2*pi)*10.5));
T6Im(22)=-(pi*D^2*r/4)*(Ap(22)*sin((2*pi)*11)+Bp(22)*cos((2*pi)*11));
T6Im(23)=-(pi*D^2*r/4)*(Ap(23)*sin((2*pi)*11.5)+Bp(23)*cos((2*pi)*11.5));
T6Im(24)=-(pi*D^2*r/4)*(Ap(24)*sin((2*pi)*12)+Bp(24)*cos((2*pi)*12));

% Absolute dampings and shaft stiffnesses and inertias

c1=2.8;
c2=5.7;
c3=5.7;
c4=5.7;
c5=5.7;
c6=5.7;
c7=5.7;
c8=0;

k1=1.54E6;
k2=1.78E6;
k3=1.78E6;
k4=1.78E6;
k5=1.78E6;
k6=1.78E6;
k7=2.38E6;

J1=0.035;
J2=0.0545;
J3=0.0335;
J4=0.0545;
J5=0.0545;
J6=0.0335;
J7=0.0545;
J8=2.12;

format long
```

```
%0.5th order

P1_1=[1 0 0 0 0;-J1*(omega/2)^2 1 -c1*(omega/2) 0 0;0 0 1 0 0;c1*(omega/2) 0 -J1*(omega/2)^2 1 0;0 0 0 0
1];
P2_1=[1 0 0 0 0;-J2*(omega/2)^2 1 -c2*(omega/2) 0 -T1Re(1);0 0 1 0 0;c2*(omega/2) 0 -J2*(omega/2)^2 1 -
T1Im(1);0 0 0 0 1];
P3_1=[1 0 0 0 0;-J3*(omega/2)^2 1 -c3*(omega/2) 0 -T2Re(1);0 0 1 0 0;c3*(omega/2) 0 -J3*(omega/2)^2 1 -
T2Im(1);0 0 0 0 1];
P4_1=[1 0 0 0 0;-J4*(omega/2)^2 1 -c4*(omega/2) 0 -T3Re(1);0 0 1 0 0;c4*(omega/2) 0 -J4*(omega/2)^2 1 -
T3Im(1);0 0 0 0 1];
P5_1=[1 0 0 0 0;-J5*(omega/2)^2 1 -c5*(omega/2) 0 -T4Re(1);0 0 1 0 0;c5*(omega/2) 0 -J5*(omega/2)^2 1 -
T4Im(1);0 0 0 0 1];
P6_1=[1 0 0 0 0;-J6*(omega/2)^2 1 -c6*(omega/2) 0 -T5Re(1);0 0 1 0 0;c6*(omega/2) 0 -J6*(omega/2)^2 1 -
T5Im(1);0 0 0 0 1];
P7_1=[1 0 0 0 0;-J7*(omega/2)^2 1 -c7*(omega/2) 0 -T6Re(1);0 0 1 0 0;c7*(omega/2) 0 -J7*(omega/2)^2 1 -
T6Im(1);0 0 0 0 1];
P8_1=[1 0 0 0 0;-J8*(omega/2)^2 1 0 0 0;0 0 1 0 0;0 0 -J8*(omega/2)^2 1 0;0 0 0 0 1];

F1_1=[1 1/k1 0 0 0;0 1 0 0 0;0 0 1 1/k1 0;0 0 0 1 0;0 0 0 0 1];
F2_1=[1 1/k2 0 0 0;0 1 0 0 0;0 0 1 1/k2 0;0 0 0 1 0;0 0 0 0 1];
F3_1=[1 1/k3 0 0 0;0 1 0 0 0;0 0 1 1/k3 0;0 0 0 1 0;0 0 0 0 1];
F4_1=[1 1/k4 0 0 0;0 1 0 0 0;0 0 1 1/k4 0;0 0 0 1 0;0 0 0 0 1];
F5_1=[1 1/k5 0 0 0;0 1 0 0 0;0 0 1 1/k5 0;0 0 0 1 0;0 0 0 0 1];
F6_1=[1 1/k6 0 0 0;0 1 0 0 0;0 0 1 1/k6 0;0 0 0 1 0;0 0 0 0 1];
F7_1=[1 1/k7 0 0 0;0 1 0 0 0;0 0 1 1/k7 0;0 0 0 1 0;0 0 0 0 1];

H1=P8_1*F7_1*P7_1*F6_1*P6_1*F5_1*P5_1*F4_1*P4_1*F3_1*P3_1*F2_1*P2_1*F1_1*P1_1;

theta1_1Re=((H1(4,5)*H1(2,3))-(H1(2,5)*H1(4,3)))/((H1(2,1)*H1(4,3))-(H1(2,3)*H1(4,1)));
theta1_1Im=((H1(2,5)*H1(4,1))-(H1(4,5)*H1(2,1)))/((H1(2,1)*H1(4,3))-(H1(2,3)*H1(4,1)));

Z1_1L=[theta1_1Re;0;theta1_1Im;0;1]
Z1_1R=P1_1*Z1_1L;
theta1_1=sqrt((Z1_1L(1))^2+(Z1_1L(3))^2)*180/pi
torque1_1L=sqrt((Z1_1L(2))^2+(Z1_1L(4))^2)
torque1_1R=sqrt((Z1_1R(2))^2+(Z1_1R(4))^2)

Z2_1L=F1_1*Z1_1R;
Z2_1R=P2_1*Z2_1L;
theta2_1=sqrt((Z2_1L(1))^2+(Z2_1L(3))^2)*180/pi
torque2_1R=sqrt((Z2_1R(2))^2+(Z2_1R(4))^2)

Z3_1L=F2_1*Z2_1R;
Z3_1R=P3_1*Z3_1L;
theta3_1=sqrt((Z3_1L(1))^2+(Z3_1L(3))^2)*180/pi
torque3_1R=sqrt((Z3_1R(2))^2+(Z3_1R(4))^2)

Z4_1L=F3_1*Z3_1R;
Z4_1R=P4_1*Z4_1L;
theta4_1=sqrt((Z4_1L(1))^2+(Z4_1L(3))^2)*180/pi
torque4_1R=sqrt((Z4_1R(2))^2+(Z4_1R(4))^2)

Z5_1L=F4_1*Z4_1R;
Z5_1R=P5_1*Z5_1L;
theta5_1=sqrt((Z5_1L(1))^2+(Z5_1L(3))^2)*180/pi
torque5_1R=sqrt((Z5_1R(2))^2+(Z5_1R(4))^2)

Z6_1L=F5_1*Z5_1R;
Z6_1R=P6_1*Z6_1L;
```

```
theta6_1=sqrt((Z6_1L(1))^2+(Z6_1L(3))^2)*180/pi
torque6_1R=sqrt((Z6_1R(2))^2+(Z6_1R(4))^2)

Z7_1L=F6_1*Z6_1R;
Z7_1R=P7_1*Z7_1L;
theta7_1=sqrt((Z7_1L(1))^2+(Z7_1L(3))^2)*180/pi
torque7_1R=sqrt((Z7_1R(2))^2+(Z7_1R(4))^2)

Z8_1L=F7_1*Z7_1R;
Z8_1R=P8_1*Z8_1L;
theta8_1=sqrt((Z8_1L(1))^2+(Z8_1L(3))^2)*180/pi
torque8_1R=sqrt((Z8_1R(2))^2+(Z8_1R(4))^2)


%1st order

P1_2=[1 0 0 0 0;-J1*(omega)^2 1 -c1*(omega) 0 0;0 0 1 0 0;c1*(omega) 0 -J1*(omega)^2 1 0;0 0 0 0 1];
P2_2=[1 0 0 0 0;-J2*(omega)^2 1 -c2*(omega) 0 -T1Re(2);0 0 1 0 0;c2*(omega) 0 -J2*(omega)^2 1 -
T1Im(2);0 0 0 0 1];
P3_2=[1 0 0 0 0;-J3*(omega)^2 1 -c3*(omega) 0 -T2Re(2);0 0 1 0 0;c3*(omega) 0 -J3*(omega)^2 1 -
T2Im(2);0 0 0 0 1];
P4_2=[1 0 0 0 0;-J4*(omega)^2 1 -c4*(omega) 0 -T3Re(2);0 0 1 0 0;c4*(omega) 0 -J4*(omega)^2 1 -
T3Im(2);0 0 0 0 1];
P5_2=[1 0 0 0 0;-J5*(omega)^2 1 -c5*(omega) 0 -T4Re(2);0 0 1 0 0;c5*(omega) 0 -J5*(omega)^2 1 -
T4Im(2);0 0 0 0 1];
P6_2=[1 0 0 0 0;-J6*(omega)^2 1 -c6*(omega) 0 -T5Re(2);0 0 1 0 0;c6*(omega) 0 -J6*(omega)^2 1 -
T5Im(2);0 0 0 0 1];
P7_2=[1 0 0 0 0;-J7*(omega)^2 1 -c7*(omega) 0 -T6Re(2);0 0 1 0 0;c7*(omega) 0 -J7*(omega)^2 1 -
T6Im(2);0 0 0 0 1];
P8_2=[1 0 0 0 0;-J8*(omega)^2 1 0 0 0;0 0 1 0 0;0 0 -J8*(omega)^2 1 0;0 0 0 0 1];

F1_2=[1 1/k1 0 0 0;0 1 0 0 0;0 0 1 1/k1 0;0 0 0 1 0;0 0 0 0 1];
F2_2=[1 1/k2 0 0 0;0 1 0 0 0;0 0 1 1/k2 0;0 0 0 1 0;0 0 0 0 1];
F3_2=[1 1/k3 0 0 0;0 1 0 0 0;0 0 1 1/k3 0;0 0 0 1 0;0 0 0 0 1];
F4_2=[1 1/k4 0 0 0;0 1 0 0 0;0 0 1 1/k4 0;0 0 0 1 0;0 0 0 0 1];
F5_2=[1 1/k5 0 0 0;0 1 0 0 0;0 0 1 1/k5 0;0 0 0 1 0;0 0 0 0 1];
F6_2=[1 1/k6 0 0 0;0 1 0 0 0;0 0 1 1/k6 0;0 0 0 1 0;0 0 0 0 1];
F7_2=[1 1/k7 0 0 0;0 1 0 0 0;0 0 1 1/k7 0;0 0 0 1 0;0 0 0 0 1];

H2=P8_2*F7_2*P7_2*F6_2*P6_2*F5_2*P5_2*F4_2*P4_2*F3_2*P3_2*F2_2*P2_2*F1_2*P1_2;

theta1_2Re=((H2(4,5)*H2(2,3))-(H2(2,5)*H2(4,3)))/((H2(2,1)*H2(4,3))-(H2(2,3)*H2(4,1)));
theta1_2Im=((H2(2,5)*H2(4,1))-(H2(4,5)*H2(2,1)))/((H2(2,1)*H2(4,3))-(H2(2,3)*H2(4,1)));

Z1_2L=[theta1_2Re;0;theta1_2Im;0;1]
Z1_2R=P1_2*Z1_2L;
theta1_2=sqrt((Z1_2L(1))^2+(Z1_2L(3))^2)*180/pi
torque1_2L=sqrt((Z1_2L(2))^2+(Z1_2L(4))^2)
torque1_2R=sqrt((Z1_2R(2))^2+(Z1_2R(4))^2)

Z2_2L=F1_2*Z1_2R;
Z2_2R=P2_2*Z2_2L;
theta2_2=sqrt((Z2_2L(1))^2+(Z2_2L(3))^2)*180/pi
torque2_2R=sqrt((Z2_2R(2))^2+(Z2_2R(4))^2)

Z3_2L=F2_2*Z2_2R;
Z3_2R=P3_2*Z3_2L;
theta3_2=sqrt((Z3_2L(1))^2+(Z3_2L(3))^2)*180/pi
torque3_2R=sqrt((Z3_2R(2))^2+(Z3_2R(4))^2)
```

```
Z4_2L=F3_2*Z3_2R;
Z4_2R=P4_2*Z4_2L;
theta4_2=sqrt((Z4_2L(1))^2+(Z4_2L(3))^2)*180/pi
torque4_2R=sqrt((Z4_2R(2))^2+(Z4_2R(4))^2)

Z5_2L=F4_2*Z4_2R;
Z5_2R=P5_2*Z5_2L;
theta5_2=sqrt((Z5_2L(1))^2+(Z5_2L(3))^2)*180/pi
torque5_2R=sqrt((Z5_2R(2))^2+(Z5_2R(4))^2)

Z6_2L=F5_2*Z5_2R;
Z6_2R=P6_2*Z6_2L;
theta6_2=sqrt((Z6_2L(1))^2+(Z6_2L(3))^2)*180/pi
torque6_2R=sqrt((Z6_2R(2))^2+(Z6_2R(4))^2)

Z7_2L=F6_2*Z6_2R;
Z7_2R=P7_2*Z7_2L;
theta7_2=sqrt((Z7_2L(1))^2+(Z7_2L(3))^2)*180/pi
torque7_2R=sqrt((Z7_2R(2))^2+(Z7_2R(4))^2)

Z8_2L=F7_2*Z7_2R;
Z8_2R=P8_2*Z8_2L;
theta8_2=sqrt((Z8_2L(1))^2+(Z8_2L(3))^2)*180/pi
torque8_2R=sqrt((Z8_2R(2))^2+(Z8_2R(4))^2)


%1.5th order

P1_3=[1 0 0 0 0;-J1*(3*omega/2)^2 1 -c1*(3*omega/2) 0 0;0 0 1 0 0;c1*(3*omega/2) 0 -J1*(3*omega/2)^2
1 0;0 0 0 0 1];
P2_3=[1  0  0  0  0;-J2*(3*omega/2)^2  1  -c2*(3*omega/2)  0  -T1Re(3);0  0  1  0  0;c2*(3*omega/2)  0  -
J2*(3*omega/2)^2 1 -T1Im(3);0 0 0 0 1];
P3_3=[1  0  0  0  0;-J3*(3*omega/2)^2  1  -c3*(3*omega/2)  0  -T2Re(3);0  0  1  0  0;c3*(3*omega/2)  0  -
J3*(3*omega/2)^2 1 -T2Im(3);0 0 0 0 1];
P4_3=[1  0  0  0  0;-J4*(3*omega/2)^2  1  -c4*(3*omega/2)  0  -T3Re(3);0  0  1  0  0;c4*(3*omega/2)  0  -
J4*(3*omega/2)^2 1 -T3Im(3);0 0 0 0 1];
P5_3=[1  0  0  0  0;-J5*(3*omega/2)^2  1  -c5*(3*omega/2)  0  -T4Re(3);0  0  1  0  0;c5*(3*omega/2)  0  -
J5*(3*omega/2)^2 1 -T4Im(3);0 0 0 0 1];
P6_3=[1  0  0  0  0;-J6*(3*omega/2)^2  1  -c6*(3*omega/2)  0  -T5Re(3);0  0  1  0  0;c6*(3*omega/2)  0  -
J6*(3*omega/2)^2 1 -T5Im(3);0 0 0 0 1];
P7_3=[1  0  0  0  0;-J7*(3*omega/2)^2  1  -c7*(3*omega/2)  0  -T6Re(3);0  0  1  0  0;c7*(3*omega/2)  0  -
J7*(3*omega/2)^2 1 -T6Im(3);0 0 0 0 1];
P8_3=[1 0 0 0 0;-J8*(3*omega/2)^2 1 0 0 0;0 0 1 0 0;0 0 -J8*(3*omega/2)^2 1 0;0 0 0 0 1];

F1_3=[1 1/k1 0 0 0;0 1 0 0 0;0 0 1 1/k1 0;0 0 0 1 0;0 0 0 0 1];
F2_3=[1 1/k2 0 0 0;0 1 0 0 0;0 0 1 1/k2 0;0 0 0 1 0;0 0 0 0 1];
F3_3=[1 1/k3 0 0 0;0 1 0 0 0;0 0 1 1/k3 0;0 0 0 1 0;0 0 0 0 1];
F4_3=[1 1/k4 0 0 0;0 1 0 0 0;0 0 1 1/k4 0;0 0 0 1 0;0 0 0 0 1];
F5_3=[1 1/k5 0 0 0;0 1 0 0 0;0 0 1 1/k5 0;0 0 0 1 0;0 0 0 0 1];
F6_3=[1 1/k6 0 0 0;0 1 0 0 0;0 0 1 1/k6 0;0 0 0 1 0;0 0 0 0 1];
F7_3=[1 1/k7 0 0 0;0 1 0 0 0;0 0 1 1/k7 0;0 0 0 1 0;0 0 0 0 1];

H3=P8_3*F7_3*P7_3*F6_3*P6_3*F5_3*P5_3*F4_3*P4_3*F3_3*P3_3*F2_3*P2_3*F1_3*P1_3;

theta1_3Re=((H3(4,5)*H3(2,3))-(H3(2,5)*H3(4,3)))/((H3(2,1)*H3(4,3))-(H3(2,3)*H3(4,1)));
theta1_3Im=((H3(2,5)*H3(4,1))-(H3(4,5)*H3(2,1)))/((H3(2,1)*H3(4,3))-(H3(2,3)*H3(4,1)));

Z1_3L=[theta1_3Re;0;theta1_3Im;0;1]
```

```
Z1_3R=P1_3*Z1_3L;
theta1_3=sqrt((Z1_3L(1))^2+(Z1_3L(3))^2)*180/pi
torque1_3L=sqrt((Z1_3L(2))^2+(Z1_3L(4))^2)
torque1_3R=sqrt((Z1_3R(2))^2+(Z1_3R(4))^2)

Z2_3L=F1_3*Z1_3R;
Z2_3R=P2_3*Z2_3L;
theta2_3=sqrt((Z2_3L(1))^2+(Z2_3L(3))^2)*180/pi
torque2_3R=sqrt((Z2_3R(2))^2+(Z2_3R(4))^2)

Z3_3L=F2_3*Z2_3R;
Z3_3R=P3_3*Z3_3L;
theta3_3=sqrt((Z3_3L(1))^2+(Z3_3L(3))^2)*180/pi
torque3_3R=sqrt((Z3_3R(2))^2+(Z3_3R(4))^2)

Z4_3L=F3_3*Z3_3R;
Z4_3R=P4_3*Z4_3L;
theta4_3=sqrt((Z4_3L(1))^2+(Z4_3L(3))^2)*180/pi
torque4_3R=sqrt((Z4_3R(2))^2+(Z4_3R(4))^2)

Z5_3L=F4_3*Z4_3R;
Z5_3R=P5_3*Z5_3L;
theta5_3=sqrt((Z5_3L(1))^2+(Z5_3L(3))^2)*180/pi
torque5_3R=sqrt((Z5_3R(2))^2+(Z5_3R(4))^2)

Z6_3L=F5_3*Z5_3R;
Z6_3R=P6_3*Z6_3L;
theta6_3=sqrt((Z6_3L(1))^2+(Z6_3L(3))^2)*180/pi
torque6_3R=sqrt((Z6_3R(2))^2+(Z6_3R(4))^2)

Z7_3L=F6_3*Z6_3R;
Z7_3R=P7_3*Z7_3L;
theta7_3=sqrt((Z7_3L(1))^2+(Z7_3L(3))^2)*180/pi
torque7_3R=sqrt((Z7_3R(2))^2+(Z7_3R(4))^2)

Z8_3L=F7_3*Z7_3R;
Z8_3R=P8_3*Z8_3L;
theta8_3=sqrt((Z8_3L(1))^2+(Z8_3L(3))^2)*180/pi
torque8_3R=sqrt((Z8_3R(2))^2+(Z8_3R(4))^2)


%2nd order

P1_4=[1 0 0 0 0;-J1*(2*omega)^2 1 -c1*(2*omega) 0 0;0 0 1 0 0;c1*(2*omega) 0 -J1*(2*omega)^2 1 0;0 0
0 0 1];
P2_4=[1 0 0 0 0;-J2*(2*omega)^2 1 -c2*(2*omega) 0 -T1Re(4);0 0 1 0 0;c2*(2*omega) 0 -J2*(2*omega)^2
1 -T1Im(4);0 0 0 0 1];
P3_4=[1 0 0 0 0;-J3*(2*omega)^2 1 -c3*(2*omega) 0 -T2Re(4);0 0 1 0 0;c3*(2*omega) 0 -J3*(2*omega)^2
1 -T2Im(4);0 0 0 0 1];
P4_4=[1 0 0 0 0;-J4*(2*omega)^2 1 -c4*(2*omega) 0 -T3Re(4);0 0 1 0 0;c4*(2*omega) 0 -J4*(2*omega)^2
1 -T3Im(4);0 0 0 0 1];
P5_4=[1 0 0 0 0;-J5*(2*omega)^2 1 -c5*(2*omega) 0 -T4Re(4);0 0 1 0 0;c5*(2*omega) 0 -J5*(2*omega)^2
1 -T4Im(4);0 0 0 0 1];
P6_4=[1 0 0 0 0;-J6*(2*omega)^2 1 -c6*(2*omega) 0 -T5Re(4);0 0 1 0 0;c6*(2*omega) 0 -J6*(2*omega)^2
1 -T5Im(4);0 0 0 0 1];
P7_4=[1 0 0 0 0;-J7*(2*omega)^2 1 -c7*(2*omega) 0 -T6Re(4);0 0 1 0 0;c7*(2*omega) 0 -J7*(2*omega)^2
1 -T6Im(4);0 0 0 0 1];
P8_4=[1 0 0 0 0;-J8*(2*omega)^2 1 0 0 0;0 0 1 0 0;0 0 -J8*(2*omega)^2 1 0;0 0 0 0 1];
```

```
F1_4=[1 1/k1 0 0 0;0 1 0 0 0;0 0 1 1/k1 0;0 0 0 1 0;0 0 0 0 1];
F2_4=[1 1/k2 0 0 0;0 1 0 0 0;0 0 1 1/k2 0;0 0 0 1 0;0 0 0 0 1];
F3_4=[1 1/k3 0 0 0;0 1 0 0 0;0 0 1 1/k3 0;0 0 0 1 0;0 0 0 0 1];
F4_4=[1 1/k4 0 0 0;0 1 0 0 0;0 0 1 1/k4 0;0 0 0 1 0;0 0 0 0 1];
F5_4=[1 1/k5 0 0 0;0 1 0 0 0;0 0 1 1/k5 0;0 0 0 1 0;0 0 0 0 1];
F6_4=[1 1/k6 0 0 0;0 1 0 0 0;0 0 1 1/k6 0;0 0 0 1 0;0 0 0 0 1];
F7_4=[1 1/k7 0 0 0;0 1 0 0 0;0 0 1 1/k7 0;0 0 0 1 0;0 0 0 0 1];

H4=P8_4*F7_4*P7_4*F6_4*P6_4*F5_4*P5_4*F4_4*P4_4*F3_4*P3_4*F2_4*P2_4*F1_4*P1_4;

theta1_4Re=((H4(4,5)*H4(2,3))-(H4(2,5)*H4(4,3)))/((H4(2,1)*H4(4,3))-(H4(2,3)*H4(4,1)));
theta1_4Im=((H4(2,5)*H4(4,1))-(H4(4,5)*H4(2,1)))/((H4(2,1)*H4(4,3))-(H4(2,3)*H4(4,1)));

Z1_4L=[theta1_4Re;0;theta1_4Im;0;1]
Z1_4R=P1_4*Z1_4L;
theta1_4=sqrt((Z1_4L(1))^2+(Z1_4L(3))^2)*180/pi
torque1_4L=sqrt((Z1_4L(2))^2+(Z1_4L(4))^2)
torque1_4R=sqrt((Z1_4R(2))^2+(Z1_4R(4))^2)

Z2_4L=F1_4*Z1_4R;
Z2_4R=P2_4*Z2_4L;
theta2_4=sqrt((Z2_4L(1))^2+(Z2_4L(3))^2)*180/pi
torque2_4R=sqrt((Z2_4R(2))^2+(Z2_4R(4))^2)

Z3_4L=F2_4*Z2_4R;
Z3_4R=P3_4*Z3_4L;
theta3_4=sqrt((Z3_4L(1))^2+(Z3_4L(3))^2)*180/pi
torque3_4R=sqrt((Z3_4R(2))^2+(Z3_4R(4))^2)

Z4_4L=F3_4*Z3_4R;
Z4_4R=P4_4*Z4_4L;
theta4_4=sqrt((Z4_4L(1))^2+(Z4_4L(3))^2)*180/pi
torque4_4R=sqrt((Z4_4R(2))^2+(Z4_4R(4))^2)

Z5_4L=F4_4*Z4_4R;
Z5_4R=P5_4*Z5_4L;
theta5_4=sqrt((Z5_4L(1))^2+(Z5_4L(3))^2)*180/pi
torque5_4R=sqrt((Z5_4R(2))^2+(Z5_4R(4))^2)

Z6_4L=F5_4*Z5_4R;
Z6_4R=P6_4*Z6_4L;
theta6_4=sqrt((Z6_4L(1))^2+(Z6_4L(3))^2)*180/pi
torque6_4R=sqrt((Z6_4R(2))^2+(Z6_4R(4))^2)

Z7_4L=F6_4*Z6_4R;
Z7_4R=P7_4*Z7_4L;
theta7_4=sqrt((Z7_4L(1))^2+(Z7_4L(3))^2)*180/pi
torque7_4R=sqrt((Z7_4R(2))^2+(Z7_4R(4))^2)

Z8_4L=F7_4*Z7_4R;
Z8_4R=P8_4*Z8_4L;
theta8_4=sqrt((Z8_4L(1))^2+(Z8_4L(3))^2)*180/pi
torque8_4R=sqrt((Z8_4R(2))^2+(Z8_4R(4))^2)


%2.5th order

P1_5=[1 0 0 0 0;-J1*(5*omega/2)^2 1 -c1*(5*omega/2) 0 0;0 0 1 0 0;c1*(5*omega/2) 0 -J1*(5*omega/2)^2
1 0;0 0 0 0 1];
```

```
P2_5=[1 0 0 0 0;-J2*(5*omega/2)^2 1 -c2*(5*omega/2) 0 -T1Re(5);0 0 1 0 0;c2*(5*omega/2) 0 -
J2*(5*omega/2)^2 1 -T1Im(5);0 0 0 0 1];
P3_5=[1 0 0 0 0;-J3*(5*omega/2)^2 1 -c3*(5*omega/2) 0 -T2Re(5);0 0 1 0 0;c3*(5*omega/2) 0 -
J3*(5*omega/2)^2 1 -T2Im(5);0 0 0 0 1];
P4_5=[1 0 0 0 0;-J4*(5*omega/2)^2 1 -c4*(5*omega/2) 0 -T3Re(5);0 0 1 0 0;c4*(5*omega/2) 0 -
J4*(5*omega/2)^2 1 -T3Im(5);0 0 0 0 1];
P5_5=[1 0 0 0 0;-J5*(5*omega/2)^2 1 -c5*(5*omega/2) 0 -T4Re(5);0 0 1 0 0;c5*(5*omega/2) 0 -
J5*(5*omega/2)^2 1 -T4Im(5);0 0 0 0 1];
P6_5=[1 0 0 0 0;-J6*(5*omega/2)^2 1 -c6*(5*omega/2) 0 -T5Re(5);0 0 1 0 0;c6*(5*omega/2) 0 -
J6*(5*omega/2)^2 1 -T5Im(5);0 0 0 0 1];
P7_5=[1 0 0 0 0;-J7*(5*omega/2)^2 1 -c7*(5*omega/2) 0 -T6Re(5);0 0 1 0 0;c7*(5*omega/2) 0 -
J7*(5*omega/2)^2 1 -T6Im(5);0 0 0 0 1];
P8_5=[1 0 0 0 0;-J8*(5*omega/2)^2 1 0 0 0;0 0 1 0 0;0 0 -J8*(5*omega/2)^2 1 0;0 0 0 0 1];

F1_5=[1 1/k1 0 0 0;0 1 0 0 0;0 0 1 1/k1 0;0 0 0 1 0;0 0 0 0 1];
F2_5=[1 1/k2 0 0 0;0 1 0 0 0;0 0 1 1/k2 0;0 0 0 1 0;0 0 0 0 1];
F3_5=[1 1/k3 0 0 0;0 1 0 0 0;0 0 1 1/k3 0;0 0 0 1 0;0 0 0 0 1];
F4_5=[1 1/k4 0 0 0;0 1 0 0 0;0 0 1 1/k4 0;0 0 0 1 0;0 0 0 0 1];
F5_5=[1 1/k5 0 0 0;0 1 0 0 0;0 0 1 1/k5 0;0 0 0 1 0;0 0 0 0 1];
F6_5=[1 1/k6 0 0 0;0 1 0 0 0;0 0 1 1/k6 0;0 0 0 1 0;0 0 0 0 1];
F7_5=[1 1/k7 0 0 0;0 1 0 0 0;0 0 1 1/k7 0;0 0 0 1 0;0 0 0 0 1];

H5=P8_5*F7_5*P7_5*F6_5*P6_5*F5_5*P5_5*F4_5*P4_5*F3_5*P3_5*F2_5*P2_5*F1_5*P1_5;

theta1_5Re=((H5(4,5)*H5(2,3))-(H5(2,5)*H5(4,3)))/((H5(2,1)*H5(4,3))-(H5(2,3)*H5(4,1)));
theta1_5Im=((H5(2,5)*H5(4,1))-(H5(4,5)*H5(2,1)))/((H5(2,1)*H5(4,3))-(H5(2,3)*H5(4,1)));

Z1_5L=[theta1_5Re;0;theta1_5Im;0;1]
Z1_5R=P1_5*Z1_5L;
theta1_5=sqrt((Z1_5L(1))^2+(Z1_5L(3))^2)*180/pi
torque1_5L=sqrt((Z1_5L(2))^2+(Z1_5L(4))^2)
torque1_5R=sqrt((Z1_5R(2))^2+(Z1_5R(4))^2)

Z2_5L=F1_5*Z1_5R;
Z2_5R=P2_5*Z2_5L;
theta2_5=sqrt((Z2_5L(1))^2+(Z2_5L(3))^2)*180/pi
torque2_5R=sqrt((Z2_5R(2))^2+(Z2_5R(4))^2)

Z3_5L=F2_5*Z2_5R;
Z3_5R=P3_5*Z3_5L;
theta3_5=sqrt((Z3_5L(1))^2+(Z3_5L(3))^2)*180/pi
torque3_5R=sqrt((Z3_5R(2))^2+(Z3_5R(4))^2)

Z4_5L=F3_5*Z3_5R;
Z4_5R=P4_5*Z4_5L;
theta4_5=sqrt((Z4_5L(1))^2+(Z4_5L(3))^2)*180/pi
torque4_5R=sqrt((Z4_5R(2))^2+(Z4_5R(4))^2)

Z5_5L=F4_5*Z4_5R;
Z5_5R=P5_5*Z5_5L;
theta5_5=sqrt((Z5_5L(1))^2+(Z5_5L(3))^2)*180/pi
torque5_5R=sqrt((Z5_5R(2))^2+(Z5_5R(4))^2)

Z6_5L=F5_5*Z5_5R;
Z6_5R=P6_5*Z6_5L;
theta6_5=sqrt((Z6_5L(1))^2+(Z6_5L(3))^2)*180/pi
torque6_5R=sqrt((Z6_5R(2))^2+(Z6_5R(4))^2)

Z7_5L=F6_5*Z6_5R;
```

```
Z7_5R=P7_5*Z7_5L;
theta7_5=sqrt((Z7_5L(1))^2+(Z7_5L(3))^2)*180/pi
torque7_5R=sqrt((Z7_5R(2))^2+(Z7_5R(4))^2)

Z8_5L=F7_5*Z7_5R;
Z8_5R=P8_5*Z8_5L;
theta8_5=sqrt((Z8_5L(1))^2+(Z8_5L(3))^2)*180/pi
torque8_5R=sqrt((Z8_5R(2))^2+(Z8_5R(4))^2)


%3rd order

P1_6=[1 0 0 0 0;-J1*(3*omega)^2 1 -c1*(3*omega) 0 0;0 0 1 0 0;c1*(3*omega) 0 -J1*(3*omega)^2 1 0;0 0
0 0 1];
P2_6=[1 0 0 0 0;-J2*(3*omega)^2 1 -c2*(3*omega) 0 -T1Re(6);0 0 1 0 0;c2*(3*omega) 0 -J2*(3*omega)^2
1 -T1Im(6);0 0 0 0 1];
P3_6=[1 0 0 0 0;-J3*(3*omega)^2 1 -c3*(3*omega) 0 -T2Re(6);0 0 1 0 0;c3*(3*omega) 0 -J3*(3*omega)^2
1 -T2Im(6);0 0 0 0 1];
P4_6=[1 0 0 0 0;-J4*(3*omega)^2 1 -c4*(3*omega) 0 -T3Re(6);0 0 1 0 0;c4*(3*omega) 0 -J4*(3*omega)^2
1 -T3Im(6);0 0 0 0 1];
P5_6=[1 0 0 0 0;-J5*(3*omega)^2 1 -c5*(3*omega) 0 -T4Re(6);0 0 1 0 0;c5*(3*omega) 0 -J5*(3*omega)^2
1 -T4Im(6);0 0 0 0 1];
P6_6=[1 0 0 0 0;-J6*(3*omega)^2 1 -c6*(3*omega) 0 -T5Re(6);0 0 1 0 0;c6*(3*omega) 0 -J6*(3*omega)^2
1 -T5Im(6);0 0 0 0 1];
P7_6=[1 0 0 0 0;-J7*(3*omega)^2 1 -c7*(3*omega) 0 -T6Re(6);0 0 1 0 0;c7*(3*omega) 0 -J7*(3*omega)^2
1 -T6Im(6);0 0 0 0 1];
P8_6=[1 0 0 0 0;-J8*(3*omega)^2 1 0 0 0;0 0 1 0 0;0 0 -J8*(3*omega)^2 1 0;0 0 0 0 1];

F1_6=[1 1/k1 0 0 0;0 1 0 0 0;0 0 1 1/k1 0;0 0 0 1 0;0 0 0 0 1];
F2_6=[1 1/k2 0 0 0;0 1 0 0 0;0 0 1 1/k2 0;0 0 0 1 0;0 0 0 0 1];
F3_6=[1 1/k3 0 0 0;0 1 0 0 0;0 0 1 1/k3 0;0 0 0 1 0;0 0 0 0 1];
F4_6=[1 1/k4 0 0 0;0 1 0 0 0;0 0 1 1/k4 0;0 0 0 1 0;0 0 0 0 1];
F5_6=[1 1/k5 0 0 0;0 1 0 0 0;0 0 1 1/k5 0;0 0 0 1 0;0 0 0 0 1];
F6_6=[1 1/k6 0 0 0;0 1 0 0 0;0 0 1 1/k6 0;0 0 0 1 0;0 0 0 0 1];
F7_6=[1 1/k7 0 0 0;0 1 0 0 0;0 0 1 1/k7 0;0 0 0 1 0;0 0 0 0 1];

H6=P8_6*F7_6*P7_6*F6_6*P6_6*F5_6*P5_6*F4_6*P4_6*F3_6*P3_6*F2_6*P2_6*F1_6*P1_6;

theta1_6Re=((H6(4,5)*H6(2,3))-(H6(2,5)*H6(4,3)))/((H6(2,1)*H6(4,3))-(H6(2,3)*H6(4,1)));
theta1_6Im=((H6(2,5)*H6(4,1))-(H6(4,5)*H6(2,1)))/((H6(2,1)*H6(4,3))-(H6(2,3)*H6(4,1)));

Z1_6L=[theta1_6Re;0;theta1_6Im;0;1]
Z1_6R=P1_6*Z1_6L;
theta1_6=sqrt((Z1_6L(1))^2+(Z1_6L(3))^2)*180/pi
torque1_6L=sqrt((Z1_6L(2))^2+(Z1_6L(4))^2)
torque1_6R=sqrt((Z1_6R(2))^2+(Z1_6R(4))^2)

Z2_6L=F1_6*Z1_6R;
Z2_6R=P2_6*Z2_6L;
theta2_6=sqrt((Z2_6L(1))^2+(Z2_6L(3))^2)*180/pi
torque2_6R=sqrt((Z2_6R(2))^2+(Z2_6R(4))^2)

Z3_6L=F2_6*Z2_6R;
Z3_6R=P3_6*Z3_6L;
theta3_6=sqrt((Z3_6L(1))^2+(Z3_6L(3))^2)*180/pi
torque3_6R=sqrt((Z3_6R(2))^2+(Z3_6R(4))^2)

Z4_6L=F3_6*Z3_6R;
Z4_6R=P4_6*Z4_6L;
```

```
theta4_6=sqrt((Z4_6L(1))^2+(Z4_6L(3))^2)*180/pi
torque4_6R=sqrt((Z4_6R(2))^2+(Z4_6R(4))^2)

Z5_6L=F4_6*Z4_6R;
Z5_6R=P5_6*Z5_6L;
theta5_6=sqrt((Z5_6L(1))^2+(Z5_6L(3))^2)*180/pi
torque5_6R=sqrt((Z5_6R(2))^2+(Z5_6R(4))^2)

Z6_6L=F5_6*Z5_6R;
Z6_6R=P6_6*Z6_6L;
theta6_6=sqrt((Z6_6L(1))^2+(Z6_6L(3))^2)*180/pi
torque6_6R=sqrt((Z6_6R(2))^2+(Z6_6R(4))^2)

Z7_6L=F6_6*Z6_6R;
Z7_6R=P7_6*Z7_6L;
theta7_6=sqrt((Z7_6L(1))^2+(Z7_6L(3))^2)*180/pi
torque7_6R=sqrt((Z7_6R(2))^2+(Z7_6R(4))^2)

Z8_6L=F7_6*Z7_6R;
Z8_6R=P8_6*Z8_6L;
theta8_6=sqrt((Z8_6L(1))^2+(Z8_6L(3))^2)*180/pi
torque8_6R=sqrt((Z8_6R(2))^2+(Z8_6R(4))^2)


%3.5th order

P1_7=[1 0 0 0 0;-J1*(7*omega/2)^2 1 -c1*(7*omega/2) 0 0;0 0 1 0 0;c1*(7*omega/2) 0 -J1*(7*omega/2)^2
1 0;0 0 0 0 1];
P2_7=[1  0  0  0  0;-J2*(7*omega/2)^2  1  -c2*(7*omega/2)  0  -T1Re(7);0  0  1  0  0;c2*(7*omega/2)  0  -
J2*(7*omega/2)^2 1 -T1Im(7);0 0 0 0 1];
P3_7=[1  0  0  0  0;-J3*(7*omega/2)^2  1  -c3*(7*omega/2)  0  -T2Re(7);0  0  1  0  0;c3*(7*omega/2)  0  -
J3*(7*omega/2)^2 1 -T2Im(7);0 0 0 0 1];
P4_7=[1  0  0  0  0;-J4*(7*omega/2)^2  1  -c4*(7*omega/2)  0  -T3Re(7);0  0  1  0  0;c4*(7*omega/2)  0  -
J4*(7*omega/2)^2 1 -T3Im(7);0 0 0 0 1];
P5_7=[1  0  0  0  0;-J5*(7*omega/2)^2  1  -c5*(7*omega/2)  0  -T4Re(7);0  0  1  0  0;c5*(7*omega/2)  0  -
J5*(7*omega/2)^2 1 -T4Im(7);0 0 0 0 1];
P6_7=[1  0  0  0  0;-J6*(7*omega/2)^2  1  -c6*(7*omega/2)  0  -T5Re(7);0  0  1  0  0;c6*(7*omega/2)  0  -
J6*(7*omega/2)^2 1 -T5Im(7);0 0 0 0 1];
P7_7=[1  0  0  0  0;-J7*(7*omega/2)^2  1  -c7*(7*omega/2)  0  -T6Re(7);0  0  1  0  0;c7*(7*omega/2)  0  -
J7*(7*omega/2)^2 1 -T6Im(7);0 0 0 0 1];
P8_7=[1 0 0 0 0;-J8*(7*omega/2)^2 1 0 0 0;0 0 1 0 0;0 0 -J8*(7*omega/2)^2 1 0;0 0 0 0 1];

F1_7=[1 1/k1 0 0 0;0 1 0 0 0;0 0 1 1/k1 0;0 0 0 1 0;0 0 0 0 1];
F2_7=[1 1/k2 0 0 0;0 1 0 0 0;0 0 1 1/k2 0;0 0 0 1 0;0 0 0 0 1];
F3_7=[1 1/k3 0 0 0;0 1 0 0 0;0 0 1 1/k3 0;0 0 0 1 0;0 0 0 0 1];
F4_7=[1 1/k4 0 0 0;0 1 0 0 0;0 0 1 1/k4 0;0 0 0 1 0;0 0 0 0 1];
F5_7=[1 1/k5 0 0 0;0 1 0 0 0;0 0 1 1/k5 0;0 0 0 1 0;0 0 0 0 1];
F6_7=[1 1/k6 0 0 0;0 1 0 0 0;0 0 1 1/k6 0;0 0 0 1 0;0 0 0 0 1];
F7_7=[1 1/k7 0 0 0;0 1 0 0 0;0 0 1 1/k7 0;0 0 0 1 0;0 0 0 0 1];

H7=P8_7*F7_7*P7_7*F6_7*P6_7*F5_7*P5_7*F4_7*P4_7*F3_7*P3_7*F2_7*P2_7*F1_7*P1_7;

theta1_7Re=((H7(4,5)*H7(2,3))-(H7(2,5)*H7(4,3)))/((H7(2,1)*H7(4,3))-(H7(2,3)*H7(4,1)));
theta1_7Im=((-H7(4,5)*H7(2,1))+(H7(2,5)*H7(4,1)))/((H7(2,1)*H7(4,3))-(H7(2,3)*H7(4,1)));

Z1_7L=[theta1_7Re;0;theta1_7Im;0;1]
Z1_7R=P1_7*Z1_7L;
theta1_7=sqrt((Z1_7L(1))^2+(Z1_7L(3))^2)*180/pi
torque1_7L=sqrt((Z1_7L(2))^2+(Z1_7L(4))^2)
```

```
torque1_7R=sqrt((Z1_7R(2))^2+(Z1_7R(4))^2)

Z2_7L=F1_7*Z1_7R;
Z2_7R=P2_7*Z2_7L;
theta2_7=sqrt((Z2_7L(1))^2+(Z2_7L(3))^2)*180/pi
torque2_7R=sqrt((Z2_7R(2))^2+(Z2_7R(4))^2)

Z3_7L=F2_7*Z2_7R;
Z3_7R=P3_7*Z3_7L;
theta3_7=sqrt((Z3_7L(1))^2+(Z3_7L(3))^2)*180/pi
torque3_7R=sqrt((Z3_7R(2))^2+(Z3_7R(4))^2)

Z4_7L=F3_7*Z3_7R;
Z4_7R=P4_7*Z4_7L;
theta4_7=sqrt((Z4_7L(1))^2+(Z4_7L(3))^2)*180/pi
torque4_7R=sqrt((Z4_7R(2))^2+(Z4_7R(4))^2)

Z5_7L=F4_7*Z4_7R;
Z5_7R=P5_7*Z5_7L;
theta5_7=sqrt((Z5_7L(1))^2+(Z5_7L(3))^2)*180/pi
torque5_7R=sqrt((Z5_7R(2))^2+(Z5_7R(4))^2)

Z6_7L=F5_7*Z5_7R;
Z6_7R=P6_7*Z6_7L;
theta6_7=sqrt((Z6_7L(1))^2+(Z6_7L(3))^2)*180/pi
torque6_7R=sqrt((Z6_7R(2))^2+(Z6_7R(4))^2)

Z7_7L=F6_7*Z6_7R;
Z7_7R=P7_7*Z7_7L;
theta7_7=sqrt((Z7_7L(1))^2+(Z7_7L(3))^2)*180/pi
torque7_7R=sqrt((Z7_7R(2))^2+(Z7_7R(4))^2)

Z8_7L=F7_7*Z7_7R;
Z8_7R=P8_7*Z8_7L;
theta8_7=sqrt((Z8_7L(1))^2+(Z8_7L(3))^2)*180/pi
torque8_7R=sqrt((Z8_7R(2))^2+(Z8_7R(4))^2)


%4th order

P1_8=[1 0 0 0 0;-J1*(4*omega)^2 1 -c1*(4*omega) 0 0;0 0 1 0 0;c1*(4*omega) 0 -J1*(4*omega)^2 1 0;0 0
0 0 1];
P2_8=[1 0 0 0 0;-J2*(4*omega)^2 1 -c2*(4*omega) 0 -T1Re(8);0 0 1 0 0;c2*(4*omega) 0 -J2*(4*omega)^2
1 -T1Im(8);0 0 0 0 1];
P3_8=[1 0 0 0 0;-J3*(4*omega)^2 1 -c3*(4*omega) 0 -T2Re(8);0 0 1 0 0;c3*(4*omega) 0 -J3*(4*omega)^2
1 -T2Im(8);0 0 0 0 1];
P4_8=[1 0 0 0 0;-J4*(4*omega)^2 1 -c4*(4*omega) 0 -T3Re(8);0 0 1 0 0;c4*(4*omega) 0 -J4*(4*omega)^2
1 -T3Im(8);0 0 0 0 1];
P5_8=[1 0 0 0 0;-J5*(4*omega)^2 1 -c5*(4*omega) 0 -T4Re(8);0 0 1 0 0;c5*(4*omega) 0 -J5*(4*omega)^2
1 -T4Im(8);0 0 0 0 1];
P6_8=[1 0 0 0 0;-J6*(4*omega)^2 1 -c6*(4*omega) 0 -T5Re(8);0 0 1 0 0;c6*(4*omega) 0 -J6*(4*omega)^2
1 -T5Im(8);0 0 0 0 1];
P7_8=[1 0 0 0 0;-J7*(4*omega)^2 1 -c7*(4*omega) 0 -T6Re(8);0 0 1 0 0;c7*(4*omega) 0 -J7*(4*omega)^2
1 -T6Im(8);0 0 0 0 1];
P8_8=[1 0 0 0 0;-J8*(4*omega)^2 1 0 0 0;0 0 1 0 0;0 0 -J8*(4*omega)^2 1 0;0 0 0 0 1];

F1_8=[1 1/k1 0 0 0;0 1 0 0 0;0 0 1 1/k1 0;0 0 0 1 0;0 0 0 0 1];
F2_8=[1 1/k2 0 0 0;0 1 0 0 0;0 0 1 1/k2 0;0 0 0 1 0;0 0 0 0 1];
F3_8=[1 1/k3 0 0 0;0 1 0 0 0;0 0 1 1/k3 0;0 0 0 1 0;0 0 0 0 1];
```

```
F4_8=[1 1/k4 0 0 0;0 1 0 0 0;0 0 1 1/k4 0;0 0 0 1 0;0 0 0 0 1];
F5_8=[1 1/k5 0 0 0;0 1 0 0 0;0 0 1 1/k5 0;0 0 0 1 0;0 0 0 0 1];
F6_8=[1 1/k6 0 0 0;0 1 0 0 0;0 0 1 1/k6 0;0 0 0 1 0;0 0 0 0 1];
F7_8=[1 1/k7 0 0 0;0 1 0 0 0;0 0 1 1/k7 0;0 0 0 1 0;0 0 0 0 1];

H8=P8_8*F7_8*P7_8*F6_8*P6_8*F5_8*P5_8*F4_8*P4_8*F3_8*P3_8*F2_8*P2_8*F1_8*P1_8;

theta1_8Re=((H8(4,5)*H8(2,3))-(H8(2,5)*H8(4,3)))/((H8(2,1)*H8(4,3))-(H8(2,3)*H8(4,1)));
theta1_8Im=((-H8(4,5)*H8(2,1))+(H8(2,5)*H8(4,1)))/((H8(2,1)*H8(4,3))-(H8(2,3)*H8(4,1)));

Z1_8L=[theta1_8Re;0;theta1_8Im;0;1]
Z1_8R=P1_8*Z1_8L;
theta1_8=sqrt((Z1_8L(1))^2+(Z1_8L(3))^2)*180/pi
torque1_8L=sqrt((Z1_8L(2))^2+(Z1_8L(4))^2)
torque1_8R=sqrt((Z1_8R(2))^2+(Z1_8R(4))^2)

Z2_8L=F1_8*Z1_8R;
Z2_8R=P2_8*Z2_8L;
theta2_8=sqrt((Z2_8L(1))^2+(Z2_8L(3))^2)*180/pi
torque2_8R=sqrt((Z2_8R(2))^2+(Z2_8R(4))^2)

Z3_8L=F2_8*Z2_8R;
Z3_8R=P3_8*Z3_8L;
theta3_8=sqrt((Z3_8L(1))^2+(Z3_8L(3))^2)*180/pi
torque3_8R=sqrt((Z3_8R(2))^2+(Z3_8R(4))^2)

Z4_8L=F3_8*Z3_8R;
Z4_8R=P4_8*Z4_8L;
theta4_8=sqrt((Z4_8L(1))^2+(Z4_8L(3))^2)*180/pi
torque4_8R=sqrt((Z4_8R(2))^2+(Z4_8R(4))^2)

Z5_8L=F4_8*Z4_8R;
Z5_8R=P5_8*Z5_8L;
theta5_8=sqrt((Z5_8L(1))^2+(Z5_8L(3))^2)*180/pi
torque5_8R=sqrt((Z5_8R(2))^2+(Z5_8R(4))^2)

Z6_8L=F5_8*Z5_8R;
Z6_8R=P6_8*Z6_8L;
theta6_8=sqrt((Z6_8L(1))^2+(Z6_8L(3))^2)*180/pi
torque6_8R=sqrt((Z6_8R(2))^2+(Z6_8R(4))^2)

Z7_8L=F6_8*Z6_8R;
Z7_8R=P7_8*Z7_8L;
theta7_8=sqrt((Z7_8L(1))^2+(Z7_8L(3))^2)*180/pi
torque7_8R=sqrt((Z7_8R(2))^2+(Z7_8R(4))^2)

Z8_8L=F7_8*Z7_8R;
Z8_8R=P8_8*Z8_8L;
theta8_8=sqrt((Z8_8L(1))^2+(Z8_8L(3))^2)*180/pi
torque8_8R=sqrt((Z8_8R(2))^2+(Z8_8R(4))^2)


%4.5th order

P1_9=[1 0 0 0 0;-J1*(9*omega/2)^2 1 -c1*(9*omega/2) 0 0;0 0 1 0 0;c1*(9*omega/2) 0 -J1*(9*omega/2)^2
1 0;0 0 0 0 1];
P2_9=[1  0  0  0  0;-J2*(9*omega/2)^2  1  -c2*(9*omega/2)  0  -T1Re(9);0  0  1  0  0;c2*(9*omega/2)  0  -
J2*(9*omega/2)^2 1 -T1Im(9);0 0 0 0 1];
```

```
P3_9=[1 0 0 0 0;-J3*(9*omega/2)^2 1 -c3*(9*omega/2) 0 -T2Re(9);0 0 1 0 0;c3*(9*omega/2) 0 -
J3*(9*omega/2)^2 1 -T2Im(9);0 0 0 0 1];
P4_9=[1 0 0 0 0;-J4*(9*omega/2)^2 1 -c4*(9*omega/2) 0 -T3Re(9);0 0 1 0 0;c4*(9*omega/2) 0 -
J4*(9*omega/2)^2 1 -T3Im(9);0 0 0 0 1];
P5_9=[1 0 0 0 0;-J5*(9*omega/2)^2 1 -c5*(9*omega/2) 0 -T4Re(9);0 0 1 0 0;c5*(9*omega/2) 0 -
J5*(9*omega/2)^2 1 -T4Im(9);0 0 0 0 1];
P6_9=[1 0 0 0 0;-J6*(9*omega/2)^2 1 -c6*(9*omega/2) 0 -T5Re(9);0 0 1 0 0;c6*(9*omega/2) 0 -
J6*(9*omega/2)^2 1 -T5Im(9);0 0 0 0 1];
P7_9=[1 0 0 0 0;-J7*(9*omega/2)^2 1 -c7*(9*omega/2) 0 -T6Re(9);0 0 1 0 0;c7*(9*omega/2) 0 -
J7*(9*omega/2)^2 1 -T6Im(9);0 0 0 0 1];
P8_9=[1 0 0 0 0;-J8*(9*omega/2)^2 1 0 0 0;0 0 1 0 0;0 0 -J8*(9*omega/2)^2 1 0;0 0 0 0 1];

F1_9=[1 1/k1 0 0 0;0 1 0 0 0;0 0 1 1/k1 0;0 0 0 1 0;0 0 0 0 1];
F2_9=[1 1/k2 0 0 0;0 1 0 0 0;0 0 1 1/k2 0;0 0 0 1 0;0 0 0 0 1];
F3_9=[1 1/k3 0 0 0;0 1 0 0 0;0 0 1 1/k3 0;0 0 0 1 0;0 0 0 0 1];
F4_9=[1 1/k4 0 0 0;0 1 0 0 0;0 0 1 1/k4 0;0 0 0 1 0;0 0 0 0 1];
F5_9=[1 1/k5 0 0 0;0 1 0 0 0;0 0 1 1/k5 0;0 0 0 1 0;0 0 0 0 1];
F6_9=[1 1/k6 0 0 0;0 1 0 0 0;0 0 1 1/k6 0;0 0 0 1 0;0 0 0 0 1];
F7_9=[1 1/k7 0 0 0;0 1 0 0 0;0 0 1 1/k7 0;0 0 0 1 0;0 0 0 0 1];

H9=P8_9*F7_9*P7_9*F6_9*P6_9*F5_9*P5_9*F4_9*P4_9*F3_9*P3_9*F2_9*P2_9*F1_9*P1_9;

theta1_9Re=((H9(4,5)*H9(2,3))-(H9(2,5)*H9(4,3)))/((H9(2,1)*H9(4,3))-(H9(2,3)*H9(4,1)));
theta1_9Im=((-H9(4,5)*H9(2,1))+(H9(2,5)*H9(4,1)))/((H9(2,1)*H9(4,3))-(H9(2,3)*H9(4,1)));

Z1_9L=[theta1_9Re;0;theta1_9Im;0;1]
Z1_9R=P1_9*Z1_9L;
theta1_9=sqrt((Z1_9L(1))^2+(Z1_9L(3))^2)*180/pi
torque1_9L=sqrt((Z1_9L(2))^2+(Z1_9L(4))^2)
torque1_9R=sqrt((Z1_9R(2))^2+(Z1_9R(4))^2)

Z2_9L=F1_9*Z1_9R;
Z2_9R=P2_9*Z2_9L;
theta2_9=sqrt((Z2_9L(1))^2+(Z2_9L(3))^2)*180/pi
torque2_9R=sqrt((Z2_9R(2))^2+(Z2_9R(4))^2)

Z3_9L=F2_9*Z2_9R;
Z3_9R=P3_9*Z3_9L;
theta3_9=sqrt((Z3_9L(1))^2+(Z3_9L(3))^2)*180/pi
torque3_9R=sqrt((Z3_9R(2))^2+(Z3_9R(4))^2)

Z4_9L=F3_9*Z3_9R;
Z4_9R=P4_9*Z4_9L;
theta4_9=sqrt((Z4_9L(1))^2+(Z4_9L(3))^2)*180/pi
torque4_9R=sqrt((Z4_9R(2))^2+(Z4_9R(4))^2)

Z5_9L=F4_9*Z4_9R;
Z5_9R=P5_9*Z5_9L;
theta5_9=sqrt((Z5_9L(1))^2+(Z5_9L(3))^2)*180/pi
torque5_9R=sqrt((Z5_9R(2))^2+(Z5_9R(4))^2)

Z6_9L=F5_9*Z5_9R;
Z6_9R=P6_9*Z6_9L;
theta6_9=sqrt((Z6_9L(1))^2+(Z6_9L(3))^2)*180/pi
torque6_9R=sqrt((Z6_9R(2))^2+(Z6_9R(4))^2)

Z7_9L=F6_9*Z6_9R;
Z7_9R=P7_9*Z7_9L;
theta7_9=sqrt((Z7_9L(1))^2+(Z7_9L(3))^2)*180/pi
```

```
torque7_9R=sqrt((Z7_9R(2))^2+(Z7_9R(4))^2)

Z8_9L=F7_9*Z7_9R;
Z8_9R=P8_9*Z8_9L;
theta8_9=sqrt((Z8_9L(1))^2+(Z8_9L(3))^2)*180/pi
torque8_9R=sqrt((Z8_9R(2))^2+(Z8_9R(4))^2)


%5th order

P1_10=[1 0 0 0 0;-J1*(10*omega/2)^2 1 -c1*(10*omega/2) 0 0;0 0 1 0 0;c1*(10*omega/2) 0 -
J1*(10*omega/2)^2 1 0;0 0 0 0 1];
P2_10=[1 0 0 0 0;-J2*(10*omega/2)^2 1 -c2*(10*omega/2) 0 -T1Re(10);0 0 1 0 0;c2*(10*omega/2) 0 -
J2*(10*omega/2)^2 1 -T1Im(10);0 0 0 0 1];
P3_10=[1 0 0 0 0;-J3*(10*omega/2)^2 1 -c3*(10*omega/2) 0 -T2Re(10);0 0 1 0 0;c3*(10*omega/2) 0 -
J3*(10*omega/2)^2 1 -T2Im(10);0 0 0 0 1];
P4_10=[1 0 0 0 0;-J4*(10*omega/2)^2 1 -c4*(10*omega/2) 0 -T3Re(10);0 0 1 0 0;c4*(10*omega/2) 0 -
J4*(10*omega/2)^2 1 -T3Im(10);0 0 0 0 1];
P5_10=[1 0 0 0 0;-J5*(10*omega/2)^2 1 -c5*(10*omega/2) 0 -T4Re(10);0 0 1 0 0;c5*(10*omega/2) 0 -
J5*(10*omega/2)^2 1 -T4Im(10);0 0 0 0 1];
P6_10=[1 0 0 0 0;-J6*(10*omega/2)^2 1 -c6*(10*omega/2) 0 -T5Re(10);0 0 1 0 0;c6*(10*omega/2) 0 -
J6*(10*omega/2)^2 1 -T5Im(10);0 0 0 0 1];
P7_10=[1 0 0 0 0;-J7*(10*omega/2)^2 1 -c7*(10*omega/2) 0 -T6Re(10);0 0 1 0 0;c7*(10*omega/2) 0 -
J7*(10*omega/2)^2 1 -T6Im(10);0 0 0 0 1];
P8_10=[1 0 0 0 0;-J8*(10*omega/2)^2 1 0 0 0;0 0 1 0 0;0 0 -J8*(10*omega/2)^2 1 0;0 0 0 0 1];

F1_10=[1 1/k1 0 0 0;0 1 0 0 0;0 0 1 1/k1 0;0 0 0 1 0;0 0 0 0 1];
F2_10=[1 1/k2 0 0 0;0 1 0 0 0;0 0 1 1/k2 0;0 0 0 1 0;0 0 0 0 1];
F3_10=[1 1/k3 0 0 0;0 1 0 0 0;0 0 1 1/k3 0;0 0 0 1 0;0 0 0 0 1];
F4_10=[1 1/k4 0 0 0;0 1 0 0 0;0 0 1 1/k4 0;0 0 0 1 0;0 0 0 0 1];
F5_10=[1 1/k5 0 0 0;0 1 0 0 0;0 0 1 1/k5 0;0 0 0 1 0;0 0 0 0 1];
F6_10=[1 1/k6 0 0 0;0 1 0 0 0;0 0 1 1/k6 0;0 0 0 1 0;0 0 0 0 1];
F7_10=[1 1/k7 0 0 0;0 1 0 0 0;0 0 1 1/k7 0;0 0 0 1 0;0 0 0 0 1];

H10=P8_10*F7_10*P7_10*F6_10*P6_10*F5_10*P5_10*F4_10*P4_10*F3_10*P3_10*F2_10*P2_10*F1_
10*P1_10;

theta1_10Re=((H10(4,5)*H10(2,3))-(H10(2,5)*H10(4,3)))/((H10(2,1)*H10(4,3))-(H10(2,3)*H10(4,1)));
theta1_10Im=((-H10(4,5)*H10(2,1))+(H10(2,5)*H10(4,1)))/((H10(2,1)*H10(4,3))-(H10(2,3)*H10(4,1)));

Z1_10L=[theta1_10Re;0;theta1_10Im;0;1]
Z1_10R=P1_10*Z1_10L;
theta1_10=sqrt((Z1_10L(1))^2+(Z1_10L(3))^2)*180/pi
torque1_10L=sqrt((Z1_10L(2))^2+(Z1_10L(4))^2)
torque1_10R=sqrt((Z1_10R(2))^2+(Z1_10R(4))^2)

Z2_10L=F1_10*Z1_10R;
Z2_10R=P2_10*Z2_10L;
theta2_10=sqrt((Z2_10L(1))^2+(Z2_10L(3))^2)*180/pi
torque2_10R=sqrt((Z2_10R(2))^2+(Z2_10R(4))^2)

Z3_10L=F2_10*Z2_10R;
Z3_10R=P3_10*Z3_10L;
theta3_10=sqrt((Z3_10L(1))^2+(Z3_10L(3))^2)*180/pi
torque3_10R=sqrt((Z3_10R(2))^2+(Z3_10R(4))^2)

Z4_10L=F3_10*Z3_10R;
Z4_10R=P4_10*Z4_10L;
theta4_10=sqrt((Z4_10L(1))^2+(Z4_10L(3))^2)*180/pi
```

```
torque4_10R=sqrt((Z4_10R(2))^2+(Z4_10R(4))^2)

Z5_10L=F4_10*Z4_10R;
Z5_10R=P5_10*Z5_10L;
theta5_10=sqrt((Z5_10L(1))^2+(Z5_10L(3))^2)*180/pi
torque5_10R=sqrt((Z5_10R(2))^2+(Z5_10R(4))^2)

Z6_10L=F5_10*Z5_10R;
Z6_10R=P6_10*Z6_10L;
theta6_10=sqrt((Z6_10L(1))^2+(Z6_10L(3))^2)*180/pi
torque6_10R=sqrt((Z6_10R(2))^2+(Z6_10R(4))^2)

Z7_10L=F6_10*Z6_10R;
Z7_10R=P7_10*Z7_10L;
theta7_10=sqrt((Z7_10L(1))^2+(Z7_10L(3))^2)*180/pi
torque7_10R=sqrt((Z7_10R(2))^2+(Z7_10R(4))^2)

Z8_10L=F7_10*Z7_10R;
Z8_10R=P8_10*Z8_10L;
theta8_10=sqrt((Z8_10L(1))^2+(Z8_10L(3))^2)*180/pi
torque8_10R=sqrt((Z8_10R(2))^2+(Z8_10R(4))^2)


%5.5th order

P1_11=[1  0  0  0  0;-J1*(11*omega/2)^2  1  -c1*(11*omega/2)  0  0;0  0  1  0  0;c1*(11*omega/2)  0  -
J1*(11*omega/2)^2 1 0;0 0 0 0 1];
P2_11=[1  0  0  0  0;-J2*(11*omega/2)^2  1  -c2*(11*omega/2)  0  -T1Re(11);0  0  1  0  0;c2*(11*omega/2)  0  -
J2*(11*omega/2)^2 1 -T1Im(11);0 0 0 0 1];
P3_11=[1  0  0  0  0;-J3*(11*omega/2)^2  1  -c3*(11*omega/2)  0  -T2Re(11);0  0  1  0  0;c3*(11*omega/2)  0  -
J3*(11*omega/2)^2 1 -T2Im(11);0 0 0 0 1];
P4_11=[1  0  0  0  0;-J4*(11*omega/2)^2  1  -c4*(11*omega/2)  0  -T3Re(11);0  0  1  0  0;c4*(11*omega/2)  0  -
J4*(11*omega/2)^2 1 -T3Im(11);0 0 0 0 1];
P5_11=[1  0  0  0  0;-J5*(11*omega/2)^2  1  -c5*(11*omega/2)  0  -T4Re(11);0  0  1  0  0;c5*(11*omega/2)  0  -
J5*(11*omega/2)^2 1 -T4Im(11);0 0 0 0 1];
P6_11=[1  0  0  0  0;-J6*(11*omega/2)^2  1  -c6*(11*omega/2)  0  -T5Re(11);0  0  1  0  0;c6*(11*omega/2)  0  -
J6*(11*omega/2)^2 1 -T5Im(11);0 0 0 0 1];
P7_11=[1  0  0  0  0;-J7*(11*omega/2)^2  1  -c7*(11*omega/2)  0  -T6Re(11);0  0  1  0  0;c7*(11*omega/2)  0  -
J7*(11*omega/2)^2 1 -T6Im(11);0 0 0 0 1];
P8_11=[1 0 0 0 0;-J8*(11*omega/2)^2 1 0 0 0;0 0 1 0 0;0 0 -J8*(11*omega/2)^2 1 0;0 0 0 0 1];

F1_11=[1 1/k1 0 0 0;0 1 0 0 0;0 0 1 1/k1 0;0 0 0 1 0;0 0 0 0 1];
F2_11=[1 1/k2 0 0 0;0 1 0 0 0;0 0 1 1/k2 0;0 0 0 1 0;0 0 0 0 1];
F3_11=[1 1/k3 0 0 0;0 1 0 0 0;0 0 1 1/k3 0;0 0 0 1 0;0 0 0 0 1];
F4_11=[1 1/k4 0 0 0;0 1 0 0 0;0 0 1 1/k4 0;0 0 0 1 0;0 0 0 0 1];
F5_11=[1 1/k5 0 0 0;0 1 0 0 0;0 0 1 1/k5 0;0 0 0 1 0;0 0 0 0 1];
F6_11=[1 1/k6 0 0 0;0 1 0 0 0;0 0 1 1/k6 0;0 0 0 1 0;0 0 0 0 1];
F7_11=[1 1/k7 0 0 0;0 1 0 0 0;0 0 1 1/k7 0;0 0 0 1 0;0 0 0 0 1];

H11=P8_11*F7_11*P7_11*F6_11*P6_11*F5_11*P5_11*F4_11*P4_11*F3_11*P3_11*F2_11*P2_11*F1_
11*P1_11;

theta1_11Re=((H11(4,5)*H11(2,3))-(H11(2,5)*H11(4,3)))/((H11(2,1)*H11(4,3))-(H11(2,3)*H11(4,1)));
theta1_11Im=((-H11(4,5)*H11(2,1))+(H11(2,5)*H11(4,1)))/((H11(2,1)*H11(4,3))-(H11(2,3)*H11(4,1)));

Z1_11L=[theta1_11Re;0;theta1_11Im;0;1]
Z1_11R=P1_11*Z1_11L;
theta1_11=sqrt((Z1_11L(1))^2+(Z1_11L(3))^2)*180/pi
torque1_11L=sqrt((Z1_11L(2))^2+(Z1_11L(4))^2)
```

```
torque1_11R=sqrt((Z1_11R(2))^2+(Z1_11R(4))^2)

Z2_11L=F1_11*Z1_11R;
Z2_11R=P2_11*Z2_11L;
theta2_11=sqrt((Z2_11L(1))^2+(Z2_11L(3))^2)*180/pi
torque2_11R=sqrt((Z2_11R(2))^2+(Z2_11R(4))^2)

Z3_11L=F2_11*Z2_11R;
Z3_11R=P3_11*Z3_11L;
theta3_11=sqrt((Z3_11L(1))^2+(Z3_11L(3))^2)*180/pi
torque3_11R=sqrt((Z3_11R(2))^2+(Z3_11R(4))^2)

Z4_11L=F3_11*Z3_11R;
Z4_11R=P4_11*Z4_11L;
theta4_11=sqrt((Z4_11L(1))^2+(Z4_11L(3))^2)*180/pi
torque4_11R=sqrt((Z4_11R(2))^2+(Z4_11R(4))^2)

Z5_11L=F4_11*Z4_11R;
Z5_11R=P5_11*Z5_11L;
theta5_11=sqrt((Z5_11L(1))^2+(Z5_11L(3))^2)*180/pi
torque5_11R=sqrt((Z5_11R(2))^2+(Z5_11R(4))^2)

Z6_11L=F5_11*Z5_11R;
Z6_11R=P6_11*Z6_11L;
theta6_11=sqrt((Z6_11L(1))^2+(Z6_11L(3))^2)*180/pi
torque6_11R=sqrt((Z6_11R(2))^2+(Z6_11R(4))^2)

Z7_11L=F6_11*Z6_11R;
Z7_11R=P7_11*Z7_11L;
theta7_11=sqrt((Z7_11L(1))^2+(Z7_11L(3))^2)*180/pi
torque7_11R=sqrt((Z7_11R(2))^2+(Z7_11R(4))^2)

Z8_11L=F7_11*Z7_11R;
Z8_11R=P8_11*Z8_11L;
theta8_11=sqrt((Z8_11L(1))^2+(Z8_11L(3))^2)*180/pi
torque8_11R=sqrt((Z8_11R(2))^2+(Z8_11R(4))^2)


%6th order

P1_12=[1 0 0 0 0;-J1*(6*omega)^2 1 -c1*(6*omega) 0 0;0 0 1 0 0;c1*(6*omega) 0 -J1*(6*omega)^2 1 0;0 0
0 0 1];
P2_12=[1  0  0  0  0;-J2*(6*omega)^2  1  -c2*(6*omega)  0  -T1Re(12);0  0  1  0  0;c2*(6*omega)  0  -
J2*(6*omega)^2 1 -T1Im(12);0 0 0 0 1];
P3_12=[1  0  0  0  0;-J3*(6*omega)^2  1  -c3*(6*omega)  0  -T2Re(12);0  0  1  0  0;c3*(6*omega)  0  -
J3*(6*omega)^2 1 -T2Im(12);0 0 0 0 1];
P4_12=[1  0  0  0  0;-J4*(6*omega)^2  1  -c4*(6*omega)  0  -T3Re(12);0  0  1  0  0;c4*(6*omega)  0  -
J4*(6*omega)^2 1 -T3Im(12);0 0 0 0 1];
P5_12=[1  0  0  0  0;-J5*(6*omega)^2  1  -c5*(6*omega)  0  -T4Re(12);0  0  1  0  0;c5*(6*omega)  0  -
J5*(6*omega)^2 1 -T4Im(12);0 0 0 0 1];
P6_12=[1  0  0  0  0;-J6*(6*omega)^2  1  -c6*(6*omega)  0  -T5Re(12);0  0  1  0  0;c6*(6*omega)  0  -
J6*(6*omega)^2 1 -T5Im(12);0 0 0 0 1];
P7_12=[1  0  0  0  0;-J7*(6*omega)^2  1  -c7*(6*omega)  0  -T6Re(12);0  0  1  0  0;c7*(6*omega)  0  -
J7*(6*omega)^2 1 -T6Im(12);0 0 0 0 1];
P8_12=[1 0 0 0 0;-J8*(6*omega)^2 1 0 0 0;0 0 1 0 0;0 0 -J8*(6*omega)^2 1 0;0 0 0 0 1];

F1_12=[1 1/k1 0 0 0;0 1 0 0 0;0 0 1 1/k1 0;0 0 0 1 0;0 0 0 0 1];
F2_12=[1 1/k2 0 0 0;0 1 0 0 0;0 0 1 1/k2 0;0 0 0 1 0;0 0 0 0 1];
F3_12=[1 1/k3 0 0 0;0 1 0 0 0;0 0 1 1/k3 0;0 0 0 1 0;0 0 0 0 1];
```

```
F4_12=[1 1/k4 0 0 0;0 1 0 0 0;0 0 1 1/k4 0;0 0 0 1 0;0 0 0 0 1];
F5_12=[1 1/k5 0 0 0;0 1 0 0 0;0 0 1 1/k5 0;0 0 0 1 0;0 0 0 0 1];
F6_12=[1 1/k6 0 0 0;0 1 0 0 0;0 0 1 1/k6 0;0 0 0 1 0;0 0 0 0 1];
F7_12=[1 1/k7 0 0 0;0 1 0 0 0;0 0 1 1/k7 0;0 0 0 1 0;0 0 0 0 1];

H12=P8_12*F7_12*P7_12*F6_12*P6_12*F5_12*P5_12*F4_12*P4_12*F3_12*P3_12*F2_12*P2_12*F1_
12*P1_12;

theta1_12Re=((H12(4,5)*H12(2,3))-(H12(2,5)*H12(4,3)))/((H12(2,1)*H12(4,3))-(H12(2,3)*H12(4,1)));
theta1_12Im=((-H12(4,5)*H12(2,1))+(H12(2,5)*H12(4,1)))/((H12(2,1)*H12(4,3))-(H12(2,3)*H12(4,1)));

Z1_12L=[theta1_12Re;0;theta1_12Im;0;1]
Z1_12R=P1_12*Z1_12L;
theta1_12=sqrt((Z1_12L(1))^2+(Z1_12L(3))^2)*180/pi
torque1_12L=sqrt((Z1_12L(2))^2+(Z1_12L(4))^2)
torque1_12R=sqrt((Z1_12R(2))^2+(Z1_12R(4))^2)

Z2_12L=F1_12*Z1_12R;
Z2_12R=P2_12*Z2_12L;
theta2_12=sqrt((Z2_12L(1))^2+(Z2_12L(3))^2)*180/pi
torque2_12R=sqrt((Z2_12R(2))^2+(Z2_12R(4))^2)

Z3_12L=F2_12*Z2_12R;
Z3_12R=P3_12*Z3_12L;
theta3_12=sqrt((Z3_12L(1))^2+(Z3_12L(3))^2)*180/pi
torque3_12R=sqrt((Z3_12R(2))^2+(Z3_12R(4))^2)

Z4_12L=F3_12*Z3_12R;
Z4_12R=P4_12*Z4_12L;
theta4_12=sqrt((Z4_12L(1))^2+(Z4_12L(3))^2)*180/pi
torque4_12R=sqrt((Z4_12R(2))^2+(Z4_12R(4))^2)

Z5_12L=F4_12*Z4_12R;
Z5_12R=P5_12*Z5_12L;
theta5_12=sqrt((Z5_12L(1))^2+(Z5_12L(3))^2)*180/pi
torque5_12R=sqrt((Z5_12R(2))^2+(Z5_12R(4))^2)

Z6_12L=F5_12*Z5_12R;
Z6_12R=P6_12*Z6_12L;
theta6_12=sqrt((Z6_12L(1))^2+(Z6_12L(3))^2)*180/pi
torque6_12R=sqrt((Z6_12R(2))^2+(Z6_12R(4))^2)

Z7_12L=F6_12*Z6_12R;
Z7_12R=P7_12*Z7_12L;
theta7_12=sqrt((Z7_12L(1))^2+(Z7_12L(3))^2)*180/pi
torque7_12R=sqrt((Z7_12R(2))^2+(Z7_12R(4))^2)

Z8_12L=F7_12*Z7_12R;
Z8_12R=P8_12*Z8_12L;
theta8_12=sqrt((Z8_12L(1))^2+(Z8_12L(3))^2)*180/pi
torque8_12R=sqrt((Z8_12R(2))^2+(Z8_12R(4))^2)


%6.5th order

P1_13=[1  0  0  0  0;-J1*(13*omega/2)^2  1  -c1*(13*omega/2)  0  0;0  0  1  0  0;c1*(13*omega/2)  0  -
J1*(13*omega/2)^2 1 0;0 0 0 0 1];
P2_13=[1  0  0  0  0;-J2*(13*omega/2)^2  1  -c2*(13*omega/2)  0  -T1Re(13);0  0  1  0  0;c2*(13*omega/2)  0  -
J2*(13*omega/2)^2 1 -T1Im(13);0 0 0 0 1];
```

```
P3_13=[1 0 0 0 0;-J3*(13*omega/2)^2 1 -c3*(13*omega/2) 0 -T2Re(13);0 0 1 0 0;c3*(13*omega/2) 0 -
J3*(13*omega/2)^2 1 -T2Im(13);0 0 0 0 1];
P4_13=[1 0 0 0 0;-J4*(13*omega/2)^2 1 -c4*(13*omega/2) 0 -T3Re(13);0 0 1 0 0;c4*(13*omega/2) 0 -
J4*(13*omega/2)^2 1 -T3Im(13);0 0 0 0 1];
P5_13=[1 0 0 0 0;-J5*(13*omega/2)^2 1 -c5*(13*omega/2) 0 -T4Re(13);0 0 1 0 0;c5*(13*omega/2) 0 -
J5*(13*omega/2)^2 1 -T4Im(13);0 0 0 0 1];
P6_13=[1 0 0 0 0;-J6*(13*omega/2)^2 1 -c6*(13*omega/2) 0 -T5Re(13);0 0 1 0 0;c6*(13*omega/2) 0 -
J6*(13*omega/2)^2 1 -T5Im(13);0 0 0 0 1];
P7_13=[1 0 0 0 0;-J7*(13*omega/2)^2 1 -c7*(13*omega/2) 0 -T6Re(13);0 0 1 0 0;c7*(13*omega/2) 0 -
J7*(13*omega/2)^2 1 -T6Im(13);0 0 0 0 1];
P8_13=[1 0 0 0 0;-J8*(13*omega/2)^2 1 0 0 0;0 0 1 0 0;0 0 -J8*(13*omega/2)^2 1 0;0 0 0 0 1];

F1_13=[1 1/k1 0 0 0;0 1 0 0 0;0 0 1 1/k1 0;0 0 0 1 0;0 0 0 0 1];
F2_13=[1 1/k2 0 0 0;0 1 0 0 0;0 0 1 1/k2 0;0 0 0 1 0;0 0 0 0 1];
F3_13=[1 1/k3 0 0 0;0 1 0 0 0;0 0 1 1/k3 0;0 0 0 1 0;0 0 0 0 1];
F4_13=[1 1/k4 0 0 0;0 1 0 0 0;0 0 1 1/k4 0;0 0 0 1 0;0 0 0 0 1];
F5_13=[1 1/k5 0 0 0;0 1 0 0 0;0 0 1 1/k5 0;0 0 0 1 0;0 0 0 0 1];
F6_13=[1 1/k6 0 0 0;0 1 0 0 0;0 0 1 1/k6 0;0 0 0 1 0;0 0 0 0 1];
F7_13=[1 1/k7 0 0 0;0 1 0 0 0;0 0 1 1/k7 0;0 0 0 1 0;0 0 0 0 1];

H13=P8_13*F7_13*P7_13*F6_13*P6_13*F5_13*P5_13*F4_13*P4_13*F3_13*P3_13*F2_13*P2_13*F1_
13*P1_13;

theta1_13Re=((H13(4,5)*H13(2,3))-(H13(2,5)*H13(4,3)))/((H13(2,1)*H13(4,3))-(H13(2,3)*H13(4,1)));
theta1_13Im=((-H13(4,5)*H13(2,1))+(H13(2,5)*H13(4,1)))/((H13(2,1)*H13(4,3))-(H13(2,3)*H13(4,1)));

Z1_13L=[theta1_13Re;0;theta1_13Im;0;1]
Z1_13R=P1_13*Z1_13L;
theta1_13=sqrt((Z1_13L(1))^2+(Z1_13L(3))^2)*180/pi
torque1_13L=sqrt((Z1_13L(2))^2+(Z1_13L(4))^2)
torque1_13R=sqrt((Z1_13R(2))^2+(Z1_13R(4))^2)

Z2_13L=F1_13*Z1_13R;
Z2_13R=P2_13*Z2_13L;
theta2_13=sqrt((Z2_13L(1))^2+(Z2_13L(3))^2)*180/pi
torque2_13R=sqrt((Z2_13R(2))^2+(Z2_13R(4))^2)

Z3_13L=F2_13*Z2_13R;
Z3_13R=P3_13*Z3_13L;
theta3_13=sqrt((Z3_13L(1))^2+(Z3_13L(3))^2)*180/pi
torque3_13R=sqrt((Z3_13R(2))^2+(Z3_13R(4))^2)

Z4_13L=F3_13*Z3_13R;
Z4_13R=P4_13*Z4_13L;
theta4_13=sqrt((Z4_13L(1))^2+(Z4_13L(3))^2)*180/pi
torque4_13R=sqrt((Z4_13R(2))^2+(Z4_13R(4))^2)

Z5_13L=F4_13*Z4_13R;
Z5_13R=P5_13*Z5_13L;
theta5_13=sqrt((Z5_13L(1))^2+(Z5_13L(3))^2)*180/pi
torque5_13R=sqrt((Z5_13R(2))^2+(Z5_13R(4))^2)

Z6_13L=F5_13*Z5_13R;
Z6_13R=P6_13*Z6_13L;
theta6_13=sqrt((Z6_13L(1))^2+(Z6_13L(3))^2)*180/pi
torque6_13R=sqrt((Z6_13R(2))^2+(Z6_13R(4))^2)

Z7_13L=F6_13*Z6_13R;
Z7_13R=P7_13*Z7_13L;
```

```
theta7_13=sqrt((Z7_13L(1))^2+(Z7_13L(3))^2)*180/pi
torque7_13R=sqrt((Z7_13R(2))^2+(Z7_13R(4))^2)

Z8_13L=F7_13*Z7_13R;
Z8_13R=P8_13*Z8_13L;
theta8_13=sqrt((Z8_13L(1))^2+(Z8_13L(3))^2)*180/pi
torque8_13R=sqrt((Z8_13R(2))^2+(Z8_13R(4))^2)


%7th order

P1_14=[1 0 0 0 0;-J1*(14*omega/2)^2 1 -c1*(14*omega/2) 0 0;0 0 1 0 0;c1*(14*omega/2) 0 -
J1*(14*omega/2)^2 1 0;0 0 0 0 1];
P2_14=[1 0 0 0 0;-J2*(14*omega/2)^2 1 -c2*(14*omega/2) 0 -T1Re(14);0 0 1 0 0;c2*(14*omega/2) 0 -
J2*(14*omega/2)^2 1 -T1Im(14);0 0 0 0 1];
P3_14=[1 0 0 0 0;-J3*(14*omega/2)^2 1 -c3*(14*omega/2) 0 -T2Re(14);0 0 1 0 0;c3*(14*omega/2) 0 -
J3*(14*omega/2)^2 1 -T2Im(14);0 0 0 0 1];
P4_14=[1 0 0 0 0;-J4*(14*omega/2)^2 1 -c4*(14*omega/2) 0 -T3Re(14);0 0 1 0 0;c4*(14*omega/2) 0 -
J4*(14*omega/2)^2 1 -T3Im(14);0 0 0 0 1];
P5_14=[1 0 0 0 0;-J5*(14*omega/2)^2 1 -c5*(14*omega/2) 0 -T4Re(14);0 0 1 0 0;c5*(14*omega/2) 0 -
J5*(14*omega/2)^2 1 -T4Im(14);0 0 0 0 1];
P6_14=[1 0 0 0 0;-J6*(14*omega/2)^2 1 -c6*(14*omega/2) 0 -T5Re(14);0 0 1 0 0;c6*(14*omega/2) 0 -
J6*(14*omega/2)^2 1 -T5Im(14);0 0 0 0 1];
P7_14=[1 0 0 0 0;-J7*(14*omega/2)^2 1 -c7*(14*omega/2) 0 -T6Re(14);0 0 1 0 0;c7*(14*omega/2) 0 -
J7*(14*omega/2)^2 1 -T6Im(14);0 0 0 0 1];
P8_14=[1 0 0 0 0;-J8*(14*omega/2)^2 1 0 0 0;0 0 1 0 0;0 0 -J8*(14*omega/2)^2 1 0;0 0 0 0 1];

F1_14=[1 1/k1 0 0 0;0 1 0 0 0;0 0 1 1/k1 0;0 0 0 1 0;0 0 0 0 1];
F2_14=[1 1/k2 0 0 0;0 1 0 0 0;0 0 1 1/k2 0;0 0 0 1 0;0 0 0 0 1];
F3_14=[1 1/k3 0 0 0;0 1 0 0 0;0 0 1 1/k3 0;0 0 0 1 0;0 0 0 0 1];
F4_14=[1 1/k4 0 0 0;0 1 0 0 0;0 0 1 1/k4 0;0 0 0 1 0;0 0 0 0 1];
F5_14=[1 1/k5 0 0 0;0 1 0 0 0;0 0 1 1/k5 0;0 0 0 1 0;0 0 0 0 1];
F6_14=[1 1/k6 0 0 0;0 1 0 0 0;0 0 1 1/k6 0;0 0 0 1 0;0 0 0 0 1];
F7_14=[1 1/k7 0 0 0;0 1 0 0 0;0 0 1 1/k7 0;0 0 0 1 0;0 0 0 0 1];

H14=P8_14*F7_14*P7_14*F6_14*P6_14*F5_14*P5_14*F4_14*P4_14*F3_14*P3_14*F2_14*P2_14*F1_
14*P1_14;

theta1_14Re=((H14(4,5)*H14(2,3))-(H14(2,5)*H14(4,3)))/((H14(2,1)*H14(4,3))-(H14(2,3)*H14(4,1)));
theta1_14Im=((-H14(4,5)*H14(2,1))+(H14(2,5)*H14(4,1)))/((H14(2,1)*H14(4,3))-(H14(2,3)*H14(4,1)));

Z1_14L=[theta1_14Re;0;theta1_14Im;0;1]
Z1_14R=P1_14*Z1_14L;
theta1_14=sqrt((Z1_14L(1))^2+(Z1_14L(3))^2)*180/pi
torque1_14L=sqrt((Z1_14L(2))^2+(Z1_14L(4))^2)
torque1_14R=sqrt((Z1_14R(2))^2+(Z1_14R(4))^2)

Z2_14L=F1_14*Z1_14R;
Z2_14R=P2_14*Z2_14L;
theta2_14=sqrt((Z2_14L(1))^2+(Z2_14L(3))^2)*180/pi
torque2_14R=sqrt((Z2_14R(2))^2+(Z2_14R(4))^2)

Z3_14L=F2_14*Z2_14R;
Z3_14R=P3_14*Z3_14L;
theta3_14=sqrt((Z3_14L(1))^2+(Z3_14L(3))^2)*180/pi
torque3_14R=sqrt((Z3_14R(2))^2+(Z3_14R(4))^2)

Z4_14L=F3_14*Z3_14R;
Z4_14R=P4_14*Z4_14L;
```

```
theta4_14=sqrt((Z4_14L(1))^2+(Z4_14L(3))^2)*180/pi
torque4_14R=sqrt((Z4_14R(2))^2+(Z4_14R(4))^2)

Z5_14L=F4_14*Z4_14R;
Z5_14R=P5_14*Z5_14L;
theta5_14=sqrt((Z5_14L(1))^2+(Z5_14L(3))^2)*180/pi
torque5_14R=sqrt((Z5_14R(2))^2+(Z5_14R(4))^2)

Z6_14L=F5_14*Z5_14R;
Z6_14R=P6_14*Z6_14L;
theta6_14=sqrt((Z6_14L(1))^2+(Z6_14L(3))^2)*180/pi
torque6_14R=sqrt((Z6_14R(2))^2+(Z6_14R(4))^2)

Z7_14L=F6_14*Z6_14R;
Z7_14R=P7_14*Z7_14L;
theta7_14=sqrt((Z7_14L(1))^2+(Z7_14L(3))^2)*180/pi
torque7_14R=sqrt((Z7_14R(2))^2+(Z7_14R(4))^2)

Z8_14L=F7_14*Z7_14R;
Z8_14R=P8_14*Z8_14L;
theta8_14=sqrt((Z8_14L(1))^2+(Z8_14L(3))^2)*180/pi
torque8_14R=sqrt((Z8_14R(2))^2+(Z8_14R(4))^2)


%7.5th order

P1_15=[1  0  0  0  0;-J1*(15*omega/2)^2  1  -c1*(15*omega/2)  0  0;0  0  1  0  0;c1*(15*omega/2)  0  -
J1*(15*omega/2)^2 1 0;0 0 0 0 1];
P2_15=[1  0  0  0  0;-J2*(15*omega/2)^2  1  -c2*(15*omega/2)  0  -T1Re(15);0  0  1  0  0;c2*(15*omega/2)  0  -
J2*(15*omega/2)^2 1 -T1Im(15);0 0 0 0 1];
P3_15=[1  0  0  0  0;-J3*(15*omega/2)^2  1  -c3*(15*omega/2)  0  -T2Re(15);0  0  1  0  0;c3*(15*omega/2)  0  -
J3*(15*omega/2)^2 1 -T2Im(15);0 0 0 0 1];
P4_15=[1  0  0  0  0;-J4*(15*omega/2)^2  1  -c4*(15*omega/2)  0  -T3Re(15);0  0  1  0  0;c4*(15*omega/2)  0  -
J4*(15*omega/2)^2 1 -T3Im(15);0 0 0 0 1];
P5_15=[1  0  0  0  0;-J5*(15*omega/2)^2  1  -c5*(15*omega/2)  0  -T4Re(15);0  0  1  0  0;c5*(15*omega/2)  0  -
J5*(15*omega/2)^2 1 -T4Im(15);0 0 0 0 1];
P6_15=[1  0  0  0  0;-J6*(15*omega/2)^2  1  -c6*(15*omega/2)  0  -T5Re(15);0  0  1  0  0;c6*(15*omega/2)  0  -
J6*(15*omega/2)^2 1 -T5Im(15);0 0 0 0 1];
P7_15=[1  0  0  0  0;-J7*(15*omega/2)^2  1  -c7*(15*omega/2)  0  -T6Re(15);0  0  1  0  0;c7*(15*omega/2)  0  -
J7*(15*omega/2)^2 1 -T6Im(15);0 0 0 0 1];
P8_15=[1 0 0 0 0;-J8*(15*omega/2)^2 1 0 0 0;0 0 1 0 0;0 0 -J8*(15*omega/2)^2 1 0;0 0 0 0 1];

F1_15=[1 1/k1 0 0 0;0 1 0 0 0;0 0 1 1/k1 0;0 0 0 1 0;0 0 0 0 1];
F2_15=[1 1/k2 0 0 0;0 1 0 0 0;0 0 1 1/k2 0;0 0 0 1 0;0 0 0 0 1];
F3_15=[1 1/k3 0 0 0;0 1 0 0 0;0 0 1 1/k3 0;0 0 0 1 0;0 0 0 0 1];
F4_15=[1 1/k4 0 0 0;0 1 0 0 0;0 0 1 1/k4 0;0 0 0 1 0;0 0 0 0 1];
F5_15=[1 1/k5 0 0 0;0 1 0 0 0;0 0 1 1/k5 0;0 0 0 1 0;0 0 0 0 1];
F6_15=[1 1/k6 0 0 0;0 1 0 0 0;0 0 1 1/k6 0;0 0 0 1 0;0 0 0 0 1];
F7_15=[1 1/k7 0 0 0;0 1 0 0 0;0 0 1 1/k7 0;0 0 0 1 0;0 0 0 0 1];

H15=P8_15*F7_15*P7_15*F6_15*P6_15*F5_15*P5_15*F4_15*P4_15*F3_15*P3_15*F2_15*P2_15*F1_
15*P1_15;

theta1_15Re=((H15(4,5)*H15(2,3))-(H15(2,5)*H15(4,3)))/((H15(2,1)*H15(4,3))-(H15(2,3)*H15(4,1)));
theta1_15Im=((-H15(4,5)*H15(2,1))+(H15(2,5)*H15(4,1)))/((H15(2,1)*H15(4,3))-(H15(2,3)*H15(4,1)));

Z1_15L=[theta1_15Re;0;theta1_15Im;0;1]
Z1_15R=P1_15*Z1_15L;
theta1_15=sqrt((Z1_15L(1))^2+(Z1_15L(3))^2)*180/pi
```

```
torque1_15L=sqrt((Z1_15L(2))^2+(Z1_15L(4))^2)
torque1_15R=sqrt((Z1_15R(2))^2+(Z1_15R(4))^2)

Z2_15L=F1_15*Z1_15R;
Z2_15R=P2_15*Z2_15L;
theta2_15=sqrt((Z2_15L(1))^2+(Z2_15L(3))^2)*180/pi
torque2_15R=sqrt((Z2_15R(2))^2+(Z2_15R(4))^2)

Z3_15L=F2_15*Z2_15R;
Z3_15R=P3_15*Z3_15L;
theta3_15=sqrt((Z3_15L(1))^2+(Z3_15L(3))^2)*180/pi
torque3_15R=sqrt((Z3_15R(2))^2+(Z3_15R(4))^2)

Z4_15L=F3_15*Z3_15R;
Z4_15R=P4_15*Z4_15L;
theta4_15=sqrt((Z4_15L(1))^2+(Z4_15L(3))^2)*180/pi
torque4_15R=sqrt((Z4_15R(2))^2+(Z4_15R(4))^2)

Z5_15L=F4_15*Z4_15R;
Z5_15R=P5_15*Z5_15L;
theta5_15=sqrt((Z5_15L(1))^2+(Z5_15L(3))^2)*180/pi
torque5_15R=sqrt((Z5_15R(2))^2+(Z5_15R(4))^2)

Z6_15L=F5_15*Z5_15R;
Z6_15R=P6_15*Z6_15L;
theta6_15=sqrt((Z6_15L(1))^2+(Z6_15L(3))^2)*180/pi
torque6_15R=sqrt((Z6_15R(2))^2+(Z6_15R(4))^2)

Z7_15L=F6_15*Z6_15R;
Z7_15R=P7_15*Z7_15L;
theta7_15=sqrt((Z7_15L(1))^2+(Z7_15L(3))^2)*180/pi
torque7_15R=sqrt((Z7_15R(2))^2+(Z7_15R(4))^2)

Z8_15L=F7_15*Z7_15R;
Z8_15R=P8_15*Z8_15L;
theta8_15=sqrt((Z8_15L(1))^2+(Z8_15L(3))^2)*180/pi
torque8_15R=sqrt((Z8_15R(2))^2+(Z8_15R(4))^2)


%8th order

P1_16=[1  0  0  0  0;-J1*(16*omega/2)^2  1  -c1*(16*omega/2)  0  0;0  0  1  0  0;c1*(16*omega/2)  0  -
J1*(16*omega/2)^2 1 0;0 0 0 0 1];
P2_16=[1  0  0  0  0;-J2*(16*omega/2)^2  1  -c2*(16*omega/2)  0  -T1Re(16);0  0  1  0  0;c2*(16*omega/2)  0  -
J2*(16*omega/2)^2 1 -T1Im(16);0 0 0 0 1];
P3_16=[1  0  0  0  0;-J3*(16*omega/2)^2  1  -c3*(16*omega/2)  0  -T2Re(16);0  0  1  0  0;c3*(16*omega/2)  0  -
J3*(16*omega/2)^2 1 -T2Im(16);0 0 0 0 1];
P4_16=[1  0  0  0  0;-J4*(16*omega/2)^2  1  -c4*(16*omega/2)  0  -T3Re(16);0  0  1  0  0;c4*(16*omega/2)  0  -
J4*(16*omega/2)^2 1 -T3Im(16);0 0 0 0 1];
P5_16=[1  0  0  0  0;-J5*(16*omega/2)^2  1  -c5*(16*omega/2)  0  -T4Re(16);0  0  1  0  0;c5*(16*omega/2)  0  -
J5*(16*omega/2)^2 1 -T4Im(16);0 0 0 0 1];
P6_16=[1  0  0  0  0;-J6*(16*omega/2)^2  1  -c6*(16*omega/2)  0  -T5Re(16);0  0  1  0  0;c6*(16*omega/2)  0  -
J6*(16*omega/2)^2 1 -T5Im(16);0 0 0 0 1];
P7_16=[1  0  0  0  0;-J7*(16*omega/2)^2  1  -c7*(16*omega/2)  0  -T6Re(16);0  0  1  0  0;c7*(16*omega/2)  0  -
J7*(16*omega/2)^2 1 -T6Im(16);0 0 0 0 1];
P8_16=[1 0 0 0 0;-J8*(16*omega/2)^2 1 0 0 0;0 0 1 0 0;0 0 -J8*(16*omega/2)^2 1 0;0 0 0 0 1];

F1_16=[1 1/k1 0 0 0;0 1 0 0 0;0 0 1 1/k1 0;0 0 0 1 0;0 0 0 0 1];
F2_16=[1 1/k2 0 0 0;0 1 0 0 0;0 0 1 1/k2 0;0 0 0 1 0;0 0 0 0 1];
```

```
F3_16=[1 1/k3 0 0 0;0 1 0 0 0;0 0 1 1/k3 0;0 0 0 1 0;0 0 0 0 1];
F4_16=[1 1/k4 0 0 0;0 1 0 0 0;0 0 1 1/k4 0;0 0 0 1 0;0 0 0 0 1];
F5_16=[1 1/k5 0 0 0;0 1 0 0 0;0 0 1 1/k5 0;0 0 0 1 0;0 0 0 0 1];
F6_16=[1 1/k6 0 0 0;0 1 0 0 0;0 0 1 1/k6 0;0 0 0 1 0;0 0 0 0 1];
F7_16=[1 1/k7 0 0 0;0 1 0 0 0;0 0 1 1/k7 0;0 0 0 1 0;0 0 0 0 1];

H16=P8_16*F7_16*P7_16*F6_16*P6_16*F5_16*P5_16*F4_16*P4_16*F3_16*P3_16*F2_16*P2_16*F1_
16*P1_16;

theta1_16Re=((H16(4,5)*H16(2,3))-(H16(2,5)*H16(4,3)))/((H16(2,1)*H16(4,3))-(H16(2,3)*H16(4,1)));
theta1_16Im=((-H16(4,5)*H16(2,1))+(H16(2,5)*H16(4,1)))/((H16(2,1)*H16(4,3))-(H16(2,3)*H16(4,1)));

Z1_16L=[theta1_16Re;0;theta1_16Im;0;1]
Z1_16R=P1_16*Z1_16L;
theta1_16=sqrt((Z1_16L(1))^2+(Z1_16L(3))^2)*180/pi
torque1_16L=sqrt((Z1_16L(2))^2+(Z1_16L(4))^2)
torque1_16R=sqrt((Z1_16R(2))^2+(Z1_16R(4))^2)

Z2_16L=F1_16*Z1_16R;
Z2_16R=P2_16*Z2_16L;
theta2_16=sqrt((Z2_16L(1))^2+(Z2_16L(3))^2)*180/pi
torque2_16R=sqrt((Z2_16R(2))^2+(Z2_16R(4))^2)

Z3_16L=F2_16*Z2_16R;
Z3_16R=P3_16*Z3_16L;
theta3_16=sqrt((Z3_16L(1))^2+(Z3_16L(3))^2)*180/pi
torque3_16R=sqrt((Z3_16R(2))^2+(Z3_16R(4))^2)

Z4_16L=F3_16*Z3_16R;
Z4_16R=P4_16*Z4_16L;
theta4_16=sqrt((Z4_16L(1))^2+(Z4_16L(3))^2)*180/pi
torque4_16R=sqrt((Z4_16R(2))^2+(Z4_16R(4))^2)

Z5_16L=F4_16*Z4_16R;
Z5_16R=P5_16*Z5_16L;
theta5_16=sqrt((Z5_16L(1))^2+(Z5_16L(3))^2)*180/pi
torque5_16R=sqrt((Z5_16R(2))^2+(Z5_16R(4))^2)

Z6_16L=F5_16*Z5_16R;
Z6_16R=P6_16*Z6_16L;
theta6_16=sqrt((Z6_16L(1))^2+(Z6_16L(3))^2)*180/pi
torque6_16R=sqrt((Z6_16R(2))^2+(Z6_16R(4))^2)

Z7_16L=F6_16*Z6_16R;
Z7_16R=P7_16*Z7_16L;
theta7_16=sqrt((Z7_16L(1))^2+(Z7_16L(3))^2)*180/pi
torque7_16R=sqrt((Z7_16R(2))^2+(Z7_16R(4))^2)

Z8_16L=F7_16*Z7_16R;
Z8_16R=P8_16*Z8_16L;
theta8_16=sqrt((Z8_16L(1))^2+(Z8_16L(3))^2)*180/pi
torque8_16R=sqrt((Z8_16R(2))^2+(Z8_16R(4))^2)


%8.5th order

P1_17=[1  0  0  0  0;-J1*(17*omega/2)^2  1  -c1*(17*omega/2)  0  0;0  0  1  0  0;c1*(17*omega/2)  0  -
J1*(17*omega/2)^2 1 0;0 0 0 0 1];
```

```
P2_17=[1 0 0 0 0;-J2*(17*omega/2)^2 1 -c2*(17*omega/2) 0 -T1Re(17);0 0 1 0 0;c2*(17*omega/2) 0 -
J2*(17*omega/2)^2 1 -T1Im(17);0 0 0 0 1];
P3_17=[1 0 0 0 0;-J3*(17*omega/2)^2 1 -c3*(17*omega/2) 0 -T2Re(17);0 0 1 0 0;c3*(17*omega/2) 0 -
J3*(17*omega/2)^2 1 -T2Im(17);0 0 0 0 1];
P4_17=[1 0 0 0 0;-J4*(17*omega/2)^2 1 -c4*(17*omega/2) 0 -T3Re(17);0 0 1 0 0;c4*(17*omega/2) 0 -
J4*(17*omega/2)^2 1 -T3Im(17);0 0 0 0 1];
P5_17=[1 0 0 0 0;-J5*(17*omega/2)^2 1 -c5*(17*omega/2) 0 -T4Re(17);0 0 1 0 0;c5*(17*omega/2) 0 -
J5*(17*omega/2)^2 1 -T4Im(17);0 0 0 0 1];
P6_17=[1 0 0 0 0;-J6*(17*omega/2)^2 1 -c6*(17*omega/2) 0 -T5Re(17);0 0 1 0 0;c6*(17*omega/2) 0 -
J6*(17*omega/2)^2 1 -T5Im(17);0 0 0 0 1];
P7_17=[1 0 0 0 0;-J7*(17*omega/2)^2 1 -c7*(17*omega/2) 0 -T6Re(17);0 0 1 0 0;c7*(17*omega/2) 0 -
J7*(17*omega/2)^2 1 -T6Im(17);0 0 0 0 1];
P8_17=[1 0 0 0 0;-J8*(17*omega/2)^2 1 0 0 0;0 0 1 0 0;0 0 -J8*(17*omega/2)^2 1 0;0 0 0 0 1];

F1_17=[1 1/k1 0 0 0;0 1 0 0 0;0 0 1 1/k1 0;0 0 0 1 0;0 0 0 0 1];
F2_17=[1 1/k2 0 0 0;0 1 0 0 0;0 0 1 1/k2 0;0 0 0 1 0;0 0 0 0 1];
F3_17=[1 1/k3 0 0 0;0 1 0 0 0;0 0 1 1/k3 0;0 0 0 1 0;0 0 0 0 1];
F4_17=[1 1/k4 0 0 0;0 1 0 0 0;0 0 1 1/k4 0;0 0 0 1 0;0 0 0 0 1];
F5_17=[1 1/k5 0 0 0;0 1 0 0 0;0 0 1 1/k5 0;0 0 0 1 0;0 0 0 0 1];
F6_17=[1 1/k6 0 0 0;0 1 0 0 0;0 0 1 1/k6 0;0 0 0 1 0;0 0 0 0 1];
F7_17=[1 1/k7 0 0 0;0 1 0 0 0;0 0 1 1/k7 0;0 0 0 1 0;0 0 0 0 1];

H17=P8_17*F7_17*P7_17*F6_17*P6_17*F5_17*P5_17*F4_17*P4_17*F3_17*P3_17*F2_17*P2_17*F1_
17*P1_17;

theta1_17Re=((H17(4,5)*H17(2,3))-(H17(2,5)*H17(4,3)))/((H17(2,1)*H17(4,3))-(H17(2,3)*H17(4,1)));
theta1_17Im=((-H17(4,5)*H17(2,1))+(H17(2,5)*H17(4,1)))/((H17(2,1)*H17(4,3))-(H17(2,3)*H17(4,1)));

Z1_17L=[theta1_17Re;0;theta1_17Im;0;1]
Z1_17R=P1_17*Z1_17L;
theta1_17=sqrt((Z1_17L(1))^2+(Z1_17L(3))^2)*180/pi
torque1_17L=sqrt((Z1_17L(2))^2+(Z1_17L(4))^2)
torque1_17R=sqrt((Z1_17R(2))^2+(Z1_17R(4))^2)

Z2_17L=F1_17*Z1_17R;
Z2_17R=P2_17*Z2_17L;
theta2_17=sqrt((Z2_17L(1))^2+(Z2_17L(3))^2)*180/pi
torque2_17R=sqrt((Z2_17R(2))^2+(Z2_17R(4))^2)

Z3_17L=F2_17*Z2_17R;
Z3_17R=P3_17*Z3_17L;
theta3_17=sqrt((Z3_17L(1))^2+(Z3_17L(3))^2)*180/pi
torque3_17R=sqrt((Z3_17R(2))^2+(Z3_17R(4))^2)

Z4_17L=F3_17*Z3_17R;
Z4_17R=P4_17*Z4_17L;
theta4_17=sqrt((Z4_17L(1))^2+(Z4_17L(3))^2)*180/pi
torque4_17R=sqrt((Z4_17R(2))^2+(Z4_17R(4))^2)

Z5_17L=F4_17*Z4_17R;
Z5_17R=P5_17*Z5_17L;
theta5_17=sqrt((Z5_17L(1))^2+(Z5_17L(3))^2)*180/pi
torque5_17R=sqrt((Z5_17R(2))^2+(Z5_17R(4))^2)

Z6_17L=F5_17*Z5_17R;
Z6_17R=P6_17*Z6_17L;
theta6_17=sqrt((Z6_17L(1))^2+(Z6_17L(3))^2)*180/pi
torque6_17R=sqrt((Z6_17R(2))^2+(Z6_17R(4))^2)
```

```
Z7_17L=F6_17*Z6_17R;
Z7_17R=P7_17*Z7_17L;
theta7_17=sqrt((Z7_17L(1))^2+(Z7_17L(3))^2)*180/pi
torque7_17R=sqrt((Z7_17R(2))^2+(Z7_17R(4))^2)

Z8_17L=F7_17*Z7_17R;
Z8_17R=P8_17*Z8_17L;
theta8_17=sqrt((Z8_17L(1))^2+(Z8_17L(3))^2)*180/pi
torque8_17R=sqrt((Z8_17R(2))^2+(Z8_17R(4))^2)


%9th order

P1_18=[1 0 0 0 0;-J1*(18*omega/2)^2 1 -c1*(18*omega/2) 0 0;0 0 1 0 0;c1*(18*omega/2) 0 -
J1*(18*omega/2)^2 1 0;0 0 0 0 1];
P2_18=[1 0 0 0 0;-J2*(18*omega/2)^2 1 -c2*(18*omega/2) 0 -T1Re(18);0 0 1 0 0;c2*(18*omega/2) 0 -
J2*(18*omega/2)^2 1 -T1Im(18);0 0 0 0 1];
P3_18=[1 0 0 0 0;-J3*(18*omega/2)^2 1 -c3*(18*omega/2) 0 -T2Re(18);0 0 1 0 0;c3*(18*omega/2) 0 -
J3*(18*omega/2)^2 1 -T2Im(18);0 0 0 0 1];
P4_18=[1 0 0 0 0;-J4*(18*omega/2)^2 1 -c4*(18*omega/2) 0 -T3Re(18);0 0 1 0 0;c4*(18*omega/2) 0 -
J4*(18*omega/2)^2 1 -T3Im(18);0 0 0 0 1];
P5_18=[1 0 0 0 0;-J5*(18*omega/2)^2 1 -c5*(18*omega/2) 0 -T4Re(18);0 0 1 0 0;c5*(18*omega/2) 0 -
J5*(18*omega/2)^2 1 -T4Im(18);0 0 0 0 1];
P6_18=[1 0 0 0 0;-J6*(18*omega/2)^2 1 -c6*(18*omega/2) 0 -T5Re(18);0 0 1 0 0;c6*(18*omega/2) 0 -
J6*(18*omega/2)^2 1 -T5Im(18);0 0 0 0 1];
P7_18=[1 0 0 0 0;-J7*(18*omega/2)^2 1 -c7*(18*omega/2) 0 -T6Re(18);0 0 1 0 0;c7*(18*omega/2) 0 -
J7*(18*omega/2)^2 1 -T6Im(18);0 0 0 0 1];
P8_18=[1 0 0 0 0;-J8*(18*omega/2)^2 1 0 0 0;0 0 1 0 0;0 0 -J8*(18*omega/2)^2 1 0;0 0 0 0 1];

F1_18=[1 1/k1 0 0 0;0 1 0 0 0;0 0 1 1/k1 0;0 0 0 1 0;0 0 0 0 1];
F2_18=[1 1/k2 0 0 0;0 1 0 0 0;0 0 1 1/k2 0;0 0 0 1 0;0 0 0 0 1];
F3_18=[1 1/k3 0 0 0;0 1 0 0 0;0 0 1 1/k3 0;0 0 0 1 0;0 0 0 0 1];
F4_18=[1 1/k4 0 0 0;0 1 0 0 0;0 0 1 1/k4 0;0 0 0 1 0;0 0 0 0 1];
F5_18=[1 1/k5 0 0 0;0 1 0 0 0;0 0 1 1/k5 0;0 0 0 1 0;0 0 0 0 1];
F6_18=[1 1/k6 0 0 0;0 1 0 0 0;0 0 1 1/k6 0;0 0 0 1 0;0 0 0 0 1];
F7_18=[1 1/k7 0 0 0;0 1 0 0 0;0 0 1 1/k7 0;0 0 0 1 0;0 0 0 0 1];

H18=P8_18*F7_18*P7_18*F6_18*P6_18*F5_18*P5_18*F4_18*P4_18*F3_18*P3_18*F2_18*P2_18*F1_
18*P1_18;

theta1_18Re=((H18(4,5)*H18(2,3))-(H18(2,5)*H18(4,3)))/((H18(2,1)*H18(4,3))-(H18(2,3)*H18(4,1)));
theta1_18Im=((-H18(4,5)*H18(2,1))+(H18(2,5)*H18(4,1)))/((H18(2,1)*H18(4,3))-(H18(2,3)*H18(4,1)));

Z1_18L=[theta1_18Re;0;theta1_18Im;0;1]
Z1_18R=P1_18*Z1_18L;
theta1_18=sqrt((Z1_18L(1))^2+(Z1_18L(3))^2)*180/pi
torque1_18L=sqrt((Z1_18L(2))^2+(Z1_18L(4))^2)
torque1_18R=sqrt((Z1_18R(2))^2+(Z1_18R(4))^2)

Z2_18L=F1_18*Z1_18R;
Z2_18R=P2_18*Z2_18L;
theta2_18=sqrt((Z2_18L(1))^2+(Z2_18L(3))^2)*180/pi
torque2_18R=sqrt((Z2_18R(2))^2+(Z2_18R(4))^2)

Z3_18L=F2_18*Z2_18R;
Z3_18R=P3_18*Z3_18L;
theta3_18=sqrt((Z3_18L(1))^2+(Z3_18L(3))^2)*180/pi
torque3_18R=sqrt((Z3_18R(2))^2+(Z3_18R(4))^2)
```

```
Z4_18L=F3_18*Z3_18R;
Z4_18R=P4_18*Z4_18L;
theta4_18=sqrt((Z4_18L(1))^2+(Z4_18L(3))^2)*180/pi
torque4_18R=sqrt((Z4_18R(2))^2+(Z4_18R(4))^2)

Z5_18L=F4_18*Z4_18R;
Z5_18R=P5_18*Z5_18L;
theta5_18=sqrt((Z5_18L(1))^2+(Z5_18L(3))^2)*180/pi
torque5_18R=sqrt((Z5_18R(2))^2+(Z5_18R(4))^2)

Z6_18L=F5_18*Z5_18R;
Z6_18R=P6_18*Z6_18L;
theta6_18=sqrt((Z6_18L(1))^2+(Z6_18L(3))^2)*180/pi
torque6_18R=sqrt((Z6_18R(2))^2+(Z6_18R(4))^2)

Z7_18L=F6_18*Z6_18R;
Z7_18R=P7_18*Z7_18L;
theta7_18=sqrt((Z7_18L(1))^2+(Z7_18L(3))^2)*180/pi
torque7_18R=sqrt((Z7_18R(2))^2+(Z7_18R(4))^2)

Z8_18L=F7_18*Z7_18R;
Z8_18R=P8_18*Z8_18L;
theta8_18=sqrt((Z8_18L(1))^2+(Z8_18L(3))^2)*180/pi
torque8_18R=sqrt((Z8_18R(2))^2+(Z8_18R(4))^2)


%9.5th order

P1_19=[1  0  0  0  0;-J1*(19*omega/2)^2  1  -c1*(19*omega/2)  0  0;0  0  1  0  0;c1*(19*omega/2)  0  -
J1*(19*omega/2)^2 1 0;0 0 0 0 1];
P2_19=[1 0 0 0 0;-J2*(19*omega/2)^2 1 -c2*(19*omega/2) 0 -T1Re(19);0 0 1 0 0;c2*(19*omega/2) 0 -
J2*(19*omega/2)^2 1 -T1Im(19);0 0 0 0 1];
P3_19=[1 0 0 0 0;-J3*(19*omega/2)^2 1 -c3*(19*omega/2) 0 -T2Re(19);0 0 1 0 0;c3*(19*omega/2) 0 -
J3*(19*omega/2)^2 1 -T2Im(19);0 0 0 0 1];
P4_19=[1 0 0 0 0;-J4*(19*omega/2)^2 1 -c4*(19*omega/2) 0 -T3Re(19);0 0 1 0 0;c4*(19*omega/2) 0 -
J4*(19*omega/2)^2 1 -T3Im(19);0 0 0 0 1];
P5_19=[1 0 0 0 0;-J5*(19*omega/2)^2 1 -c5*(19*omega/2) 0 -T4Re(19);0 0 1 0 0;c5*(19*omega/2) 0 -
J5*(19*omega/2)^2 1 -T4Im(19);0 0 0 0 1];
P6_19=[1 0 0 0 0;-J6*(19*omega/2)^2 1 -c6*(19*omega/2) 0 -T5Re(19);0 0 1 0 0;c6*(19*omega/2) 0 -
J6*(19*omega/2)^2 1 -T5Im(19);0 0 0 0 1];
P7_19=[1 0 0 0 0;-J7*(19*omega/2)^2 1 -c7*(19*omega/2) 0 -T6Re(19);0 0 1 0 0;c7*(19*omega/2) 0 -
J7*(19*omega/2)^2 1 -T6Im(19);0 0 0 0 1];
P8_19=[1 0 0 0 0;-J8*(19*omega/2)^2 1 0 0 0;0 0 1 0 0;0 0 -J8*(19*omega/2)^2 1 0;0 0 0 0 1];

F1_19=[1 1/k1 0 0 0;0 1 0 0 0;0 0 1 1/k1 0;0 0 0 1 0;0 0 0 0 1];
F2_19=[1 1/k2 0 0 0;0 1 0 0 0;0 0 1 1/k2 0;0 0 0 1 0;0 0 0 0 1];
F3_19=[1 1/k3 0 0 0;0 1 0 0 0;0 0 1 1/k3 0;0 0 0 1 0;0 0 0 0 1];
F4_19=[1 1/k4 0 0 0;0 1 0 0 0;0 0 1 1/k4 0;0 0 0 1 0;0 0 0 0 1];
F5_19=[1 1/k5 0 0 0;0 1 0 0 0;0 0 1 1/k5 0;0 0 0 1 0;0 0 0 0 1];
F6_19=[1 1/k6 0 0 0;0 1 0 0 0;0 0 1 1/k6 0;0 0 0 1 0;0 0 0 0 1];
F7_19=[1 1/k7 0 0 0;0 1 0 0 0;0 0 1 1/k7 0;0 0 0 1 0;0 0 0 0 1];

H19=P8_19*F7_19*P7_19*F6_19*P6_19*F5_19*P5_19*F4_19*P4_19*F3_19*P3_19*F2_19*P2_19*F1_
19*P1_19;

theta1_19Re=((H19(4,5)*H19(2,3))-(H19(2,5)*H19(4,3)))/((H19(2,1)*H19(4,3))-(H19(2,3)*H19(4,1)));
theta1_19Im=((-H19(4,5)*H19(2,1))+(H19(2,5)*H19(4,1)))/((H19(2,1)*H19(4,3))-(H19(2,3)*H19(4,1)));

Z1_19L=[theta1_19Re;0;theta1_19Im;0;1]
```

```
Z1_19R=P1_19*Z1_19L;
theta1_19=sqrt((Z1_19L(1))^2+(Z1_19L(3))^2)*180/pi
torque1_19L=sqrt((Z1_19L(2))^2+(Z1_19L(4))^2)
torque1_19R=sqrt((Z1_19R(2))^2+(Z1_19R(4))^2)

Z2_19L=F1_19*Z1_19R;
Z2_19R=P2_19*Z2_19L;
theta2_19=sqrt((Z2_19L(1))^2+(Z2_19L(3))^2)*180/pi
torque2_19R=sqrt((Z2_19R(2))^2+(Z2_19R(4))^2)

Z3_19L=F2_19*Z2_19R;
Z3_19R=P3_19*Z3_19L;
theta3_19=sqrt((Z3_19L(1))^2+(Z3_19L(3))^2)*180/pi
torque3_19R=sqrt((Z3_19R(2))^2+(Z3_19R(4))^2)

Z4_19L=F3_19*Z3_19R;
Z4_19R=P4_19*Z4_19L;
theta4_19=sqrt((Z4_19L(1))^2+(Z4_19L(3))^2)*180/pi
torque4_19R=sqrt((Z4_19R(2))^2+(Z4_19R(4))^2)

Z5_19L=F4_19*Z4_19R;
Z5_19R=P5_19*Z5_19L;
theta5_19=sqrt((Z5_19L(1))^2+(Z5_19L(3))^2)*180/pi
torque5_19R=sqrt((Z5_19R(2))^2+(Z5_19R(4))^2)

Z6_19L=F5_19*Z5_19R;
Z6_19R=P6_19*Z6_19L;
theta6_19=sqrt((Z6_19L(1))^2+(Z6_19L(3))^2)*180/pi
torque6_19R=sqrt((Z6_19R(2))^2+(Z6_19R(4))^2)

Z7_19L=F6_19*Z6_19R;
Z7_19R=P7_19*Z7_19L;
theta7_19=sqrt((Z7_19L(1))^2+(Z7_19L(3))^2)*180/pi
torque7_19R=sqrt((Z7_19R(2))^2+(Z7_19R(4))^2)

Z8_19L=F7_19*Z7_19R;
Z8_19R=P8_19*Z8_19L;
theta8_19=sqrt((Z8_19L(1))^2+(Z8_19L(3))^2)*180/pi
torque8_19R=sqrt((Z8_19R(2))^2+(Z8_19R(4))^2)


%10th order

P1_20=[1  0  0  0  0;-J1*(20*omega/2)^2  1  -c1*(20*omega/2)  0  0;0  0  1  0  0;c1*(20*omega/2)  0  -
J1*(20*omega/2)^2 1 0;0 0 0 0 1];
P2_20=[1 0 0 0 0;-J2*(20*omega/2)^2 1 -c2*(20*omega/2) 0 -T1Re(20);0 0 1 0 0;c2*(20*omega/2) 0 -
J2*(20*omega/2)^2 1 -T1Im(20);0 0 0 0 1];
P3_20=[1 0 0 0 0;-J3*(20*omega/2)^2 1 -c3*(20*omega/2) 0 -T2Re(20);0 0 1 0 0;c3*(20*omega/2) 0 -
J3*(20*omega/2)^2 1 -T2Im(20);0 0 0 0 1];
P4_20=[1 0 0 0 0;-J4*(20*omega/2)^2 1 -c4*(20*omega/2) 0 -T3Re(20);0 0 1 0 0;c4*(20*omega/2) 0 -
J4*(20*omega/2)^2 1 -T3Im(20);0 0 0 0 1];
P5_20=[1 0 0 0 0;-J5*(20*omega/2)^2 1 -c5*(20*omega/2) 0 -T4Re(20);0 0 1 0 0;c5*(20*omega/2) 0 -
J5*(20*omega/2)^2 1 -T4Im(20);0 0 0 0 1];
P6_20=[1 0 0 0 0;-J6*(20*omega/2)^2 1 -c6*(20*omega/2) 0 -T5Re(20);0 0 1 0 0;c6*(20*omega/2) 0 -
J6*(20*omega/2)^2 1 -T5Im(20);0 0 0 0 1];
P7_20=[1 0 0 0 0;-J7*(20*omega/2)^2 1 -c7*(20*omega/2) 0 -T6Re(20);0 0 1 0 0;c7*(20*omega/2) 0 -
J7*(20*omega/2)^2 1 -T6Im(20);0 0 0 0 1];
P8_20=[1 0 0 0 0;-J8*(20*omega/2)^2 1 0 0 0;0 0 1 0 0;0 0 -J8*(20*omega/2)^2 1 0;0 0 0 0 1];
```

```
F1_20=[1 1/k1 0 0 0;0 1 0 0 0;0 0 1 1/k1 0;0 0 0 1 0;0 0 0 0 1];
F2_20=[1 1/k2 0 0 0;0 1 0 0 0;0 0 1 1/k2 0;0 0 0 1 0;0 0 0 0 1];
F3_20=[1 1/k3 0 0 0;0 1 0 0 0;0 0 1 1/k3 0;0 0 0 1 0;0 0 0 0 1];
F4_20=[1 1/k4 0 0 0;0 1 0 0 0;0 0 1 1/k4 0;0 0 0 1 0;0 0 0 0 1];
F5_20=[1 1/k5 0 0 0;0 1 0 0 0;0 0 1 1/k5 0;0 0 0 1 0;0 0 0 0 1];
F6_20=[1 1/k6 0 0 0;0 1 0 0 0;0 0 1 1/k6 0;0 0 0 1 0;0 0 0 0 1];
F7_20=[1 1/k7 0 0 0;0 1 0 0 0;0 0 1 1/k7 0;0 0 0 1 0;0 0 0 0 1];

H20=P8_20*F7_20*P7_20*F6_20*P6_20*F5_20*P5_20*F4_20*P4_20*F3_20*P3_20*F2_20*P2_20*F1_
20*P1_20;

theta1_20Re=((H20(4,5)*H20(2,3))-(H20(2,5)*H20(4,3)))/((H20(2,1)*H20(4,3))-(H20(2,3)*H20(4,1)));
theta1_20Im=((-H20(4,5)*H20(2,1))+(H20(2,5)*H20(4,1)))/((H20(2,1)*H20(4,3))-(H20(2,3)*H20(4,1)));

Z1_20L=[theta1_20Re;0;theta1_20Im;0;1]
Z1_20R=P1_20*Z1_20L;
theta1_20=sqrt((Z1_20L(1))^2+(Z1_20L(3))^2)*180/pi
torque1_20L=sqrt((Z1_20L(2))^2+(Z1_20L(4))^2)
torque1_20R=sqrt((Z1_20R(2))^2+(Z1_20R(4))^2)

Z2_20L=F1_20*Z1_20R;
Z2_20R=P2_20*Z2_20L;
theta2_20=sqrt((Z2_20L(1))^2+(Z2_20L(3))^2)*180/pi
torque2_20R=sqrt((Z2_20R(2))^2+(Z2_20R(4))^2)

Z3_20L=F2_20*Z2_20R;
Z3_20R=P3_20*Z3_20L;
theta3_20=sqrt((Z3_20L(1))^2+(Z3_20L(3))^2)*180/pi
torque3_20R=sqrt((Z3_20R(2))^2+(Z3_20R(4))^2)

Z4_20L=F3_20*Z3_20R;
Z4_20R=P4_20*Z4_20L;
theta4_20=sqrt((Z4_20L(1))^2+(Z4_20L(3))^2)*180/pi
torque4_20R=sqrt((Z4_20R(2))^2+(Z4_20R(4))^2)

Z5_20L=F4_20*Z4_20R;
Z5_20R=P5_20*Z5_20L;
theta5_20=sqrt((Z5_20L(1))^2+(Z5_20L(3))^2)*180/pi
torque5_20R=sqrt((Z5_20R(2))^2+(Z5_20R(4))^2)

Z6_20L=F5_20*Z5_20R;
Z6_20R=P6_20*Z6_20L;
theta6_20=sqrt((Z6_20L(1))^2+(Z6_20L(3))^2)*180/pi
torque6_20R=sqrt((Z6_20R(2))^2+(Z6_20R(4))^2)

Z7_20L=F6_20*Z6_20R;
Z7_20R=P7_20*Z7_20L;
theta7_20=sqrt((Z7_20L(1))^2+(Z7_20L(3))^2)*180/pi
torque7_20R=sqrt((Z7_20R(2))^2+(Z7_20R(4))^2)

Z8_20L=F7_20*Z7_20R;
Z8_20R=P8_20*Z8_20L;
theta8_20=sqrt((Z8_20L(1))^2+(Z8_20L(3))^2)*180/pi
torque8_20R=sqrt((Z8_20R(2))^2+(Z8_20R(4))^2)


%10.5th order
```

```
P1_21=[1 0 0 0 0;-J1*(21*omega/2)^2 1 -c1*(21*omega/2) 0 0;0 0 1 0 0;c1*(21*omega/2) 0 -
J1*(21*omega/2)^2 1 0;0 0 0 0 1];
P2_21=[1 0 0 0 0;-J2*(21*omega/2)^2 1 -c2*(21*omega/2) 0 -T1Re(21);0 0 1 0 0;c2*(21*omega/2) 0 -
J2*(21*omega/2)^2 1 -T1Im(21);0 0 0 0 1];
P3_21=[1 0 0 0 0;-J3*(21*omega/2)^2 1 -c3*(21*omega/2) 0 -T2Re(21);0 0 1 0 0;c3*(21*omega/2) 0 -
J3*(21*omega/2)^2 1 -T2Im(21);0 0 0 0 1];
P4_21=[1 0 0 0 0;-J4*(21*omega/2)^2 1 -c4*(21*omega/2) 0 -T3Re(21);0 0 1 0 0;c4*(21*omega/2) 0 -
J4*(21*omega/2)^2 1 -T3Im(21);0 0 0 0 1];
P5_21=[1 0 0 0 0;-J5*(21*omega/2)^2 1 -c5*(21*omega/2) 0 -T4Re(21);0 0 1 0 0;c5*(21*omega/2) 0 -
J5*(21*omega/2)^2 1 -T4Im(21);0 0 0 0 1];
P6_21=[1 0 0 0 0;-J6*(21*omega/2)^2 1 -c6*(21*omega/2) 0 -T5Re(21);0 0 1 0 0;c6*(21*omega/2) 0 -
J6*(21*omega/2)^2 1 -T5Im(21);0 0 0 0 1];
P7_21=[1 0 0 0 0;-J7*(21*omega/2)^2 1 -c7*(21*omega/2) 0 -T6Re(21);0 0 1 0 0;c7*(21*omega/2) 0 -
J7*(21*omega/2)^2 1 -T6Im(21);0 0 0 0 1];
P8_21=[1 0 0 0 0;-J8*(21*omega/2)^2 1 0 0 0;0 0 1 0 0;0 0 -J8*(21*omega/2)^2 1 0;0 0 0 0 1];

F1_21=[1 1/k1 0 0 0;0 1 0 0 0;0 0 1 1/k1 0;0 0 0 1 0;0 0 0 0 1];
F2_21=[1 1/k2 0 0 0;0 1 0 0 0;0 0 1 1/k2 0;0 0 0 1 0;0 0 0 0 1];
F3_21=[1 1/k3 0 0 0;0 1 0 0 0;0 0 1 1/k3 0;0 0 0 1 0;0 0 0 0 1];
F4_21=[1 1/k4 0 0 0;0 1 0 0 0;0 0 1 1/k4 0;0 0 0 1 0;0 0 0 0 1];
F5_21=[1 1/k5 0 0 0;0 1 0 0 0;0 0 1 1/k5 0;0 0 0 1 0;0 0 0 0 1];
F6_21=[1 1/k6 0 0 0;0 1 0 0 0;0 0 1 1/k6 0;0 0 0 1 0;0 0 0 0 1];
F7_21=[1 1/k7 0 0 0;0 1 0 0 0;0 0 1 1/k7 0;0 0 0 1 0;0 0 0 0 1];

H21=P8_21*F7_21*P7_21*F6_21*P6_21*F5_21*P5_21*F4_21*P4_21*F3_21*P3_21*F2_21*P2_21*F1_
21*P1_21;

theta1_21Re=((H21(4,5)*H21(2,3))-(H21(2,5)*H21(4,3)))/((H21(2,1)*H21(4,3))-(H21(2,3)*H21(4,1)));
theta1_21Im=((-H21(4,5)*H21(2,1))+(H21(2,5)*H21(4,1)))/((H21(2,1)*H21(4,3))-(H21(2,3)*H21(4,1)));

Z1_21L=[theta1_21Re;0;theta1_21Im;0;1]
Z1_21R=P1_21*Z1_21L;
theta1_21=sqrt((Z1_21L(1))^2+(Z1_21L(3))^2)*180/pi
torque1_21L=sqrt((Z1_21L(2))^2+(Z1_21L(4))^2)
torque1_21R=sqrt((Z1_21R(2))^2+(Z1_21R(4))^2)

Z2_21L=F1_21*Z1_21R;
Z2_21R=P2_21*Z2_21L;
theta2_21=sqrt((Z2_21L(1))^2+(Z2_21L(3))^2)*180/pi
torque2_21R=sqrt((Z2_21R(2))^2+(Z2_21R(4))^2)

Z3_21L=F2_21*Z2_21R;
Z3_21R=P3_21*Z3_21L;
theta3_21=sqrt((Z3_21L(1))^2+(Z3_21L(3))^2)*180/pi
torque3_21R=sqrt((Z3_21R(2))^2+(Z3_21R(4))^2)

Z4_21L=F3_21*Z3_21R;
Z4_21R=P4_21*Z4_21L;
theta4_21=sqrt((Z4_21L(1))^2+(Z4_21L(3))^2)*180/pi
torque4_21R=sqrt((Z4_21R(2))^2+(Z4_21R(4))^2)

Z5_21L=F4_21*Z4_21R;
Z5_21R=P5_21*Z5_21L;
theta5_21=sqrt((Z5_21L(1))^2+(Z5_21L(3))^2)*180/pi
torque5_21R=sqrt((Z5_21R(2))^2+(Z5_21R(4))^2)

Z6_21L=F5_21*Z5_21R;
Z6_21R=P6_21*Z6_21L;
theta6_21=sqrt((Z6_21L(1))^2+(Z6_21L(3))^2)*180/pi
```

```
torque6_21R=sqrt((Z6_21R(2))^2+(Z6_21R(4))^2)

Z7_21L=F6_21*Z6_21R;
Z7_21R=P7_21*Z7_21L;
theta7_21=sqrt((Z7_21L(1))^2+(Z7_21L(3))^2)*180/pi
torque7_21R=sqrt((Z7_21R(2))^2+(Z7_21R(4))^2)

Z8_21L=F7_21*Z7_21R;
Z8_21R=P8_21*Z8_21L;
theta8_21=sqrt((Z8_21L(1))^2+(Z8_21L(3))^2)*180/pi
torque8_21R=sqrt((Z8_21R(2))^2+(Z8_21R(4))^2)


%11th order

P1_22=[1 0 0 0 0;-J1*(22*omega/2)^2 1 -c1*(22*omega/2) 0 0;0 0 1 0 0;c1*(22*omega/2) 0 -
J1*(22*omega/2)^2 1 0;0 0 0 0 1];
P2_22=[1 0 0 0 0;-J2*(22*omega/2)^2 1 -c2*(22*omega/2) 0 -T1Re(22);0 0 1 0 0;c2*(22*omega/2) 0 -
J2*(22*omega/2)^2 1 -T1Im(22);0 0 0 0 1];
P3_22=[1 0 0 0 0;-J3*(22*omega/2)^2 1 -c3*(22*omega/2) 0 -T2Re(22);0 0 1 0 0;c3*(22*omega/2) 0 -
J3*(22*omega/2)^2 1 -T2Im(22);0 0 0 0 1];
P4_22=[1 0 0 0 0;-J4*(22*omega/2)^2 1 -c4*(22*omega/2) 0 -T3Re(22);0 0 1 0 0;c4*(22*omega/2) 0 -
J4*(22*omega/2)^2 1 -T3Im(22);0 0 0 0 1];
P5_22=[1 0 0 0 0;-J5*(22*omega/2)^2 1 -c5*(22*omega/2) 0 -T4Re(22);0 0 1 0 0;c5*(22*omega/2) 0 -
J5*(22*omega/2)^2 1 -T4Im(22);0 0 0 0 1];
P6_22=[1 0 0 0 0;-J6*(22*omega/2)^2 1 -c6*(22*omega/2) 0 -T5Re(22);0 0 1 0 0;c6*(22*omega/2) 0 -
J6*(22*omega/2)^2 1 -T5Im(22);0 0 0 0 1];
P7_22=[1 0 0 0 0;-J7*(22*omega/2)^2 1 -c7*(22*omega/2) 0 -T6Re(22);0 0 1 0 0;c7*(22*omega/2) 0 -
J7*(22*omega/2)^2 1 -T6Im(22);0 0 0 0 1];
P8_22=[1 0 0 0 0;-J8*(22*omega/2)^2 1 0 0 0;0 0 1 0 0;0 0 -J8*(22*omega/2)^2 1 0;0 0 0 0 1];

F1_22=[1 1/k1 0 0 0;0 1 0 0 0;0 0 1 1/k1 0;0 0 0 1 0;0 0 0 0 1];
F2_22=[1 1/k2 0 0 0;0 1 0 0 0;0 0 1 1/k2 0;0 0 0 1 0;0 0 0 0 1];
F3_22=[1 1/k3 0 0 0;0 1 0 0 0;0 0 1 1/k3 0;0 0 0 1 0;0 0 0 0 1];
F4_22=[1 1/k4 0 0 0;0 1 0 0 0;0 0 1 1/k4 0;0 0 0 1 0;0 0 0 0 1];
F5_22=[1 1/k5 0 0 0;0 1 0 0 0;0 0 1 1/k5 0;0 0 0 1 0;0 0 0 0 1];
F6_22=[1 1/k6 0 0 0;0 1 0 0 0;0 0 1 1/k6 0;0 0 0 1 0;0 0 0 0 1];
F7_22=[1 1/k7 0 0 0;0 1 0 0 0;0 0 1 1/k7 0;0 0 0 1 0;0 0 0 0 1];

H22=P8_22*F7_22*P7_22*F6_22*P6_22*F5_22*P5_22*F4_22*P4_22*F3_22*P3_22*F2_22*P2_22*F1_
22*P1_22;

theta1_22Re=((H22(4,5)*H22(2,3))-(H22(2,5)*H22(4,3)))/((H22(2,1)*H22(4,3))-(H22(2,3)*H22(4,1)));
theta1_22Im=((-H22(4,5)*H22(2,1))+(H22(2,5)*H22(4,1)))/((H22(2,1)*H22(4,3))-(H22(2,3)*H22(4,1)));

Z1_22L=[theta1_22Re;0;theta1_22Im;0;1]
Z1_22R=P1_22*Z1_22L;
theta1_22=sqrt((Z1_22L(1))^2+(Z1_22L(3))^2)*180/pi
torque1_22L=sqrt((Z1_22L(2))^2+(Z1_22L(4))^2)
torque1_22R=sqrt((Z1_22R(2))^2+(Z1_22R(4))^2)

Z2_22L=F1_22*Z1_22R;
Z2_22R=P2_22*Z2_22L;
theta2_22=sqrt((Z2_22L(1))^2+(Z2_22L(3))^2)*180/pi
torque2_22R=sqrt((Z2_22R(2))^2+(Z2_22R(4))^2)

Z3_22L=F2_22*Z2_22R;
Z3_22R=P3_22*Z3_22L;
theta3_22=sqrt((Z3_22L(1))^2+(Z3_22L(3))^2)*180/pi
```

```
torque3_22R=sqrt((Z3_22R(2))^2+(Z3_22R(4))^2)

Z4_22L=F3_22*Z3_22R;
Z4_22R=P4_22*Z4_22L;
theta4_22=sqrt((Z4_22L(1))^2+(Z4_22L(3))^2)*180/pi
torque4_22R=sqrt((Z4_22R(2))^2+(Z4_22R(4))^2)

Z5_22L=F4_22*Z4_22R;
Z5_22R=P5_22*Z5_22L;
theta5_22=sqrt((Z5_22L(1))^2+(Z5_22L(3))^2)*180/pi
torque5_22R=sqrt((Z5_22R(2))^2+(Z5_22R(4))^2)

Z6_22L=F5_22*Z5_22R;
Z6_22R=P6_22*Z6_22L;
theta6_22=sqrt((Z6_22L(1))^2+(Z6_22L(3))^2)*180/pi
torque6_22R=sqrt((Z6_22R(2))^2+(Z6_22R(4))^2)

Z7_22L=F6_22*Z6_22R;
Z7_22R=P7_22*Z7_22L;
theta7_22=sqrt((Z7_22L(1))^2+(Z7_22L(3))^2)*180/pi
torque7_22R=sqrt((Z7_22R(2))^2+(Z7_22R(4))^2)

Z8_22L=F7_22*Z7_22R;
Z8_22R=P8_22*Z8_22L;
theta8_22=sqrt((Z8_22L(1))^2+(Z8_22L(3))^2)*180/pi
torque8_22R=sqrt((Z8_22R(2))^2+(Z8_22R(4))^2)


%11.5th order

P1_23=[1  0  0  0  0;-J1*(23*omega/2)^2  1  -c1*(23*omega/2)  0  0;0  0  1  0  0;c1*(23*omega/2)  0  -
J1*(23*omega/2)^2 1 0;0 0 0 0 1];
P2_23=[1  0  0  0  0;-J2*(23*omega/2)^2  1  -c2*(23*omega/2)  0  -T1Re(23);0  0  1  0  0;c2*(23*omega/2)  0  -
J2*(23*omega/2)^2 1 -T1Im(23);0 0 0 0 1];
P3_23=[1  0  0  0  0;-J3*(23*omega/2)^2  1  -c3*(23*omega/2)  0  -T2Re(23);0  0  1  0  0;c3*(23*omega/2)  0  -
J3*(23*omega/2)^2 1 -T2Im(23);0 0 0 0 1];
P4_23=[1  0  0  0  0;-J4*(23*omega/2)^2  1  -c4*(23*omega/2)  0  -T3Re(23);0  0  1  0  0;c4*(23*omega/2)  0  -
J4*(23*omega/2)^2 1 -T3Im(23);0 0 0 0 1];
P5_23=[1  0  0  0  0;-J5*(23*omega/2)^2  1  -c5*(23*omega/2)  0  -T4Re(23);0  0  1  0  0;c5*(23*omega/2)  0  -
J5*(23*omega/2)^2 1 -T4Im(23);0 0 0 0 1];
P6_23=[1  0  0  0  0;-J6*(23*omega/2)^2  1  -c6*(23*omega/2)  0  -T5Re(23);0  0  1  0  0;c6*(23*omega/2)  0  -
J6*(23*omega/2)^2 1 -T5Im(23);0 0 0 0 1];
P7_23=[1  0  0  0  0;-J7*(23*omega/2)^2  1  -c7*(23*omega/2)  0  -T6Re(23);0  0  1  0  0;c7*(23*omega/2)  0  -
J7*(23*omega/2)^2 1 -T6Im(23);0 0 0 0 1];
P8_23=[1 0 0 0 0;-J8*(23*omega/2)^2 1 0 0 0;0 0 1 0 0;0 0 -J8*(23*omega/2)^2 1 0;0 0 0 0 1];

F1_23=[1 1/k1 0 0 0;0 1 0 0 0;0 0 1 1/k1 0;0 0 0 1 0;0 0 0 0 1];
F2_23=[1 1/k2 0 0 0;0 1 0 0 0;0 0 1 1/k2 0;0 0 0 1 0;0 0 0 0 1];
F3_23=[1 1/k3 0 0 0;0 1 0 0 0;0 0 1 1/k3 0;0 0 0 1 0;0 0 0 0 1];
F4_23=[1 1/k4 0 0 0;0 1 0 0 0;0 0 1 1/k4 0;0 0 0 1 0;0 0 0 0 1];
F5_23=[1 1/k5 0 0 0;0 1 0 0 0;0 0 1 1/k5 0;0 0 0 1 0;0 0 0 0 1];
F6_23=[1 1/k6 0 0 0;0 1 0 0 0;0 0 1 1/k6 0;0 0 0 1 0;0 0 0 0 1];
F7_23=[1 1/k7 0 0 0;0 1 0 0 0;0 0 1 1/k7 0;0 0 0 1 0;0 0 0 0 1];

H23=P8_23*F7_23*P7_23*F6_23*P6_23*F5_23*P5_23*F4_23*P4_23*F3_23*P3_23*F2_23*P2_23*F1_
23*P1_23;

theta1_23Re=((H23(4,5)*H23(2,3))-(H23(2,5)*H23(4,3)))/((H23(2,1)*H23(4,3))-(H23(2,3)*H23(4,1)));
theta1_23Im=((-H23(4,5)*H23(2,1))+(H23(2,5)*H23(4,1)))/((H23(2,1)*H23(4,3))-(H23(2,3)*H23(4,1)));
```

```
Z1_23L=[theta1_23Re;0;theta1_23Im;0;1]
Z1_23R=P1_23*Z1_23L;
theta1_23=sqrt((Z1_23L(1))^2+(Z1_23L(3))^2)*180/pi
torque1_23L=sqrt((Z1_23L(2))^2+(Z1_23L(4))^2)
torque1_23R=sqrt((Z1_23R(2))^2+(Z1_23R(4))^2)

Z2_23L=F1_23*Z1_23R;
Z2_23R=P2_23*Z2_23L;
theta2_23=sqrt((Z2_23L(1))^2+(Z2_23L(3))^2)*180/pi
torque2_23R=sqrt((Z2_23R(2))^2+(Z2_23R(4))^2)

Z3_23L=F2_23*Z2_23R;
Z3_23R=P3_23*Z3_23L;
theta3_23=sqrt((Z3_23L(1))^2+(Z3_23L(3))^2)*180/pi
torque3_23R=sqrt((Z3_23R(2))^2+(Z3_23R(4))^2)

Z4_23L=F3_23*Z3_23R;
Z4_23R=P4_23*Z4_23L;
theta4_23=sqrt((Z4_23L(1))^2+(Z4_23L(3))^2)*180/pi
torque4_23R=sqrt((Z4_23R(2))^2+(Z4_23R(4))^2)

Z5_23L=F4_23*Z4_23R;
Z5_23R=P5_23*Z5_23L;
theta5_23=sqrt((Z5_23L(1))^2+(Z5_23L(3))^2)*180/pi
torque5_23R=sqrt((Z5_23R(2))^2+(Z5_23R(4))^2)

Z6_23L=F5_23*Z5_23R;
Z6_23R=P6_23*Z6_23L;
theta6_23=sqrt((Z6_23L(1))^2+(Z6_23L(3))^2)*180/pi
torque6_23R=sqrt((Z6_23R(2))^2+(Z6_23R(4))^2)

Z7_23L=F6_23*Z6_23R;
Z7_23R=P7_23*Z7_23L;
theta7_23=sqrt((Z7_23L(1))^2+(Z7_23L(3))^2)*180/pi
torque7_23R=sqrt((Z7_23R(2))^2+(Z7_23R(4))^2)

Z8_23L=F7_23*Z7_23R;
Z8_23R=P8_23*Z8_23L;
theta8_23=sqrt((Z8_23L(1))^2+(Z8_23L(3))^2)*180/pi
torque8_23R=sqrt((Z8_23R(2))^2+(Z8_23R(4))^2)


%12th order

P1_24=[1 0 0 0 0;-J1*(24*omega/2)^2 1 -c1*(24*omega/2) 0 0;0 0 1 0 0;c1*(24*omega/2) 0 -
J1*(24*omega/2)^2 1 0;0 0 0 0 1];
P2_24=[1 0 0 0 0;-J2*(24*omega/2)^2 1 -c2*(24*omega/2) 0 -T1Re(24);0 0 1 0 0;c2*(24*omega/2) 0 -
J2*(24*omega/2)^2 1 -T1Im(24);0 0 0 0 1];
P3_24=[1 0 0 0 0;-J3*(24*omega/2)^2 1 -c3*(24*omega/2) 0 -T2Re(24);0 0 1 0 0;c3*(24*omega/2) 0 -
J3*(24*omega/2)^2 1 -T2Im(24);0 0 0 0 1];
P4_24=[1 0 0 0 0;-J4*(24*omega/2)^2 1 -c4*(24*omega/2) 0 -T3Re(24);0 0 1 0 0;c4*(24*omega/2) 0 -
J4*(24*omega/2)^2 1 -T3Im(24);0 0 0 0 1];
P5_24=[1 0 0 0 0;-J5*(24*omega/2)^2 1 -c5*(24*omega/2) 0 -T4Re(24);0 0 1 0 0;c5*(24*omega/2) 0 -
J5*(24*omega/2)^2 1 -T4Im(24);0 0 0 0 1];
P6_24=[1 0 0 0 0;-J6*(24*omega/2)^2 1 -c6*(24*omega/2) 0 -T5Re(24);0 0 1 0 0;c6*(24*omega/2) 0 -
J6*(24*omega/2)^2 1 -T5Im(24);0 0 0 0 1];
P7_24=[1 0 0 0 0;-J7*(24*omega/2)^2 1 -c7*(24*omega/2) 0 -T6Re(24);0 0 1 0 0;c7*(24*omega/2) 0 -
J7*(24*omega/2)^2 1 -T6Im(24);0 0 0 0 1];
```

```
P8_24=[1 0 0 0 0;-J8*(24*omega/2)^2 1 0 0 0;0 0 1 0 0;0 0 -J8*(24*omega/2)^2 1 0;0 0 0 0 1];

F1_24=[1 1/k1 0 0 0;0 1 0 0 0;0 0 1 1/k1 0;0 0 0 1 0;0 0 0 0 1];
F2_24=[1 1/k2 0 0 0;0 1 0 0 0;0 0 1 1/k2 0;0 0 0 1 0;0 0 0 0 1];
F3_24=[1 1/k3 0 0 0;0 1 0 0 0;0 0 1 1/k3 0;0 0 0 1 0;0 0 0 0 1];
F4_24=[1 1/k4 0 0 0;0 1 0 0 0;0 0 1 1/k4 0;0 0 0 1 0;0 0 0 0 1];
F5_24=[1 1/k5 0 0 0;0 1 0 0 0;0 0 1 1/k5 0;0 0 0 1 0;0 0 0 0 1];
F6_24=[1 1/k6 0 0 0;0 1 0 0 0;0 0 1 1/k6 0;0 0 0 1 0;0 0 0 0 1];
F7_24=[1 1/k7 0 0 0;0 1 0 0 0;0 0 1 1/k7 0;0 0 0 1 0;0 0 0 0 1];

H24=P8_24*F7_24*P7_24*F6_24*P6_24*F5_24*P5_24*F4_24*P4_24*F3_24*P3_24*F2_24*P2_24*F1_
24*P1_24;

theta1_24Re=((H24(4,5)*H24(2,3))-(H24(2,5)*H24(4,3)))/((H24(2,1)*H24(4,3))-(H24(2,3)*H24(4,1)));
theta1_24Im=((-H24(4,5)*H24(2,1))+(H24(2,5)*H24(4,1)))/((H24(2,1)*H24(4,3))-(H24(2,3)*H24(4,1)));

Z1_24L=[theta1_24Re;0;theta1_24Im;0;1]
Z1_24R=P1_24*Z1_24L;
theta1_24=sqrt((Z1_24L(1))^2+(Z1_24L(3))^2)*180/pi
torque1_24L=sqrt((Z1_24L(2))^2+(Z1_24L(4))^2)
torque1_24R=sqrt((Z1_24R(2))^2+(Z1_24R(4))^2)

Z2_24L=F1_24*Z1_24R;
Z2_24R=P2_24*Z2_24L;
theta2_24=sqrt((Z2_24L(1))^2+(Z2_24L(3))^2)*180/pi
torque2_24R=sqrt((Z2_24R(2))^2+(Z2_24R(4))^2)

Z3_24L=F2_24*Z2_24R;
Z3_24R=P3_24*Z3_24L;
theta3_24=sqrt((Z3_24L(1))^2+(Z3_24L(3))^2)*180/pi
torque3_24R=sqrt((Z3_24R(2))^2+(Z3_24R(4))^2)

Z4_24L=F3_24*Z3_24R;
Z4_24R=P4_24*Z4_24L;
theta4_24=sqrt((Z4_24L(1))^2+(Z4_24L(3))^2)*180/pi
torque4_24R=sqrt((Z4_24R(2))^2+(Z4_24R(4))^2)

Z5_24L=F4_24*Z4_24R;
Z5_24R=P5_24*Z5_24L;
theta5_24=sqrt((Z5_24L(1))^2+(Z5_24L(3))^2)*180/pi
torque5_24R=sqrt((Z5_24R(2))^2+(Z5_24R(4))^2)

Z6_24L=F5_24*Z5_24R;
Z6_24R=P6_24*Z6_24L;
theta6_24=sqrt((Z6_24L(1))^2+(Z6_24L(3))^2)*180/pi
torque6_24R=sqrt((Z6_24R(2))^2+(Z6_24R(4))^2)

Z7_24L=F6_24*Z6_24R;
Z7_24R=P7_24*Z7_24L;
theta7_24=sqrt((Z7_24L(1))^2+(Z7_24L(3))^2)*180/pi
torque7_24R=sqrt((Z7_24R(2))^2+(Z7_24R(4))^2)

Z8_24L=F7_24*Z7_24R;
Z8_24R=P8_24*Z8_24L;
theta8_24=sqrt((Z8_24L(1))^2+(Z8_24L(3))^2)*180/pi
torque8_24R=sqrt((Z8_24R(2))^2+(Z8_24R(4))^2)
```

```
%synthesis


for i=1:720

theta1(i)=(theta1_1Re*cos(i*pi/180/2)+theta1_2Re*cos(i*pi/180)+theta1_3Re*cos(3*i*pi/180/2)+theta1_4R
e*cos(4*i*pi/180/2)+theta1_5Re*cos(5*i*pi/180/2)+theta1_6Re*cos(6*i*pi/180/2)+theta1_7Re*cos(7*i*pi/
180/2)+theta1_8Re*cos(8*i*pi/180/2)+theta1_9Re*cos(9*i*pi/180/2)+theta1_10Re*cos(10*i*pi/180/2)+thet
a1_11Re*cos(11*i*pi/180/2)+theta1_12Re*cos(12*i*pi/180/2)+theta1_13Re*cos(13*i*pi/180/2)+theta1_14
Re*cos(14*i*pi/180/2)+theta1_15Re*cos(15*i*pi/180/2)+theta1_16Re*cos(16*i*pi/180/2)+theta1_17Re*co
s(17*i*pi/180/2)+theta1_18Re*cos(18*i*pi/180/2)+theta1_19Re*cos(19*i*pi/180/2)+theta1_20Re*cos(20*i
*pi/180/2)+theta1_21Re*cos(21*i*pi/180/2)+theta1_22Re*cos(22*i*pi/180/2)+theta1_23Re*cos(23*i*pi/18
0/2)+theta1_24Re*cos(24*i*pi/180/2))-
(theta1_1Im*sin(1*i*pi/180/2)+theta1_2Im*sin(2*i*pi/180/2)+theta1_3Im*sin(3*i*pi/180/2)+theta1_4Im*si
n(4*i*pi/180/2)+theta1_5Im*sin(5*i*pi/180/2)+theta1_6Im*sin(6*i*pi/180/2)+theta1_7Im*sin(7*i*pi/180/2
)+theta1_8Im*sin(8*i*pi/180/2)+theta1_9Im*sin(9*i*pi/180/2)+theta1_10Im*sin(10*i*pi/180/2)+theta1_11I
m*sin(11*i*pi/180/2)+theta1_12Im*sin(12*i*pi/180/2)+theta1_13Im*sin(13*i*pi/180/2)+theta1_14Im*sin(
14*i*pi/180/2)+theta1_15Im*sin(15*i*pi/180/2)+theta1_16Im*sin(16*i*pi/180/2)+theta1_17Im*sin(17*i*pi
/180/2)+theta1_18Im*sin(18*i*pi/180/2)+theta1_19Im*sin(19*i*pi/180/2)+theta1_20Im*sin(20*i*pi/180/2)
+theta1_21Im*sin(21*i*pi/180/2)+theta1_22Im*sin(22*i*pi/180/2)+theta1_23Im*sin(23*i*pi/180/2)+theta1
_24Im*sin(24*i*pi/180/2));
end
theta1=theta1*180/pi;
plot(theta1)



for i=1:720

theta8(i)=((Z8_1L(1))*cos(i*pi/180/2)+(Z8_2L(1))*cos(i*pi/180)+(Z8_3L(1))*cos(3*i*pi/180/2)+(Z8_4L(1)
)*cos(4*i*pi/180/2)+(Z8_5L(1))*cos(5*i*pi/180/2)+(Z8_6L(1))*cos(6*i*pi/180/2)+(Z8_7L(1))*cos(7*i*pi/
180/2)+(Z8_8L(1))*cos(8*i*pi/180/2)+(Z8_9L(1))*cos(9*i*pi/180/2)+(Z8_10L(1))*cos(10*i*pi/180/2)+(Z8
_11L(1))*cos(11*i*pi/180/2)+(Z8_12L(1))*cos(12*i*pi/180/2)+(Z8_13L(1))*cos(13*i*pi/180/2)+(Z8_14L(
1))*cos(14*i*pi/180/2)+(Z8_15L(1))*cos(15*i*pi/180/2)+(Z8_16L(1))*cos(16*i*pi/180/2)+(Z8_17L(1))*co
s(17*i*pi/180/2)+(Z8_18L(1))*cos(18*i*pi/180/2)+(Z8_19L(1))*cos(19*i*pi/180/2)+(Z8_20L(1))*cos(20*i
*pi/180/2)+(Z8_21L(1))*cos(21*i*pi/180/2)+(Z8_22L(1))*cos(22*i*pi/180/2)+(Z8_23L(1))*cos(23*i*pi/18
0/2)+(Z8_24L(1))*cos(24*i*pi/180/2))-
((Z8_1L(3))*sin(1*i*pi/180/2)+(Z8_2L(3))*sin(2*i*pi/180/2)+(Z8_3L(3))*sin(3*i*pi/180/2)+(Z8_4L(3))*si
n(4*i*pi/180/2)+(Z8_5L(3))*sin(5*i*pi/180/2)+(Z8_6L(3))*sin(6*i*pi/180/2)+(Z8_7L(3))*sin(7*i*pi/180/2
)+(Z8_8L(3))*sin(8*i*pi/180/2)+(Z8_9L(3))*sin(9*i*pi/180/2)+(Z8_10L(3))*sin(10*i*pi/180/2)+(Z8_11L(
3))*sin(11*i*pi/180/2)+(Z8_12L(3))*sin(12*i*pi/180/2)+(Z8_13L(3))*sin(13*i*pi/180/2)+(Z8_14L(3))*sin(
14*i*pi/180/2)+(Z8_15L(3))*sin(15*i*pi/180/2)+(Z8_16L(3))*sin(16*i*pi/180/2)+(Z8_17L(3))*sin(17*i*pi
/180/2)+(Z8_18L(3))*sin(18*i*pi/180/2)+(Z8_19L(3))*sin(19*i*pi/180/2)+(Z8_20L(3))*sin(20*i*pi/180/2)
+(Z8_21L(3))*sin(21*i*pi/180/2)+(Z8_22L(3))*sin(22*i*pi/180/2)+(Z8_23L(3))*sin(23*i*pi/180/2)+(Z8_2
4L(3))*sin(24*i*pi/180/2));
end


for i=1:719
   omega8(i)=(theta8(i+1)-theta8(i))/(pi/(180*omega));
end

figure;
plot(omega8)

theta8=theta8*180/pi;
figure;
plot(theta8)
```

```
%torque values


for i=1:720

torque_pulley_cyl1(i)=((Z1_1R(2))*cos(i*pi/180/2)+(Z1_2R(2))*cos(i*pi/180)+(Z1_3R(2))*cos(3*i*pi/180/
2)+(Z1_4R(2))*cos(4*i*pi/180/2)+(Z1_5R(2))*cos(5*i*pi/180/2)+(Z1_6R(2))*cos(6*i*pi/180/2)+(Z1_7R(2
))*cos(7*i*pi/180/2)+(Z1_8R(2))*cos(8*i*pi/180/2)+(Z1_9R(2))*cos(9*i*pi/180/2)+(Z1_10R(2))*cos(10*i
*pi/180/2)+(Z1_11R(2))*cos(11*i*pi/180/2)+(Z1_12R(2))*cos(12*i*pi/180/2)+(Z1_13R(2))*cos(13*i*pi/18
0/2)+(Z1_14R(2))*cos(14*i*pi/180/2)+(Z1_15R(2))*cos(15*i*pi/180/2)+(Z1_16R(2))*cos(16*i*pi/180/2)+(
Z1_17R(2))*cos(17*i*pi/180/2)+(Z1_18R(2))*cos(18*i*pi/180/2)+(Z1_19R(2))*cos(19*i*pi/180/2)+(Z1_2
0R(2))*cos(20*i*pi/180/2)+(Z1_21R(2))*cos(21*i*pi/180/2)+(Z1_22R(2))*cos(22*i*pi/180/2)+(Z1_23R(2)
)*cos(23*i*pi/180/2)+(Z1_24R(2))*cos(24*i*pi/180/2))-
((Z1_1R(4))*sin(1*i*pi/180/2)+(Z1_2R(4))*sin(2*i*pi/180/2)+(Z1_3R(4))*sin(3*i*pi/180/2)+(Z1_4R(4))*s
in(4*i*pi/180/2)+(Z1_5R(4))*sin(5*i*pi/180/2)+(Z1_6R(4))*sin(6*i*pi/180/2)+(Z1_7R(4))*sin(7*i*pi/180/
2)+(Z1_8R(4))*sin(8*i*pi/180/2)+(Z1_9R(4))*sin(9*i*pi/180/2)+(Z1_10R(4))*sin(10*i*pi/180/2)+(Z1_11R
(4))*sin(11*i*pi/180/2)+(Z1_12R(4))*sin(12*i*pi/180/2)+(Z1_13R(4))*sin(13*i*pi/180/2)+(Z1_14R(4))*si
n(14*i*pi/180/2)+(Z1_15R(4))*sin(15*i*pi/180/2)+(Z1_16R(4))*sin(16*i*pi/180/2)+(Z1_17R(4))*sin(17*i
*pi/180/2)+(Z1_18R(4))*sin(18*i*pi/180/2)+(Z1_19R(4))*sin(19*i*pi/180/2)+(Z1_20R(4))*sin(20*i*pi/180
/2)+(Z1_21R(4))*sin(21*i*pi/180/2)+(Z1_22R(4))*sin(22*i*pi/180/2)+(Z1_23R(4))*sin(23*i*pi/180/2)+(Z
1_24R(4))*sin(24*i*pi/180/2));
end

figure;
plot(torque_pulley_cyl1)


for i=1:720

torque_cyl1_cyl2(i)=((Z2_1R(2))*cos(i*pi/180/2)+(Z2_2R(2))*cos(i*pi/180)+(Z2_3R(2))*cos(3*i*pi/180/2)
+(Z2_4R(2))*cos(4*i*pi/180/2)+(Z2_5R(2))*cos(5*i*pi/180/2)+(Z2_6R(2))*cos(6*i*pi/180/2)+(Z2_7R(2))
*cos(7*i*pi/180/2)+(Z2_8R(2))*cos(8*i*pi/180/2)+(Z2_9R(2))*cos(9*i*pi/180/2)+(Z2_10R(2))*cos(10*i*p
i/180/2)+(Z2_11R(2))*cos(11*i*pi/180/2)+(Z2_12R(2))*cos(12*i*pi/180/2)+(Z2_13R(2))*cos(13*i*pi/180/
2)+(Z2_14R(2))*cos(14*i*pi/180/2)+(Z2_15R(2))*cos(15*i*pi/180/2)+(Z2_16R(2))*cos(16*i*pi/180/2)+(Z
2_17R(2))*cos(17*i*pi/180/2)+(Z2_18R(2))*cos(18*i*pi/180/2)+(Z2_19R(2))*cos(19*i*pi/180/2)+(Z2_20
R(2))*cos(20*i*pi/180/2)+(Z2_21R(2))*cos(21*i*pi/180/2)+(Z2_22R(2))*cos(22*i*pi/180/2)+(Z2_23R(2))
*cos(23*i*pi/180/2)+(Z2_24R(2))*cos(24*i*pi/180/2))-
((Z2_1R(4))*sin(1*i*pi/180/2)+(Z2_2R(4))*sin(2*i*pi/180/2)+(Z2_3R(4))*sin(3*i*pi/180/2)+(Z2_4R(4))*s
in(4*i*pi/180/2)+(Z2_5R(4))*sin(5*i*pi/180/2)+(Z2_6R(4))*sin(6*i*pi/180/2)+(Z2_7R(4))*sin(7*i*pi/180/
2)+(Z2_8R(4))*sin(8*i*pi/180/2)+(Z2_9R(4))*sin(9*i*pi/180/2)+(Z2_10R(4))*sin(10*i*pi/180/2)+(Z2_11R
(4))*sin(11*i*pi/180/2)+(Z2_12R(4))*sin(12*i*pi/180/2)+(Z2_13R(4))*sin(13*i*pi/180/2)+(Z2_14R(4))*si
n(14*i*pi/180/2)+(Z2_15R(4))*sin(15*i*pi/180/2)+(Z2_16R(4))*sin(16*i*pi/180/2)+(Z2_17R(4))*sin(17*i
*pi/180/2)+(Z2_18R(4))*sin(18*i*pi/180/2)+(Z2_19R(4))*sin(19*i*pi/180/2)+(Z2_20R(4))*sin(20*i*pi/180
/2)+(Z2_21R(4))*sin(21*i*pi/180/2)+(Z2_22R(4))*sin(22*i*pi/180/2)+(Z2_23R(4))*sin(23*i*pi/180/2)+(Z
2_24R(4))*sin(24*i*pi/180/2));
end

figure;
plot(torque_cyl1_cyl2)


for i=1:720

torque_cyl2_cyl3(i)=((Z3_1R(2))*cos(i*pi/180/2)+(Z3_2R(2))*cos(i*pi/180)+(Z3_3R(2))*cos(3*i*pi/180/2)
+(Z3_4R(2))*cos(4*i*pi/180/2)+(Z3_5R(2))*cos(5*i*pi/180/2)+(Z3_6R(2))*cos(6*i*pi/180/2)+(Z3_7R(2))
*cos(7*i*pi/180/2)+(Z3_8R(2))*cos(8*i*pi/180/2)+(Z3_9R(2))*cos(9*i*pi/180/2)+(Z3_10R(2))*cos(10*i*p
i/180/2)+(Z3_11R(2))*cos(11*i*pi/180/2)+(Z3_12R(2))*cos(12*i*pi/180/2)+(Z3_13R(2))*cos(13*i*pi/180/
2)+(Z3_14R(2))*cos(14*i*pi/180/2)+(Z3_15R(2))*cos(15*i*pi/180/2)+(Z3_16R(2))*cos(16*i*pi/180/2)+(Z
```

```
3_17R(2))*cos(17*i*pi/180/2)+(Z3_18R(2))*cos(18*i*pi/180/2)+(Z3_19R(2))*cos(19*i*pi/180/2)+(Z3_20
R(2))*cos(20*i*pi/180/2)+(Z3_21R(2))*cos(21*i*pi/180/2)+(Z3_22R(2))*cos(22*i*pi/180/2)+(Z3_23R(2))
*cos(23*i*pi/180/2)+(Z3_24R(2))*cos(24*i*pi/180/2))-
((Z3_1R(4))*sin(1*i*pi/180/2)+(Z3_2R(4))*sin(2*i*pi/180/2)+(Z3_3R(4))*sin(3*i*pi/180/2)+(Z3_4R(4))*s
in(4*i*pi/180/2)+(Z3_5R(4))*sin(5*i*pi/180/2)+(Z3_6R(4))*sin(6*i*pi/180/2)+(Z3_7R(4))*sin(7*i*pi/180/
2)+(Z3_8R(4))*sin(8*i*pi/180/2)+(Z3_9R(4))*sin(9*i*pi/180/2)+(Z3_10R(4))*sin(10*i*pi/180/2)+(Z3_11R
(4))*sin(11*i*pi/180/2)+(Z3_12R(4))*sin(12*i*pi/180/2)+(Z3_13R(4))*sin(13*i*pi/180/2)+(Z3_14R(4))*si
n(14*i*pi/180/2)+(Z3_15R(4))*sin(15*i*pi/180/2)+(Z3_16R(4))*sin(16*i*pi/180/2)+(Z3_17R(4))*sin(17*i
*pi/180/2)+(Z3_18R(4))*sin(18*i*pi/180/2)+(Z3_19R(4))*sin(19*i*pi/180/2)+(Z3_20R(4))*sin(20*i*pi/180
/2)+(Z3_21R(4))*sin(21*i*pi/180/2)+(Z3_22R(4))*sin(22*i*pi/180/2)+(Z3_23R(4))*sin(23*i*pi/180/2)+(Z
3_24R(4))*sin(24*i*pi/180/2));
end

figure;
plot(torque_cyl2_cyl3)


for i=1:720

torque_cyl3_cyl4(i)=((Z4_1R(2))*cos(i*pi/180/2)+(Z4_2R(2))*cos(i*pi/180)+(Z4_3R(2))*cos(3*i*pi/180/2)
+(Z4_4R(2))*cos(4*i*pi/180/2)+(Z4_5R(2))*cos(5*i*pi/180/2)+(Z4_6R(2))*cos(6*i*pi/180/2)+(Z4_7R(2))
*cos(7*i*pi/180/2)+(Z4_8R(2))*cos(8*i*pi/180/2)+(Z4_9R(2))*cos(9*i*pi/180/2)+(Z4_10R(2))*cos(10*i*p
i/180/2)+(Z4_11R(2))*cos(11*i*pi/180/2)+(Z4_12R(2))*cos(12*i*pi/180/2)+(Z4_13R(2))*cos(13*i*pi/180/
2)+(Z4_14R(2))*cos(14*i*pi/180/2)+(Z4_15R(2))*cos(15*i*pi/180/2)+(Z4_16R(2))*cos(16*i*pi/180/2)+(Z
4_17R(2))*cos(17*i*pi/180/2)+(Z4_18R(2))*cos(18*i*pi/180/2)+(Z4_19R(2))*cos(19*i*pi/180/2)+(Z4_20
R(2))*cos(20*i*pi/180/2)+(Z4_21R(2))*cos(21*i*pi/180/2)+(Z4_22R(2))*cos(22*i*pi/180/2)+(Z4_23R(2))
*cos(23*i*pi/180/2)+(Z4_24R(2))*cos(24*i*pi/180/2))-
((Z4_1R(4))*sin(1*i*pi/180/2)+(Z4_2R(4))*sin(2*i*pi/180/2)+(Z4_3R(4))*sin(3*i*pi/180/2)+(Z4_4R(4))*s
in(4*i*pi/180/2)+(Z4_5R(4))*sin(5*i*pi/180/2)+(Z4_6R(4))*sin(6*i*pi/180/2)+(Z4_7R(4))*sin(7*i*pi/180/
2)+(Z4_8R(4))*sin(8*i*pi/180/2)+(Z4_9R(4))*sin(9*i*pi/180/2)+(Z4_10R(4))*sin(10*i*pi/180/2)+(Z4_11R
(4))*sin(11*i*pi/180/2)+(Z4_12R(4))*sin(12*i*pi/180/2)+(Z4_13R(4))*sin(13*i*pi/180/2)+(Z4_14R(4))*si
n(14*i*pi/180/2)+(Z4_15R(4))*sin(15*i*pi/180/2)+(Z4_16R(4))*sin(16*i*pi/180/2)+(Z4_17R(4))*sin(17*i
*pi/180/2)+(Z4_18R(4))*sin(18*i*pi/180/2)+(Z4_19R(4))*sin(19*i*pi/180/2)+(Z4_20R(4))*sin(20*i*pi/180
/2)+(Z4_21R(4))*sin(21*i*pi/180/2)+(Z4_22R(4))*sin(22*i*pi/180/2)+(Z4_23R(4))*sin(23*i*pi/180/2)+(Z
4_24R(4))*sin(24*i*pi/180/2));
end

figure;
plot(torque_cyl3_cyl4)


for i=1:720

torque_cyl4_cyl5(i)=((Z5_1R(2))*cos(i*pi/180/2)+(Z5_2R(2))*cos(i*pi/180)+(Z5_3R(2))*cos(3*i*pi/180/2)
+(Z5_4R(2))*cos(4*i*pi/180/2)+(Z5_5R(2))*cos(5*i*pi/180/2) ...

+(Z5_6R(2))*cos(6*i*pi/180/2)+(Z5_7R(2))*cos(7*i*pi/180/2)+(Z5_8R(2))*cos(8*i*pi/180/2)+(Z5_9R(2))
*cos(9*i*pi/180/2)+(Z5_10R(2))*cos(10*i*pi/180/2) ...

+(Z5_11R(2))*cos(11*i*pi/180/2)+(Z5_12R(2))*cos(12*i*pi/180/2)+(Z5_13R(2))*cos(13*i*pi/180/2)+(Z5_
14R(2))*cos(14*i*pi/180/2)+(Z5_15R(2))*cos(15*i*pi/180/2) ...

+(Z5_16R(2))*cos(16*i*pi/180/2)+(Z5_17R(2))*cos(17*i*pi/180/2)+(Z5_18R(2))*cos(18*i*pi/180/2)+(Z5_
19R(2))*cos(19*i*pi/180/2)+(Z5_20R(2))*cos(20*i*pi/180/2) ...

+(Z5_21R(2))*cos(21*i*pi/180/2)+(Z5_22R(2))*cos(22*i*pi/180/2)+(Z5_23R(2))*cos(23*i*pi/180/2)+(Z5_
24R(2))*cos(24*i*pi/180/2)) ...
```

```
      -
((Z5_1R(4))*sin(1*i*pi/180/2)+(Z5_2R(4))*sin(2*i*pi/180/2)+(Z5_3R(4))*sin(3*i*pi/180/2)+(Z5_4R(4))*s
in(4*i*pi/180/2)+(Z5_5R(4))*sin(5*i*pi/180/2) ...

+(Z5_6R(4))*sin(6*i*pi/180/2)+(Z5_7R(4))*sin(7*i*pi/180/2)+(Z5_8R(4))*sin(8*i*pi/180/2)+(Z5_9R(4))*s
in(9*i*pi/180/2)+(Z5_10R(4))*sin(10*i*pi/180/2) ...

+(Z5_11R(4))*sin(11*i*pi/180/2)+(Z5_12R(4))*sin(12*i*pi/180/2)+(Z5_13R(4))*sin(13*i*pi/180/2)+(Z5_1
4R(4))*sin(14*i*pi/180/2)+(Z5_15R(4))*sin(15*i*pi/180/2) ...

+(Z5_16R(4))*sin(16*i*pi/180/2)+(Z5_17R(4))*sin(17*i*pi/180/2)+(Z5_18R(4))*sin(18*i*pi/180/2)+(Z5_1
9R(4))*sin(19*i*pi/180/2)+(Z5_20R(4))*sin(20*i*pi/180/2) ...

+(Z5_21R(4))*sin(21*i*pi/180/2)+(Z5_22R(4))*sin(22*i*pi/180/2)+(Z5_23R(4))*sin(23*i*pi/180/2)+(Z5_2
4R(4))*sin(24*i*pi/180/2));
end

figure;
plot(torque_cyl4_cyl5)


for i=1:720

torque_cyl5_cyl6(i)=((Z6_1R(2))*cos(i*pi/180/2)+(Z6_2R(2))*cos(i*pi/180)+(Z6_3R(2))*cos(3*i*pi/180/2)
+(Z6_4R(2))*cos(4*i*pi/180/2)+(Z6_5R(2))*cos(5*i*pi/180/2) ...

+(Z6_6R(2))*cos(6*i*pi/180/2)+(Z6_7R(2))*cos(7*i*pi/180/2)+(Z6_8R(2))*cos(8*i*pi/180/2)+(Z6_9R(2))
*cos(9*i*pi/180/2)+(Z6_10R(2))*cos(10*i*pi/180/2) ...

+(Z6_11R(2))*cos(11*i*pi/180/2)+(Z6_12R(2))*cos(12*i*pi/180/2)+(Z6_13R(2))*cos(13*i*pi/180/2)+(Z6_
14R(2))*cos(14*i*pi/180/2)+(Z6_15R(2))*cos(15*i*pi/180/2) ...

+(Z6_16R(2))*cos(16*i*pi/180/2)+(Z6_17R(2))*cos(17*i*pi/180/2)+(Z6_18R(2))*cos(18*i*pi/180/2)+(Z6_
19R(2))*cos(19*i*pi/180/2)+(Z6_20R(2))*cos(20*i*pi/180/2) ...

+(Z6_21R(2))*cos(21*i*pi/180/2)+(Z6_22R(2))*cos(22*i*pi/180/2)+(Z6_23R(2))*cos(23*i*pi/180/2)+(Z6_
24R(2))*cos(24*i*pi/180/2)) ...
      -
((Z6_1R(4))*sin(1*i*pi/180/2)+(Z6_2R(4))*sin(2*i*pi/180/2)+(Z6_3R(4))*sin(3*i*pi/180/2)+(Z6_4R(4))*s
in(4*i*pi/180/2)+(Z6_5R(4))*sin(5*i*pi/180/2) ...

+(Z6_6R(4))*sin(6*i*pi/180/2)+(Z6_7R(4))*sin(7*i*pi/180/2)+(Z6_8R(4))*sin(8*i*pi/180/2)+(Z6_9R(4))*s
in(9*i*pi/180/2)+(Z6_10R(4))*sin(10*i*pi/180/2) ...

+(Z6_11R(4))*sin(11*i*pi/180/2)+(Z6_12R(4))*sin(12*i*pi/180/2)+(Z6_13R(4))*sin(13*i*pi/180/2)+(Z6_1
4R(4))*sin(14*i*pi/180/2)+(Z6_15R(4))*sin(15*i*pi/180/2) ...

+(Z6_16R(4))*sin(16*i*pi/180/2)+(Z6_17R(4))*sin(17*i*pi/180/2)+(Z6_18R(4))*sin(18*i*pi/180/2)+(Z6_1
9R(4))*sin(19*i*pi/180/2)+(Z6_20R(4))*sin(20*i*pi/180/2) ...

+(Z6_21R(4))*sin(21*i*pi/180/2)+(Z6_22R(4))*sin(22*i*pi/180/2)+(Z6_23R(4))*sin(23*i*pi/180/2)+(Z6_2
4R(4))*sin(24*i*pi/180/2));
end

figure;
plot(torque_cyl5_cyl6)


for i=1:720
```

```
torque_cyl6_flywheel(i)=((Z7_1R(2))*cos(i*pi/180/2)+(Z7_2R(2))*cos(i*pi/180)+(Z7_3R(2))*cos(3*i*pi/1
80/2)+(Z7_4R(2))*cos(4*i*pi/180/2)+(Z7_5R(2))*cos(5*i*pi/180/2) ...

+(Z7_6R(2))*cos(6*i*pi/180/2)+(Z7_7R(2))*cos(7*i*pi/180/2)+(Z7_8R(2))*cos(8*i*pi/180/2)+(Z7_9R(2))
*cos(9*i*pi/180/2)+(Z7_10R(2))*cos(10*i*pi/180/2) ...

+(Z7_11R(2))*cos(11*i*pi/180/2)+(Z7_12R(2))*cos(12*i*pi/180/2)+(Z7_13R(2))*cos(13*i*pi/180/2)+(Z7_
14R(2))*cos(14*i*pi/180/2)+(Z7_15R(2))*cos(15*i*pi/180/2) ...

+(Z7_16R(2))*cos(16*i*pi/180/2)+(Z7_17R(2))*cos(17*i*pi/180/2)+(Z7_18R(2))*cos(18*i*pi/180/2)+(Z7_
19R(2))*cos(19*i*pi/180/2)+(Z7_20R(2))*cos(20*i*pi/180/2) ...

+(Z7_21R(2))*cos(21*i*pi/180/2)+(Z7_22R(2))*cos(22*i*pi/180/2)+(Z7_23R(2))*cos(23*i*pi/180/2)+(Z7_
24R(2))*cos(24*i*pi/180/2)) ...
    -
((Z7_1R(4))*sin(1*i*pi/180/2)+(Z7_2R(4))*sin(2*i*pi/180/2)+(Z7_3R(4))*sin(3*i*pi/180/2)+(Z7_4R(4))*s
in(4*i*pi/180/2)+(Z7_5R(4))*sin(5*i*pi/180/2) ...

+(Z7_6R(4))*sin(6*i*pi/180/2)+(Z7_7R(4))*sin(7*i*pi/180/2)+(Z7_8R(4))*sin(8*i*pi/180/2)+(Z7_9R(4))*s
in(9*i*pi/180/2)+(Z7_10R(4))*sin(10*i*pi/180/2) ...

+(Z7_11R(4))*sin(11*i*pi/180/2)+(Z7_12R(4))*sin(12*i*pi/180/2)+(Z7_13R(4))*sin(13*i*pi/180/2)+(Z7_1
4R(4))*sin(14*i*pi/180/2)+(Z7_15R(4))*sin(15*i*pi/180/2) ...

+(Z7_16R(4))*sin(16*i*pi/180/2)+(Z7_17R(4))*sin(17*i*pi/180/2)+(Z7_18R(4))*sin(18*i*pi/180/2)+(Z7_1
9R(4))*sin(19*i*pi/180/2)+(Z7_20R(4))*sin(20*i*pi/180/2) ...

+(Z7_21R(4))*sin(21*i*pi/180/2)+(Z7_22R(4))*sin(22*i*pi/180/2)+(Z7_23R(4))*sin(23*i*pi/180/2)+(Z7_2
4R(4))*sin(24*i*pi/180/2));
end

figure;
plot(torque_cyl6_flywheel)



for i=1:720

torque_zero(i)=((Z8_1R(2))*cos(i*pi/180/2)+(Z8_2R(2))*cos(i*pi/180)+(Z8_3R(2))*cos(3*i*pi/180/2)+(Z8
_4R(2))*cos(4*i*pi/180/2)+(Z8_5R(2))*cos(5*i*pi/180/2) ...

+(Z8_6R(2))*cos(6*i*pi/180/2)+(Z8_7R(2))*cos(7*i*pi/180/2)+(Z8_8R(2))*cos(8*i*pi/180/2)+(Z8_9R(2))
*cos(9*i*pi/180/2)+(Z8_10R(2))*cos(10*i*pi/180/2) ...

+(Z8_11R(2))*cos(11*i*pi/180/2)+(Z8_12R(2))*cos(12*i*pi/180/2)+(Z8_13R(2))*cos(13*i*pi/180/2)+(Z8_
14R(2))*cos(14*i*pi/180/2)+(Z8_15R(2))*cos(15*i*pi/180/2) ...

+(Z8_16R(2))*cos(16*i*pi/180/2)+(Z8_17R(2))*cos(17*i*pi/180/2)+(Z8_18R(2))*cos(18*i*pi/180/2)+(Z8_
19R(2))*cos(19*i*pi/180/2)+(Z8_20R(2))*cos(20*i*pi/180/2) ...

+(Z8_21R(2))*cos(21*i*pi/180/2)+(Z8_22R(2))*cos(22*i*pi/180/2)+(Z8_23R(2))*cos(23*i*pi/180/2)+(Z8_
24R(2))*cos(24*i*pi/180/2)) ...
    -
((Z8_1R(4))*sin(1*i*pi/180/2)+(Z8_2R(4))*sin(2*i*pi/180/2)+(Z8_3R(4))*sin(3*i*pi/180/2)+(Z8_4R(4))*s
in(4*i*pi/180/2)+(Z8_5R(4))*sin(5*i*pi/180/2) ...

+(Z8_6R(4))*sin(6*i*pi/180/2)+(Z8_7R(4))*sin(7*i*pi/180/2)+(Z8_8R(4))*sin(8*i*pi/180/2)+(Z8_9R(4))*s
in(9*i*pi/180/2)+(Z8_10R(4))*sin(10*i*pi/180/2) ...
```

```
+(Z8_11R(4))*sin(11*i*pi/180/2)+(Z8_12R(4))*sin(12*i*pi/180/2)+(Z8_13R(4))*sin(13*i*pi/180/2)+(Z8_1
4R(4))*sin(14*i*pi/180/2)+(Z8_15R(4))*sin(15*i*pi/180/2) ...

+(Z8_16R(4))*sin(16*i*pi/180/2)+(Z8_17R(4))*sin(17*i*pi/180/2)+(Z8_18R(4))*sin(18*i*pi/180/2)+(Z8_1
9R(4))*sin(19*i*pi/180/2)+(Z8_20R(4))*sin(20*i*pi/180/2) ...

+(Z8_21R(4))*sin(21*i*pi/180/2)+(Z8_22R(4))*sin(22*i*pi/180/2)+(Z8_23R(4))*sin(23*i*pi/180/2)+(Z8_2
4R(4))*sin(24*i*pi/180/2));
end

figure;
plot(torque_zero)


W=pi*0.077^3/16;


%stress related to crankpin

stress_pulley_cyl1=torque_pulley_cyl1/W;
figure;
plot(stress_pulley_cyl1)

stress_cyl1_cyl2=torque_cyl1_cyl2/W;
figure;
plot(stress_cyl1_cyl2)

stress_cyl2_cyl3=torque_cyl2_cyl3/W;
figure;
plot(stress_cyl2_cyl3)

stress_cyl3_cyl4=torque_cyl3_cyl4/W;
figure;
plot(stress_cyl3_cyl4)

stress_cyl4_cyl5=torque_cyl4_cyl5/W;
figure;
plot(stress_cyl4_cyl5)

stress_cyl5_cyl6=torque_cyl5_cyl6/W;
figure;
plot(stress_cyl5_cyl6)

stress_cyl6_flywheel=torque_cyl6_flywheel/W;
figure;
plot(stress_cyl6_flywheel)
```

APPENDIX B
STRESS RESULTS FOR BEAM CRANKSHAFT MODEL

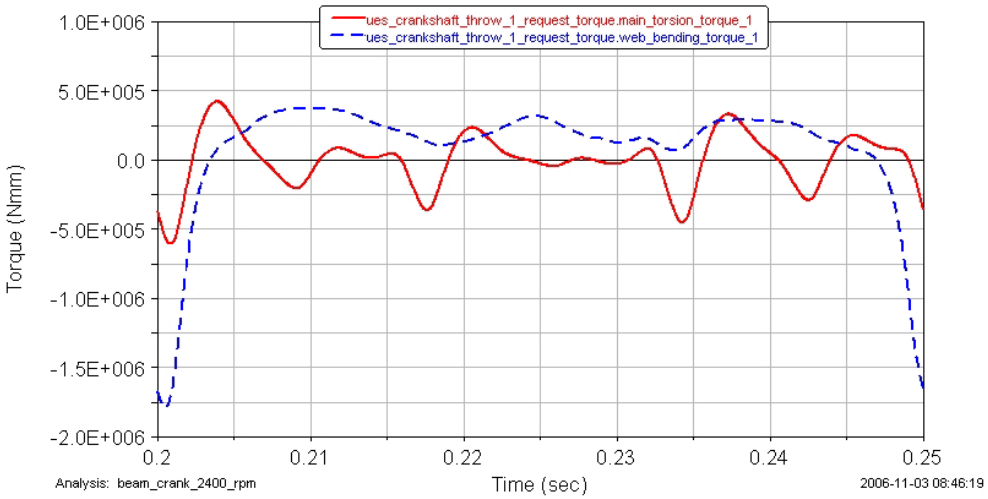

Figure B1. Web 1 (main torque and web bending moment)

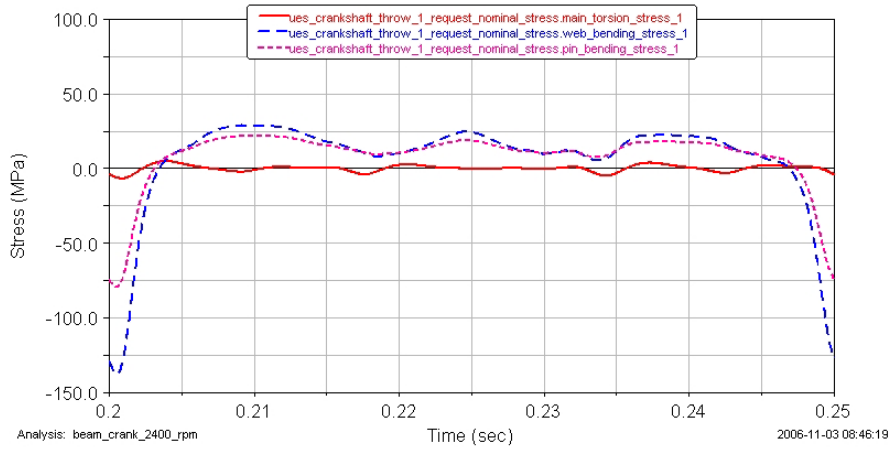

Figure B2. Web 1 (main torsion, web bending and pin bending stresses)

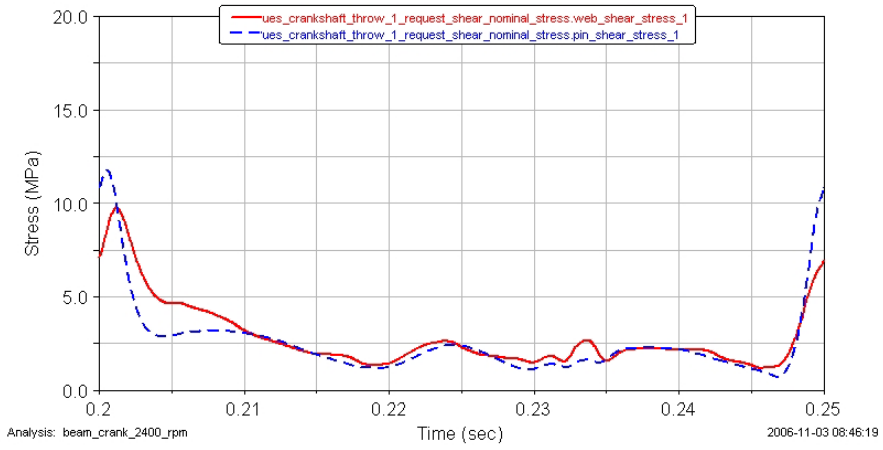

Figure B3. Web 1 (web and pin shear stresses)

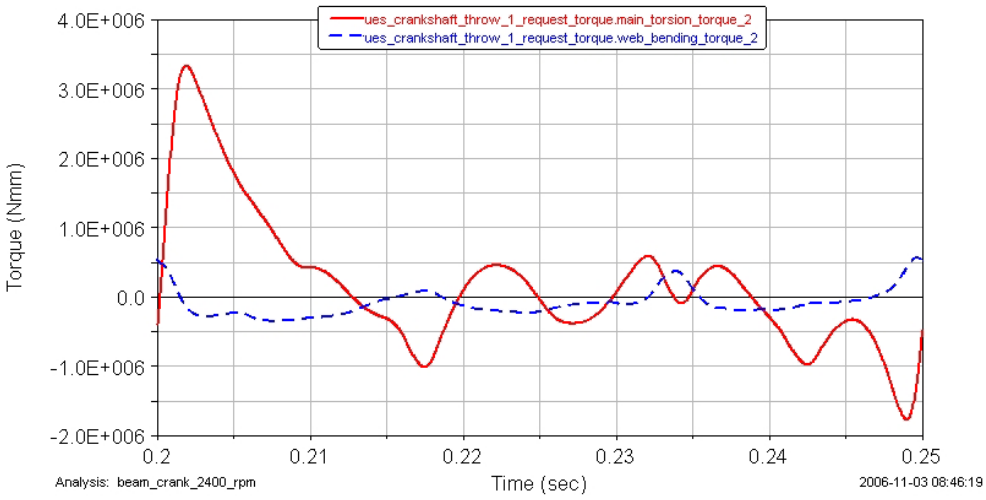

Figure B4. Web 2 (main torque and web bending moment)

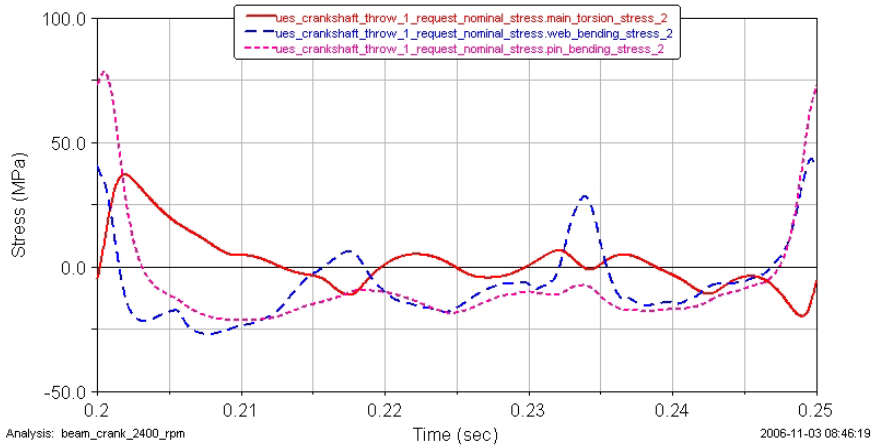

Figure B5. Web 2 (main torsion, web bending and pin bending stresses)

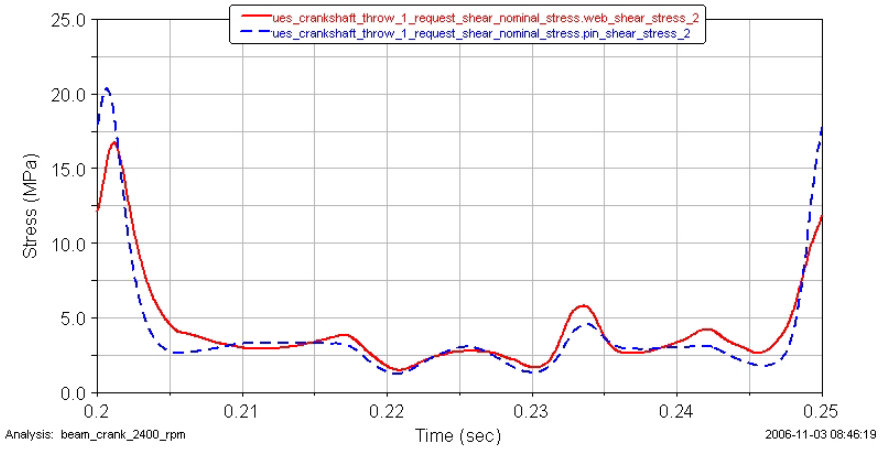

Figure B6. Web 2 (web and pin shear stresses)

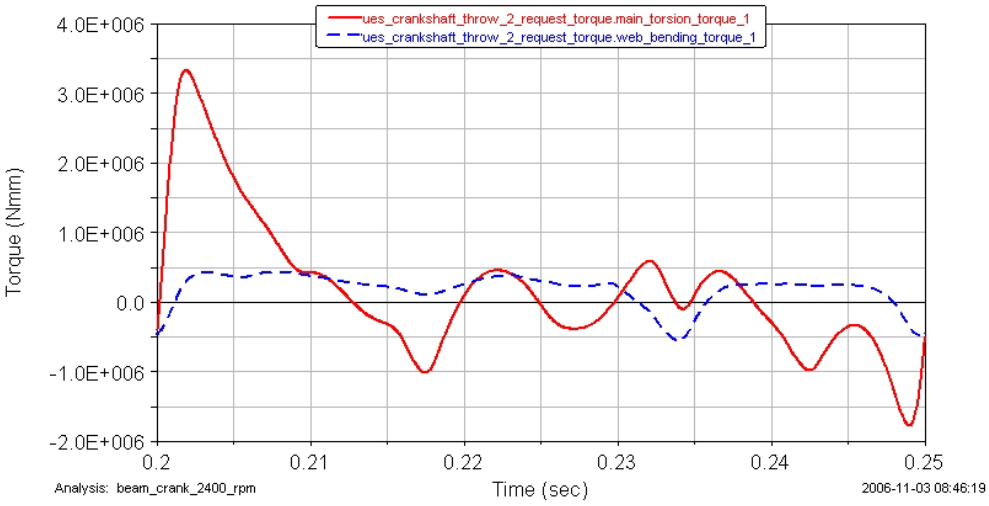

Figure B7. Web 3 (main torque and web bending moment)

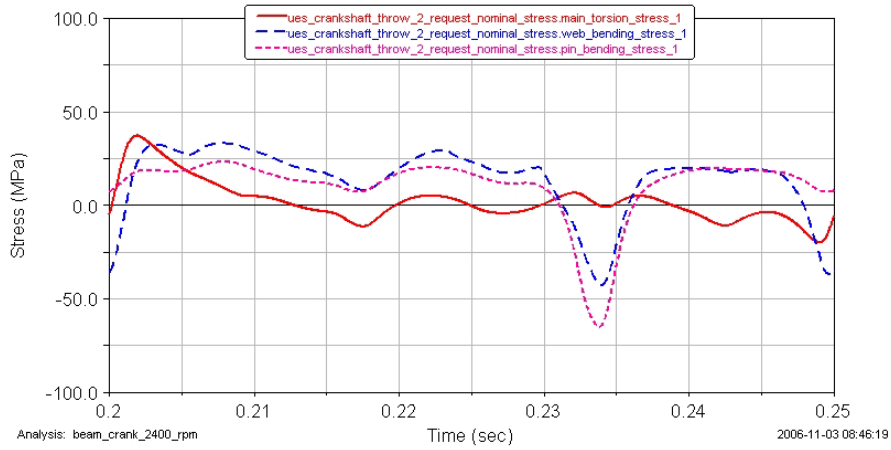

Figure B8. Web 3 (main torsion, web bending and pin bending stresses)

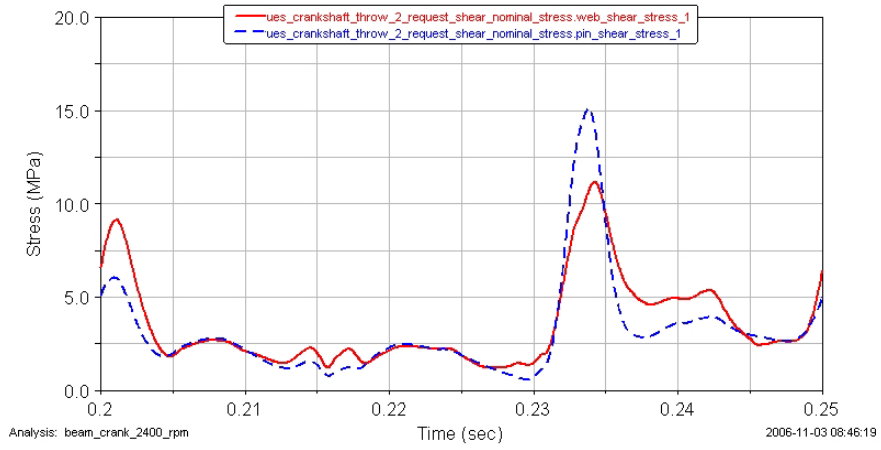

Figure B9. Web 3 (web and pin shear stresses)

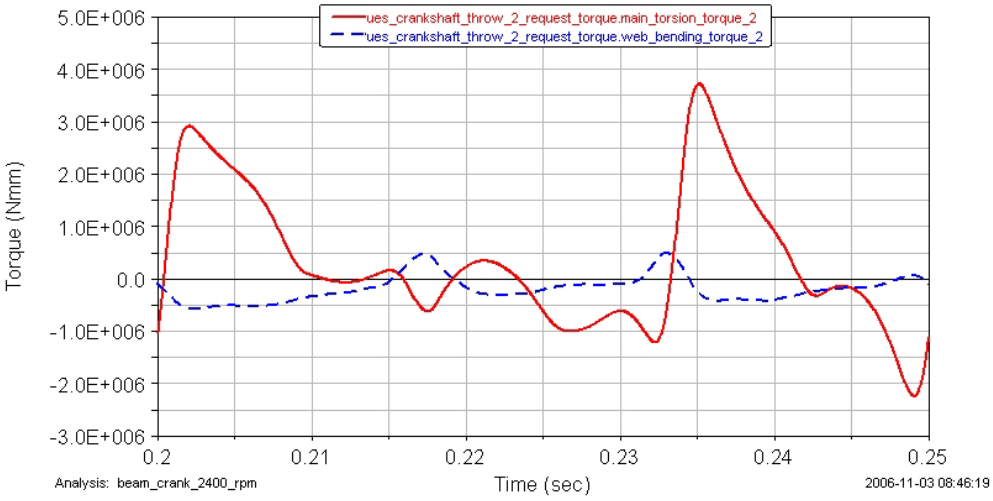

Figure B10. Web 4 (main torque and web bending moment)

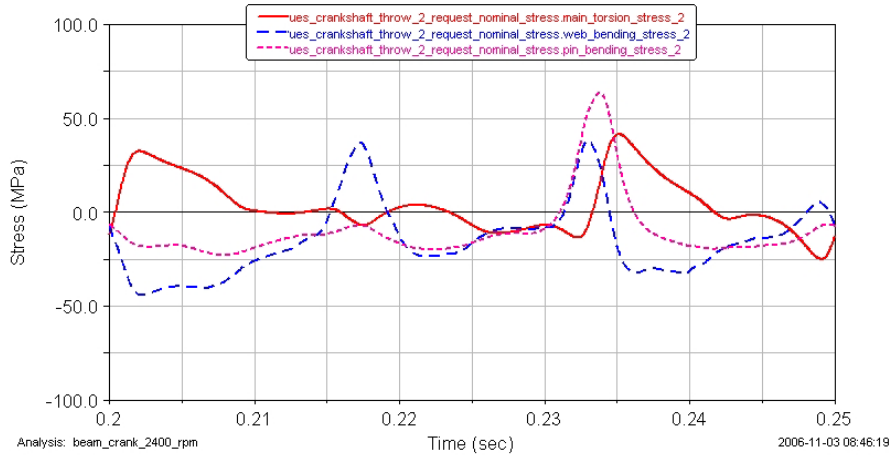

Figure B11. Web 4 (main torsion, web bending and pin bending stresses)

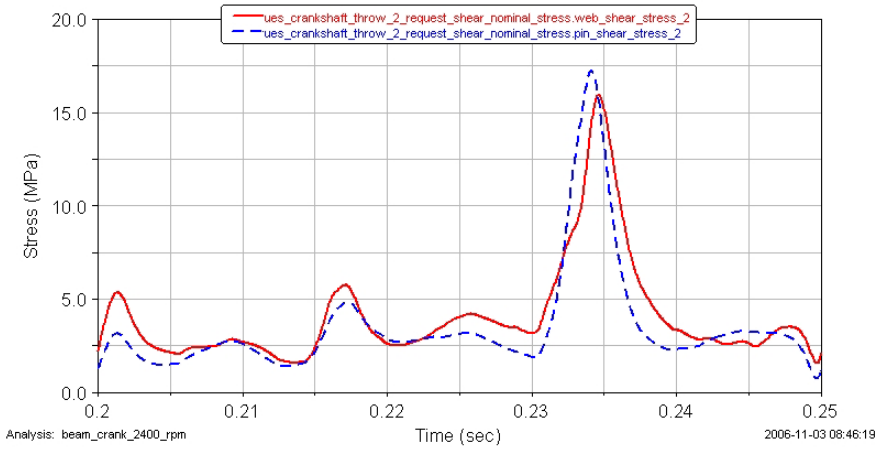

Figure B12. Web 4 (web and pin shear stresses)

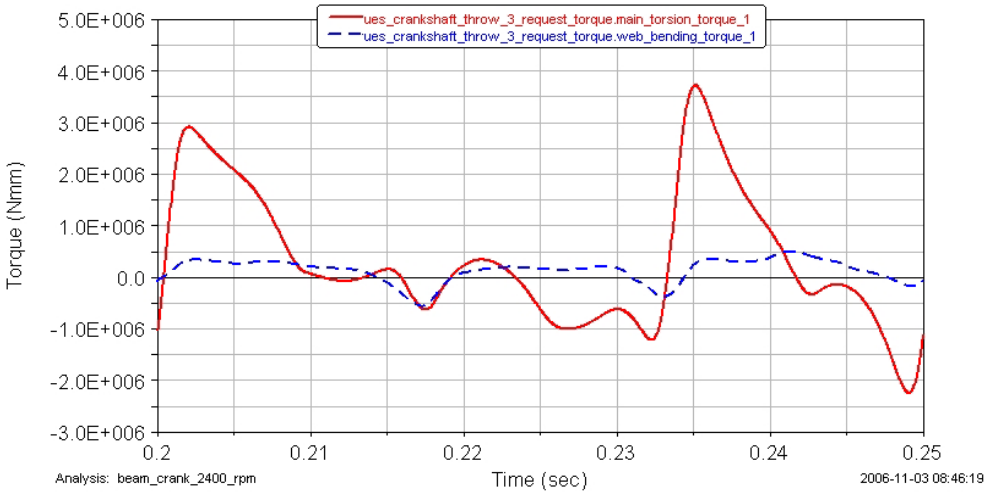

Figure B13. Web 5 (main torque and web bending moment)

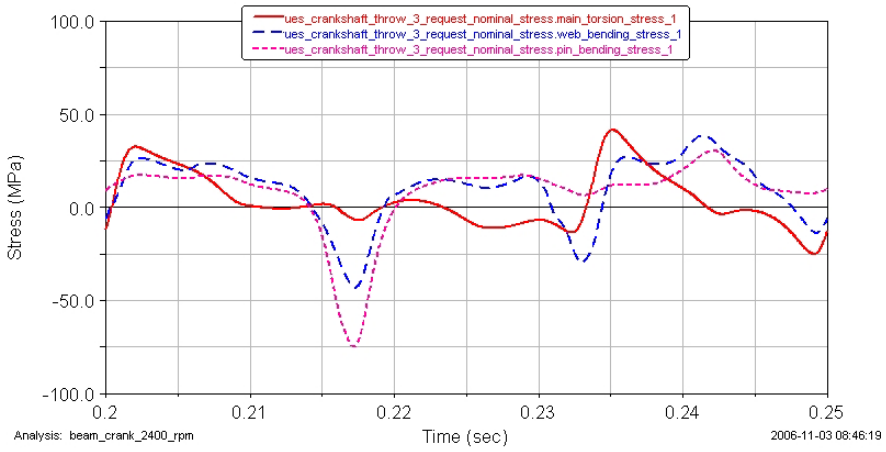

Figure B14. Web 5 (main torsion, web bending and pin bending stresses)

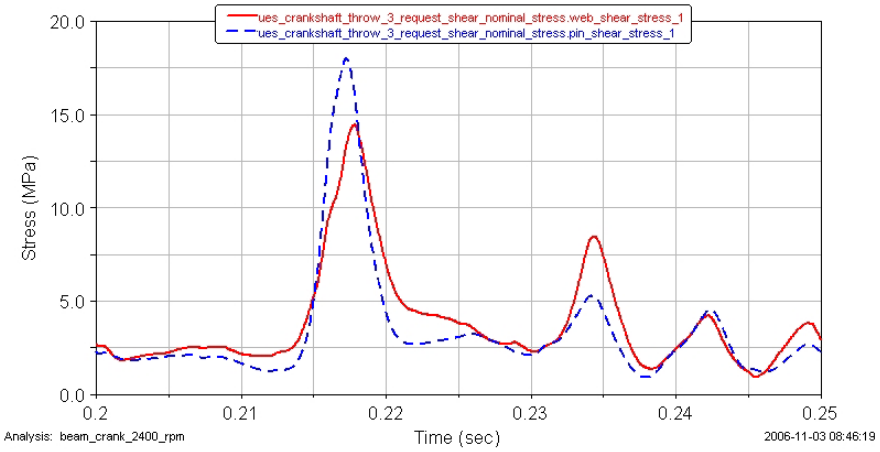

Figure B15. Web 5 (web and pin shear stresses)

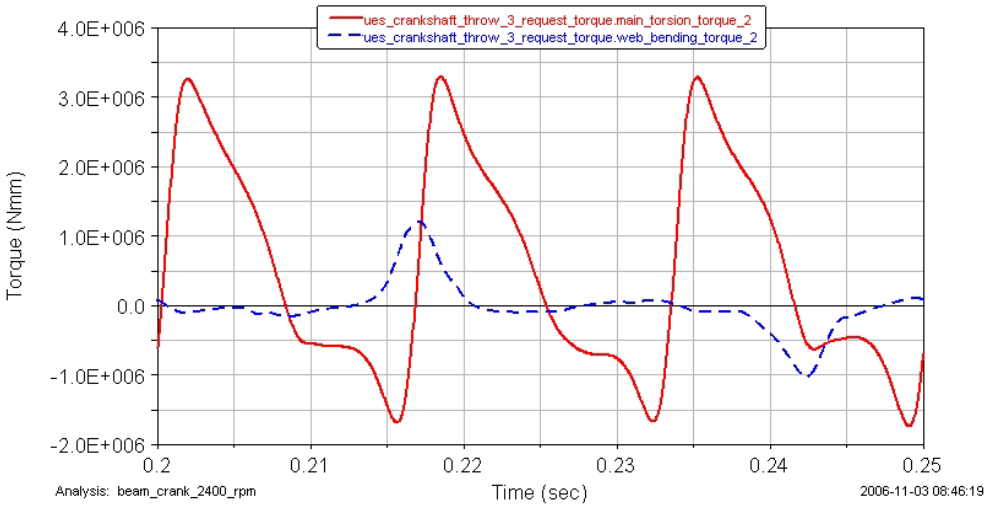

Figure B16. Web 6 (main torque and web bending moment)

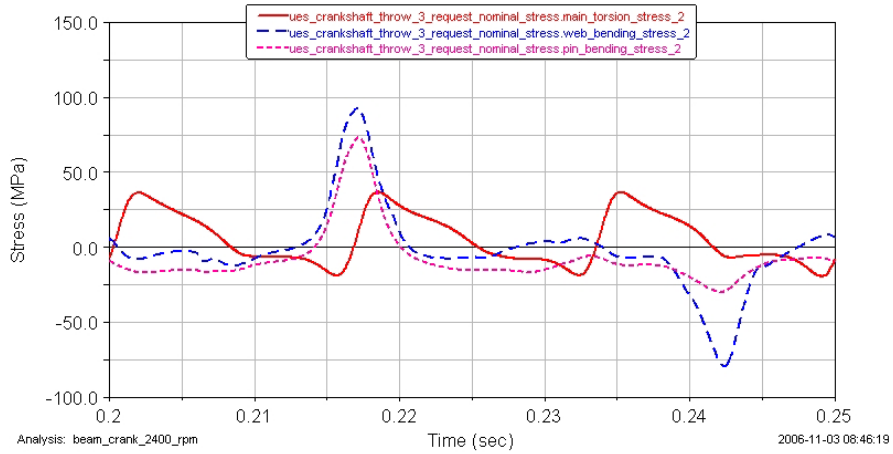

Figure B17. Web 6 (main torsion, web bending and pin bending stresses)

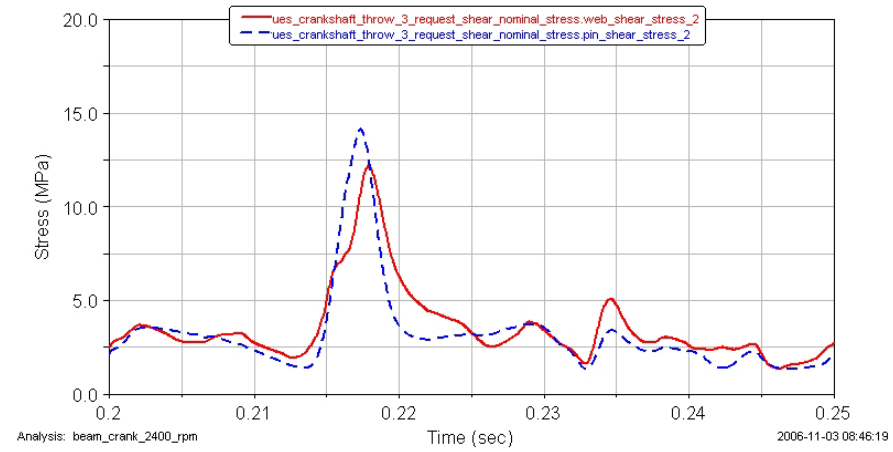

Figure B18. Web 6 (web and pin shear stresses)

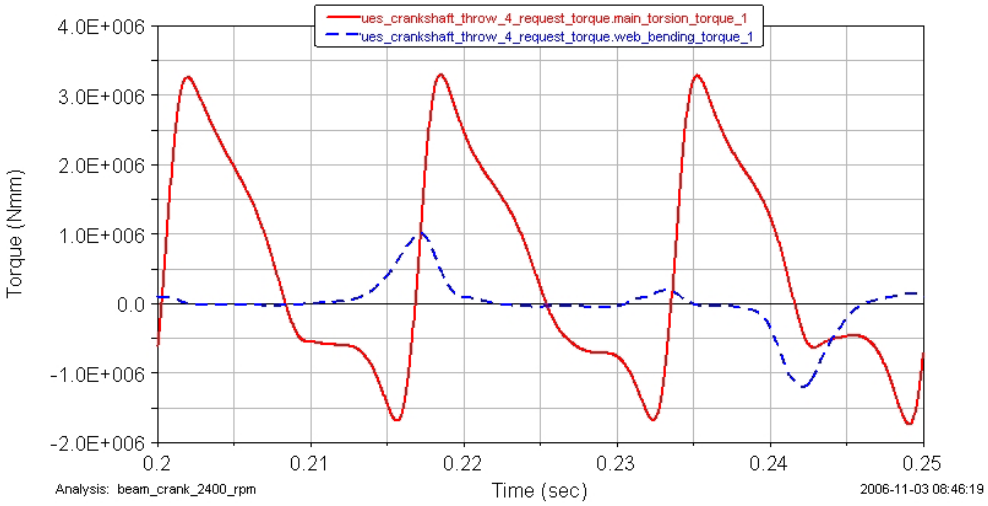

Figure B19. Web 7 (main torque and web bending moment)

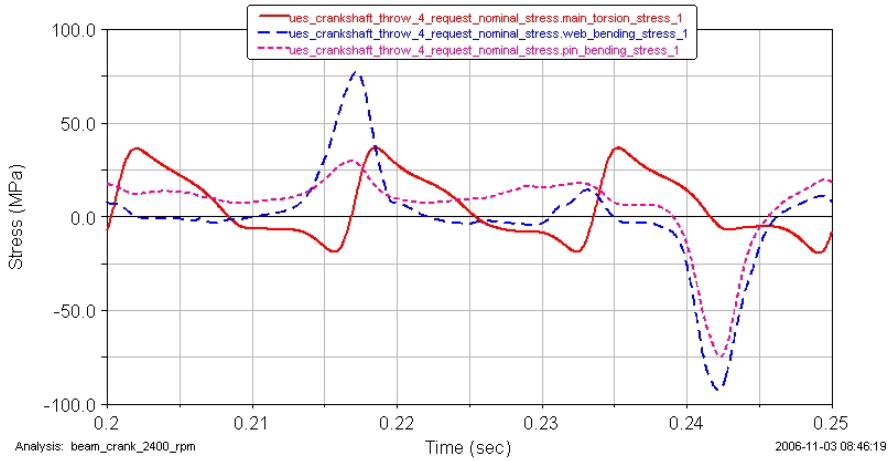

Figure B20. Web 7 (main torsion, web bending and pin bending stresses)

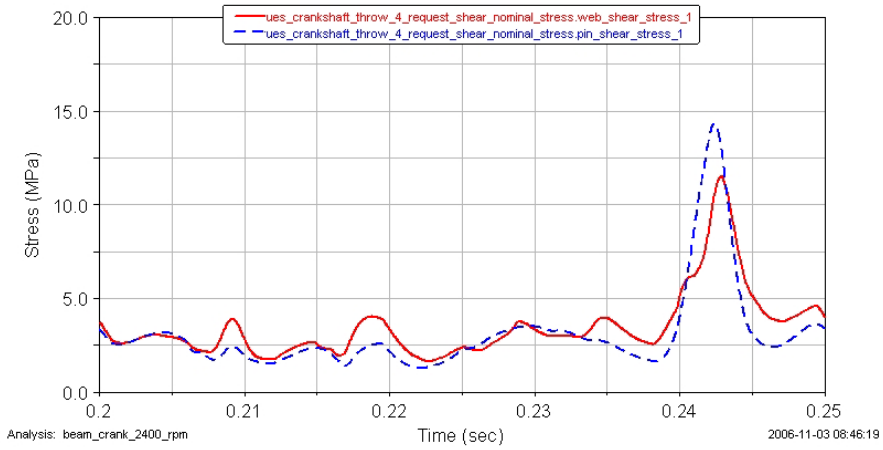

Figure B21. Web 7 (web and pin shear stresses)

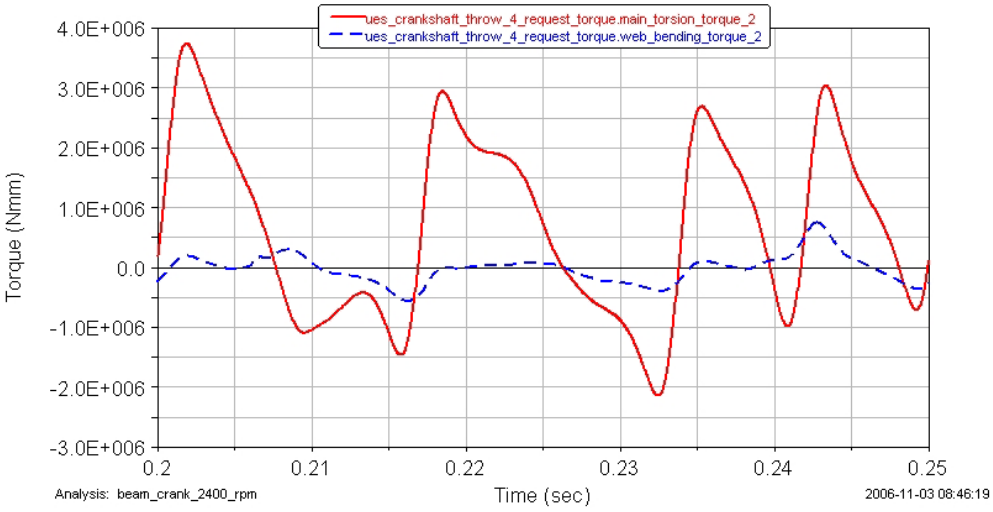

Figure B22. Web 8 (main torque and web bending moment)

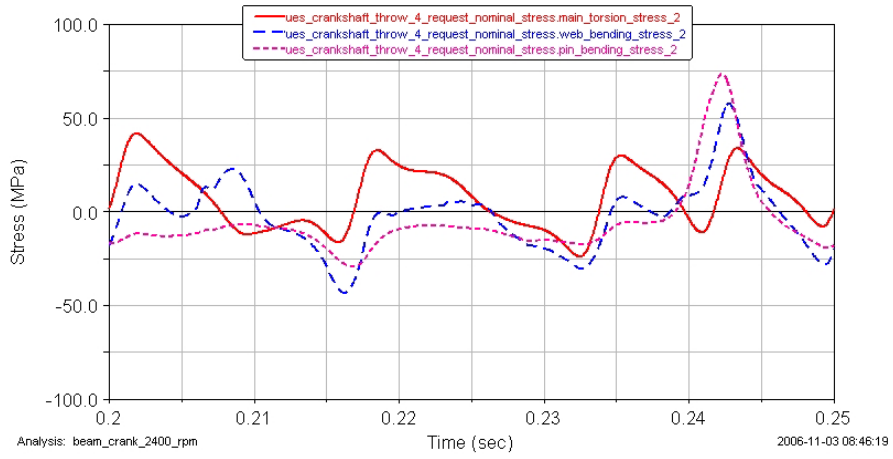

Figure B23. Web 8 (main torsion, web bending and pin bending stresses)

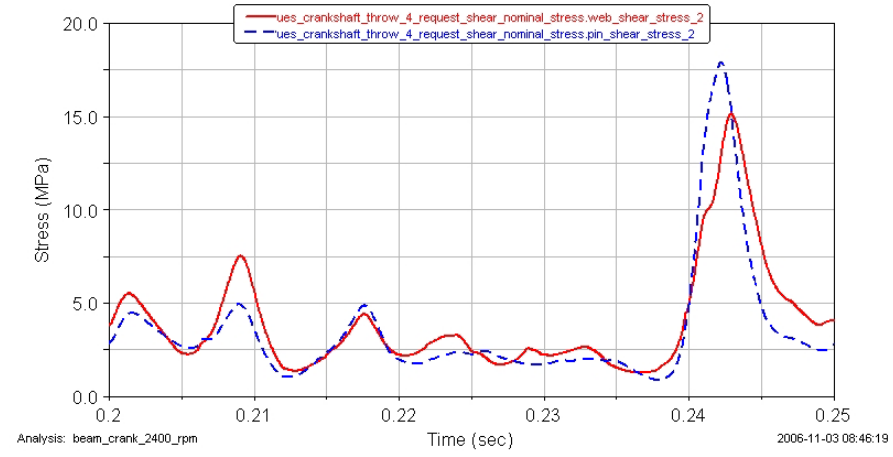

Figure B24. Web 8 (web and pin shear stresses)

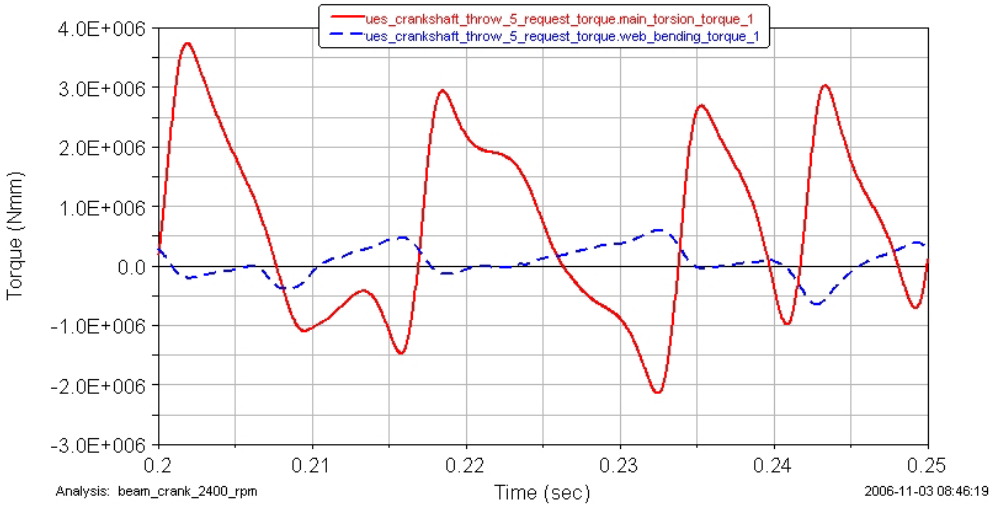

Figure B25. Web 9 (main torque and web bending moment)

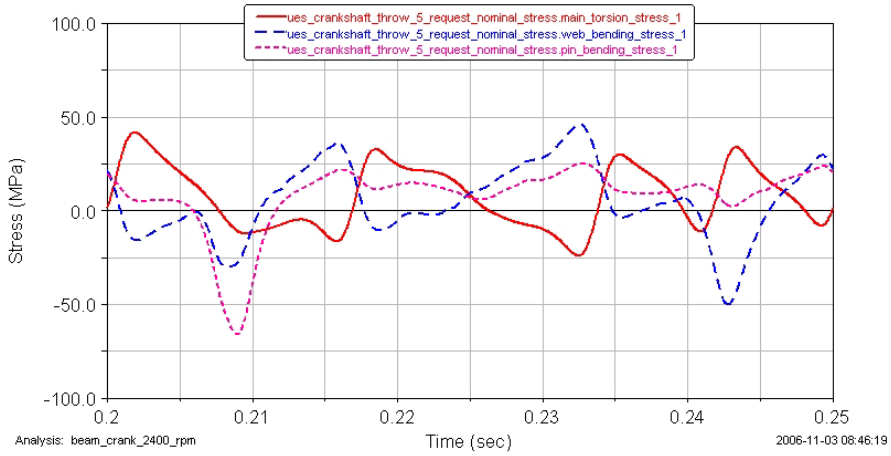

Figure B26. Web 9 (main torsion, web bending and pin bending stresses)

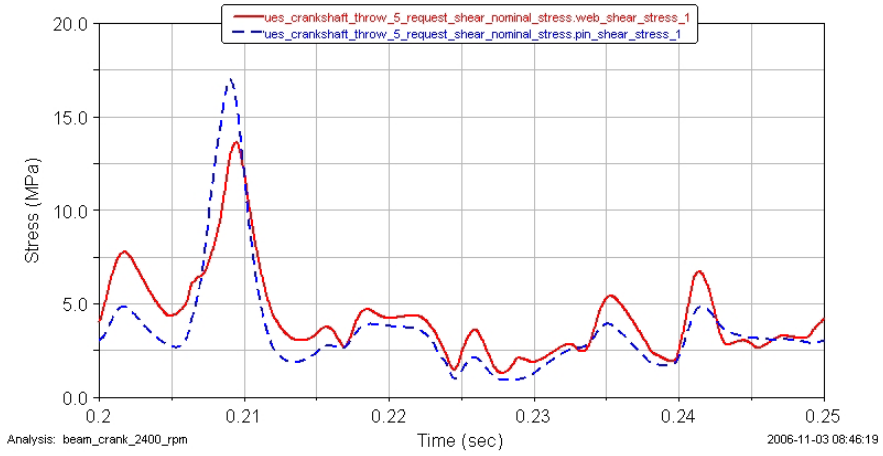

Figure B27. Web 9 (web and pin shear stresses)

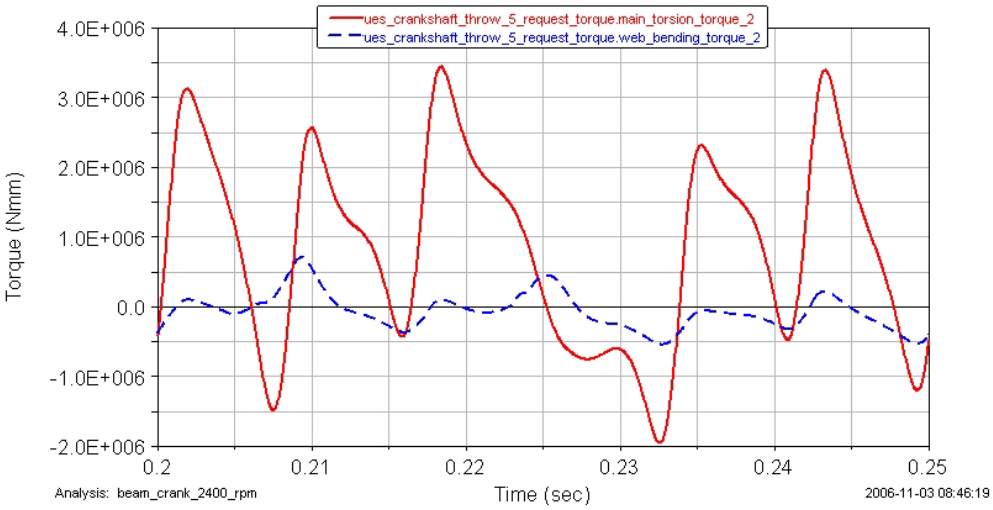

Figure B28. Web 10 (main torque and web bending moment)

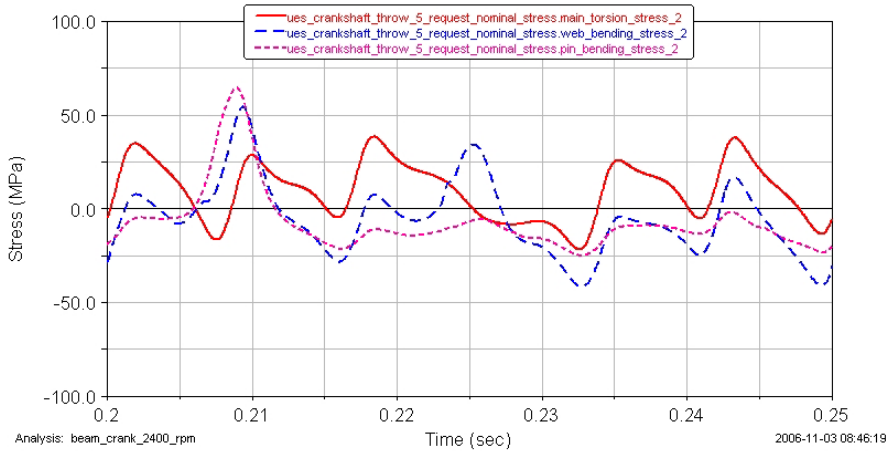

Figure B29. Web 10 (main torsion, web bending and pin bending stresses)

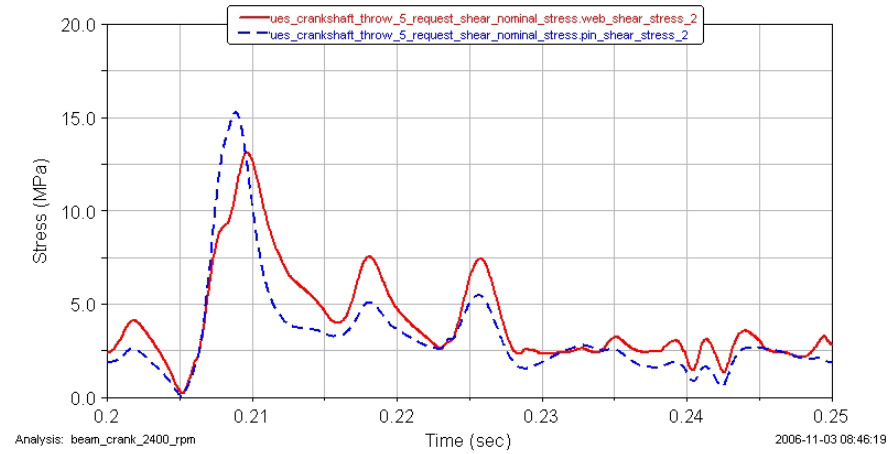

Figure B30. Web 10 (web and pin shear stresses)

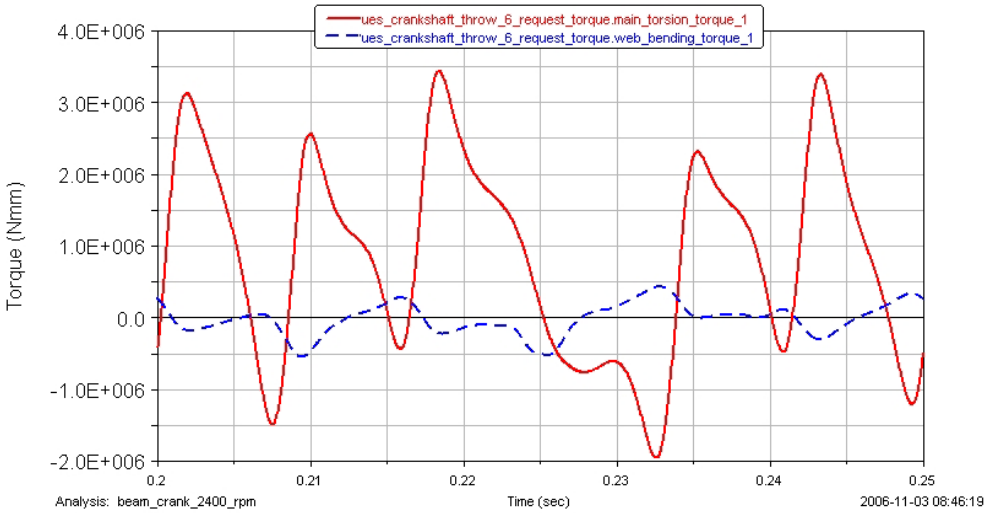

Figure B31. Web 11 (main torque and web bending moment)

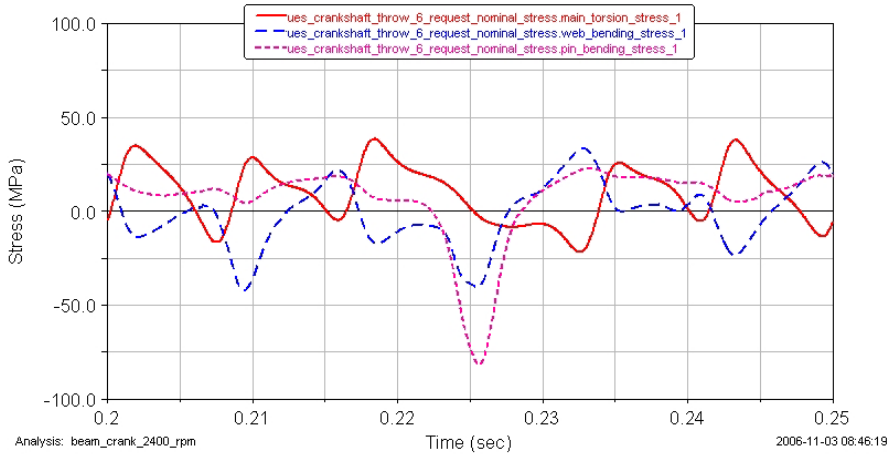

Figure B32. Web 11 (main torsion, web bending and pin bending stresses)

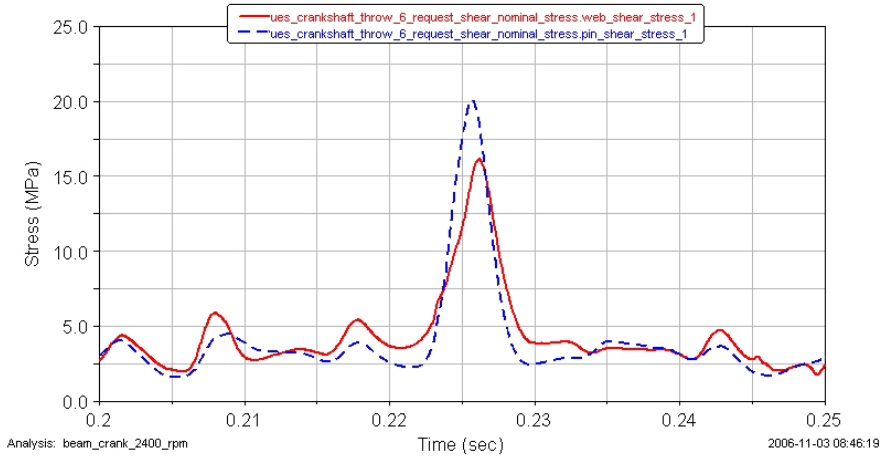

Figure B33. Web 11 (web and pin shear stresses)

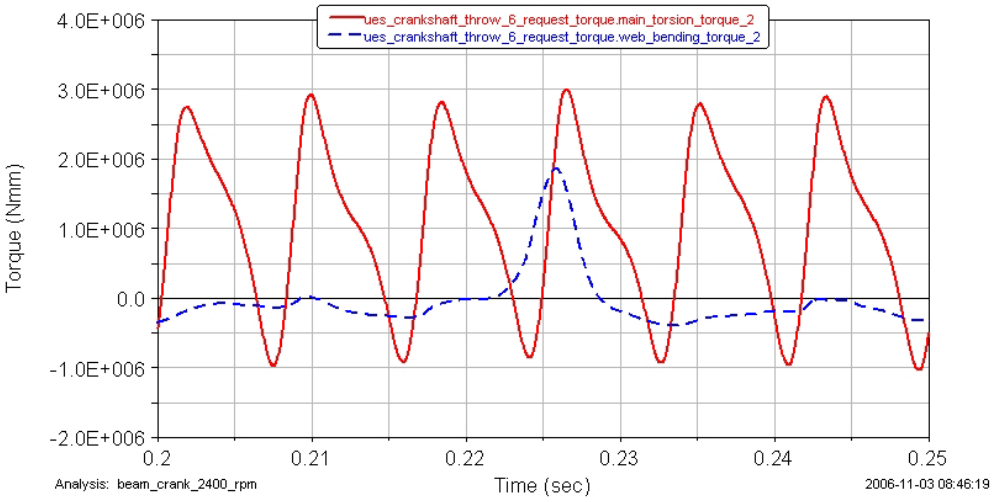

Figure B34. Web 12 (main torque and web bending moment)

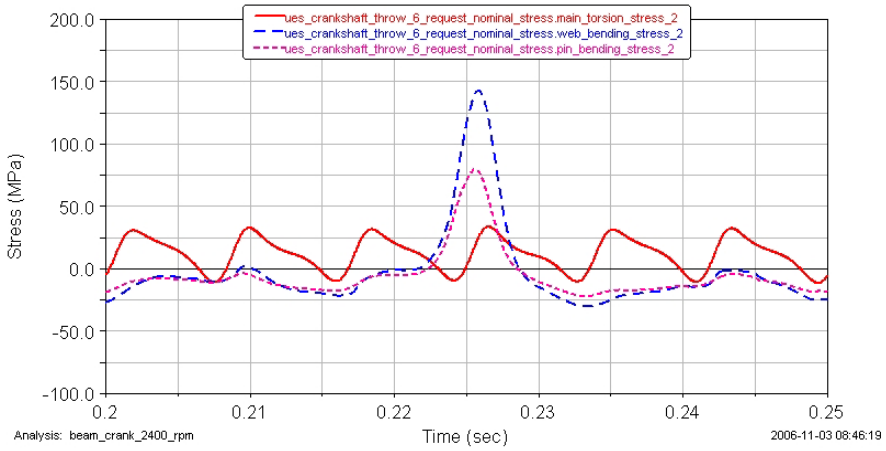

Figure B35. Web 12 (main torsion, web bending and pin bending stresses)

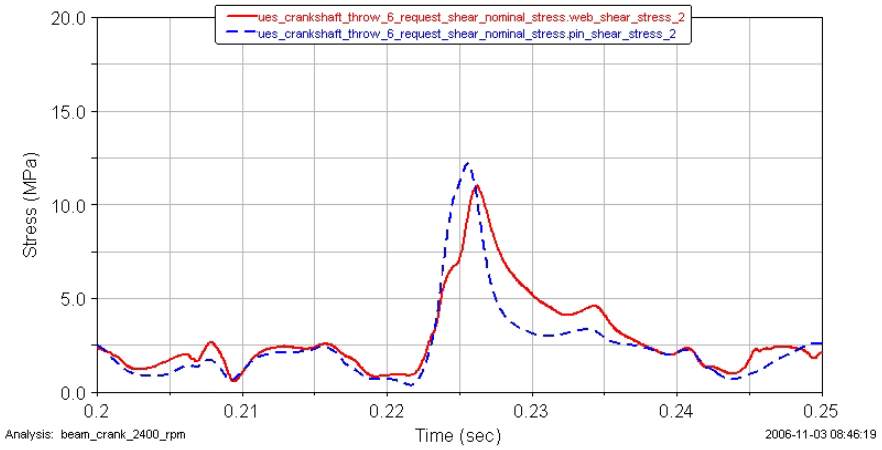

Figure B36. Web 12 (web and pin shear stresses)

REFERENCES

1. Heywood, J. B., *Internal Combustion Engine Fundamentals*, McGraw Hill, ISBN 0-07-100499-8, 1988.

2. Ferguson, C. R., *Internal Combustion Engines*, John Wiley & Sons, ISBN 0-471-88129-5, 1986.

3. Rebbert, M. and P. Kley, "Strategies for mechanical engine simulations", 14th European ADAMS Users' Conference, Berlin, 1999.

4. Okamura, H., A. Shinno, T. Yamanaka, A. Suzuki and K. Sogabe, "Simple modeling and analysis for crankshaft three-dimensional vibrations, Part 1: Background and application to free vibrations", *Journal of Vibration and Acoustics*, Vol. 117, pp. 70-79, 1995.

5. Morita, T. and H. Okamura, "Simple modeling and analysis for crankshaft three-dimensional vibrations, Part 2: Application to an operating engine crankshaft", *Journal of Vibration and Acoustics*, Vol.117, pp. 80-86, 1995.

6. Rajendran, S., M. V. Narasimhan, "Effect of inertia variation due to reciprocating parts and connecting rod on coupled free vibration of crankshaft", *Journal of Engineering for Gas Turbines and Power*, Vol. 119, pp. 257-263, 1997.

7. Boysal, A. and H. Rahnejat, "Torsional vibration analysis of a multi-body single cylinder internal combustion engine model", *Applied Mathematical Modeling*, Vol. 21, pp. 481-493, 1997.

8. Brusa, E., C. Delprete and G. Genta, "Torsional vibration of crankshafts: Effects of non-constant moments of inertia", *Journal of Sound and Vibration*, Vol. 205, No. 2, pp. 135-150, 1997.

9. Kang, Y., G. J. Sheen and M. H. Tseng, “Modal analyses and experiments for engine crankshafts”, *Journal of Sound and Vibration*, Vol. 214, No. 3, pp. 413-430, 1998.

10. Nehme, H., N. G. Chalhoub and N. Henein, “Development of a dynamic model for predicting the rigid and flexible motions of the crank slider mechanism”, *Journal of Engineering for Gas Turbines and Power*, Vol. 120, pp. 678-686, 1998.

11. Chalhoub, N. G., H. Nehme and N. A. Henein, “Effects of structural deformations of the crank-slider mechanism on the estimation of the instantaneous engine friction torque”, *Journal of Sound and Vibration*, Vol. 224, No. 3, pp. 489-503, 1999.

12. Nehme, H., N. G. Chalhoub, and N. A. Henein, “Effects of filtering the angular motion of the crankshaft on the estimation of the instantaneous engine friction torque”, *Journal of Sound and Vibration*, Vol. 236, No 5, pp. 881-894, 2000.

13. Mourelatos, Z. P., “An efficient crankshaft dynamic analysis using substructuring with Ritz vectors”, *Journal of Sound and Vibration*, Vol. 238, No 3, pp. 495-527, 2000.

14. Mourelatos, Z. P., “A crankshaft system model for structural dynamic analysis of internal combustion engines”, *Computers & Structures*, Vol. 79, pp. 2009-2027, 2001.

15. Hoffman, D. M. W. and D. R. Dowling, “Fully coupled rigid internal combustion engine dynamics and vibration-Part 1: Model development”, *Journal of Engineering for Gas Turbines and Power*, Vol. 123, pp. 677-684, 2001.

16. Hoffman, D. M. W. and D. R. Dowling, “Fully coupled rigid internal combustion engine dynamics and vibration-Part II: Model-experiment comparisons”, *Journal of Engineering for Gas Turbines and Power*, Vol. 123, pp. 677-684, 2001.

17. Ma, Z. D. and N. C. Perkins, “An efficient multibody dynamics model for internal combustion engine systems”, *Multibody System Dynamics*, Vol. 10, pp. 363-391, 2003.

18. Metallidis, P. and S. Natsiavas, “Linear and nonlinear dynamics of reciprocating engines”, *International Journal of Non-Linear Mechanics*, Vol. 38, pp. 723-738, 2003.

19. Zweiri, Y. H., J. F. Whidborne and L. D. Seneviratne, “Dynamic simulation of a single-cylinder diesel engine including dynamometer modeling and friction”, *Proceedings of the Institution of Mechanical Engineers Part D Journal of Automobile Engineering*, Vol. 213, pp. 391-402, 1999.

20. Zweiri, Y. H., J. F. Whidborne and L. D. Seneviratne, “Instantaneous friction components model for transient engine operation”, *Proceedings of the Institution of Mechanical Engineers Part D Journal of Automobile Engineering*, Vol. 214, pp. 809-824, 2000.

21. Zweiri, Y. H., J. F. Whidborne and L. D. Seneviratne, “Detailed analytical model of a single-cylinder diesel engine in the crank angle domain”, *Proceedings of the Institution of Mechanical Engineers Part D Journal of Automobile Engineering*, Vol. 215, pp. 1197-1216, 2001.

22. Pasricha, M. S. and W. D. Carnegie, “Effects of variable inertia on the damped torsional vibrations of diesel engine systems”, *Journal of sound and vibration*, Vol. 46, No. 3, pp. 339-345, 1976.

23. Drew, S. J., D. C. Hesterman and B. J. Stone, “The torsional excitation of variable inertia effects in a reciprocating engine”, *Mechanical Systems and Signal Processing*, Vol. 13, No. 1, pp. 125-144, 1999.

24. Geveci, M., A. W. Osburn and M. A. Franchek, “An investigation of crankshaft oscillations for cylinder health diagnostics”, *Mechanical Systems and Signal Processing*, Vol. 19, pp. 1107-1134, 2005.

25. Burla, R. V., P. Seshu, H. Hirani, P. R. Sajanpawar and H. S. Suresh, “Three dimensional finite element analysis of crankshaft torsional vibrations using parametric modeling techniques”, *SAE Technical Paper*, No. 2003-01-2711, 2003.

26. Parakash, V., K. Aprameyan and U. Shrinivasa, “An FEM based approach to crankshaft dynamics and life estimation”, *SAE Technical Paper*, No. 980565, 1998.

27. Raub, J., J. D. Jones, P. Kley and M. Rebbert, “Analytical investigation of crankshaft dynamics as a virtual engine module”, *SAE Technical Paper*, No. 1999-01-1750, 1999.

28. Ortjohann, T., M. Rebbert, F. Maassen and M. Robers, “3D-Durability analysis of crankshafts via coupled dynamic simulation including modal reduction”, *SAE Technical Paper*, No. 2006-01-0823, 2006.

29. Kodama, T., K. Wakabayashi, Y. Honda and S. Iwamoto, “Three dimensional vibration characteristics of high-speed automobile diesel engine crankshaft system with a viscous fluid damper”, *SAE Technical Paper*, No. 2002-01-0165, 2002.

30. Henry, J. P., J. Toplosky and M. Abramczuk, “Crankshaft durability prediction – a new 3-D approach”, *SAE Technical Paper*, No. 920087, 1992.

31. Kreuter, P. and F. Pischinger, “Status of rules and methods for assessment of stresses in crankshafts of I.C. engines”, *SAE Technical Paper*, No: 851197, 1995.

32. Borges, A. C. C., L. C. Oliveira and P. S. Neto, “Stress distribution in a crankshaft crank using a geometrically restricted finite element model”, *SAE Technical Paper*, No. 2002-01-2183, 2002.

33. Montazersadgh, F. H. and A. Fatemi, “Dynamic load and stress analysis of a crankshaft”, *SAE Technical Paper*, No. 2007-01-0258, 2002.

34. Wu, J. S. and I. H. Yang, “Computer method for torsion-and-flexure-coupled forced vibration of shafting system with damping”, *Journal of sound and vibration*, Vol. 180, No. 3, pp. 417-435, 1995.

35. Koser, K. and F. Pasin, “Continuous modeling of the torsional vibrations of the drive shaft of mechanisms”, *Journal of Sound and Vibration*, Vol. 188, No. 1, pp. 17-24, 1995.

36. Heath, A. R. and P. M. McNamara, “Crankshaft stress analysis – combination of finite element and classical analysis techniques”, *Journal of Engineering for Gas Turbines and Power*, Vol. 112, pp. 268-275, 1990.

37. Priebsch, H. H., J. Affenzeller and S. Gran, “Prediction technique for stress and vibration of nonlinear supported, rotating crankshafts”, *Journal of Engineering for Gas Turbines and Power*, Vol. 115, pp. 711-720, 1993.

38. Fessler, H. and V. K. Sood, “Stress distributions in some diesel engine crankshafts”, *Journal of Engineering for Power*, pp. 1-10, 1972.

39. Bickley, I., V. D’Olier, H. Fessler, T. H. Hyde and N. A. Warrior, “Stresses and deformations in overlapped diesel engine crankshafts. Part 1: experimental results” *Proc. Instn Mech. Engrs, Part D, Journal of Automobile Engineering*, Vol. 212, pp. 187-204, 1998.

40. Bickley, I., V. D’Olier, H. Fessler, T. H. Hyde and N. A. Warrior, “Stresses and deformations in overlapped diesel engine crankshafts. Part 2: evaluation of results” *Proc. Instn Mech. Engrs, Part D, Journal of Automobile Engineering*, Vol. 212, pp. 255-270, 1998.

41. Fessler, H., T. H. Hyde, A. P. Sime and N. A. Warrior, “The effect of regrinding bearing surfaces on stresses in overlapped crankshafts”, *Journal of Strain Analysis*, Vol. 33, No. 4, pp. 305-313, 1998.

42. Warrior, N. A., A. P. Sime, T. H. Hyde and H. Fessler, “The design of overlapped crankshafts. Part 1: crankpin fillets” *Proc. Instn Mech. Engrs, Part D, Journal of Automobile Engineering*, Vol. 215, pp. 503-513, 2001.

43. Warrior, N. A., A. P. Sime, T. H. Hyde and H. Fessler, "The design of overlapped crankshafts. Part 2: web shape" *Proc. Instn Mech. Engrs, Part D, Journal of Automobile Engineering*, Vol. 216, pp. 655-662, 2002.

44. Warrior, N. A., A. P. Sime, T. H. Hyde and H. Fessler, "Design of overlapped crankshafts. Part 3: holes in crankpin and journal" *Proc. Instn Mech. Engrs, Part D, Journal of Automobile Engineering*, Vol. 217, pp. 899-906, 2003.

45. Filipi, Z. S. and D. N. Assanis, "A nonlinear, transient, single-cylinder diesel engine simulation for predictions of instantaneous engine speed and torque" *Journal of Engineering for Gas Turbines and Power*, Vol. 123, pp. 951-959, 2001.

46. Taraza, D., N. A. Henein and W. Bryzik, "Determination of the gas-pressure torque of a multicylinder engine from measurements of the crankshaft's speed variation" *SAE Technical Paper*, No. 980164, 1998.

47. Taraza, D., N. A. Henein and W. Bryzik, "Friction losses in multi-cylinder diesel engines" *SAE Technical Paper*, No. 2000-01-0921, 2001.

48. Stanley, R. and D. Taraza, "A characteristic parameter to estimate the optimum counterweight mass of symmetric in-line engines" *Journal of Engineering for Gas Turbines and Power*, Vol. 126, pp. 645-655, 2004.

49. Lu, X., Z. Huang and G. Shu, "Modeling and experimental study on bending vibration of a diesel engine crankshaft" *Proc. Instn Mech. Engrs, Part D, Journal of Automobile Engineering*, Vol. 218, pp. 385-394, 2004.

50. Aminudin, B. A., J. E. Oh, J. Y. Lee, "Analysis of an in-line engine crankshaft under the firing condition" " *Proc. Instn Mech. Engrs, Part D, Journal of Automobile Engineering*, Vol. 219, pp. 345-353, 2005.

51. Engine and Powertrain Systems, Ford Otosan, Golcuk, Kocaeli, Turkey.

52. Yamauchi, T., Y. Yamazaki and J. Kimura, “Experiment and computation analyses for torsional vibration of crankshaft system with viscous torsional damper on diesel engine” *SAE Technical Paper*, No. 1999-01-1748, 1999.

53. Kimura, J., R. Kai and S. Shibata, “Six-cylinder in-line turbo-charged diesel engine crankshaft torsional vibration characteristics” *SAE Technical Paper*, No. 2001-01-2719, 2001.

54. Chen, S. K. and T. Chang, “Crankshaft torsional and damping simulation - an update and correlation with test results” *SAE Technical Paper*, No. 861226, 1986.

55. Citron, S. J., J. E. O’Higgins and L. Y. Chen, “Cylinder by cylinder engine pressure and pressure torque waveform determination utilizing speed fluctuations” *SAE Technical Paper*, No. 890486, 1989.

56. Taraza, D., “Estimation of the mean indicated pressure from measurements of the crankshaft angular speed variation” *SAE Technical Paper*, No. 932413, 1993.

57. Salzgeber, K., “Ford Otosan NHDD engine torsion vibration measurement” AVL Report AX0279, Graz, 2002.

58. Shiao, Y. and J. J. Moskwa, “An investigation of load force and dynamic error magnitude using the lumped mass connecting rog model” *SAE Technical Paper*, No. 930617, 1993.

59. EXCITE Designer Theory, AVL, Graz, 2003.

60. Altendorfer, H., “Design Analysis for the Ford Otosan NHDD engine”, AVL Report BC0178, Graz, 1999.

61. ADAMS/Engine Documentation, MSC.ADAMS 2005 r2, 2005.

62. ADAMS/Flex Documentation, MSC.ADAMS 2005 r2, 2005.

63. Craig, R. R. and M. C. C. Bampton, “Coupling of substructures for dynamic analyses” *AIAA Journal*, Vol. 6, No. 7, pp. 1313-1319, 1968.

64. Craig, R. R., *Structural dynamics – an introduction to computer methods*, John Wiley & Sons, New York, ISBN 0-04499-7, 1981.

65. Rebbert, M. and P. Kley, “Powertrain Dynamics Applications using "ADAMS/Engine powered by FEV" Part II: Cranktrain Dynamics”, International ADAMS Users Conference, Rome, 2000.

66. Rebbert, M., R. Lach and P. Kley, “Dynamic Crankshaft Stress Calculation using a combination of MSS and FEA”, International ADAMS User Meeting, Orlando, 2000.

67. AVL Report BT0070, “Ford Otosan new DI TCI 6-cylinder heavy duty diesel engine with two ratings (230 HP/300 HP): Thermodynamic calculations”, Graz 1999.

68. AVL Report BC0213, “EHD main bearing analysis for the Otosan NHDD engine”, Graz, 2000.

69. Shigley J and Mischke C, *Mechanical Engineering Design*, McGraw-Hill, New York, 1989.